

**GEOLOGICAL AND STRUCTURAL CONTROLS
ON
LA GARROTXA MONOGENETIC VOLCANIC FIELD
(NE IBERIA)**



Xavier de Bolós Granados
PhD Thesis

Universitat de Barcelona
Faculty of Geology
Department of Geodynamics and Geophysics

Barcelona 2014

**GEOLOGICAL AND STRUCTURAL CONTROLS
ON
LA GARROTXA MONOGENETIC VOLCANIC FIELD
(NE IBERIA)**

Xavier de Bolós Granados

Doctorat en Ciències de la Terra

Department of Geodynamic and Geophysics
Universitat de Barcelona - UB

Institute of Earth Science Jaume Almera
Consejo Superior de Investigaciones Científicas - CSIC

Supervisors

Prof. Joan Martí Molist

Dra. Stéphanie Barde-Cabusson

Tutor:

Prof. Joan Manuel Vilaplana

Barcelona 2014

*Als meus pares
i a la meva terra*

Contents

Agraiments

Abstract

Resum

Chapter 1. Introduction	1
1.1. Motivation	3
1.2. State of the art	3
1.2.1. Monogenetic volcanism	3
1.2.2. A review of the research history in La Garrotxa Volcanic Field	5
1.3. Main objectives	6
1.3. Outline	7
Chapter 2. Structural control of monogenetic volcanism in the Garrotxa volcanic field (Northeastern Spain) from gravity and self-potential measurements	9
2.1. Abstract	11
2.2. Introduction	11
2.3. Field investigations, data post-processing and modelling	14
2.3.1. Joint gravimetric and GPS surveys	14
2.3.2. Gravimetric data uncertainties and adjustment of geodetic reference frames	15
2.3.3. 3D inversion of Bouguer gravity anomaly data	16
2.3.4. Self-potential survey	17
2.4. Results	18
2.4.1. Local gravity anomaly	18
2.4.2. Gravity inversion results	19
2.4.3. Self-potential	20
2.5. Discussion	22
2.5.1. Distribution of volcanism related to local tectonics from gravity and self-potential data	22
2.5.2. Density anomaly models of volcanic roots	24
2.5.3. Volcano-tectonics of the Garrotxa monogenetic field	25
2.6. Conclusions	26
References	26
Supplementary material	30
Chapter 3. Geophysical exploration on the subsurface geology of La Garrotxa monogenetic Volcanic Field (NE Iberian Peninsula)	35
3.1. Abstract	37
3.2. Introduction	37
3.3. Geological settings	39

3.4. Methods	41
3.5. Results	42
3.5.1. Self-potential map	42
3.5.2. Electric resistivity tomography	44
Profile 1: Montsacopa volcano	44
Profile 2: Montolivet volcano.....	45
Profile 3, 4 and 5: Pujalós volcano	45
Profile 6: La Pomareda spatter cone.....	47
Profile 7 and 8: Croscat volcano.....	47
Profile 9: Santa Margarida volcano	50
3.6. Discussion	50
3.7. Conclusions	53
References	54
Chapter 4. Investigation of the inner structure of La Crosa de Sant Dalmai maar (Catalan Volcanic Zone, Spain)	59
4.1. Abstract	61
4.2. Introduction	61
4.3. Geological setting and general characteristics of La Crosa de Sant Dalmai	62
4.4. Methodology	65
4.5. Results	67
4.5.1. Geological data	67
4.5.2. Gravimetry	67
4.5.3. Magnetometry	69
4.5.4. Self-potential (SP)	69
4.5.5. Electrical resistivity tomography (ERT)	70
4.6. Discussion	72
4.6.1. Phreatomagmatic activity	72
4.6.2. Strombolian activity	72
4.6.3. Post-eruptive phase	72
4.6.4. Geological control on the eruptive activity	74
4.6. Conclusions	76
References	77
Chapter 5. Electrical resistivity tomography revealing the internal structure of monogenetic volcanoes	79
5.1. Abstract	81
5.2. Introduction	81
5.3. Monogenetic Volcanism in the Garrotxa Volcanic Field	82
5.3. Data Acquisition and Processing	83
5.3. Results	85
5.3. Discussion	86
5.3. Conclusions	88
References	89
Chapter 6. Volcanic stratigraphy of the Quaternary La Garrotxa Volcanic Field (NE Iberian Peninsula)	91
6.1. Abstract	93
6.2. Introduction	93

6.3. Geological settings	94
6.4. Methodology	97
6.5. Volcanic stratigraphy vs. conventional stratigraphy	100
6.6. Results	101
6.7. Discussion and conclusions	110
References	111
Supplementary material	116
Chapter 7. Volcano-structural analysis of La Garrotxa Volcanic Field (NE Iberia): implications for the plumbing system	121
7.1. Abstract	123
7.2. Introduction	123
7.3. Geological settings	124
7.4. Methodology	126
7.5. Results	134
7.6. Discussion and conclusions	136
References	140
Supplementary material	146
Chapter 8. Summary of results and discussion	153
Chapter 9. Conclusions	159
References	163
Appendix 1. Contribution to the papers	173
Appendix 2. Structural control of monogenetic volcanism in the Garrotxa volcanic field (Northeastern Spain) from gravity and self-potential measurements	177
Appendix 3. Geophysical exploration on the subsurface geology of La Garrotxa monogenetic Volcanic Field (NE Iberian Peninsula)	193
Appendix 4. Investigation of the inner structure of La Crosa de Sant Dalmai maar (Catalan Volcanic Zone, Spain)	209
Appendix 5. Electrical resistivity tomography revealing the internal structure of monogenetic volcanoes	223
Appendix 6. Volcanic stratigraphy of the Quaternary La Garrotxa Volcanic Field (NE Iberian Peninsula)	231
Appendix 6.1. Acceptance proof of the paper	376
Appendix 7. Volcano-structural analysis of La Garrotxa Volcanic Field (NE Iberia): implications for the plumbing system	277
Appendix 7.1. Proof of delivery of the paper	325

Agraïments

Són moltes les persones que han contribuït durant la realització de la present Tesi Doctoral, no només des d'un punt de vista professional sinó també personal. A totes elles moltes gràcies!

En primer lloc vull donar les gràcies al meu director el Prof. Joan Martí, per donar-me la oportunitat de formar part del Grup de Vulcanologia de Barcelona i sobretot per guiar-me i formar-me durant aquests darrers anys. Vull agrair-li també d'una forma molt especial a la meva codirectora la Dra. Stéphanie Barde-Cabusson per tots els coneixements que m'ha transmès i pel suport que m'ha donat en tot moment.

Al meu company de viatge Dario Pedrazzi, per totes les dures jornades al camp, i per totes les aventures i viatges que hem viscut junts pel món. Grazie Dario!

Vull agrair especialment al company olotí Llorenç Planagumà el suport que m'ha donat en els darrers anys a més de totes les contribucions, discussions i ratafies fetes. Aquesta Tesi no hagués estat possible sense la seva ajuda.

Gràcies als companys del Grup de Vulcanologia i en general de l'Institut de Ciències de la Terra Jaume Almera del CSIC pel seu suport i amiatat, en especial a la Stefania Bartolini, la Laura Becerril, la Sílvia Aragó, l'Adelina Geyer i l'Alberto Carballo.

Al Prof. Albert Casas de la Universitat de Barcelona per la seva entrega i per la inestimable col·laboració que m'ha mostrat sempre i en tot moment.

De l'estància d'investigació a Orleans em vaig endur, no només una gran experiència professional, sinó també uns bons amics. Gràcies Joan Andujar, Prof. Michel Pichavant, Pierangelo Romano i Arnaud Villaros, per fer fàcil lo difícil.

Als companys d'Olot per la col·laboració en les campanyes de camp, tot i fer vida lluny de la nostra terra sempre trobaven una excusa per ajudar. No voldria oblidar-me del meu amic Fok, junts hem cartografiat i trepitjat totes i cadascuna de les valls de la comarca.

Gràcies a tot el personal del Parc Natural, en especial a l'Emili Bassols pel suport i l'interès que m'han mostrat sempre.

Sense la financiació del projecta "VUELCO" (European Commission, FT7 Theme: ENV.2011.1.3.3-1; Grant 282759) com també de la Beca Ciutat d'Olot en Ciències Naturals, res del que reflexa aquesta memòria hagués estat possible.

Vull agrair molt especialment a la Núria Bagués tot el suport, comprensió, carinyo i ajuda que em mostra a diari. Moltes gràcies Núria!!

Per acabar, vull donar les gràcies i agrair d'una forma molt especial als meus pares Josep de Bolós i Dolors Granados tot l'esforç, voluntat i sacrifici que han fet sempre! per tal que jo avui estigui escrivint les últimes paraules de la Tesi Doctoral, la qual ús dedico.

Gràcies a tots!

Xavier

Barcelona, 12 de Juny del 2014

Abstract

Basaltic monogenetic volcanism is widely distributed around the World and is characterised by the formation of volcanoes that erupt small amounts (0.01–0.2 km³) of mafic magma in short lived eruptions typically lasting from few days to few months. Monogenetic volcanoes are often grouped in volcanic fields, the distribution of which depends in each case on their regional and local tectonic controls. The great variety of eruptive styles, edifice morphologies, and deposits shown by monogenetic volcanoes is the result of a complex combination of internal (magma composition, gas content, magma rheology, magma volume, etc.) and external (regional and local stress fields, stratigraphic and rheological contrasts of substrate rock, hydrogeology, etc.) parameters during magma transport from the source region to the surface.

The present PhD Thesis focuses on the geological and structural controls of monogenetic volcanism. It pays particular attention to the uppermost part of the lithosphere and its role to determine the distribution of eruptive vents and eruptive styles. We have selected La Garrotxa Volcanic Field (GVF) as a case study. This Quaternary volcanic field is located in the Northeast of the Iberian Peninsula and includes more than 50 well-preserved volcanoes. It covers an area of 600 km², between the cities of Olot and Girona and belongs to the Catalan Volcanic Zone, one of the alkaline volcanic provinces of the European Rift System. The GVF is still poorly known and has become an ideal place for the application of the multidisciplinary studies, including geophysical methods, geological fieldwork and geomorphological and structural analyses, which constitute this PhD Thesis.

The first work was carried out at the Northern sector of the GVF. This study was mainly based on the application of gravimetry and self-potential techniques, in order to identify the main tectonic structures of the volcanic area at depth. A second work was performed in order to obtain a much better detail of the shallower structures and to relate the subsurface geology to the feeding system of these monogenetic volcanoes. In this case, we applied the electrical resistivity tomography method, comparing the new data with the self-potential results. A third work was carried out at the Southern sector of the GVF, at La Crosa de Sant Dalmai volcano (10 km SW of Girona), one of the biggest maar-diatreme edifices of the Iberian Peninsula. Here, several geophysical techniques were applied, including gravimetry, magnetometry, self-potential and electrical resistivity tomography. A model of the uppermost part of the diatreme was obtained, determining the internal structure and its origin. The results obtained with the application of these geophysical methods in this volcanic field suggest that electrical resistivity tomography is a useful tool for the study the internal structures of different types of monogenetic landforms. In this way we present a short work that illustrates different examples of internal structures of monogenetic volcanic cones from GVF. Furthermore, combining the results from these geophysical studies with the geological informations obtained by fieldwork, we performed the first volcanic

stratigraphy map of the GVF. Finally, we also led a detailed volcano-structural analysis of the whole volcanic field, including geostatistical distribution of faults, fissures and vents, morpho-structural lineaments identified by remote sensing, a morphometrical analysis of the volcanic cones and craters, location of regional seismic events recorded in the area (since 1978), and mantle derived gases in springs and water wells, as a guide to identify active faults and open fractures and to define the structural controls of this volcanism.

The results obtained from all these studies have permitted understanding how magma was transported into the lithosphere and erupted at the surface, and represent an essential tool for a correct volcanic hazard assessment of the GVF. Furthermore, the methodologies described in this PhD Thesis establish general guidelines to study active monogenetic volcanic fields and we hope that it will contribute to improve their understanding.

Resum

El vulcanisme basàltic monogenètic està extensament distribuït arreu del món i es caracteritza per la formació de volcans amb poc volum de material emès ($0,01$ a $0,2 \text{ km}^3$) de magma màfic en erupcions de curta durada, habitualment amb períodes de pocs dies fins a mesos. Els volcans monogenètics sovint estan agrupats en camps volcànics, la distribució dels quals depèn del control tectònic regional i local al qual estan sotmesos en cada cas. La gran varietat d'estils eruptius, morfologies volcàniques i dipòsits, que presenta el vulcanisme monogenètic són el resultat d'una complexa combinació de paràmetres interns (composició del magma, contingut de gas, reologia del magma, volum de magma, etc.) i externs (camps d'esforços locals i regionals, contrastos estratigràfics i reològics del substrat, hidrogeologia, etc.) durant el transport del magma des de la zona d'origen fins la superfície.

La present Tesi Doctoral es centra en els controls geològics i estructurals del vulcanisme monogenètic. S'ha posat especial atenció a la part més superficial de la litosfera i en el paper que juga aquesta zona en determinar la distribució de punts emissors i estils eruptius. S'ha seleccionat com a cas estudi el Camp Volcànic de la Garrotxa (GVF), localitzat al nord-est de la Península Ibèrica, el qual comprèn més de 50 volcans ben preservats. Aquest camp volcànic Quaternari s'estén per una àrea de més 600 km^2 , entre les ciutats d'Olot i Girona, i forma part de la Zona Volcànica Catalana, una de les províncies volcàniques alcalines del Rift Europeu. El GVF és encara poc conegut i ha esdevingut un lloc ideal per l'aplicació d'estudis multidisciplinaris com els treballs que constitueixen aquesta Tesi Doctoral, integrant mètodes geofísics, treballs de camp, i anàlisis geomorfològics i estructurals.

El primer treball s'ha portat a terme al sector Nord del GVF. Aquest estudi s'ha basat principalment en l'aplicació de les tècniques de gravimetria i potencial espontani, per tal d'identificar les estructures tectòniques principals de la zona volcànica en profunditat. Un segon treball s'ha realitzat per tal d'obtenir un major detall de les estructures superficials i relacionar la geologia subsuperficial amb el sistema d'ascens magmàtic d'aquest volcans monogenètics. En aquest cas, s'ha aplicat el mètode geofísic de la tomografia elèctrica comparant les noves dades amb els resultats de potencial espontani. Un tercer treball s'ha dut a terme en el sector Sud del GVF, concretament en el volcà de la Crosa de Sant Dalmai (a 10 km al SO de Girona), un dels maar-diatrema més grans de la Península Ibèrica. Per portar-ho a terme, s'han usat diverses tècniques geofísiques, incloent gravimetria, magnetometria, potencial espontani i tomografia elèctrica. D'aquesta manera s'ha obtingut un model de la part superior de la diatrema, determinant la seva estructura interna i el seu origen. El resultat obtingut amb l'aplicació d'aquests mètodes geofísics en aquest camp volcànic, suggereix que la tomografia elèctrica resulta una eina eficaç per l'estudi de l'estructura interna en diferents tipus d'edificis monogenètics. D'aquesta manera es presenta un treball breu amb diferents exemples il·lustratius de l'estructura interna de cons volcànics del camp monogenètic del

GVF. A més, combinant els resultats d'aquests estudis geofísics amb la informació geològica obtinguda a partir de treballs de camp, s'ha realitzat la primera cartografia vulcanoestratigràfica del GVF. Finalment, també s'ha portat a terme un anàlisi detallat de la volcano-estructura de tot el camp volcànic, el qual inclou la distribució geoestadística de falles, fissures eruptives i punts emissors, identificació morfo-estructural de lineacions a partir de teledetecció, un anàlisi morfomètric dels cons i els cràters, localització de la sismicitat registrada de la zona (des de 1978) i gasos derivats del mantell en surgències i pous, com a guia per identificar falles actives o fractures obertes, per tal de definir els controls estructurals d'aquest vulcanisme.

Els resultats obtinguts a partir de tots aquests estudis han permès entendre com el magma va ser transportat des de la litosfera fins fer erupció a la superfície, i representa un eina essencial per una correcta avaluació de la perillositat volcànica al GVF. Tanmateix, les metodologies descrites en aquesta Tesi Doctoral estableixen una pauta general per l'estudi dels camps volcànics monogenètics actius, i s'espera que contribueixi a millorar-ne el seu coneixement.

1

Introduction

1.1. Motivation

Scoria cone and maar-diatreme edifices are the main manifestations of monogenetic volcanism and are often grouped into volcanic fields that are found in any geotectonic settings. Due to the abundance of this volcanism, about 10% of the world population lives in active volcanic areas (Baxter, 2000; Lorenz, 2007).

The Neogene-Quaternary European Cenozoic Rift System contains several volcanic areas, all related to the same geodynamic environment but with different local tectonics affecting volcanism (Wilson and Downes 1991, 1992; Downes 2001; Dèzes et al. 2004). The stratigraphic and volcano-structural evolution of the different volcanic fields of this rift system is still poorly known. Moreover, one of the least studied of these recent European volcanic areas is the Catalan Volcanic Zone (CVZ) (Martí et al., 1992) located in the northeast of Iberia.

As part of the CVZ, La Garrotxa monogenetic Volcanic Field (GVF) is the youngest (Middle Pleistocene to Early Holocene) and the best-preserved volcanic area of the Iberian Peninsula. This volcanic field offers exceptional conditions, in terms of size and distribution of volcanic vents and products, to study the evolution of the dynamics of volcanism. During the last years, several studies have been conducted in this area mostly addressed to characterise the volcanic activity and petrology of volcanic products (Bianchini et al., 2007; Di Traglia et al., 2009; Gisbert et al., 2009; Martí et al., 2011; Cimarelli et al., 2012, 2013; Pedrazzi et al., 2014). However, the geological and structural controls of this magmatism and related volcanism are still poorly constrained. This is why we have addressed this PhD Thesis to the study of the GVF in order to characterise how regional and local tectonics have influenced and controlled the volcanic activity in the area. In addition, the purpose of this PhD Thesis is to make the results obtained applicable to other volcanic areas of similar characteristics, thus contributing to the general understanding on monogenetic volcanism.

Moreover, the characterisation of the geological and structural controls of this volcanic field will constitute the basis to build a comprehensive hazard assessment of the area. Despite, volcanic activity stopped about Early Holocene, the fact that volcanism in CVZ started more than 12 Ma ago (Araña et al., 1983) and continued nearly to present, suggests that this is not an extinct area. In fact, since 2013, this volcanic field has been considered, in legal terms, as an active volcanic area jointly to other Spanish volcanic zones (e.g.: Canary Islands) by the Spanish government. This is illustrated in the Spanish for Official Bulletin of the State (B.O.E) of February 11th of 2013, which establishes the actions procedure for a correct volcanic risk assessment, including a correct knowledge of the area. This implicates that hazard assessment, together with volcano monitoring, is a necessary requisite to reduce potential volcanic risk in this area.

1.2. State of the art

1.2.1. Monogenetic volcanism

Monogenetic volcanism represents the most common volcano type on Earth (Wood, 1980; Cas and Wright (1987), Wohletz and Heiken (1992), Vespermann and Schmincke (2000), Schmincke (2004), Lorenz (2007), and Le Corvec (2013). Monogenetic volcanoes are commonly clustered within volcanic fields and are present in any geotectonic and environmental setting

(Connor and Conway, 2000; Valentine and Gregg, 2008; Kereszturi and Németh, 2012). Basaltic monogenetic volcanism is characterised by the formation of volcanoes that erupt small amounts (0.01–0.2 km³) of mafic magma in short lived eruptions typically lasting from few days to few months (Fiske and Jackson, 1972; Walker, 1999). Each volcanic eruption is the end process of a magma rising from its source in the upper mantle to the surface (e.g., Brenna et al., 2011; McGee et al., 2011). Monogenetic volcanoes distribution inside a volcanic field depends in each case on their regional and local tectonic controls. The great variety of eruptive styles, edifice morphologies, and deposits shown by monogenetic volcanoes are the result of a complex combination of internal (magma composition, gas content, magma rheology, magma volume, etc.) and external (regional and local stress fields, stratigraphic and rheological contrasts of substrate rock, hydrogeology, etc.) parameters, during the magma transport from the source region to the surface (Gretener, 1969; Clemens and Mawer, 1992; Gudmundsson, 2003; Tibaldi, 2003; Acocella and Tibaldi, 2005; Gudmundsson and Philipp, 2006; Kavanagh et al., 2006; Tibaldi et al., 2014). These recent findings highlight the need to view volcanic fields in the same manner as we view composite volcanoes in terms of dangerousness (Németh, 2010).

A monogenetic basaltic volcanic field may contain an average 10 to 100 volcanoes of cumulative volume about 10 km³, and may span 50 ka to 5 Ma (Connor and Conway, 2000) during which dramatic climatic and paleoenvironmental changes can take place (Németh, 2010). However, some volcanic fields are much larger than the average. This is the case of the Michoacan-Guanajuato volcanic field in Mexico that contains more than 1000 volcanoes and covers an area about 40,000 km² (Hasenaka and Carmichael, 1985; Connor, 1987; Hasenaka, 1994).

Eruptions in monogenetic volcanic fields are difficult to forecast because the factors controlling the precursory activity are still poorly understood. Furthermore, in monogenetic volcanism each new eruption creates a different vent, suggesting that volcanic susceptibility (i.e.: the probability of vent opening, Martí and Felpeto, 2010) contains a high degree of randomness and that accurate spatial forecasting is highly uncertain. Recent studies of monogenetic volcanism reveal how sensitive magma migration is to changes in regional and/or local stress fields caused by structural or lithological contrasts (e.g. former magmatic intrusions) (Martí et al. 2013). This may induce variations in the pattern of further magma movements and thus affect the location of future eruption sites. Furthermore, the interaction between monogenetic volcanoes and the uppermost part of the basement plays an important role in the evolution of volcanic fields (Tibaldi and Lagmay, 2006), as shown by changes in eruption dynamics occurring at different vents located at relatively short distances.

Studies of monogenetic volcanic fields are among the earliest works in Volcanology. One of the first surveys was carried out by Nicholas Desmarest, a geologist that mapped the cinder cones of Auvergne, France, around 1766. The major contribution of Desmarest was the relative volcano-stratigraphy of cinder cones in Auvergne using the superposition of lava flows deposits that he carefully correlated to eruptive vents when possible. Subsequently, all mappings in volcanic fields have emulated the techniques used by Desmarest. The 1759–1774 eruption of Jorullo volcano in the Michoacán-Guanajuato volcanic field (Mexico) focused additional attention on this type of volcanism. Geologists such as Von Humboldt, Scrope, and Lyell noted the great number of cones around Jorullo and realized that these cones formed during episodes of similar eruptive styles. The 1943–1952 eruptions of Parícutin volcano, also in the Michoacán-Guanajuato volcanic field, led to more systematic mapping in this area. In his

pioneer work on volcanoes of the Parícutin region, Williams (1950) conducted petrologic investigations, mapping, and relative dating of volcanoes in this area, resulting in the first comprehensive, modern treatment of basaltic volcanic fields. During the sixties and seventies, the NASA lunar programme started several studies of monogenetic volcanoes on Earth. These research projects were focused on morphological aspects of monogenetic volcanic landforms in order to relate these morphologies to analogous extra terrestrial landforms. In the last decades, the number of studies devoted to characterise the distribution patterns of monogenetic volcanic fields and the tectonic environment in which they occur has increased (e.g. Rout et al., 1993; Nishi et al., 1996; Bibby et al., 1998; Di Maio et al., 1998, 2000; Németh et al., 2001; Schulz et al., 2005; Ross et al., 2011; Blaikie et al., 2014).

Due to the complexity that magmatic plumbing systems in monogenetic volcanism entails, the geologists need other methods for understanding the structural and stratigraphic setting of a volcanic area and the pathways of the magma in its ascent to the Earth's surface. In this way, geophysical exploration and more specifically geoelectrical methods have been used in different volcanic areas around the world. For example, in Ethiopian Rift Valley, Emilia et al. (1977) applied magnetic anomaly and resistivity measurements to investigate the evolution of a volcanic crater. Nishi et al. (1996), in New Zealand, applied self-potential surveys to study the hydrothermal system of White Island Volcano. Bibby et al. (1998) used electrical resistivity imaging to characterise the upper crust of the Taupo Volcanic Zone. In Italy Di Maio et al (1998, 2000) applied electrical and electromagnetic methods to study the structure of Mount Somma and Campi Flegrei. In Japan Hase et al (2005) studied the hydrothermal system beneath Aso volcano with self-potential and resistivity measurements. In Massif Central of France Portal et al (2013) explored the inner structure of Puy de Dôme volcano from electrical resistivity tomography, gravity and muon imaging. These studies have proven the efficiency of geoelectrical methods in the characterisation of the inner structure of volcanic systems. For this reason they have been also applied recently to the study of monogenetic volcanic fields (Brunner et al., 1999; López-Loera et al., 2008; Mrlina et al., 2009; Martin-Serrano et al., 2009; Cassidy and Locke, 2010; Blaikie et al., 2012; Valenta et al., 2014), and constitute one of the main contributions of this PhD Thesis.

1.2.2. A review of the research history in La Garrotxa Volcanic Field

The early naturalistic and geological works in La Garrotxa Volcanic Field (GVF) were carried out by the pharmacist and naturalist Francesc X. Bolós (1776, published in 1820 and 1841). In 1808 the geologist William Maclure came to the region of Olot accompanied by Bolós (Bolós 1841; Riba 1996). Soon after, Maclure published the first scientific note about the volcanic region of Catalonia (Maclure 1808) without ever mentioning the communications given by Bolós. Lyell visited the GVF in 1830 and he was helped in the fieldwork around the Olot area by Bolós (Lyell 1833; Bolós 1841; Riba 1996). Lyell, on the basis of his field observations, included a very well illustrated geological study of "*Volcanic region of Olot in Catalonia*" in the "*Principles of Geology*" (Lyell 1833). Since then, several national and foreign researchers have published about this volcanic area in the main European scientific journals and geological societies.

At the beginning of 20th century the works by Gelabert (1904), Sapper (1904), Calderon et al. (1906), Washington (1907), San Miguel de la Cámara (1918, 1936), San Miguel de la

Cámara and Marcet Riba (1926), Chevalier (1926, 1927, 1931a, 1931b); Bolós (1931), and Loewinson-Lessin (1931) include detailed descriptions about the main volcanoes of the GVF, as well as the first petrographic and geochemical studies of their rocks and an improvement of the geological maps of the area.

During the Spanish Civil War (1936 – 1939), all scientific activity on this region was interrupted. More than 20 years were required to reactivate the research activity on the area. After this inactivity period, Solé Sabarís and Marcet Riba (1953), Solé Sabarís (1957, 1962), Bolós (1957), Cardelús (1957), and Guardia (1964), restored the research in the GVF giving the first chronology of this Quaternary monogenetic volcanism. During the seventies the number of authors working on the GVF increased (e.g.: Donville 1973; Fayas and Doménech 1974; Riba 1975; Coy-Yll et al., 1975; Mallarach 1976; Bech et al., 1976; Solé Sograñes 1978) with the research work focused on several subjects (i.e.: geochronology, geomorphology, geothermalism, geochemistry and structural geology).

Mallarach and Riera (1981), Mallarach (1982, 1998), Araña, et al. (1983), and Martí and Mallarach (1987) provided the first insights into the eruptive mechanisms of the GVF, pointing out the presence of a large number of volcanoes with phreatomagmatic activity. Martí et al. (1992) published for the first time an overview of regional and global settings of the GVF, outlining the relationship between the volcanism in this area and the rift system related to the Valencia Trough. From that time, the most abundant research articles about the area were related to petrological and geochemical aspects of the basaltic rocks and their xenoliths (Llobera 1983; López-Ruiz and Badiola 1985; Neumann et al., 1999; Cebrià et al., 2000; Enrique and Toribio 2009; Oliveras and Galán 2006, 2009; Bianchini et al., 2007; Galán et al., 2008; Oliveras 2009; Gisbert et al., 2011; Cimorelli et al., 2012). However, some insights about the geophysical, tectonic and structural aspects of the area were also published by Gallart et al. (1984, 1991), Fernández et al. (1990), Vegas (1994), Saula et al. (1996), Goula et al. (1999), Lewis et al. (2000), Zarroca et al. (2012), and Moreno et al. (2014).

During the last decade new data addressed to characterise the volcanic activity of this volcanic field were produced (Di Traglia et al., 2009; Gisbert et al., 2009; Martí et al., 2011; Cimorelli et al., 2013; Pedrazzi et al., 2014).

The inheritance of the whole naturalists and researchers that investigated the GVF is an essential starting point in order to allow further geological studies in this area. Furthermore, the GVF is an ideal place to apply several geological and geophysical methods in order to understand the different aspects that conform the volcanology of the area, to compare it with other monogenetic volcanic fields worldwide, and to assess its potential hazard and risk.

1.3. Main objectives

The present PhD Thesis aims to characterise how regional and local tectonics have influenced and controlled the volcanic activity in the GVF, in order to understand how magma was transported through the lithosphere and erupted at the surface. Particular attention has been paid on the geology of the uppermost part of the lithosphere and its role to determine the distribution of eruptive vents and eruptive styles. Therefore, the main overall objective has been to establish general guidelines to study the structural controls on active monogenetic volcanism, thus contributing to improve their understanding. This was

achieved by applying different methods, such as geophysical methods, fieldwork and geomorphological and structural analyses.

The specific aims of this PhD Thesis are: (a) to study the relationship between the distribution of monogenetic volcanic landforms and the subsurface structure of the GVF, (b) to clarify the control exerted by the substrate geology in this volcanic field, (c) to explore the internal structure of simple and complex monogenetic volcanoes including a tuff cone and the biggest maar-diatreme of the GVF, (d) to reconstruct the eruptive history and geochronological evolution of the whole study area, and (e) to establish the tectonic controls and the geodynamic origin of this volcanic field.

The specific results obtained from this multidisciplinary work represent an essential tool to lead a correct volcanic hazard assessment of the area, but also a step forward in the preservation of the geological heritage of the GVF.

1.4. Outline

This PhD dissertation is structured into several chapters each one corresponding to a different research paper that constitutes independent but interrelated scientific contributions. In this sense, each work reflects the main objectives of the PhD Thesis and describes the different methodologies applied in the GVF, in order to develop a conceptual model of magma transport through the lithosphere and its eruption at surface, which will contribute to improve our understanding of the volcanic evolution of this region and to undertake hazard assessment in this monogenetic volcanic field.

Chapter 1 is this general introduction. Chapters 2 to 5 correspond to research papers consisting of several geophysical surveys performed in different specific areas of the GVF, and which have allowed to reconstruct the internal structure of these volcanoes and the geology of the substrate on which they built up. Combining these results with geological information obtained from new fieldwork and remote sensing studies, chapters 6 and 7 offer the volcanic stratigraphy of the whole volcanic field and its volcano-structural analysis, respectively.

The first geophysical survey (Chapter 2) was performed at the Northern sector of the study area. This study was mainly based on the application of gravimetry and self-potential techniques, in order to identify the main tectonic structures of the volcanic area at depth. This work was published in *Bulletin of Volcanology* (Barde-Cabusson et al., 2014).

A second work (Chapter 3) was performed in order to obtain a much better resolution of the shallowest structures and to relate the subsurface geology to the feeding system of these monogenetic volcanoes and to their eruptive style. In this case, we applied the electrical resistivity tomography method, comparing the new data with the previous self-potential results. The study is presented in Bolós et al. (2014) in *International Journal of Earth Science*.

A third work (Chapter 4) was carried out at the Southern sector of the GVF, at La Crosa de Sant Dalmai volcano (10 km SW of Girona), one of the biggest Quaternary maar-diatreme edifices of the Iberian Peninsula. Here, several geophysical techniques were applied: gravimetry, magnetometry, self-potential and electrical resistivity tomography. A model of the uppermost part of the diatreme was proposed, determining the internal

structure and its origin. The results were published in *Journal of Volcanology and Geothermal Research* (Bolós et al., 2012).

The results obtained with the application of geophysical methods in the mentioned works, suggested that electrical resistivity tomography is a useful tool to study the internal structures of different types of monogenetic landforms. In this way we present a short work (Chapter 5), published in *Geophysical Research Letters* (Barde-Cabusson et al., 2013) that illustrates various examples of internal structures of monogenetic volcanic cones from GVF.

The fifth work conducted in the area (Chapter 6) as part of this PhD Thesis, consisted in studying and cataloguing all new ephemeral outcrops, water wells, and geotechnical boreholes (almost 100). This enabled us to establish the first volcanic stratigraphy of the whole volcanic succession, completing a detailed volcanological map of this volcanic field, which includes the geology below the city of Olot. Likewise, the knowledge of the relative geochronology and extension of the most recent volcanic deposits has also improved. This work is presented in Bolós et al. (2014 in-press) in *Journal of Quaternary Science*.

The final study (Chapter 7) corresponds to a detailed volcano-structural analysis of the whole volcanic field. This includes geostatistical distribution of faults, fissures and vents, morpho-structural lineaments identified by remote sensing, a morphometrical analysis of the volcanic cones and craters, location of regional seismic events recorded in the area (since 1978), and mantle derived gases in springs and water wells, used as a guide to identify active faults and open fractures and to define the structural controls of this volcanism. This study is currently under review in *Tectonophysics* (Bolós et al., under-review).

The last chapters (Chapters 8 and 9) correspond to the summary of the results and discussion and to the general conclusions of the whole work, respectively.

Therefore, the structure of this PhD Thesis follows a logical sequence in which the reader first identifies the main aims of the work, thereby enhancing the coherence of the working approach. Then, the main geological and structural features of this monogenetic volcanism are progressively defined in order to provide at the end a coherent conceptual model of the magmatic plumbing system of this volcanic field.

2

Structural control of monogenetic volcanism in the Garrotxa volcanic field (Northeastern Spain) from gravity and self-potential measurements

Published in:

Bulletin of Volcanology

Authors of the paper:

Stéphanie Barde-Cabusson ^(a)

Joachim Gottsmann ^(b)

Joan Martí ^(a)

Xavier Bolós ^(a)

Antonio Gonzalez Camacho ^(c)

Adelina Geyer ^(a)

Llorenç Planagumà ^(d)

Erika Ronchin ^(a)

Anna Sánchez ^(a)

a) Institute of Earth Sciences Jaume Almera, ICTJA-CSIC, Group of Volcanology. SIMGEO (UB-CSIC) Lluís Sole i Sabarís s/n, 08028 Barcelona, Spain

b) Department of Earth Sciences, University of Bristol, Wills Memorial Building, Queens Road, Bristol BS8 1RJ, UK

c) Instituto de Geociencias (CSIC, UCM), Plaza de Ciencias 3, 28040 Madrid, Spain

d) Tosca, Environment Services of Education, Casal dels Volcans, Av. Santa Coloma, 17800 Olot, Spain

2.1. Abstract

We report new geophysical observations on the distribution of subsurface structures associated with monogenetic volcanism in the Garrotxa volcanic field (Northern Spain). As part of the Catalan Volcanic Zone, this Quaternary volcanic field is associated with the European rifts system. It contains the most recent and best preserved volcanic edifices of the Catalan Volcanic Zone with 38 monogenetic volcanoes identified in the Garrotxa Natural Park. We conducted new gravimetric and self-potential surveys to enhance our understanding of the relationship between the local geology and the spatial distribution of the monogenetic volcanoes. The main finding of this study is that the central part of the volcanic field is dominated by a broad negative Bouguer anomaly of around -0.5 mGal, within which a series of gravity minima are found with amplitudes of up to -2.3 mGal. Inverse modelling of the Bouguer data suggests that surficial low-density material dominates the volcanic field, most likely associated with effusive and explosive surface deposits. In contrast, an arcuate cluster of gravity minima to the NW of the Croscat volcano, the youngest volcano of this zone, is modelled by vertically extended low-density bodies, which we interpret as a complex ensemble of fault damage zones and the roots of young scoria cones. A ground-water infiltration zone identified by a self-potential anomaly is associated with a steep horizontal Bouguer gravity gradient and interpreted as a fault zone and/or magmatic fissure, which fed the most recent volcanic activity in the Garrotxa. Gravimetric and self-potential data are well correlated and indicate a control on the locations of scoria cones by NNE–SSW and NNW–SSE striking tectonic features, which intersect the main structural boundaries of the study area to the north and south. Our interpretation of the data is that faults facilitated magma ascent to the surface. Our findings have major implications for understanding the relationship between subsurface structures and potential future volcanic activity in the Garrotxa volcanic field.

Keywords: Self-potential · Gravimetry · Garrotxa · Structural control · Monogenetic volcanism

2.2. Introduction

The temporal and spatial distribution of monogenetic volcanoes and the probability of future activity in monogenetic volcanic fields are subjects of increasing interest (e.g. Scandone 1979; Connor and Hill 1995; Connor et al. 2000; Alberico et al. 2002; Martin et al. 2003; Valentine and Perry 2006; Alberico et al. 2008). Statistical analyses indicate that deep and near-surface geological structures may control the distribution of magmatic complexes and volcanic vents (Zhang and Lutz 1989; Lutz and

Gutmann 1995; Paulsen and Wilson 2010), but geological structures are often hidden and their identification from surface geology alone can be difficult. Statistical, numerical and geological studies are ideally combined with geophysical investigations to build geologically meaningful models (Kiyosugi et al. 2010; Cebrià et al. 2011). In addition, geophysical methods have already been shown to be useful in studying dispersed volcanic fields and their relation to local tectonics (e.g. Rout et al. 1993 with detailed gravity and aeromagnetic studies on the Auckland volcanic field, New Zealand; Blakely et al. 1997 with gravity data on the Cascade Range, Oregon and California; Connor et al. 2000 with a combination of gravity data and magnetic data at Yucca Mountain (Nevada); Kiyosugi et al. 2010 with P wave tomography from the Abu Monogenetic Volcano Group, Japan).

In a monogenetic volcanic field, from one eruption to another, magma must be transported from source to surface at different places. Depending on stress conditions, magma injection parameters and geometry, pre-existing crustal fractures may influence the propagation of magmas (Valentine and Krogh 2006; Gaffney et al. 2007; Wetmore et al. 2009). In a set of analogue experiments, Le Corvec et al. (2013) investigate the conditions leading a dyke to interact with preexisting fractures into the crust, by varying (1) the volume of injected magma, (2) the distance between a dike and a preexisting fracture and (3) the impact of a deviatoric stress. They find that, in nature, the interaction between propagating dikes and pre-existing fractures is likely to occur when the horizontal distance that separates them becomes less than about 200 m, and they determine that dikes with a volume less than about $10\text{--}2\text{ km}^3$ would experience a decrease in their propagation velocity owing to the presence of surrounding fractures.

The Garrotxa monogenetic volcanic field is part of the Catalan Volcanic Zone (Martí et al. 1992) and hosts one of the Spanish Peninsula's youngest volcanic fields (Fig. 1).

The Catalan Volcanic Zone is itself part of a major European belt of young volcanic zones and rift valleys (Wilson and Downes 1991) including the Eger graben and the Rhone–Rhine valley systems. Despite eruptive activity as recently as 10 ka BP (Cébria et al. 2000), the hazard potential of the Garrotxa volcanic field has been little studied and needs to be accurately assessed. Most of the volcanic activity of the Garrotxa took place along a WNW–ESE trending depression, corresponding to an eroded anticline of Eocene rocks (Martí et al. 2011; Fig. 1). The volcanic activity within the Garrotxa volcanic field is concentrated along structural lineaments (Martí et al. 2011; Cimarelli et al. 2013). Martí et al. (2011) described the main characteristics of the volcanism and the stratigraphic sequences of some key volcanic edifices in this area. They conclude that the main cause of the complex eruptive behaviour observed in the Garrotxa volcanic field resides in the lithological, structural and hydrogeological characteristics of the substrate beneath the volcanoes. However, knowledge of the subsurface architecture from geophysical data has so far only been available on a regional scale.

Here, we present results from a study of the subsurface structure beneath the Garrotxa volcanic field using new gravity and self-potential data to assess the relationship between the distribution of volcanic landforms and the subsurface structure of the field (Fig. 2).

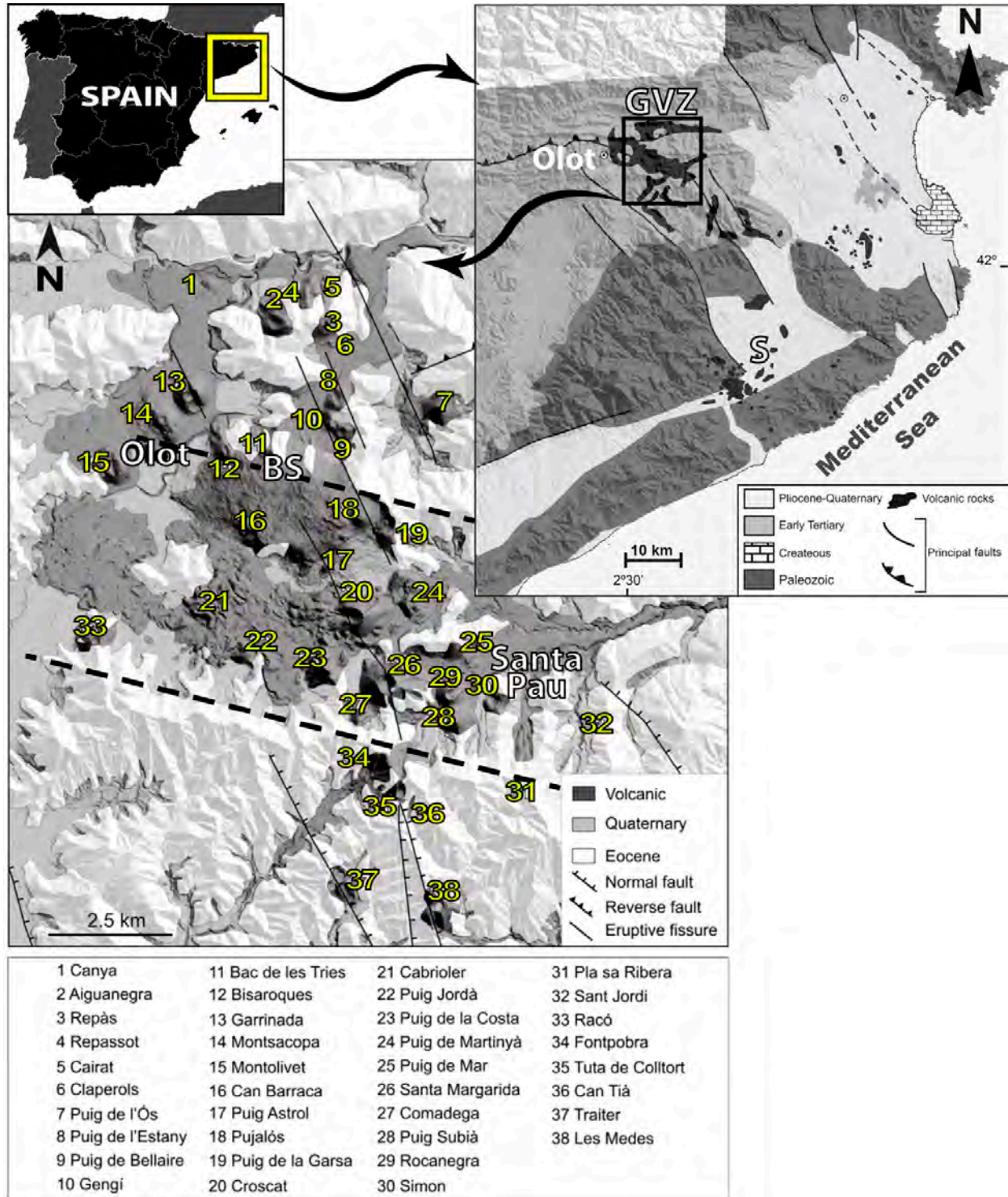


Fig. 1. Index and simplified geological and structural map of the studied area (modified from Martí et al. 2011). BS stands for Batet de la Serra village, and black dashed lines highlight the Garrotxa eroded anticline depression. Upper right inset Simplified geological map of the Catalan Volcanic Zone and its surroundings (modified from Guérin et al. 1985). GVZ Garrotxa Volcanic Zone, S La Selva.

2.3. Field investigations, data post-processing and modelling

2.3.1. Joint gravimetric and GPS surveys

Gravimetric data were obtained over 80 km² in the Natural Park of La Garrotxa, including all volcanic edifices outside the township of Olot. The survey area extends roughly between the townships of Olot and Santa Pau and follows the east–west elongated depression where most of the volcanic edifices are built (Fig. 1).

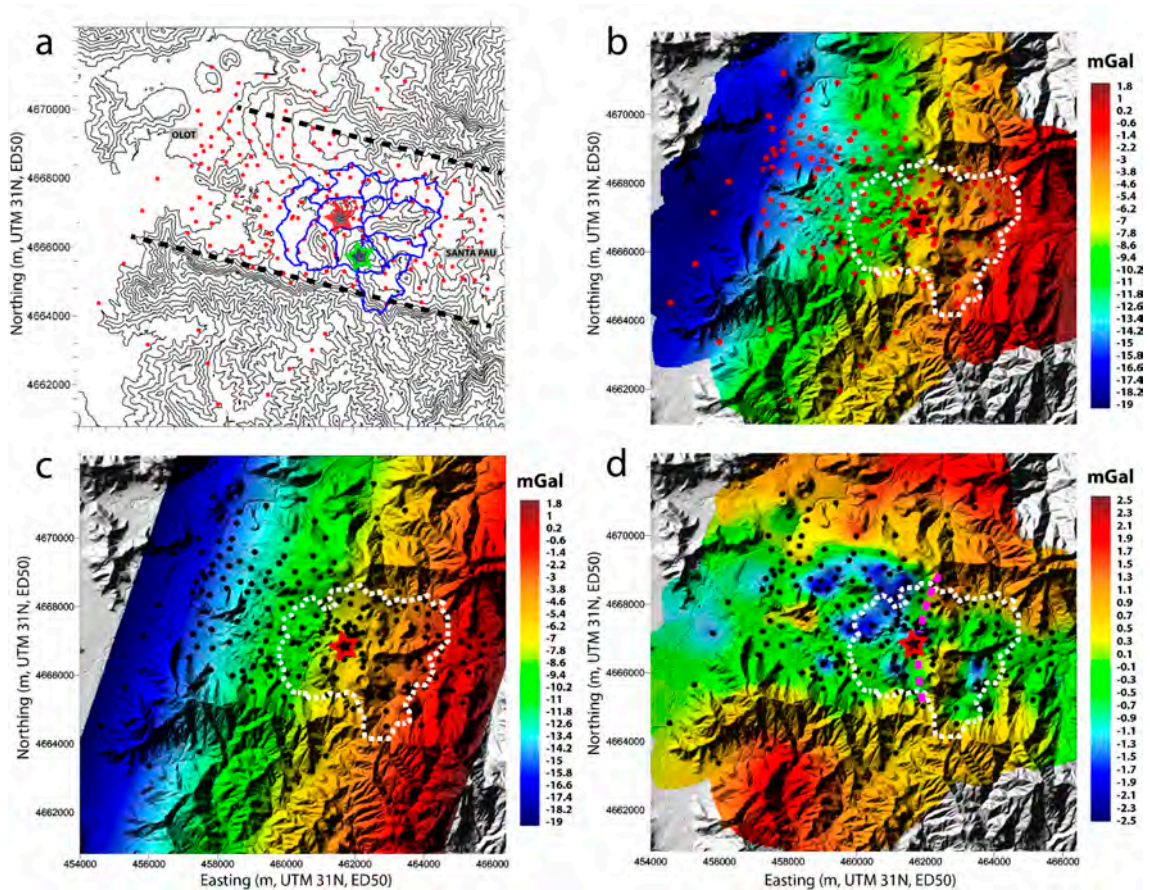


Fig. 2. a) Topographic contours for the area, overlain by the gravity data benchmarks (red dots) and the self-potential data points (blue dots). b) Bouguer anomaly map and index for the self-potential map (white dashed line). c) Regional anomaly. d) Residual gravity map obtained by subtracting the regional anomaly from the observed one; this residual anomaly is built to extract the short-wavelength signal. The pink dashed line highlights a steep gravity gradient described in the text. Red and black dots Gravimetry-survey benchmarks, red star Croscat volcano, green star Santa Margarida cone. Coordinates in metres (UTM31N–ED50).

Data were collected in September 2007 and March 2008 at 205 individual benchmarks (Fig. 2). Maximum distance between individual benchmarks in the central zone was about 1.5 km, and average distance between benchmarks around volcanic vents was <500 m. Gravimetric measurements were performed using an automated Burris gravimeter (B-028). Data at each benchmark were obtained by averaging a data stream from the gravimeter collected automatically by a handheld controller. The data collection is unbiased by the operator as the process of data

collection and processing to an observed gravity value is automated by the system. Individual measurements were obtained at an instrumental repeatability of better than 6 μGal ($1 \mu\text{Gal} = 10^{-8} \text{ m/s}^2$). Data at benchmarks was recorded relative to a reference located at 4665916mN, 459604 mE (m, UTM 31 N, ED50).

We calculated the complete Bouguer anomaly (with terrain correction to a distance of 60 km). Raw data was reduced for the effects of instrument drift (approximately linear at $-37.5 \mu\text{Gal/day}$), Solid Earth tides, latitude variations, difference of elevation between individual benchmarks and terrain effects using standard procedures. A terrain density of $2,450 \text{ kg/m}^3$ was derived based on a minimum correlation between observed gravity variations and topography, inferred from digital elevation data of 15 m spatial resolution. This mathematically derived density value is in broad agreement with the densities of sedimentary surface rocks of the area. Gravity data are reported relative to absolute gravity reference value calculated theoretically at 980,240 mGal (see supplementary Table 1).

Benchmark locations and elevations were determined using a Global Satellite Navigation System composed of two LEICA SR20 Global Positioning System (GPS) single- frequency receivers. GPS data were collected simultaneously at benchmarks and at a reference station. The reference included an antenna mounted on a metal pole, which was fixed to the ground by a buried socket and a data logger. In total, we recorded more than 100 h of reference data at 10-s intervals. The roving receiver collected data in static mode from an antenna, which was carried on a pole housed in a backpack. GPS observation times varied inversely with signal quality between 6 and 30 min. One operator took GPS measurements at each benchmark, while another operated the gravimeter.

Benchmark locations were calculated with respect to the reference using LEICA SKIPRO software. We obtained an average precision on benchmark locations of <0.5 and 1 m in the horizontal and vertical, respectively. This precision is sufficient to correct the gravimetric data for the effect of elevation changes from benchmark to benchmark over the survey area in order to obtain a resolution of Bouguer gravity variations $<1 \text{ mGal}$ ($=10^{-5} \text{ m/s}^2$), which is deemed appropriate for the study. This contrasts with existing regional Bouguer anomaly data, which is associated with an uncertainty of at least a factor of 5 higher.

2.3.2. Gravimetric data uncertainties and adjustment of geodetic reference frames

Error analysis gives a mean precision of the differential gravity values of $\pm 21 \mu\text{Gal}$, which represents an excellent value for structural gravimetric observations. Nevertheless, final anomaly data also contain uncertainties coming from elevation data and from terrain corrections. We estimate a precision level of $0.3 \mu\text{Gal}$, for this combined data. Some complexities in processing the terrain effect arise from differences between the geodetic reference frame of the survey (ellipsoidal WGS84) and the reference frame of available digital topographic data (local reference frame with geoidal orthometric heights). We applied a mathematical correlation procedure to compare Northing, Easting and ellipsoidal height values of both frames. Fixing several reference points in either framework, we were able to derive the following relationships to match the DEM framework to our GPS positions and vice versa:

- 1: Easting = Easting_{DEM} - 88 m;
- 2: Northing = Northing_{DEM} - 220.8 m
- 3: Geoid Height = Ellipsoidal heights from GPS measurements + 47.1 m

Three-dimensional (3D) positions of benchmarks between our GPS data and the available digital elevation data are thus offset according to the following shift values:

$$dz = 47.1 \text{ m} \qquad dx = 88.0 \text{ m} \qquad dy = 220.8 \text{ m}$$

The value of dz of 47.1 m clearly corresponds to the height of the geoid in the zone (orthometric to geometric height translation). The values for dx and dy would correspond to a translation or horizontal discrepancy between the two reference systems. Cross-correlating both datasets, we obtain an average vertical precision of the digital elevation data of 2.52 m, which appears a reasonable value given that the DEM is based on gridded data with 15m precision. Supplementary Table 1 gives details on UTM benchmark coordinates (Zone T31), GPS heights and correlation with available digital elevation data of the survey area as well as the obtained gravity data.

2.3.3. 3D inversion of Bouguer gravity anomaly data

We performed a non-linear inversion of resulting local Bouguer anomaly data to construct a 3D model of the anomalous sub-surface density distribution (Fig. 3). The inversion routine is described in detail in Gottsmann et al. (2008) and Camacho et al. (2011) including sensitivity tests. In summary, the inversion constructs a subsurface model defined by a 3-D aggregation of M parallelepiped cells, which are filled, in a “growth” process, by means of prescribed positive and/or negative density contrasts.

We addressed the problem of non-uniqueness by adopting a mixed minimisation condition, based on model “fitness” (least square fitness) and “smoothness” (total anomalous mass):

$$\mathbf{v}^T \mathbf{Q}_D^{-1} \mathbf{v} + \lambda \mathbf{m}^T \mathbf{Q}_M^{-1} \mathbf{m} = \min, \quad (1)$$

where $\mathbf{m} = (\Delta\rho_{1_1}, \dots, \Delta\rho_M)^T$ (superscript T denotes transpose of a matrix) are density contrast values for the M cells of the model, $\mathbf{v} = (v_1, \dots, v_N)^T$ are residual values for the N data points, QD is an a priori covariance matrix for uncertainties of the gravity data, QM is an a priori covariance matrix for uncertainties of the model parameters, and λ is a factor for selected balance fitness/smoothness of the model (Camacho et al. 2011).

Key for the inversion is the selection of an optimal balance between data “fitness” (least-square fitness) and model “smoothness” (total anomalous mass) expressed by the dimensional optimisation factor λ . For low values of λ , the inversion results in the generation of an excessively complex model of the subsurface structure with very good fit to the data. For high values of λ , the inversion produces a simple model but with poor fit to the data. L-curve criterion is a popular approach to select the trade-off parameter (e.g., Aster et al., 2004). We adopt the optimisation procedure proposed in Camacho et al. (2011) as producing uncorrelated inversion residuals. In fact, for too high a value of λ , model residuals are large and auto-correlated with respect to their mutual distance. For too low a value of λ , model residuals show negative values of autocorrelation for small distances due to accounting for noise. The optimal value satisfies the condition of a zero autocorrelation of residuals with respect to the mutual distance between benchmarks.

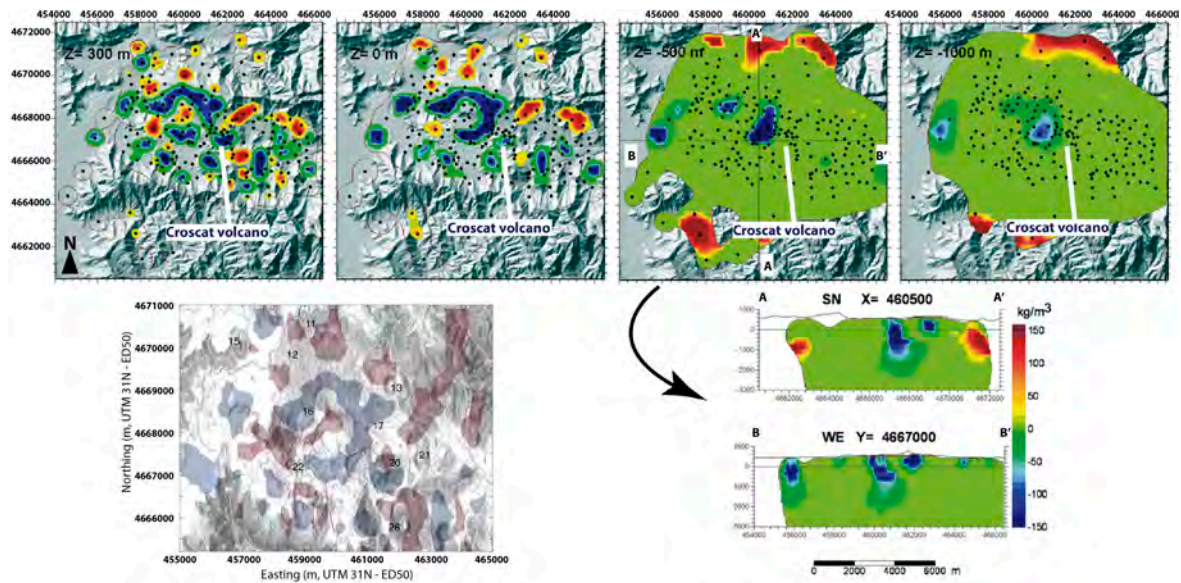


Fig. 3. Horizontal and vertical sections through the preferred density anomaly model of the Garrotxa depression (upper panel and lower right-hand side). Lower left-hand side depicts the modelled distribution of anomalous density bodies overlain by a digital elevation model. Isopycnic surfaces show the $+120 \text{ kg/m}^3$ (red) and -120 kg/m^3 (blue) contrasts. Numbers of volcanoes refer to those shown in Fig. 1. The low density bodies are interpreted to result from a combination of tectonic lineaments and the sub-volcanic roots of the dominant volcanic landforms in the Garrotxa monogenetic volcanic field. High-density bodies in the centre of the modelling domain are interpreted as surficial features of the landforms such as lava flows. High-density bodies at the periphery of the modelling domain are poorly constrained due to low data coverage. Coordinates in meters (UTM31N–ED50)

3.3.4. Self-potential survey

The self-potential method measures the distribution of the electric potential at the surface of Earth or in boreholes, with respect to a reference electrode. Sources of self-potential fields include chemical potential gradients (Maineult et al. 2005, 2006), redox potentials (Linde and Revil 2007), rapid fluid disruption (Johnston et al. 2001) and electrokinetic conversion associated with fluid movement through porous materials (the so-called streaming potential). In active volcanic areas, the main source of self-potential variations is related to the flow of groundwater (e.g. Massenet and Pham 1985; Ishido et al. 1997; Bedrosian et al. 2007; Barde-Cabusson et al. 2009; Mauri et al. 2010; Pearson et al. 2012).

We used a pair of non-polarizing Cu/CuSO₄ electrodes. The microporous nature of the end contacts of these electrodes (made of a low-permeability wood) avoids leakage of the CuSO₄ solution during contact with the ground. The difference of electrical potential between a fixed reference and a moving electrode was measured with a calibrated high impedance voltmeter (Extech EX520, sensitivity of 0.1 mV, input impedance >10 MΩ).

Before and after each series of measurements, the reference electrode and the moving electrode were put face-to-face to check that the difference of potential between the two electrodes was <2 mV (if this is not the case, the static value is removed to all the measurements). For each self-potential measurement, the value of the electrical resistance was also measured prior the self-potential measurement in order to check the quality of the

electrical contact between the scanning electrode and the ground (less than a few tens kilohms).

Self-potential measurements were obtained with a 300-m-long wire connecting the two electrodes. We performed a series of closed profiles between Olot and Santa Pau (2,073 measurements). The distance between two successive measurement stations was 20 m. Using a long cable avoids cumulative errors by changing the reference too often along the same profile. As the profiles are several kilometres long, a new reference station was established every 300 m. After the survey, the entire self-potential dataset was corrected using the first reference station as the unique reference. Usually, the 0 mV reference for self-potential measurements is taken at the sea or a water table as it provides a constant value in time. Because no such stable reference was available and self-potential is intrinsically a relative measurement, our self-potential data set is referenced arbitrarily to a point northeast of Santa Margarida (Fig. 1). A closure correction (below 50 mV for eight profiles and as much as 100 mV for three profiles) was applied to distribute the calculated data drift linearly on the profiles forming the dataset in order to limit cumulative errors.

Measurements of self-potential were only carried out in a small part of the area investigated by gravimetric measurements. Our aim was to test if near-surface structures such as fracture and faults have corresponding expressions at greater depth as revealed by the inversion of the gravimetric data and if the joint application of these potential field techniques in the Garrotxa yields useful insights.

2.4. Results

2.4.1. Local gravity anomaly

Figure 2b shows the resultant gravity anomaly data for the survey area with values between -19 and 2 mGal. The gravity data appears to follow a strong linear trend, which we modelled with a horizontal slope of $1,928$ $\mu\text{Gal}/\text{km}$ and azimuth $\text{N}108^\circ\text{E}$ (Fig. 2c). We attribute this trend to regional large wavelength deep-seated geological structures associated with the topography of the metamorphic basement below a thrust belt at the SE part of the Pyrenees (Martinez et al. 1997). In order to derive the local gravity anomaly data (Bouguer anomaly), we subtracted the predicted gravity anomaly of the regional component from the observed data. The resultant anomaly map is given in Fig. 2d.

The obtained Bouguer anomaly map shows a range in gravity variations in the survey area between -2.5 and $+2.5$ mGal. Neutral to mildly negative (up to -0.7 mGal) gravity anomalies dominate a central elongated sector striking WNW–ESE and following the Garrotxa depression, which hosts the volcanic zone. A pronounced negative gravity anomaly with amplitudes of up to -2.5 mGal lays in the central part of the survey area bordering the high ground to the north. There is, however, no indication for a spatially extended large amplitude and coherent low-density structure beneath the entire volcanic zone, but rather for a series of spatially concentrated low-density bodies. The overall surficial shape of the dominant gravity-low resembles a horseshoe, which opens towards the SW (Fig. 2d).

Parts of the area dominated by low gravity values correspond to prominent volcanic edifices such as, the Crosca, Can Barraca, Puig Astrol and Pujalós volcanoes (see Figs. 1 and 2d with Crosca taken as a reference for localization). The anomaly is clearly bounded to the North (by areas of higher topography) as well as to the East with a steep horizontal gravity gradient towards neutral gravity. This transition occurs across a line striking roughly N–S (pink dashed line in Fig. 2d).

In addition, a linear element of relative higher gravity (+0.3 to +0.7 mGal; depicted by yellow colors in Fig. 2d; roughly at 4 666 000 mN and 463,000 mE) separates two zones with negative anomalies. This gravity high strikes NNE–SSW, coincides with a break in slope from the volcanic centres towards the town of Santa Pau and runs roughly parallel to the Eastern border of the dominant negative horseshoe-shaped gravity anomaly.

2.4.2. Gravity inversion results

The resultant gravity model is illustrated in Fig. 3, and the distribution of inversion residuals is shown in Fig. 4. Anomalous density contrasts range between -150 and 150 kg/m^3 , where neutral contrasts with terrain rocks are expressed by values of 0 kg/m^3 .

Bodies of positive and negative density contrasts dominate the near surface of the volcanic field. However, only low density bodies modelled in the centre of the survey area and underlying major volcanic landforms (predominantly scoria cones) appear to be rooted at greater depth with traceable extents to depths greater than -500 m . In particular, the size and extent of the dominant low-density bodies beneath the Crosca cone and its adjacent NW side are revealed. The lower left hand of Fig. 3 depicts the modelled distribution of anomalous density bodies overlain by a digital elevation model. Isopycnic surfaces show the $+120 \text{ kg/m}^3$ (red) and -120 kg/m^3 (blue) contrasts (see Fig. 1 for numbered volcano names).

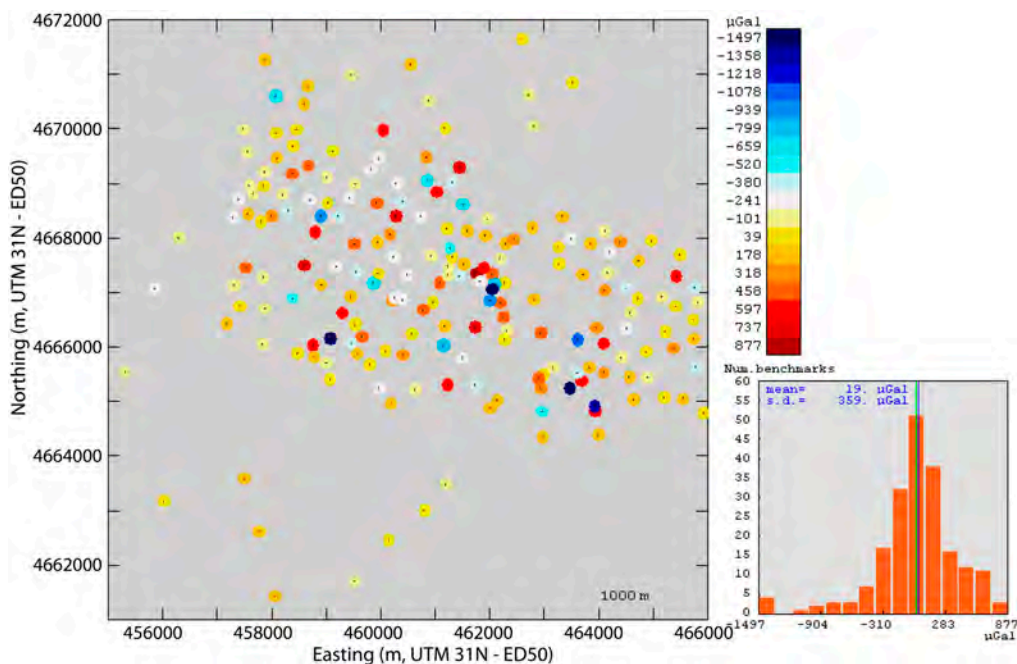


Fig. 4. Map showing the distribution of the inversion residuals as a proxy for the quality of fit of the model to the observations. The mean residual is 0.019 mGal with a standard deviation of 0.359 mGal , reflecting the best fit to the data as well as satisfying constraints of model smoothness ($\lambda = 40$)

2.4.3. Self-potential

The most striking feature of the self-potential map is a sharp transition in the self-potential values from east to west, where the lowest values are registered (Fig. 5a). This transition takes place along a NNE–SSW axis in the northern part of the study area and along a NNW–SSE axis south of the Croscat volcanic cone. The NNW–SSE axis is outlined by sharp self-potential spatial variations northwest of the Croscat cone, south of the Croscat cone and a more gradual variation through the Santa Margarida cone. The self-potential map shows a total variation of ~ 340 mV. Maximum self-potential values have been measured in the eastern half of the study area with poor spatial variations (< 30 mV) and no specific pattern identified through the orientation of the self-potential isolines. In this sector, however, as it coincides with a negative gravity anomaly (~ -1.7 mGal; Fig. 5b), we note the presence of a low self-potential minimum (< 20 mV under the local values) just north of the Rocanegra scoria cone. This variation is less than the background noise in the area, but it is clearly above the local noise (see profile a–b in Fig. 5a).

The Puig Subià cone shows a strong self-potential minimum of 150 mV below the surrounding background self-potential. A self-potential vs elevation graph of the whole dataset (Fig. 6) shows different distributions of the measurements for the eastern and western parts of the map, separated by the NNE–SSW and NNW–SSE lineations identified with self-potential. The eastern zone shows a linear trend with a self-potential vs elevation gradient of -0.19 mV/m, typical of hydrogeological zones on volcanoes (e.g. Lénat 2007). This contrasts with data from the western zone, which does not follow a particular trend. Only the isolated minima or maxima registered in the eastern part of the map diverge from this trend. As an example, the self-potential measurements corresponding to the strong minimum registered on Puig Subià plot outside of the hydrogeological trend (Fig. 6). At the south-western end of the map the self-potential signal tends to increase again. Additionally, some small-scale (a few tens of metres wide) self-potential minima or maxima are visible along single profiles. In particular, a self-potential minimum has been mapped in the Puig de Martinyà area (see profile c–d in Fig. 5a). The NNE–SSW and NNW–SSE self-potential axes coincide with the orientation of the residual gravity anomaly isolines corresponding to the gravity lows reported in the previous section (Fig. 5). Overall we find an excellent correlation between the gravity and self-potential anomalies as depicted in Fig. 7.

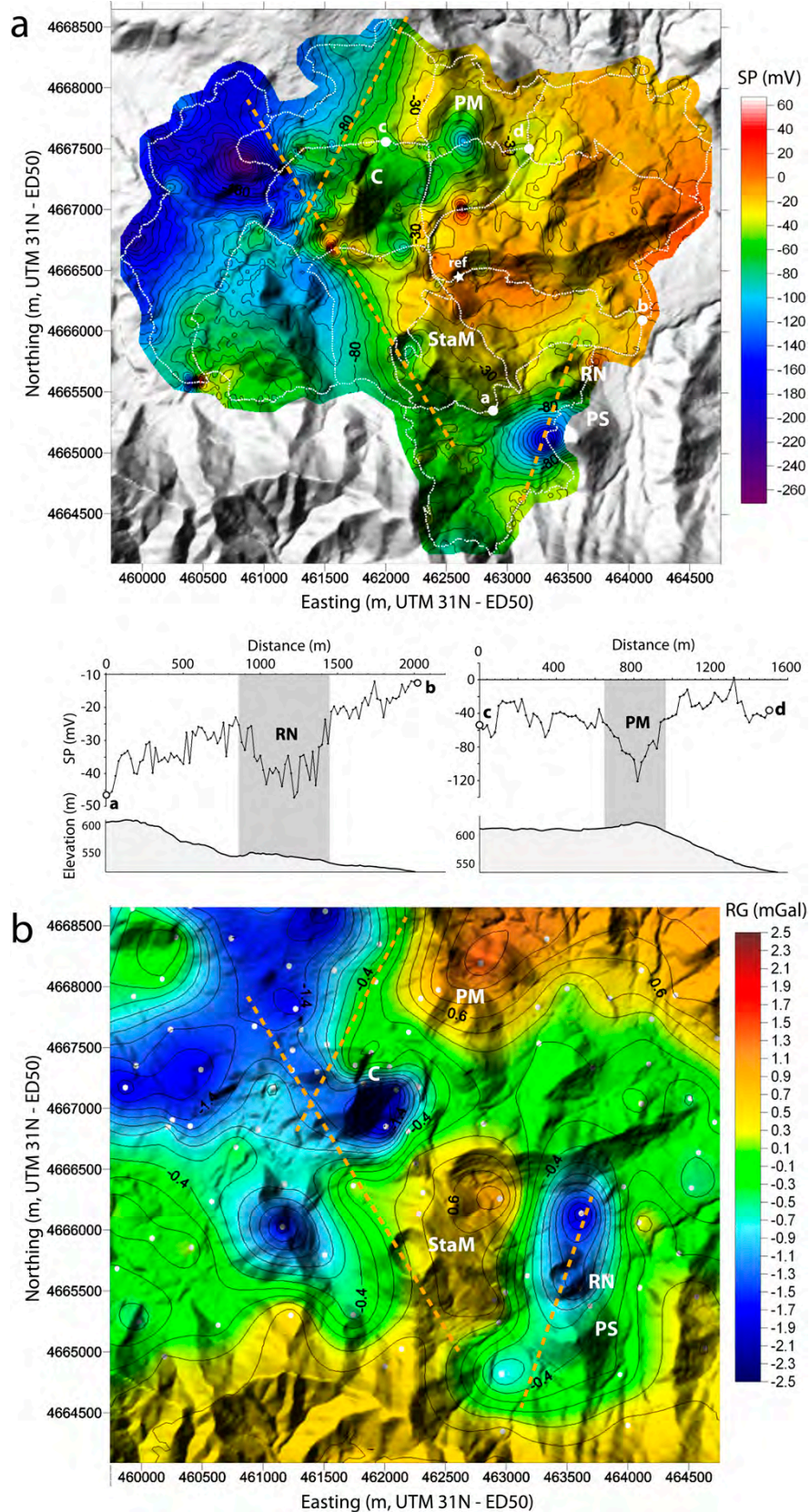


Fig. 5. a) Self-potential map overlain on a digital elevation model. In the lower part, two SP vs distance graphs and corresponding topography (ab and cd). b) Residual gravity anomaly map in the same area. Note how both self-potential and gravimetric data highlight NNE–SSW and NNW–SSE lineaments (orange broken lines). ref stands for the SP reference point, C Croscat, PM Puig de Martinyà, Sta M Santa Margarida, RN Rocanegra, PS Puig Subià.

2.5. Discussion

2.5.1. Distribution of volcanism related to local tectonics from gravity and self-potential data

The localized gravity lows (Fig. 2d) are interpreted to result from relatively low rock densities. These densities could reflect either volcanic surface deposits or rocks of the shallow plumbing system of individual volcanic centres. The rather abrupt change from neutral to both pronounced negative and positive gravity values and vice versa (horizontal gravity gradients $> \pm 1$ mGal/km) might indicate a structural confinement of the main anomalous density zones by conjugated faults. The data allow us to suggest a WNW–ESE orientation, which finds expression in the main structural lineaments of the Garrotxa graben. In addition, NNE–SSW and NNW–SSE axes are highlighted in the central part of the volcanic field (Fig. 5). Although the self-potential data covers only part of the gravimetry map, it supports the same NNE–SSW and NNW–SSE orientations with the strong transition observed from east to west (100 mV over a few hundred metres). The NNW–SSE axis matches the lineament drawn by the gravity high near Croscat and Santa Margarida cones (Fig. 5). Marti et al. (2011) interpret the Santa Margarida/Croscat/La Pomareda alignment as the result of a single eruptive episode along a NNW–SSE trending, 3 km long fissure. Our data provides geophysical evidence for a correlation between volcanism and tectonic structures, which may imply a structural control on magma at depth, establishing a basis for interpreting the self-potential variations associated with gravity anomalies in our study area.

The north-western sector of the self-potential map presents another sharp variation highlighting a NNE–SSW lineament. This coincides with the eastern limit of the north-western negative gravity anomaly (Fig. 5). No volcanic edifice is evident along this lineament, but our geophysical data might indicate the presence of a NNE–SSW-oriented structural boundary, similar to the NNW–SSE axis detected between the Croscat and Santa Margarida volcanoes. The former can be interpreted as a fault zone or a zone of failed shallow intrusions along an existing structural anisotropy. Due to the substantial vegetation cover and poor accessibility, there is a lack of precise geological data on the extent of surface deposits from individual eruptions or indeed small-scale volcanic edifices in this area. Volcanological field observations to the north and south of the Croscat volcano indicate that there is indeed no correlation between the spatial distribution of the surface deposits and the spatial limits of the geophysical structures. The stark difference in self-potential values between the western and eastern zone (Fig. 6) suggests lateral heterogeneity of the medium (Lénat 2007). This indicates that the corresponding NNW–SSE and NNE–SSW lineaments might not simply mark eruptive fissures but may indicate faults separating two blocks with different hydrogeological properties and/or different global resistivity values. The presence of pre-existing faults is not necessary to explain the observed self-potential signal because the presence of dykes might impede groundwater movement, creating this contrast between the eastern and the western zones. Both interpretations, independently or combined, are compatible with the results.

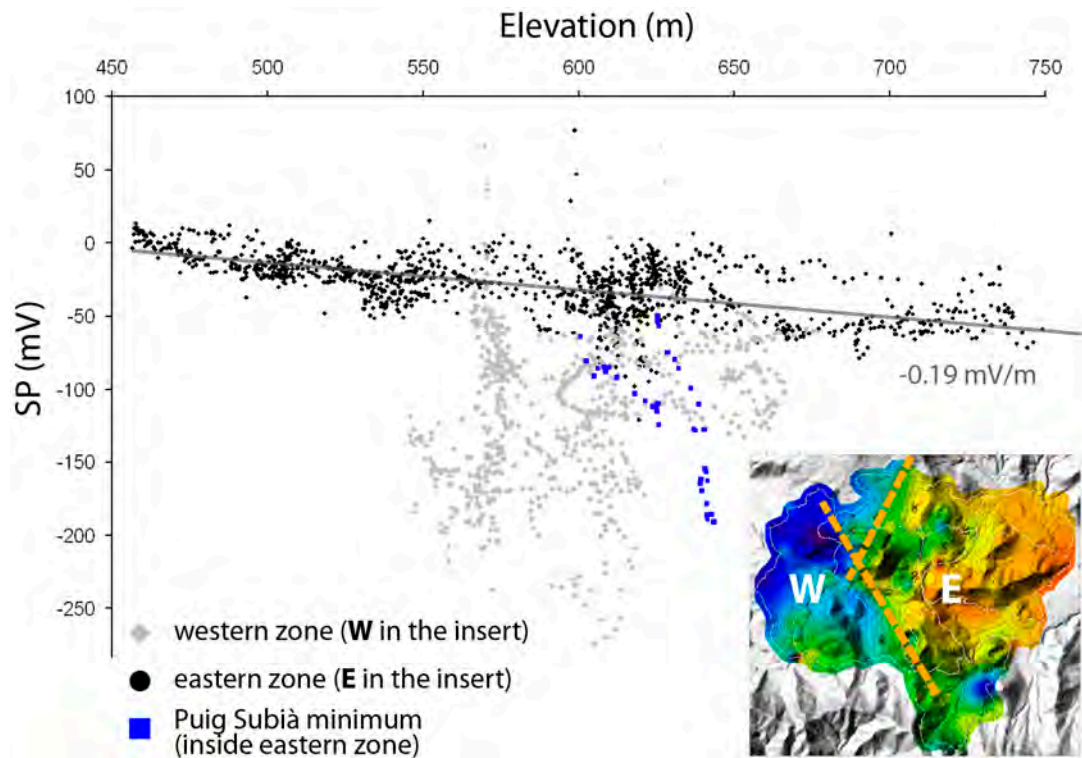


Fig. 6. Plot of the self-potential data as a function of elevation. A global trend illustrates the correlation between SP and elevation in the eastern zone of the SP map, with a SP/elevation gradient of -0.19 mV m^{-1} , while this correlation does not exist in the western zone. Only punctual minima or maxima registered in the eastern part of the SP map plot outside this trend, as exemplified by the Puig Subià minimum (blue squares).

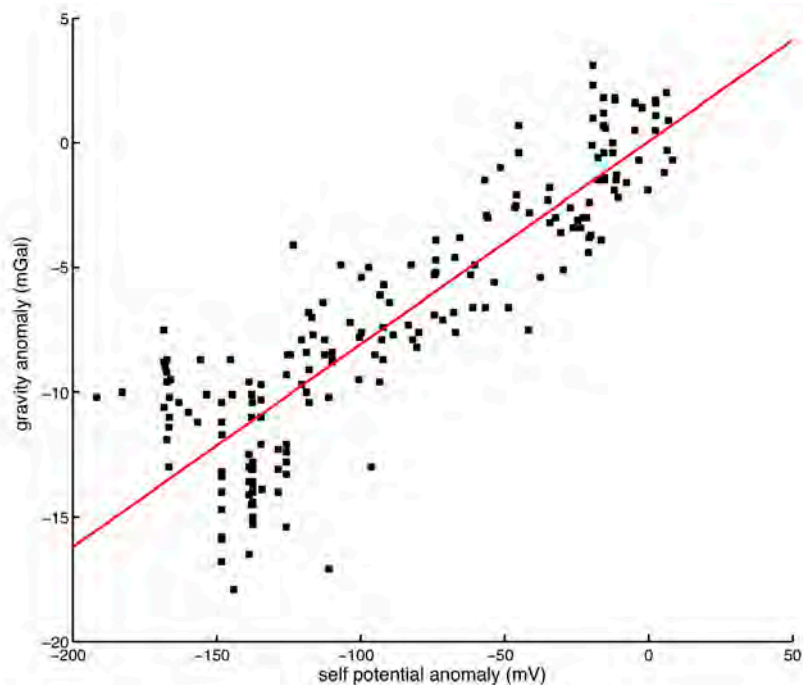


Fig. 7. There is a positive linear relationship between the gravity and self potential anomalies with a regression coefficient $R = 0.88$. Due to different locations of the individual measurement points for the two techniques, the SP data have been interpolated at the gravity benchmark to test for a possible correlation.

North of the Rocanegra cone, the eastern negative gravity anomaly (Fig. 5) is associated with a weak self-potential minimum showing a sharp variation at the limits (see profile a–b in Fig. 5). This minimum is of ~ 20 mV with respect to the surrounding area, which is significantly higher than the signal noise along the corresponding profile. South of Rocanegra, on the Puig Subià cone, we also measured a strong self-potential minimum of ~ 150 mV. Again, no relationship could be established with the surface lithology. These self-potential minima are thought to be related to preferential meteoric infiltration or to a sharp lateral resistivity variation. The association and sharp limits of the self-potential minima and the negative gravity anomaly might indicate a structural limit such as a fault or a fissure, guiding infiltration of groundwater. The respective location of Rocanegra and Puig Subià, two well-preserved volcanic edifices, establish a NNE–SSW alignment with the measured anomalies. This direction and the similar preservation state of the two cones are consistent with a genetic link between them along a NNE–SSW oriented structural weakness (Fig. 5).

It is interesting to note that volcanic edifices occur only within the depression formed by the eroded anticline. Wetmore et al. (2009) discuss the relationship between intrusions and folding on local scale and give the example of the Trachyte Mesa intrusion (Utah, USA), which was emplaced into a series of northeast trending upright and open folds formed during the Jurassic. The fold axes strike sub-parallel to the long axis of the Trachyte Mesa intrusion, and the geometry of the basal contact of the intrusion appears to follow the morphology of the fold limbs. The majority of the intrusion is confined within the axis of a syncline bounded by anticlines on either side. The authors suggest that both pre-existing structures and the density of the magma relative to that of the host rocks fundamentally controlled the emplacement of this intrusion. In the case of the Garrotxa volcanic field, we cannot unambiguously establish a causal relationship between the anticline and the volcanic activity, but note that there are strong indications for the presence of structural lineaments that cut across the anticline and contributed to the localisation of magma pathways (see below).

2.5.2. Density anomaly models of volcanic roots

The 3D density anomaly model shows a dominant body of negative density contrast, with an annulus of isolated density lows of similar amplitude (up to -150 g/m³). The centre of the main anomalous body is located ~ 1 km WNW of the ~ 14 ka Croscat volcano, the youngest volcano in this area (Puiguirguer et al. 2012). The -2 mGal Bouguer anomaly is explained in the model by a coherent arcuate and rather shallow-seated (to depths of around sea level) low-density structure. The anomaly is well defined by numerous gravity stations and its diameter at the surface is about 2 km. Its northern border appears buried beneath the morphological high of the plateau between Batet de la Serra village and Pujalós volcano (Fig. 1). Beneath the main central depression of the Garrotxa (between Olot and the Croscat cone), the anomaly is modelled for an optimisation factor $\lambda = 40$ by a shallow zone extending at least 1 km deep over a zone about 1.5 km wide and characterized by up to -150 kg/m³ density contrast (see cross-sections in Fig. 3). A possible explanation of this dominant structure is that it represents a combination of the (pyroclastic) sub-volcanic root of the surficial scoria cones and fault/fissure damage zones. The portions of these structures beneath Batet de la Serra village and Pujalós volcano appear to be shallow intrusions

branching from the main low-density bodies, which fed the scoria cones in the central depression as depicted in the N–S cross-section and by the -120 kg/m^3 isopycnic surfaces (Fig. 3). The roughly NNE–SSW extension of the western arc and the roughly NNW–SSE extension of the eastern arc may delineate magma pathways along the dominant structural features of the Garrotxa. It is perhaps interesting to note that the deeper portions of the low density bodies resemble cylindrical geometries, which may delineate the shallow magmatic feeder systems of individual volcanoes in the western part of the study (near Olot), as well as the scoria cone cluster at the centre of the volcanic field (Croscat and its neighbouring volcanoes to the SW and W). From west to east, the Garrinada, Can Barraca, Cabrioler, Puig Jordà, Puig de la Costa, Croscat, Puig Subià, Rocanegra, Puig de Mar and Simon volcanoes are modelled to contain low density roots to several hundred metres depth.

The origin of the main low-density body near Croscat deserves further examination. First, it appears that the cluster of volcanic cones in the centre of the Garrotxa has been fed by a common fault-bounded magmatic feeder system from which conduit-like structures fan away at surficial levels ($<1,000 \text{ m}$ depth) to feed monogenetic volcanoes of the central zone. Second, the stratigraphic record of the Croscat edifice shows evidence for violent Strombolian activity during its generation (Marti et al. 2011). This implies an increase in intensity of eruption, inferred to result from deepening of the fragmentation level. Therefore, in addition to a tectonic origin for the low-density structure, the body could also be a testament of pyroclastic roots beneath the cones.

In contrast to Croscat, a pronounced negative density body is absent beneath Santa Margarida volcano, which appears bounded in the north by a high-density body next to the low density volume beneath Croscat. Such a sharp change in density contrasts is striking and our interpretation is that a NNE–SSW trending fault zone and potentially a second zone striking perpendicular to it separates the plumbing systems of Croscat and Santa Margarida, masking a potential low-density root beneath Santa Margarida. In addition, the eruptive history of Santa Margarida volcano is profoundly different from that of Croscat. Santa Margarida is almost exclusively built of phreatomagmatic lithic-rich deposits from surges. The absence of a dominant density low beneath Santa Margarida could also result from a fundamentally different fragmentation process of its magma, which according to its stratigraphic record never attained the substantial violent Strombolian character that its neighbour Croscat did (Marti et al. 2011).

2.5.3. Volcano-tectonics of the Garrotxa monogenetic field

The main lineaments identified by the geophysical study intersect the edges of the depression formed by the Garrotxa eroded anticline (Martinez et al. 1997). The NNW–SSE trending lineaments run parallel to major regional structures expressed by major normal faults (see insert in Fig. 1). One could thus envisage a mini-(half) graben almost perpendicular to the main WNW–ESE striking eroded anticline defining the location of the central volcanic zone of the Garrotxa, between Olot and Santa Pau. In order to explain the negative density contrasts, a substantial amount of pyroclastic material or porous lavas with lower than average bulk densities must be present. In this context and based on the data and modelling presented herein, we surmise that the presence and location of the volcanic centres is tectonically controlled by a network of conjugate faults intersecting the anticline axis.

2.5. Conclusions

The main finding of this study is that the central part of the Garrotxa volcanic field is underlain by low-density material. Porous volcanoclastic deposits including the pyroclastic roots of volcanic edifices in combination with fault and fissure damage zones appear to be the main candidates to explain the observed gravity anomalies. Volcanism appears to be controlled by NNE–SSW and NNW–SSE tectonic structures identified by both gravimetric and self-potential data. The Croscat, Santa Margarida and Roca Negra volcanoes lie atop a conjugated fault system. The combination of the two geophysical methods has helped us to explore and link the surficial expressions of monogenetic volcanism and characteristic fault/fissure zones of the volcanic field with magma pathways and their sub-surface structures to depths of about 1 km. Identification of such volcano-morpho-tectonic structures and their mutual relationships is critical for better understanding the dynamics of monogenetic volcanic fields. Our study demonstrates the close link between tectonic structures and magma pathways in the evolution of the Garrotxa volcanic field with potential to guide future eruptive activity. This subject is of substantial interest for the assessment of causes and consequences of future volcano-tectonic unrest and volcanic reactivation in the Garrotxa and other monogenetic volcanic fields.

Acknowledgements:

We thank the Natural Park of the La Garrotxa Volcanic Zone and its staff for their support throughout this study. SBC acknowledges the JAE-Doc postdoctoral personal grant program of Consejo Superior de Investigaciones Científicas (JAEDoc_09_01319), JG acknowledges funding from a Royal Society University Research Fellowship and an International Joint Project grant with JM and AG acknowledges her post-doctoral Juan de la Cierva Grant (JCI-2010-06092). X. Bolós has been funded by grant Beca d’investigació “Oriol de Bolós” en Ciències Naturals (Olot, Spain). AGC has been supported by the MICINN research project AYA2010-17448. The work was also partially supported by the European Commission (FP7 Theme: ENV.2011.1.3.3-1; Grant 282759: “VUELCO”). We sincerely thank the Executive Editor James D. L. White, Editor Takeshi Nishimura, and reviewers Charles Connor and Koki Aizawa for their constructive and helpful comments on our manuscript.

References:

- Alberico I, Lirer L, Petrosino P, Scandone R (2002) A methodology for the evaluation of long-term volcanic risk from pyroclastic flows in Campi Flegrei (Italy). *J Volcanol Geotherm Res* 116:63-78
- Alberico I, Lirer L, Petrosino P, Scandone R (2008) Volcanic hazard and risk assessment from pyroclastic flows at Ischia island (southern Italy). *J Volcanol Geotherm Res* 171:118-136

- Aster R, Borchers B, Thurber C (2004) *Parameter Estimation and Inverse Problems*. Elsevier Academic Press, 301 pp.
- Barde-Cabusson S, Levieux G, Lénat JF, Finizola A, Revil A, Chaput M, Dumont S, Duputel Z, Guy A, Mathieu L, Saumet S, Sorbadère F, Vieille M (2009) Transient self-potential anomalies associated with recent lava flows at Piton de la Fournaise volcano (Réunion Island, Indian Ocean). *J Volcanol Geotherm Res* 187:158–166. doi:10.1016/j.jvolgeores.2009.09.003.
- Bedrosian PA, Unsworth MJ, Johnston MJS (2007) Hydrothermal circulation at Mount St. Helens determined by self-potential measurements. *J Volcanol Geotherm Res* 160:137–146
- Blakely RJ, Christiansen RL, Guffanti M, Wells RE, Donnelly-Nolan JM, Muffler LJP, Clynne MA, Smith JG (1997) Gravity anomalies, Quaternary vents, and Quaternary faults in the southern Cascade Range, Oregon and California: Implications for arc and backarc evolution. *J Geophys Res* 102(B10): 22513-22527
- Camacho AG, Fernandez J, Gottsmann J (2011) A new gravity inversion method for multiple subhorizontal discontinuity interfaces and shallow basins. *J Geophys Res* 116:B02413. doi:10.1029/2010JB008023
- Cebriá JM, López-Ruiz J, Doblás M, Oyarzun R, Hertogen J, Benito R (2000) Geochemistry of the Quaternary alkali basalts of Garrotxa (NE Volcanic Province, Spain): a case of double enrichment of the mantle lithosphere. *J Volcanol Geotherm Res* 112:175–187.
- Cebriá JM, Martín-Escorza C, López-Ruiz J, Morán-Zenteno DJ, Martiny BM (2011) Numerical recognition of alignments in monogenetic volcanic areas: Examples from the Michoacán-Guanajuato Volcanic Field in Mexico and Calatrava in Spain. *J Volcanol Geotherm Res* 201:73-82. doi:10.1016/j.jvolgeores.2010.07.016
- Cimarelli C, Di Traglia F, de Rita D, Gimeno Torrente D, Fernandez Turiel JL (2013) Space-time evolution of monogenetic volcanism in the mafic Garrotxa Volcanic Field (NE Iberian Peninsula). *Bull Volcanol* 75:758. doi 10.1007/s00445-013-0758-6
- Connor CB, Hill BE (1995) Three nonhomogeneous Poisson models for the probability of basaltic volcanism: Application to the Yucca Mountain region, Nevada. *J Geophys Res* 100:10107–10125
- Connor CB, Stamatakos JA, Ferrill DA, Hill BE, Ofoegbu GI, Conway FM, Sagar B, Trapp J (2000) Geologic factors controlling patterns of small-volume basaltic volcanism: Application to a volcanic hazards assessment at Yucca Mountain, Nevada. *J Geophys Res* 105:417–432
- Gaffney ES, Damjanac B, Valentine GA (2007) Localization of volcanic activity: 2. Effects of pre-existing structure. *Earth Planet. Sci. Lett.* 263 (3-4): 323–338
- Gottsmann J, Camacho AG, Marti J, Wooller L, Fernandez J, Garcia A, Rymer H (2008) Shallow structure beneath the Central Volcanic Complex of Tenerife from new gravity data: Implications for its evolution and recent reactivation. *Phys Earth Planet Inter* 168(3-4):212–230
- Guérin G, Behamoun G, Mallarach JM (1985) Un exemple de fusió parcial en medi continental. El vulcanisme quaternari de la Garrotxa. Publicació del Museu Comarcal de la Garrotxa, Vitrina 19–26
- Ishido T, Kiruchi T, Matsushima N, Yano Y, Nakao S, Sugihara M, Tosha T, Takakura S, Ogawa Y (1997) Repeated self-potential profiling of Izu-Oshima Volcano, Japan. *J Geomagn Geoelectr* 49:1267-1278

- Johnston MJS, Byerlee JD, Lockner D (2001) Rapid fluid disruption: A source of self-potential anomalies on volcanoes. *J Geophys Res* 106(B3): 4327-4335
- Kiyosugi K, Connor CB, Zhao D, Connor LJ, Tanaka K (2010) Relationships between volcano distribution, crustal structure, and P-wave tomography: an example from the Abu Monogenetic Volcano Group, SW Japan. *Bull Volcanol* 72:331-340. doi: 10.1007/s00445-009-0316-4
- Le Corvec N, Menand T, Lindsay J (2013) Interaction of ascending magma with pre-existing crustal fractures in monogenetic basaltic volcanism: an experimental approach. *J. Geophys. Res.* 118: 968–984. doi: 10.1002/jgrb.50142
- Lénat JF (2007) Retrieving self-potential anomalies in a complex volcanic environment: an SP/elevation gradient approach. *Near Surf Geophys* 5:161–170
- Linde N, Revil A (2007) Comment on “Electrical tomography of La Soufrière of Guadeloupe Volcano: Field experiments, 1D inversion and qualitative interpretation”, by F. Nicollin et al.. *Earth Planet Sci Lett* 258:619-622. doi:10.1016/j.epsl.2006.02.020
- Lutz TM, Gutmann JT (1995) An improved method for determining and characterizing alignments of pointlike features and its implications for the Pinacate volcanic field, Sonora, Mexico. *J Geophys Res* 100(B9):17659-17670
- Maineult A, Bernabé Y, Ackerer P (2005) Detection of advected concentration and pH fronts from self-potential measurements. *J Geophys Res* 110:B11205. doi:10.1029/2005JB003824
- Maineult A, Bernabé Y, Ackerer P (2006) Detection of advected, reacting redox fronts from self-potential measurements. *J Contam Hydrol* 86:32-52
- Martí J, Mitjavila J, Roca E, Aparicio A (1992) Cenozoic magmatism of the Valencia trough (Western Mediterranean): relation between structural evolution and Volcanism. *Tectonophysics* 203:145–166
- Martí J, Planagumà LI, Geyer A, Canal E, Pedrazzi D (2011) Complex interaction between Strombolian and phreatomagmatic eruptions in the Quaternary monogenetic volcanism of the Catalan Volcanic Zone (NE of Spain). *J Volcanol Geotherm Res* 201(1-4):178-193. doi:10.1016/j.jvolgeores.2010.12.009
- Martin AJ, Takahashi M, Umeda K, Yusa Y (2003) Probabilistic methods for estimating the long-term spatial characteristics of monogenetic volcanoes in Japan. *Acta Geophys Pol* 51:271-291
- Martinez A, Rivero L, Casas A (1997) Integrated gravity and seismic interpretation of duplex structures and imbricate thrust systems in the southeastern Pyrenees (NE Spain). *Tectonophysics* 282: 303-329
- Massenet F, Pham VN (1985) Experimental and theoretical basis of self-potential phenomena in volcanic areas with reference to results obtained on Mount Etna (Sicily). *Earth Planet Sci Lett* 73:415-429
- Mauri G, Williams-Jones G, Saracco G (2010) Depth determinations of shallow hydrothermal systems by self-potential and multi-scale wavelet tomography. *J Volcanol Geotherm Res* 191(3): 233-244.
- Paulsen TS, Wilson TJ (2010) New criteria for systematic mapping and reliability assessment of monogenetic volcanic vent alignments and elongate volcanic vents for crustal stress analyses. *Tectonophysics* 482(1): 16-28

- Pearson SCP, Kiyosugi K, Lehto HL, Saballos JA, Connor CB, Sanford WE (2012) Integrated geophysical and hydrothermal models of flank degassing and fluid flow at Masaya volcano, Nicaragua. *Geochem. Geophys. Geosyst.*, 13 Q05011. doi:10.1029/2012GC004117.
- Puiguiriguer M, Alcalde G, Bassols E, Burjachs F, Exposito I, Planaguma L, Sana M, Yll E (2012) C-14 dating of the last Croscat volcano eruption (Garrotxa Region, NE Iberian Peninsula). *Geol. Acta* 10(1): 43-47
- Rout DJ, Cassidy J, Locke CA, Smith IE (1993) Geophysical evidence for temporal and structural relationships within the monogenetic basalt volcanoes of the Auckland volcanic field, northern New Zealand. *J Volcanol Geotherm Res* 57(1): 71-83
- Scandone R (1979) Preliminary evaluation of the volcanic hazard in the southern valley of Mexico. *Geofis Int* 18:21–35
- Valentine GA, Perry FV (2006) Decreasing magmatic footprints of individual volcanoes in a waning basaltic field. *Geophys Res Lett* 33:L14305. doi:10.1029/2006GL026743
- Valentine GA, Krogh KEC (2006). Emplacement of shallow dikes and sills beneath a small basaltic volcanic center — the role of pre-existing structure (Paiute Ridge, southern Nevada, USA). *Earth Planet. Sci. Lett.* 246 (3–4): 217–230
- Wetmore PH, Connor CB, Kruse SE, Callihan S, Pignotta G, Stremtan C, Burke A (2009) Geometry of the Trachyte Mesa intrusion, Henry Mountains, Utah: Implications for the emplacement of small melt volumes into the upper crust. *Geochem. Geophys. Geosyst.* 10: Q08006. doi:10.1029/2009GC002469
- Wilson M, Downes H (1991) Tertiary-Quaternary extension-related alkaline magmatism in Western and Central Europe. *Journal of Petrology* 32(4):811-849
- Zhang D, Lutz T (1989) Structural control of igneous complexes and kimberlites: a new statistical method. *Tectonophysics* 159:137-148

Supplemental Table 1: Detailed listing of gravity benchmarks and resultant gravity data.

Benchmark	GPS(Z+47.1m)			DEM*	Diff	Gravity **	Anomaly**
Name	Easting	Northing	Height	(m)	(m)	μGal^{**}	μGal^{**}
GPS Ref	459604	4665916	560.53	559.0	-1.5	980240000	-4331
SG0001	459567	4665876	548.95	547.0	-2.0	980236309	-10170
SG0002	459665	4666192	569.48	567.1	-2.4	980233151	-9837
SG0003	459531	4666425	553.86	551.0	-2.9	980235617	-10848
SG0004	459529	4666410	553.56	550.1	-3.4	980235603	-10895
SG0005	459294	4666626	549.53	544.4	-5.2	980236840	-10737
SG0006	459448	4666926	556.23	554.3	-1.9	980235199	-11351
SG0007	459866	4667172	559.84	557.7	-2.1	980233796	-12213
SG0008	459554	4667388	557.82	555.9	-2.0	980234151	-12374
SG0009	459183	4667476	563.95	560.3	-3.7	980232837	-12374
SG0010	458906	4667143	549.34	546.2	-3.2	980236091	-11984
SG0011	459077	4666160	530.86	530.9	.1	980237324	-13158
SG0012	460411	4665858	574.65	570.3	-4.3	980233247	-8288
SG0013	459978	4665250	564.78	562.9	-1.9	980232958	-9389
SG0014	460190	4664964	578.32	574.9	-3.4	980229985	-8070
SG0015	460631	4665222	567.34	564.2	-3.2	980233882	-7745
SG0017	464092	4666062	511.29	510.3	-1.0	980253250	-1501
SG0018	463617	4666139	555.06	552.3	-2.7	980240875	-4777
SG0019	462944	4666259	595.77	599.0	3.2	980233715	-3072
SG0020	462316	4666308	622.16	622.9	.7	980227091	-4982
SG0023	463828	4665625	526.53	528.5	1.9	980248453	-2627
SG0024	463690	4665376	533.34	535.6	2.3	980246253	-2667
SG0025	463934	4664815	552.12	555.5	3.4	980242740	-1535
SG0026	463996	4664397	601.45	604.1	2.6	980232580	-478
SG0027	463927	4664915	525.12	536.7	11.6 *	980245911	-3632
SG0028	463601	4665526	555.08	557.2	2.1	980240936	-3778
SG0029	463469	4665246	597.65	600.1	2.5	980230194	-5302
SG0030	463171	4665625	544.33	546.9	2.5	980242881	-3734
SG0031	459800	4665684	573.28	571.2	-2.1	980231953	-9673
SG0032	462993	4665490	565.21	567.1	1.9	980238836	-3486
SG0033	462933	4665243	572.22	572.9	.7	980237493	-3282
SG0034	462958	4664819	574.69	577.8	3.1	980235881	-3999
SG0035	462971	4664350	628.43	627.7	-.7	980225233	-2334
SG0036	462902	4665428	604.00	602.2	-1.8	980231196	-3026
SG0037	462277	4666133	655.00	654.8	-.2	980219992	-4812
SG0038	461228	4665301	652.99	653.4	.4	980218643	-5998
SG0039	461157	4666027	631.30	633.4	2.1	980220936	-8948
SG0040	462001	4664882	657.58	659.6	2.0	980218572	-4394
SG0041	462136	4665025	665.01	668.3	3.3	980217566	-4248
SG0042	461743	4665304	621.96	627.8	5.9	980224650	-6189
SG0043	461505	4665797	595.24	596.6	1.4	980229787	-7339
SG0044	460777	4666683	590.77	590.5	-.2	980230354	-8624
SG0045	461174	4666381	615.82	614.1	-1.7	980225631	-8047
SG0046	461740	4666367	616.95	620.5	3.6	980227013	-6110
SG0047	462255	4666548	618.02	619.7	1.7	980228081	-5150
SG0048	462189	4666812	618.18	620.5	2.4	980227329	-6193
SG0049	462008	4666853	636.45	639.2	2.7	980221241	-8162
SG0050	462274	4667174	608.18	612.8	4.6	980229279	-6562
SG0051	462042	4667341	610.03	615.0	4.9	980229058	-6596
SG0052	461757	4667355	610.93	613.1	2.2	980228373	-6861
SG0053	461445	4667302	613.58	614.8	1.2	980225165	-8813
SG0054	461244	4667480	604.50	604.4	-.1	980227759	-9178
SG0055	461313	4667649	610.03	611.6	1.6	980226911	-9014
SG0056	461527	4667524	613.31	614.7	1.4	980226920	-8215
SG0057	461887	4667455	612.65	614.4	1.8	980228566	-6685
SG0058	460576	4666238	571.31	567.2	-4.2	980233453	-8919
SG0059	460959	4666826	608.18	610.4	2.3	980226736	-8915

SG0060	461085	4667178	604.58	607.3	2.8	980227894	-8725
SG0061	461235	4667314	611.31	613.7	2.4	980226150	-9110
SG0062	461268	4667819	622.69	626.0	3.4	980223616	-9803
SG0063	462093	4667152	627.88	630.6	2.7	980223749	-7943
SG0064	461825	4667206	624.75	631.8	7.0 *	980223671	-7884
SG0065	462043	4667063	643.30	645.0	1.7	980219434	-8786
SG0066	462198	4667624	626.18	627.6	1.5	980225890	-6408
SG0067	462293	4667902	631.86	634.6	2.7	980225747	-5711
SG0068	461925	4668040	638.02	638.7	.6	980223270	-7078
SG0069	461585	4668135	653.98	656.2	2.3	980218426	-8593
SG0070	461214	4668171	669.80	672.3	2.5	980213680	-9862
SG0071	460739	4668396	669.06	667.0	-2.0	980212958	-10983
SG0072	460400	4668664	663.24	663.5	.3	980213731	-11606
SG0073	460288	4668998	664.47	663.4	-1.1	980213285	-11986
SG0074	460047	4669981	653.61	653.2	-4	980216992	-10000
SG0075	459968	4669462	636.56	635.2	-1.4	980219118	-12292
SG0076	459829	4669265	622.39	622.7	.3	980221601	-12703
SG0077	459527	4668992	596.99	595.7	-1.3	980226014	-13331
SG0078	459116	4669593	554.68	552.9	-1.8	980235266	-13240
SG0079	459006	4669106	529.16	528.8	-4	980239489	-13942
SG0080	459956	4667351	553.34	550.0	-3.3	980235887	-11548
SG0081	460241	4667647	545.74	542.8	-2.9	980237740	-11243
SG0082	460172	4668064	569.72	567.4	-2.3	980233505	-10432
SG0083	459937	4667918	536.47	533.8	-2.7	980239897	-11081
SG0084	460491	4667319	574.67	571.0	-3.7	980231892	-10922
SG0085	460929	4667676	602.68	601.7	-9	980227424	-9969
SG0086	460283	4668403	657.43	654.0	-3.5	980216001	-10221
SG0087	461029	4668845	726.91	728.0	1.1	980201771	-9910
SG0088	461314	4669019	724.92	723.2	-1.7	980202404	-9892
SG0089	460834	4669477	705.21	705.0	-.2	980206232	-9894
SG0091	460086	4665935	571.93	568.1	-3.8	980233249	-9070
SG0092	460399	4666857	580.69	578.0	-2.7	980230880	-10401
SG0093	460222	4666849	567.26	564.2	-3.1	980233926	-10118
SG0094	460256	4666903	576.94	572.9	-4.0	980231426	-10722
SG0095	459510	4667892	532.90	530.5	-2.4	980240370	-11549
SG0096	458798	4668113	513.72	512.6	-1.1	980243165	-12780
SG0097	459223	4668398	510.36	507.1	-3.3	980242694	-13888
SG0098	459434	4668732	582.43	580.6	-1.8	980228371	-13593
SG0099	459025	4668641	502.91	503.2	.3	980244207	-14150
SG0100	459925	4668641	630.81	628.5	-2.3	980220686	-11405
SG0101	461441	4669295	723.86	722.0	-1.9	980204455	-7870
SG0102	460853	4669054	709.70	709.1	-.6	980204190	-11447
SG0103	461509	4668619	709.10	710.3	1.2	980205174	-10099
SG0104	461955	4668349	669.27	671.0	1.8	980215876	-7729
SG0105	462443	4667973	634.35	636.1	1.8	980225286	-5076
SG0106	464417	4665809	483.35	486.7	3.3	980258725	-1094
SG0107	464519	4666347	488.59	490.2	1.6	980257969	-1731
SG0108	464578	4666638	471.19	473.7	2.5	980261804	-1679
SG0109	464108	4667039	473.90	477.3	3.4	980260695	-2312
SG0110	463710	4667332	500.60	503.4	2.8	980254633	-3299
SG0111	463267	4667533	517.19	519.4	2.2	980250398	-4243
SG0112	462815	4666874	571.01	572.3	1.3	980238356	-4578
SG0117	457869	4669215	430.16	429.0	-1.1	980258392	-15405
SG0118	457852	4668952	430.56	430.2	-.4	980258107	-15365
SG0120	457590	4668963	435.46	434.8	-.7	980256337	-16186
SG0121	457398	4668706	439.04	438.8	-.2	980254718	-16879
SG0122	457654	4668815	434.48	434.3	-.2	980256630	-15977
SG0123	457569	4668445	438.21	436.4	-1.8	980255872	-15618
SG0124	457300	4668379	441.67	442.7	1.0	980253995	-16761
SG0125	457800	4668300	436.80	436.8	.0	980256419	-14951
SG0126	458000	4668400	446.10	446.1	.0	980257178	-12390
SG0127	458200	4668800	435.10	435.0	-.1	980257432	-14908

SG0128	458300	4668500	454.60	454.6	.0	980253215	-14864
SG0129	458700	4668700	473.90	473.9	.0	980249625	-14724
SG0130	458900	4668400	503.70	503.8	.1	980243099	-15101
SG0131	458600	4667500	547.20	547.2	.1	980237064	-11504
SG0132	463960	4666358	503.41	505.4	2.0	980253803	-2495
SG0134	464966	4667949	526.11	527.6	1.5	980251422	-467
SG0135	464730	4667577	497.34	496.5	-8	980257265	-1011
SG0136	464508	4667083	469.20	470.7	1.5	980262007	-2151
SG0138	459462	4666072	556.04	552.1	-3.9	980234171	-11219
SG0140	458754	4666034	538.35	535.0	-3.3	980237449	-11374
SG0141	458775	4665814	531.34	528.5	-2.8	980237970	-11433
SG0142	459071	4665415	573.03	570.0	-3.0	980229209	-10684
SG0143	458996	4665711	532.34	528.4	-3.9	980237866	-11290
SG0144	458471	4665890	516.23	515.0	-1.2	980240417	-12005
SG0145	457830	4666053	513.20	512.8	-4	980239806	-13534
SG0146	457180	4666424	495.63	496.2	.6	980242542	-14649
SG0147	457421	4666751	490.89	492.1	1.2	980244534	-14658
SG0148	457311	4667132	484.21	484.2	.0	980245863	-15139
SG0149	457524	4667454	475.59	475.0	-6	980248726	-14276
SG0150	457845	4667277	490.19	490.4	.2	980245712	-14202
SG0151	458382	4666890	512.89	513.8	.9	980241268	-13565
SG0153	464712	4666885	462.28	463.8	1.5	980264145	-1320
SG0154	465158	4666928	455.22	459.2	4.0	980266355	-435
SG0155	465417	4667295	479.21	480.8	1.5	980262301	931
SG0156	465495	4667688	483.83	485.8	2.0	980261262	751
SG0158	464167	4667364	480.05	480.3	.2	980259462	-2604
SG0159	464194	4667734	498.43	499.8	1.4	980255924	-2574
SG0160	464389	4667929	519.44	521.0	1.6	980252273	-1579
SG0161	464110	4668133	523.14	523.8	.7	980250993	-2537
SG0163	463849	4667903	505.04	506.1	1.1	980254248	-2972
SG0164	463331	4668392	548.39	549.5	1.1	980244878	-3540
SG0165	463496	4667982	508.45	511.7	3.2	980252624	-4008
SG0166	462787	4668193	564.36	561.6	-2.7	980240614	-4147
SG0167	463257	4667831	518.90	518.9	.0	980250295	-4113
SG0168	465403	4666749	436.74	438.0	1.3	980270595	160
SG0169	465825	4666820	425.32	427.0	1.7	980273628	816
SG0170	465758	4667086	433.56	436.2	2.6	980271580	530
SG0171	465217	4666283	452.39	455.1	2.7	980266911	-093
SG0172	465731	4666500	431.24	433.7	2.5	980272223	739
SG0173	465741	4666151	435.72	436.5	.8	980271286	1051
SG0174	465788	4665634	436.46	438.0	1.5	980269997	723
SG0175	465546	4665050	470.60	471.7	1.1	980262637	1323
SG0176	465916	4664790	461.65	463.3	1.6	980265162	2153
SG0177	465372	4665980	473.24	475.8	2.5	980262866	607
SG0178	464869	4665916	459.32	459.5	.2	980264625	-432
SG0179	465207	4665082	517.35	519.0	1.7	980252719	727
SG0180	464893	4665441	464.20	466.1	1.9	980263076	048
SG0181	464564	4665454	511.49	508.3	-3.2	980252897	-254
SG0182	464635	4665034	494.32	494.1	-.2	980256241	210
SG0185	464093	4665528	510.26	512.0	1.7	980252661	-1465
SG0186	457566	4669584	433.77	432.0	-1.8	980257409	-16060
SG0187	457877	4666705	499.03	500.4	1.3	980243466	-14070
SG0188	457479	4669991	438.37	436.4	-2.0	980256822	-16077
SG0189	458084	4669923	428.64	425.8	-2.8	980259717	-14928
SG0190	458392	4669691	461.88	460.0	-1.9	980253678	-14048
SG0191	458374	4669176	468.93	468.7	-.2	980252021	-13894
SG0192	458675	4669322	497.44	494.0	-3.4	980246772	-13366
SG0193	458095	4669464	448.04	446.4	-1.7	980255897	-14547
SG0194	458451	4669986	448.25	446.2	-2.0	980256406	-14290
SG0195	458594	4670456	426.19	424.5	-1.7	980261326	-13942
SG0196	458665	4670792	418.85	417.1	-1.7	980263352	-13904
SG0197	459451	4670981	408.82	407.4	-1.4	980266409	-12732

SG0198	460556	4671179	464.23	459.4	-4.9	980258559	-9832
SG0199	460880	4670522	487.66	483.1	-4.5	980253089	-9753
SG0200	461181	4670011	522.47	523.4	1.0	980245348	-9019
SG0201	462598	4671647	403.84	402.4	-1.4	980274305	-6206
SG0202	462706	4670615	435.69	433.7	-2.0	980267016	-6330
SG0203	462811	4670046	430.10	428.1	-2.0	980267241	-5922
SG0204	463517	4670845	489.55	487.1	-2.5	980258404	-4127
SG0206	454591	4664374	471.50	471.3	-.2	980242295	-18081
SG0207	456026	4663175	496.04	496.7	.7	980240460	-13997
SG0208	457502	4663590	553.95	557.8	3.9	980232349	-10797
SG0209	458063	4661433	511.11	514.1	3.0	980241632	-8369
SG0210	459521	4661707	531.08	529.6	-1.5	980239976	-6345
SG0211	460151	4662466	591.09	589.3	-1.8	980229303	-5866
SG0212	461194	4663484	639.28	644.0	4.7	980220851	-5087
SG0213	460807	4663005	620.37	619.6	-.7	980224466	-5192
SG0214	457768	4662619	549.20	547.9	-1.3	980233510	-8887
SG0215	455312	4665529	467.67	469.4	1.7	980244606	-17486
SG0216	455862	4667073	459.73	458.7	-1.0	980246867	-18867
SG0217	456300	4668006	475.17	472.4	-2.7	980245940	-17806
SG0218	458082	4670595	453.34	448.7	-4.6	980253452	-16302
SG0219	457880	4671260	428.81	426.4	-2.4	980260163	-15359

Geophysical exploration on the subsurface geology of La Garrotxa monogenetic Volcanic Field (NE Iberian Peninsula)

Published in:

International Journal of Earth Science

Authors of the paper:

Xavier Bolós ^(a)

Stéphanie Barde-Cabusson ^(a)

Dario Pedrazzi ^(a)

Joan Martí ^(a)

Albert Casas ^(b)

Raúl Lovera ^(b)

Daniel Nadal-Sala ^(c)

a) Institute of Earth Sciences Jaume Almera, ICTJA-CSIC, Group of Volcanology. SIMGEO (UB-CSIC) Lluís Sole i Sabaris s/n, 08028 Barcelona, Spain

b) Economic and Environmental Geology and Hydrology Group. Department of Geochemistry, Petrology and Geophysical Prospecting. Faculty of Geology, University of Barcelona. Martí Franqués s/n, 08028 Barcelona,) Spain

c) Ecology Department, University of Barcelona, Diagonal 645, 08028 Barcelona, Spain.

3.1. Abstract

We applied self-potential and electrical resistivity tomography to the exploration of the uppermost part of the substrate geology and shallow structure of La Garrotxa monogenetic Volcanic Field, part of the European Neogene-Quaternary volcanic province. The aim of the study was to improve knowledge of the shallowest part of the feeding system of these monogenetic volcanoes and of its relationship with the subsurface geology. This study complements previous geophysical studies carried out at a less detailed scale and aimed at identifying deeper structures, and together will constitute the basis to establish volcanic susceptibility in La Garrotxa. Self-potential study complemented previous smaller-scale studies and targeted key areas where electrical resistivity tomography could be conducted. The main new results include the generation of resistivity models identifying dykes and faults associated with several monogenetic cones. The combined results confirm that shallow tectonics controlling the distribution of the foci of eruptive activity in this volcanic zone mainly correspond to NNW–SSE and accessorially by NNE–SSW Neogene extensional fissures and faults and concretely show the associated magmatic intrusions. These structures coincide with the deeper ones identified in previous studies, and show that previous Alpine tectonic structures played no apparent role in controlling the loci of this volcanism. Moreover, the results obtained show that the changes in eruption dynamics occurring at different vents located at relatively short distances in this volcanic area are controlled by shallow stratigraphical, structural, and hydrogeological differences underneath these monogenetic volcanoes.

Keywords: monogenetic volcanism · Garrotxa Volcanic Field · electrical resistivity tomography · self-potential · subsurface geology · feeding system

3.2. Introduction

Monogenetic volcanism is characterised by the formation of volcanoes that extrude small amounts of magma in each eruption ($0.01\text{--}0.2\text{ km}^3$) (Walker 2000). These short-lived eruptions are often grouped in volcanic fields (Connor and Conway 2000; Walker 2000; Valentine and Gregg 2008) and are common under a variety of geodynamic conditions (Francis 1993; Connor and Conway 2000; Walker 2000). A particular feature of this type of volcanism is the great variety of resulting eruptive styles, morphologies and deposits (Houghton et al. 1999; Connor and Conway 2000; Parfitt 2004; Valentine and Gregg 2008). This diversity is caused by compositional changes (e.g. volatile content), magma supply rate, local tectonics (e.g. stress fields, degree of fracturing, basement mechanical behaviour) or by the hydrogeological characteristics of the substrate (e.g. Vespermann and Schmincke 2000; Walker 2000; Martí et al. 2011; Bolós et al. 2012; Pedrazzi et al. 2014). A good example of the great diversity found in monogenetic volcanic fields is the European Cenozoic Rift System, which encompasses several different volcanic areas, all related to the same geodynamic environment but with different local tectonics (Wilson and Downes 1991, 1992; Downes 2001; Dèzes et al. 2004).

The location and distribution of monogenetic volcanic fields depend on the size and shape of the magmatic source, i.e. it is governed by regional geodynamics. However, the distribution of the eruptive vents within each volcanic field is the result of the geological structure and stress fields found in the upper crust at the moment of activity in each location (Zhang and Lutz 1989; Connor and Conway 2000; Cebrià et al. 2011).

The factors controlling the precursory activity in monogenetic volcanic fields are still poorly understood and so eruptions in these systems are difficult to forecast. In monogenetic volcanism each new eruption creates a different vent, suggesting that volcanic susceptibility contains a high degree of randomness and that accurate spatial forecasting is at best highly uncertain. Recent studies of monogenetic volcanism reveal how sensitive magma migration is to changes in regional and/or local stress fields caused by tectonic or lithological contrasts (e.g. former magmatic intrusions) (Martí et al. 2013). This may induce variations in the pattern of further magma movements and thus affect the location of future eruption sites.

The spatial distribution of eruptive vents may help reveal fracture patterns. At depth, magma rises towards the surface following the path that is normal to the minimum stress in the area (Connor and Conway 2000; Gudmundsson 2006; Cebrià et al. 2011). Near to the Earth's surface, it may become increasingly influenced by pre-existing structures and, for example, be captured by pre-existing faults and joints (e.g. Valentine and Gregg 2008; Le Corvec et al. 2013). Therefore, knowledge of regional and local tectonic controls and structures and the position of the eruptive vents is essential for understanding past volcanism. The relationship between the position of past eruptive focuses and these controls and structures will be important for determining the location of future vents (Martí and Felpeto 2010).

Geophysical exploration and more specifically geoelectrical methods have been used in the last decades to investigate structural geology and the feeding system in different volcanic areas around the world. For example, in New Zealand Nishi et al. (1996) applied self-potential surveys to study the hydrothermal system of White Island Volcano. Bibby et al. (1998) used electrical resistivity imaging to characterise the upper crust of the Taupo Volcanic Zone. In Italy Di Maio et al. (1998, 2000) applied electrical and electromagnetic methods to study the structure of Mount Somma and Campi Flegrei. In Japan Hase et al. (2005) studied the hydrothermal system beneath Aso volcano with self-potential and resistivity measurements. In Massif Central of France Portal et al. (2013) explored the inner structure of Puy de Dôme volcano from electrical resistivity tomography, gravity and muon imaging. These studies and others referenced therein have proven the efficiency of geoelectrical methods for studying the structure and geology of volcanoes.

A previous geophysical study has been performed in La Garrotxa Volcanic Field (GVF) by Barde-Cabusson et al. (2014) dealing with deeper structures (up to 3 km in depth) associated with the volcanism of this area. This study was based mainly on the application of gravimetry and self-potential techniques, and revealed interesting features of the internal structure of the area (e.g. the presence of low density bodies associated with the main Neogene fault and fissure systems). However, this study did not clarify the superficial aspects of the possible control exercised by the substrate geology or identify any shallow structural features. Thus, in order to obtain a much better resolution of the shallower structures of this area a new geophysical survey was carried out that covered a greater area than the previous self-potential survey and undertook electrical resistivity tomography surveys throughout the whole area. The self-potential data confirm and complement previous results, which, combined with the new electrical tomography data, offer a more detailed picture of the substrate geology and structure beneath the volcanoes of La Garrotxa.

In this paper we describe the methodology used to conduct the field surveys and to process the data gathered, and then present the data obtained. We interpret the geological meaning of the data and, finally, discuss their relevance to subsoil geology in highly built-up areas and/or areas covered by dense vegetation. We identify the local shallow tectonic controls operating on the distribution of eruptive vents in the GVF and situate them in a more complex regional context.

3.3. Geological setting

The GVF is part of the Catalan Volcanic Zone (CVZ) (NE Spain), one of the Quaternary alkaline volcanic provinces associated with the intraplate European Cenozoic Rift System (Martí et al. 1992; Downes 2001; Dèzes et al. 2004) (Figure 1). It covers an area of about 600 km² and is located between the cities of Olot and Girona (Figure 1). This basaltic volcanic field contains over 50 cones including cinder and scoria cones, tuff rings and maars, ranging in age from 0.7 Ma to early Holocene (Martí et al. 2011). Materials from the upper Palaeozoic, Eocene and Quaternary characterize the substrate. The volcanism of the GVF is mainly represented by alkaline rocks with poorly evolved magmas, i.e. basalts and basanites (Araña et al. 1983; Cebrià et al. 2000). A notable feature of this area is the presence of mantle xenoliths and lower crust cumulates (Araña et al. 1983; López-Ruiz and Rodríguez-Badiola 1985; Martí et al. 1992; Neumann et al. 1999; Cebrià et al. 2000), which suggests that some of the eruptive fissures and faults reached quite deeply into the lithosphere and that some were the same regional normal faults which bound the area's horsts and grabens (Martí et al. 2011).

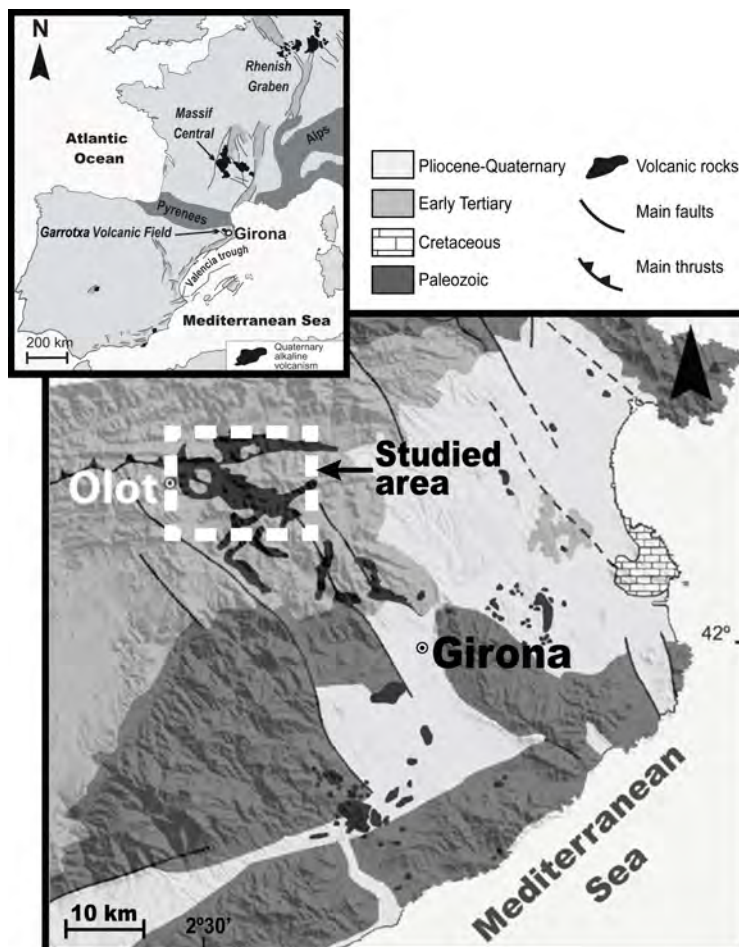


Fig. 1. a) Simplified map of the distribution of the volcanism in the European Cenozoic Rift System. b) Simplified geological map of the Catalan Volcanic Zone (modified from Guérin et al. 1985).

The GVF is laterally limited by two main NNW–SSE fault systems: the Llorà Fault to the east and the Amer Fault to the west, which are thought to be responsible for the distribution of the area's volcanism and its fluvial network (Saula et al. 1995; Martí et al. 2011; Bolós et al. 2012; Cimarelli et al. 2013). Most of the volcanoes in the study area are located between the towns of Olot and Santa Pau (Figure 2). They stand on folded Eocene basement, characterized by conglomerates, sandstones, marls, clays and gypsum (Bracons and Bellmunt Formations) that outcrops as an eroded anticline with an E–W axial plane. This anticline and the reverse faults described in the area were formed during the Alpine Orogeny (Martinez et al. 1997) (Figure 2).

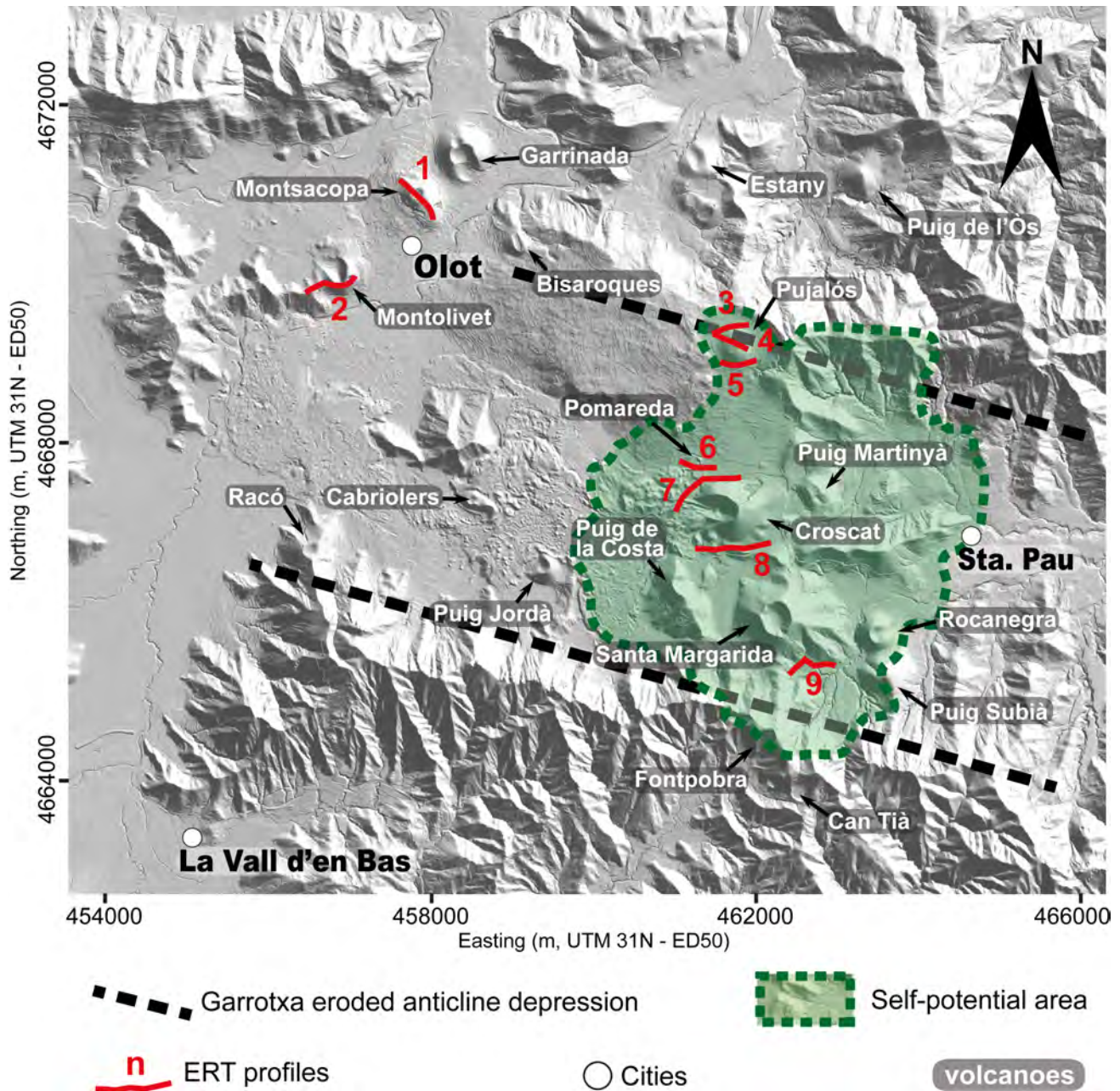


Fig. 2. Digital Elevation Model of the study area, with location of the self-potential and ERT profiles described in this study.

3.4. Methods

The study area extends roughly between the towns of Olot and Santa Pau, both inside and outside the elongated E–W-eroded anticline depression in which most of the volcanic edifices of the GVF are situated (Figure 2). The study involved the application of self-potential (SP) and electrical resistivity tomography (ERT), which generated data that, in conjunction with existing geological data, enabled us to map geological units and to delineate structural limits at the surface and in the substrate below the volcanic edifices. The SP measurements focused on a number of key volcanic edifices and provided surface information to a resolution of 20 m, thereby allowing the main structural limits to be identified; the ERT profiles, on the other hand, provided 2D geological, structural and hydrogeological information at depth.

The main mechanism responsible of self-potential signals in volcanic terrains is the electrokinetic effect. This mechanism produces a positive electrical potential in the flow direction. When the groundwater moves through a porous rock matrix or in fractures and discontinuities of the substrate, electrochemical interactions occur at the interface between a mineral and the pore water. In normal pH conditions the surface of silicate and aluminosilicates is negatively charged and the zeta-potential is negative. In order to maintain a global electroneutrality in the system, the electrical double (or triple) layer theory says that the diffuse layer has a net charge of opposite sign (positive) to the surface charge of the mineral. In this way the positive electrical charges are dragged by groundwater in the direction of the flow, creating positive self-potential anomalies over discharge areas and negative anomalies over recharge areas (e.g. Revil 2002).

The SP map drawn by Barde-Cabusson et al. (2014) was completed by means of 474 new measurements in additional profiles that covered a total of 10 km. All the SP measurements were made with a high impedance voltmeter (Extech EX520, sensitivity of 0.1 mV, input impedance >10 M Ω) using two non-polarised Cu/CuSO₄ electrodes and a 300-m section of cable. The difference in potential between the reference electrode, which was placed at the start of the profile, and the moving electrode was measured. In all, the SP surveys correspond to a series of profiles involving a total of 2,547 measurements with a distance of 20 m between successive stations. Additional data were corrected for closure errors based on the previous SP dataset correction with a single reference (Figure 3; for details of the field methodology, see Barde-Cabusson et al. 2014).

Electrical resistivity methods are based on the principle that the distribution of electrical potential in the ground around a current-carrying electrode depends on the electrical resistivities and distribution of the surrounding rocks. Resistivity measurements are commonly used for investigating various types of subsurface exploration problems. As a general principle, the acquisition techniques consist in measuring, between two electrodes (M, N), the difference of potential generated by the electrical current which is injected into the ground via two other electrodes (the transmitting line AB). Electrical resistivity tomography (ERT) surveys are normally carried out with multi-electrode resistivity systems. Such surveys use a number of electrodes deployed in a straight line at equal intervals and computer-controlled system is then used to select the active electrodes for each electrode set-up automatically (Griffiths and Barker 1993). This allows a large number of measurements to be performed and 2D resistivity high-resolution data can be obtained very quickly. The ERT data were acquired with an Iris Syscal Pro resistivity system. A Wenner-Schlumberger electrode configuration was used with 48

electrodes connected to a 470-m section of cable (10 m between electrodes) that enabled us to obtain a maximum depth of investigation of 100 m. The main reason for choosing a mixed Wenner-Schlumberger array in areas where both types of geological structures (vertical and horizontal) are expected to occur is because better results might be obtained. The signal strength of this hybrid array is weaker than the one provided by the Wenner array, but the depth of investigation is increased and lateral coverage is improved (Martorana et al. 2009). Besides, in the Wenner-Schlumberger configuration, the measured voltage signal drops to the level of electrical noise as the distance between the current electrodes becomes very large while keeping the potential dipole length constant. This is because the measured potential signal in the Schlumberger array is inversely proportional to the square of the current electrode spacing, whereas in the dipole-dipole array the measured potential signal is inversely proportional to the third power of the current electrode spacing.

A total of nine ERT profiles of different lengths were obtained from 16 acquisitions using 470-m-long sections (Figure 2). The roll-along method was used to obtain five of the profiles (profiles 1, 2, 7, 8 and 9). Profiles 7 and 8 consisted of three sections with half the cable length overlapping, giving each a total length of 950 m, while profiles 1, 2, and 9 were composed of two sections, each with a total length of 710 m. Finally, four profiles (3, 4, 5 and 6) consisted of individual sections.

The data obtained were interpreted using an inversion process to provide a resistivity section that approximates the actual subsurface structure and to locate their boundaries spatially below the surface of the site. The apparent electrical resistivity data acquired in the field were processed with the Res2dinv software from GEOTOMO© (Loke 2002), which is based on the smoothness-constrained, nonlinear least-squares optimization technique, was used to obtain the interpretative model. The inversion algorithm is an iteratively reweighted least-squared method based on the Gauss–Newton method; in addition, the Jacobian matrix of partial derivatives is always recalculated using the finite-element method. The first step in the inversion is the estimation of an initial model. Next, the solution is iteratively improved by varying the model parameters to minimize the discrepancies between the observed and the calculated responses. The inversion program uses a 2D model divided into a number of rectangular blocks (pixels of inversion models), whose arrangement is made according to the distribution of the data points in the pseudo-section (Loke and Barker 1996). In the model we also included topographical information obtained from the Digital Elevation Model (DEM) to a resolution of 15x15 m from Catalan Geographic Institute (www.icc.cat). The RMS error (representation of the reproducibility of the data from the inverted model) was in most cases less than 7% but increased in the roll-along profiles.

3.5. Results

3.5.1. Self-potential map

The SP map (Figure 3) shows a total variation of ~300 mV. The main feature of the map is the transition from east to west: in the east, low amplitude SP spatial variation (<30 mV) is observed, while in the west the SP isolines are oriented NNW–SSE and NNE–SSW. Additional more isolated negative SP peaks are visible at Rocanegra Strombolian volcano, Puig Subià and

Puig Martinyà (Figure 3). One of the most significant features of this new SP map is the abrupt E–W transition (with the lowest values recorded on the western side) observable in the northern sector centred on the Pujalós volcano. In the southernmost part of the map, the new data that complement the data generated by Barde-Cabusson et al. (2014) show a continuation of the NNW–SSE lineament crossing the volcanoes of Croscat and Santa Margarida (Figure 3). This area corresponds to the southern high-point of the anticline, where a normal fault and pyroclastic deposits from the Fontpobra volcano are found (IGC; 1:25 000, www.igc.cat).

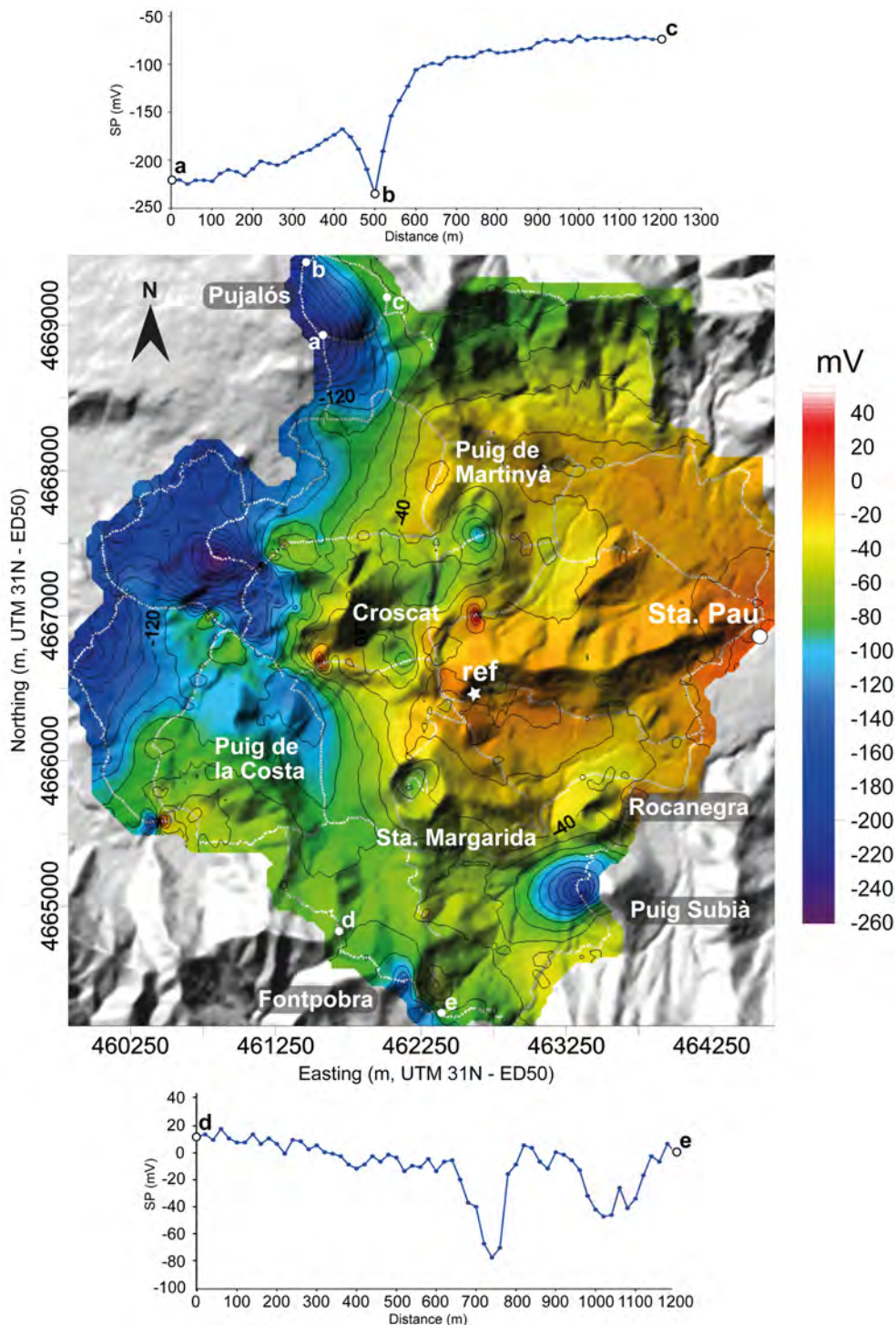


Fig. 3. Self-potential map. In the upper and lower part of the figure, the two SP vs. distance graphs correspond on the map to the 'abc' and 'de' profiles. White dots show the location of the SP measuring stations. Coordinates in UTM - 31N - ED50.

3.5.2. Electrical resistivity tomography

ERT profiles show in some cases excessively high resistivity values, ranging from less than $10 \Omega \text{ m}$ to hundreds of thousands of $\Omega \text{ m}$. These high resistivities are generated by the inversion process in Res2dinv when strong resistivity contrasts exist close to the surface. This occurs if materials with very low resistivity such as clay, silt and organic soils come into contact in parallel with materials with very high resistivity (Loke 2002). For this reason, we chose a colour scale whose maximum corresponds to values of resistivity $>26,000 \Omega \text{ m}$, the value measured for the massive basaltic intrusions that outcrop in the field that were the highest measured in the area. This enabled us to provide a more realistic picture of the subsurface repartitioning of the resistivity. In Res2dinv, however, we imposed a cell width of half the unit electrode spacing, which allowed us to obtain optimal results in profiles with high contrasts in resistivity (Loke 2002).

Profile 1: Montsacopa volcano

Profile 1 was carried out through the central part of the Montsacopa edifice (Figure 4) in a NNW–SSE direction. It is characterized by resistivity values from ~ 100 to over $26,000 \Omega \text{ m}$. The lowest values are visible in the shallowest part of the high resistivity intrusive and spatter products below the volcano's crater A. In the southeastern half of the profile, high values of resistivity are interrupted by a small zone of lower resistivities (Figure 4) corresponding to another hidden crater (crater B) (Bolós 2009; Barde-Cabusson et al. 2013). These craters are aligned in a NNW–SSE direction.

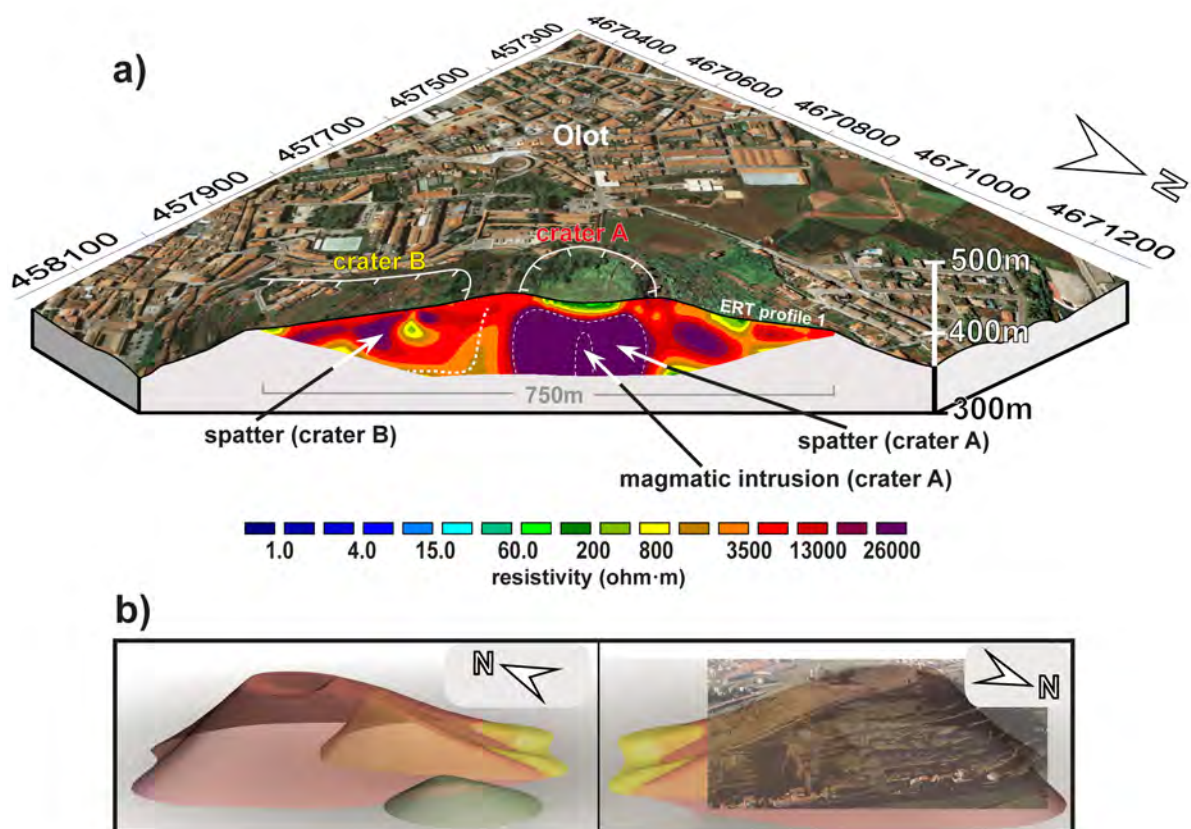


Fig. 4 a) Orthophotograph overlaid on a 3D block diagram of ERT profile 1 corresponding to Montsacopa volcano (RMS error 5.7%). b) 3D interpretation model showing the overlapping cones inside the edifice. Coordinates in UTM - 31N - ED50.

Profile 2: Montolivet volcano

An E–W profile was conducted on the southern side of the Montolivet volcano. Profile 2 (Figure 5) reveals a zone of high resistivity ($>1,000 \Omega \text{ m}$) located mainly in the eastern half of the edifice, with a thickness of over 80 m. The deepest part of this profile had lower resistivity values ($\sim 60\text{--}1,000 \Omega \text{ m}$) that define a horizontal interface with the upper resistive layer. This deep layer continues in the western part of the volcano, where the values are also lower ($\sim 20\text{--}200 \Omega \text{ m}$), and is separated from the eastern high resistivity zone by an interface dipping 45° eastwards in the cross-section defined by the ERT profile.

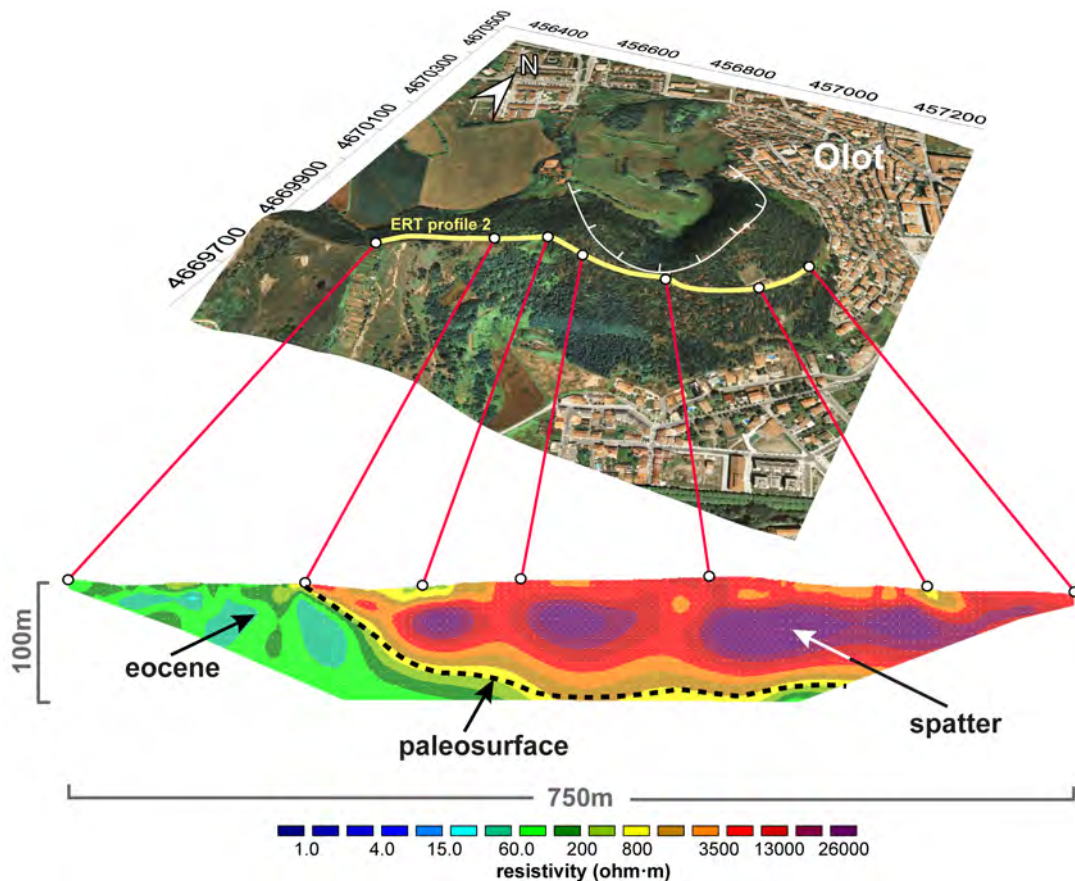


Fig. 5 Top: orthophotograph overlaid on a Digital Elevation Model with the location of ERT profile 2 (yellow line) corresponding to Montolivet volcano. Bottom: ERT model (RMS error 3.0%). Coord. in UTM - 31N - ED50.

Profiles 3, 4 and 5: Pujalós volcano

Three profiles were carried out on the Pujalós volcano as a means of comparing results with variations in the SP. Profile 3 in the northern part of the volcano (Figs. 6a and b) cuts across the NNW–SSE lineament shown by the SP. This profile reveals a shallow conductive layer ($40\text{--}400 \Omega \text{ m}$) overlaying a resistive layer ($>1,000 \Omega \text{ m}$) that continues to the maximum depth of exploration in the western half of the profile, but narrows eastwards to a thickness of $\sim 40 \text{ m}$ (Figure 6b). Profile 4 was acquired through the centre of the volcanic cone (Figs. 6a and c) and obtained a resistivity model that is very similar to that from profile 3 (Figure 6b). Profile 5 was located in the southern part of the volcano and crosses the NNW–SSE SP lineament described above (Figs. 6a and d). Although the repartition of the resistivity is not as clear in this ERT model as in the two previous profiles, an

irregular resistive layer is seen to extend from a depth of 50 m to the maximum depth of the exploration. In the upper part, a less resistive layer is sometimes interrupted in places by resistive bodies connected to the deeper layer and sometimes also to the topography surface. Strombolian fallout deposits and spatter facies have been observed on the surface, coinciding geographically with the high resistivity values in the shallow part of these profiles.

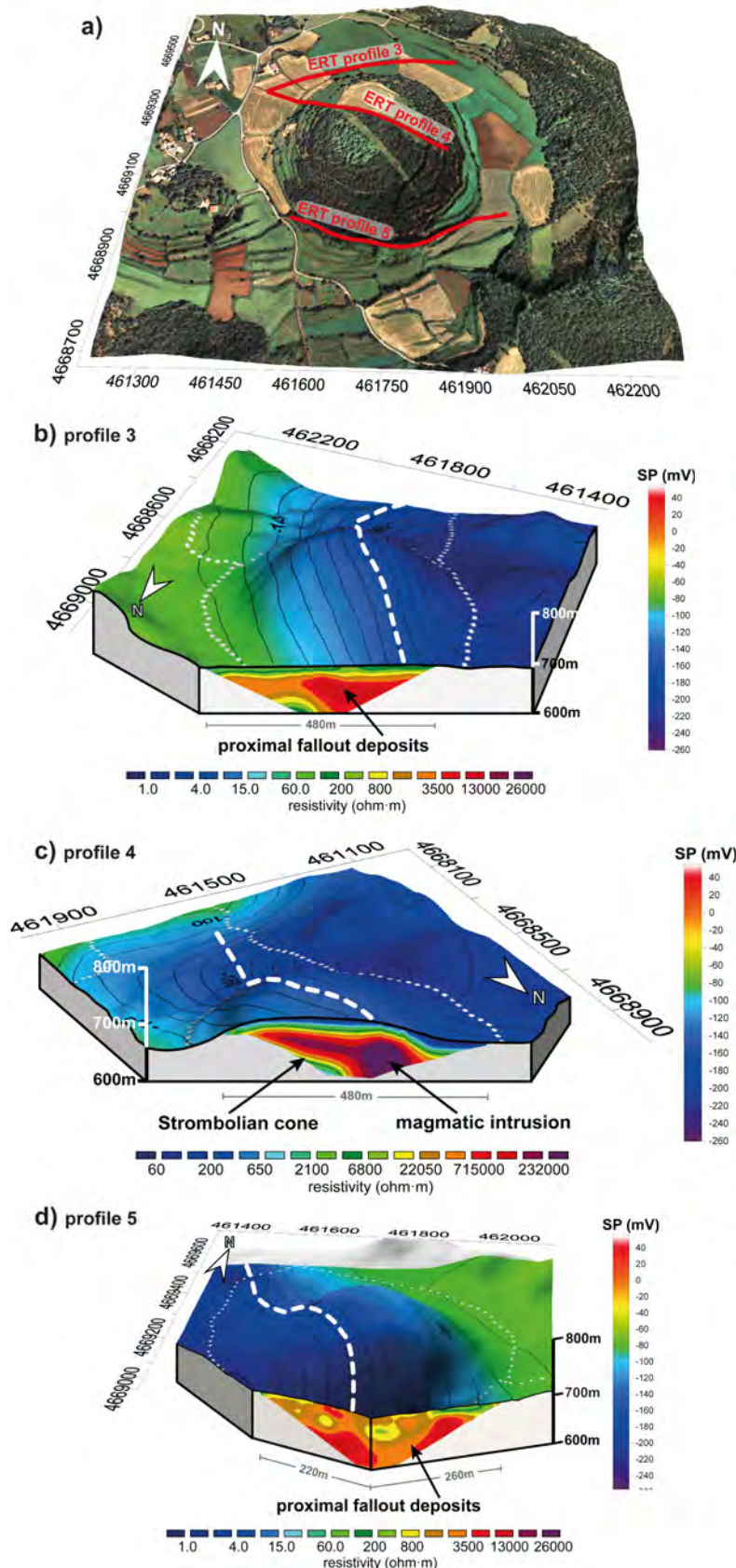


Fig. 6. a) Orthophotograph overlaid on a digital elevation model with the location of the ERT profiles (red lines). b), c) and d) 3D block diagrams of Pujalós volcano, showing the corresponding SP mapping on the surface and ERT profiles 3 (RMS error 2.9%), 4 (RMS error 15.2%) and 5 (RMS error 3.7%) in the cross-section. White dotted lines show the location of the SP measurements. White dashed line identifies the SP lineation. Coordinates in UTM - 31N - ED50.

Profile 6: La Pomareda spatter cone

Profile 6 cuts across the Pomareda volcano in an E–W direction (Figure 2) and has the highest resistivity values ($\sim 13,000 - \sim 26,000 \Omega \text{ m}$) detected at the surface in the study area (Figure 7). In the field this unit corresponds to massive basaltic lava flows and spatter deposits. A 15–20-m-thick layer appears to be connected to the deepest part of the resistivity model via a narrow channel reaching $\sim 4,000 \Omega \text{ m}$. This channel crosses a less resistive layer ($400-2,000 \Omega \text{ m}$) and joins a deep, high resistivity horizontal layer with values that range from $\sim 2,000 \Omega \text{ m}$ in the west to $\sim 10,000 \Omega \text{ m}$ in the east (Figure 7).

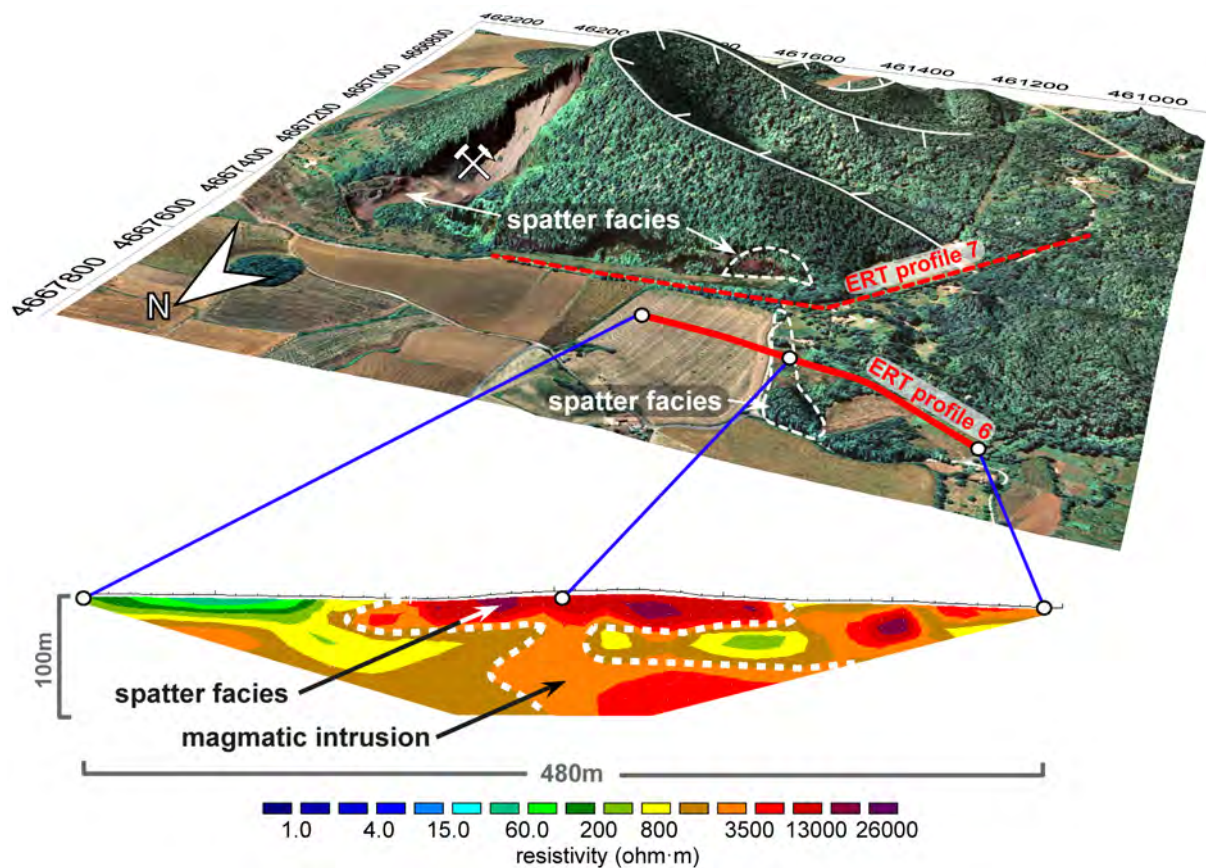


Fig. 7. Top: orthophotograph overlaid on a digital elevation model with the location of ERT profile 6 corresponding to Pomareda volcano (red line). Bottom: ERT model (RMS error 5.5%). Coordinates in UTM - 31N - ED50.

Profiles 7 and 8: Croscat volcano

Profile 7 (Figure 8) was carried out in an E–W direction (Figure 2) on the northern side of the volcano and it was composed of three different sections that were processed jointly. It has a high inversion error (RMS=22.5%) due to the poor quality of the measurements carried out in the western part of the profile. We processed each section separately and found RMS errors of 11.9%, 15.2% and 35.8% from east to west, respectively, indicating that the data from the westernmost section is the least reliable.

One of the main elements of the profile is observed in its centre (Figure 8, zone A), where a resistive body shows values over 20,000 Ω m. This body is elongated and rises vertically from the base of the resistivity model almost to the topography surface. Its lateral contacts are well defined on both sides and there is a sharp lateral transition of the resistivity. In the cross-section this body is ~30-m thick in its shallowest part and ~60-m thick at depth. In the westernmost part of the profile its resistivity values are of the same order of magnitude (Figure 8, zone B); this area is quite homogeneous from the surface to the maximum depth of exploration (Figure 8).

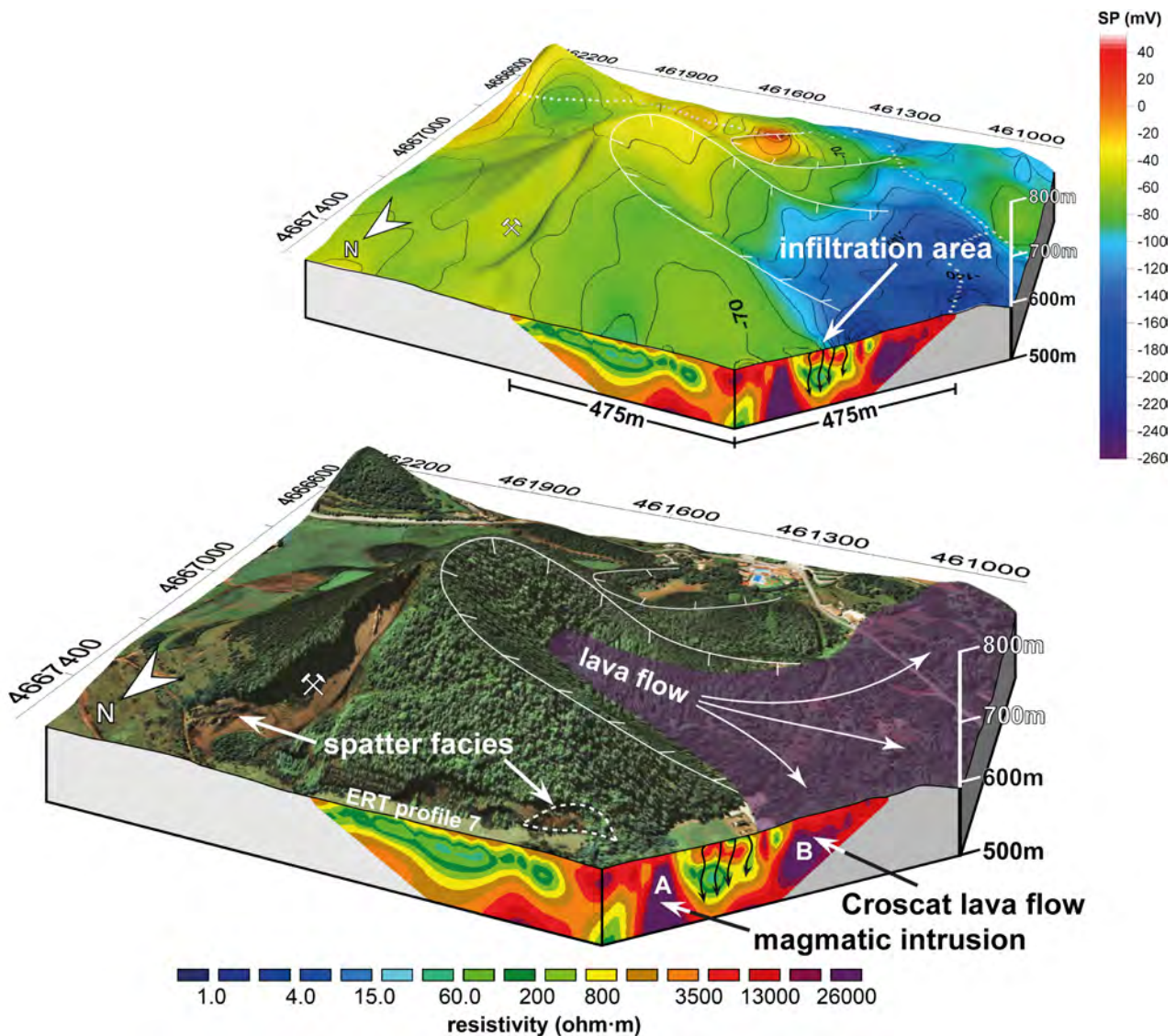


Fig. 8. 3D block diagrams for ERT profile 7 located on the northern side of Croscat volcano. The upper part of the figure shows the surface SP map overlaid on a Digital Elevation Model. In the lower part, an orthophotograph is overlaid on the same Digital Elevation Model. The corresponding ERT profile is presented in the cross-section (RMS error 22.5%). Coordinates in UTM - 31N - ED50.

Profile 8 has the same direction as profile 7 (E–W) and it is located on the southern side of the volcano (Figure 9). A resistive body borders the western part of the profile (Figure 9, zone A) and extends from the maximum depth of exploration (here ~70 m) to the

topography surface. Due to the presence of a main road we were unable to extend the profile further to the west to gain a better idea of the geometry of this resistive body. A few metres to the east a resistive bulge with no continuity at depth coincides with the deposits of Croscat’s secondary crater (Figure 9, zone B). Throughout the rest of the profile, a 30–15-m-thick resistive level (1,000–13,000 Ω m) overlies a more conductive layer (50–1,000 Ω m). In the easternmost part of the profile these layers appear to be shifted downwards by \sim 10 m, thereby defining a western and an eastern block. This separation also coincides with a discrete break-in-slope in the topography. The eastern block is overlain by a conductive layer that is just a few metres thick. The deepest layer has the highest conductive values encountered in the profile (reaching values <4 Ω m) (Figure 9, zone C), a whole order of magnitude lower than the corresponding layer in the western block.

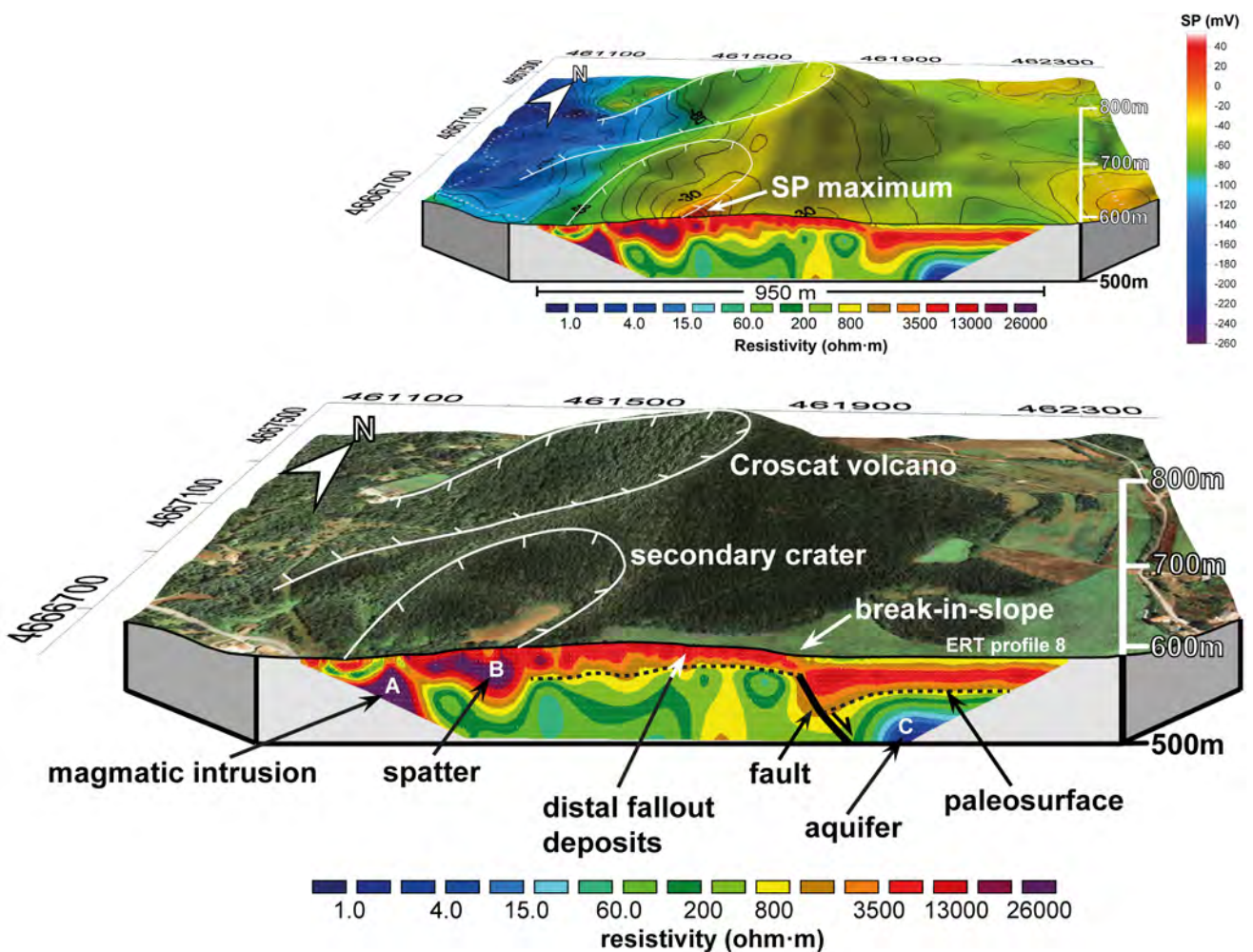


Fig. 9. 3D block diagrams for ERT profile 8 located on the southern side of Croscat volcano. The upper part of the figure shows the surface SP map overlaid on a Digital Elevation Model. In the lower part, an orthophotograph is overlaid on the same Digital Elevation Model. The corresponding ERT profile is presented in the cross-section (RMS error 11.7%). Coordinates in UTM - 31N - ED50.

Profile 9: Santa Margarida volcano

Profile 9 is located on the south of Santa Margarida volcano (Figure 10). With an RMS error of 11% after six iterations, this profile may be unreliable since it also included a lot of unrealistic data points that we removed during processing with Res2dinv. The distribution of the resistivity is not as clear as in the other resistivity models. Nevertheless, the most interesting feature here is probably the observation of a resistive body at a depth of about 70 m in the east of a resistive body ($>10,000 \Omega \text{ m}$), possibly connected to shallower layers along a narrow pathway (Figure 10, zone A).

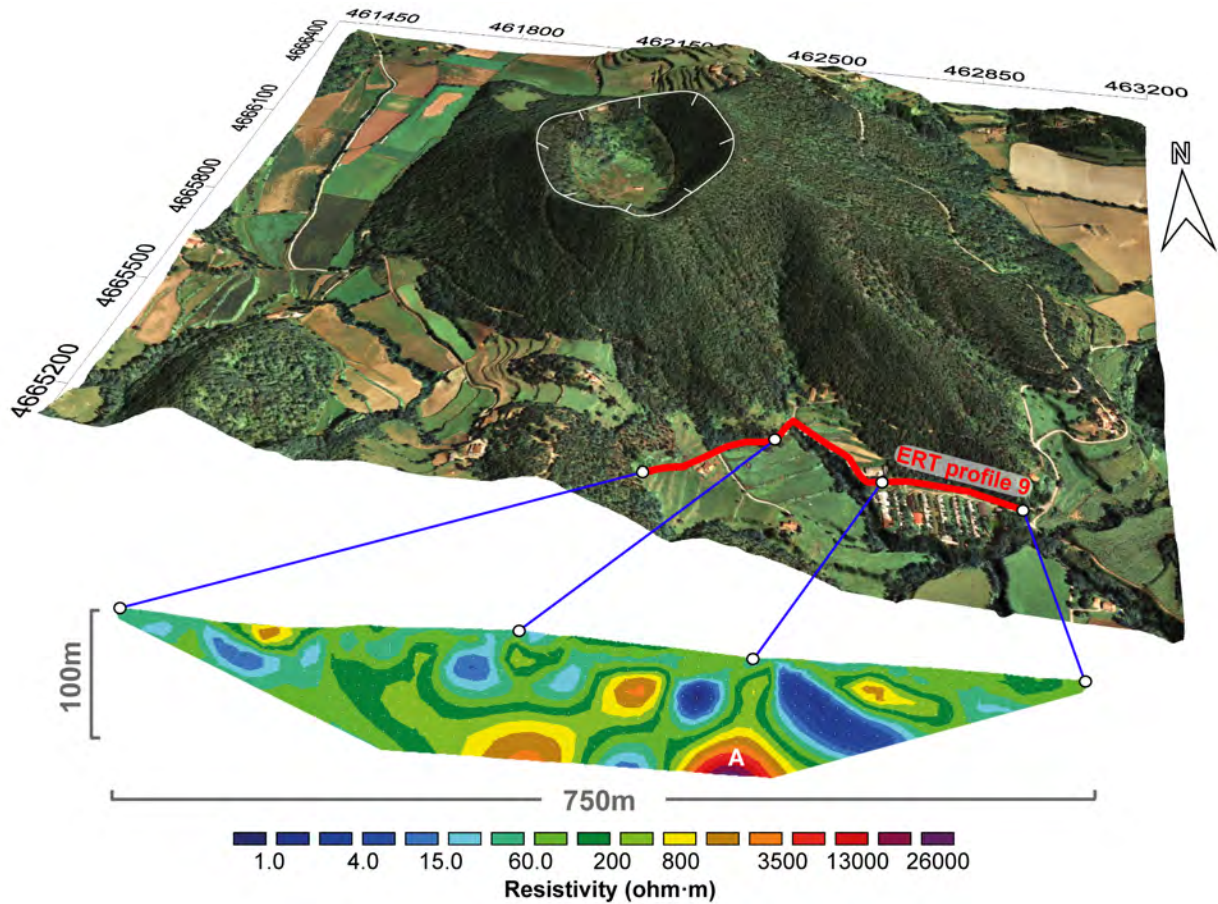


Fig. 10. Top: orthophotograph overlaid on a Digital Elevation Model with the location of ERT profile 9 on the southern side of Santa Margarida volcano (red line). Bottom: ERT model (RMS error 11.0%). Coordinates in UTM - 31N - ED50.

3.6. Discussion

Interpretations of the new SP map enable us to identify structures that were subsequently observed in two dimensions in the high-resolution ERT profiles. Surface geological information was also useful for interpreting the ERT profiles.

As proposed by Barde-Cabusson et al. (2014; Figure 5a), the main observed features are the NNW–SSE and NNE–SSW trends that show up in the SP, suggesting that the volcanic field is structurally confined by this conjugated fault system that favoured magma ascent.

This hypothesis is confirmed by the ERT profiles performed in the directions described above. We identified several very shallow intrusive bodies aligned along the profiles whose cross-sections are geometrically more or less vertical which narrow near the surface, and which are characterized by high resistivity values. This is fully compatible with the presence of feeder dykes. In the northern part of the map, at least two of the three ERT profiles (i.e. profiles 3 and 4) from Pujalós volcano (Figure 6) reveal resistive bodies that continue beyond the maximum depth of exploration. Although the distribution of the resistivity in the third southern profile (profile 5) is less clear, the direction of the line joining the main resistive bodies detected in these profiles matches the NNW–SSE SP trend detected in this volcano. Figure 3 contains a graph of SP vs. distance passing north of Pujalós that shows a clear negative peak corresponding geographically to the location of the resistive body in profile 3 that is not present in the SP profile passing south of this volcano. This peak cannot be explained by the non-linearity of the SP profile in the north and could be a consequence of meteoric water infiltration along a structural limit covered by impermeable material in the south. We believe that profiles 3 and 4 merely reveal the upper part of the feeder dyke as it flares on reaching the topography surface (Valentine 2012; Barde-Cabusson et al. 2013).

The Santa Margarida-Croscat-La Pomareda alignment in the central part of the study area was described by Martí et al. (2011) as the result of a single eruptive episode occurring along a 3-km long fissure system. Our study provides geophysical and geological evidence supporting this idea. La Pomareda ERT (profile 6) was performed across the inferred fissure zone (Figure 7) and generated high resistivity values that can be related to outcropping spatter facies. At depth, the resistive channel connecting the spatter at the surface to the deepest zone can be interpreted as the feeder dyke that supplied the eruption. The resistivity values obtained for this channel ($\sim 3,500 \Omega \text{ m}$) are lower than those obtained for the resistive bodies found along the same fissure near Croscat volcano. It is important to bear in mind, however, that the Pomareda spatter cone forms a smaller edifice than Croscat. These observations suggest that the magma flow rate – and thus the intensity of the eruptive activity – was lower at this point on the fissure. Croscat, built on the same eruptive fissure, is a complex volcano with several vents and several eruptive phases including violent Strombolian and phreatomagmatic episodes (Martí and Mallarach 1987; Martí et al. 2011). The ERT profiles performed north and south of this volcano (Figure 8 and 9, respectively) exhibit resistive bodies that are compatible with the presence of a feeder dyke aligned with the Pomareda volcano in a NNW–SSE direction (Figure 11). At the surface a spatter facies was found in profile 7 and a secondary cone is visible near profile 8. The westernmost resistive body described in profile 7 matches a lava flow that occurred during the final phase of Croscat's eruption (Figure 8). An important feature observable in the eastern part of profile 8 (Figure 9) is a clear shift of $\sim 10 \text{ m}$ at the base of the upper resistive layer, which has been mapped as fallout deposits and a lava flow from Croscat (Cimarelli et al. 2013). These volcanic deposits probably cover a pre-existing normal fault that affects the underlying Eocene units and is revealed only by a small break-in-slope visible in the surface topography. In the eastern block the underlying unit is clearly more conductive than in the western block due to the presence of an aquifer confined to the west by the fault plane (Figs. 9 and 11). This fault is likely a conjugate of a Neogene fault mapped 200 m to the southeast (IGC; 1:25 000, www.igc.cat) or a prolongation of the same. Its presence has important implications for understanding eruptive dynamics in monogenetic volcanic fields since it may explain why

hydromagmatic and Strombolian activity can take place simultaneously or within short time spans, in close proximity to each other or even in the same edifice (e.g. Martí et al. 2011; Pedrazzi et al. 2014). Thus, tectonic limits may play an important role in defining the diversity of monogenetic volcanoes owing to their impact on hydrogeology at shallow depths. In the eastern part of profile 9 (Figure 10) in the south of this area, a resistive body ($>10,000 \Omega \text{ m}$) is present at a depth of 70 metres. This body is aligned with Santa Margarida-Croscat-La Pomareda fissure system, therefore it correspond presumably to a magmatic intrusion, which did not reach the surface in this profile.

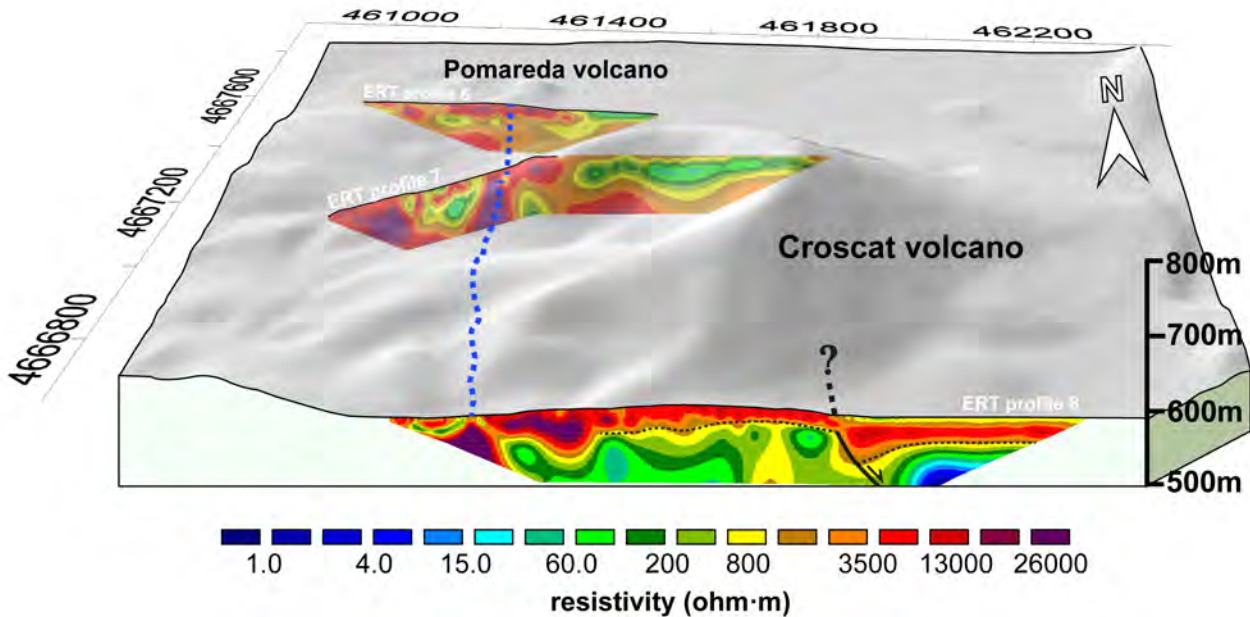


Fig. 11. 3D block diagram of Croscat and Pomareda volcanoes showing ERT profiles 6, 7 and 8. The blue dashed line highlights a NNW–SSE eruptive fissure.

The area of Olot ERT profile 1 (Figure 4) performed on the Montsacopa volcano has already been described by Barde-Cabusson (2013). The present study confirms that in addition to the obvious crater on its summit, there is a hidden vent located on the southeastern flank of this volcano, as suggested by Bolós (2009). These two coalescent cones are aligned in a NNW–SSE direction. Montsacopa and the two other volcanic edifices within the city of Olot (Garrinada and Montolivet) all have several vents that define three separate NNW–SSE lines which reflect the direction of their corresponding eruptive fissures (Martí et al. 2011). This finding contrasts with previous studies that assumed that the eruptions of Montsacopa, Garrinada and Montolivet were located along a single NE–SW fissure (Calderón et al. 1906; San Miguel de la Cámara 1918; Mallarach and Riera 1981; Gisbert et al. 2009).

ERT profile 2 crosses the southern flank of Montolivet and the outcropping Eocene basement (Bellmunt Formation) that is characterized by conglomerates, sandstones and clays. The Bellmunt Formation appears in the profiles as shades of green ($\sim 20\text{--}500 \Omega \text{ m}$) only on the western side and at depth (Figure 5). The transition towards the high resistivity values of the Montolivet volcanic deposits defines the pre-eruptive topography. The highest resistivity values have no continuity at depth, which suggests that this area is characterized only by proximal facies deposits and that this profile (profile 2) did not cross the feeder dyke

(Figure 5). Nevertheless, the horseshoe-shaped depression of Montolivet's crater indicates that the feeder fracture runs in a NNW–SSE direction (i.e. fault-strike breaching, Tibaldi 1995), as seen in other areas (Corazzato and Tibaldi 2006). Differently, Crosca's crater is open to the west, even though all the data obtained show that it is associated with a NNW–SSE fault. Crater breaching might coincide with fracture propagation (e.g. Montolivet volcano) or with the weakest zone of the cone (e.g. Crosca volcano) (see Tibaldi 1995). The NNW–SSE direction determined for the nearby Montsacopa and Garrinada volcanoes tends to support this interpretation of Montolivet. A hypothesis that explains why the feeder dyke is not visible in the ERT profile is that the edifice of Montolivet was in fact built at the southeastern tip of the fissure.

Two main fault systems were identified in the study area: an E–W compressive fault system formed during the Alpine Orogeny and a NNW–SSE normal fault system formed during the current extensive context (Martinez et al. 1997). The data obtained suggest that volcanism in the area is controlled by the recent extensive fault system and that the Alpine system played no role in controlling magma ascent and/or eruptions. These NNW–SSE normal faults are almost perpendicular to the limits of the E–W depression formed by the Garrotxa anticline.

The Pujalós and the Fontpobra volcanoes provide key information on the faults associated with the GVF volcanism. Both are located outside the depression of La Garrotxa, very close to the northern and southern limits of the anticline, respectively. However, ERT (in the case of Pujalós) and self-potential (Pujalós and Fontpobra) suggest the presence of NNW–SSE eruptive fissures, which would indicate that the tectonic limits associated with the Alpine Orogeny did not determine the volcanic intrusions in the GVF.

3.7. Conclusions

New geophysical data were combined with field geological information to explore the subsurface geology and structure of the monogenetic Garrotxa Volcanic Field. We identified feeder dykes and structural limits associated with known eruptive vents. The information derived for the subsurface provides data that is useful for interpreting the influence of shallow geological and structural settings on the eruptive dynamics of this monogenetic volcanic field and has interesting implications for similar volcanic zones.

The NNW–SSE direction highlighted by previous SP and gravimetric studies was targeted by the ERT. The 2D images obtained with this method reveal the existence of high resistivity bodies corresponding to NNW–SSE-running feeder dykes that confirm the role played by NNW–SSE tectonic structures in the volcanic manifestations in the area. In addition, the same direction is observed for the Pujalós and Fontpobra eruptive fissures, although both volcanoes are located in the vicinity of the limits of the anticline, respectively, in the northern and southern part of the study area. This suggests that Alpine tectonic structures such as the anticline and the associated regional faults were not implicated in the formation of these two volcanoes. This conclusion can be extended to the whole area given the distribution of the dykes that have been identified and available geological and geophysical data.

In ERT profile 8, we identified a normal fault confining an aquifer to the west. This configuration could have a number of different consequences on eruptive dynamics depending on the path followed by future intrusions. Both phreatomagmatic and Strombolian activity could take place simultaneously or within a short time span, in close proximity or even in the same volcanic edifice, depending on whether or not the intrusion interacts with the aquifer. The existence of such a configuration could explain the variety of eruptive dynamics in the monogenetic Garrotxa Volcanic Field and in other volcanic fields of similar characteristics without any need for change in the composition of the magma.

The results of this paper will help assess the volcanic susceptibility of the area and increase understanding of the influence of local geology on the distribution and dynamics of the eruptive activity in this area and in monogenetic fields in general.

Acknowledgements:

This study was partially funded by the *Beca Ciutat d'Olot en Ciències Naturals* and the European Commission (FT7 Theme: ENV.2011.1.3.3-1; Grant 282759: "VUELCO"). S. Barde-Cabusson was funded by JAE-Doc Program (JAEDoc_09_01319). We are grateful to La Garrotxa Volcanic Zone Natural Park and its staff for their support throughout this study. We would like to thank Llorenç Planagumà for his logistical help during this research. Thanks are also due to Núria Bagués, David Granados, Guillem Serra and Joan Puigferrer for their assistance in the field. We are also grateful to Editors Prof. Wolf-Christian Dullo and Christoph Breitzkreuz, and two anonymous reviewers for their constructive reviews of this manuscript. The English text was corrected by Michael Lockwood.

References:

- Araña V, Aparicio A, Martín-Escorza C, García Cacho L, Ortiz R, Vaquer R, Barberi F, Ferrara G, Albert J, and Gassiot X (1983) El volcanismo Neógeno-Cuaternario de Catalunya: caracteres estructurales, petrológicos y geodinámicos. *Acta Geologica Hispánica* 18, 1–17.
- Barde-Cabusson S, Bolós X, Pedrazzi D, Lovera R, Serra G, Martí J, Casas A (2013) Electrical resistivity tomography revealing the internal structure of monogenetic volcanoes. *Geophys Res Lett* 40, 2544-2549. doi:10.1002/grl.50538
- Barde-Cabusson S, Gottsmann J, Martí J, Bolós X, Camacho A, Geyer A, Planagumà LI, Ronchin E, Sánchez A (2014) Some insights on the structural control of monogenetic volcanism from gravity and self-potential measurements. *Bull Volcanol* 76:788. doi: 10.1007/s00445-013-0788-0
- Bibby HM, Caldwell TG, Risk GF (1998) Electrical resistivity image of the upper crust within the Taupo Volcanic Zone, New Zealand. *Journal Geophysical Research*, 103, 9665-9680.
- Bolós X (2009) Characterization of the Montsacopa volcano and its surroundings (in English, Spanish, and Catalan). Web access <http://bit.ly/ZqkAaY>, Garrotxa Volcanic Natural Parc, Olot, Spain.

- Bolós X, Barde-Cabusson S, Pedrazzi D, Martí J, Casas A, Himi M, Lovera R (2012) Investigation of the inner structure of La Crosa de Sant Dalmai maar (Catalan Volcanic Zone, Spain). *J Volcanol Geoth Res* 247–248, 37–48, doi: 10.1016/j.jvolgeores.2012.08.003.
- Calderón S, Cazorro M, Fernández Navarro L (1906) Memoria sobre las formaciones volcánicas de la provincia de Gerona. *Memorias de Real Sociedad Española de Historia Natural*, t. IV, memoria 5ª, Madrid, pp. 165–489.
- Catalan Geographic Institute (ICC). Digital Elevation Model 15x15 m. <http://www.icc.cat/>. Accessed 3 December 2013.
- Catalan Geologic Institute (IGC). Carta Volcanològica de la Zona Volcànica de la Garrotxa, 1:25 000. <http://www.igc.cat/>. Accessed 3 December 2013.
- Cebrià JM, López-Ruiz J, Doblás M, Oyarzun R, Hertogen J, Benito R (2000) Geochemistry of the Quaternary alkali basalts of Garrotxa (NE Volcanic Province, Spain): a case of double enrichment of the mantle lithosphere. *J Volcanol Geoth Res* 112, 175–187.
- Cebrià JM, Martín-Escorza C, López-Ruiz J, Morán-Zenteno DJ, Martiny BM (2011) Numerical recognition of alignments in monogenetic volcanic areas: Examples from the Michoacán-Guanajuato Volcanic Field in Mexico and Calatrava in Spain, *J Volcanol Geoth Res* 201, 73–82.
- Cimarelli C, Di Tragia F, de Rita D, Gimeno Torrente D, Fernandez Turiel JL (2013) Space–time evolution of monogenetic volcanism in the mafic Garrotxa Volcanic Field (NE Iberian Peninsula). *Bull Volcanol* 75:758, doi: 10.1007/s00445-013-0758-6
- Connor CB, Conway FM (2000) Basaltic volcanic fields. In: Sigurdsson, H. (Ed.), *Encyclopedia of Volcanoes*. Academic Press, San Francisco (CA), pp. 331–343.
- Corazzato C, Tibaldi A (2006) Fracture control on type, morphology and distribution of parasitic volcanic cones: an example from Mt. Etna Italy. *J Volcanol Geoth Res* 158, 177–194.
- Dèzes P, Schmid SM, and Ziegler PA (2004) Evolution of the European Cenozoic Rift System: interaction of the Alpine and Pyrenean orogens with their foreland lithosphere. *Tectonophysics* 389, 1–33.
- Di Maio R, Mauriello P, Patella D, Petrillo Z, Piscitelli S, Siniscalchi A (1998) Electric and electromagnetic outline of the Mount Somma-Vesuvius structural setting. *Journal of Volcanology and Geothermal Research* 82, 219–238.
- Di Maio R, Patella D, Petrillo Z, Siniscalchi A, Cecere G, De Martino P, (2000) Application of electric and electromagnetic methods to the definition of the Campi Flegrei caldera (Italy). *Annali di Geofisica* 43, 375–390. Catalan Geographic Institute. Digital Elevation model, Garrotxa area. <http://www.icc.cat/>. Accessed 10 October 2013
- Downes H (2001) Formation and modification of the shallow sub-continental lithospheric mantle: a review of geochemical evidence from ultramafic xenolith suites and tectonically emplaced ultramafic massifs of Western and Central Europe. *Journal of Petrology* 42, 233–250.
- Francis PW (1993) *Volcanoes: a planetary perspective*. Clarendon Press, Oxford. 443pp.
- Gisbert G, Gimeno D, Fernandez-Turiel JL (2009) Eruptive mechanisms of the Puig de La Garrinada volcano (Olot, Garrotxa volcanic field, Northeastern Spain): a methodological study based on proximal pyroclastic deposits. *J Volcanol Geoth Res* 180, 259–276.
- Griffiths DH, Barker RD (1993) Two-dimensional resistivity imaging and modelling in areas of complex geology. *Journal of Applied Geophysics* 29, 211–226.

- Gudmundsson A (2006) How local stresses control magma-chamber ruptures, dyke injections, and eruptions in composite volcanoes. *Earth Sci. Rev* 79, 1–31.
- Guérin G, Behamoun G, Mallarach JM (1985) Un exemple de fusió parcial en medi continental. El vulcanisme quaternari de la Garrotxa. Publicació del Museu Comarcal de la Garrotxa, Vitrina, pp. 19–26.
- Hase H, Hashimoto T, Sakanaka S, Kanda W, Tanaka Y (2005) Hydrothermal system beneath Aso volcano as inferred from self-potential mapping and resistivity structure. *Journal of Volcanology and Geothermal Research* 143, 259–277.
- Houghton BF, Wilson CJN, Smith IEM (1999) Shallow-seated controls on styles of explosive basaltic volcanism: a case study from New Zealand. *J Volcanol Geoth Res* 91, 97–120.
- Le Corvec N, Menand T, Lindsay J (2013) Interaction of ascending magma with pre-existing crustal fractures in monogenetic basaltic volcanism: an experimental approach. *J Geophys Res Solid Earth* 118, 968–984, doi: 10.1002/jgrb.50142
- Loke MH, Barker RD (1996) Rapid least-squares inversion of apparent resistivity pseudosections by a quasi-Newton method *Geophysical Prospecting* 44, 131–52
- Loke MH (2002) Res2dinv ver. 3.54. Rapid 2-D resistivity and IP inversion using the least square method. Geotomo Software.
- López-Ruiz J, Rodríguez-Badiola E (1985) La región volcánica Mio-Pleistocena del NE de España. *Estudios Geológicos* 41, 105–126.
- Mallarach JM, Riera M (1981) Els volcans olotins i el seu paisatge. Editorial Serpa, Barcelona. 250 pp.
- Martí J, Mallarach JM (1987) Erupciones hidromagmáticas en el volcanismo cuaternario de Olot. *Estudios Geológicos* 43, 31–40.
- Martí J, Mitjavila J, Roca E, Aparicio A (1992) Cenozoic magmatism of the Valencia trough (Western Mediterranean): relation between structural evolution and Volcanism. *Tectonophysics* 203, 145–166.
- Martí J, Felpeto A (2010), Methodology for the computation of volcanic susceptibility: An example mafic and felsic eruptions on Tenerife (Canary Islands). *J Volcanol Geoth Res* 195, 69–7.
- Martí J, Planagumà LI, Geyer A, Canal E, Pedrazzi D (2011) Complex interaction between Strombolian and phreatomagmatic eruptions in the Quaternary monogenetic volcanism of the Catalan Volcanic Zone (NE of Spain). *J Volcanol Geoth Res* 201 (1–4), 178–193.
- Martí J, Pinel V, López C, Geyer A, Abella R, Tárraga M, Blanco MJ, Castro A, Rodríguez C (2013) Causes and mechanisms of the 2011–2012 El Hierro (Canary Islands) submarine eruption. *J Geophys Res Solid Earth* 118, 823–839, doi: 10.1002/jgrb.50087
- Martinez A, Rivero L, Casas A (1997) Integrated gravity and seismic interpretation of duplex structures and imbricate thrust systems in the southeastern Pyrenees (NE Spain). *Tectonophysics* 282: 303–329
- Martorana R, Fiandaca G, Casas A, Cosentino PL (2009) Comparative tests on different multi-electrode arrays using models in near-surface geophysics. *Journal of Geophysics and Engineering* 6, 1–20.
- Neumann ER, Martí J, Mitjavila J, Wulff-Pedersen E (1999) Origin and implications of mafic xenoliths associated with Cenozoic extension-related volcanism in the València Trough, NE Spain. *Mineralogy and Petrology* 65, 113–139.

- Nishi Y, Ishido T, Matsushima N, Ogawa Y, Tosha T, Myazaki J, Yasuda A, Scott BJ, Sherburn S, Bromley C (1996) Self-Potential and audio-magnetotelluric survey in White Island Volcano. New Zealand Geothermal Workshop.
- Parfitt EA (2004) A discussion on the mechanisms of explosive basaltic eruptions. *J Volcanol Geoth Res* 134, 77–107.
- Pedrazzi D, Bolós X, Martí J (2014) Phreatomagmatic volcanism in complex hydrogeological environments: La Crosa de Sant Dalmai maar (Catalan Volcanic Zone, NE Spain). *Geosphere*. doi: 10.1130/GES00959.1
- Portal A, Labazuy P, Lénat JF, Béné S, Boivin P, Busato E, Cârloganu C, Combaret C, Dupieux P, Fehr F, Gay P, Laktineh I, Miallier D, Mirabito L, Niess V, Vulpescu B (2013) Inner structure of the Puy de Dôme volcano: cross-comparison of geophysical models (ERT, gravimetry, muon imaging). *Geosci. Instrum. Method. Data Syst.* 2, 47–54.
- Revil A (2002) Comment on “Rapid fluid disruption: a source for self-potential anomalies on volcanoes” by M. J. S. Johnston, J. D. Byerlee, and D. Lockner. *Journal of Geophysical Research* 107 (B8). doi:10.1029/2001JB000788.
- San Miguel de la Cámara M (1918) El volcanismo en España. *Boletín de la Real Academia de Ciencias y Artes de Barcelona* 244–254.
- Saula E, Picart J, Mató E, Llenas M, Losantos M, Berasategui X, Agustí J (1995), Evolución geodinámica de la fosa del Empordà y de las Sierras Transversales. *Acta Geologica Hispánica* 29, 55–75.
- Tibaldi, A., 1995. Morphology of pyroclastic cones and tectonics. *Journal of Geophysical Research* 100.
- Valentine GA, Gregg TKP (2008) Continental basaltic volcanism—process and problems. *J Volcanol Geoth Res* 177, 857–873.
- Valentine GA (2012) Shallow plumbing systems for small-volume basaltic volcanoes, 2: Evidence from crustal xenoliths at scoria cones and maars. *J Volcanol Geoth Res* 223–224, 47–63. doi: 10.1016/j.jvolgeores.2012.01.012
- Vespermann D, Schmincke HU (2000) Scoria cones and tuff rings. In: Sigurdsson, H.(Ed.), *Encyclopedia of Volcanoes*. Academic Press, San Diego, pp. 683–694.
- Walker GPL (2000) Basaltic volcanoes and volcanic systems. In: Sigurdsson, H. (Ed.), *Encyclopedia of Volcanoes*. Academic Press, San Francisco (CA), pp. 283–289.
- Wilson M, Downes H (1991) Tertiary–Quaternary extension-related alkaline magmatism in Western and Central Europe. *Journal of Petrology* 32, 811–849.
- Wilson M, Downes H (1992) Mafic alkaline magmatism associated with the European Cenozoic rift system. *Tectonophysics* 208, 173–182.
- Zhang D, Lutz T (1989) Structural control of igneous complexes and kimberlites: a new statistical method. *Tectonophysics* 159, 137–148.

4

Investigation of the inner structure of La Crosa de Sant Dalmai maar (Catalan Volcanic Zone, Spain)

Published in:

Journal of Volcanology and Geothermal Research

Authors of the paper:

Xavier Bolós ^(a)

Stéphanie Barde-Cabusson ^(a)

Dario Pedrazzi ^(a)

Joan Martí ^(a)

Albert Casas ^(b)

Mahjoub Himi ^(b)

Raúl Lovera ^(b)

a) Institute of Earth Sciences Jaume Almera, ICTJA-CSIC, Group of Volcanology. SIMGEO (UB-CSIC) Lluís Sole i Sabaris s/n, 08028 Barcelona, Spain

b) Economic and Environmental Geology and Hydrology Group. Department of Geochemistry, Petrology and Geophysical Prospecting. Faculty of Geology, University of Barcelona. Martí Franqués s/n, 08028 Barcelona,) Spain

4.1. Abstract

La Crosa de Sant Dalmai volcano is the largest volcanic edifice of the Catalan Volcanic Zone (NE Spain). It is a very well preserved maar-type structure, 1.5 km in diameter, excavated at the contact between a hard substrate and a soft substrate formed by Palaeozoic granites and Pliocene and Quaternary gravels, respectively. In order to infer the uppermost inner structure of La Crosa de Sant Dalmai maar and to characterise its main geological and tectonic constraints, we have performed a multiparametric geophysical study including gravimetry, magnetometry, self-potential, and electrical resistivity tomography. The results obtained together with a field geology revision and additional geological data from two drill cores, provide a detailed picture of the post-eruptive maar infill sequence as well as of the uppermost part of the maar-diatreme structure. This information helps in understanding the origin and subsequent evolution of the volcano, which included an alternation of phreatomagmatic and Strombolian phases. Geophysical data show that the last Strombolian phase, which culminated with the formation of a scoria cone inside the maar, was associated with a NW–SE trending regional fault. The little erosion and degradation of the original tephra ring suggest a much younger age of La Crosa de Sant Dalmai maar than was previously stated.

Keywords: Catalan Volcanic Zone · Maar-diatreme · Geoelectrical methods · Gravity survey · Magnetic survey · Drill core

4.2. Introduction

Phreatomagmatic explosions result from brief, near-surface magma/water interactions occurring during the ascent of magma towards the surface, which leads to violent explosions (Lorenz, 1973; Sheridan and Wohletz, 1981, 1983; Wohletz, 1983). Unlike magmatic eruptions that are entirely controlled by the composition and physical properties of the magma (i.e. volatile content, viscosity), phreatomagmatic eruptions may vary considerably depending on external factors such as the stratigraphic, structural and hydrogeological characteristics of the substrate through which the volcanoes are emplaced. Phreatomagmatism is common in all subaerial volcanic settings as continental rifts, active continental volcanic island arc, foreland basins, late orogenic intermontane basins of orogenic belts, basin and range, cratons, and hot spots (Lorenz, 2007). In monogenetic volcanic fields, as well as in polygenetic volcanoes, a large variety of volcanic morphologies and eruption sequences can be observed associated with this type of volcanism (Wohletz and Sheridan, 1983).

A maar is a type of phreatomagmatic volcanic structure characterised by the formation of a tephra ring due to the accumulation of pyroclastic deposits around a circular crater, whose floor lies below the pre-eruption ground surface (Lorenz, 1973, 2007; Lorenz and Kurszlaukis, 2007; White and Ross, 2011). The presence of meteoric water and/or groundwater, after the eruption's end, might lead to the development of a lake inside the

crater (Schmincke, 1988; Büchel, 1993). Due to the surface geomorphology and the internal structure, these volcanoes are called maar-diatremes. The term used is descriptive and not genetic, so it does not refer to any specific place or suite of processes (Lorenz, 1975, 1986). The maar-diatreme volcanoes, although representing examples of monogenetic activity, represent a significant degree of hazard, as has been shown by past eruptions with a number of human casualties in the historical record around the world (White and Ross, 2011).

The reconstruction of the internal structure of individual young maar-diatreme systems can only be based on geophysical studies and drill cores and other type of mechanical excavations. In deeply eroded systems it is possible to observe the deepest parts of the diatreme but the uppermost sections have been lost in most cases. Therefore, to get an idealised picture of the maar-diatreme system it is necessary to combine both approaches.

This study is aimed at obtaining a 3D geological model of the internal structure of the topmost part of La Crosa de Sant Dalmai maar, in the Catalan Volcanic Zone (NE Spain), in order to determine the structure of the substrate below the tephra ring and the post-eruptive infill sequence of the maar crater and the uppermost level inside the diatreme. In order to accomplish this objective we applied several geophysical techniques, including gravity, magnetic, self-potential and electrical resistivity tomography methods. These methods combined with field geology and the study of samples from two drill cores located inside the maar-crater, provided the necessary information to image the shallow internal structure of the La Crosa de Sant Dalmai maar-diatreme volcano.

4.3. Geological setting and general characteristics of La Crosa de Sant Dalmai

The Catalan Volcanic Zone (CVZ), situated in the NE part of the Iberian Peninsula (Girona Province), is one of the Quaternary alkaline volcanic provinces belonging to the European Cenozoic Rift System (Martí et al., 1992; Dèzes et al., 2004) (Fig. 1). The CVZ ranges in age from >12 Ma to early Holocene and it is mainly represented by alkali basalts and basanites (Martí et al., 1992; Cebrià et al., 2000).

This basaltic monogenetic volcanic zone comprises more than 50 well preserved monogenetic cones including scoria cones, tuff cones, tephra rings, and maars. The area has traditionally been divided into three different sub-zones: L'Empordà to the Northeast (12–8 Ma), La Selva (7.9–1.7 Ma) to the South and La Garrotxa (0.5–0.01 Ma) to the West (Araña et al., 1983; Martí et al., 1992) (Fig. 1). In the CVZ volcanism, small-sized cinder cones formed along widely dispersed fissure zones during monogenetic, short-lived eruptions. Hydromagmatic events were also common. Each eruption was probably caused by an individual batch of magma that was transported rapidly from the source region, each batch representing the products of an individual partial melting event (Martí et al., 1992, 2011).

La Crosa de Sant Dalmai maar belongs to the La Selva subzone, which corresponds to a tectonic depression bounded by an ENE–WSW and a NW–SE fault system (Fig. 1). The basement of this area consists of granites and metamorphic rocks of Palaeozoic age, which crop out defining a nonconformity with the Pliocene and Quaternary sediments. These last

filled the La Selva depression with variable thicknesses of 35 to 200 m in the Sant Dalmai area (Trilla and Pallí, 1977; Barnolas et al., 1979). The volcanic deposits cover an area of about 7 km² among the municipalities of Aiguaviva and Sant Dalmai, 2 km northwest of the Girona airport, overlying basement and Pliocene and Quaternary rocks (Fig. 2).

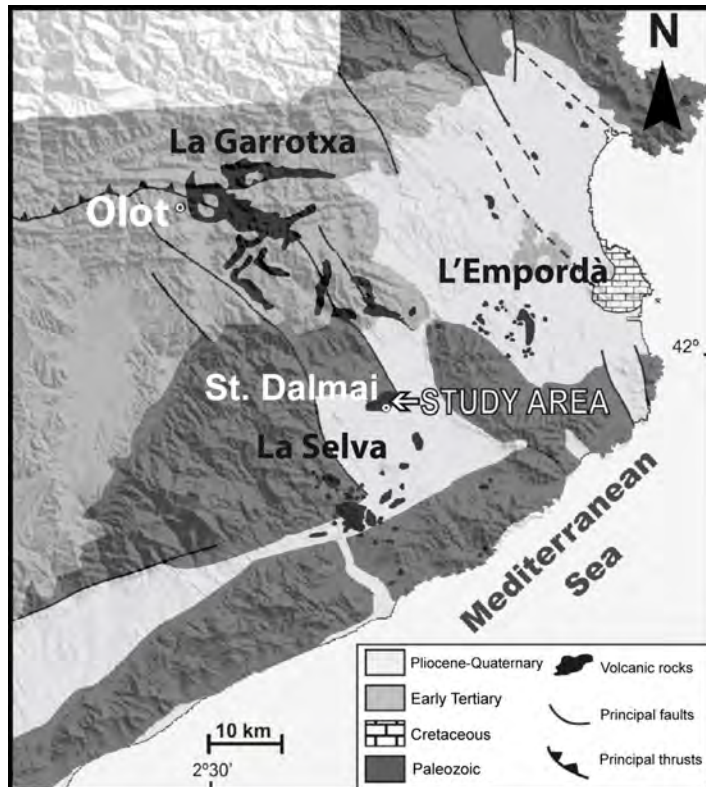


Fig. 1. Simplified geological map of the Catalan Volcanic Zone and its surroundings. Location of La Garrotxa, La Selva and L'Empordà volcanic fields. (Modified from Guérin et al., 1986).

The ejecta of this maar volcano are mostly composed of phreatomagmatic deposits that form a circular tephra ring around a shallow crater 1250 m in diameter and a few tens of metres in depth. The tephra ring is asymmetrical, being higher in the west (maximum height of 50 m), where the internal and external slopes are also steeper, than in the east (maximum height of 30 m). Also, the deposits surrounding the rim show a wider distribution towards the east (Fig. 2). The succession of deposits shows the same stratigraphy all around the tephra ring but not in equal proportions. They reached distances of nearly 4 km towards the east and only of a few hundred metres towards the west. This asymmetrical distribution of the deposits was attributed to different strength of the rocks that form the substrate at each side below the volcano (Martí et al., 1986). The initial topography, the direction of the wind during the eruption, and the possible inclination of the eruptive conduit could also have influenced the distribution of the deposits around the vent (e.g. Büchel and Lorenz, 1993).

The lowermost unit of the succession of deposits of La Crosa de Sant Dalmai volcano is not fully exposed and corresponds to >1 m thick coarse lithic-rich breccia with blocks up to 70 cm in diameter. The lithics consist of granites and schists with subordinate scoria lapilli and cauliflower bombs (Pedrazzi, et al., 2012). Above them lies a 10 m thick uniform sequence of lithic-rich deposits alternating with crudely stratified, coarse-grained pyroclastic surge deposits. The next unit in the stratigraphic succession is a 1 m thick Strombolian, non-welded scoria lapilli deposit, which is followed by 8 m thick sequence of alternating units of lithic-rich breccia and pyroclastic surges. The eruption ended with a new Strombolian episode

from a new vent opened at the interior of the maar. This episode formed a small scoria cone partially overlapping the maar tephra ring and a lava flow emplaced inside the maar (see below). As most maar-diatreme volcanoes are related to basic magmas, most final magmatic phases inside maar craters lead to the formation of scoria cones or even lava lakes in a final magmatic phase (Lorenz, 2007).

The age of this volcano is not well constrained. Although it is located in the La Selva sector where most of the outcropping volcanic rocks have ages older than 1.7 Ma (Araña et al., 1983), it is evident from the state of preservation of its morphology and juvenile components that La Crosa de Sant Dalmai volcano might be younger.

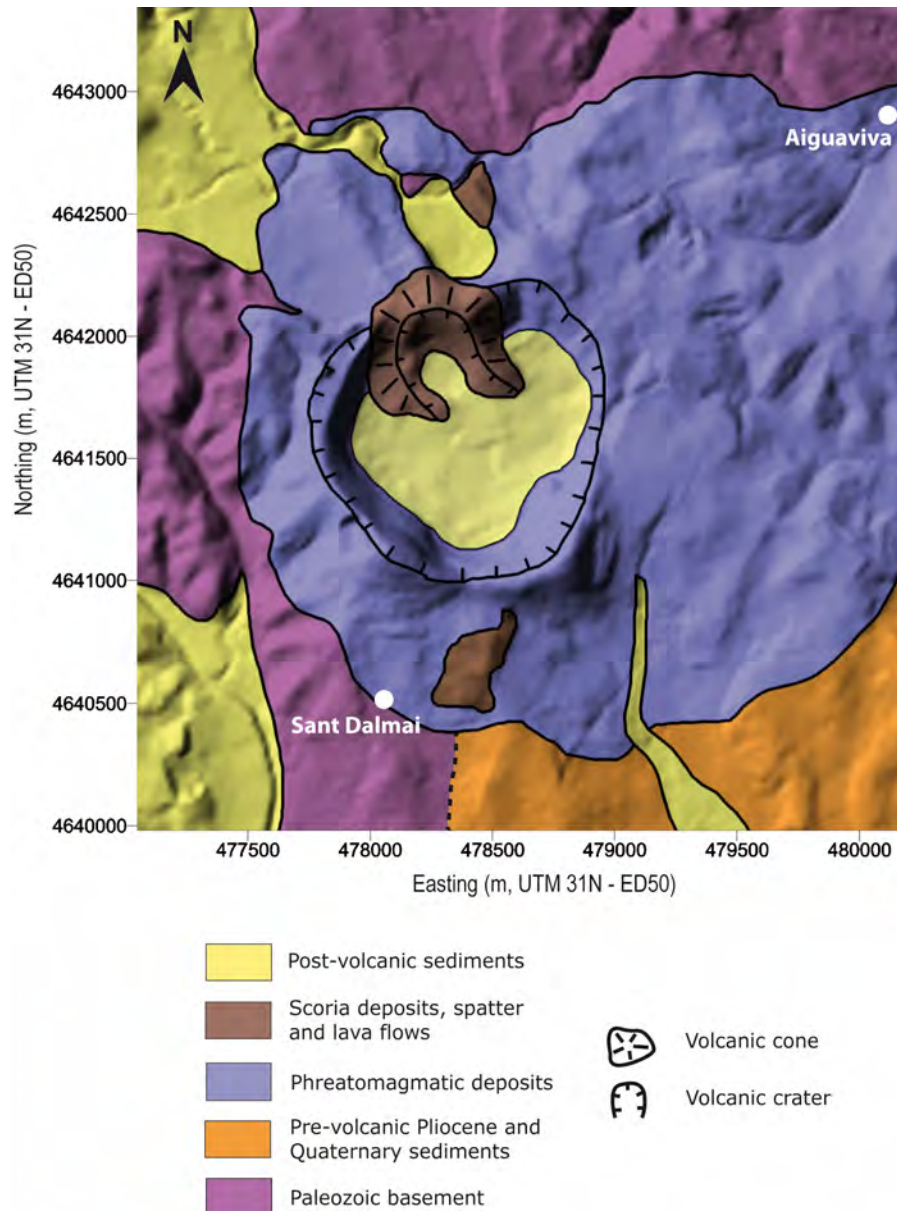


Fig. 2. Geological map of la Crosa de Sant Dalmai volcano. Coordinates in metres (UTM31N — ED50). Topographic base is taken from the ICC, at 1:5000 scale. The mapping of the deposits has been developed from the simplified map of Martí and Mallarach (1987) and analysis from new outcrops in the field. The figure shows the main crater and the scoria cone the latter formed during the final stages of activity of the volcano, along with the extent of the phreatomagmatic deposits.

4.4. Methodology

The methodology used to carry out this work comprises multidisciplinary tasks. A preliminary geological map of the area at 1:5000 scale was produced starting from the one elaborated by Martí, et al. (1986) and conducting new field work (Fig. 2). This allowed us to understand field relationships among the different geological units, to determine the extent of the deposits, and to identify the most significant geomorphological features. All the geological information collected was incorporated into a georeferenced database and processed through a Geographical Information System managed by ©Global Mapper 12.00 and Arcgis 9.2 (© ESRI) software. The projection system of coordinates used was the ED50 DATUM, UTM 31 N.

Additional geological data came from two drill cores (S1 and S2, Fig. 3). S1, reaching a depth of 15 m, was made in December 2009 at the western side of La Crosa de Sant Dalmai maar crater. S2, with a total depth of 61 m, was made in April 2012 at the north-eastern side of the maar crater (Fig. 3) The data collected from these cores were helpful in studying the post-eruptive sedimentary fill of the crater and correlating these deposits with the resistivity profiles obtained through the electrical resistivity tomography (ERT) (Fig. 3).

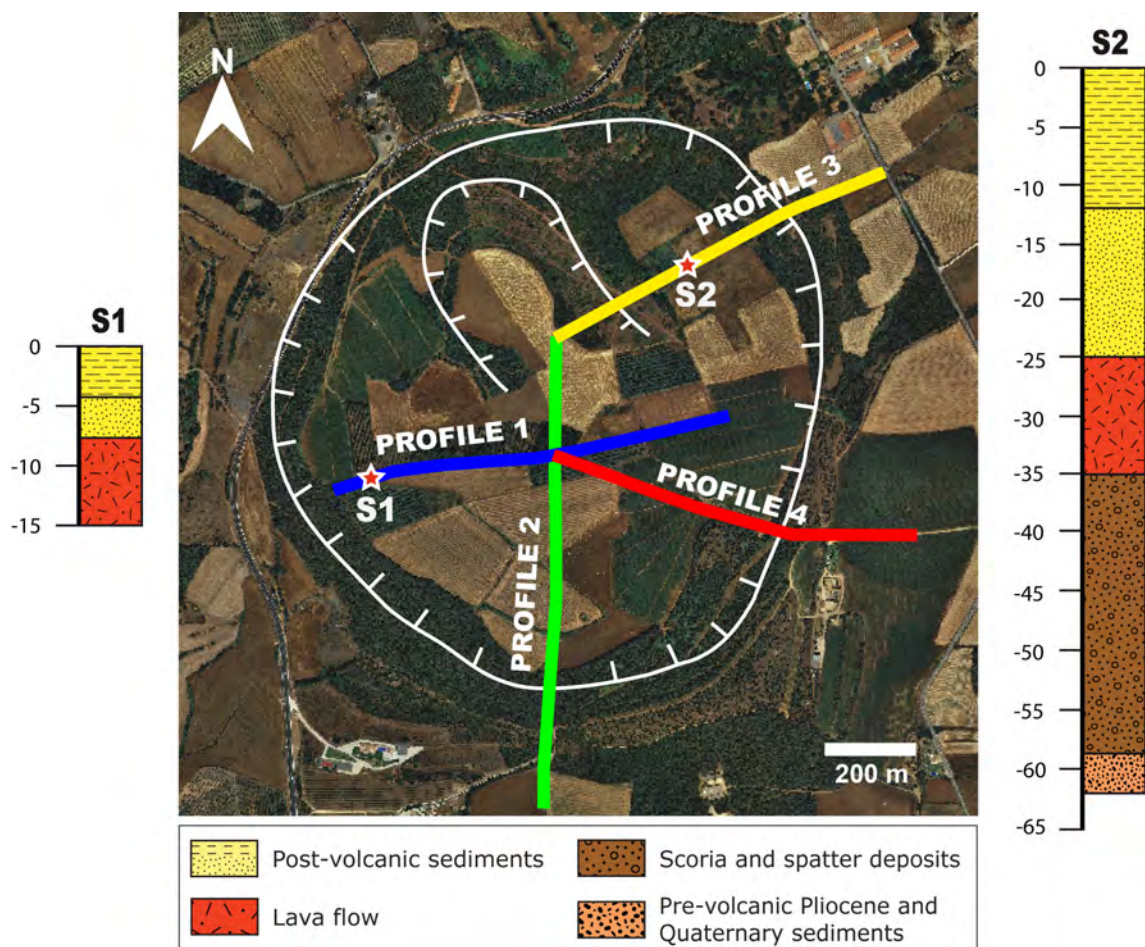


Fig. 3. Orthophotomap from the Institut Cartogràfic de Catalunya (ICC) web site, showing the location of each ERT profile. It also shows the location of the two drill cores (S1 and S2) and their respective synthetic stratigraphic sections.

Subsequently, various geophysical techniques, including gravity, magnetics, self-potential and electrical resistivity tomography, were applied. Some unpublished data from several geophysical surveys carried out in 1995 by some of the authors of this publication already existed. We incorporated these data into this study and in some cases they were recollected and reprocessed.

The gravity survey covered a total area of 8 km² inside and around La Crosa de Sant Dalmai maar, and included a total of 158 stations. Gravity readings were taken with a Lacoste and Romberg G831 gravimeter and referred to the IGSN-71 international gravity system. Station altitude was measured with an Air HB-1A high precision quartz altimeter or derived from ± 0.1 m benchmarks. The gravity data were corrected for effects caused by variations in latitude, elevation, topography, instrumental drift and earth tides caused by the sun and moon. The corrected values generated Bouguer anomalies, which represent the gravity effect of crustal and shallower geological structures. In order to get the residual anomaly, due to the local density changes, it was necessary to subtract the regional component that in this area shows a well defined west–east trend with values ranging from -0.2 to -4.4 mGal that mostly express the depth of the Moho discontinuity (Casas et al., 1986).

Total field magnetic measurements were performed in 1995 with a proton magnetometer Geometrics model G-816. In this study we used the 226 original stations without adding new measurements. The correction for diurnal variation was previously performed on the data set and as with the gravity data, a regional field was defined from stations distant from the volcano and subtracted to give the residual anomaly. After this step, the magnetic data were interpolated to a regular grid. The residual values are around the zero level far away from the volcano indicating a successful removal of the regional field.

The self-potential (SP) measurements were made with a high impedance voltmeter (~ 10 M Ω) with a sensitivity of 0.1 mV, using two non-polarised Cu/CuSO₄ electrodes and a 300 m long cable. The difference of potential was measured between the reference electrode, which was placed at the beginning of the profile and the moving electrode. The measurements were performed every 20 m with several profiles forming an interconnected network covering the entire surface of the crater of La Crosa de Sant Dalmai. During the measurements, the reference and moving electrodes were switched every few hundred metres in order to avoid the systematic error due to electrode offset. In the data-processing we applied a closure correction along the profiles, in order to limit cumulative errors.

The electrical resistivity tomography (ERT) is a technique in which the process of data acquisition is fully automated. This allows performing a great number of measurements, obtaining 2D resistivity high-resolution data in a short time. The electrical resistivity data were acquired with an Iris Syscal Pro resistivity system. The electrode configuration was the Wenner-Schlumberger array using 48 electrodes connected to a 470 m long cable (10 m spacing between electrodes), obtaining a maximum depth of investigation of about 100 m. The main reason for choosing a Wenner-Schlumberger electrode array was the good relationship between signal intensity and good horizontal and vertical sensitivity analysis (Binley and Kemna, 2005).

We used the roll-along method to complete some of the profiles (Fig. 3). Profile 1 and profile 3 were composed of two sections overlapping on one-third of the cable length, resulting in 800 m long profiles. Profile 4 sections overlapped on half of the cable length giving a total length of 710 m. Finally, the two sections composing profile 2 did not share any electrode.

The apparent electrical resistivity data acquired in the field were processed with the RES2DINV software from GEOTOMO© (Loke, 2002) including topography information. The topography was obtained from the Digital Elevation Model (DEM) of 15Å~15 m resolution from Institut Cartogràfic de Catalunya. In all our profiles the RMS error, indicator of the reliability of the inversion, was less than 7%, giving a high viability for the resistivity models obtained (Loke and Barker, 1996).

4.5. Results

4.5.1. Geological data

The geological map in Fig. 2 shows that the maar is located near the nonconformity between Palaeozoic basement (mainly outcropping at the northern and western side of the map) and the pre-volcanic Pliocene and Quaternary sediments, which the fill La Selva depression mainly at the southern side. The maar pyroclastic deposits show an asymmetrical distribution mostly extending towards the east for more than 4 km (Martí et al., 1986). The tephra ring morphology and deposits around the crater are very well preserved as well as the Strombolian cone located on the northern side of the maar crater (Fig. 2).

Relevant geological information was also obtained from the analysis of the two drill cores S1 and S2 (Fig. 3). S1 shows a phreatic water table at a depth of 10 m. The first 7.6 m below the crater floor are composed of alternating fine-grained silt and clay deposits. Deeper, the drilling encounters a basaltic lava flow from the final Strombolian episode related to La Crosa de Sant Dalmai eruption. S2 shows a phreatic water table at a depth of 18 m. The first 12 m of the core are composed of fine silt and clay deposits, and the following 14 m show grained sand and colluvial deposits from the tephra ring and the Strombolian cone. The basaltic lava flow appears at a depth of 26 m and shows a total thickness of 10 m. Below, there is a 20 m thick succession of alternating fine and coarse-grained lapilli beds from the intra-maar Strombolian cone. At a depth of 61 m, S2 shows Pliocene and Quaternary sediments containing organic material, which correspond to the contact between the diatreme and the substratum.

4.5.2. Gravimetry

The residual Bouguer anomaly map (Fig. 4c) shows slightly negative to neutral values in the western sector of the map, increasing towards the east, up to 3.5 mGal. The global pattern in the eastern sector shows a NW–SE orientation. The map shows negative values for the stations located right on the rim of the tephra cone. In the north, a minimum is centred on the ring, where the Strombolian scoria cone was emplaced. In the south another minimum coincides with the thicker deposits of the tephra ring. Inside the maar, neutral values are found while reaching the central area. The gravity model of the maar structure has not been developed because the main gravity signature is a circular gravity low produced by the accumulation of pyroclastic material and there is no evidence of the deep root of the structure.

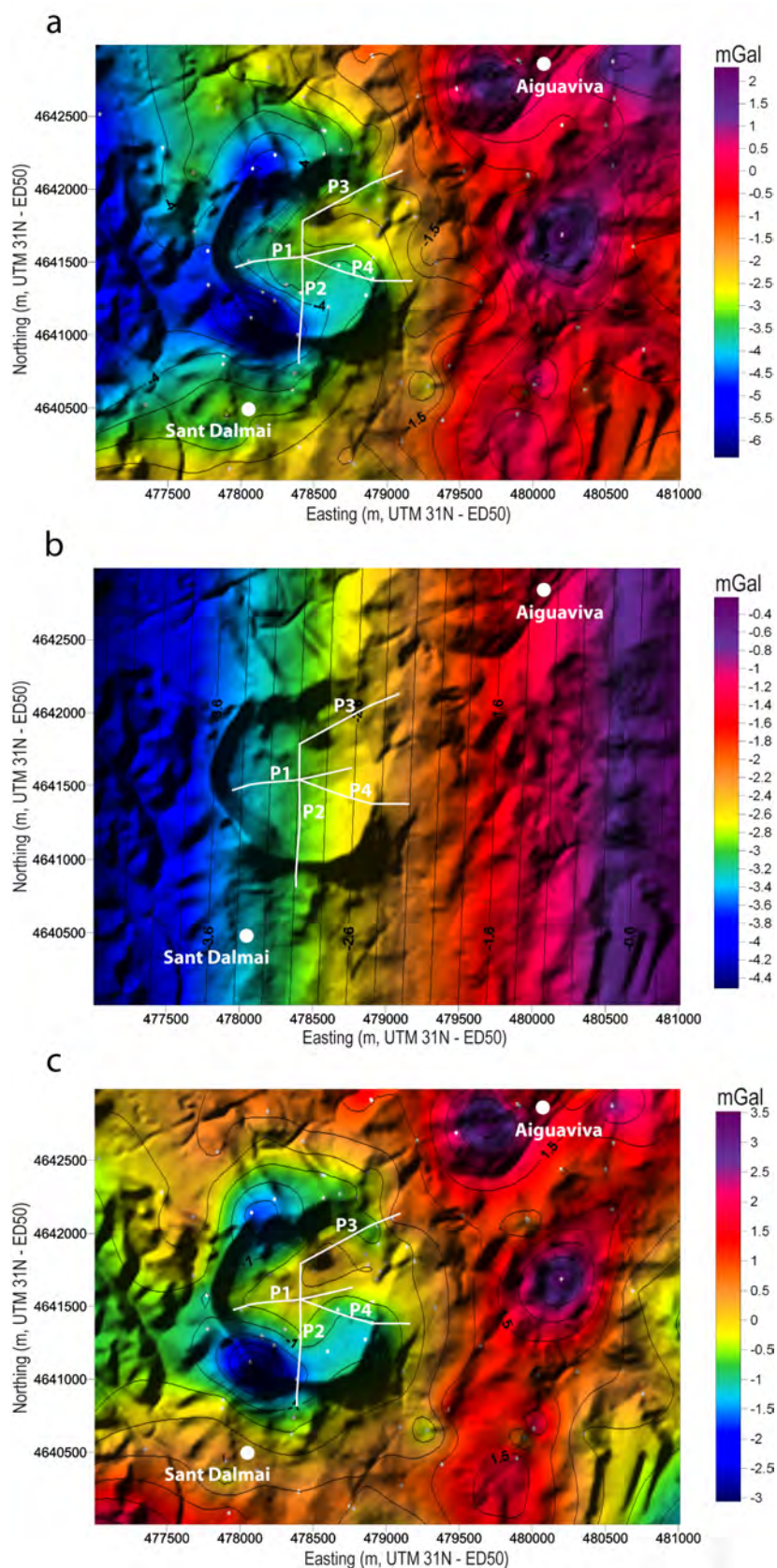


Fig. 4. a. Bouguer anomaly map; b. regional anomaly; c. residual gravity map obtained by subtracting the regional anomaly from the Bouguer anomaly map. Coordinates in metres (UTM31N — ED50). In white: location of ERT the profiles P1, P2, P3, and P4. Small white dots correspond to the gravimetry stations.

4.5.3. Magnetometry

The resulting magnetometry map (Fig. 5) shows the distribution of the local magnetic field for the superficial geological layers. The surface structures detected by this method correspond to rocks with a high proportion of magnetic minerals. Concentric magnetic isolines characterise the interior of the maar crater, with an increase from 1600 nT along the ring to 3200 nT toward the central area. A magnetic maximum is measured at the northern side of the maar, on the eastern side of the Strombolian cone rim with values up to 5000 nT.

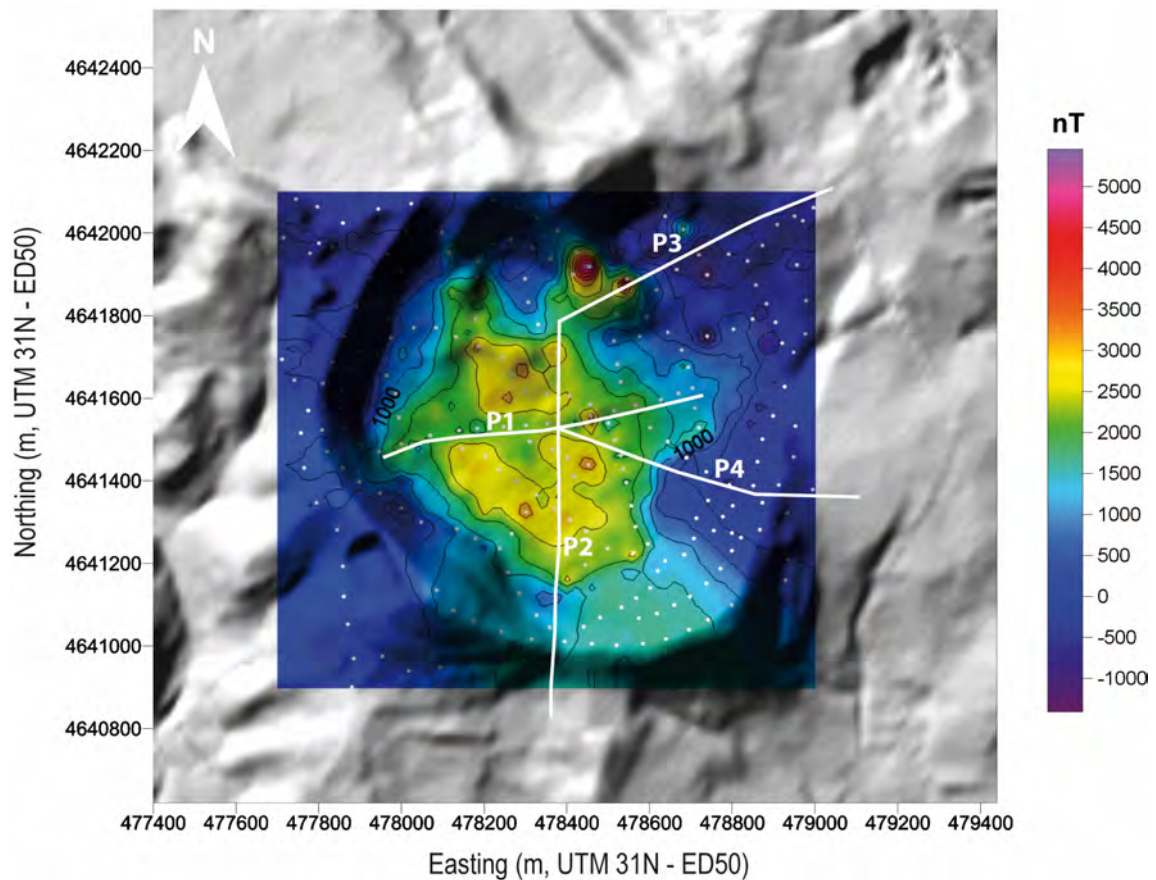


Fig. 5. Residual total field magnetic anomaly map. The white dots correspond to the measurements. The white lines show the location of ERT profiles (P).

4.5.4. Self-potential (SP)

The SP map (Fig. 6) shows an increase of 120 mV from SW to NE, describing a sharp transition highlighting a NW–SE lineament across the maar. The northern end of this lineament overlaps the magnetic anomaly high centred on the Strombolian edifice located at the northern side of the maar crater. In the western side the maar no significant variation of self-potential is observed.

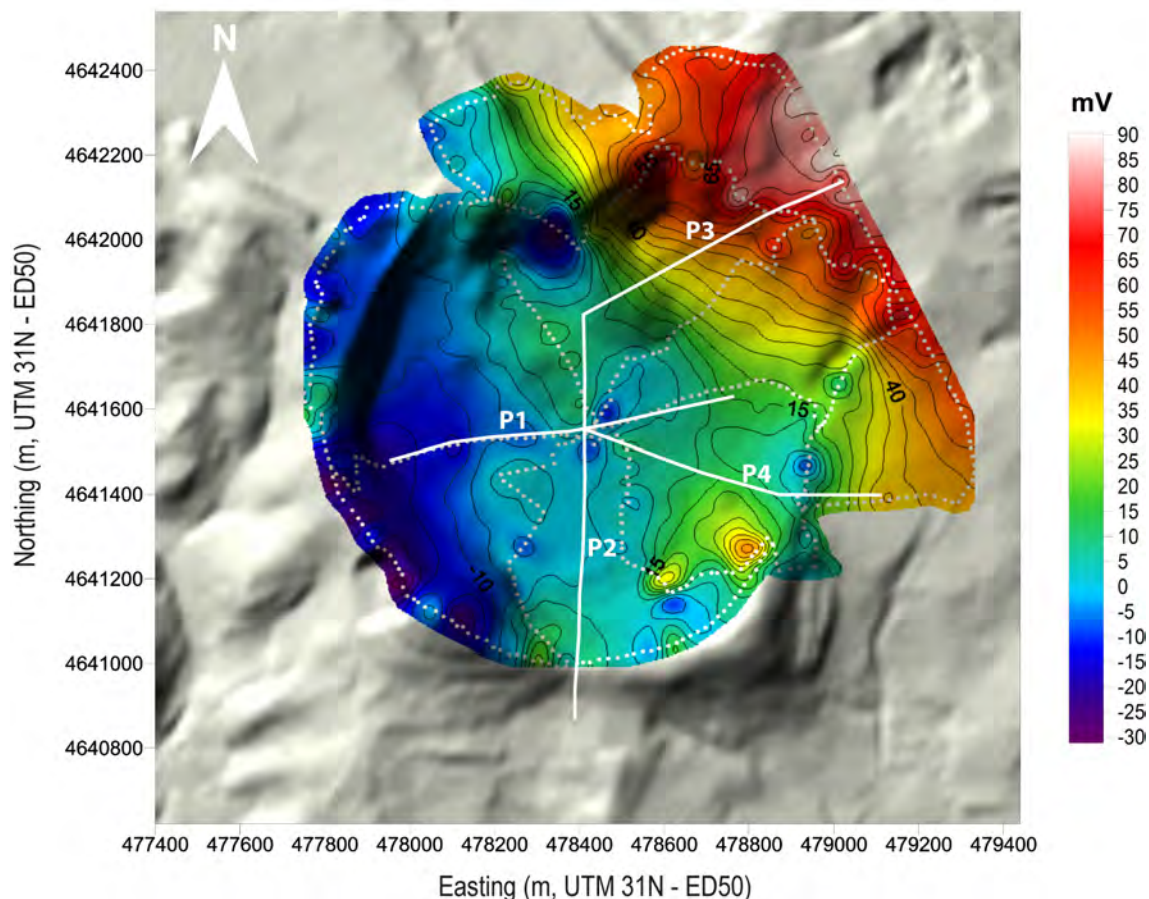


Fig. 6. Self-potential map. The white dots correspond to the measurements. The white lines show the location of ERT profiles (P).

4.5.5. Electrical resistivity tomography (ERT)

ERT models show high resistivity values (1000 $\Omega\cdot\text{m}$ to more than 8000 $\Omega\cdot\text{m}$) matching the areas where the profiles cut the tephra ring (Fig. 7). Inside the main crater the profiles show a ~ 10 to 20 m thick superficial planar layer of low resistivity (10 $\Omega\cdot\text{m}$ to 200 $\Omega\cdot\text{m}$) (Fig. 7).

In profiles 1 and 2, this layer overlies a thick high resistivity layer (~ 2000 to 5000 $\Omega\cdot\text{m}$) visible until the maximum depth of investigation. However, in the last 20 m, resistivity tends to be lower so that we can estimate the thickness of this layer at ~ 60 m.

Profile 3 crosses the eastern flank of the Strombolian cone and the eastern side of the maar rim. We observe a high resistivity body (from 2000 to more than 8000 $\Omega\cdot\text{m}$) in the Strombolian cone area. This resistive zone spreads from 30 m under the surface and is rooted beyond the depth of investigation. Between the Strombolian cone and the maar rim (from 380 to 520 m distance on the resistivity model) the conductive superficial layer overlies a resistive layer, slightly thinner than the one described in profiles 1 and 2. This resistive layer overlies a conductive layer (a few $\Omega\cdot\text{m}$ to 100 $\Omega\cdot\text{m}$), visible until depth of investigation.

In profile 4, high resistivity in the tephra ring narrows from 30 m under the topography and extends at depth. Inside the maar, under the superficial low resistivity layer encountered in all the profiles, lies a resistive layer. As well as in profile 3, it is thinner than those encountered in the same position on profiles 1 and 2. At greater depth the resistivity lowers to ~ 100 $\Omega\cdot\text{m}$.

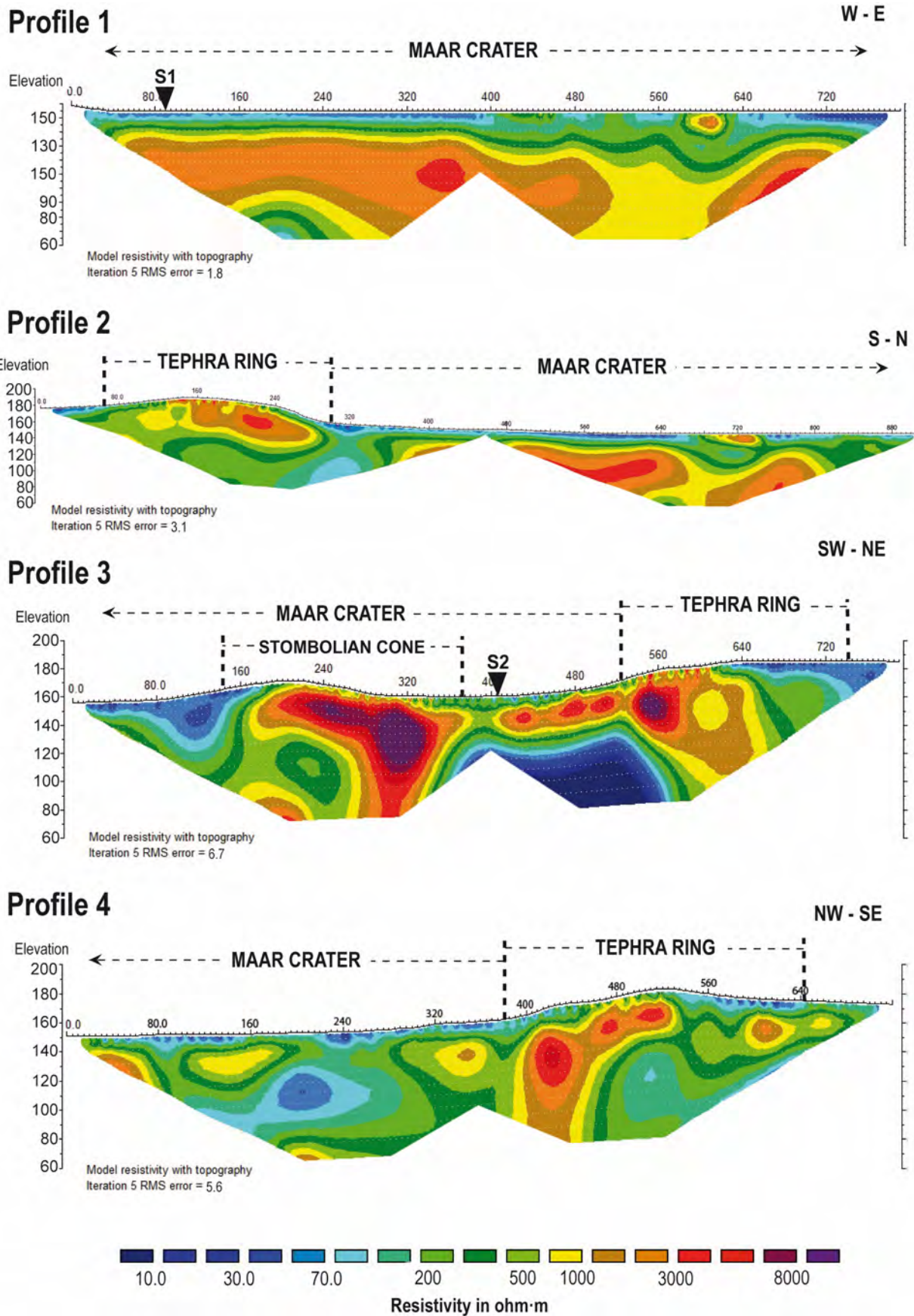


Fig. 7. ERT models with topography.

4.6. Discussion

4.6.1. Phreatomagmatic activity

The residual gravity anomaly map shows negative anomalies coinciding with resistive structures imaged with ERT. The southwest main gravity anomaly reaches values of about -2.5 mGal and coincides with an area of maximum accumulation of poorly consolidated pyroclastic materials, i.e. unwelded breccia, that form the tephra ring. This is consistent with the high resistivity observed in the tephra ring as this material is highly vesiculated. This physical characteristic confers a high resistivity to these levels.

4.6.2. Strombolian activity

The strong gravity anomaly located at the northern side of the tephra ring shows negative values of up to -2 mGal. This anomaly marks the zone of maximum accumulation of scoria deposits belonging to the Strombolian cone formed inside the maar crater. Resistivity profile 3, crossing the Strombolian cone more in the South, gives high resistivity values. The shape of the corresponding resistivity body, narrowing from 30 m under the topographic surface might correspond to the base of the Strombolian cone, highlighting the former depth of the maar crater before the Strombolian episode in this part of the crater. The resistive root found under the Strombolian cone might correspond to the eruptive conduit or a secondary dyke.

The ERT images show an area inside the maar crater ranging from 1100 to 3000 $\Omega\cdot\text{m}$ (coloured orange and red in Fig. 8a). This is interpreted to correspond to the basaltic lava flow emitted during the Strombolian phase at the end of La Crosa de Sant Dalmai eruption, and which was also intersected by the drill core S1 (see position in Fig. 3). In some places, this basaltic lava flow is detected until the maximum depth of investigation of the ERT profiles (95 m). The positive magnetic anomaly covers almost the whole maar crater, outlining the extent of the lava below the post-maar sediments (Fig. 8b). In the eastern part of the maar crater floor, no significant magnetic anomaly is detected while the S2 drill core shows the presence of the lava flow at a depth of 26 m, with a thickness of 10 m. The lava flow is not detected by the magnetic measurements probably because it is thin and located too deep for the resolution of the method.

4.6.3. Post-eruptive phase

The drill cores show that the post-volcanic infill sequence of the maar crater has an average thickness of 10 m in the eastern part of the maar, and 26 m in the north-western zone. This is in the order of magnitude of the 10–25 m thick superficial conductive layer observed in the ERT models. These data indicate that the corresponding post-maar sediments (ranging from ~ 30 $\Omega\cdot\text{m}$ to 500 $\Omega\cdot\text{m}$) form a regular layer extending in the whole maar crater around the Strombolian cone, burying the associated lava flow (Fig. 8).

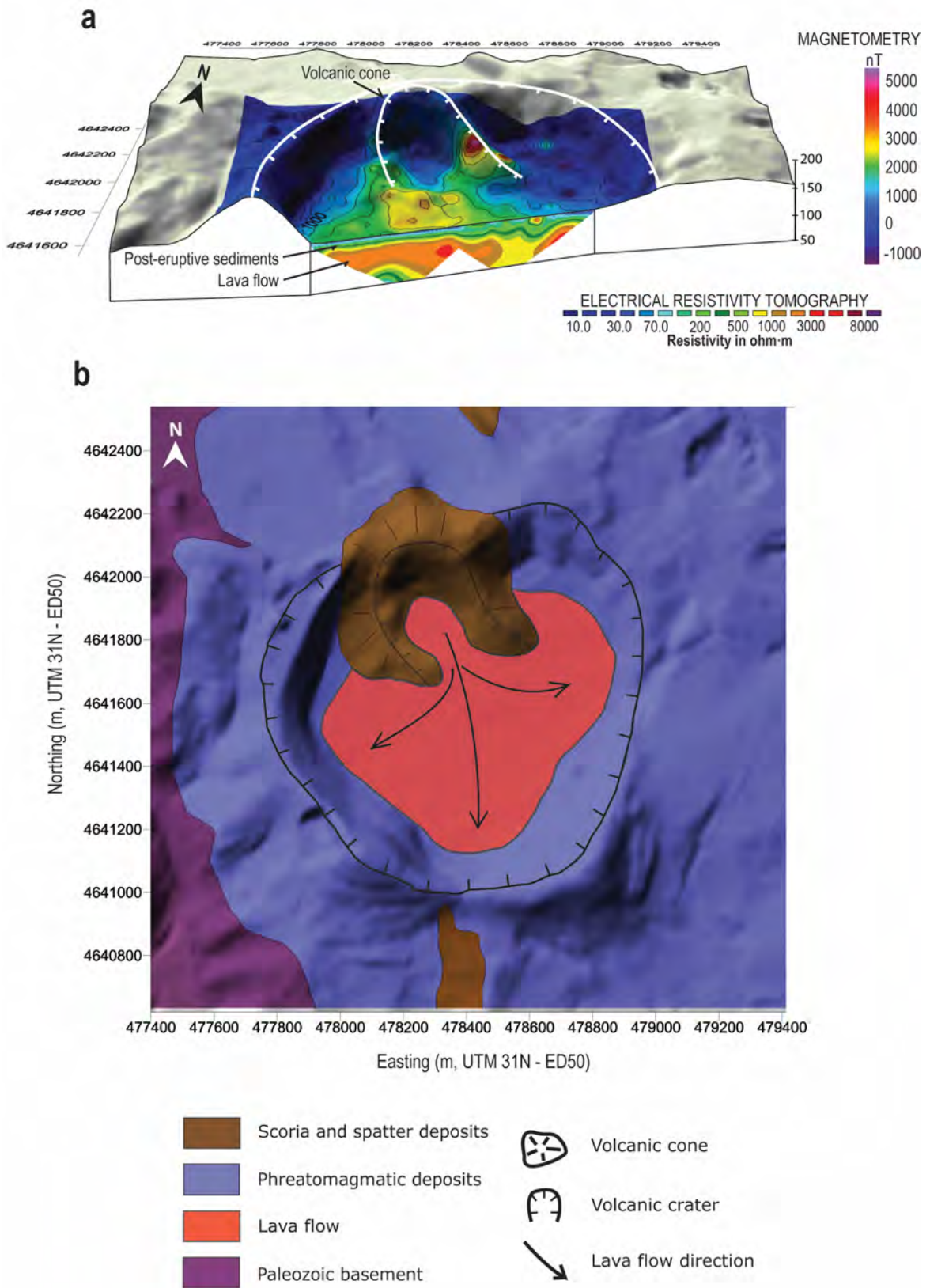


Fig. 8. a) 3D block diagram of the residual total field magnetic anomaly map and the ERT profile 1. b) Mapping of the interpreted lava flow.

4.6.4. Geological control on the eruptive activity

The SP map displays a sharp transition from negative (–25 mV) to positive values (75 mV), following a NW–SE trend. This lineament may be interpreted as a fault associated with the regional trend, guiding the ascending magma (Fig 1). The resistive body (2000 to more than 8000 Ω .m) detected at depth in the ERT profile 3 and rooted below the maximum depth of investigation is located on this fault (Fig. 9). We interpret this high resistivity root as a basaltic intrusion that fed the last episode of La Crosa de Sant Dalmai eruption, i.e. the last Strombolian phase. It is difficult to estimate the dimensions of this intrusion (eruptive conduit or secondary dyke). Our ERT data provide only 2 day information and the resolution decreases exponentially with depth making difficult concluding on the nature of this intrusion. However, the superficial section of this intrusion could be estimated between 20 and 30 m wide. This is not concordant with the usual dyke dimensions in such small volcanic edifices. However, White and Ross (2011) and Lefebvre et al. (2012) show that dykes can widen through several processes near the surface and produce such large superficial intrusions from a dyke or from the coalescence of dyke segments.

The problem is whether this fracture also controlled the ascent of magma in the phreatomagmatic phases corresponding to the opening and development of the maar crater and its diatreme. Although the deeper internal structure of the diatreme cannot be defined with the geophysical methods we have applied in this study, it is possible to know the geological unit where the phreatomagmatic explosions occurred. This may be done by simply looking at the populations of the lithic fragments present in the maar deposits, which correspond exclusively to Palaeozoic granites. These fragments are decimetric to less than 1 mm in size, show angular to subangular shapes, and in some cases are strongly hydrothermally altered. These lithic fragments were directly broken and ejected from the Palaeozoic substrate of the volcano by the phreatomagmatic explosions. This suggests that the maar-forming explosions and, therefore, the magma/water interaction did not occur at the contact between the Palaeozoic basement and the Pliocene and Quaternary infill of the La Selva depression as was initially suggested by Martí et al (1986), but occurred directly in an aquifer located in the fractured granitic basement (Pedrazzi et al., 2012).

Therefore, if the fracture detected with SP is the main pathway by which the magma ascended to the surface, this should be branched into the granite causing interaction of ascending magma with its aquifer, thus generating violent explosions leading to the formation of the maar and its diatreme. Later, after the maar-diatreme formation, the rise and eruption of the magma would be restricted to the main fracture without the possibility of interacting with the granite aquifer, probably already exhausted, resulting in a final purely Strombolian phase.

Finally, it is important to mention that the geophysical imaging of the maar confirms the lack of significant erosion and modification of its original morphology. This is demonstrated by the preservation of the original slopes of the tephra ring and also by the scarcity of breccia deposits inside the crater, which suggests that little remobilisation of the tephra ring deposits has occurred since its formation. All this suggests that the age of the La Crosa de Sant Dalmai volcano is younger than stated previously for the La Selva sub-zone (7.9–1.7 Ma, Araña, et al. (1983)).

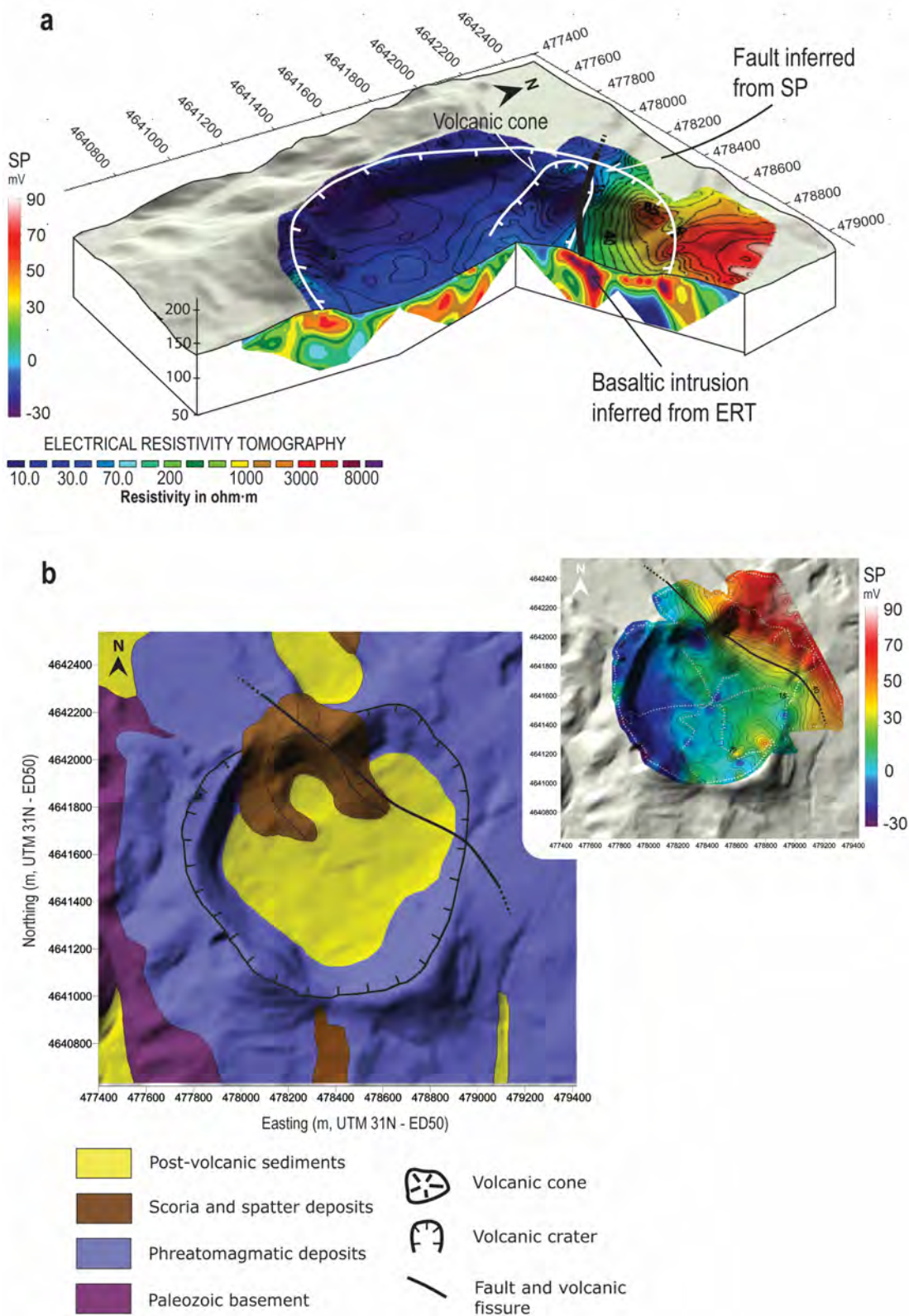


Fig. 9. a) 3D block diagram of the self-potential and the ERT profiles 2 and 3. b) NW–SE fault inferred from self-potential, in the upper right corner, and located on the geological map.

4.6. Conclusions

Combining new geophysical and geological data we have been able to elaborate a 3D model of the internal structure of the uppermost part of La Crosa de Sant Dalmai maar-diatreme system (Fig. 10), the largest volcano of the Catalan Volcanic Zone. This model helps in understanding the influence of the pre-eruptive basement on the phreatomagmatic and Strombolian activity that constructed the volcanic edifice and the characteristics of the post-eruptive deposits that infill the maar crater. In particular, we have been able to determine 1) the elevation of the maar crater floor under the Strombolian cone; 2) the extension of the lava flow formed during this last Strombolian episode, which is now buried under a 10 to 20 m thick post eruptive sedimentary layer; 3) the presence of a NW–SE lineament interpreted as a fault associated with the regional trend; and 4) the control exerted by this fault on the location of the Strombolian cone, whilst the phreatomagmatic activity resulted from the interaction with an aquifer in the granitic basement.

This multiparametric geophysical and geological research has provided relevant information on the upper structure of La Crosa de Sant Dalmai maar, offering important clues to understand its formation and evolution. However, the applied geophysical methods do not always have sufficient spatial resolution and depth of investigation, so there are still some questions about the deeper part of the diatreme, for which exploration other methods such as pole-dipole ERT profiles or seismic reflection profiles should be used.

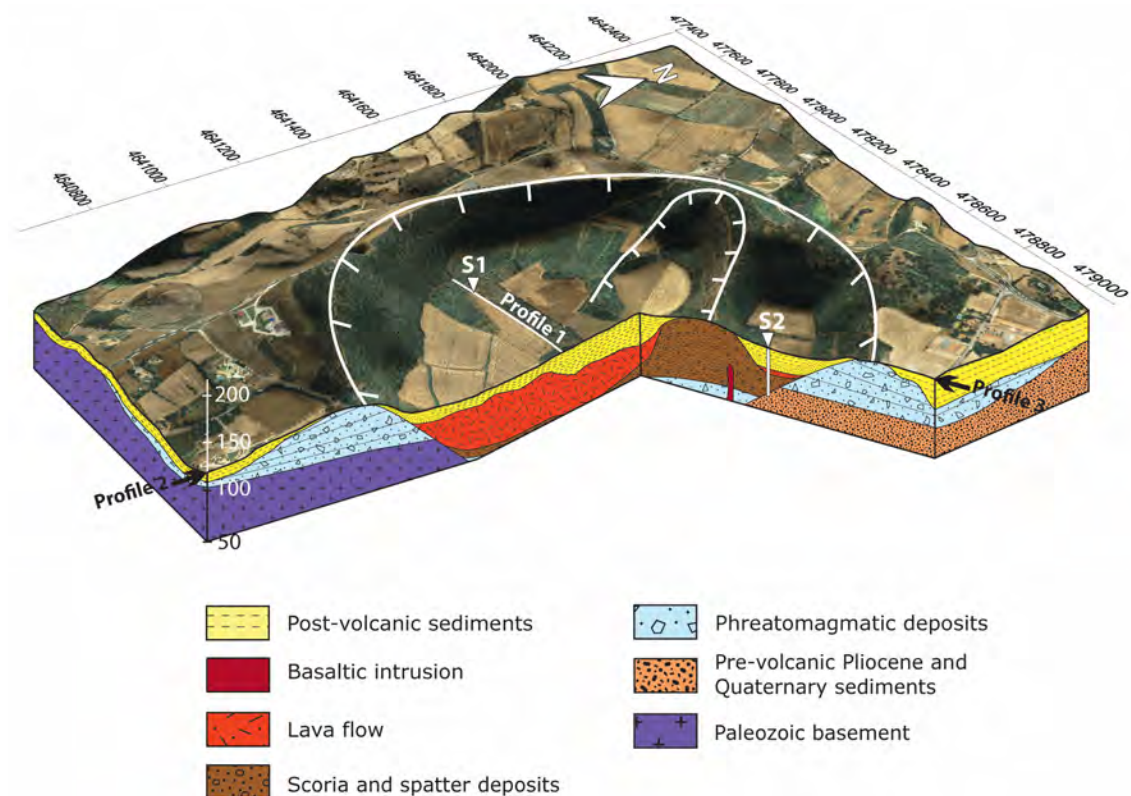


Fig. 10. Synthetic 3D model. Orthophotomap overlapped on the DEM with geologic interpretation through cross sections corresponding to ERT profile 2 (N–S direction) and 3 (SW–NE direction). The locations of S1 and S2 drillings are indicated.

Acknowledgements:

This study has been partially funded by the grants CGL2010-12338-E and CGL2009-07025 (subprogram BTE). We thank Lluís Motjé (Consortium of the Crosa de Sant Dalmaí: management of field geology at the Crosa volcanic area) for his great logistical support all along the field work. We also thank Olaya García, Adelina Geyer, Stefania Bartolini, Llorenç Planagumà, Silvina Guzmán, Ismael Casado, and Anna Sanchez for their assistance in the field. We are grateful to the Editor, Prof. Lionel Wilson, and Prof. Volker Lorenz and one anonymous referee for the constructive reviews of our manuscript.

References:

- Araña, V., Aparicio, A., Martín-Escorza, C., García Cacho, L., Ortiz, R., Vaquer, R., Barberi, F., Ferrara, G., Albert, J., Gassiot, X., 1983. El volcanismo Neógeno-Cuaternario de Catalunya: caracteres estructurales, petrológicos y geodinámicos. *Acta Geologica Hispánica* 18, 1–17.
- Barnolas, A., García, A., Muelas, A., Soubrier, J., Pallí, Ll., Carreras, J., Martínez, F., Quesada, C., Ruiz, C., 1979. Mapa Geológico de España. E. 1:50000. Santa Coloma de Farners.
- Binley, A., Kemna, A., 2005. DC resistivity and induced polarization methods. In: Rubin, Y., Hubbard, S. (Eds.), *Hydrogeophysics*. Springer, New York, pp. 129–156.
- Büchel, G., 1993. Maars of the Westeifel, Germany. In: Negendank, J.F.K., Zolitschka, B. (Eds.), *Paleolimnology of European Maar Lakes. Lecture Notes in Earth Sciences*, vol. 49. Springer, Berlin, Heidelberg, pp. 1–13.
- Büchel, G., Lorenz, V., 1993. Syn- and post-eruptive mechanism of the Alaska Ukinrek Maars in 1977. In: Negendank, J.F.W., Zolitschka, B. (Eds.), *Paleolimnology of European Maar Lakes. Lecture Notes in Earth Sciences*, 49. Springer, Berlin, Heidelberg, pp. 15–60.
- Casas, A., Torné, M., Banda, E., 1986. Mapa gravimètric de Catalunya 1:500000. Servei Geològic de Catalunya. Dpt. De Política Territorial i Obres Públiques.
- Cebriá, J.M., López-Ruiz, J., Doblas, M., Oyarzun, R., Hertogen, J., Benito, R., 2000. Geochemistry of the Quaternary alkali basalts of Garrotxa (NE Volcanic Province, Spain): a case of double enrichment of the mantle lithosphere. *Journal of Volcanology and Geothermal Research* 102 (3–4), 217–235.
- Dèzes, P., Schmid, S.M., Ziegler, P.A., 2004. Evolution of the European Cenozoic Rift System: interaction of the Alpine and Pyrenean orogens with their foreland lithosphere. *Tectonophysics* 389, 1–33.
- Digital Elevation model. Sant Dalmaí zone. <http://www.icc.cat/>, Last date of access 27 February, 2012.
- Guérin, G., Benhamou, G., Mallarach, J.M., 1986. Un exemple de fusió parcial en medi continental. *El vulcanisme quaternari de Catalunya. Vitrina* 1, 20–26.
- Lefebvre, N.S., White, J.D.L., Kjarsgaard, B.A., 2012. Spatter-dike reveals subterranean magma diversions: consequences for small multivalent basaltic eruptions. *Geology* 40, 423–426.
- Loke, M.H., 2002. RES2DINV ver. 3.54. Rapid 2-D resistivity and IP inversion using the least square method. Geotomo Software.

- Loke, M.H., Barker, R.D., 1996. Practical techniques for 3D resistivity surveys and data inversion. *Geophysical Prospecting* 44 (3), 499–523.
- Lorenz, V., 1973. On the formation of maars. *Bulletin Volcanologique* 37 (2), 183–204.
- Lorenz, V., 1975. Formation of phreatomagmatic maar-diatreme volcanoes and its relevance to kimberlite diatremes. *Physics and Chemistry of the Earth* 9, 17–27.
- Lorenz, V., 1986. On the growth of maars and diatremes and its relevance to the formation of tuff rings. *Bulletin of Volcanology* 48 (5), 265–274.
- Lorenz, V., 2007. Syn- and post-eruptive hazards of maar-diatreme-volcanoes. *Journal of Volcanology and Geothermal Research* 150, 285–312.
- Lorenz, V., Kurszlaukis, S., 2007. Root zone processes in the phreatomagmatic pipe emplacement model and consequences for the evolution of maar-diatreme volcanoes. *Journal of Volcanology and Geothermal Research* 159 (1–3), 4–32.
- Martí, J., Mallarach, J.M., 1987. Erupciones hidromagmáticas en el volcanismo cuaternario de Olot. *Estudios Geológicos* 43, 31–40.
- Martí, J., Ortiz, R., Claudin, F., Mallarach, J.M., 1986. Mecanismos eruptivos del volcán de la Closa de Sant Dalmai (Prov. Girona). *Anales de Física* (82), 143–153 Vol. esp. serie B.
- Martí, J., Mitjavila, J., Roca, E., Aparicio, A., 1992. Cenozoic magmatism of the Valencia trough (western Mediterranean): relationship between structural evolution and volcanism. *Tectonophysics* 203 (1–4), 145–165.
- Martí, J., Planagumà, L., Geyer, A., Canal, E., Pedrazzi, D., 2011. Complex interaction between Strombolian and phreatomagmatic eruptions in the Quaternary monogenetic volcanism of the Catalan Volcanic Zone (NE of Spain). *Journal of Volcanology and Geothermal Research* 201 (1–4), 178–193.
- Pedrazzi, D., Martí, J., Bolós, X., 2012. Interaction between Strombolian and phreatomagmatic eruptions in the Catalan Volcanic Field: La Crosa de Sant Dalmai maar. *Volcanpark International Congress, Olot, Spain*, pp. 22–52.
- Schmincke, H.-U., 1988. *Vulkane im Laacher See-Gebiet, ihre Entstehung und heutige Bedeutung*. Doris Bode Verlag, Haltern, pp. 1–119.
- Sheridan, M.F., Wohletz, K.H., 1981. Hydrovolcanic explosions: the systematics of water-pyroclast equilibrium. *Science* 212, 1387–1389.
- Sheridan, M.F., Wohletz, K.H., 1983. Hydrovolcanism: basic considerations and review. *Journal of Volcanology and Geothermal Research* 17 (1–4), 1–29.
- Trilla, J., Pallí, L., 1977. Vulnerabilidad a la polución como temática hidrogeológica. Aplicación en una zona de los alrededores de Girona. *Cámara of. de Com. e Ind. Gerona*, p. 75.
- White, J.D.L., Ross, P.-S., 2011. Maar-diatreme volcanoes: a review. *Journal of Volcanology and Geothermal Research* 201 (1–4), 1–29.
- Wohletz, K.H., 1983. Mechanisms of hydrovolcanic pyroclast formation: grain-size, scanning electron microscopy, and experimental studies. *Journal of Volcanology and Geothermal Research* 17 (1–4), 31–63.
- Wohletz, K.H., Sheridan, M.F., 1983. Hydrovolcanic explosions II, evolution of basaltic tuff rings and tuff cones. *American Journal of Science* 283 (5), 385–413.

Electrical resistivity tomography revealing the internal structure of monogenetic volcanoes

Published in:

Geophysical Research Letters

Authors of the paper:

Stéphanie Barde-Cabusson^(a)

Xavier Bolós^(a)

Dario Pedrazzi^(a)

Raúl Lovera^(b)

Guillem Serra^(b)

Joan Martí^(a)

Albert Casas^(b)

a) Institute of Earth Sciences Jaume Almera, ICTJA-CSIC, Group of Volcanology. SIMGEO (UB-CSIC) Lluís Sole i Sabaris s/n, 08028 Barcelona, Spain

b) Economic and Environmental Geology and Hydrology Group. Department of Geochemistry, Petrology and Geophysical Prospecting. Faculty of Geology, University of Barcelona. Martí Franqués s/n, 08028 Barcelona,) Spain

c) Polytechnic University of Catalonia, Barcelona, Spain

5.1. Abstract

Eruptive activity of individual monogenetic volcanoes usually lasts a few days or weeks. However, their short lifetime does not always mean that their dynamics and structure are simple. Monogenetic cones construction is rarely witnessed from the beginning to the end, and conditions for observing their internal structure are hardly reached. We provide high-resolution electrical resistivity sections (10m electrode spacing) of three monogenetic cones from northeastern Spain, comparing our results to geological observations to interpret their underground continuation. The 100m maximum depth of exploration provides information on almost the entire edifices, highlighting the relationships between Strombolian and hydromagmatic deposits in two multiphase edifices. A main observation is a column of distinct resistivity centered on the Puig d' Àdri volcano, which we interpret as the eruptive conduit. This method can provide valuable information on the past volcanic dynamics of monogenetic volcanic fields, which has real implications for the forecast of future activity.

Keywords: Exploration Geophysics · Magnetic and electrical methods · Volcanology · Instruments and techniques

5.2. Introduction

Monogenetic volcanoes are small volcanic edifices built-up in a short period of time, (e.g., few hours or days in the East-Izu monogenetic volcano group and several years for Jorullo in 1759 ~ 1766 and Parícutín in 1943 ~ 1952), so that their complexity is sometimes underestimated (De la Cruz-Reyna and Yokoyama, 2011). Monogenetic volcanic edifices go from simple one-phase volcanoes to complex edifices built from several distinct phases of activity (Walker, 2000; Valentine and Gregg, 2008). A complex eruptive dynamics can, for example, result in the accumulation of highly vesicular scoria (Strombolian-style explosive events) and compact, fine-enriched ash (phreatomagmatic explosive events), forming a complex layercake-style edifice alternating horizons of different electric resistivity material in a reduced space. This makes high-resolution electrical resistivity tomography (ERT) a valuable tool to investigate the internal structure of monogenetic volcanoes. In contrast with polygenetic volcanoes and despite being the most common type of activity, eruptions giving birth to monogenetic volcanoes are much less witnessed and less described in scientific reports (Kereszturi and Németh, 2012). Only a few events of this type have occurred worldwide in historical times such as Al Madinah (1256), Jorullo (1759 ~ 1766) and Parícutín (1943 ~ 1952), and the Ukinrek maar (1977) (De la Cruz-Reyna and Yokoyama, 2011; Kereszturi and Németh, 2012). Monogenetic cones can be weathered, exhibiting part of their internal structure. Mathieu et al. (2008) presented natural examples of monogenetic cones from the Chaîne des Puys (French Massif Central) and of parasitic cones from the northeast rift of Teide (Canary Islands) where the shape of shallow volcanic intrusions are well-preserved. Other examples exist (e.g., Geshi et al., 2011); however, no unified model or

similar attempted to connect field observations of this type with some geophysical approach until now.

Valentine (2012) used crustal xenoliths to study the shallow plumbing systems of small-volume scoria cones and maars. In particular, he showed that their conduits or dikes flare mainly in the uppermost ~150m of the crust.

Geophysics has been successfully used to model (Cassidy et al., 2007; Mrlina et al., 2009; Blaikie et al., 2012) or to image (e.g., Gebhardt et al., 2011; Martín-Serrano et al., 2009; Bolós et al., 2012) the subsurface structure of maar volcanoes. ERT was applied on polygenetic volcanoes, providing valuable information on their structure and hydrothermal systems (e.g., Revil et al., 2008, 2011). Portal et al. (2013) also presented preliminary results on a model of monogenetic dome using joint interpretation of ERT, gravimetry, and muonic imagery models. However, a detailed study of the internal structure of monogenetic volcanoes remains poorly documented, particularly edifices built up after multiple phases of activity.

The Catalan Volcanic Zone (CVZ), at the north of Spain (Figure 1a), is mostly unknown compared to the contemporaneous alkaline volcanism in other parts of western and central Europe (Cenozoic alkaline volcanism in the Rhenish massif and Rhinegraben of Germany, the Massif Central of France, and the western Pannonian Basin in Eastern Europe; e.g., Downes (2001)) but it offers an excellent opportunity for a detailed exploration of monogenetic volcanoes' internal structure. In this study, we present ERT models from three monogenetic volcanoes giving a detailed image of the entire edifices. Key observations are made from the two more complex edifices because they offer the most important diversity of deposits and structural features.

5.3. Monogenetic Volcanism in the Garrotxa Volcanic Field

The CVZ is one of the Quaternary alkaline volcanic provinces of the European rifts system (Martí et al., 1992, 2011). It has been active during the last 12 Ma and the volcanism is mainly characterized by alkali basalts and basanites. Inside the CVZ, the Garrotxa volcanic field is a subzone registering the latest volcanic activity (0.5–0.01 Ma) (Araña et al., 1983; Martí et al., 1992). It comprises more than 50 well-preserved monogenetic volcanoes including scoria cones, tephra rings, and maars. Some of these eruptions alternated Strombolian and hydromagmatic phases, giving rise to complex stratigraphic successions not only within the monogenetic field but also at the scale of individual edifices (Martí and Mallarach, 1987; Martí et al., 2011; Pedrazzi and Marti, 2011; Bolós et al., 2012). Martí et al. (2011) classify monogenetic volcanoes depending on whether or not hydromagmatic activity contributed to their construction. Volcanoes exclusively derived from magmatic activity correspond to scoria cones with occasional lava flows while volcanic cones including hydromagmatic activity, although morphologically similar to scoria cones, are much more complex. They may alternate phreatic, phreatomagmatic, and Strombolian phases, generating a wide diversity of pyroclastic density currents and fallout deposits, including explosive and effusive episodes.

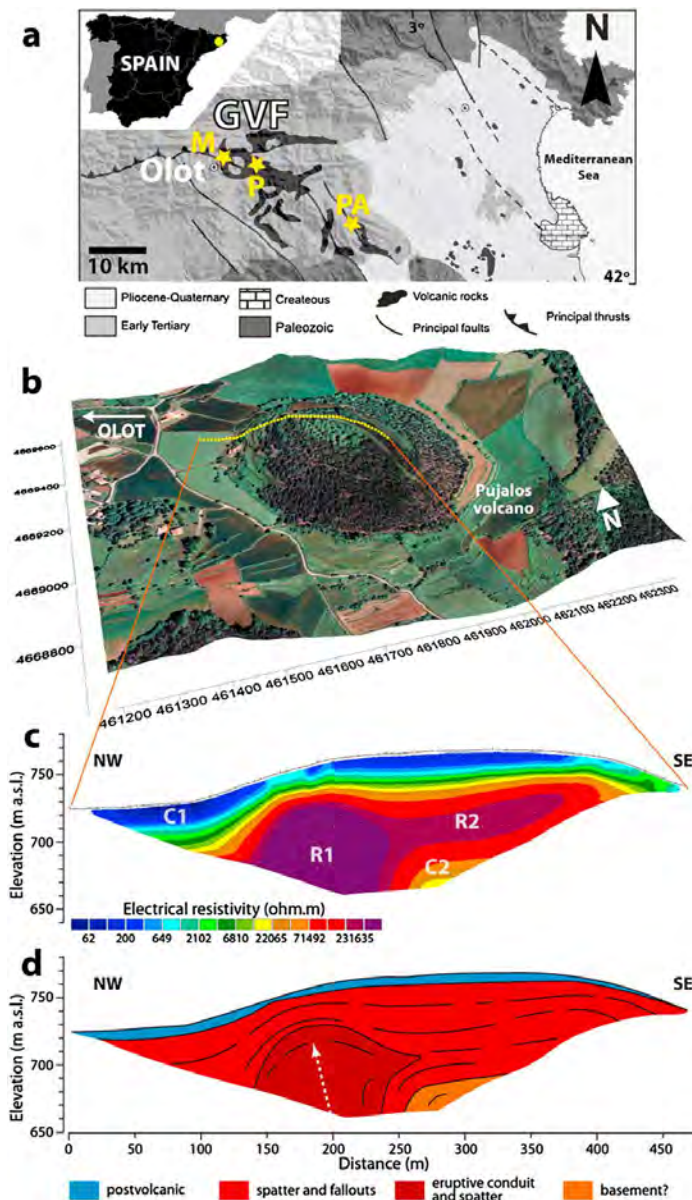


Fig. 1. (a) Localization maps of the Garrotxa volcanic field (GVF) and of our three monogenetic volcanoes: Pujalós (P), Montsacopa (M), and Puig d'Àdri (PA) volcanoes (modified from Martí et al. (2011)). (b) Orthophotography of the Pujalós volcano, a monogenetic Strombolian volcano, overlaid on a digital Elevation Model with localization of the ERT profile (yellow dotted line). (c) ERT model (RMS error 15.2% after five iterations). R and C stands for resistive and conductive bodies or layers respectively. (d) Geological interpretation.

5.4. Data Acquisition and Processing

Multielectrode ERT was used to obtain 2-D resistivity high-resolution data on three monogenetic volcanoes from the Garrotxa volcanic field. We used an Iris Syscal Pro resistivity system with 48 electrodes connected to a 470m long cable (10m electrode spacing) in Wenner-Schlumberger configuration (maximum depth of investigation of about 100 m). We used the roll-along method to complete some of the profiles. No reciprocal measurements were taken but data quality was assessed by averaging or stacking several measurements and very good quality factors were obtained ($q < 3.5\%$). Low contact resistances of the electrodes were achieved because of the high moisture of the soils and the special design of the stainless steel electrodes directly in contact with the multicore cable (maximum values < 3 k Ω). Current injected was automatically adjusted by the system to optimize the input voltage and to ensure the best signal-to-noise ratio. The maximum power of the instrument is 800V and the maximum current is 320mA at 2.5 k Ω contact resistance. In our survey, depending on

the distance between current electrodes, the current intensity ranged from 275 to 5mA. The typical standard deviation was less than 1% with maximum standard deviation values lower than 3.5%. (8) The resistivity data were inverted with RES2DINV (Loke, 2002). Covariance matrix is commonly used to assess the accuracy of the inversion for models that consist of a small number of parameters but RES2DINV, like most nonlinear inversion programs, carries out an optimization process that tries to reduce the difference between the calculated and measured apparent resistivity values. The inversion routine used by the program is based on the smoothness constrained least-squares method (de Groot-Hedlin and Constable, 1990; Sasaki, 1992) which allows to adjust the damping factor. This parameter is designed to accommodate noisier data sets, without which the inversion attempts to fit noise as data and becomes unstable. A larger damping factor was used for the Pujalós volcano data set (Figure 1). When data show large resistivity variations near the surface, it is also recommended to use a model where the cell width is half the unit electrode spacing. This was applied to the Pujalós and Montsacopa profiles. This strategy allowed us to improve the results but RMS error, estimating the difference between the calculated and measured apparent resistivity, was still high for Pujalós. The results are discussed taking this fact into account.

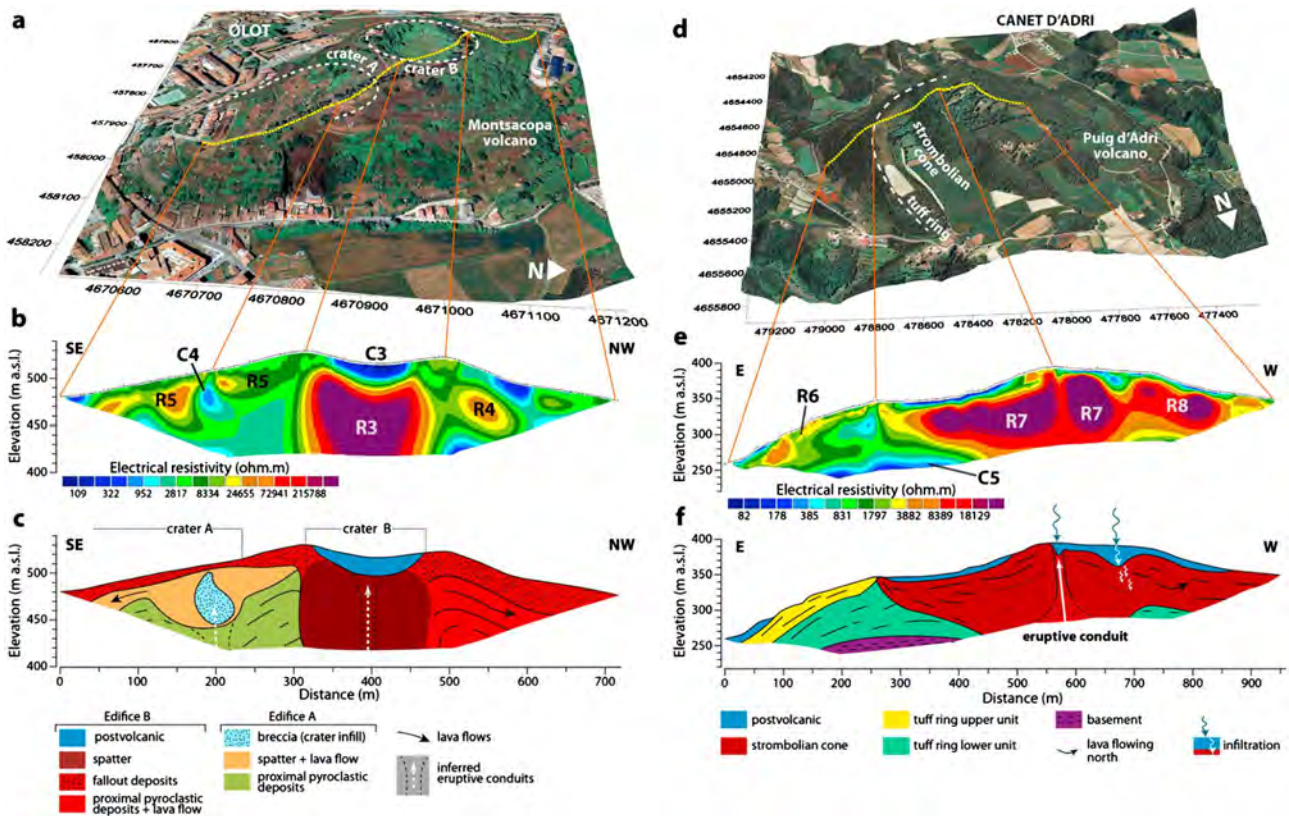


Fig. 2. The Montsacopa and Puig d'Àdri volcanoes, two complex monogenetic volcanoes built by hydromagmatic and Strombolian activity. (a and d) Orthophotography overlaid on a digital elevation model with localization of the ERT profile (yellow dotted line). (b and e) ERT model (vertical exaggeration 1.17, RMS error 5.7% after four iterations for Montsacopa and vertical exaggeration 1.17, RMS error 6.1% after five iterations for Puig d'Àdri). R and C stands for resistive and conductive units respectively. (c and f) Geological interpretation.

5.5. Results

The following results relate to our three example monogenetic volcanoes. A first ERT profile was performed on the Pujalós volcano, near the city of Olot, in the Garrotxa volcanic field (Figure 1). The ERT cable was laid out from the northwestern side of the Pujalós, passing through the summit up to the southeastern flank (Figure 1b). The resistivity model (Figure 1c) shows a globally simple distribution of the resistivity. We found a superficial conductive layer C1 ($< 650 \Omega\text{m}$), 10 to 20m thick, and slightly thicker beyond the fields located at the NW of the cone. A rounded resistive body R1 ($> 250,000 \Omega\text{m}$) appears at $\sim 30\text{m}$ depth. R1 is offset with respect to the cone summit and extends beyond the maximum depth of investigation. This resistive body seems to be connected to the SE with an elongated shape of slightly lower resistivity values that follows a 15 slope (R2). Under this layer, the resistivity values decrease progressively up to one order of magnitude (C2).

The second test was performed in the same area, on Montsacopa, a volcano located inside the city of Olot itself. This volcano presents a NW-SE elongated shape with a well-preserved circular crater in the summit (crater B in Figure 2a). A previous study based on stratigraphy indicates the presence of a second eruptive vent (crater A in Figure 2a) on the SE flank (Bolós, 2009). Our ERT profile (Figure 2b) covers the volcano nearly from one extreme to the other, crossing the two craters. This 710m long profile is composed of two sections acquired with a roll-along of half the cable length. After four iterations, the data inversion gave a good RMS error value of 5.7%. The most striking feature is a 150m wide high-resistivity body R3 ($> 200,000 \Omega\text{m}$) under crater B. It presents a concave upper limit, nearly vertical laterals, and extends beyond the maximum depth of exploration. On top of this body lies a lenticular conductive body marked as C3, $\sim 20\text{m}$ thick at its maximum (~ 950 to $100 \Omega\text{m}$). At the NW we observe a resistive elongated body (R4), dipping NW at an angle of 20° . It is surrounded by lower resistivity values (~ 3000 to $300 \Omega\text{m}$). The resistivity distribution in the SE flank is more complex. It shows a few meters-thick superficial layer, displaying resistivity $< 3000 \Omega\text{m}$. It overlays an irregular resistive layer with several tens of thousands Ωm resistivity (R5). Surrounded by these high-resistivity values, the model shows a drop-shaped zone C4, of lower resistivity ($\sim 1000 \Omega\text{m}$). Deeper, the inversion model shows resistivity values of about $3000 \Omega\text{m}$.

Still in the Garrotxa, we acquired a third ERT profile on the Puig d' Àdri volcano (Figures 2d, 2e, 2f, and 1a for localization). These data were acquired along three sections overlapping by half the cable length, i.e., we obtained a profile of 950m in total. After five iterations we obtained an RMS error of 6.1% for this model, confirming the quality of the inversion. The eastern part of the resistivity model shows several layers identified through their respective resistivity. In particular, we can notice the presence of a horizontal conductive layer ($< 400 \Omega\text{m}$) at depth (C5). Going upward, an area of 1000 to $3000 \Omega\text{m}$ seems to change progressively from horizontal to $\sim 20^\circ$ dip. It lays under a more resistive (up to $8000 \Omega\text{m}$) 20m thick layer (R6). The rest of the resistivity model is occupied by a large resistive unit, R7, ($> 4000 \Omega\text{m}$) overlaid by a conductive layer ($< 400 \Omega\text{m}$). The resistive unit displays a V-shaped base, intersected by the lower limit of the model. Nearly in the center of the V, a less-resistive (light-red color in Figure 2e) vertical column connects the deepest layer to the surface. At 100m to the west the conductive superficial layer enters deeper into the resistive unit. This last follows the slope of the western flank, forming a thick resistive layer (R8).

5.6. Discussion

Our three example monogenetic volcanoes are a good illustration of the difference made by Martí et al. (2011) concerning monogenetic volcanoes affected or not by hydromagmatic phases during their construction. For the three sites, the water table is located in the sedimentary basement, at depths greater than our maximum depth of exploration so that we do not take it into account in the interpretation. Available geological information describes the Pujalós volcano as a scoria cone, possibly originating a lava flow covering an area of about 6 km² to the west (IGC et al., 2007). Despite the elevated RMS error (15.2% after five iterations), the resistivity model seems to fit well this description (Figure 1). Moreover, a strong likeness exists with natural examples from eroded areas such as the one we observed in El Hierro (Canary Islands, Spain). Figure 3 shows two buried monogenetic cones intersected by a vertical scarp on the coast of El Hierro. This situation allows observing a cross-section of both cones with their feeding dykes enlarging to flattened rounded massive units at the center of the volcanoes. This would correspond to the resistive heart R1 of the Pujalós volcano (Figure 1c). The conduit enlarging in the very superficial part of the eruptive system is quite compatible with conclusions made by Valentine (2012). It can be interpreted as spatter deposits, which are the most proximal products to volcanic vents and directly connected to the eruptive conduit. In the Pujalós, resistive layer R2 can be compared to the stratified accumulation of scoria visible in the monogenetic cones of El Hierro. The resistivity values decreasing at depth (C2) may correspond to the basement, dipping NW. Because of the position of the profile we cannot confirm or infer the presence of a lava flow to the west. Finally, the conductive superficial layer C1 corresponds to the postvolcanic cover, thicker in the northwestern cultivated fields area.

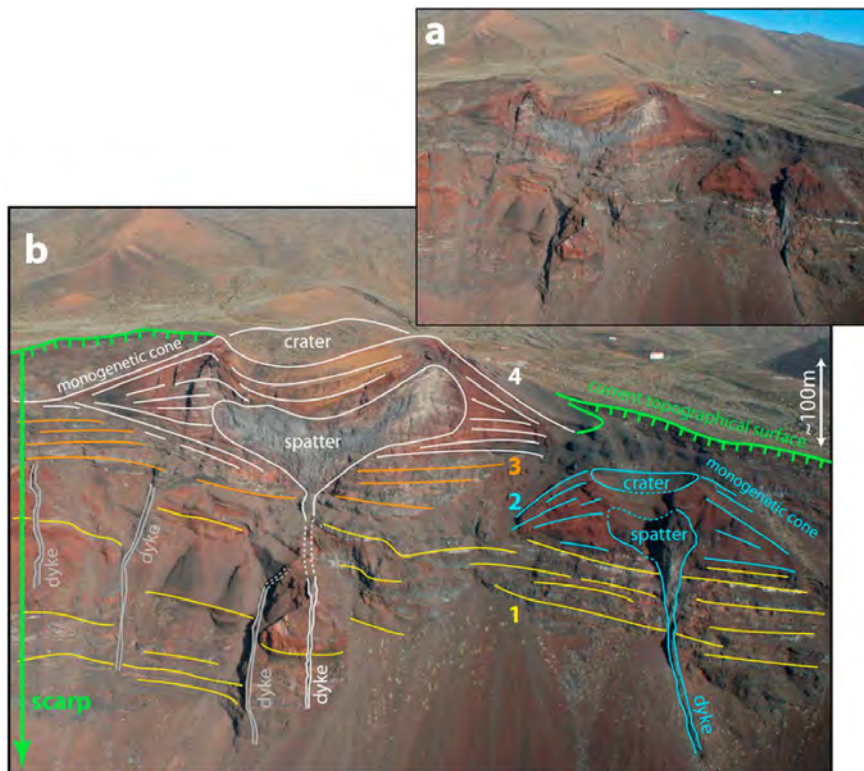


Fig. 3. (a) Photography of two monogenetic cones intersected by a cliff at the western point of El Hierro (Canary Islands, Spain). (b) Interpretation. Numbers associated to a color code corresponds to a chronological order.

The repartition of the resistivity inside Montsacopa and Puig d'Àdri appears more complex than for the Pujalós volcano, reflecting their more complex eruptive histories. Montsacopa shows a sequence involving a Strombolian phase at the beginning and a hydromagmatic one at the end (Martí et al., 2011). In addition to the summit well-visible crater, stratigraphical study of the volcanic deposits suggest the existence of a hidden vent on the southeastern flank (Bolós, 2009), which is confirmed by ERT. In the SE flank, we interpret the lower resistivity body C4 as crater A infill, i.e., breccias associated to Strombolian explosions (Figure 2b). This unit is likely surrounded by spatter deposits (R5). The connection with a feeding conduit is not visible on the tomogram, most probably because the profile is offset on a side of the crater. The continuation of R5 to the SE can be

interpreted as a lava flow (Figure 2c). Under this system, the lower resistivity values may correspond to material with a higher open porosity and/or alteration (Loke, 2002). According to the position of this unit in the edifice, it is compatible with fallout deposits that can be associated to the early activity of crater A. These deposits may have been cut-off to the NW by an explosion giving birth to crater B. This ~150m wide cavity was likely filled by welded deposits forming R3 high-resistivity body. However, note that the inversion process may be affected by superficial strong resistivity contrasts (Loke, 2002) and the resistivity values of this body may be overestimated. These rocks being inaccessible and no similar rocks outcropping, no laboratory measurement of the real resistivity could be performed. The lenticular conductive layer C3 consists of postvolcanic products filling crater B. The NW flank of the volcano can be interpreted as an accumulation of proximal fallout deposits associated to crater B, with intercalation of more resistive lava flows (R4). Indeed, outcrops at the NW of the volcano, close to our profile, show a superposition of two lava flows attributed to the activity of Montsacopa (Bolós, 2009).

Martí et al. (2011) describe a complex eruptive history for the Puig d'Àdri volcano, involving successive hydromagmatic and Strombolian phases. On the corresponding ERT profile the hydromagmatic deposits of the eastern side of the profile and the Strombolian deposits inside the limits of the tuff-cone (Pujadas et al., 1997; Martí et al., 2011) are well-identifiable (Figures 2e and 2f). In the east, the successive layers of different resistivity values correspond, from the surface to the base, to postvolcanic deposits on two hydromagmatic units. The upper hydromagmatic deposits (R6) show higher resistivity values with respect to the underlying deposits possibly because of a higher degree of compaction, reducing its permeability and then its water content. The underlying tuff ring deposits (Figure 2f) consist mainly of surges, explosion breccias, and a pyroclastic flow (Martí et al., 2011). Conductive layer C5, visible at the inferior limit of the tomogram, likely corresponds to marls and sandstones constituting the basement. Its spatial relationship with both the hydromagmatic and Strombolian units and its resistivity, are fully compatible with this interpretation. The most uncommon observation provided by our ERT data concerns the Strombolian unit, represented in red tones in Figure 2f and corresponding to the highest resistivity values. A less-resistive 10 to 20m large column occupies a central position inside the Strombolian cone and connects the deep layer to the surface. We believe that this lower resistivity values correspond to an accumulation of brecciated material partly consolidated,

plugging the feeding conduit of the Strombolian cone. To our knowledge this is the first time that this has been shown with geophysical imaging. Finally, we interpret R8, at the western side of the profile, as the two lava flows described by Martí et al. (2011) that caused the breaching of the northwestern flank of the scoria cone. The underlying deposits are likely to be attributed to the hydromagmatic anterior phase. The interface between the lava flows and the Strombolian cone may constitute a preferential path for meteoric water infiltration, triggering progressive weathering of rocks and thus leading to decrease the resistivity. This would explain the deepening of the conductive superficial layer observed (blue arrow in Figure 2f). A similar explanation can be proposed for the slight deepening of the conductive superficial layer into the eruptive conduit, even if we are here at the limit of the spatial resolution of the ERT measurements.

5.7. Conclusion

We show that volcanic cones exclusively derived from magmatic activity, built by the accumulation of scoria with occasional emission of lava flows, are easily distinguished from more complex edifices affected by hydromagmatic phases. ERT offers a strong advantage regarding spatial resolution and depth of exploration with respect to other geophysical methods, for the study of monogenetic volcanoes. With complementary surface geological observations either on site or using other natural examples, we could highlight various elements of the structure of these volcanoes and evidence several types of volcanic products such as (1) spatter deposits in the central part of the cones, (2) contrasts between hydromagmatic and Strombolian deposits, (3) buried lava flows, (4) the hidden eruptive vent of the Montsacopa volcano, and (5) the eruptive conduit of the Puig d'Àdri Strombolian cone. We think that high-resolution ERT is a powerful tool for the study of the internal structure of monogenetic volcanoes. The detailed structural and geological interpretation of such data is a valuable contribution to enhance knowledge about volcanic hazards in monogenetic volcanic fields in general. Because this method gives information about the past volcanic dynamics, it is particularly interesting for the forecast of future activity in a given monogenetic volcanic field.

Acknowledgements:

S. Barde-Cabusson was funded by JAE-Doc Program (JAEDoc_09_01319). This study was partially funded by the European Commission (FP7 Theme: ENV.2011.1.3.3-1; grant 282759: "VUELCO"), and by the grant Beca d'investigació "Oriol de Bolós" en Ciències Naturals (Olot, Spain). We thank the Natural Park of the Garrotxa Volcanic Zone for its support. We sincerely thank the Editor Andrew Newman, Karoly Nemeth and an anonymous reviewer for the improvements made from their comments.

References:

- Araña, V., A. Aparicio, C. Martín-Escorza, L. García Cacho, R. Ortiz, R. Vaquer, F. Barberi, G. Ferrara, J. Albert, and X. Gassiot (1983), El volcanismo Neógeno-Cuaternario de Catalunya: caracteres estructurales, petrológicos y geodinámicos, *Acta Geol. Hisp.*, 18, 1–17.
- Blaikie, T. N., L. Ailleres, R. A. F. Cas, and P. G. Betts (2012), Threedimensional potential field modelling of a multi-vent maar-diatreme - The Lake Coragulac maar, Newer Volcanics Province, south-eastern Australia, *J. Volcanol. Geoth. Res.*, 235–236, 70–83, doi:10.1016/j.jvolgeores.2012.05.002.
- Bolós, X. (2009), Characterization of the Montsacopa volcano and its surroundings (in English, Spanish, and Catalan). Web access <http://bit.ly/ZqkAaY>, Garrotxa Volcanic Natural Parc, Olot, Spain.
- Bolós, X., S. Barde-Cabusson, D. Pedrazzi, J. Martí, A. Casas, M. Himi, and R. Lovera (2012), Investigation of the inner structure of La Crosa de Sant Dalmai maar (Catalan Volcanic Zone, Spain), *J. Volcanol. Geoth. Res.*, 247–248, 37–48, doi:10.1016/j.jvolgeores.2012.08.003.
- Cassidy, J., S. J. France, and C. A. Locke (2007), Gravity and magnetic investigation of maar volcanoes, Auckland volcanic field, New Zealand, *J. Volcanol. Geoth. Res.*, 159, 153–163, doi:10.1016/j.jvolgeores.2006.06.007.
- De la Cruz-Reyna, S., and I. Yokoyama (2011), A geophysical characterization of monogenetic volcanism, *Geofis. Int.*, 50(4), 465–484.
- Downes, H. (2001), Formation and modification of the shallow subcontinental lithospheric mantle: a review of geochemical evidence from ultramafic xenolith suites and tectonically emplaced ultramafic massifs of Western and Central Europe, *J. Petrol.*, 42, 233–250.
- Gebhardt, A. C., M. De Batist, F. Niessen, F. S. Anselmetti, D. Ariztegui, T. Habertzettl, C. Kopsch, C. Ohlendorf, and B. Zolitschka (2011), Deciphering lake and maar geometries from seismic refraction and reflection surveys in Laguna Potrok Aike (southern Patagonia, Argentina), *J. Volcanol. Geoth. Res.*, 201, 357–363, doi:10.1016/j.jvolgeores.2010.12.019.
- Geshi, N., K. Németh, and T. Oikawa (2011), Growth of phreatomagmatic explosion craters: A model inferred from Suoana crater in Miyakejima Volcano, Japan, *J. Volcanol. Geoth. Res.*, 201(1–4), 30–38, doi:10.1016/j.jvolgeores.2010.11.012.
- de Groot-Hedlin, C., and S. Constable (1990), Occam's inversion to generate smooth, two-dimensional models from magnetotelluric data, *Geophysics*, 55, 1613–1624.
- Institut Geològic de Catalunya (IGC), Institut Cartogràfic de Catalunya (ICC), and Parc Natural de la Zona Volcànica de la Garrotxa (PNZVG) (2007), Carta Vulcanològica de la Zona Volcànica de la Garrotxa, 1:25.000, Ed.: Institut Cartogràfic de Catalunya, Barcelona.
- Kereszturi G., and K. Németh (2012), Monogenetic Basaltic Volcanoes: Genetic Classification, Growth, Geomorphology and Degradation, in *Updates in Volcanology - New Advances in Understanding Volcanic Systems*, edited by K.
- Nemeth, Jeddah, Kingdom of Saudi Arabia, ISBN: 978-953-51-0915-0, InTech, doi:10.5772/51387.
- Loke, M. H. (2002). RES2DINV ver. 3.54. Rapid 2-D resistivity and IP inversion using the least square method. Geotomo Software.

- Martí, J., and J. M. Mallarach (1987), Erupciones hidromagmáticas en el volcanismo cuaternario de Olot, *Estudios Geológicos*, 43, 31–40.
- Martí, J., J. Mitjavila, E. Roca, and A. Aparicio (1992), Cenozoic magmatism of the Valencia trough (WesternMediterranean): relation between structural evolution and Volcanism, *Tectonophysics*, 203, 145–166.
- Martí, J., L. Planagumà, A. Geyer, E. Canal, and D. Pedrazzi (2011), Complex interaction between Strombolian and phreatomagmatic eruptions in the Quaternary monogenetic volcanism of the Catalan Volcanic Zone (NE of Spain), *J. Volcanol. Geoth. Res.*, 201(1–4), 178–193.
- Martín-Serrano, A., J. Vegas, A. García-Cortés, L. Galán, J. L. Gallardo-Millán, S. Martín-Alfageme, F. M. Rubio, P. I. Ibarra, A. Granda, A. Pérez-González, and J. L. García-Lobón (2009), Morphotectonic setting of maar lakes in the Campo de Calatrava Volcanic Field (Central Spain, SW Europe), *Sediment. Geol.*, 222, 52–63.
- Mathieu, L., B. van Wyk de Vries, E. P. Holohan, and V. R. Troll (2008), Dykes, cups, saucers and sills: Analogue experiments on magma intrusion into brittle rocks, *Earth Planet. Sci. Lett.*, 271(1–4), 1–13, doi:10.1016/j.epsl.2008.02.020.
- Mrlina, J., H. Kämpf, C. Kroner, J. Mingram, M. Stebich, A. Brauer, W. H. Geissler, J. Kallmeyer, H. Matthes, and M. Seidl (2009), Discovery of the first Quaternary maar in the Bohemian Massif, Central Europe, based on combined geophysical and geological surveys, *J. Volcanol. Geoth. Res.*, 182, 97–112, doi:10.1016/j.jvolgeores.2009.01.027.
- Pedrazzi, D., and J. Marti (2011), Interaction between Strombolian and phreatomagmatic eruptions in the monogenetic volcanic fields of the Iberian Peninsula and Lanzarote Island, A. Rittmann Conference, Nicolosi (Catania), 7–9 June 2011.
- Portal, A., et al. (2013), Inner structure of the Puy de Dôme volcano: crosscomparison of geophysical models (ERT, gravimetry, muon imaging), *Geosci. Instrum. Method. Data Syst.*, 2, 47–54, doi:10.5194/gi-2-47-2013.
- Pujadas, A., L. Pallí, D. Brusi, and C. Roqué (1997), *El Vulcanisme de la Vall de Llémena*, Universitat de Girona, Spain (Eds.).
- Revil, A., et al. (2008), Inner structure of La Fossa di Vulcano (Vulcano Island, southern Tyrrhenian Sea, Italy) revealed by high resolution electric resistivity tomography coupled with self-potential, temperature, and soil CO₂ diffuse degassing measurements, *J. Geophys. Res.*, 113, B07207, doi:10.1029/2007JB005394.
- Revil, A., et al. (2011), Hydrogeology of Stromboli volcano, Aeolian Islands (Italy) from the interpretation of resistivity tomograms, self-potential, soil temperature, and soil CO₂ concentration measurements, *Geophys. J. Int.*, 186, 1078–1094, doi:10.1111/j.1365-246X.2011.05112.x.
- Sasaki, Y. (1992), Resolution of resistivity tomography inferred from numerical simulation, *Geophys. Prospect.*, 40, 453–464.
- Valentine, G. A. (2012), Shallow plumbing systems for small-volume basaltic volcanoes, 2: Evidence from crustal xenoliths at scoria cones and maars, *J. Volcanol. Geoth. Res.*, 223–224, 47–63, doi:10.1016/j.jvolgeores.2012.01.012.
- Valentine, G. A., and T. K. P. Gregg (2008), Continental basaltic volcanism—processs and problems, *J. Volcanol. Geoth. Res.*, 177, 857–873.
- Walker, G. P. L. (2000), Basaltic volcanoes and volcanic systems, in *Encyclopedia of Volcanoes*, edited by Sigurdsson, H., pp. 283–289, Academic Press, San Francisco (CA).

6

Volcanic stratigraphy of the Quaternary La Garrotxa Volcanic Field (NE Iberian Peninsula)

Accepted for publication in:

Journal of Quaternary Science

Authors of the paper:

Xavier Bolós^(a)

Llorenç Planagumà^(b)

Joan Martí^(a)

a) Institute of Earth Sciences Jaume Almera, ICTJA-CSIC, Group of Volcanology. SIMGEO (UB-CSIC) Lluís Sole i Sabaris s/n, 08028 Barcelona, Spain

b) Tosca, Environment Services of Education, Casal dels Volcans, Av. Santa Coloma, 17800 Olot, Spain

6.1. Abstract

The monogenetic Quaternary La Garrotxa Volcanic Field forms part of the Catalan Volcanic Zone (NE Iberian Peninsula), one of the alkaline volcanic provinces of the European rift system. It harbours in total more than 50 basaltic monogenetic cones that range in age from the Middle Pleistocene to the early Holocene and include cinder and scoria cones, lava flows, tuff rings and maars. This study is the result of 10 years work, during which we conducted extensive fieldwork, including the study of ephemeral outcrops and the stratigraphic logging of new water wells and geotechnical drill holes, taking also into account the existing information gathered by recent geophysical studies that have applied shallow geophysical methods to establish the substrate geology of this volcanic field. As a result we have obtained a comprehensive volcanic stratigraphy of the area that identifies the products of each single eruption, their relative stratigraphy and their surface area. This volcanic stratigraphy constitutes an essential tool for understanding the evolution of this volcanic field and for establishing a correct volcanic hazard assessment of the area, but it also provides a precise reference for the Quaternary tephrochronology of the lake sediments in neighbouring areas.

Keywords: Quaternary volcanism · volcano-stratigraphy · monogenetic volcanism · Garrotxa volcanic field · hazard assessment

6.2. Introduction

Volcanic terrains are characterised by the complex stratigraphic relationships of their products whose causes include, variously, the extremely rapid depositional rates compared with conventional sub-aerial and submarine sedimentary environments, the friable character of many volcanic deposits, which facilitate their rapid erosion, the contrasting influence of topography on the emplacement of volcanic products, and rapid changes in facies. Such complexity constitutes one of the main obstacles when reconstructing the geological evolution of volcanic areas. This is even more problematic in highly urbanised areas where construction activities modify the original morphology of the area and hide many natural features, and where deposits are often lost to quarrying. This may impose a limitation to construct a volcanic hazard model from such active volcanic areas, as establishing correct stratigraphic relationships may be challenged due to the ignorance of part of the volcanological record.

The stratigraphic and volcanological evolution of the different volcanic fields of the Neogene-Quaternary volcanism associated with the European Cenozoic Rift System are still poorly known. Although several detailed petrological and geochemical studies of this magmatic episode have been conducted in recent decades aimed at understanding its petrogenesis and geodynamic constraints (Wilson and Downes, 1991, 1992, 2006; Hoernle et al., 1995; Wilson and Bianchini, 1999; Wilson and Petterson, 2001; Lustrino and Wilson, 2007), the eruptive history and geochronology of the different areas where this volcanic activity occurred, are not well constrained. In many cases this has hindered the definition of

the evolution of the volcanism in each area, thereby generating uncertainty around the relative age of volcanic episodes and recurrence cycles. It also complicates any comprehensive hazard assessment in these areas, some of which have been active into Mid-Holocene.

One of the least studied of these recent European volcanic areas is the Catalan Volcanic Zone (Martí et al., 1992) located in the northeast of the Iberian Peninsula. Its activity started over 12 Ma ago and continued until the early Holocene. The Quaternary La Garrotxa Volcanic Field (GVF) (Martí et al., 2011) is the youngest (Middle Pleistocene to early Holocene) and best preserved of these volcanic areas. However, its surface outcrops are just part of the complex geology that has been constructed during the over 700 ka of intermittent volcanism in this area. In this paper we present a comprehensive volcanic stratigraphy of the GVF. This work is based on ten years of systematic recognition and characterisation of all ephemeral outcrops exposed on construction sites and data from all new wells and geotechnical boreholes. Geological data have been complemented with results from recent geophysical studies on the substrate geology of the GVF (Bolós et al., 2012, in press; Barde-Cabusson et al., 2013, 2014;), in order to obtain a more precise picture of the subsoil geology of the area and to better define the corresponding stratigraphic relationships. We describe the results obtained and discuss their implications for the study of the evolution of this volcanic area and for assessing potential hazard and tephrochronological correlations in the area.

6.3. Geological setting

Situated in the northeast of the Iberian Peninsula, the Garrotxa Volcanic Field (GVF) is part of the Catalan Volcanic Zone and one of the provinces of the Neogene-Quaternary alkaline volcanism associated with the European rift system. It covers about 600 km² and is located between the cities of Olot and Girona (Fig. 1). This basaltic volcanic field contains over 50 cones (including both cinder and scoria cones), lava flows, tuff rings and maars dating from the Middle Pleistocene to early Holocene that rest on upper Palaeozoic granites and schists, or on sedimentary Eocene and Quaternary substrates. Available petrological and geochemical data indicate that the products of this volcanic region range from strongly silica-undersaturated to nearly silica-saturated compositions (Araña et al., 1983; López-Ruiz and Rodríguez-Badiola, 1985; Cebriá et al., 2000; Martí et al., 1992). This region comprises a suite of intracontinental leucite, basanites, nepheline basanites and alkali olivine basalts, which in most cases represent primary or nearly primary liquids (Cebriá et al., 2000). The geochemical characteristics of these lavas are very similar to the analogous petrologic types of other Cenozoic volcanics of Europe, which are intermediate between HIMU, DM and EM1 (Cebriá et al., 2000; Downes, 2001).

The GVF embraces two geographically distinct zones, the larger one located in the north in the area of La Garrotxa and a southerly area that contains fewer but larger and more complex volcanic edifices (Martí et al., 2011) (Fig. 1). Although both corresponding to tectonically controlled depressions, the northern zone has a substrate of thick layers of Tertiary and Quaternary sediments, whereas the southern zone is floored by unconsolidated Quaternary sediments in combination with the Palaeozoic basement.

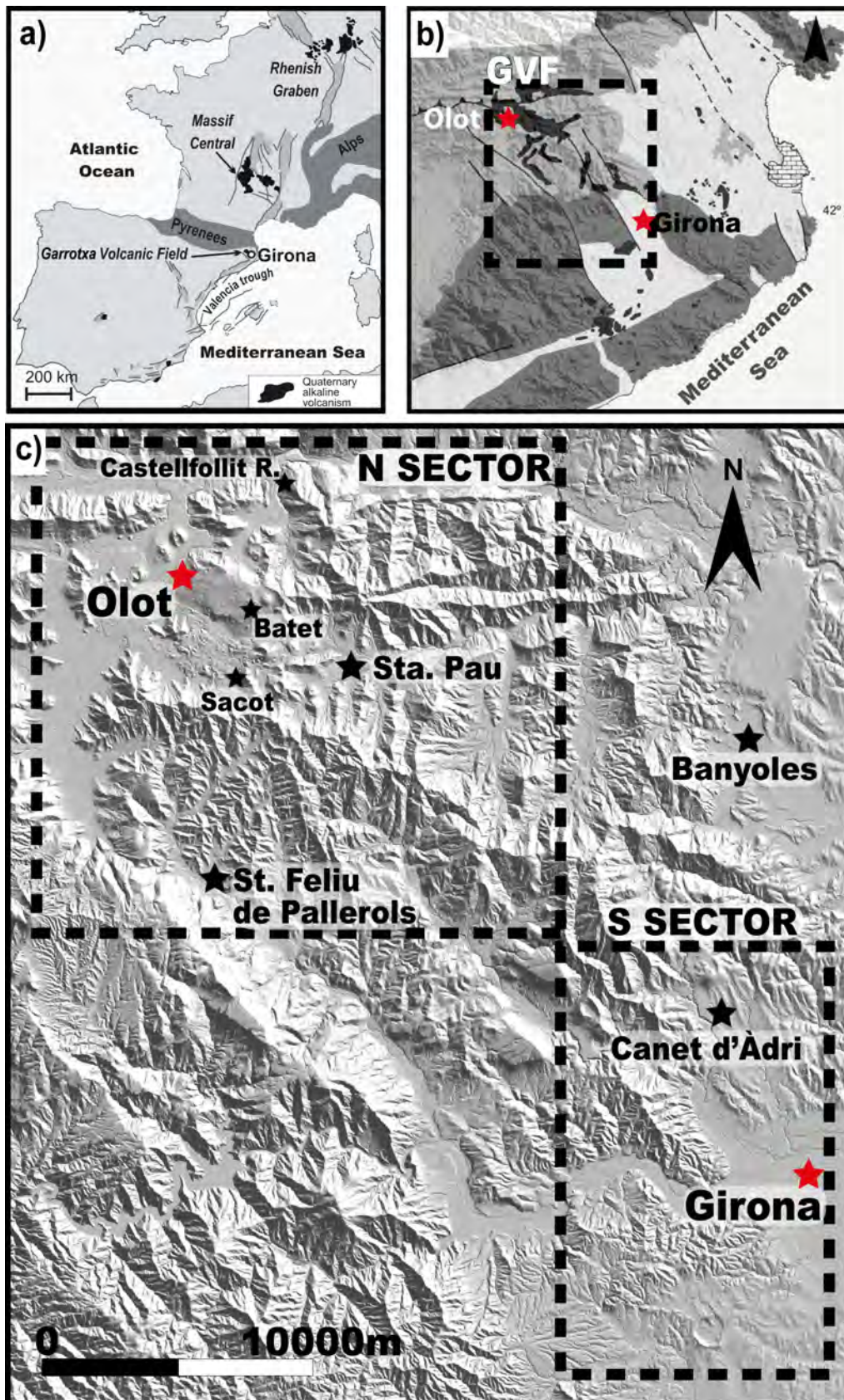


Fig. 1. Map of the study area. a) Simplified map of the distribution of the European rift system. b) Simplified geological map of the Catalan Volcanic Zone (Modified from Guérin et al., 1985). c) Geographic distribution of the Garrotxa Quaternary volcanic field

Volcanic activity in the GVF is characterised by numerous small cinder cones built during short-lived monogenetic eruptions along tectonic related volcanic fissures. The total volume of extruded magma in each eruption was between 0.01 and 0.2 km³ (DRE). Strombolian and phreatomagmatic episodes alternated in most of these eruptions and gave rise to complex stratigraphic sequences composed of a broad range of pyroclastic deposits (Martí et al., 2011; Cimarelli et al., 2013). The eruption sequences differ from one cone to another and demonstrate that the eruptions did not follow a common pattern, particularly in cases of magma/water interaction. This complex eruptive behaviour may be related to the differing stratigraphic, structural and hydrogeological characteristics of the substrate below each volcano rather than to any differences in the physicochemistry of the erupting magmas, which are generally fairly homogeneous throughout the GVF (Martí et al., 2011).

The eruptive fissures that controlled the volcanic activity in the GVF correspond to NNW-SSE and NNE-SSW oriented Neogene tectonic structures (Cimarelli et al., 2013; Barde-Cabusson et al., 2013, 2014; Bolós et al., in press). This suggests that the ascent and eruption of the magmas originated at the base of the lithosphere (Martí et al., 1992) was guided by the same regional faults system that bound the area's horsts and grabens. This explains the high magma ascent velocities (0.2m/s) found in these volcanic materials, which together with the presence of mantle xenoliths and lower crust cumulates suggest that some of the eruptive fissures and faults extended to the base of the lithosphere (Martí et al., 1992).

An important part of the northern zone of the GVF now lies underneath the city of Olot (almost 40,000 inhabitants), a highly industrialised and urbanised area covering about 30 km². The deposits of the five recent volcanic cones (Montolivet, Montsacopa, La Garrinada, Bisaroques and Ca l'Isidret) located in the middle of the city (Fig. 2) have been partially covered by or removed due to urban and industrial construction. Furthermore, a dense carpet of vegetation covers other parts of the GVF and thus the surface geology of the area is not always visible. Traditionally, these factors have hampered geological mapping and stratigraphic correlations and in part explain the incomplete knowledge of the volcanological evolution of this area.



Fig. 2. Aerial view of the city of Olot and its volcanic cones. Photography by SIGMA

6.4. Methodology

The lack of continuous outcrops due to partial erosion of the deposits, coverage by younger products and/or human-induced modification of terrains due construction activities, as well as the apparent similarity of most of these deposits, mean that stratigraphic correlation and the determination of the relative ages of these outcrops is not a straightforward task. To sort out these limitations we carried out extensive fieldwork including the study of ephemeral outcrops and the stratigraphic logging of water wells and geotechnical drill holes (Fig. 3).

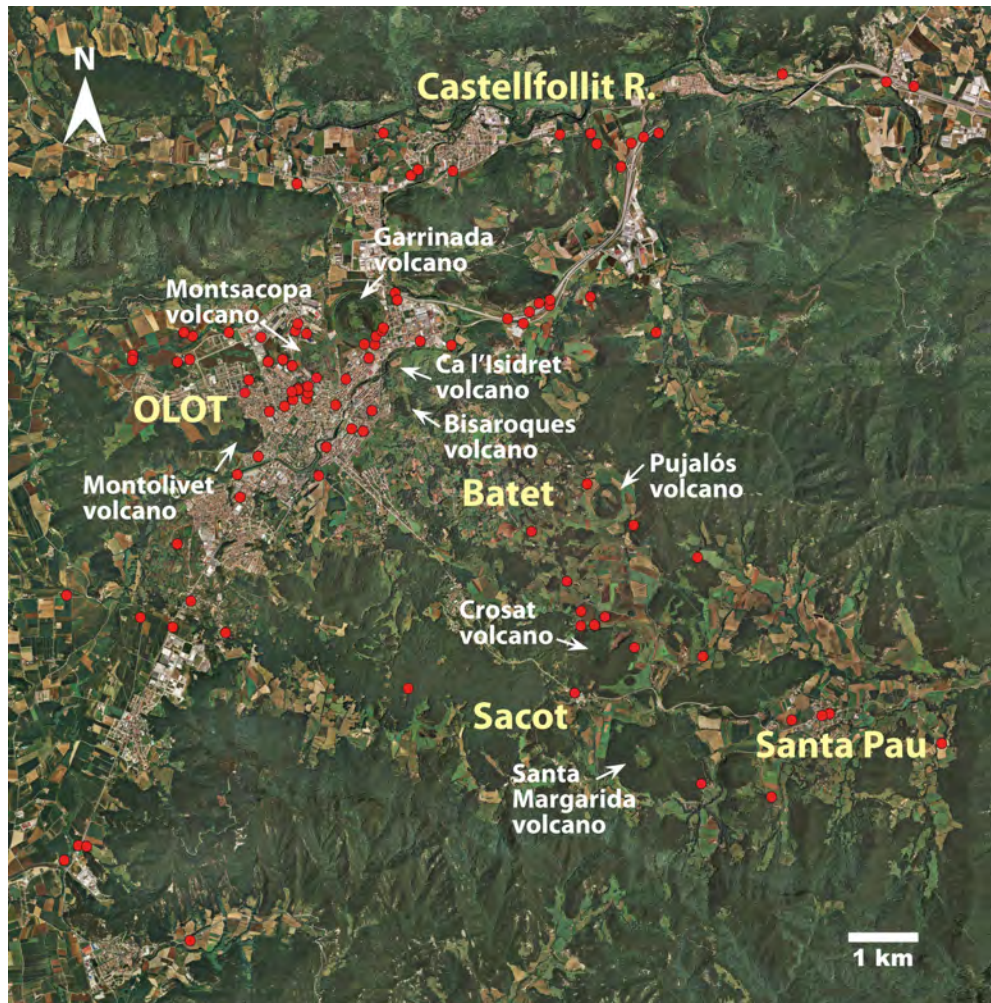


Fig. 3. Location of the studied ephemeral outcrops, water wells and geotechnical drill holes.

In addition, we also considered the existing information gathered by recent geophysical studies that have applied shallow geophysical methods to establish the substrate geology of the GVF (Bolós et al., 2012, in press; Barde-Cabusson et al., 2013, 2014). Finally, we also used basic petrology and geochemistry including mineral chemistry to identify possible fingerprints that could establish a precise correlation between these deposits and determine their relative stratigraphy, as it has been done in similar studies (e.g.: García et al., 2014). However, in this case the results obtained were not relevant to establish a systematic distinction of deposits from different eruptions based on petrological criteria, so these results were not considered to establish our volcanic stratigraphy and are not presented in this study. The use of precise

petrological fingerprints with this type of volcanic rock would require a much more detailed petrological study, which is beyond the main purpose of this study.

We used as a reference the geological 1:25,000-scale maps of the Catalan Geological Survey (IGC, 2003, 2007), which were substantially modified by the new data obtained in this work. A shape file containing the new digital geological maps was combined with a 2-m resolution DEM of the area using an open GIS platform (QGIS) to obtain a graphic representation of the volcanic stratigraphy of the area. The legend of the maps includes the relative stratigraphy of the different mappable units that were identified.

Field geology consisted of a revision of the existing geological maps and the remapping of certain areas at different scales (1:5000 and 1:1000) using as a basis the topographic maps and orthophotographs produced by the Catalan Geographic Institute (www.icc.cat). These resources permitted us to identify most of the characteristics of the surface geology and, in particular, the contact between the volcanic and non-volcanic units, the superficial extent of the volcanic units, the direction of emplacement and position of vents, and a number of volcanic-related structural lineations.

Fieldwork was completed via the study of ephemeral outcrops (Fig. 4) and the stratigraphic logging of water wells and geotechnical drill holes (Fig. 3), which also provided information on the subsoil geology. Construction in built-up areas occasionally exposes new outcrops and large stratigraphic sections. However, the temporary nature of these outcrops is an important drawback and if they are not documented immediately they run the risk of being quickly lost. The same applies to geotechnical boreholes and wells. This information is frequently poorly recorded and often lost among the myriad of documents handled by local administrative bodies.

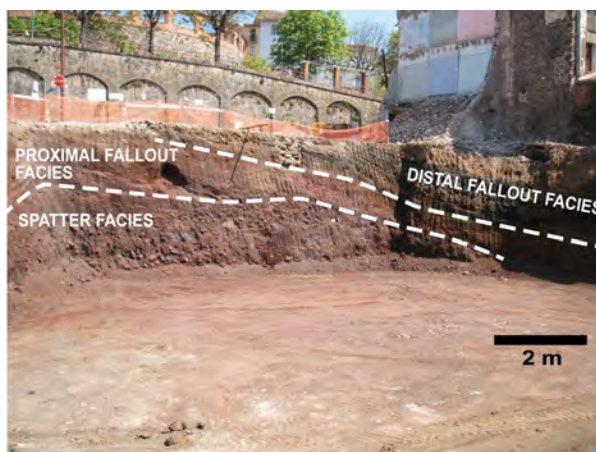


Fig. 4. Example of an ephemeral outcrop from Montsacopa member, visible during the construction of a new building.

Over the previous ten years we systematically studied most of the ephemeral outcrops in the GVF created by urban, industrial and infrastructure construction, as well as new water wells and geotechnical boreholes. In all, we described and catalogued almost 100 ephemeral outcrops (Fig. 3). The methodology applied consisted of three different steps that were followed in all cases. First, we designed a series of data sheets or templates for the systematic description of each ephemeral outcrop (Fig. 5) with space for notes on a series of variables including outcrop code, type of construction work, name of reviewer of the outcrop, location (UTM coordinates), a detailed field description, photographs, geological cross-sections, a stratigraphic column, an interpretation of the outcrop in the general geological context of the area, and other relevant observations. Second, we maintained close links with local authorities and the Catalan Geological Survey to ensure that we were warned well in advance of any new construction work in the area or any new wells or boreholes. We also developed a protocol for obtaining information from any public construction work planned at national level that was to

be carried out in the study area. Lastly, all the information obtained was incorporated into a geographical database developed using an open-access GIS platform (QGIS, www.qgis.org). A shape file containing all the new digital geological map sections was created with a 2-m-resolution DEM of the area.

Fig. 5. Data sheet designed for the systematic study and cataloguing of ephemeral outcrops (see text for explanation).

During the period of data collection we conducted stratigraphic logging of the geotechnical boreholes and water wells included in this study directly at each site during drilling operations. This allowed us to identify the different stratigraphic units and to obtain samples that were later studied at the laboratory. In most cases only cuttings were obtained from the drilling operations but they permitted to identify the different stratigraphic units with a high degree of accuracy. Also, we revised and incorporated, when relevant, information from previous boreholes recorded and classified by the Catalan Geological Survey.

The criteria used to establish the relative stratigraphy of the volcanic units were their field relationships, the stratigraphic relationships observed in boreholes and wells, morphometry-based relative dating using the degradation of volcanic cones (see Kereszturi et al., 2013), paleomagnetic correlations (Ll. Planagumà, unpublished data), the degree of alteration (weathering) of the volcanic materials, the presence of interbedded fluvial terraces, and absolute dates (if available). To estimate the volume of the deposits corresponding to the products of each eruption we took into account their spatial distribution and thickness variations. We measured in the laboratory densities from field samples from all types of volcanic materials (lavas, scoria, lapilli size pyroclasts, juvenile fragments in PDC deposits) and obtained an average density for each type. Then, the calculated volumes were converted into Dense Rock Equivalent volumes using a density of 2,53 for the magma that we obtained from a

glass made from a natural sample (Crosca lava flow) and applying the equation: $DRE (km^3) = \text{volume of volcanic deposit (km}^3) * \text{density of volcanic deposit (kg/m}^3) / \text{magma density (kg/m}^3)$, for each type of deposit belonging to the same eruption and then adding all the values to obtain the total volume in DRE for each eruption.

To complement the geological information obtained from the field studies, we also took into account the available geophysical information of the area, including gravity data, self-potential (SP) maps and electrical resistivity tomography (ERT), obtained in previous studies by the same working group (Bolós et al., 2012; in press; Barde-Cabusson et al., 2013, 2014). The combined interpretation of the geological and geophysical data provided detailed information on the internal structure of certain volcanic cones and the stratigraphy and shallow structure of the substrate on which the volcanoes were emplaced.

6.5. Volcanic stratigraphy vs. conventional stratigraphy

Before presenting and discussing the results of this study it is worthwhile first analysing the stratigraphic criteria used in this work. One of the key questions in understanding the evolution of an active volcano or a recent volcanic field is the volcanic stratigraphy, that is, the stratigraphic and chronological order in which the products of each eruption appear in the geological record. Volcanic stratigraphy is an essential part of field studies in volcanic areas everywhere and is necessary for generating geological maps, reconstructing the volcanological evolution and eruptive dynamics, and studying the physical volcanology and tephrostratigraphy (Connor, 1990; Nemeth et al., 2001, 2012; Palladino et al., 2010; Branca et al., 2011; Guillbaud et al., 2011; Groppelli and Martí, 2013).

Fisher and Schmincke (1984) proposed the use of volcanic activity units combining stratigraphic and volcanological criteria, a method that has the advantage of directly linking volcanic activity with the resulting stratigraphic record; the main unit is considered to be the individual eruption (Member) (Table 1). Another advantage of volcanic stratigraphic units is that they are very useful for understanding the eruptive dynamics of a given eruption or set of eruptions. However, they do not take into account inter-eruptive phenomena (e.g. debris flow, lahars, etc.), which may represent important elements in the life of a volcano and can have important chronological implications (Groppelli and Martí, 2013). Instead of this some authors (e.g. Groppelli et al., 2005; Giordano et al., 2010; Palladino et al., 2010; Branca et al., 2011; Cimarelli et al., 2013) prefer to use unconformity related units (synthems) in the study of volcanic successions. These type of stratigraphic units, initially defined by Chang (1975) and Salvador (1987) for sedimentary terrains, enable the time evolution of a volcanic area to be correlated with geological events acting on local, regional or global scales; an example would be the correlation of the timing and styles of volcanism in a volcanic province with regional tectonics (Palladino et al., 2010). In a similar way, volcanic activity may lead to the incorporation of a large amount of debris into a sedimentary system, thereby changing its dynamics and the sedimentation vs. erosional rates (Smith, 1991). All this may create normally low-rank unconformities in the stratigraphic record of an area that correspond to distinct volcanological-geological events. However, unconformity based units often show non-isochronous boundaries. This is the reason why geological units, members, formations and groups are preferred in many volcano-stratigraphic studies and also in this study.

In the GVF the recorded volcanism dates from the Middle Pleistocene to the early Holocene (Araña et al., 1983; Guerin et al., 1985; Lewis et al., 2000). During this period no significant geological changes have been recorded in the region (Martí et al., 1992) and so the observed stratigraphic unconformities are very local in scale and due to the irregular emplacement of volcanic products and not to any more widespread geological changes. In addition to this, the lack of geochronological data hampers the identification of groups of volcanic eruptions that could have occurred during the same time interval. For these reasons, we chose to use the formal volcano-stratigraphic unit member - in the sense defined by Fisher and Schminke (1984) – and mapped the eruptive units associated with each of the volcanic structures of this field.

Using the member as the fundamental volcano-stratigraphic unit we grouped all the products of a single eruption into the same stratigraphic member and distinguished each one from those pertaining to other eruptions or members. In each member, we distinguished different units corresponding to the products of the different pulses of a single eruption. This permitted us to characterise the eruption sequences and their mechanisms and understand how volcanism evolved with time; this in turn enabled us to identify any changes in the eruption style, the location of the vents, the size of the eruptions, the characteristics of their products, and their relative stratigraphy (age) and areal extent (Figs. 4 and 5). The information provided in this format is crucial not only for understanding the evolution of this volcanic area but also for the description of any potential hazards.

6.6. Results

The main outcome of this study is a new digital volcano-stratigraphic map of the GVF at scale 1:2000, which is summarised in Figs. 6 and 7. These new volcano-stratigraphic framework complements a previous study focused on the description of the successions of deposits characteristic of the GVF volcanoes (Martí et al., 2011), and improves the recent stratigraphy proposed by Cimarelli et al., 2013, which is based on different stratigraphic criteria (synthoms) and is partially incomplete due to the lack of subsoil information and that from the ephemeral outcrops. Table 2 summarises all the stratigraphic members (55 in all) that were identified in this study. The members are placed from the youngest (top) to the oldest (bottom) according to their relative stratigraphy (Fig. 8). Also given is an indication of whether the age is relative (i.e. it was established on the basis of observable stratigraphic relationships) or absolute (i.e. a geochronological – isotopic or paleontologic – date is available), as well as the corresponding reference source and the calculated erupted volumes (in Dense Rock Equivalent, DRE) when available.

The precision in establishing the stratigraphic relationships between the volcanic materials studied decreased progressively with their age, as the younger materials were better exposed and preserved, and located at shallower depths than the older ones, which were often only accessible through boreholes and wells or deep ephemeral outcrops. Due to the incomplete exposure some of the older units could have been missed. However, the systematics used in the construction of this volcanic stratigraphy will allow the incorporation of new stratigraphic units or the modification of their relative stratigraphic position in an easy way and without disturbing the rest of the information included.

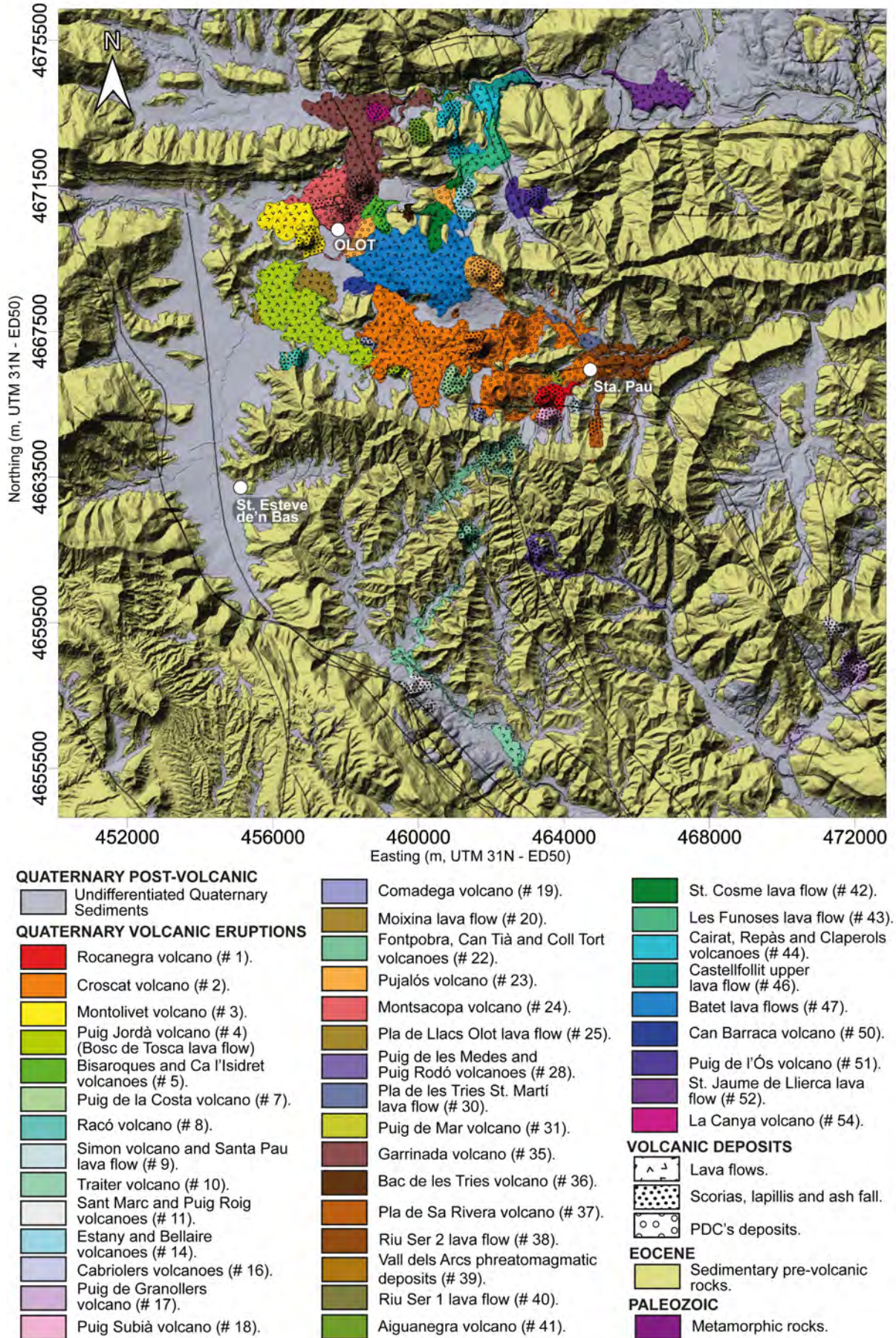


Fig. 6. Volcanic stratigraphy map of the northern sector of the Garrotxa Volcanic Field. A different colour based on the RGB scale was assigned to each member and different kinds of hatching were used to indicate different types of deposits (PDCs, lava flows, fallout, etc.). Numbers correspond to the stratigraphic order of Table 2. Numbers missing in this legend correspond to non-mappable (i.e.: only observable in boreholes and wells) stratigraphic units.

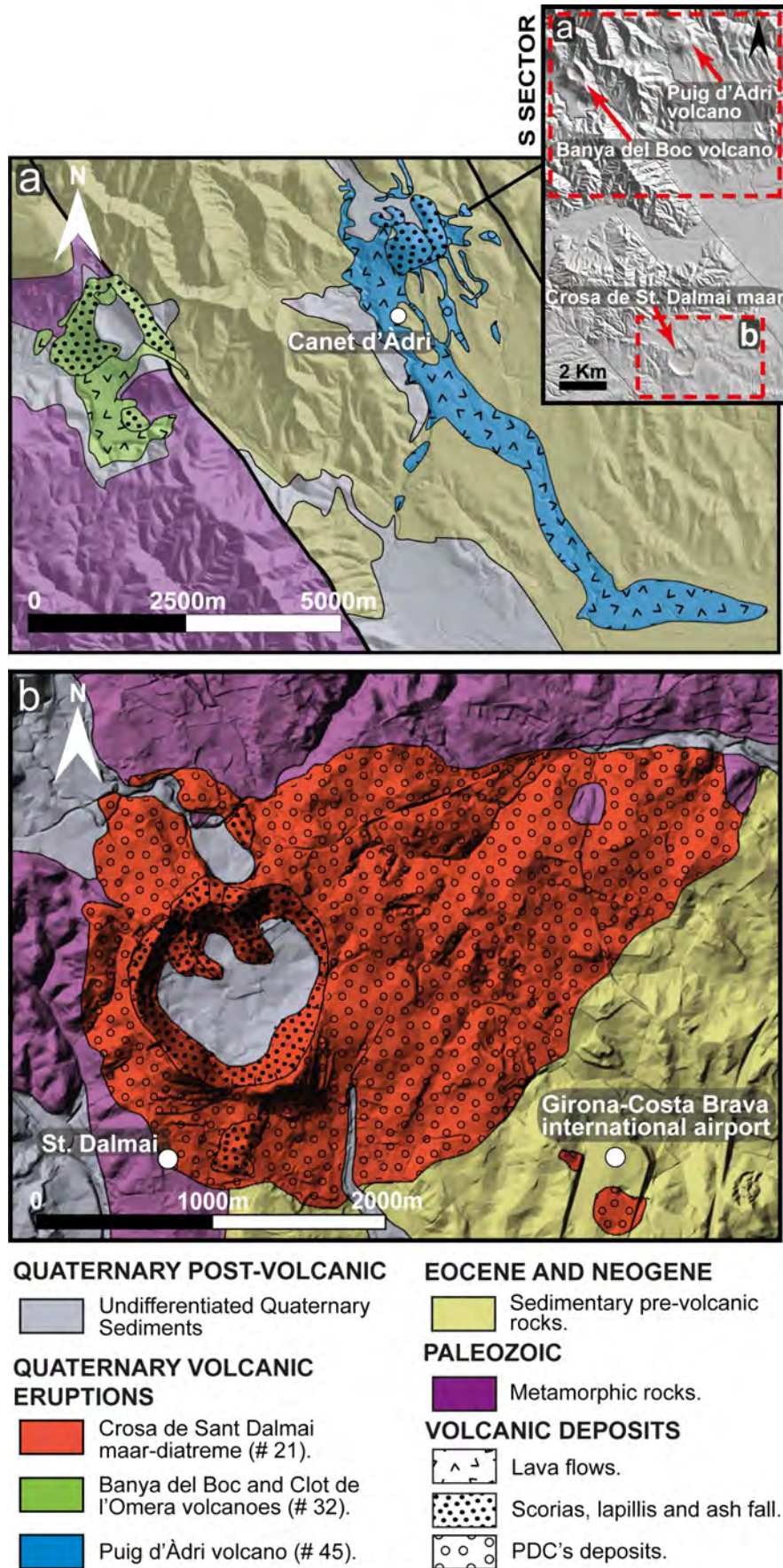


Figure 7. Volcanic stratigraphy map of the southern sector of the Garrotxa Volcanic Field.

When the source area or vent of the different volcano-stratigraphic units or members was plotted on a structural map of the area with the successive numbers of their relative ages (1 for the youngest, 55 for the oldest) indicated (Fig. 9), it becomes evident that most members are located on NNW-SSE-oriented Neogene fractures and faults, thereby confirming the findings of other authors (Martí et al, 2011; Cimarelli et al., 2013; Barde-Cabusson et al., 2014; Bolós et al., in press). These members have a rather scattered time-space distribution, albeit with a tendency for older eruptions (Middle Pleistocene) to be concentrated towards the north of the area. However, we observed no structural indicator that could suggest a similar tendency in the Neogene faults as suggested by Cimarelli et al (2013). Some of the eruptions developed in multiple phases and with multiple vents along the same eruption fissure (Martí et al., 2011), and are thus responsible for some of the clusters of vents that appear in Fig 8. However, a comparison of the different eruptions failed to identify any apparent concentration of vents at any specific location or at any specific time.

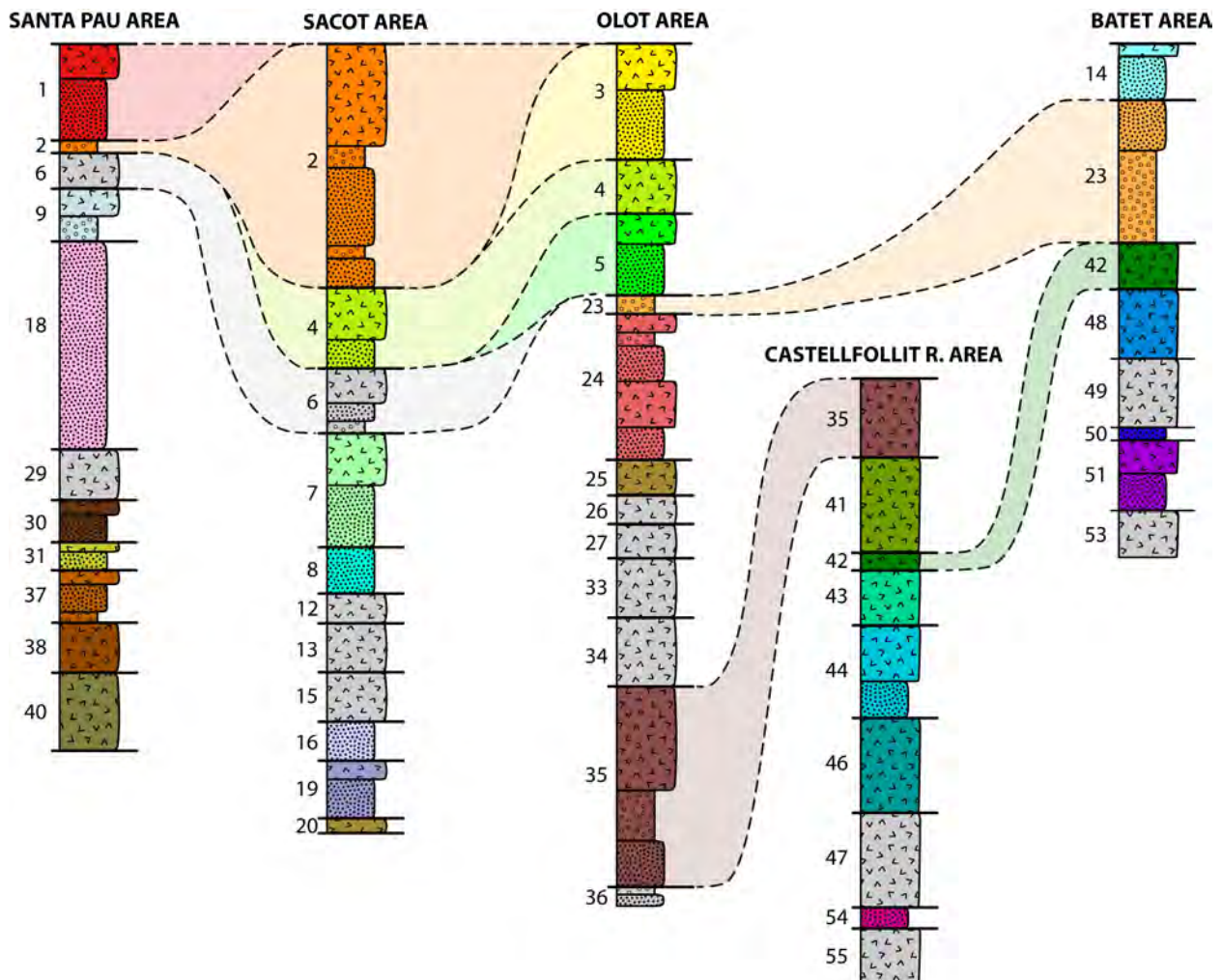
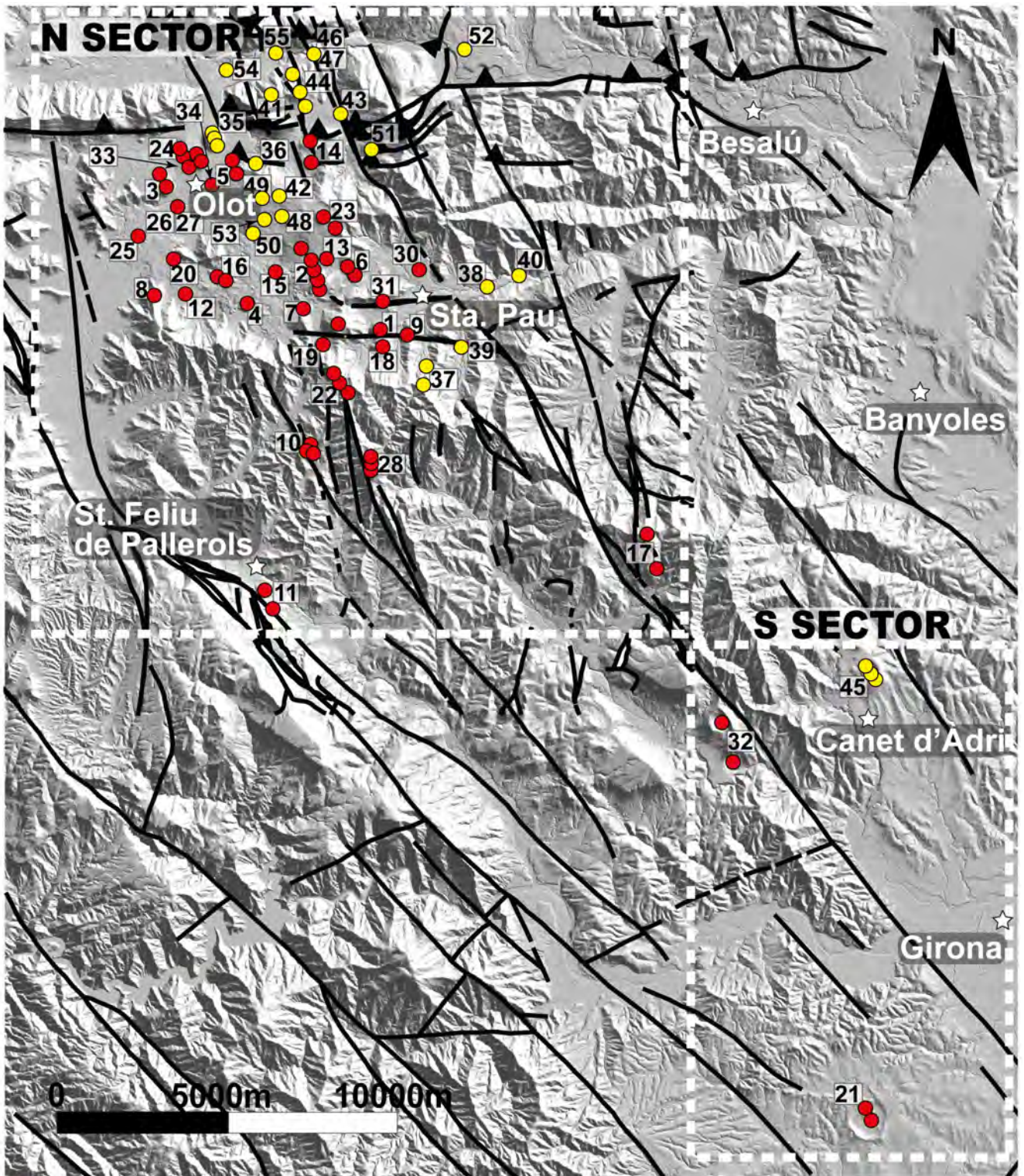


Fig. 8. Correlation of the main stratigraphic members identified in the northern sector of the GVF. Colours of different units are the same than in Fig. 6. In grey, units not observable at surface (i.e.: only visible in boreholes and wells). Numbers of different members as listed in Table 2. See Figures 1 and 3 for location of the stratigraphic logs.



- Holocene and Upper Pleistocene eruptions (0 to 126,000 years)
- Middle Pleistocene eruptions (126,000 to 781,000 years)
- Neogene normal faults
- ▲ Alpine thrusts

Fig. 9. Map of the vents and source areas of the different eruptions (members) listed in Table 2.

The volcanic materials of the studied stratigraphic units consist of lava flows and different types of fallout and pyroclastic density current deposits derived from Strombolian and phreatomagmatic eruptions. Martí et al. (2011) pointed out that different eruption sequences, corresponding either to purely magmatic or phreatomagmatic episodes and alternating Strombolian and phreatomagmatic phases, characterise the volcanoes of La Garrotxa. However, they did not identify neither the spatial relationships among the products of the different eruptions nor their relative stratigraphy. Our field stratigraphic study did not reveal any apparent time or space variation in the style of volcanism, thereby suggesting that differences in eruptive behaviour could be related to local variations in the characteristics (e.g. hydrogeology) of the substrate rather than to geological changes on a major scale.

The calculated volumes shown in Table 2 are all minimum estimates of the DRE and represent the minimum volume of magma erupted in each case and, consequently, the magnitude of the eruption. Not all calculated volumes have the same degree of accuracy, since not all deposits are completely exposed. This implies that the record presented here is incomplete and should be treated with care if used in further studies. The volumes obtained lie between 0.01–0.03 km³. However, a few eruptions (Crosca (2), Puig Subià (18), Crosca de Sant Dalmau (21), Puig de Banya del Boc (32), Garrinada (35), Puig d'Àdri (45) and Puig de l'Ós (51)) generated larger volumes, up to 0.2 km³, in the case of Crosca.

Other important results derive from this stratigraphic study at a more local and detailed level. The use of ephemeral outcrops, wells and boreholes (this work), in combination with results from the application of shallow geophysical methods (Bolós et al., 2012, in press; Barde-Cabusson, et al., 2013, 2014), permitted to obtain the volcanic stratigraphy of the highly urbanised – and, consequently, with a poorly exposed geology – area of Olot (Fig. 9), thus improving previous maps (Mallarach, 1982; IGC, 2003, 2007; Cimarelli et al., 2013) that could not show the same degree of detail. In this sector of the GVF we found very complex stratigraphic relationships between the city's five volcanic cones (Garrinada, Montsacopa, Bisaroques, Ca l'Isidret and Montolivet) (Fig. 10). In previous studies based on the surface geology observable in this built-up area, three of these volcanoes (Montolivet, Garrinada and Montsacopa) were assumed to belong either to the same eruption (Calderón et al, 1906; Sant Miguel de la Cámara and Marcet Riba, 1926; Mallarach and Riera, 1981) or to different eruptions occurring along the same NE-SW fracture (Gisbert et al., 2009). Our study reveals that, in fact, each cone corresponds to a different eruption, all of which are situated along NNW-SSE-oriented fissures. The study of the ephemeral outcrops enabled us to identify the stratigraphic relationships between deposits and discover that each succession of deposits was separated from the next by stratigraphic discontinuities (i.e. erosion surfaces, and paleosoils), which suggest that several thousand years elapsed between each eruption. The oldest of these volcanoes is now thought to be La Garrinada and the youngest Montolivet. In addition, we identified a previously unrevealed volcanic cone (Ca l'Isidret) that formed from a separate vent during the eruption of the Bisaroques volcano (Fig. 10). The volcanic fissures that formed these five cones run all in a NNW-SSE direction, as do most of the other eruptive fissures identified in this study.

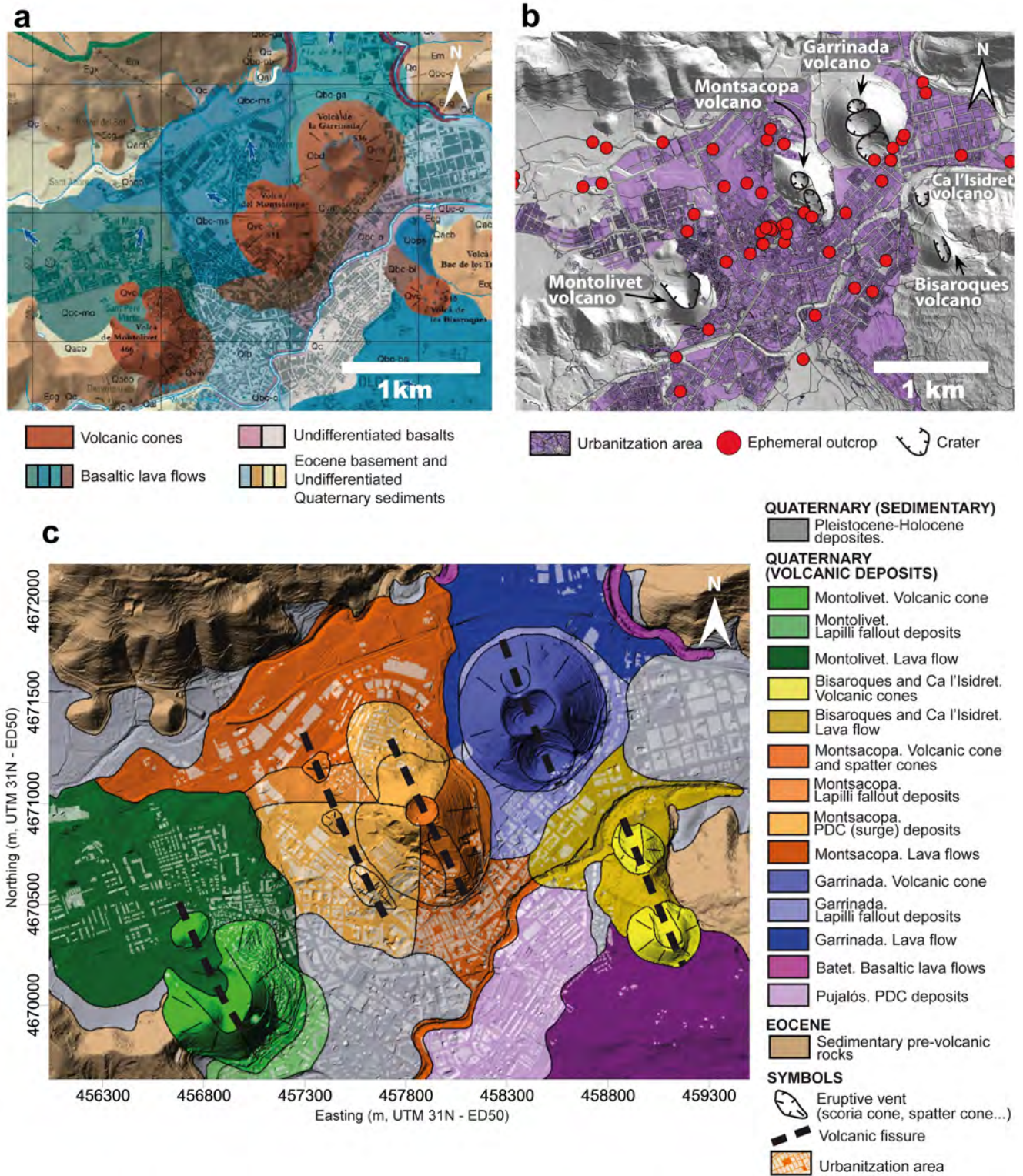


Fig. 10. a) Geological map of the Olot area made by the Catalan Geological Survey (IGC, 2007). (b) Main urbanised area (violet colour) and location of the studied ephemeral outcrops and boreholes. c) New geological map of the Olot area made in this study.

Moreover, in the case of La Garrinada, we used an ephemeral outcrop to complete the stratigraphic sequence partially established by Gisbert et al. (2009), thus providing better constraints to interpret its eruption sequence. Also, the study of 30 ephemeral outcrops

around Montsacopa (Fig. 11), combined with a revision of existing conventional outcrops, enabled us to identify the different vents and products generated during its construction, not envisaged in previous studies (e.g.: Martí et al., 2011; Cimarelli et al., 2013). The construction of this volcano resulted from a multivent fissural eruption. In total we identified up to five different vents on Montsacopa: a central cone and crater, which was the only previously known cone, two other vents whose products are mostly covered by those emitted from the main crater, and scoria deposits that were generated by two further vents. This multivent eruption included Strombolian and phreatomagmatic phases that generated a large variety of deposits including fallout, ballistic ejecta, pyroclastic density currents and lava flows (Fig. 10).

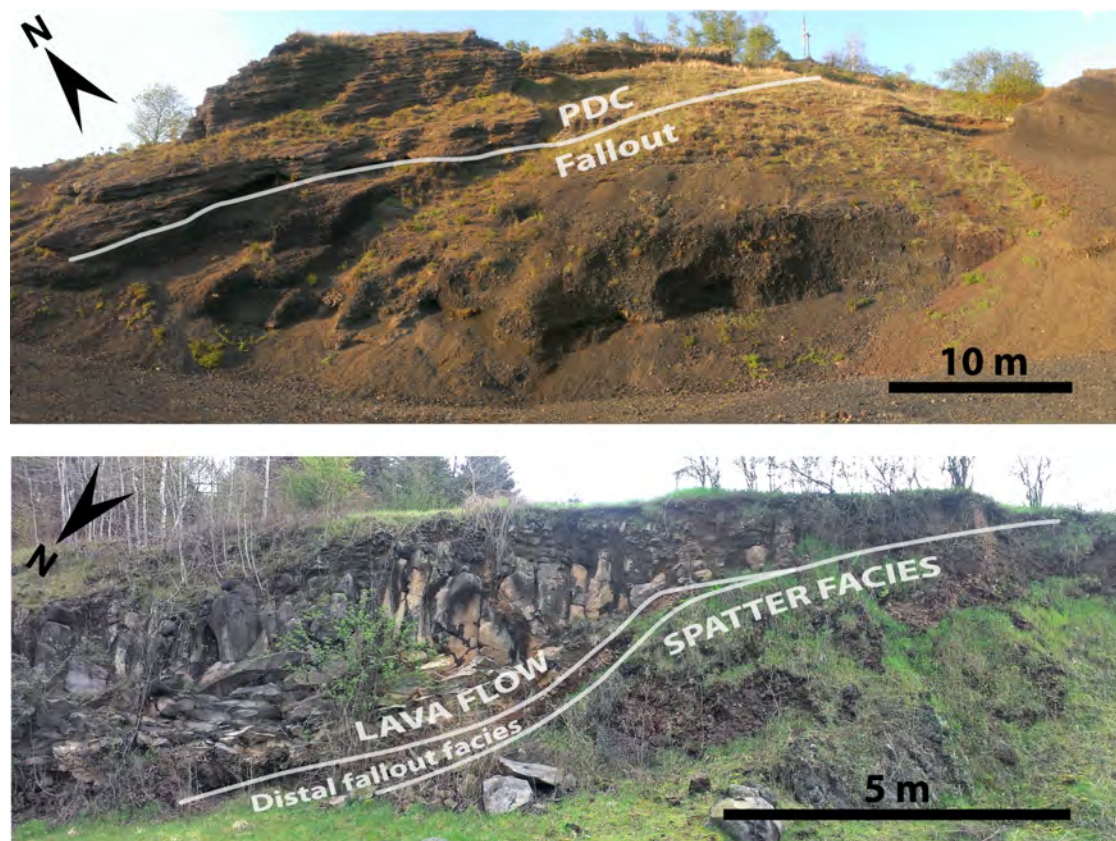


Fig. 11. Field photographs showing Montsacopa deposits and their the stratigraphic relationships. Upper) Conformable contact between Strombolian (lapilli scoria) and phreatomagmatic (PDC) deposits from the main cone building phase of the Montsacopa eruption. Lower) Syn-eruptive succession formed by welded scoria (spatter) at the base and a lava flow on top erupted from a marginal vent with an intercalated distal fallout deposits from the main Montsacopa vent.

Another example of complex multivent fissure fed eruption is illustrated by two of the largest volcanoes in the GVF, Croscat and Santa Margarida (Figs. 8 and 12). Our results confirm what was envisaged by Martí et al (2011) in the sense these two volcanoes, together with La Pomareda scoria vent, formed during the same eruption along the same fissure and showing very different eruption dynamics. The data obtained in this study from two boreholes and one ephemeral outcrop confirm the existence of a phreatomagmatic ash layer formed during the opening phase of the Santa Margarida crater, which is conformably underlying La Pomareda and Croscat successions. This ash layer lies on a thick paleosoil, thus indicating the existence in this area of a significant temporal interruption of volcanic activity before this last eruption.

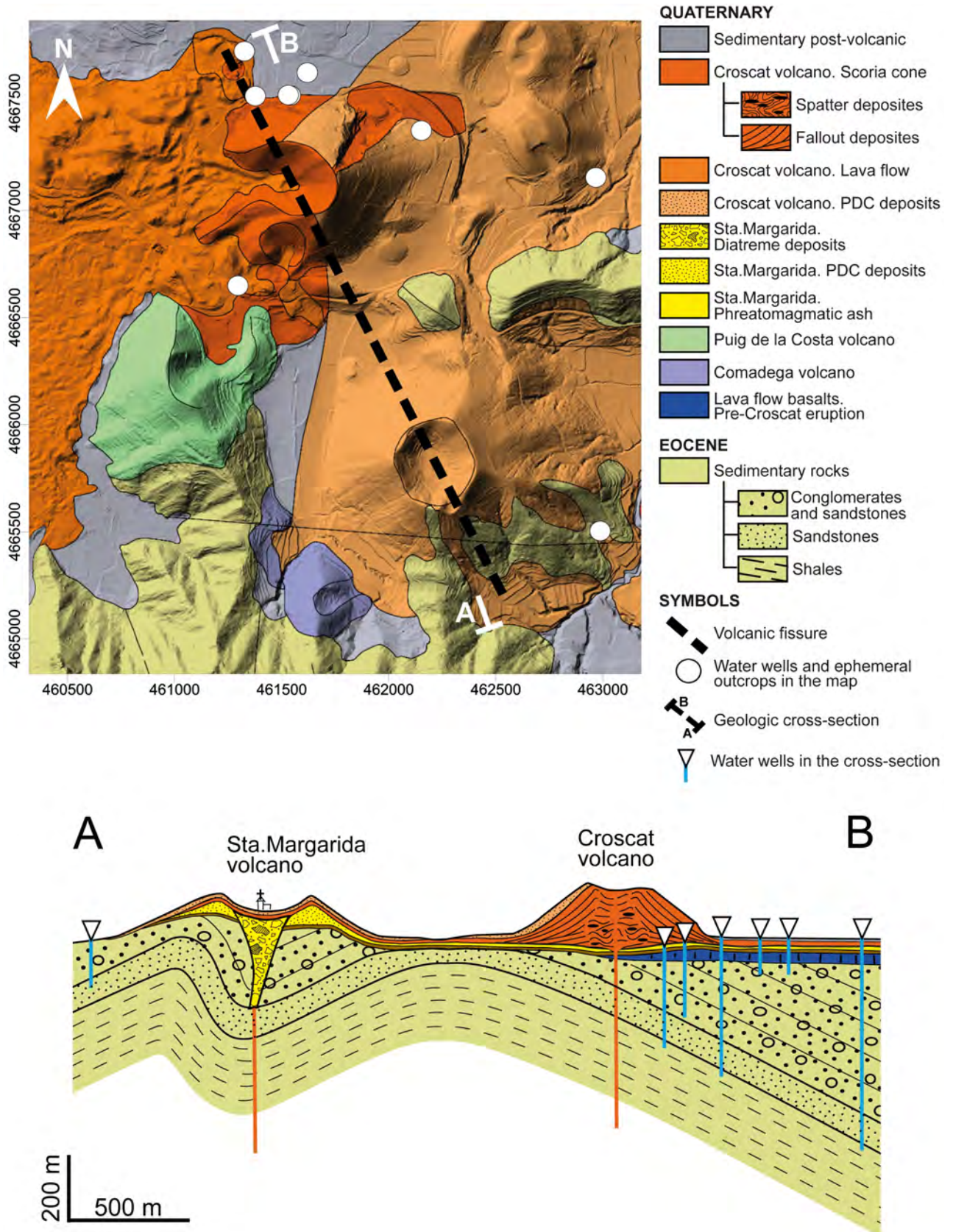


Fig. 12. New geological map (this study) and cross section showing the stratigraphic correlation (modified from Martí et al. 2011) of the central sector of the Garrotxa Volcanic Field obtained through the study of ephemeral outcrops and the stratigraphic logging of wells.

These boreholes also show the existence of more than 100 m of pyroclastic materials from La Pomareda and Crosca not exposed at surface, and how the La Pomareda scoria conformably underlies the Crosca succession (Fig. 8), mostly formed by an initial scoria and a thick sequence of lapilli size fallout, which mostly extend towards the east, conformably overlying the Santa Margarida crater and deposits. These conformable stratigraphic relationships and the absence of paleosoils or erosion surfaces between the deposits suggest that these three vents, in fact, formed during the same eruption.

6.7. Discussion and conclusions

The study of ephemeral outcrops and the stratigraphic logging of water wells and geotechnical drill holes, combined with surface geology and results from shallow geophysical studies, proves to be an efficient way of reconstructing the geology and volcanic stratigraphy of recent volcanic fields and, in particular, of highly urbanised areas in which increasing construction and the occupation of the soil hamper direct observation. The pioneering work conducted in La Garrotxa Volcanic Field, studying and cataloguing all new ephemeral outcrops and water wells and geotechnical boreholes (almost 100) over a period of ten years, has enabled us to (i) establish a detailed stratigraphy of the whole volcanic succession, from the Middle Pleistocene to the early Holocene, (ii) complete a detailed volcanological map of this volcanic field (which includes the city of Olot), and (iii) reinterpret a number of eruptive events. Likewise, our knowledge of the relative geochronology and extension of the most recent volcanic deposits has also improved. Despite revealing no clear pattern of the time-space evolution of this volcanism without a more precise statistical analysis, a concentration of the oldest eruptions towards the north and east of the area can be inferred from the results. Most of the volcanic eruptions (members) identified in this study concentrate in what we refer to as the northern sector of the GVF (Fig. 6) and far fewer are found in the southern sector (Fig. 7). This difference in the concentrations of the volcanic vents between the two sectors is not time-controlled since eruptions of similar ages have occurred in both sectors (see Table 2).

Despite their complexity, we observed no major geological changes in the area that could justify the stratigraphic relationships in the volcanic materials of the GVF. We attribute all the observed stratigraphic discontinuities and unconformities to either minor, inter-eruptive and syn-eruptive erosional and depositional episodes, to non-depositional hiatus corresponding to the non-uniform aerial distribution of the volcanic materials erupting from the vents, or – above all – to the fact that volcanic materials do not always emplace according to the principle of superposition, in particular when younger materials emplace on deeply eroded older ones. The style of the volcanism does not show any significant variation along the stratigraphic succession. The differences observed in the deduced eruption sequences (e.g. the alternation of Strombolian and phreatomagmatic phases) (see Martí et al 2011 and Cimarelli et al 2013) of the different members should be interpreted as due to local variations in the characteristics of the substrate rather than to any geological changes on a major scale. Similarly, the volume of erupted magma in those cases for which it could be calculated is mostly of the order of $0.02 \text{ km}^3 \pm 0.01$, which indicates that most of the eruptions were low magnitude monogenetic eruptions. The trends and outliers observed in these estimated volumes require a more detailed investigation that was beyond the scope of this study.

At a more detailed level, the results obtained help demonstrate the importance of access to the subsoil geology if a correct interpretation of such a complex stratigraphic succession, marked by multiple but relatively small and irregularly distributed depositional (and erosional) events, is to be attempted; this is the case of many Quaternary monogenetic volcanic fields and, in particular, in highly urbanised areas. In this study we were able to identify the volcanic stratigraphy buried below the city of Olot and other sectors of the volcanic field, thereby providing a correct interpretation that previously had always depended on incomplete observations. This complicates the reconstruction of the eruption dynamics and may induce significant miscalculations in hazard assessments due to errors in the inferred eruptive scenarios resulting from a lack of geological information from built-up areas.

In conclusion, the proposed volcanic stratigraphy offers the basis on which to build further studies on the GVF. It also provides a precise reference for the Quaternary tephrochronology of the lake sediments in neighbouring areas. The role of these studies in the reconstruction of the palaeoclimate histories is important to understand sedimentological variability and climate change. In the case of northeastern Iberian Peninsula the presence of Late Pleistocene tephra layers coming from the GVF in some lake sediments (e.g. Höbig et al., 2012) help to establish stratigraphic and geochronological markers. A precise correlation with eruptive episodes identified in this study will provide a constraint for the Pleistocene evolution of this area, but will also contribute to better estimate the size of these eruption by characterising more precisely their areal extend and volume of erupted magma. Finally, studies like this one represent a step forward in the preservation of the geological heritage of areas such as the GVF, by providing the basic knowledge on their evolution but also by enhancing the importance of their geological values in front of potential threats imposed by the demographic expansion of modern societies.

Acknowledgments

This study was partially funded by the *Beca Ciutat d'Olot* and the European Commission (FT7 Theme: ENV.2011.1.3.3-1; Grant 282759: "VUELCO"). We would like to thank La Garrotxa Volcanic Zone Natural Park for their support and logistical help during this research. With thank Shan Cronin, Patrick Bachelery and Antonio Brum da Silveira for their throughout and constructive reviews. The English text was corrected by Michael Lockwood.

References:

- Araña, V., Aparicio, A., Martín-Escorza, C., García Cacho, L., Ortiz, R., Vaquer, R., Barberi, F., Ferrara, G., Albert, J., Gassiot, X., 1983. El volcanismo Neógeno-Cuaternario de Catalunya: caracteres estructurales, petrológicos y geodinámicos. *Acta Geologica Hispánica* 18, 1–17.
- Barde-Cabusson, S., Bolós, X., Pedrazzi, D., Lovera, R., Serra, G., Martí, J., Casas, A., 2013. Electric resistivity tomography revealing the internal structure of monogenetic volcanoes. *Geophysical Research Journal*, 40, 1–6, doi:10.1002/grl.50538.
- Barde-Cabusson, S., Gottsmann, J., Martí, J., Bolós, X., Camacho, A., Geyer, A., Planagumà, Ll., Ronchin, E., Sánchez, A., 2014. New insights on a monogenetic volcanic field from gravity

- and self-potential measurements. *Bulletin of Volcanology*, 76:788. doi:[10. 1007/ s00445-013-0788-0](https://doi.org/10.1007/s00445-013-0788-0)
- Branca S., Coltelli M., Gropelli G., Lentini F., 2011. Geological map of Etna volcano, 1:50,000 scale, *Italian Journal of Geoscience*, 130, n. 3, pp. 265-291.
- Bolós, A., 1925. L'estació paleontològica del Pont de Ferro i algunes consideracions sobre el vulcanisme olotí. *But. ICHN*, 2^a sèrie. V, 4. Barcelona.
- Bolós, X., Barde-Cabusson, S., Pedrazzi, D., Martí, J., Casas, A., Himi, M., Lovera, R., 2012. Investigation of the inner structure of La Crosa de Sant Dalmai maar (Catalan Volcanic Zone, Spain). *Journal of Volcanology and Geothermal Research* 247–248, 37-48.
- Bolós, X., Barde-Cabusson, S., Pedrazzi, D., Martí, J., Casas, A., Lovera, R., Nadal-Sala, D., in press. Geophysical exploration on the subsurface geology of La Garrotxa monogenetic Volcanic Field (NE Iberian Peninsula). *International Journal of Earth Science*.
- Burjachs, F., 1985. Evolució de la vegetació i paleoclimatologia des de fa més de 85.000 anys a la regió d'Olot. Anàlisi pol·línica del Pla de l'Estany (Sant Joan les Fonts, la Garrotxa). *Vitrina: publicació del Museu Comarcal de la Garrotxa, a Recerca Científica del Parc Natural de la Zona Volcànica de la Garrotxa*. 1982-1992. 1, 49-56.
- Cebriá. J. M., López-Ruiz, J., Doblas, M., Oyarzun, R., Hertogen, J., Benito, R., 2000. Geochemistry of the Quaternary alkali basalts of Garrotxa (NE Volcanic Province, Spain): a case of double enrichment of the mantle lithosphere. *Journal of Volcanology and Geothermal Research*, 112, 175-187.
- Calderón, S., Cazorro, M., Fernández Navarro, L., 1906. Memoria sobre las formaciones volcánicas de la provincia de Gerona. *Memorias de Real Sociedad Española de Historia Natural*, t. IV, memoria 5^a, Madrid, 165–489.
- Cimarelli, C., Di Traglia, F., de Rita, D., Gimeno Torrente, D., Fernandez Turiel, J.L., 2013. Space–time evolution of monogenetic volcanism in the mafic Garrotxa Volcanic Field (NE Iberian Peninsula). *Bulletin of Volcanology* 75, 758.
- Chang K.H., 1975. Unconformity bounded stratigraphic units, *Geological Society of America Bulletin*, 86, 11, 1544-1552,
- Connor, C.B., 1990. Cinder cone clustering in the TransMexican volcanic belt: implication for structural and petrologic models. *Journal of Geophysical Research* 95, 19395–19405
- Di Traglia, F., Cimarelli, C., de Rita, D., Gimeno Torrente, D., 2009. Changing eruptive styles in basaltic explosive volcanism: examples from Croscat complex scoria cone, Garrotxa Volcanic Field (NE Iberian Peninsula). *Journal of Volcanology and Geothermal Research* 180, 89–109.
- Donville, B., 1973. Géologie Néogène et ages des éruptions volcaniques de la Catalogne orientale. These doct. Fac. Sciences. Université Paul Sabatier. Tolosa de Llenguadoc.
- Downes, H., 2001. Formation and modification of the shallow sub-continental lithospheric mantle: a review of geochemical evidence from ultramafic xenolith suites and tectonically emplaced ultramafic massifs of Western and Central Europe. *Journal of Petrology*, 42, 233-250.
- Fisher, R.V., Schmincke, H.U., 1984. *Pyroclastic rocks*, Springer Verlag, 472 pp.
- García, O., Guzmán, S., Martí, J., 2014. Stratigraphic correlation of Holocene phonolitic explosive episodes of the Teide–Pico Viejo Volcanic Complex, Tenerife. *Journal of the Geological Society, London* 86. <http://dx.doi.org/10.1144/jgs2013-086>

- Gisbert, G., Gimeno, D., Fernandez-Turiel, J.L., 2009. Eruptive mechanisms of the Puig de La Garrinada volcano (Olot, Garrotxa volcanic field, Northeastern Spain): a methodological study based on proximal pyroclastic deposits. *Journal of Volcanology and Geothermal Research* 180, 259–276.
- Giordano G., Mattei M., Funicello F., 2010. Geological map of the Colli Albani Volcano, in Funicello F. Giordano G. (Eds), *The Colli Albano Volcano*, Special Publication of IAVCEI, 3, Geological Society, London.
- Groppelli G., Norini G., 2005. From geological map to volcanic hazard evaluation on Mount Etna, Italy: Methodology and examples based on GIS analyses, in J.C. Thouret, C. Ollier, B. Joyce (Eds), *Zeitschrift für Geomorphologie*, Special Issue on “Volcanic landforms, processes and hazards”, vol. 140, pp. 167-179.
- Groppelli, G., Martí, J., 2013. Volcanic Stratigraphy – State of the art. *Proceedings of STRATI 2013, First International Congress on Stratigraphy*, Ciències de la Terra (UNL), Lisboa, 18, 99-104.
- Guérin, G., Behamoun, G., Mallarach, J.M., 1985. Un exemple de fusió parcial en medi continental. *El vulcanisme quaternari de la Garrotxa*. Publicació del Museu Comarcal de la Garrotxa, *Vitrina* 1, 19–26.
- Guérin, G., Valladas, G., 1980. Un exemple de fusió parcial en medi continental. *El vulcanisme quaternari de la Garrotxa*. Thermoluminescence dating of volcanic plagioclases. *Nature*, 286, 697-699.
- Guilbaud, M.N, Siebe, C., Layer, P., Salinas, S., Castro-Govea, R., Garduño-Monroy, V.H., Le Corvec, N., 2011. Geology, geochronology, tectonic setting of the Jorullo volcano region, Michoacán, México. *Journal of Volcanology and Geothermal Research* 201, 97–112
- Hedberg, H.D. (ed.), 1976, *International Stratigraphic Guide - A guide to stratigraphic classification, terminology, and procedure*, 1st edition. Wiley & Sons, Inc., 200 pp.
- Höbig, N., Weber, M. E., Kehl, M., Weniger, G. C., Julià, R., Melles, M., Fülöp, R. H., Vogel, H., Reicherter, K., 2012. Lake Banyoles (northeastern Spain): A Last Glacial to Holocene multi-proxy study with regard to environmental variability and human occupation. *Quaternary International*, 274, 205-218.
- Hoernle, K., Zhang, Y.S., Graham, D., 1995. Seismic and geochemical evidence for large-scale mantle upwelling beneath the eastern Atlantic and western and central Europe. *Nature* 374, 34–9.
- IGC (Institut Geològic de Catalunya), 2003. Cartografia Temàtica. Sèrie Mapa Geològic de Catalunya. Olot. Available at http://www1.igc.cat/web/gcontent/pdf/mapes/igc_GT1_257q12_75x22_v1g.pdf
- IGC (Institut Geològic de Catalunya), 2007. Carta vulcanològica de la Zona Volcànica de La Garrotxa. Institut Geològic de Catalunya. scale 1:25,000
- Kereszturi, G., Geyer, A., Martí, J., Nemeth, K., Dóniz-Pérez, F. J., 2013. Evaluation of morphometry-based dating of monogenetic volcanoes—a case study from Bandas del Sur, Tenerife (Canary Islands). *Bulletin of Volcanology* 75:734 DOI 10.1007/s00445-013-0734-1
- Lewis, C. L., Vergés, J., Marzo, M. 2000. High mountains in a zone of extended crust: Insights into the Neogeno-Quaternary topographic development of Northeastern Iberia. *Tectonics*, 19, 86-102
- López-Ruiz, J., Rodríguez-Badiola, E., 1985. La región volcánica Mio-Pleistocena del NE de España. *Estudios Geológicos*, 41, 105-126.

- Lustrino, M., Wilson, M., 2007. The circum-Mediterranean anorogenic Cenozoic igneous province. *Earth-Science Reviews* 81 1–65
- Mallarach, J.M., 1982. Carta geològica de la regió volcànica d'Olot. *Litologia i geomorfologia*. 1120.000. Ed Maber, Ajuntament d'Olot.
- Mallarach, J.M., 1984. Nota sobre les darreres erupcions volcàniques quaternàries olotines. *Revista de Girona*. Núm. 107.
- Mallarach, J.M., 1998. El vulcanisme prehistòric de Catalunya *Revista de Girona*. Núm. 107. 322.
- Mallarach, J.M., Riera, M., 1981. Els volcans olotins i el seu paisatge. Editorial Serpa, Barcelona. 250 pp.
- Martí, J., Mallarach, J.M., 1987. Erupciones hidromagmáticas en el volcanismo cuaternario de Olot. *Estudios Geológicos* 43, 31–40.
- Martí, J., Mitjavila, J., Roca, E., Aparicio, A., 1992. Cenozoic magmatism of the Valencia trough (Western Mediterranean): relation between structural evolution and Volcanism. *Tectonophysics* 203, 145–166.
- Martí, J., Planagumà, L., Geyer, A., Canal, E., Pedrazzi, D., 2011. Complex interaction between Strombolian and phreatomagmatic eruptions in the Quaternary monogenetic volcanism of the Catalan Volcanic Zone (NE of Spain). *Journal of Volcanology and Geothermal Research* 201, 178–193.
- Murphy M.A., Salvador A., (eds.), 1999. *International Stratigraphic Guide -An abridged edition*, Episodes, 22, no. 4, pp. 255-271.
- Nemeth, K., Martin, U., Harangi, S., 2001. Miocene phreatomagmatic volcanism at Tihany (Pannonian Basin, Hungary). *Journal of Volcanology and Geothermal Research* 111 (1–4), 111–135.
- Nemeth, K., Cronin, S. J., Smith, I. E. M., Flores, J. A., 2012. Amplified hazard of small-volume monogenetic eruptions due to environmental controls, Orakei Basin, Auckland Volcanic Field, New Zealand. *Bulletin of Volcanology*, DOI 10.1007/s00445-012-0653-6
- Owen, D., 2009. How to use stratigraphic terminology in papers, illustrations, and talks. *Stratigraphy*, 6, 106-116.
- Palladino D.M., Simei S., Sottili G., Trigila R., 2010. Integrated approach for the reconstruction of stratigraphy and geology of Quaternary volcanic terrains: an application to the Vulsini Volcanoes (central Italy), in G. Gropelli & L. Viereck-Goette (Eds.), *Stratigraphy and geology of volcanic areas*, The Geological Society of America Special Paper 464, pp. 63-84.
- Salvador A., 1987. Unconformity-bounded stratigraphic units. *Geological Society of America Bulletin*, 98, 232-237.
- Salvador A. (Ed.), 1994, *International Stratigraphic Guide. A guide to stratigraphic classification, terminology, and procedure*. The International Union of Geological Sciences and the Geological Society of America, 214 pp.
- San Miguel de la Cámara, M., Marcet Riba, J., 1926. Región Volcánica de Olot, Extracto de la Guía “Cataluña” Excursión C-4, XIV Congreso Geológico Internacional, Imprenta Sobrinos de López Robert y Cia., Barcelona, 39–214.
- Wilson, M., Bianchini, G., 1999. Tertiary–Quaternary magmatism within the Mediterranean and surrounding regions. In: Durand, B., Jolivet, L., Horvath, F., Seranne, M. (Eds.), *The Mediterranean Basins: Tertiary extension within the Alpine Orogen*. Geological Society of London, vol. 156, pp. 141–168.

- Wilson, M., Downes, H., 1991. Tertiary–Quaternary extension related alkaline magmatism in western and central Europe. *Journal of Petrology*. 32, 811–849.
- Wilson, M., Downes, H., 1992. Mafic alkaline magmatism associated with the European Cenozoic rift system. *Tectonophysics* 208, 173– 182.
- Wilson, M., Downes, H., 2006. Tertiary–Quaternary intra-plate magmatism in Europe and its relationship to mantle dynamics. In: Gee, D., Stephenson, R. (eds.) *European Lithosphere Dynamics*, Geological Society of London Memoire 32, 147–166.
- Wilson, M., Patterson, R., 2001. Intraplate magmatism related to short wavelength convective instabilities in the upper mantle: evidence from the Tertiary–Quaternary volcanic province of western and central Europe. In: Ernst, R.E., Buchan, K.L. (Eds.), *Mantle Plumes: Their Identification Through Time*. Geological Society of America Special Paper, vol. 352, pp. 37–58.

Supplemental Table 1: Volcanic activity units and formal volcano-stratigraphic units (modified from Fisher and Schmincke, 1984)

Volcanic Activity Units	Duration	Products and Volcanic Landforms	General Genetic designation	Volcano-stratigraphic Units (Formal units)
Eruptive pulse	seconds, minutes	Single airfall bed, PDC deposit, lahar, lava flow, etc	Eruption units (one or several beds, bedding sets, flows, ...)	Bed or level
Eruptive phase (several pulses)	minutes, hours, days	One or several deposits (several beds) of airfall, PDC, lava flows, lahars	One or several deposits (several beds) corresponding to a particular eruption dynamics	Unit
Eruption (several phases)	days, months, years	Succession of volcanic deposits of any nature (airfall, PDCs, lahars, lava flows, etc	Sequence of volcanic and related deposits formed during the same eruption	Member
Eruptive epoch (includes several eruptions and inter-eruptive - calm- episodes)	tens, hundreds or thousands of years	Single poligenetic volcanoes (stratovolcanoes, shield volcanoes, calderas, etc) or single monogenetic volcanic fields	Multiple members that may be grouped in cycles, depending on age, composition, eruptive style, etc	Formation
Eruptive period (includes several epochs and calm periods)	thousands or millions of years	Volcanic fields and regions consisting of many volcanoes and volcanic forms	Multiple Formations	Group

Supplemental Table 2. Volcanic stratigraphy of the La Garrotxa Volcanic Field. Source: (1) Burjachs (1983). C14 dating. (2) Guérin and Valladas (1980). Thermoluminescence dating of volcanic plagioclases. (3) Guerin i Benhamou (1985). Thermoluminescence dating of volcanic plagioclases and K/Ar Isotopic dating. (4) Bolós A. (1925). Relative dating by biostratigraphy. (5) Pedrazzi et al. (2014). U-Th and C14 dating. (6) Mallarach, JM. (1981, 1982, 1998). Relative dating by stratigraphy. (7) Donville (1973). K/Ar Isotopic dating. (8) Lewis, C (2000). Ar/Ar Isotopic dating. (9) Gòmez B. (personal communication, 2014) Thermoluminescence (TL) dating of sediments.

Time period	Relative Stratigraphy (from younger to older)	Age	Member	Source	Description	DRE (Km ³)
Holocene	1	Relative	Rocanegra volcano	(1)	These deposits overlie the Croscat volcano (# 2) phreatomagmatic deposits and are not covered by the Croscat volcano fallout.	0,01
Upper Pleistocene	2	11.5 – 13 ka	Santa Margarida – Croscat – Pomareda eruptive fissure	(2) (3)		0,18
	3	Relative < 18000	Montolivet volcano	(4)	These deposits overlie those of Montsacopa volcano (# 24), which in turn overlay La Garrinada (# 35) volcano deposits.	0,02
	4	17.1 ka	Puig Jordà volcano	(2) (3)	Lava flow with rootless volcanoes, locally known as Bosc de Tosca.	0,03
	5	Relative	Bisaroques and Ca l'Isidret volcanoes		Young aspect and poorly eroded materials overlying La Garrinada (# 35) volcano deposits.	0,01
	6	Relative	Puig de Martinyà volcano		There is a paleosol that separates these deposits from the Croscat volcano (# 2) deposits.	
	7	Relative	Puig de la Costa volcano (Lava flow below Croscat volcano member (# 2))		Several lava flows were recognised in the Croscat borehole (see Figs. 8 and 12) below the Croscat and Puig Martinyà (# 6) deposits. The uppermost lava flow can be stratigraphically correlated with the Puig de la Costa volcano, so it should be younger than 30 ka.	
	8	Relative	Racó volcano			0,02
	9	28.1 ka	Simon volcano and Santa Pau lava flow	(2)	Santa Pau lava flow could be related to the Simon volcano according to its location and stratigraphic position.	
	10	30 to 46.3 ka	Traiter volcano	(2)		0,03
	11	Relative	Sant Marc and Puig Roig volcano			
	12	Relative	Lava flow below Bosc de Tosca		Appears underlying the Bosc de Tosca (Puig Jordà volcano (# 4)) lava flow and Racó volcano (# 8) deposits.	
	13	Relative	Pla de Massandell borehole upper lava flow			

14	Relative (< 45 ka)	L'Estany and Bellaire volcanoes	(1)		0,02
15	Relative	Pla de Massandell borehole lower lava flow			
16	Relative	Cabriolers volcanoes			
17	Relative	Puig de Granollers volcano			0,03
18	Relative	Puig Subià volcano		Its deposits appear below the Santa Pau lava flow (# 9).	0.1 – 0.2
19	Relative	Comadega volcano		Underlying deposits from Croscat and Santa Margarida (# 2) and other volcanoes deposits in the Santa Pau area.	
20	Relative	La Moixina lava flow			
21	43 - 120 ka	Crosa de Sant Dalmai volcano	(1) (5)		0,13
22	73.5 ka	Fontpobra, Can Tià and Coll Tort volcanoes	(2)		0,03
23	Relative	Pujalós volcano			0,03-0.07
24	Relative	Volcà del Montsacopa		Its deposits overlay La Garrinada volcano (# 35) and are covered by thus from the Bisaroques and Ca l'Isidret volcanoes (# 5).	0.02-0.06
25	Relative	Pla de Llacs lava flow			
26	Relative	Pla d'Olot lava flow		Below Pla de Llacs (# 25). Only observable in boreholes.	
27	Relative	Pla d'Olot lava flows		Undetermined number of lava flows that fill the Olot depression.	
28	100 ka	Puig de les Medes and Puig Rodó volcanoes	(2)		0,02
29	Relative	Lava flow in borehole at Croscat northern flank			
30	110 ka	Pla de les Tries lava flow	(2)		

	31	110 ka	Puig de Mar volcano	(6) (2) (7) (6) (2) (7)		
	32	121 ka	Puig de la Banya del Boch and Clot de l'Omera volcanoes	(2) (3)		
	33	Relative	Olot 2 lava flow		Only observable in boreholes.	
	34	Relative	Olot 1 lava flow		Only observable in boreholes.	
Middle Pleistocene	35	133 ka	Garrinada volcano	(2) (8)		0,08
	36	Relative	Bac de les Tries volcano		Deposits observable below la Garrinada volcano (# 35).	
	37	Relative	Pla sa Ribera volcano			
	38	Relative	Riu Ser lava flow 2		Appearing above the Riu Ser lava flow 1 (# 40).	
	39	Relative	Vall dels Arcs phreatomagmatic deposits		Underlying the Riu Ser lava flow 2 (# 39).	
	40	Relative	Riu Ser lava flow 1			
	41	150 ka	Sant Joan les Fonts lava flow and Aiguanegra volcano	(8)		
	42	Relative	Sant Cosme lava flow (from Batet)		Above the Funoses lava flow (# 42).	
	43	Relative	Les Funoses lava flow		Above the Castellfollit lava flows (# 46 and # 47).	
	44	Relative	Cairat-Repàs-Claperols eruptive fissure			
	45	168 ka	Puig d'Àdri volcano	(9)		0,09
	46	192 ka	Castellfollit de la Roca upper lava flow	(8)		
	47	217 ka	Castellfollit de la Roca lower lava flow	(8)		
	48	Relative	Batet upper lava flows			

49	247 ka	Batet middle lava flows	(2)		
50	Relative	Barraca volcano		These products are covered by the Batet lavas (# 48 and # 49).	
51	250 ka	Puig de l'Ós volcano	(8)		0,02
52	Relative	Sant Jaume de Llierca lava flow			
53	Relative	Batet lower lava flows		Lava flows identified in a borehole at the Batet high (Fig. 3).	
54	Relative	La Canya volcano			
55	590 – 700 ka	Sant Joan les Fonts lava flows	(8)	The oldest lava emission recognised in this volcanic field.	

Volcano-structural analysis of La Garrotxa Volcanic Field (NE Iberia): implications for the plumbing system

Submitted to:

Tectonophysics

Authors of the paper:

Xavier Bolós ^(a)

Joan Martí ^(a)

Laura Becerril ^(a)

Llorenç Planagumà ^(b)

Pablo Grosse ^(c)

Stéphanie Barde-Cabusson ^(a)

a) Institute of Earth Sciences Jaume Almera, ICTJA-CSIC, Group of Volcanology. SIMGEO (UB-CSIC) Lluís Sole i Sabaris s/n, 08028 Barcelona, Spain

b) Tosca, Environment Services of Education, Casal dels Volcans, Av. Santa Coloma, 17800 Olot, Spain.

c) CONICET and Fundación Miguel Lillo, Tucumán, Argentina.

7.1. Abstract

The Garrotxa Volcanic Field is related to the Neogene-Quaternary European Rift system and is the youngest representation of monogenetic volcanism in the Iberian Peninsula. It encompasses over 50 well-preserved volcanoes in an area of about 600 km² lying between the cities of Olot and Girona (NE Spain). In this paper we investigate the relationship between the Neogene extensional tectonics and the spatial distribution of the volcanoes in the area. The analysis includes the geostatistical distribution of faults, fissures and vents, as well as morpho-structural lineaments, and the morphometrical analysis of volcanic cones and craters. As well, we use the location of the regional seismicity registered since 1978 and the sites of freshwater springs and mantle-derived gases as indicators of active faults and open fractures. Finally, we consider the location of the volcanoes with ultramafic xenoliths as a way of identifying the deepest fractures in the zone and estimating magma ascent velocities. The results obtained show that this volcanic area consists of an extensional basin delimited by two principal faults that permitted the ascent of magma from either the source region or from shallower reservoirs located at the base of the crust. Towards the upper part of the crust, magma transport was captured by shallow extensional secondary faults whose formation is linked to the slight transtensional movement of the main bounding faults. Our study provides evidence of how the local stress field and contrasts in rheology could have controlled magma migration, which suggests that precise knowledge of the stress configuration and distribution of rheological and structural discontinuities in such regions is crucial in the forecasting of monogenetic volcanism.

Keywords: Volcano-structural · Garrotxa Volcanic Field · monogenetic volcanism · magma ascent rates · plumbing system

7.2. Introduction

Basaltic monogenetic volcanic fields related to rift zones are found world-over and are expressed on the Earth's surface by the alignments of pyroclastic cones and vents and parallel faults and eruptive fissures (Fiske and Jackson, 1972; Walker, 1999). A volcanic eruption signals the end of the process whereby magma rises from its source in the upper mantle to the surface (e.g. Brenna et al., 2011; McGee et al., 2011). The final geometry of the magma pathway towards the surface is directly controlled by the stress field and always follows a path normal to the minimum stress and parallel to the maximum principal stress (Rubin, 1995; Connor and Conway, 2000; Gudmundsson and Philipp, 2006, Cebrià et al., 2011; Le Corvec et al., 2013). In monogenetic volcanic fields the distributions and magnitudes of different stress fields can be related to the tectonic and gravitational forces that, in turn, are linked to (a) basement geometry, (b) local topography, (c) stress changes occurring during dyke propagation, and (d) stress barriers related to structural discontinuities and rheological changes in stratigraphic successions (Gretnener, 1969; Clemens and Mawer, 1992; Gudmundsson, 2003; Tibaldi, 2003; Acocella and Tibaldi, 2005; Gudmundsson and Philipp, 2006; Kavanagh et al., 2006; Tibaldi et al., 2014).

Deciphering the potential pathways that magma uses to reach the surface is of crucial importance when conducting hazard assessment in volcanic areas.

The complexity of subsurface plumbing systems in monogenetic volcanic fields ensures that such systems are difficult to predict and rarely accessible for study and so other methods are needed for understanding the structural setting of a volcanic area and the pathways used by magma on its ascent to the Earth's surface. Over the last twenty years, several geophysical studies have been devoted to geostructural characterisations of the feeding systems of monogenetic volcanic areas (or, more generally, of active volcanic districts) (e.g. Nishi et al., 1996; Bibby et al., 1998; Di Maio et al., 1998, 2000; Portal et al., 2013; Blaikie et al 2014). In La Garrotxa Volcanic Field geophysical studies of this type have been conducted in recent years and have been successful in describing the stratigraphy of the area and the shallow structure beneath the volcanic deposits (Bolós et al., 2012, 2014a, 2014b; Barde-Cabusson et al., 2013, 2014). Results have confirmed in general terms that this volcanism is mainly controlled by NW-SE faults that are the very faults that control the post-Alpine structural evolution of the area. However, the exact structural control and the role played by the major and subordinated faults in determining the distribution of vents and the frequency and size of the eruptions is not known.

In order to improve our understanding of the structural constraints of La Garrotxa volcanism we combined the results of these previous geophysical works with new volcano-structural analysis that includes data on the geostatistical distribution of faults, fissures and eruptive vents, the identification of morpho-structural lineaments by remote sensing, and a morphometrical analysis of the field's volcanic cones and craters. In addition, we took into account all of the epicentres of regional seismic events recorded by the Geological Survey of Catalonia (IGC) since 1978, as well as the distribution of CO₂-rich freshwater springs, and springs and wells with high radon levels, as a guide to active faults and open fractures, respectively. Finally, we analysed the distribution of upper mantle xenoliths and lower crust cumulates as an indication of the depth reached by certain fractures and faults, and used the largest of these enclaves to estimate magma ascent velocities. The data obtained was combined into a conceptual model describing how magma was transported from source to the surface in La Garrotxa Volcanic Field, which can bring some clues for such processes in other monogenetic volcanic fields.

7.3. Geological setting

Mafic alkaline volcanism is widely distributed along the European Cenozoic Rift System that comprises four main volcanic areas: the Rhenohercynian in Germany, the western Panonian Basin in Eastern Europe, the Massif Central in France and the Valencia Trough in Spain (Ziegler, 1992; Downes, 2001; Dèzes et al, 2004, Michon and Merle, 2005). The study area is part of the Valencia Trough, a NE-SW-oriented Neogene basin lying offshore between the Iberian Peninsula and the Balearic promontory in northeastern Spain (Fig. 1). The most important concentration of Middle Miocene-to-recent volcanism in the Valencia Trough is found in the Catalan Volcanic zone (CVZ) in the NE Iberian Peninsula (Martí et al., 1992; Martí et al., 2011). This area is characterised by a series of graben and horst structures that have controlled Neogene-Quaternary volcanism and sedimentation.

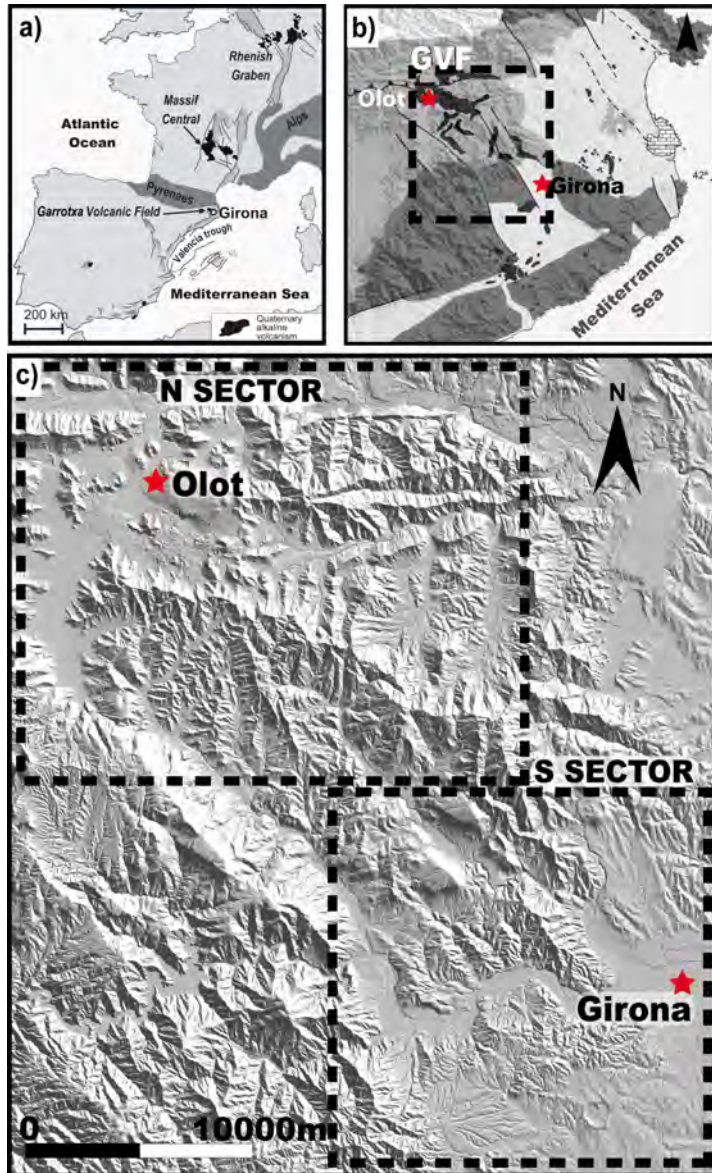


Fig. 1. Location of the study area. a) Simplified map of the distribution of the European rift system. b) Simplified geological map of the Catalan Volcanic Zone (modified from Guérin et al., 1985). c) Geographic distribution of La Garrotxa Quaternary volcanic field.

The most recent episode in this volcanism corresponds to La Garrotxa Volcanic Field (GVF) (0.7 Ma to early Holocene) (Araña et al., 1983; Bolós et al., 2014b). This field covers an area of about 600 km² located between the cities of Olot and Girona (Fig. 1) and is bounded by two regional conjugated Neogene normal faults with a transtensional component (Goula et al., 1999; Olivera et al., 2003): the Amer Fault to the east and the Llorà Fault to the west. These two faults are responsible for the distribution of the area's volcanism, as well as its seismicity and fluvial network (Saula et al., 1996; Martí et al., 2011; Cimarelli et al., 2013; Barde-Cabusson et al. 2014). The northern part of this volcanic field is limited by an E-W reverse fault system, which is not related to the subsequent magmatism. The GVF contains over 50 well-preserved cones, the main concentration being located in the northern sector of the area (Fig. 1). The morphologies of these volcanoes include cinder and scoria cones, spatter cones, tuff rings and maars, and in composition mainly correspond to basanites and alkaline basalts (Araña et al., 1983; Cebrià et al., 2000; Martí et al., 1992). Some volcanoes contain ultramafic to mafic xenoliths including pyroxenites, melanogabbros, amphibolites and spinel lherzolites, of which the pyroxenites are the most abundant (Llobera, 1983;

Neumann et al., 1999, Bianchini et al., 2007; Galán et al., 2008). Pressure and temperature estimates suggest that the pyroxenites, melanogabbros and amphibolites may have crystallised in magma chambers located at the crust–mantle boundary (Neumann et al., 1999), which, according to geophysical estimates, are located at a depth of ~30 km (Fernández et al., 1990; Gallart et al., 1984, 1991); on the other hand, the spinel lherzolites may derive from the source region in the asthenospheric mantle (Bianchini et al., 2007).

7.4. Methodology

New fieldwork and remote sensing analyses were conducted in order to identify and measure the main volcano-structural features such as vents lineaments, fissures and faults (Fig. 2). Structural mapping was performed with the software ArcGIS 10 by ESRI® at a scale of 1:5 000 using orthophotographs (1:2500), aerial photographs (1:18 000) and Digital Elevation Models (DEM; 5- and 2-m resolutions) produced by the Cartographic Institute of Catalonia (ICC; www.icc.cat). Geological maps produced by the Geological Survey of Spain and Geological Survey of Catalonia (IGME; 1:50 000, <http://cuarzo.igme.es/sigeco/>, 2011; IGC; 1:25 000; www.igc.cat) were also used. The morpho-tectonic analysis included the determination and comparison of lineaments obtained from orthophotomaps and different illumination-shaded relief DEMs, as well as a statistical analysis of the length and orientation of lineations. To avoid any artefact that could be attributed to the lighting direction of the DEM we used different lighting models. We also analysed the profile and direction of several streams and rivers in order to detect abrupt changes in slope direction that could be related to tectonic movements (Fig. 3).

Eruptive vents were mapped as individual points of magma emission on the surface, which allowed us to delineate eruptive fissures corresponding to lines connecting volcanic vents opened during the same eruption (e.g. Tibaldi; 1995, Paulsen and Wilson, 2010; Becerril et al., 2013). Fieldwork allowed us to verify the number of existing vents and to check fissure lengths and strikes.

A morphometrical analysis of the most representative well-preserved volcanoes was also performed. We analysed a total of 28 cones and craters in both the northern and southern sectors of the GVF using a DEM with resolutions of 2 and 5 m, respectively. The cone and crater outlines were manually delimited by consulting slope breaks and geological maps. Morphometric parameters of each cone and crater were extracted using the MORVOLC program (Grosse et al., 2009, 2012). The following parameters were considered: (a) Ellipticity Index (EI) of the cone and crater outlines (EI is a measure of elongation equal to:

$$EI = \frac{PI * \left(\frac{L}{2}\right)^2}{A} \quad (1)$$

where L is the maximum/major outline axis and A is the outline area), (b) the average EI of the closed elevation contours (at 5 m equidistance) within the cone base, (c) the major axis azimuths of the cone and crater outlines, (d) the circular average azimuth of the major axes of the closed elevation contours within the cone, and (e) the calculated azimuth and direction of breaching in breached craters.

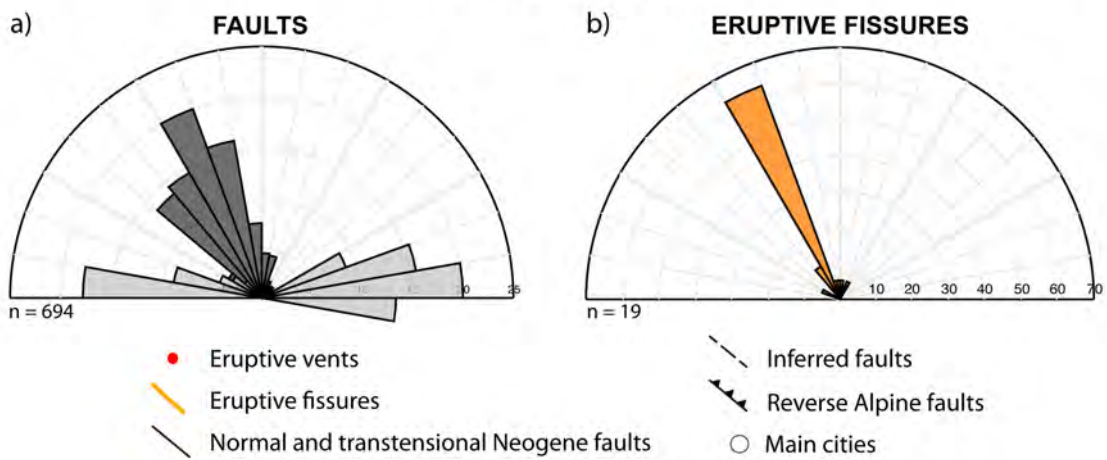
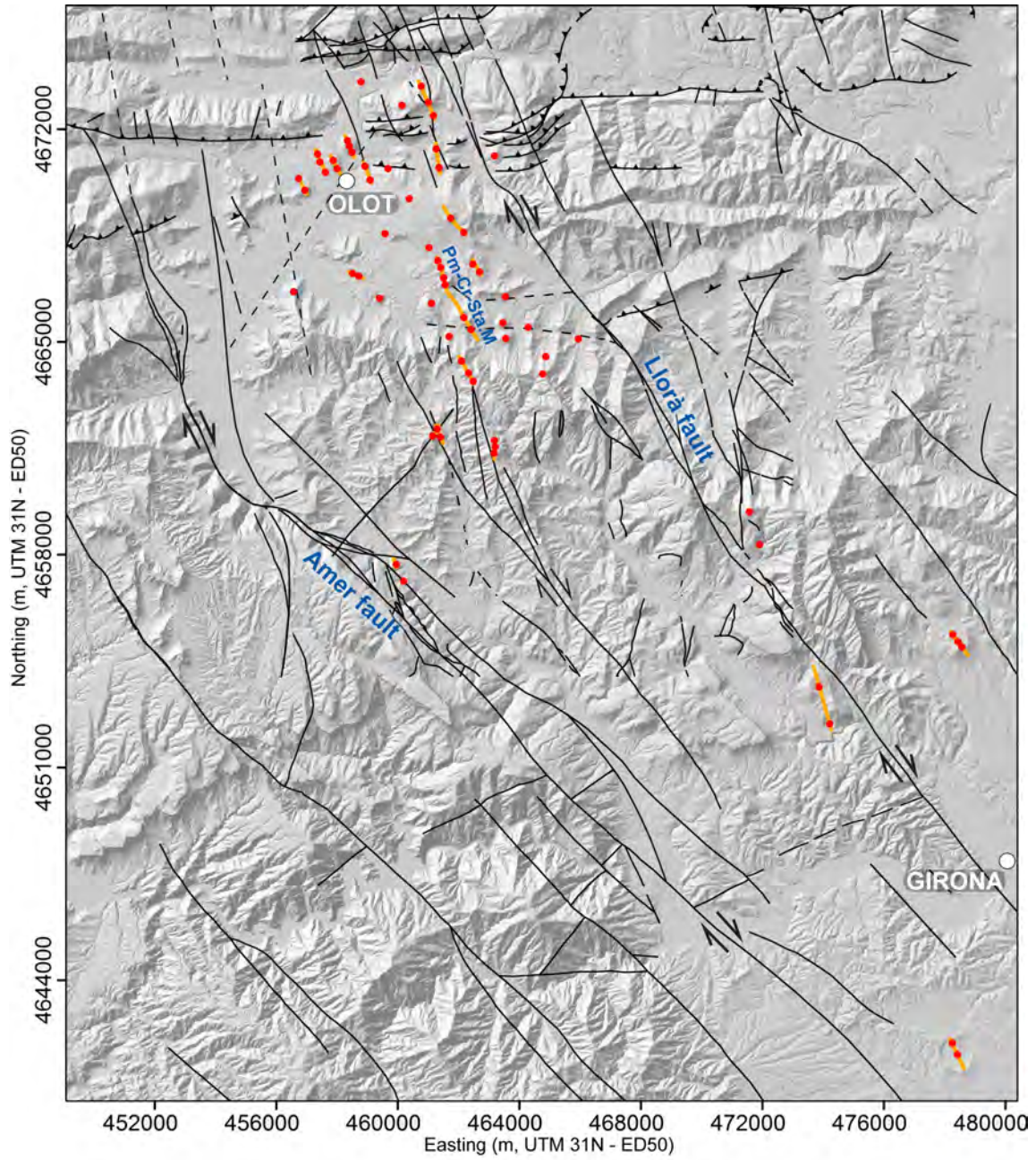


Fig. 2. Volcano-structural map of La Garrotxa Volcanic Field. a) Rose diagram of faults; Neogene faults are represented in dark grey and Alpine reverse faults in light grey. b) Rose diagram of eruptive fissures.

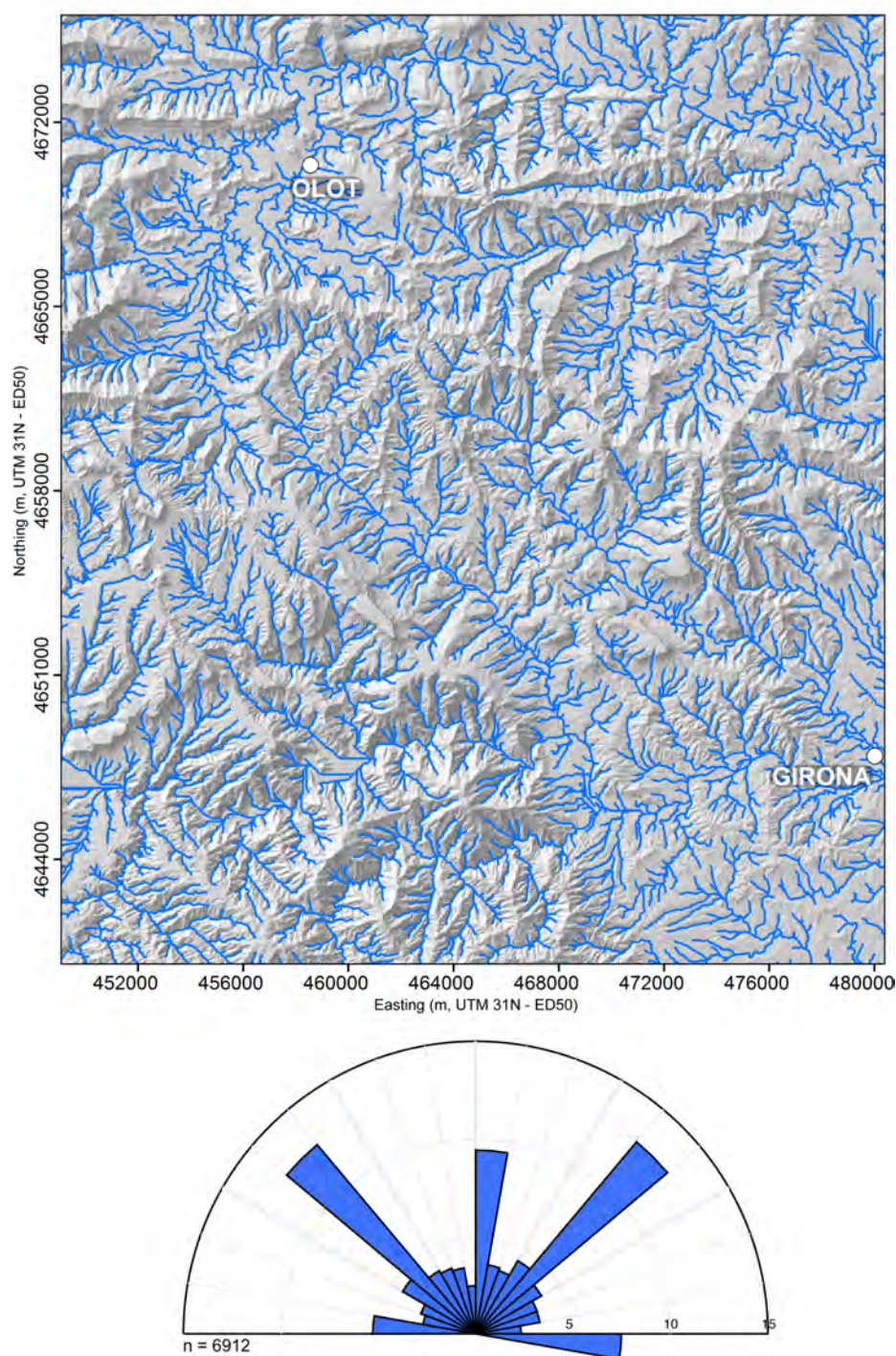


Fig. 3. Drainage network of La Garrotxa Volcanic Field. Trends are represented in a rose diagram.

A statistical analysis based on the nearest-neighbour concept (see Cebrià et al., 2011) was applied to eruptive vents in order to obtain the angles of the lines that connect all pairs of eruptive vents. Previous studies have demonstrated that the main lineaments obtained from the union of eruptive vents can reveal stress field patterns (Lutz, 1986; Cebrià et al., 2011). To carry out this analysis we considered lineaments of up to 12 km in maximum length, corresponding to the maximum distance between two eruptive vents inside the northern sector. We choose this sector since it has the major concentration of volcanoes (Fig. 4).

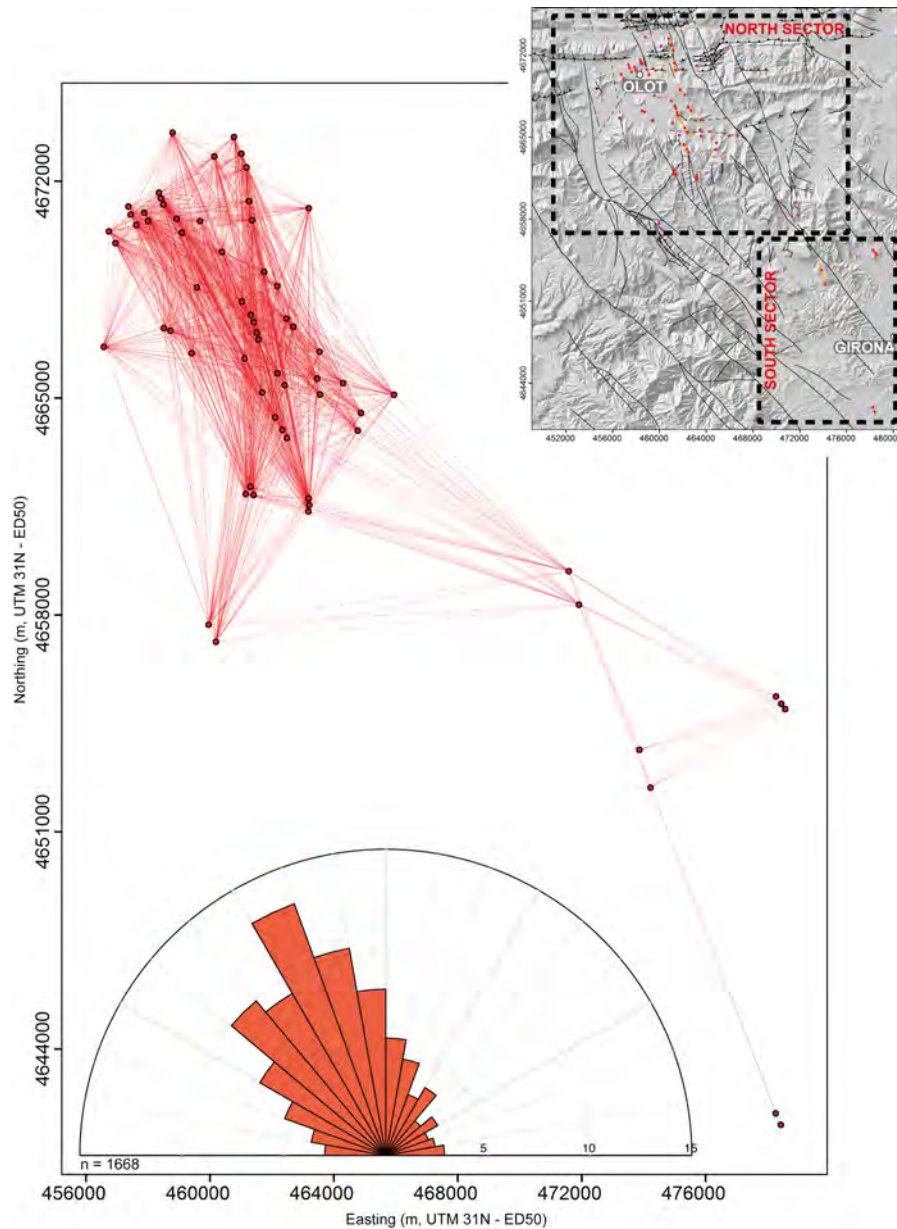


Fig. 4. Eruptive vent lineaments obtained using the nearest-neighbour technique. The rose diagram shows the distribution of the alignments.

No outcropping dykes were identified in the studied area due to its recent age and lack of significant erosion. However, several feeder dykes hidden by their own deposits were identified using Electric Resistivity Tomography (Bolós et al., 2012, 2014a). Preliminary interpretations of geological maps were carried out in order to compile and to check previous mapped faults (IGC and IGME geological maps) and to identify new ones. Stress patterns were also obtained from the drainage network map extracted using a DEM spatial analysis. Rose diagrams of fissures, faults and drainage networks were performed with the software Stereonet 8.8.4 (Cardozo and Allmendinger, 2013). We also took into account the distribution of the main freshwater springs existing in the study area (Fig. 5) to indicate the presence of open fractures and faults. We georeferenced a total of 254 springs shown on the topographic maps of the Catalan Geographic Institute (www.icc.cat), along with others identified during fieldwork. High concentrations of

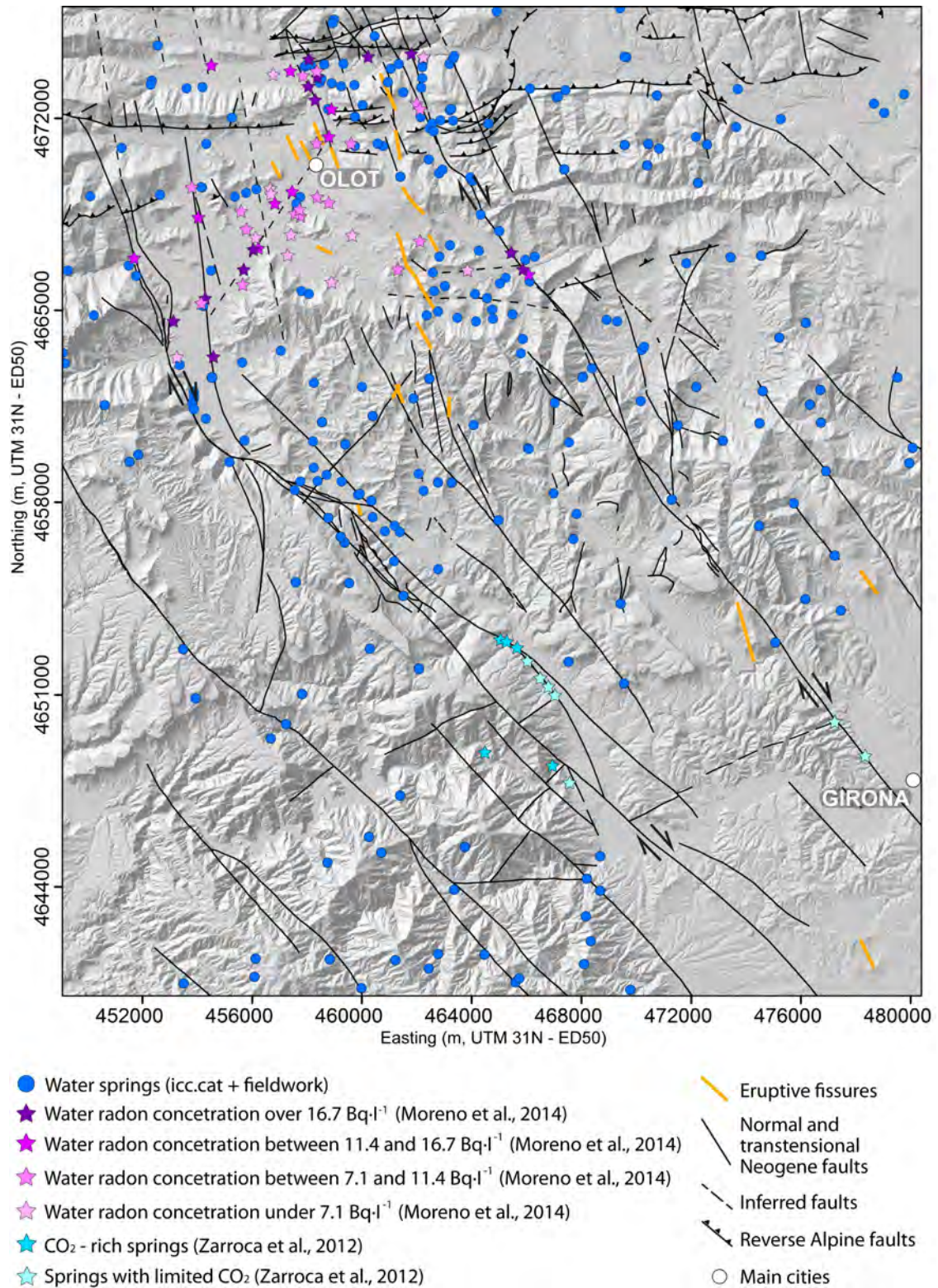


Fig. 5. Map of freshwater springs (blue dots) and water radon concentrations (purple stars) obtained by Moreno et al. (2014), and CO_2 -rich springs (blue stars) obtained by Zarroca et al. (2012).

endogenous gases (i.e. radon, CO_2) in freshwater springs are assumed to indicate the presence of deep fractures with high permeability values (Wattananikorn et al., 1998; Kresic, 2010), which is this case where they are directly linked to active Quaternary faults (Zarroca et al., 2012). In a small part of the study area (southern sector; 463216, 4646403 (UTM 31N - ED50)) we also used

12 measurements of CO₂ in freshwater springs taken by Zarroca et al. (2012). In the northern part of the study area (449194, 4662424 (UTM 31N - ED50)), Moreno et al. (2014) catalogued 53 groundwater radon measurements in water wells and springs. All these data were incorporated into a database and are presented in this work, together with data from other springs (Fig. 5).

The location of seismic events was also incorporated into the dataset used in this study (Fig. 6). Although seismic events are not that abundant in the northeastern part of the Iberian Peninsula, it was possible to collect accurate data regarding the earthquakes recorded since 1978 by the Geological Survey of Catalonia (www.igc.cat). This data provides information regarding the current tectonic stresses in the GVF. We compiled the location, depth and magnitude of the seismic events; locations of seismic events were represented on the structural map. The average distance between seismic stations is 30 km and data pertaining to earthquakes located within this network have an accuracy of 2–3 km for epicentres and 5 km for depths (Goula et al., 1999).

The presence of upper-mantle and lower-crust xenoliths in volcanic products has been used as an indicator of the depth of magma pathways and to estimate magma ascent velocities (Sparks et al., 1977, 2006; Spera, 1984; Tsuchiyama 1986; Sachs and Stange, 1993; Klügel, 1998; Mattsson 2012; Jankovics et al., 2013). In this study we mapped the distribution of the volcanoes containing lower-crust xenoliths, mantle-derived xenoliths or both (Fig. 7) as a way of estimating the depth of the fractures and faults through which magma is transported to the surface. Calculations of magma ascent velocities were made on the basis of the assumption that magma (melt) was – in rheological and petrological terms – similar throughout the study area (i.e. basalts and basanites) (Araña et al., 1983; Cebriá et al., 2000; Martí et al., 1992), although the distribution of xenoliths does in fact vary. In addition, we assumed that during its ascent the magma did not undergo any significant temperature variations, as has been suggested by Cimarelli et al. (2012), and that its rheology was close to that of a Newtonian fluid, as should occur in the case of a magma of this composition with a crystal content of less than 15% (see Vona et al, 2011). With these assumptions in mind, we applied the method of Spera (1980, 1984), which defines:

$$Re_n = \frac{\rho_l D_n u_n}{\eta_l} \quad (2)$$

$$u_n = \left(\frac{8R_n \Delta \rho g}{3C_d \rho_l} \right)^{1/2} \quad (3)$$

where η_l , u_n , R_n , $\Delta \rho$, ρ_l , g and C_d represent the Newtonian viscosity, nodule settling velocity, radius, density difference between melt and xenolith, density of melt, gravity value, and drag coefficient, respectively. C_d is related to the nodule settling velocity and hence to Re_n . For our samples we considered $Re_n > 0.1$ and therefore we applied:

$$C_d = 18Re_n^{-3/5} \quad (4)$$

In order to estimate the minimum ascent rate we took into account the maximum size of xenoliths found in the area. The density of the melt was measured from natural rock glass by remelting a representative sample in a Pt crucible at 1400° C for 5 hours in an open atmosphere to remove vesiculation. The density obtained was 2.53 g/cm³. Finally, we used the method of Vona et al. (2011) to estimate the viscosity (40 to 50 Pa.s).

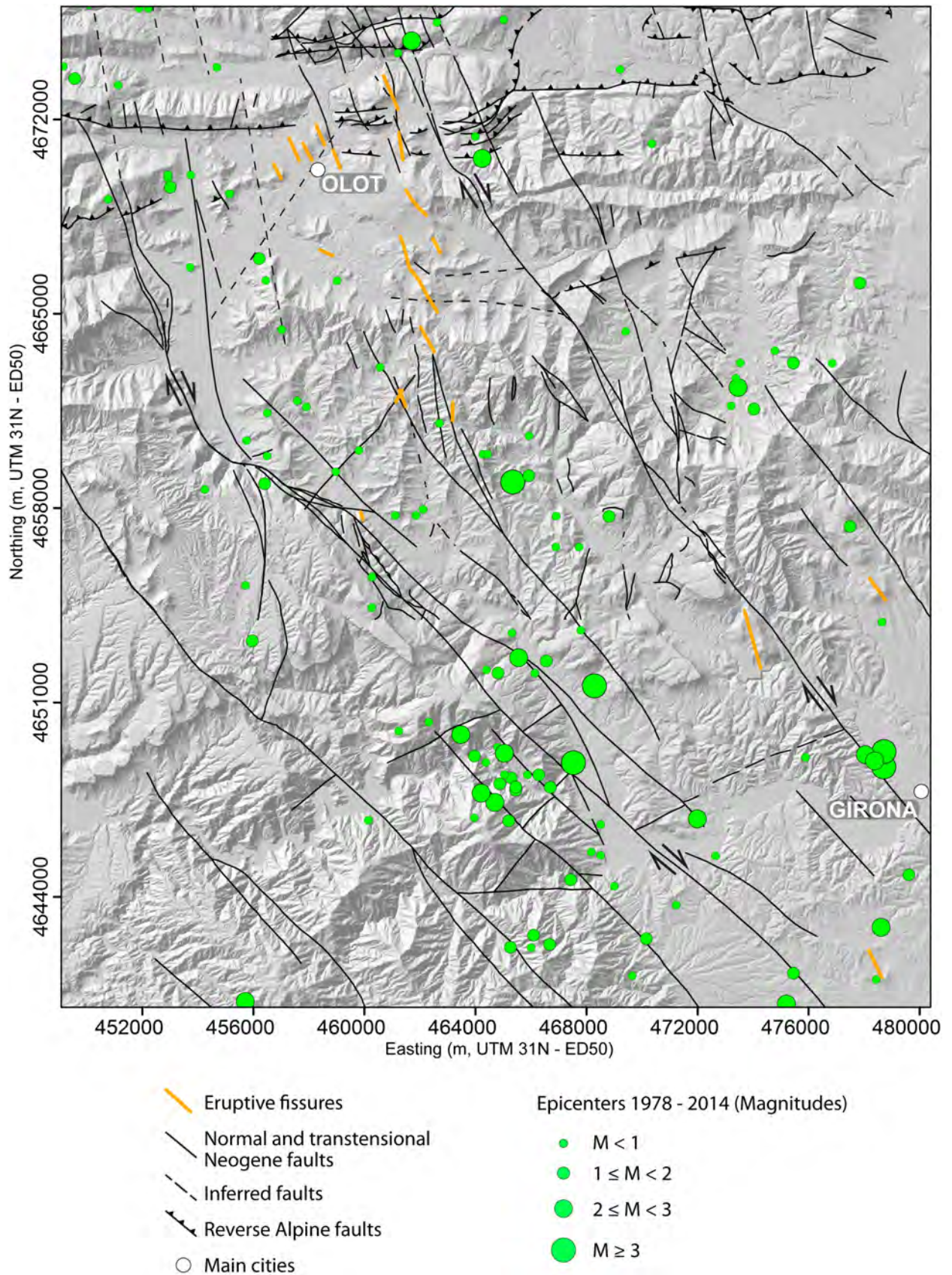


Fig. 6. Epicentral map of regional seismic events recorded by the Geological Survey of Catalonia (IGC) since 1978.

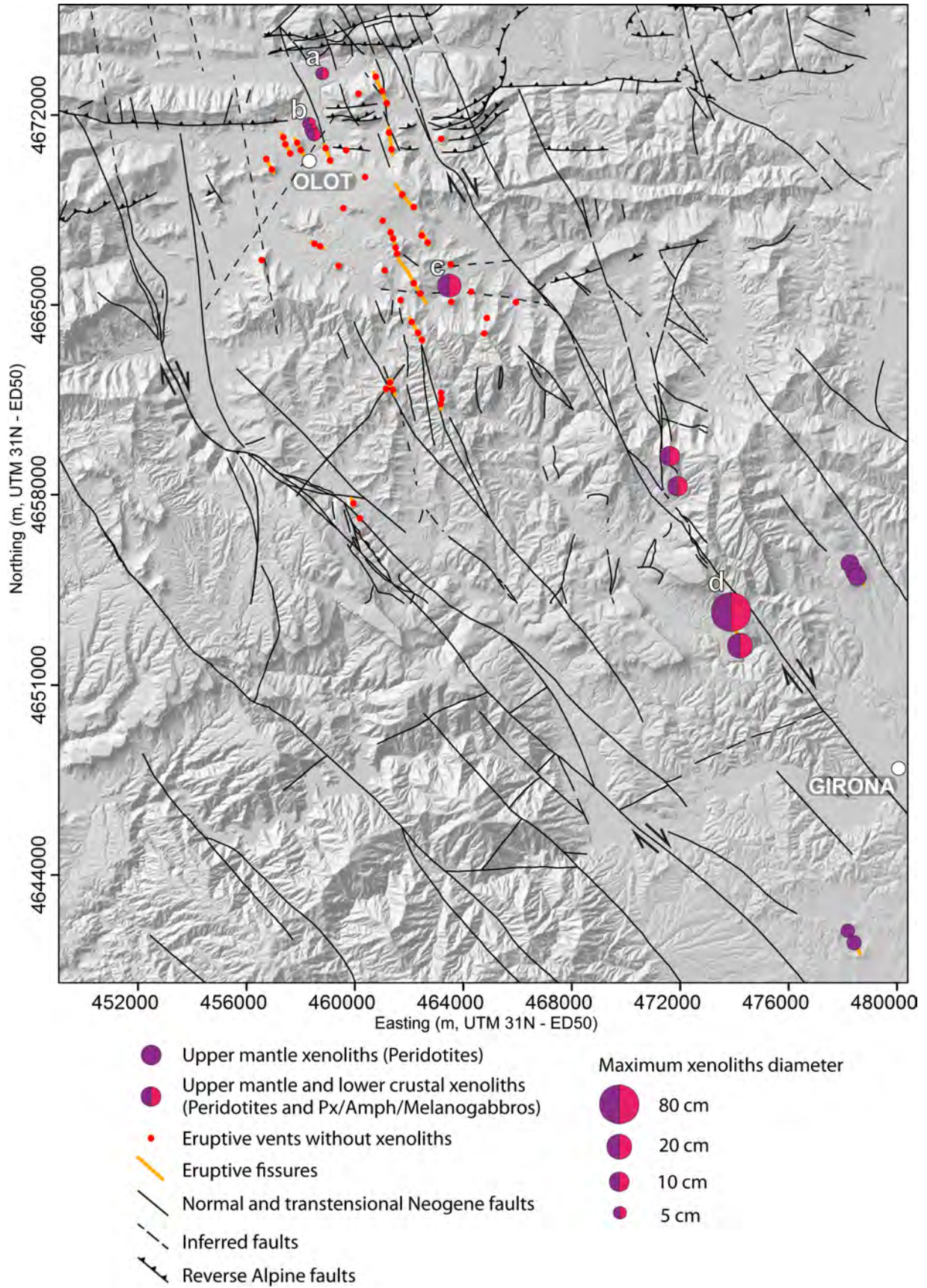


Fig. 7. Volcano-structural map with the distribution of all ultramafic xenoliths (upper-mantle and lower-crust xenoliths) found in the study area, with an indication of their maximum size. a: La Canya; b: La Garrinada; c: Rocanegra; d: Puig de la Banya del Boc.

7.5. Results

Although the GVF is constrained above all between two Neogene faults, the Amer and Llorà faults, there are a few other volcanic outcrops and vents located outside these structural limits, mainly east of the Llorà fault (Fig. 2). No vents are directly located on the Amer and Llorà faults. All the vents identified in this study are located on subordinated faults. In the field it is clear that the majority of volcanic deposits have not been affected by the Neogene faults. Only the main Amer fault affects the central sector of the volcanic deposits (Fig. 8). Most of the volcanic deposits located in the north of the study area cover the basement rocks, which prevents the subordinate faults in this zone from being identified. Towards the north, a set of E-W reverse faults and thrusts formed during the Alpine Orogeny delimits the volcanic field but is intersected (crossed) by the same NW-SW Neogene fault system that constrains the volcanic field further to the south (Fig. 2) (Table 1, Supp. material).



Fig. 8. Outcrops of Quaternary volcanic deposits affected by the Amer fault.

A total of 67 eruptive vents were mapped in the study area and are represented on our map (Fig. 2) by points corresponding to the middle of the craters of isolated cinder cones and of coalescent cinder cones that belong to the same eruptive fissure. The majority of eruptive vents (83.5%) are located in the northern sector of the GVF, around the city of Olot (Fig. 2), while only a few (16.5%) are located in the southern sector (Fig. 2) (Table 1, Supp. material). However, the volcanoes in the southern sector are larger and emitted more magma than those in the northern sector (Bolós et al., 2014a). Several volcanic deposits that cannot be associated with any eruptive vent, either because they have been eroded or covered by more recent volcanic materials, were not considered in our structural analysis.

The alignments defined by 44 eruptive vents allowed us to infer up to 19 eruptive fissures (Fig. 2). All fissures have the same trend, with a strike average of $\sim N155^{\circ}E$; the exception is a fissure with a strike of $N29^{\circ}E$ subparallel to a related. The longest fissure was measured at ~ 3050 m and is located in the central area of the northern sector (Pomareda - Crosca - Santa Margarida eruptive fissure) (Pm-Cr-Sta.M in Fig. 2), and was recognized through geological fieldwork and geophysical studies (Barde-Cabusson et al., 2013; Barde-Cabusson et al., 2014). The shortest fissure measures 287 m and the average fissure length is 968 m, although most fissures measure between 400 and 1200 m (Table 1, Supp. material).

The 28 analysed cones have basal widths between 160 and 1430 m (average 610 m) and heights between 20 and 170 m (average 73 m). 23 of the 28 cones have visible craters, with some cones having 2 or 3 coalescing craters. Additionally, 4 craters not associated to any cone, were also mapped. Of a total of 36 analysed craters, 21 are breached. Closed craters have widths between 40 and 390 m (average 220 m; excluding one large crater with a width of 1160 m) and depths between 5 and 60 m (average 20 m). Cone bases EI vary between 1.2 and 2.1, and for the closed crater outlines between 1.2 and 1.5; EI average of elevation contours vary between 1.3 and 4.9. Elongation azimuths of the cone bases, closed crater outlines and elevation contours, together with breaching directions of the breached craters, defines two orientation trends: a main NW-SE to NNW-SSE trend (with crater breaching mostly to the NNW), and a secondary NE-SW trend (with crater breaching towards the NE) (see Table 2 in Supp. material).

The analysis of the drainage network also allowed us to distinguish different trends that confirm the main structural features of the area; the four principal stream directions identified were NW-SE, NE-SW, N-S and E-W (Fig. 3).

In order to obtain an unbiased analysis of the main direction of the alignments, we performed a statistical study based on the nearest-neighbour concept. The results obtained show a lineament distribution that clearly follows a NNW-SSE trend (Fig. 4). Secondary directions ranging from NE-SW to E-W were also obtained.

The majority of freshwater springs identified and plotted on the structural map coincide with the main tectonic elements such as Neogene faults and the Alpine reverse faults (Fig 5). However, a few springs are not associated to any structural element. Moreno et al. (2014) analysed the endogenous gas content of springs and water wells in the northern part of the study area. A total of 41 measurements of water radon concentration with values between 16.7 and 7.1 Bq.l⁻¹ were made, with most located on the Amer and Llorà faults and others on other Neogene secondary faults (Fig. 5). As well, Zarroca et al. (2012) measured a total of 12 CO₂-rich springs located in the southern part of our study area on the central part of the Amer fault (Fig.5). The emissions of CO₂ in this area are clearly measurable in the field as sustained bubbling in freshwater springs.

A total of 144 seismic events have been recorded in the GVF since 1978 (Fig. 6) and are mostly distributed along the Neogene faults clustered between the Amer and Llorà faults. Moreover, there is a greater density of seismic events in the central part of the Amer fault that coincides with high CO₂ emissions. The maximum earthquake magnitude registered in this period was 3.5 (local magnitude) in 1983 on the Amer fault (Fig. 6) (Table 3, Supp. material). Despite the low present-day seismicity, a swarm of powerful earthquakes that took place in 1427-1428 with epicentral intensities ranging between VI and VIII has been attributed to a movement of the Amer fault (Fontserè and Iglésies, 1971; Goula et al., 1999; Olivera et al., 2003, 2006; Perea, 2009; Zarroca et al., 2012).

As explained above, we also considered the distribution of mantle-derived xenolith and crustal cumulates as a way of indicating the depth of the faults and fissures through which they were transported to the surface, and of estimating magma ascent velocities. The distribution of all ultramafic xenoliths found in the area along with their maximum sizes is shown in Figure 7. We observed that the presence of xenoliths is related to the volcanoes located near – but not on – the main Llorà fault. In the area with the greatest density of volcanic cones (northern area), only three volcanoes (Rocanegra, La Garrinada and La Canya;

see Fig. 7) have ultramafic xenoliths, whilst in the southern sector all the volcanoes have this type of xenoliths. Moreover, we observed that the presence of upper-mantle cumulates (i.e. spinel lherzolites) coincides with the volcanoes that have xenoliths, whereas the presence of lower-crust cumulates (i.e. Pyroxenites/Amphybolites) is restricted to volcanoes located in the northern sector and just one volcano in the south sector (Puig de la Banya del Boc; see Fig. 7). The maximum sizes of the ultramafic xenoliths found in the GVF correspond to pyroxenites, with diameters of up to 80 cm (Fig. 9). However, most xenoliths range in size from a few centimetres to 20 cm in diameter, for both mantle-derived nodules and lower-crust cumulates. Velocities of 0.19 to 0.21 m/s have been obtained using equations 2, 3, 4, assuming a Newtonian viscosity of 40–50 Pa.s, the largest xenolith encountered (80 cm), a melt density of 2.53 g/cm³, a xenolith density of 3.55 g/cm³, and a gravity value of 9.8 m/s². The velocities obtained are in accordance with those suggested for other monogenetic volcanic fields (Szabó and Bodnar, 1996; Klügel, 1998; Sparks et al., 2006; Mattsson, 2012; Harangi et al., 2013; Jankovics et al., 2013).



Fig. 9. Photograph of the largest xenolith (pyroxenite) found in the study area (Banya del Boc volcano, southern sector of the GVF, see Fig. 7).

7.6. Discussion and conclusions

The morphological and structural data presented above reveal that the evolution of the GVF has been mostly controlled by two major Neogene faults, the Amer and Llorà faults. They are both oriented NW-SE as are most of the major post-Alpine extensional faults that have defined a horst and graben structural pattern in NE Iberia. However, most of the eruptive fissures and secondary structural lineaments identified in this study show a NNW-SSE trend that runs slightly obliquely to the main faults.

The pattern shown by the eruptive fissures and subordinated structural lineaments is compatible with a slight dextral transtensional component in the two main faults, as previously suggested by previous studies (Goula et al., 1999; Olivera et al., 2003) and indicates that magma ascent in the uppermost crust and subsequent eruptions were controlled by these subordinated fissures. This structural configuration would have favoured the opening of these fractures and the transport of magma through them, at least in the final pre-eruptive stages. Similar behaviour has been described in other volcanic zones (e.g.

Karakhianian et al., 2002). However, it is not clear how deep these fractures are nor what exactly was their role in transporting magma from deeper levels.

The presence of mantle-derived xenoliths and lower-crust cumulates suggests that the magmas that erupted in the GVF came either directly from the source region in the upper mantle or from intermediate reservoirs located at the base of the crust. No evidence exists for the presence of shallower reservoirs under this volcanic field. This is also confirmed by existing petrological and geochemical data (Martí et al., 1992; Neuman et al., 1999; Cebriá et al., 2000). Therefore, what remains to be discerned is how deep the structures observed on the surface extend and how they were used by magma to reach the surface. It is worth noting that most of the area's freshwater springs are associated with relatively shallow stratigraphic or structural discontinuities, while the presence of high radon and CO₂ concentrations mainly occurs along the major Neogene faults (Moreno et al., 2014; Zarroca et al., 2012), thereby indicating that the deep circulation of these mantle-derived gases is permitted through these faults (Redondo and Yélamos, 2005; Zarroca et al., 2012). Likewise, the recorded seismicity also reveals that Neogene faults have been active recently, mainly along the Amer fault. Finally, the obtained magma ascent rates indicate that only a relatively short time was required for magma to reach the surface, thereby suggesting the existence of preferential pathways for magma when ascending from source or accumulation regions to the eruption sites.

Taking into account all this evidence we speculate that the Llorà fault played the most important role in driving magma from the source region, either to the base of the crust where magma occasionally accumulated (underplating) and differentiated or directly to much shallower levels where it was captured by the subordinated fractures that allowed it to erupt to the surface. As indicated by the presence of lower-crust cumulates and the location of vents and eruptive fissures, the extraction of magma from the lower crust reservoir(s) was mainly controlled by the Llorà fault and, to a lesser extent, by the Amer fault, which would have acted as a conjugate major fault reaching down the base of the crust. Shallow subordinated fractures to the Amer fault would have also captured the ascending magma in its last stages and have controlled its eruption to the surface (Fig. 10).

Confirming the proposed model would require the undertaking of a detailed petrological study, which is beyond the purpose of this paper. However, the fact that the mantle-derived xenoliths and the largest lower-crust cumulates are restricted to the vents related to the Llorà fault is strong support for this model. Likewise, the volcanoes associated with this fault have the largest erupted volumes (Bolós et al., 2014b) of all volcanoes in this volcanic field, which also suggests that the Llorà fault was the main magma pathway.

The reason why magma eruptions have occurred through different NNW-SSE eruptive fissures during the history of the GVF – despite its constant and common feeding system at depth – seems to be related to the role played by these subordinate shallow fractures. They captured magma during the final stages of its ascent to the surface and so determined the point of each eruption. The shallow character of these fractures suggests that the local stress field, which was mostly controlled by the movement of the two main (Llorà and Amer) faults, only made a weak contribution. Under these circumstances, these shallow fractures could be easily sealed by residual magma that solidified within and it was easier for a new eruptive episode to open a fresh fracture than to reuse a previously sealed one. The sealing of these eruptive fissures by intruding magma would also obstruct the

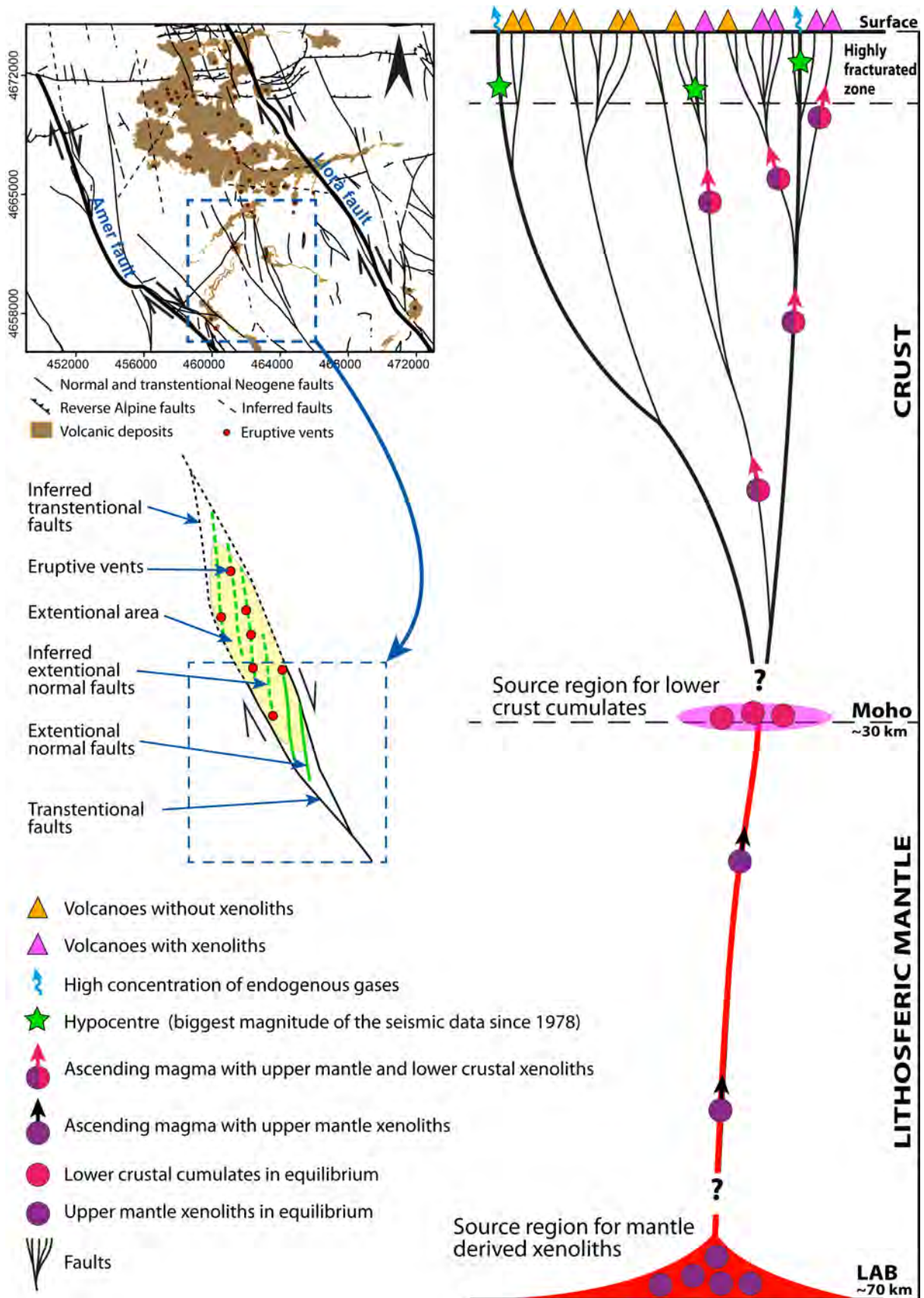


Fig. 10. Schematic representation of the relationships between regional/local tectonic faulting and the plumbing system of La Garrotxa Volcanic Field. (Right) cross section. (Left) top view.

circulation of the endogenous gases, as is shown in the northern sector around Olot, where most eruptive vents have no associated volcanic gas emissions. This would also suggest – in accordance with the intermittent character of this volcanism (Martí et al., 1992) – that each eruptive episode corresponds to an intermittent reactivation of the main fault system every 5 000 – 20 000 years. These tectonic reactivations would permit the ascent of deep magma and the opening of subordinate fractures in the uppermost crust, which would erupt on the surface each time in a different location in the volcanic field. Volcanism in the GVF is mainly concentrated in its northern sector, which suggests that the basin in this area is larger, where the accumulation of post-Alpine sediments is thicker. Moreover, the difference in basement lithology between the northern (Tertiary and Quaternary sediments) and southern (Paleozoic granites and schists) sectors of the volcanic field may also have played a significant role in controlling the ability for magma to find pathways to reach the surface. The fact that there is no magmatism north of the GVF may be due to the important increase in thickness of the crust due to the Alpine Orogeny (Fig. 2).

Although the GVF is the best-preserved area in the Catalan Volcanic zone, it is not the only one containing important volumes of volcanic rocks. Older zones such as the Empordà or La Selva (Araña et al., 1983; Martí et al., 1992) also have numerous volcanic features that can be observed on the surface (highly eroded outcrops) or in the subsoil in seismic profiles and gravity and aeromagnetic maps (Casas et al., 1986; Zeyen and Banda, 1988). The tectonic evolution of the area has been controlled by a similar system of Neogene NW-SE-oriented faults, which seems to have evolved over time from NE to SW. We believe that a similar model to the one proposed in this study for the GVF could be applied to other areas in the Catalan Volcanic Zone.

In conclusion, the GVF provides a good example of the structural complexity that governs monogenetic volcanism. Although magma ascent from the depths has always been controlled by the same Neogene extensional fault system that reaches the base of the lithosphere, magma transport in the uppermost crust and the eruptions were controlled by subordinated fractures originating in response to the transtensional component of the main faults. These shallow fractures were sealed by the remaining magma after each eruption and so new fractures had to be opened in each new eruptive episode, probably in association with a sporadic reactivation of the main faults. The model proposed has important implications for hazard assessment as this pattern of magma flow makes this type of volcanism largely unpredictable in terms of the eruption location since the exact position of new vents does not necessarily follow a statistically pre-defined law. Any point located in the area affected by the tectonic stresses constrained by the two main faults could host a new vent if no major basement rheological discontinuities exist. Moreover, the calculated ascent velocities imply that magma may travel either from the source region in the mantle or from the base of the crust to the surface in just a few days, as has been proposed in other monogenetic fields. It is likely that most of this journey occurred aseismically due to the relatively large dimensions of the path provided by the main faults and the absence of shear movement between the fault planes, as occurred in the 2011-2012 El Hierro eruption (Martí et al., 2013). Only when magma had to open the shallow subordinate fractures did the hydraulic fracturing cause any shallow seismicity that could warn of the imminence of the eruption. Therefore, precise knowledge of the stress configuration and distribution of rheological and structural discontinuities in monogenetic fields is crucial when attempting to forecast monogenetic volcanism.

Acknowledgments

This study was partially funded by the European Commission (FT7 Theme: ENV.2011.1.3.3-1; Grant 282759: "VUELCO") and Beca Ciutat d'Olot en Ciències Naturals. We are grateful to La Garrotxa Volcanic Zone Natural Park for their support throughout this study. We would like to thank Emilio Casciello, Núria Bagués, Joan Andujar, Pierangelo Romano, Dario Pedrazzi, Daniele Giordano, Jorge Pedro Galve, Xavier Castelltort and Daniel Nadal for their suggestions during this research. We also thank Enric Vinyals for providing us with unpublished information on seismic studies in the study area. The English text was corrected by Michael Lockwood.

References:

- Acocella, V., Tibaldi, A., 2005. Dike propagation driven by volcano collapse: a general model tested at Stromboli, Italy. *Geophysical Research Letters* 32.
- Araña, V., Aparicio, A., Martín Escorza, C., García Cacho, L., Ortiz, R., Vaquer, R., Barberi, F., Ferrara, G., Albert, J., Gassiot, X., 1983. Neogene-Quaternary volcanism of Catalunya: structural, petrological, and geodynamic characteristics. *Acta Geol. Hisp.* 18, 1-17.
- Barde-Cabusson, S., Bolós, X., Pedrazzi, D., Lovera, R., Serra, G., Martí, J., Casas, A., 2013. Electrical resistivity tomography revealing the internal structure of monogenetic volcanoes. *Geophysical Research Letters* 40, 2544-2549.
- Barde-Cabusson, S., Gottsman, J., Martí, J., Bolós, X., Camacho, A.G., Geyer, A., Planagumà, L., Ronchin, E., Sanchez, A., 2014. Structural control of monogenetic volcanism in the Garrotxa volcanic field (Northeastern Spain) from gravity and self-potential measurements. *Bulletin of Volcanology* 76, 788.
- Becerril, L., Cappello, A., Galindo, I., Neri, M., Del Negro, C., 2013. Spatial probability distribution of future volcanic eruptions at El Hierro Island (Canary Islands, Spain). *Journal of Volcanology and Geothermal Research* 257, 21-30.
- Bibby H. M., Caldwell T. G., Risk G. F., 1998: Electrical resistivity image of the upper crust within the Taupo Volcanic Zone, New Zealand. *Journal Geophysical Research*, 103, 9665-9680.
- Bianchini, G., Beccaluva, L., Bonadiman, C., Nowell, G., Pearson, G., Siena, F., Wilson, M., 2007. Evidence of diverse depletion and metasomatic events in harzburgite–lherzolite mantle xenoliths from the Iberian plate (Olot, NE Spain) implications for lithosphere accretionary processes. *Lithos* 94, 25-45.
- Blaikie, T. N., Ailleres, L., Betts, P. G., Cas, R.A.F., 2014, A geophysical comparison of the diatremes of simple and complex maar volcanoes, Newer Volcanics Province, south-eastern Australia. *Journal of Volcanology and Geothermal Research* 276 (2014) 64–81
- Bolós, X., Barde-Cabusson, S., Pedrazzi, D., Martí, J., Casas, A., Himi, M., Lovera, R., 2012. Investigation of the inner structure of La Crosa de Sant Dalmai maar (Catalan Volcanic Zone, Spain). *Journal of Volcanology and Geothermal Research* 247–248, 37-48.
- Bolós, X., Barde-Cabusson, S., Pedrazzi, D., Martí, J., Casas, A., Lovera, R., Nadal-Sala, D., 2014a (in press). Geophysical exploration on the subsurface geology of La Garrotxa

- monogenetic Volcanic Field (NE Iberian Peninsula). *International Journal of Earth Science*.
- Bolós, X., Planagumà, L., Martí, J., 2014b (in press). Volcanic stratigraphy and evolution of the Quaternary monogenetic volcanism in the Catalan Volcanic Zone (NE Spain). *Journal of Quaternary Science*.
- Brenna, M., Cronin, S.J., Németh, K., Smith, I.E.M., Sohn, Y.K., 2011. The influence of magma plumbing complexity on monogenetic eruptions, Jeju Island, Korea. *Terra Nova* 23(2), 70-75.
- Catalan Geographic Institute (ICC). <http://www.icc.cat/>. Accessed 15 January 2014
- Catalan Geologic Institute (IGC). <http://www.igc.cat/>. Accessed 15 January 2014
- Cardozo, N., Allmendinger, R.W., 2013. Spherical projections with OSXStereonet Computers & Geosciences 51, 193-205.
- Casas, A., Torné, M., Banda, E., 1986. Mapa gravimètric de Catalunya 1:500000. Servei Geològic de Catalunya . Dpt. De Política Territorial i Obres Públiques.
- Cebrià, J.M., López-Ruiz, J., Doblas, M., Oyarzun, R., Hertogen, J., Benito, R., 2000. Geochemistry of the Quaternary alkali basalts of Garrotxa (NE Volcanic Province, Spain): a case of double enrichment of the mantle lithosphere. *Journal of Volcanology and Geothermal Research* 102, 217-235.
- Cebrià, J.M., Martín-Escorza, C., López-Ruiz, J., Morán-Zenteno, D.J., Martiny, B.M., 2011. Numerical recognition of alignments in monogenetic volcanic areas: Examples from the Michoacán-Guanajuato Volcanic Field in Mexico and Calatrava in Spain. *Journal of Volcanology and Geothermal Research* 201, 73-82.
- Cimarelli, C., Di Traglia, F., de Rita, D., Gimeno Torrente, D., Fernandez Turiel, J.L., 2013. Space-time evolution of monogenetic volcanism in the mafic Garrotxa Volcanic Field (NE Iberian Peninsula). *Bulletin of Volcanology* 75, 758.
- Cimarelli, C., Di Traglia, F., Taddeucci, J., 2012. Basaltic scoria textures from a zoned conduit as precursors to violent Strombolian activity. *Geology* 38, 439-442.
- Clemens, J.D., Mawer, C.K., 1992. Granitic magma transport by fracture propagation. *Tectonophysics* 204, 339-360.
- Connor, C.B., Conway, F.M., 2000. Basaltic volcanic fields. In: Sigurdsson, H., Houghton, B.F., McNutt, S.R., Rymer H., Stix J. (Editors), *Encyclopedia of Volcanoes*. Academic Press, San Diego, p. 331–343.
- Dèzes, P., Schmid, S.M., Ziegler, P.A., 2004. Evolution of the European Cenozoic Rift System: interaction of the Alpine and Pyrenean orogens with their foreland lithosphere. *Tectonophysics* 389, 1–33.
- Di Maio, R., Mauriello, P., Patella, D., Petrillo, Z., Piscitelli, S., Siniscalchi, A., 1998. Electric and electromagnetic outline of the Mount Somma-Vesuvius structural setting. *Journal of Volcanology and Geothermal Research*, 82, 219-238.
- Di Maio R., Patella D., Petrillo Z., Siniscalchi A., Cecere G., De Martino P., 2000: Application of electric and electromagnetic methods to the definition of the Campi Flegrei caldera (Italy). *Annali di Geofisica*, 43, 375-390.
- Downes, H., 2001. Formation and modification of the shallow sub-continental lithospheric mantle: a review of geochemical evidence from ultramafic xenolith suites and tectonically emplaced ultramafic massifs of Western and Central Europe. *Journal of Petrology* 42, 233-250.

- Fernández, M., Torné, M., Zeyen, H., 1990. Lithospheric thermal structure of NE Spain and the North-Balearic basin. *Journal of Geodynamics* 12, 253–267.
- Fiske, R.S., Jackson, E.D., 1972. Orientation and growth of Hawaiian volcanic rifts: the effect of regional structure and gravitational stresses. *Proc. R. Soc. Lond.* 329, 299-326.
- Fontserè, E., Iglésies, J., 1971. Recopilació de dades sísmiques de les terres catalanes entre 1100 i 1906. Fundació Salvador Vives Casajuana, Barcelona, 548.
- Galán, G., Oliveras, V., Paterson, B.A., 2008. Types of metasomatism in mantle xenoliths enclosed in Neogene–Quaternary alkaline mafic lavas from Catalonia (NE Spain). *Geological Society of London* 293, 121-153.
- Gallart, J., Olivera, C., Correig, A., 1984. Aproximació geofísica a la zona volcànica de Olot (Girona). Estudio local de sismicidad. *Revista de Geofísica* 40, 205-226.
- Gallart, J., Pous, J., Boix, F., Hirn, A., 1991. Geophysical constraints on the structure of the Olot Volcanic Area, north-eastern Iberian Peninsula. *Journal of Volcanology and Geothermal Research* 47, 33–44.
- Goula, X., Olivera, C., Fleta, J., Grellet, B., Lindo, R., Rivera, L.A., Cisternas, A., Carbon, D., 1999. Present and recent stress regime in the eastern part of the Pyrenees. *Tectonophysics* 308, 487–502.
- Gretnener, P.E., 1969. On the mechanics of the intrusion of sills. *Canadian Journal of Earth Sciences* 6, 1415–1419.
- Grosse, P., van Wyk de Vries, B., Petrinovic, I.A., Euillades, P.A., Alvarado, G., 2009. Morphometry and evolution of arc volcanoes. *Geology* 37, 651–654. Gudmundsson, A., 2003. Surface stresses associated with arrested dykes in rift zones. *Bulletin of Volcanology* 65, 606-619.
- Grosse, P., B. van Wyk de Vries, P. A. Euillades, M. Kervyn, and I. Petrinovic (2012), Systematic morphometric characterization of volcanic edifices using digital elevation models, *Geomorphology*, 136, 114–131, doi:10.1016/j.geomorph.2011.06.001.
- Gudmundsson, A., Philipp, S.L., 2006. How local stress fields prevent volcanic eruptions. *J. Volcanol. Geotherm. Res.* 158, 257-268.
- Guérin, G., Behamoun, G., Mallarach, J.M., 1985. Un exemple de fusió parcial en medi continental. El vulcanisme quaternari de la Garrotxa. Publicació del Museu Comarcal de la Garrotxa, *Vitrina* 1, 19–26.
- Harangi, S., Sági, T., Seghedi, I., Ntaflos, T., 2013. Origin of basaltic magmas of Perşani volcanic field, Romania: a combined whole rock and mineral scale investigation. *Lithos* 180-181, 43–57 (in this issue).
- IGME, 2011. Continuous Digital Geological Map of Spain, Canary Islands, 1:25.000, <http://cuarzo.igme.es/sigeco/>. Accessed 15 January 2014
- Jankovics, M.É., Dobosi, G., Embey-Isztin, A., Kiss, B., Sági, T., Harangi, S., Ntaflos, T., 2013. Origin and ascent history of unusually crystal-rich alkaline basaltic magmas from the western Pannonian Basin. *Bulletin of Volcanology* 75, 1–23. DOI 10.1007/s00445-013-0749-7
- Karakhian, A., Djrbashian, R., Trifonov, V., Philip, H., Arakelian, S., 2002 holocene-historical volcanism and active faults as natural risk factors for Armenia and adjacent countries. *Journal of Volcanology and Geothermal Research* 113, 319-344
- Kavanagh, J.L., Menand, T., Sparks, R.S.J., 2006. An experimental investigation of sill formation and propagation in layered elastic media. *Earth Planetary Science Letters* 245, 799-813.

- Klügel, A., 1998. Reactions between mantle xenoliths and host magma beneath La Palma (Canary Islands): constraints on magma ascent rates and crustal reservoirs. *Contrib Mineral Petrol* 131(2):237–257
- Kresic, N., 2010. Types and classifications of springs, in: Kresic, N., Stevanovic, Z. (Eds.), *Groundwater Hydrology of Springs: Engineering, Theory, Management and Sustainability*. Butterworth-Heinemann, p. 592.
- Le Corvec, N., Menand, T., Lindsay, J., 2013. Spatial distribution and alignments of volcanic centers: Clues to the formation of monogenetic volcanic fields. *Earth-Science Reviews* 124, 96-114.
- Llobera, P., 1983. Petrologia de los enclaves del volcán Roca Negra (Olot, NE España). *Acta Geológica Hispánica* 18, 19-25.
- Lutz, T.M., 1986. An analysis of the orientations of large-scale crustal structures: a statistical approach based on areal distributions of pointlike feature. *Journal of Geophysical Research* 91 (B1), 421–434.
- Martí, J., Mitjavila, J., Roca, E., Aparicio, A., 1992. Cenozoic magmatism of the Valencia trough (western Mediterranean): relationship between structural evolution and volcanism. *Tectonophysics* 203, 145-165.
- Martí, J., Planagumà, L., Geyer, A., Canal, E., Pedrazzi, D., 2011. Complex interaction between Strombolian and phreatomagmatic eruptions in the Quaternary monogenetic volcanism of the Catalan Volcanic Zone (NE of Spain). *Journal of Volcanology and Geothermal Research* 201, 178-193.
- Martí, J., Pinel, V., López, C., Geyer, A., Abella, R., Tárraga, M., Blanco, M.J., Castro, A., Rodríguez, C., 2013. Causes and mechanisms of the 2011-2012 El Hierro (Canary Islands) submarine eruption, *J. Geophys. Res. Solid Earth*, 118, 823–839, doi:10.1002/jgrb.50087.
- Mattsson, H.B., 2012. Rapid magma ascent and short eruption durations in the Lake Natron–Engaruka monogenetic volcanic field (Tanzania): a case study of the olivine melilititic Pello Hill scoria cone. *Journal of Volcanology and Geothermal Research* 247–248, 16–25.
- McGee, L., Beier, C., Smith, I., Turner, S., 2011. Dynamics of melting beneath a smallscale basaltic system: a U-Th–Ra study from Rangitoto volcano, Auckland volcanic field, New Zealand. *Contributions to Mineralogy and Petrology*, 1-17.
- Michon, L., Merle, O., 2005. Discussion on “Evolution of the European Cenozoic Rift System: interaction of the Alpine and Pyrenean orogens with their foreland lithosphere”. *Tectonophysics* 401, 251-256.
- Moreno, V., Bach, J., Baixeras, C., Font, L., 2014. Radon levels in groundwaters and natural radioactivity in soils of the volcanic region of La Garrotxa, Spain. *Journal of Environmental Radioactivity* 128, 1-8.
- Neumann, E.R., Martí, J., Mitjavila, J., Wulff-Pedersen, E., 1999. Origin and implications of mafic xenoliths associated with Cenozoic extension-related volcanism in the Valencia Trough, NE Spain. *Mineralogy and Petrology* 65, 113-139.
- Nishi Y., Ishido T., Matsushima N., Ogawa Y., Tosha T., Myazaki J., Yasuda A., Scott B.J., Sherburn S., Bromley C., 1996: Self-Potential and audio-magnetotelluric survey in White Island Volcano. *New Zealand Geothermal Workshop* (<http://www.geothermal-energy.org/pdf/IGStandard/NZGW/1996/Nishi.pdf>).

- Olivera, C., Fleta, J., Susagna, T., Figueras, S., Goula, X., Roca, A., 2003. Seismicity and recent deformations in the northeastern of the Iberian Peninsula. *Física de la Tierra* 15, 111-114.
- Olivera, C., Redondo, E., Lambert, J., Riera Melis, A., Roca, A., 2006. Els terratrèmols dels segles XIV i XV a Catalunya. Institut Cartogràfic de Catalunya, Barcelona Monografies no. 30, 407.
- Paulsen, T.S., Wilson, T.J., 2010. New criteria for systematic mapping and reliability assessment of monogenetic volcanic vent alignments and elongate volcanic vents for crustal stress analyses. *Tectonophysics* 482, 16–28.
- Perea, H., 2009. The Catalan seismic crisis (1427 and 1428; NE Iberian Peninsula): Geological sources and earthquake triggering. *Journal of Geodynamics* 47, 259-270.
- Portal, A., Labazuy, P., Lénat, J.F., Béné, S., Boivin, P., Busato, E., Cârloganu, C., Combaret, C., Dupieux, P., Fehr, F., Gay, P., Laktineh, I., Miallier, D., Mirabito, L., Niess, V., Vulpescu, B., 2013. Inner structure of the Puy de Dôme volcano: cross-comparison of geophysical models (ERT, gravimetry, muon imaging). *Geosci. Instrum. Method. Data Syst.* 2, 47–54.
- Rubin, A.M., 1995. Propagation of magma-filled cracks. *Annual Review of Earth & Planetary Sciences* 23, 287-336.
- Sachs, P.M., Stange, S., 1993. Fast assimilation of xenoliths in mag-mas. *J Geophys Res* 98(B11): 19741-19754
- Saula, E., Picart, J., Mató, E., Llenas, M., Losantos, M., Berasategui, X., Agustí, J., 1996. Evolución geodinámica de la fosa del Empordà y de las Sierras Transversales. *Acta Geologica Hispánica* 29, 55–75.
- Sparks, R.S.J., Pinkerton, H., Macdonald, R., 1977. The transport of xenoliths in magmas. *Earth Planet Sci Lett* 35(2):234–238.
- Sparks, R.S.J., Baker, L., Brown, R.J., Field, M., Schumacher, J., Stripp, G., Walters, A., 2006. Dynamical constraints on kimberlite volcanism. *J Volcanol Geotherm Res* 155(1–2):18–48.
- Spera, F.J., 1980. Aspects of magma transport, in: Hargraves, R.B. (Ed.), *Physics of magmatic processes*. Princeton University Press, p. 265-323.
- Spera, F.J., 1984. Carbon dioxide in petrogenesis III: role of volatiles in the ascent of alkaline magma with special reference to xenolith-bearing mafic lavas. *Contrib. Mineral. Petrol.* 88, 217-232.
- Szabó, C., Bodnar, R.J., 1996. Changing magma ascent rates in the Nógrád–Gömör volcanic field, Northern Hungary/Southern Slovakia: evidence from CO₂-rich fluid inclusions in metasomatized upper mantle xenoliths. *Petrology* 4(3):221–230
- Tibaldi, A., 1995. Morphology of pyroclastic cones and tectonics. *Journal of Geophysical Research* 100.
- Tibaldi, A., 2003. Influence of cone morphology on dykes, Stromboli, Italy. *Journal of Volcanology and Geothermal Research* 126, 79-95.
- Tibaldi, A., Bonali, F.L., Corazzato, C., 2014. The diverging volcanic rift system. *Tectonophysics* 611, 94-113.
- Tsuchiyama, A., 1986. Melting and dissolution kinetics: application to partial melting and dissolution of xenoliths. *J Geophys Res* 91(B9): 9395-9406

- Vona, A., Romano, C., Dinwell, D.B., Giordano, D., 2011. The rheology of crystal-bearing basaltic magmas from Stromboli and Etna. *Geochimica et Cosmochimica Acta* 75, 3214–3236.
- Walker, G.P.L., 1999. Volcanic rift zones and their intrusion swarms. *Journal of Volcanology and Geothermal Research* 94, 21–34.
- Wattananikorn, K., Kanaree, M., Wiboolsake, S., 1998. Soil gas radon as an earthquake precursor: some considerations on data improvement. *Radiate Measurements* 29, 593–598.
- Zarroca, M., Linares, R., Bach, J., Roqué, C., Moreno, V., Font, L., Baixeras, C., 2012. Integrated geophysics and soil gas profiles as a tool to characterize active faults: the Amer fault example (Pyrenees, NE Spain). *Environment Earth Science* 67, 889–910.
- Zeyen, H. J. Banda, E., 1988. Geophysical mapping in Catalonia. Aeromagnetic map. *Rev. Soc. Geol. España*, 1, (1-2), 73–79.
- Ziegler, P.A., 1992. European Cenozoic rift system. In: P.A. Ziegler (ed), *Geodynamics of Rifting, Volume I. Case History Studies on Rift: Europe and Asia*. *Tectonophysics*, 208:91–111.

Supplemental Table 1: Summary of the structural data.

		Total Nº	North Sector %	South Sector %	Mean Trend	Min. length (m)	Max. length (m)
Eruptive vents		67	83.5	16.5	-	-	-
Fissures		19	84.2	15.8	N155°E	287	3050
Faults	Main transtensional Neogen	604	-	-	NW-SW	-	-
	Secondary extensional Neogen				NNW-SSE		
	Reverse Alpine	90			E-W		

Supplemental Table 2. Summary of the morphometric data. ND: not determined. * Azimuth of crater

Name	X (m UTM 31N ED-50)	Y (m UTM 31N ED-50)	Basal Width (m)	Height (m)	Ellipticity index [basal outline]	Ellipticity index [avg. contours]	Azimuth Major Basal Axis (0-180°)	Avg. Azimuth Elevation contours (0-180°)	Crater [type]	Crater Width (m)	Crater Depth (m)	Ellipticity index [crater outline]	Azimuth Major Crater Axis (0-180°)	Breaching Direction (0-360°)
<i>Northern Sector</i>														
Aiguanegra volcano	460148	4672798	605	69	1.40	ND	114	ND	breached	296	28	ND	ND	307
Puig de l'Òs volcano	463197	4671125	614	83	1.27	1.70	49	162	breached	ND	ND	ND	ND	220
Puig de l'Estany volcano	461363	4670747	505	48	1.46	ND	45	ND	breached	245	19	ND	ND	336
Puig de Bellaire volcano	461268	4671371	472	36	1.80	ND	122	ND	closed	188	9	1.34	58	ND
Gengi volcano	461219	4670962	248	22	1.38	ND	41	ND	<i>no crater</i>	ND	ND	ND	ND	ND
Bisaroques volcano	459082	4670358	304	42	1.20	ND	79	ND	breached	156	4	ND	ND	342
Ca l'Isidret volcano	458924	4670777	238	26	1.38	ND	109	ND	breached	125	9	ND	ND	332
Garrinada volcano	458417	4671430	726	116	1.15	1.50	10	36	multiple (3); 2 closed & 1 breached	ND	ND	ND	163*	335
Montsacopa volcano	457906	4670935	669	83	1.62	1.69	148	137	multiple (2); closed & breached	ND	ND	ND	148*	151
Montolivet volcano	456937	4670015	644	87	1.48	ND	27	ND	breached	251	19	ND	ND	320
Puig Astrol volcano	461039	4668110	160	25	1.22	1.32	139	17	closed	41	5	1.25	61	ND
Pujalós volcano	461748	4669070	473	56	1.19	1.28	159	165	<i>no crater</i>	ND	ND	ND	ND	ND
Croscat volcano	461518	4667115	964	169	1.70	1.98	67	134	multiple (2); breached	ND	ND	ND	ND	203
Cabrioler volcanoes	458620	4667237	355	38	2.06	2.79	122	113	multiple (2); closed & breached	122	8	1.49	125	212

Puig Jordà v.	459401	4666446	343	54	1.51	2.22	68	36	breached	178	10	ND	ND	294
Puig de la Costa volcano	461117	4666257	793	115	1.81	4.28	43	150	breached	220	29	ND	ND	22
Santa Margarida volcano	462184	4665796	1296	161	1.64	1.44	126	105	closed	392	59	1.29	169	ND
Comadega volcano	461685	4665177	382	53	1.29	ND	167	ND	breached	147	10	ND	ND	65
Puig Subià volcano	463558	4665103	652	119	1.48	1.35	104	159	<i>no crater</i>	ND	ND	ND	ND	ND
Rocanegra volcano	463466	4665636	536	98	1.32	2.06	67	173	breached	261	24	ND	ND	54
Simon volcano	464297	4665482	480	33	1.26	ND	159	ND	breached	287	25	ND	ND	319
Racó volcano	456565	4666649	653	87	2.00	ND	50	ND	closed	149	12	1.43	67	ND
Fontpobra volcano	462100	4664362	562	38	1.36	ND	142	ND	breached	293	24	ND	ND	188
Traiter volcano	461298	4661940	582	60	1.39	ND	174	ND	multiple (3); 2 closed & 1 breached	ND	ND	ND	35*	151
Les Medes volcano	463179	4661343	701	62	1.61	ND	145	ND	multiple (2); closed & breached	ND	ND	ND	14*	170
Puig de Granollers volcanoes	471822	4658670	ND	ND	ND	ND	ND	ND	multiple (2); closed & breached	246; 416	16; 19	1.42	113	137
Southern Sector														
Banya del Boc volcano	473917	4653698	1428	118	1.87	4.86	122	141	breached	716	53	ND	ND	162
Clot de l'Omera v.	474197	4652475	ND	ND	ND	ND	ND	ND	closed	391	45	1.25	156	ND
Puig d'Àdri volcano	478554	4655037	1234	118	1.34	1.57	78	36	multiple (3); 1 tuff cone & 2 scoria cones breached	239	5	ND	ND	315
Crosa de Sant Dalmai maar	478402	4641591	466	21	1.95	2.11	117	102	multiple (2); tephra ring & scoria cone (intra-maar) breached	1163,3; 271,7	49; 9	1.21	33.00	149

Supplemental Table 3: Seismic events recorded by the Geological Survey of Catalonia (IGC) since 1978. ND: not determined.

Year	Month	Day	Hour	X (m UTM 31N ED-50)	Y (m UTM 31N ED-50)	Z (km)	Magnitude
1978	7	19	15:46	448637,7	4671031,3	2	2,9
1979	5	24	19:47	467528,9	4648822,6	1	3
1979	5	25	01:42	478711,2	4648669,2	1	3,3
1979	5	25	01:47	478712,9	4649224,4	ND	3
1979	5	25	07:32	478049,9	4649115,3	ND	2,9
1979	5	26	21:21	478380,6	4648892,3	ND	2,7
1981	6	22	15:22	455712,4	4640225,7	ND	2,7
1982	4	12	02:24	475202,3	4640131,1	ND	2,6
1982	4	12	14:55	463475,1	4649841,6	24	2,7
1982	4	12	15:21	465559,2	4652607,1	ND	2,6
1985	8	24	02:16	458974,6	4659304,4	ND	0
1986	8	25	22:17	462318,0	4650291,8	ND	0
1986	10	26	21:56	468286,8	4651595,0	3	3,5
1988	1	13	23:58	460105,5	4639755,6	ND	0
1988	2	11	04:50	478381,5	4676207,0	ND	0
1988	8	29	09:35	452479,0	4677333,7	ND	0
1988	10	7	19:46	446877,2	4678484,2	ND	0
1988	12	12	09:29	455723,1	4655215,6	ND	0
1990	4	16	08:14	449563,5	4673467,5	ND	1,6
1991	3	8	02:31	464798,1	4649390,8	2,8	
1991	10	29	12:54	468580,3	4680241,4	ND	2,5
1992	2	9	22:00	464242,9	4670601,7	1	2,9
1992	5	28	04:29	460410,4	4679283,3	ND	0
1992	8	16	13:20	450436,0	4680123,9	1	2,9
1992	9	5	20:59	466669,8	4642275,6	ND	1,9
1992	9	18	07:58	447960,3	4679919,7	8	2,8
1993	3	9	20:31	455865,7	4677977,9	ND	2
1993	4	19	12:24	446793,9	4678373,8	ND	0
1993	6	30	22:33	471994,1	4646805,0	ND	2
1993	8	2	21:54	478644,1	4653888,0	ND	0
1993	8	22	20:06	477496,2	4657333,6	ND	1,7
1993	9	2	12:39	456209,9	4666982,7	ND	1,8
1994	5	19	13:27	475895,9	4649011,3	ND	0
1994	11	15	01:54	464705,3	4647392,6	ND	2
1995	2	20	04:09	465341,8	4658937,2	1	3,2
1995	4	6	06:53	461705,9	4674834,5	9	2,3
1996	2	9	07:34	447942,2	4677476,9	4	2,4
1996	2	10	10:55	449114,1	4679800,2	ND	1,9
1996	3	25	21:33	459586,3	4679399,0	3	2,4
1996	11	7	12:23	472284,2	4678449,2	ND	1,6
1997	4	6	05:24	474036,9	4661564,8	ND	1,8
1997	4	6	05:25	475448,3	4663225,3	9	1,3
1997	4	6	05:45	473210,4	4661678,9	ND	0,7
1997	4	6	06:00	473461,0	4662344,2	7	2
1997	4	6	06:02	473379,6	4662677,6	ND	0,7
1997	4	25	23:14	466645,4	4637057,1	ND	1,5
1998	9	27	21:23	470153,0	4642482,2	ND	1,6
1998	12	29	00:20	452222,4	4676002,9	0,7	0

1999	5	8	11:46	446532,9	4676599,1	ND	0,7
1999	5	27	09:49	470356,2	4671128,5	ND	0,5
1999	11	9	02:41	478611,0	4642895,8	ND	2,1
2000	1	3	18:28	459011,5	4679846,5	1	3
2000	1	3	18:44	459006,3	4678958,2	ND	0,4
2000	1	3	18:55	459588,8	4679843,2	10	0,7
2000	1	3	19:17	459503,2	4679288,5	3	0,9
2000	1	3	19:48	459836,2	4679841,8	2	0
2000	1	3	19:49	461071,5	4679501,7	11	1,8
2000	1	3	20:18	459095,9	4680179,2	4	0,9
2000	1	3	21:45	459338,8	4679400,5	ND	0,1
2000	1	4	01:33	459013,5	4680179,7	13	0,5
2000	1	4	03:23	459257,0	4679512,0	3	0,6
2000	1	4	03:26	459498,0	4678400,2	ND	0,1
2000	1	4	03:40	459590,7	4680176,3	3	2,2
2000	1	4	03:45	458756,9	4678626,6	ND	0,3
2000	1	4	04:03	459421,3	4679400,0	6	1,5
2000	1	4	06:20	459422,6	4679622,1	3	1,4
2000	1	4	13:08	459340,1	4679622,5	3	0,9
2000	1	7	04:49	459423,2	4679733,1	3	1,1
2000	1	12	23:28	459421,3	4679400,0	6	0,3
2000	1	27	04:47	459833,1	4679286,6	7	0,4
2000	3	2	22:10	459421,3	4679400,0	7	0,7
2000	3	14	14:21	456453,0	4666203,9	ND	0,8
2000	5	13	06:09	466091,0	4642611,4	ND	1,4
2001	4	26	19:42	448224,0	4670923,3	14	1,4
2001	5	7	21:54	477854,7	4666104,3	ND	1,5
2001	10	24	18:12	456506,2	4661428,9	ND	0,5
2001	10	25	04:50	456496,6	4659874,4	ND	0,1
2001	10	26	14:04	457583,8	4661866,5	0,5	0
2001	10	29	19:28	457913,2	4661642,4	9	0,2
2001	10	30	05:55	455755,8	4660434,2	0,2	
2001	10	30	18:29	460567,2	4663070,6	ND	0,2
2002	1	2	06:50	459917,5	4679619,2	1	1,7
2002	1	25	15:33	451130,4	4673234,4	ND	0,1
2002	3	31	23:12	479611,3	4644780,4	ND	1,1
2002	6	10	15:55	450508,3	4678679,8	3	1,4
2002	6	13	23:23	463999,2	4671380,2	ND	0
2002	6	27	19:32	464811,3	4652055,6	3	1,1
2002	8	4	02:56	469649,9	4641151,9	ND	0,9
2002	8	11	07:54	446391,2	4668827,2	10	0,1
2002	11	3	04:17	465928,9	4660599,9	ND	0
2002	11	3	22:12	459806,1	4660076,9	ND	0,6
2002	11	5	02:03	456407,8	4658875,6	3	1,6
2002	11	17	20:50	461317,1	4679167,2	11	0,6
2003	4	21	22:42	475454,9	4641240,5	ND	1,2
2003	4	22	02:18	482025,5	4648993,1	ND	0,9
2003	4	22	23:36	467426,7	4644603,8	ND	1
2003	7	9	10:46	468332,9	4680242,5	ND	0
2003	8	3	13:14	466552,2	4652491,3	4	1,1
2003	9	3	13:55	446486,6	4659610,0	ND	0

2003	7	2	03:50	460240,4	4678395,9	7	1,6
2004	2	18	10:04	459503,8	4679399,5	2	1,3
2004	3	2	04:13	460251,1	4680283,6	3	1,7
2004	3	24	20:31	468810,5	4657699,7	6	1,6
2004	3	26	04:25	463968,1	4649061,9	ND	1,7
2004	4	13	19:05	460144,8	4646750,6	ND	0,6
2004	6	4	01:54	461387,4	4676946,0	10	1
2004	8	25	23:12	461239,5	4649964,5	ND	0,8
2004	11	21	21:56	448136,5	4670257,6	12	1,5
2004	11	22	00:22	448056,4	4670591,4	12	0,5
2004	11	27	06:19	448303,3	4670478,5	13	0,7
2005	2	9	15:20	464209,9	4647728,2	3	2,9
2005	3	18	13:32	466284,3	4648384,3	3	1,4
2005	3	18	13:49	465870,1	4648386,2	1,6	0
2005	7	26	12:08	465453,2	4647833,1	3	1,7
2005	8	17	11:09	464874,3	4648058,0	3	1,8
2005	10	7	02:18	459014,6	4666188,6	ND	0,2
2005	10	18	12:26	465259,8	4642171,3	13	1,3
2006	4	1	01:20	478842,9	4637232,5	ND	0,6
2006	4	1	03:29	480585,2	4637227,5	ND	0,7
2006	5	26	18:00	466136,1	4652049,1	13	0,4
2006	5	27	07:02	454255,7	4658667,1	ND	0,7
2006	5	30	18:01	453004,6	4669557,2	10	1
2006	6	4	13:24	465921,9	4659156,5	8	1,5
2006	7	10	11:08	464271,6	4659941,9	ND	0
2006	9	1	05:20	462706,0	4661060,3	0,9	0
2006	11	10	11:28	466696,4	4647938,2	ND	1,4
2006	12	11	18:41	462110,5	4657954,4	13	0,5
2006	12	27	12:19	463956,9	4646841,2	12	0
2007	1	11	11:47	465045,5	4649167,5	3	2,2
2007	2	19	11:56	465199,2	4646724,0	3	1,4
2007	4	26	11:02	465289,6	4648278,0	3	1,5
2007	4	30	03:21	468177,1	4645599,7	5	0,9
2007	5	14	10:44	465453,7	4647944,1	5	1,4
2007	6	29	02:00	478677,3	4637344,0	ND	0
2007	7	5	21:23	479423,7	4637230,8	9	0,9
2007	12	20	03:57	455150,6	4669321,2	3	0,3
2008	2	3	02:16	461861,2	4657733,7	4	0,3
2008	4	24	00:50	467799,1	4653595,9	0,5	0
2008	6	22	19:49	465151,9	4637064,3	ND	0,1
2008	7	25	02:04	465235,9	4637285,9	ND	0,3
2009	1	1	04:42	480341,5	4639115,7	ND	0,3
2009	2	16	02:37	447873,7	4679365,1	ND	0,5
2009	9	21	05:08	462617,3	4675495,8	ND	0,7
2009	10	25	06:15	465011,0	4675594,6	5	0
2009	11	8	01:11	452650,7	4678331,9	10	0,6
2010	4	12	20:59	465779,6	4680920,7	10	0
2010	7	27	01:47	471235,8	4643699,1	9	0,8
2010	9	14	23:09	469318,6	4679349,8	7	0,4
2010	12	28	18:14	474788,6	4663671,8	9	0,5
2010	12	31	04:43	448036,8	4667926,5	ND	0

2011	1	7	17:49	460476,7	4676395,9	5	0
2011	1	18	03:20	465905,0	4638393,0	4	0,8
2011	1	18	03:21	466319,3	4638280,0	ND	0,4
2011	3	19	19:48	451892,3	4676005,2	ND	0
2011	3	19	20:24	451495,8	4678339,8	ND	0
2011	3	31	01:39	469211,8	4673798,3	1	0,4
2011	4	30	19:14	450771,5	4669128,3	18	0,2
2011	5	24	02:23	455959,0	4653215,4	7	1,4
2011	6	3	21:44	450077,7	4676128,9	ND	0,2
2011	7	27	10:36	452924,3	4669890,9	7	0,4
2011	8	17	06:38	449154,0	4673914,6	15	0,3
2011	9	10	01:18	465315,2	4653496,6	ND	0,7
2011	9	17	03:08	465041,7	4648390,3	5	0,9
2011	12	11	03:26	471789,2	4636923,9	2	0,5
2011	12	11	03:39	454684,4	4673876,9	ND	0
2011	12	13	02:44	470796,2	4637594,0	8	1,5
2011	12	13	02:50	470548,3	4637817,1	8	1
2011	12	15	01:33	469000,5	4644374,7	3	0,3
2011	12	26	06:48	452745,9	4680219,0	ND	0,2
2011	12	26	08:47	453159,0	4680327,3	5	0,3
2011	12	26	18:02	453244,4	4680770,9	ND	0,2
2011	12	26	20:23	452912,3	4680440,0	6	0,2
2011	12	27	12:17	452999,2	4681105,7	8	0,4
2011	12	27	13:20	452916,0	4680995,2	7	0
2011	12	27	20:56	453078,7	4680661,0	5	0,7
2011	12	27	22:30	453571,3	4680324,6	5	0,3
2011	12	30	06:44	453245,1	4680881,9	ND	1,8
2012	3	30	10:52	464381,2	4648837,7	2	1,5
2012	4	20	00:06	469418,5	4664359,2	12	0,3
2012	5	11	00:56	453750,9	4669996,5	13	0,4
2012	6	5	01:03	453729,0	4666665,4	8	0
2012	7	1	19:03	460270,6	4654411,4	4	0,9
2012	8	31	19:31	464437,0	4659941,0	4	0,9
2012	8	31	21:27	464397,9	4652168,7	2	0,8
2012	11	4	04:00	461208,3	4674393,1	4	0
2013	2	28	05:16	473547,0	4663232,2	14	0
2013	3	16	00:27	478439,5	4641008,8	2	0,4
2013	3	26	13:50	457020,6	4664423,8	1	0,2
2013	5	25	09:03	447945,1	4666705,7	13	1,2
2013	7	23	17:27	452925,0	4670001,9	12	2
2013	7	24	11:26	476853,6	4663220,5	13	0
2013	7	24	14:40	472651,8	4645470,0	ND	0,1
2013	8	17	01:58	466006,0	4642167,7	18	0
2013	8	26	16:11	461116,6	4657737,8	4	0,4
2013	9	19	16:31	466907,7	4657708,3	ND	0,2
2013	9	20	03:04	467730,0	4656594,1	4	1,1
2013	9	20	03:17	466902,5	4656598,0	4	0,4
2013	11	19	01:51	468513,1	4646597,5	4	0,9
2013	12	2	02:45	468508,1	4645487,2	4	0,9
2014	2	17	02:01	470142,3	4639928,4	4	0
2014	2	17	05:24	460276,8	4655521,7	8	0

8

Summary of results and discussion

This PhD Thesis consists of six research papers that are currently published, in-press or under-review in international journals. The results obtained in the whole work show that the influence of local tectonics and geology of the substrate determine the controls and eruption styles in the GVF. Several methodologies were implemented, described and discussed, in order to investigate the role played by the structural and geological controls, but also to explore the internal structure of monogenetic volcanoes and to reconstruct the relative stratigraphy of this volcanic field.

The first work allowed identifying the main tectonic structures of the volcanic area at depth. This study was performed in the Northern sector of the study area, as it presents the greatest density of volcanic cones of the whole volcanic field. As reported in Barde-Cabusson et al. (2014), volcanism appears to be controlled by NNE–SSW and NNW–SSE tectonic structures identified by gravimetric and self-potential surveys. Moreover, another finding of this study was that the central part of the northern sector is dominated by a broad negative Bouguer anomaly of around -0.5 mGal, within which a series of gravity minima are found with amplitudes of up to -2.3 mGal. Porous volcanoclastic deposits, including the pyroclastic roots of volcanic edifices, in combination with fault and fissure damage zones appear to be the main candidates to explain the observed gravity anomalies. This suggests that there is not evidence of a large magma chamber in the upper part of the crust that controlled any eruption. The combination of both geophysical methods helped us to explore and link the superficial expressions of monogenetic volcanism and characteristic fissure zones of the GVF with magma pathways at depths.

From the identification of the tectonic structures that play a main role on this volcanism, we carried out a second work (see Bolós et al., 2014) in order to obtain a much better resolution of the shallower structures and to better identify the role played by the geology of the substrate on the uppermost part of the feeding system. The self-potential dataset was complemented from the previous smaller-scale studies and electrical resistivity tomography was conducted on some key areas. The main new results include the generation of resistivity models from 9 electrical resistivity tomography profiles. The 2D images obtained revealed the existence of high resistivity bodies corresponding to NNW–SSE-running feeder dykes, confirming the role played by NNW–SSE Neogene extensional faults in the volcanic manifestations in the area. These structures coincide with the deeper ones identified in the previous work, and show that anterior Alpine tectonic structures played no apparent role in controlling the loci of this volcanism. In addition, the results obtained showed that the phreatomagmatic and Strombolian activity could take place simultaneously or within a short time span, in close proximity or even in the same volcanic edifice, because of the controlled exerted by shallow stratigraphical, structural, and hydrogeological differences underneath these monogenetic volcanoes. The existence of such a configuration could explain the variety of eruptive dynamics in the monogenetic GVF and in other volcanic fields of similar characteristics without any need for change in the composition of the magma.

A further investigation was carried out at the southern sector of the GVF, specifically in La Crosa de Sant Dalmai volcano (10 km SW of Girona) one of the most representative volcanic landform of the GVF. This volcano is a very well preserved maar-diatreme, 1.5 km in diameter, excavated at the contact between a hard substrate and a soft substrate formed by Palaeozoic granites and squits and Pliocene and Quaternary gravels, respectively. This work applied gravimetry, magnetometry, self-potential and electrical resistivity tomography in

order to infer the inner structure of the maar-diatreme and to characterise the main geological and tectonic constraints, as reported in Bolós et al. (2012). This multiparametric geophysical study together with new field geology and additional geological data from two drill cores provided a detailed picture of the post-eruptive maar infill sequence as well as of the uppermost part of the maar-diatreme structure. The model obtained helps to understand the influence of the pre-eruptive basement on the phreatomagmatic and Strombolian activity that constructed the volcanic edifice and the characteristics of the post-eruptive deposits that infill the maar crater. In addition, geophysical data showed that the last Strombolian phase, which culminated with the formation of a scoria cone inside the maar, was associated with a NW–SE oriented fault, in accordance with the regional trend already mentioned.

The results obtained with the application of these geophysical methods in the GVF demonstrate that electrical resistivity tomography is a useful tool to study the internal structure of monogenetic volcanoes. This is reported in Barde-Cabusson et al. (2013) where, this method was applied to three monogenetic cones from the GVF (Montsacopa and Pujalós volcanoes at northern sector and Puig d'Àdri tephra ring at the southern sector of the GVF), comparing the results with geological observations to interpret the inner structures of the volcanoes. Several volcanic products were identified such as (a) spatter deposits in the central part of the cones, (b) sharp contrasts between hydromagmatic and Strombolian deposits, (c) buried lava flows, (d) the hidden eruptive vent of the Montsacopa volcano, and (e) the eruptive conduit of the Puig d'Àdri Strombolian cone.

The fifth work was conducted in whole volcanic field and dealt with the study of ephemeral outcrops, the stratigraphic logging of water wells and geotechnical drill holes, combined with surface geology and the results from the previous shallow geophysical studies. As reported in Bolós et al. (2014 in-press), the methodology applied in this work proved to be an efficient way of reconstructing the geology and volcanic stratigraphy of recent volcanic fields and, in particular, of highly urbanised areas in which increasing construction and the occupation of the soil hamper direct observation. The main results obtained enabled us to (a) establish a detailed stratigraphy of the whole volcanic succession, from the Middle Pleistocene to the early Holocene, (b) complete a detailed volcanological map of this volcanic field (which includes the city of Olot), and (c) reinterpret a number of eruptive events. Likewise, the knowledge of the relative geochronology and extension of the most recent volcanic deposits has also improved. Despite revealing no clear pattern of the time-space evolution of this volcanism without a more precise statistical analysis, a concentration of the oldest eruptions towards the north and east of the area can be inferred from the results. Most of the volcanic eruptions identified in this study were concentrated in the northern sector of the GVF and only fewer are found far in the southern sector. This difference in the concentrations of the eruptive vents between the two sectors is not time-controlled since eruptions of similar ages have occurred in both sectors. In addition, the volume of erupted magma in those cases for which it could be calculated is mostly of the order of $0.02 \text{ km}^3 \pm 0.01$, which indicates that most of the eruptions were low magnitude monogenetic eruptions. The proposed volcanic stratigraphy offers the basis to build further studies on the GVF and it also provides a precise reference for the Quaternary tephrochronology of the lake sediments in neighbouring areas.

The last research paper (Bolós et al., under-review) aimed at investigating the relationship between the Neogene extensional tectonics and the spatial distribution of the volcanoes in the whole area through a volcano-structural analysis. This included the geostatistical distribution of faults, fissures and vents, as well as morpho-structural lineaments, and the morphometrical analysis of volcanic cones and craters. Furthermore, we used the location of the regional seismicity registered since 1978 and the sites of freshwater springs and mantle-derived gases as indicators of active faults and open fractures. In addition, we considered the location of the volcanoes with ultramafic xenoliths as a way for identifying the deepest fractures in the zone and estimating magma ascent velocities. The morphological and structural data obtained revealed that the evolution of the GVF was mostly controlled by two major Neogene transtensional faults oriented NW-SE, the Amer and Llorà faults. However, most of the eruptive fissures and structural lineaments identified in this study show a NNW-SSE trend that runs slightly obliquely to the main faults. The pattern shown by the eruptive fissures and subordinated extensional faults is compatible with a slight dextral transtensional component in the two main faults, as suggested by previous studies (Goula et al., 1999; Olivera et al., 2003) and indicates that magma ascent in the uppermost crust and subsequent eruptions were controlled by these subordinated fractures. The presence of mantle-derived xenoliths and lower-crust cumulates suggests that the magmas that erupted in the GVF came either directly from the source region in the upper mantle or from intermediate reservoirs located at the base of the crust. This is also confirmed by existing petrological and geochemical data (Martí et al., 1992; Neuman et al., 1999; Cebriá et al., 2000). It is worth noting that most of the area's freshwater springs are associated with relatively shallow stratigraphic or structural discontinuities, while the presence of high radon and CO₂ concentrations mainly occur along the major Neogene faults (Moreno et al., 2014; Zarroca et al., 2012), thereby indicating that the deep circulation of these mantle-derived gases is permitted through these faults (Redondo and Yélamos, 2005; Zarroca et al., 2012). Likewise, the recorded seismicity also revealed that Neogene faults have been active recently, mainly along the Amer fault. Moreover, the calculated ascent velocities (0.19 to 0.21 m/s) imply that magma may travel either from the source region in the mantle or from the base of the crust to the surface in just a few days, thereby suggesting the existence of preferential pathways for magma when ascending from source or accumulation regions to the eruption sites. The fact that the xenoliths are restricted to the eruptive vents related to the Llorà fault and that these volcanoes have also the largest erupted volumes of all the volcanoes in this volcanic field, as shown in the previous work (see Bolós et al., 2014 in-press), suggests that the Llorà fault was the main magma pathway. However, towards the upper part of the crust, magma was captured by shallow extensional secondary faults.

The results presented in this PhD Thesis evidence the importance of multidisciplinary studies to understand how magma is transported into the lithosphere and erupts at surface. The final model proposed takes into account the whole works presented and has important implications for hazard assessment as this type of volcanism is largely unpredictable in terms of eruption location (i.e. susceptibility) since the exact position of new vents does not necessarily follow a statistically pre-defined law. Furthermore, the results obtained show that the changes in eruption dynamics occurring at different vents located at relatively short distances is controlled by shallow stratigraphical, structural, and hydrogeological differences in the uppermost part of the lithosphere.

9

Conclusions

The present PhD Thesis is the first comprehensive study addressing physical volcanology, volcanic-stratigraphy and geological structure of the Quaternary La Garrotxa monogenetic Volcanic Field (GVF) in a combined approach. This study has included detailed field geology and the application of shallow geophysical methods to characterise both the surface and the subsoil geology of the area. The results obtained will allow to better understand how regional and local tectonics have influenced and controlled the volcanic activity in the GVF, and to constrain the tephrochronological evolution of the area.

The GVF provides a good example of the structural complexity that governs monogenetic volcanism. The results obtained suggest that each eruptive episode in this volcanic field corresponds to an intermittent reactivation of the main fault system every 5 000 to 20 000 years. These tectonic reactivations would have permitted the ascent of deep magma through the crust, which would have erupted at the surface each time in a different location inside the volcanic field. Volcanism in the area is mainly concentrated in the northern sector, where the tectonic depression is wider and the accumulation of post-Alpine sediments is thicker, compared to the rest of the field. Moreover, the difference in basement lithology between the northern (Tertiary and Quaternary sediments) and southern (Paleozoic granites and schists) sectors of the volcanic field may also have played a significant role in controlling the ability for the magma to find pathways to reach the surface. The absence of magmatism beyond the northern limit of the GVF may be due to the significant thickness increase of the crust due to the Alpine Orogeny (i.e. Pyrenees). Moreover, geophysical data and volcano-structural analysis show that the previous Alpine tectonic structures played no apparent role in controlling the loci of this volcanism. This last appears to be controlled mainly by NNW–SSE extensional faults related to Neogene tectonism. This PhD Thesis demonstrates the close link between tectonic structures and magma pathways in the evolution of the GVF and their potential to guide future eruptive activity. This subject is of primary interest for the assessment of volcanic hazard in the GVF and similar monogenetic volcanic fields.

Moreover, a precise stratigraphy and correlation of the identified eruptive episodes will provide a constraint for the Pleistocene to Holocene evolution of the area, but will also contribute to better estimate the size of these eruptions by characterising more precisely their areal extent and the volume of erupted magma. In addition, the results obtained show the importance of the basement geology as changes in eruption dynamics occurring at different vents located at relatively short distances are controlled by shallow stratigraphical, structural, and hydrogeological differences underneath these monogenetic volcanoes. The existence of such a configuration could explain the variety of eruptive dynamics in the GVF and in other monogenetic volcanic fields of similar characteristics without any need for changes in the composition or rheology of the magma. In this way, it has been determined that electrical resistivity tomography method is a powerful tool to study the substrate underneath monogenetic volcanoes and as well as their internal structure.

All the data acquired and presented in this thesis will help to assess volcanic susceptibility and hazard, two of the unavoidable requirements to estimate volcanic risk. In addition, this work has intended to be a step forward in the preservation of the geological heritage in La Garrotxa monogenetic Volcanic Field by providing the basic knowledge but also by enhancing the importance of their geological values in front of potential threats imposed by the demographic expansion of modern societies.

Future research in this area should focus, among other aspects, on detailed petrological studies of the volcanic rocks to carry out phase equilibrium experiments, in order to establish the precise conditions of magma transport and storage at depth. This is necessary to identify melting and melt extraction rising mechanisms governing volcanism in this region, the origin of different xenoliths erupted by magmas and, finally, to establish a comparison with other volcanic provinces of the European Rift System.

References

- Acocella, V. and Tibaldi, A., 2005. Dike propagation driven by volcano collapse: a general model tested at Stromboli, Italy. *Geophysical Research Letters*, 32.
- Araña, V., Aparicio, A., Martín Escorza, C., García Cacho, L., Ortiz, R., Vaquer, R., Barberi, F., Ferrara, G., Albert, J. and Gassiot, X., 1983. Neogene-Quaternary volcanism of Catalunya: structural, petrological, and geodynamic characteristics. *Acta Geol. Hisp.*, 18: 1-17.
- Barde-Cabusson, S., Bolós, X., Pedrazzi, D., Lovera, R., Serra, G., Martí, J. and Casas, A., 2013. Electrical resistivity tomography revealing the internal structure of monogenetic volcanoes. *Geophysical Research Letters*, 40(11): 2544-2549.
- Barde-Cabusson, S., Gottsman, J., Martí, J., Bolós, X., Camacho, A.G., Geyer, A., Planagumà, L., Ronchin, E. and Sanchez, A., 2014. Structural control of monogenetic volcanism in the Garrotxa volcanic field (Northeastern Spain) from gravity and self-potential measurements. *Bulletin of Volcanology*, 76: 788.
- Baxter, P.J., 2000. Impacts of eruptions on human health. In: H. Sigurdsson, B. Houghton, S.R. McNutt, H. Rymer and J. Stix (Editors), *Encyclopedia of Volcanoes*, Academic Press, San Diego, pp. 1035–1043.
- Bech, J., Ségalen, P. and Quantin, P., 1976. Étude des andosols d'Olot (Gérone-Espagne) Première partie: Écologie, morphologie, caractéristiques physiques et chimiques. *Tecniterrae Cahiers O.R.S.T.G.M série Pédologie(73-87. Paris)*.
- Bianchini, G., Beccaluva, L., Bonadiman, C., Nowell, G., Pearson, G., Siena, F. and Wilson, M., 2007. Evidence of diverse depletion and metasomatic events in harzburgite–lherzolite mantle xenoliths from the Iberian plate (Olot, NE Spain) implications for lithosphere accretionary processes. *Lithos*, 94: 25-45.
- Bibby, H.M., Caldwell, T.G. and Risk, G.F., 1998. Electrical resistivity image of the upper crust within the Taupo Volcanic Zone. *New Zealand Journal Geophysical Research*, 103: 9665-9680.
- Blaikie, T.N., Ailleres, L., Betts, P.G. and Cas, R.A.F., 2014. A geophysical comparison of the diatremes of simple and complex maar volcanoes, Newer Volcanics Province, south-eastern Australia. *Journal of Volcanology and Geothermal Research*, 276: 64-81.
- Blaikie, T.N., Ailleres, L., Cas, R.A.F. and Betts, P.G., 2012. Three-dimensional potential field modelling of a multi-vent maar-diatreme — The Lake Coragulac maar, Newer Volcanics Province, south-eastern Australia. *Journal of Volcanology and Geothermal Research*, 235–236: 70–83.
- Bolós, A., 1931. L'estructura del Pla d'Olot. *Géologie de la Méditerranée Occidentale*, M(IV): 20.
- Bolós, F.X., 1820. Noticia de los extinguidos volcanes de Olot, de la naturaleza de sus productos, y de sus aplicaciones. *Memorias de Agricultura y Artes*, XI: 19.
- Bolós, F.X., 1841. Noticia de los extinguidos volcanes de la villa de Olot y de sus inmediaciones hasta Amer, y de los nuevamente descubiertos y no publicados, todos en la provincial de Gerona, de la naturaleza de sus productos y de sus aplicaciones. *Imprenta Herederos Viuda Pla, Barcelona*.
- Bolós, M.T., 1957. Terrazas del rio Fluvia. *Res. des Communications Congrès Géologique*, 39 I.N.Q.U.A: 23.
- Bolós, X., Barde-Cabusson, S., Pedrazzi, D., Martí, J., Casas, A., Himi, M. and Lovera, R., 2012. Investigation of the inner structure of La Crosa de Sant Dalmai maar (Catalan Volcanic Zone, Spain). *Journal of Volcanology and Geothermal Research*, 247–248(0): 37-48.
- Bolós, X., Barde-Cabusson, S., Pedrazzi, D., Martí, J., Casas, A., Lovera, R. and Nadal-Sala, D., 2014. Geophysical exploration on the subsurface geology of La Garrotxa monogenetic Volcanic Field (NE Iberian Peninsula). *International Journal of Earth Science*.
- Bolós, X., Martí, J., Becerril, L., Planagumà, L., Grosse, P. and Barde-Cabusson, S., under-review. Volcano-structural analysis of La Garrotxa Volcanic Field (NE Iberia): implications for the plumbing system. *Tectonophysics*.

- Bolós, X., Planagumà, L. and Martí, J., 2014 in-press. Volcanic stratigraphy of the Quaternary La Garrotxa Volcanic Field (NE Iberian Peninsula). *Journal of Quaternary Science*.
- Brenna, M., Cronin, S.J., Németh, K., Smith, I.E.M. and Sohn, Y.K., 2011. The influence of magma plumbing complexity on monogenetic eruptions, Jeju Island, Korea. *Terra Nova*, 23(2): 70-75.
- Brunner, I., Friedel, S., Jacobs, F. and Danckwardt, E., 1999. Investigation of a tertiary maar structure using three-dimensional resistivity imaging. *Geophysical Journal International*, 136 (3): 771–780.
- Calderón, S., Cazorro, M. and Fernández Navarro, L., 1906. Memoria sobre las formaciones volcánicas de la provincia de Gerona. *Memorias de de Real Sociedad Española de Historia Natural*, IV memoria 5ª, Madrid: 165–489.
- Cardelús, J., 1957. *Productos volcánicos y suelos de Olot*, Universidad de Madrid.
- Cas, R.A.F. and Wright, J.V., 1987. Volcanic successions, modern and ancient. *MA geological approach to processes products and successions*. 528 pp.
- Cassidy, J. and Locke, A.C., 2010. The Auckland volcanic field, New Zealand: Geophysical evidence for structural and spatio-temporal relationships. *Journal of Volcanology and Geothermal Research*, 195: 127–137.
- Cebriá, J.M., López-Ruiz, J., Doblas, M., Oyarzun, R., Hertogen, J. and Benito, R., 2000. Geochemistry of the Quaternary alkali basalts of Garrotxa (NE Volcanic Province, Spain): a case of double enrichment of the mantle lithosphere. *Journal of Volcanology and Geothermal Research*, 102(3–4): 217-235.
- Chevalier, M., 1926. *Essai sur la physiographie de la Catalogne orientale*. Leur evolution pendant le temps quaternaire. *Butlletí Institució Catalana Història Natural*, XXVI: 25-51. Barcelona.
- Chevalier, M., 1927. Contribution á l'étude du volcanisme en Catalogne. *Comptes rendus du X I V. Congrès Géologique International*, IV.
- Chevalier, M., 1931a. Les terrasses quaternaires des environs d'Olot. *Ass. pour l'étude géologique de la Méditerranée Occidentale*, 2(IV).
- Chevalier, M., 1931b. Sur la tectonique de la région d'Olot. *Ass. pour l'étude géologique de la Méditerranée Occidentale*, 11(IV).
- Cimarelli, C., Di Traglia, F., de Rita, D., Gimeno Torrente, D. and Fernandez Turiel, J.L., 2013. Space–time evolution of monogenetic volcanism in the mafic Garrotxa Volcanic Field (NE Iberian Peninsula). *Bulletin of Volcanology*, 75: 758.
- Cimarelli, C., Di Traglia, F. and Taddeucci, J., 2012. Basaltic scoria textures from a zoned conduit as precursors to violent Strombolian activity. *Geology*, 38: 439-442.
- Clemens, J.D. and Mawer, C.K., 1992. Granitic magma transport by fracture propagation. *Tectonophysics*, 204: 339-360.
- Connor, C.B., 1987. Structure of the Michoacán-Guanajuato volcanic field, Mexico. *Journal of Volcanology and Geothermal Research*, 33(1–3): 191-200.
- Connor, C.B. and Conway, F.M., 2000. Basaltic volcanic fields. In: Sigurdsson, H., Houghton, B.F., McNutt, S.R., Rymer H., Stix J. (Editors), *Encyclopedia of Volcanoes*. Academic Press, San Diego: p. 331–343.
- Coy-Yll, R., Gunn, B.M. and Traveria-Cross, A., 1975. Geochemistry of the Catalanian Volcanics, Spain. *Acta Geológica Hispana*, Madrid.
- Dèzes, P., Schmid, S.M. and Ziegler, P.A., 2004. Evolution of the European Cenozoic Rift System: interaction of the Alpine and Pyrenean orogens with their foreland lithosphere. *Tectonophysics*, 389: 1–33.
- Di Maio, R., Mauriello, P., Patella, D., Petrillo, Z., Piscitelli, S. and Siniscalchi, A., 1998. Electric and electromagnetic outline of the Mount Somma-Vesuvius structural setting. *Journal of Volcanology and Geothermal Research*, 82: 219-238.

- Di Maio, R., Patella, D., Petrillo, Z., Siniscalchi, A., Cecere, G. and De Martino, P., 2000. Application of electric and electromagnetic methods to the definition of the Campi Flegrei caldera (Italy). *Annali di Geofisica*, 43: 375-390.
- Di Traglia, F., Cimarelli, C., de Rita, D. and Gimeno Torrente, D., 2009. Changing eruptive styles in basaltic explosive volcanism: examples from Croscat complex scoria cone, Garrotxa Volcanic Field (NE Iberian Peninsula). *J Volcanol Geotherm Res*, 180: 89–109.
- Donville, D., 1973. Géologie Néogène et ages des éruptions volcaniques de la Catalogne orientale, Tesis doct, de la Universitat de Tolosa de Llenguadoc.
- Downes, H., 2001. Formation and modification of the shallow sub-continental lithospheric mantle: a review of geochemical evidence from ultramafic xenolith suites and tectonically emplaced ultramafic massifs of Western and Central Europe. *Journal of Petrology*, 42: 233-250.
- Emilia, D.A., Last, B.J., Wood, C.A. and Dakin, F.M., 1977. Geophysics and Geology of an Explosion Crater in the Ethiopian Rift Valley. *Bulletin of Volcanology*, 40-3.
- Enrique, P. and Toribio, T., 2009. Basaltos subalcalinos en las coladas de la cuenca del Ser (Zona Volcánica de Olot). *Geogaceta*, 47.
- Fayas, J.A. and Doménech, J., 1974. Morfología volcánica de Olot y su interés geológico. *Rev, Agua*, 85. Barcelona.
- Fernández, M., Torné, M. and Zeyen, H., 1990. Lithospheric thermal structure of NE Spain and the North-Balearic basin. *Journal of Geodynamics*, 12: 253–267.
- Fiske, R.S. and Jackson, E.D., 1972. Orientation and growth of Hawaiian volcanic rifts: the effect of regional structure and gravitational stresses. *Proc. R. Soc. Lond.*, 329: 299-326.
- Galán, G., Oliveras, V. and Paterson, B.A., 2008. Types of metasomatism in mantle xenoliths enclosed in Neogene–Quaternary alkaline mafic lavas from Catalonia (NE Spain). *Geological Society of London*, 293: 121-153.
- Gallart, J., Olivera, C. and Correig, A., 1984. Aproximación geofísica a la zona volcánica de Olot (Girona). Estudio local de sismicidad. *Revista de Geofísica*, 40: 205-226.
- Gallart, J., Pous, J., Boix, F. and Hirn, A., 1991. Geophysical constraints on the structure of the Olot Volcanic Area, north-eastern Iberian Peninsula. *Journal of Volcanology and Geothermal Research*, 47: 33–44.
- Gelabert, J., 1904. Los volcanes extinguidos de la provincia de Gerona. Octavio Viader impresor, Sant Feliu de Guíxols, Girona: 120 pp, 121map.
- Gisbert, G., Gimeno Torrente, D. and Fernandez-Turiel, J.L., 2009. Eruptive mechanisms of the Puig de La Garrinada volcano (Olot, Garrotxa Volcanic Province, Northeastern Spain): a methodological study developed on proximal pyroclastic deposits. *J Volcanol Geotherm Res*, 180: 259–276.
- Goula, X., Olivera, C., Fleta, J., Grellet, B., Lindo, R., Rivera, L.A., Cisternas, A. and Carbon, D., 1999. Present and recent stress regime in the eastern part of the Pyrenees. *Tectonophysics*, 308: 487–502.
- Gretener, P.E., 1969. On the mechanics of the intrusion of sills. *Canadian Journal of Earth Sciences*, 6: 1415–1419.
- Guardia, P., 1964. Contribution á l'étude des volcanes de la province de Gérone et du paléomagnetisme de leurs coulées, Universitat. París-VI.
- Gudmundsson, A., 2003. Surface stresses associated with arrested dykes in rift zones. *Bulletin of Volcanology*, 65: 606-619.
- Gudmundsson, A. and Philipp, S.L., 2006. How local stress fields prevent volcanic eruptions. *J. Volcanol. Geotherm. Res.*, 158: 257-268.
- Hase, H., Hashimoto, T., Sakanakac, S.y., Kandad, W. and Tanakaa, Y., 2005. Hydrothermal system beneath Aso volcano as inferred from self-potential mapping and resistivity structure. *J Volcanol Geotherm Res*, 143: 259-277.

- Hasenaka, T., 1994. Size, distribution, and magma output rate for shield volcanoes of the Michoacán-Guanajuato Volcanic Field, Central Mexico. *Journal of Volcanology and Geothermal Research*, 63: 13–31.
- Hasenaka, T. and Carmichael, I.S.E., 1985. The cinder cones of Michoacán-Guanajuato, central Mexico: Their age, volume and distribution, and magma discharge rate. *Journal of Volcanology and Geothermal Research*, 25: 105–124.
- Kavanagh, J.L., Menand, T. and Sparks, R.S.J., 2006. An experimental investigation of sill formation and propagation in layered elastic media. *Earth Planetary Science Letters*, 245: 799–813.
- Kereszturi, G. and Németh, K., 2012. Monogenetic Basaltic Volcanoes: Genetic Classification, Growth, Geomorphology and Degradation. In: K. Németh (Editor), *Updates in Volcanology - New Advances in Understanding Volcanic Systems*, Jeddah, Kingdom of Saudi Arabia.
- Le Corvec, N., Menand, T. and Lindsay, J., 2013. Spatial distribution and alignments of volcanic centers: Clues to the formation of monogenetic volcanic fields. *Earth-Science Reviews*, 124: 96–114.
- Lewis, C.J., Vergés, J. and Marzo, M., 2000. High mountains in a zone of extended crust: Insights into the Neogene-Quaternary topographic development of northeastern Iberia. *Tectonics*, 19(1): 86–102.
- Llobera, P., 1983. Petrologia de los enclaves del volcán Roca Negra (Olot, NE España). *Acta Geològica Hispànica*, 18(1): 19–25.
- Loewinson-Lessing, F., 1931. Quelques considerations sur les laves basaltiques de la région volcanique d'Olot. *Ass. pour l'étude géologique de la Méditerranée Occidentale*, 2: 24, Barcelona.
- López-Loera, H., Aranda-Gómez, J.J., Arzate, J.A. and Stanley Molina-Garza, R., 2008. Geophysical surveys of the Joya Honda maar (México) and surroundings; volcanic implications. *Journal of Volcanology and Geothermal Research*, 170: 135–152.
- López-Ruiz, J. and Rodríguez-Badiola, E., 1985. La región volcánica Mio-Pleistocena del NE de España. *Estudios Geológicos*, 41: 105–126.
- Lorenz, V., 2007. Syn- and post-eruptive hazards of maar–diatreme volcanoes. *Journal of Volcanology and Geothermal Research*, 159(1–3): 285–312.
- Lyell, C., 1830. *Principles of Geology*. reprinted 1990 by University of Chicago Press, Chicago.
- Lyell, C., 1833. Volcanos of Olot, in Catalonia. In: C. Lyell (Editor), *Principles of geology*, London, J. Murray, pp. 183–193.
- Maclure, W., 1808. Extrait d'une lettre a J.c. Delamétherie, sur les volcans d'Olot, en Catalogne. *Journal de Physique, de Chimie et d'Histoire Naturelle*, 66(2): 19–220.
- Mallarach, J.M., 1976. El vulcanisme d'Olot i la seva relació amb l'arqueologia. *El Paleolític a les comarques gironines*. A.A.Girona: 105–109.
- Mallarach, J.M., 1982. Carta geològica de la Regió volcànica d'Olot. *Litologia i geomorfologia*. E 1:20.000. Editorial Maber, Ajuntament d'Olot.
- Mallarach, J.M., 1998. *El vulcanisme prehistòric de Catalunya*. Diputació de Girona.
- Mallarach, J.M. and Riera, M., 1981. *Els volcans olotins i el seu paisatge*. Editorial Serpa, Barcelona.
- Martí, J., Castro, A., Rodríguez, C., Costa, F., Carrasquilla, S., Pedreira, R. and Bolos, X., 2013. Correlation of Magma Evolution and Geophysical Monitoring during the 2011–2012 El Hierro (Canary Islands) Submarine Eruption. *Journal of Petrology*, 54(7): 1349–1373.
- Martí, J., Mallarach, J.M., 1987. Erupciones hidromagmáticas en el volcanismo cuaternario de Olot. *Estudios Geológicos*, 43: 31–40.
- Martí, J., Mitjavila, J., Roca, E. and Aparicio, A., 1992. Cenozoic magmatism of the Valencia trough (western Mediterranean): relationship between structural evolution and volcanism. *Tectonophysics*, 203: 145–165.

- Martí, J., Planagumà, L., Geyer, A., Canal, E. and Pedrazzi, D., 2011. Complex interaction between Strombolian and phreatomagmatic eruptions in the Quaternary monogenetic volcanism of the Catalan Volcanic Zone (NE of Spain). *Journal of Volcanology and Geothermal Research*, 201(1–4): 178-193.
- Martín-Serrano, A., Vegas, J., García-Cortés, A., Galán, L., Gallardo-Millán, J.L., Martín-Alfageme, S., Rubio, F.M., Ibarra, P.I., Granda, A., Pérez-González, A. and García-Lobón, J.L., 2009. Morphotectonic setting of maar lakes in the Campo de Calatrava Volcanic Field (Central Spain, SW Europe). *Sedimentary Geology*, 222(1–2): 52-63.
- McGee, L., Beier, C., Smith, I. and Turner, S., 2011. Dynamics of melting beneath a smallscale basaltic system: a U-Th–Ra study from Rangitoto volcano, Auckland volcanic field, New Zealand. *Contributions to Mineralogy and Petrology*: 1-17.
- Moreno, V., Bach, J., Baixeras, C. and Font, L., 2014. Radon levels in groundwaters and natural radioactivity in soils of the volcanic region of La Garrotxa, Spain. *Journal of Environmental Radioactivity*, 128: 1-8.
- Mrlina, J., Kampf, H., Kroner, C., Mingram, J., Stebich, M., Brauer, A., Geissler, W.H., Kallmeyer, J., Matthes, H. and Seidl, M., 2009. Discovery of the first Quaternary maar in the Bohemian Massif, Central Europe, based on combined geophysical and geological surveys. *Journal of Volcanology and Geothermal Research*, 182 (1–2): 97–112.
- Németh, K., 2010. Monogenetic volcanic fields: Origin, sedimentary record, and relationship with polygenetic volcanism. In: E. Cañón-Tapia and A. Szakács (Editors), *What Is a Volcano?* Geological Society of America, pp. 43–66.
- Németh, K., Martin, U. and Harangi, S., 2001. Miocene phreatomagmatic volcanism at Tihany (Pannonian Basin, Hungary). *Journal of Volcanology and Geothermal Research*, 111(1–4): 111-135.
- Neumann, E.R., Martí, J., Mitjavila, J. and Wulff-Pedersen, E., 1999. Origin and implications of mafic xenoliths associated with Cenozoic extension-related volcanism in the Valencia Trough, NE Spain. *Mineralogy and Petrology*, 65: 113-139.
- Nishi, Y., Ishido, T., Matsushima, N., Ogawa, Y., Toshi, T., Myazaki, J., Yasuda, A., Scott, B.J., Sherburn, S. and Bromley, C., 1996. Self-Potential and audio-magnetotelluric survey in White Island Volcano. *New Zealand Geothermal Workshop*.
- Oliveras, V., 2009. Xenòlits mantèl·lics lligats al vulcanisme Neògeno-Quaternari de Catalunya: caracterització, processos i condicions d'equilibri, Universitat Autònoma de Barcelona.
- Oliveras, V. and Galán, G., 2006. Petrología y mineralogía de los xenolitos mantélicos del volcán la Banya del Boc (Girona). *Geogaceta*, 40: 107-110.
- Oliveras, V. and Galán, G., 2007. Condiciones P-T en xenolitos mantélicos de los volcanes la Banya del Boc y el Puig d'Adri (Girona). *Geogaceta*, 43: 19-22.
- Pedrazzi, D., Bolós, X. and Martí, J., 2014. Phreatomagmatic volcanism in complex hydrogeological environments: La Crosa de Sant Dalmai maar (Catalan Volcanic Zone, NE Spain). *Geosphere*.
- Portal, A., Labazuy, P., Léna, J.F., Béné, S., Boivin, P., Busato, E., Cârloganu, C., Combaret, C., Dupieux, P., Fehr, F., Gay, P., Laktineh, I., Miallier, D., Mirabito, L., Niess, V. and Vulpescu, B., 2013. Inner structure of the Puy de Dôme volcano: cross comparison of geophysical models (ERT, gravimetry, muon imaging). *Geosci. Instrum. Method. Data Syst.*, 2: 47–54.
- Redondo, R. and Yélamos, J.G., 2005. Determination of CO₂ origin (natural or industrial) in sparkling bottled waters by ¹³C/¹²C isotope ratio analysis. *Food Chemistry*, 92: 507-514.
- Riba, O., 1975. Geotermismo de la zona volcánica de Olot. Nota preliminar sobre posibilidades geotérmicas. *Bol. Geológico y Minero*, LXXXV: 45-62.
- Riba, O., 1996. Història de la recerca vulcanològica a les nostres terres. *Revista de Girona*, 174: 60-64.
- Ross, P.-S., Delpit, S., Haller, M.J., Németh, K. and Corbella, H., 2011. Influence of the substrate on maar–diatreme volcanoes — An example of a mixed setting from the Pali

- Aike volcanic field, Argentina. *Journal of Volcanology and Geothermal Research*, 201(1–4): 253–271.
- Rout, D.J., Cassidy, J., Locke, C.A. and Smith, I.E.M., 1993. Geophysical evidence for temporal and structural relationships within the monogenetic basalt volcanoes of the Auckland volcanic field, northern New Zealand. *Journal of Volcanology and Geothermal Research*, 57(1–2): 71–83.
- San Miguel de la Cámara, M., 1918. El volcanismo en España. *Boletín de la Real Academia de Ciencias y Artes de Barcelona*: 244–254.
- San Miguel de la Cámara, M., 1936. Estudio de las rocas eruptivas de España. *Serie de Ciencias Naturales, Real Academia de Ciencias Exactas, Físicas y Naturales, Madrid*, 6: 660.
- San Miguel de la Cámara, M. and Marcet Riba, J., 1926. Región Volcánica de Olot. Extracto de la Guía “Cataluña” Excursión C-4, XIV Congreso Geológico Internacional Imprenta Sobrinos de López Robert y Cia., Barcelona: 39–214.
- Sapper, K., 1904. Die Katalonischen Vulkane. *Zeitschrift der Deutsche Geologisches Gessellschaft*, LXI: 240–248 Berlin.
- Saula, E., Picart, J., Mató, E., Llenas, M., Losantos, M., Berasategui, X. and Agustí, J., 1996. Evolución geodinámica de la fosa del Empordà y de las Sierras Transversales. *Acta Geologica Hispánica*, 29: 55–75.
- Schmincke, H.U., 2004. *Volcanism*, Springer Verlag, Berlin.
- Schulz, R., Bunn, H., Gabriel, G., Pucher, R., Rolf, C., Wiederhold, H. and Wonik, T., 2005. Detailed investigation of preserved maar structures by combined geophysical surveys. *Bulletin of Volcanology*, 68(2): 95–106.
- Solé Sabarís, L., 1957. Emporda et région volcanique d'Olot. *Congress Internationale Barcelona*.
- Solé Sabarís, L., 1962. Observaciones sobre la edad del vulcanismo gerundense. *Memorias de la Real Academia de Ciencias y Artes*, 34(12).
- Solé Sabarís, L. and Marcet Riba, H., 1953. Hoja geológica de España. Instituto Geológico y Minero, Madrid, 334.
- Solé Sugrañes, L.L., 1978. Alineaciones y fracturas en el sistema catalán según las imágenes LANDSAT-I. *Tecniterrae*, 22: 6–16.
- Tibaldi, A., 2003. Influence of cone morphology on dykes, Stromboli, Italy. *Journal of Volcanology and Geothermal Research*, 126(1–2): 79–95.
- Tibaldi, A., Bonali, F.L. and Corazzato, C., 2014. The diverging volcanic rift system. *Tectonophysics*, 611: 94–113.
- Tibaldi, A. and Lagmay, A.M.F., 2006. Preface: interaction between volcanoes and their basement. *Journal of Volcanology and Geothermal Research*, 158((1–2)): 1–5.
- Valenta, J., Rapprich, V., Skácelová, Z., Gazdová, R. and Fojtíková, L., 2014. The newly discovered Neogene maar volcano near the Mariánské Lázně, western Bohemia. *Acta Geodyn. Geomater*, 11(2): 107–116.
- Valentine, G.A. and Gregg, T.K.P., 2008. Continental basaltic volcanoes — Processes and problems. *Journal of Volcanology and Geothermal Research*, 177(4): 857–873.
- Vegas, R., 1994. A tectonic model for the volcanic province of Olot (NE Spain). *Geogaceta*, 15: 121–123.
- Vespermann, D. and Schmincke, H.U., 2000. Scoria cones and tuff rings. In: H. Sigurdsson, B.F. Houghton, S.R. McNutt, H. Rymer and J. Stix (Editors), *Encyclopedia of Volcanoes*. Academic Press, San Diego: 683–694.
- Walker, G.P.L., 1999. Volcanic rift zones and their intrusion swarms. *Journal of Volcanology and Geothermal Research*, 94: 21–34.
- Washington, H.S., 1907. The Catalan volcanoes and their rocks. *The American Journal of Science*, XXIV: 217–242.
- Williams, H., 1950. Volcanoes of the Parícutin Region. *U.S. Geol. Survey Bull.*, 965B: 165–279.

-
- Wilson, M. and Downes, H., 1991. Tertiary-Quaternary extension-related alkaline magmatism in Western and Central Europe. *J. Petrol.*(32(4)): 811–849.
- Wilson, M. and Downes, H., 1992. Mafic alkaline magmatism associated with the European Cenozoic rift system. *Tectonophysics*, 208: 173–182.
- Wohletz, K. and Heiken, G., 1992. *Volcanology and geothermal energy*. University of California Press, Berkeley, California: 432.
- Wood, C.A., 1980. Morphometric evolution of cinder cones. *Journal of Volcanology and Geothermal Research*, 7: 387–413.
- Zarroca, M., Linares, R., Bach, J., Roqué, C., Moreno, V., Font, L. and Baixeras, C., 2012. Integrated geophysics and soil gas profiles as a tool to characterize active faults: the Amer fault example (Pyrenees, NE Spain). *Environment Earth Science*, 67: 889-910.

APPENDIX 1

Contribution to the papers

Inform from the supervisors of the thesis on the impact factor or the categorization of journal publications to be found in the doctoral thesis and the report of the thesis supervisor explaining the participation in the paper of the coauthors.



MINISTERIO
DE ECONOMIA Y
COMPETITIVIDAD



CONSEJO SUPERIOR
DE INVESTIGACIONES
CIENTÍFICAS

JOAN MARTI I MOLIST, Professor d'Investigació del CSIC adscrit a l'Institut de Ciències de la Terra "Jaume Almera" de Barcelona i Director de la Tesi Doctoral realitzada per Xavier de Bolós Granados titulada "GEOLOGICAL AND STRUCTURAL CONTROLS ON LA GARROTXA MONOGENETIC VOLCANIC FIELD (NE IBERIA)"

CERTIFICA:

1) que, d'acord amb la normativa vigent de la Universitat de Barcelona referent a la presentació de Tesis Doctorals, aquesta Tesi Doctoral es presenta com a compendi de les següents publicacions científiques de les que s'indica el seu factor d'impacte a l'any de la publicació:

S. Barde-Cabusson, J. Gottsmann, J. Martí, **Xavier Bolós**, A. G. Camacho, A. Geyer, Ll. Planagumà, E. Ronchin, A. Sánchez, 2014. Structural control of monogenetic volcanism in the Garrotxa volcanic field (Northeastern Spain) from gravity and self-potential measurements. *Bulletin of Volcanology*.
<http://link.springer.com/article/10.1007%2Fs00445-013-0788-0>. Factor d'impacte: 2,653

Xavier Bolós, Stéphanie Barde-Cabusson, Dario Pedrazzi, Joan Martí, Albert Casas, Raúl Lovera, Daniel Nadal-Sala, 2014 in-press. Geophysical exploration on the subsurface geology of La Garrotxa monogenetic Volcanic Field (NE Iberian Peninsula). *International Journal of Earth Science (IJES)*. Factor d'impacte: 2,261

Xavier Bolós, Stéphanie Barde-Cabusson, Dario Pedrazzi, Joan Martí, Albert Casas, Mahjoub Himi, Raúl Lovera, 2012. Investigation of the inner structure of La Crosa de Sant Dalmai maar. *Journal of Volcanology and Geothermal Research (JVGR)*.
<http://dx.doi.org/10.1016/j.jvolgeores.2012.08.003>. Factor d'impacte: 2,19

Stéphanie Barde-Cabusson, **Xavier Bolós**, Dario Pedrazzi, Raul Lovera, Guillem Serra, Joan Martí, Albert Casas, 2013. Electrical resistivity tomography revealing the internal structure of monogenetic volcanoes. *Geophysical Research Letters (GRL)*.
<http://onlinelibrary.wiley.com/doi/10.1002/grl.50538/abstract>. Factor d'impacte: 3,98

Xavier Bolós, Llorenç Planagumà, Joan Martí, (2014 in-press). Volcanic stratigraphy and evolution of the Quaternary monogenetic volcanism in the Catalan Volcanic Zone (NE Spain). *Journal of Quaternary Science*. Factor d'impacte: 2,939

Xavier Bolós, Joan Martí, Laura Becerril, Llorenç Planagumà, Pablo Grosse, Stéphanie Barde-Cabusson (under-review). Volcano-structural analysis of La Garrotxa Volcanic Field (NE Iberia): implications for the plumbing system. *Tectonophysics*. Factor d'impacte: 2,684



ICTJA

INSTITUTO DE CIENCIAS DE LA TIERRA JAUME ALMERA

C/ SOLÉ I SABARÍS, S/N
08028 BARCELONA ESPAÑA
TELF. +34 93 409 54 10
FAX.: +34 93 411 00 12



MINISTERIO
DE ECONOMIA Y
COMPETITIVIDAD



CONSEJO SUPERIOR
DE INVESTIGACIONES
CIENTÍFICAS

2) que tots els treballs han estat realitzats en col·laboració amb altres investigadors, havent estat el doctorant la persona encarregada de realitzar la major part del treball, la seva planificació, redacció i revisió, en aquelles publicacions en que és el primer autor, en els que el paper dels altres firmants ha estat l'assessorament científic, aportació de dades complementaries i/o participació en els treballs de camp. Igualment, en els altres treballs inclosos, el paper del doctorant ha estat destacat i del tot necessari per la consecució dels resultats obtinguts.

I perquè així consti i a tots el efectes oportuns signo el present certificat a Barcelona a 9 de juny de dos mil catorze.



ICTJA

INSTITUTO DE CIENCIAS DE LA TIERRA JAUME ALMERA

C/ SOLÉ I SABARÍS, S/N
08028 BARCELONA ESPAÑA
TELF. +34 93 409 54 10
FAX.: +34 93 411 00 12

APPENDIX 2

Structural control of monogenetic volcanism in the Garrotxa volcanic field (Northeastern Spain) from gravity and self-potential measurements

Structural control of monogenetic volcanism in the Garrotxa volcanic field (Northeastern Spain) from gravity and self-potential measurements

S. Barde-Cabusson · J. Gottsmann · J. Martí · X. Bolós · A. G. Camacho · A. Geyer · Ll. Planagumà · E. Ronchin · A. Sánchez

Received: 17 May 2013 / Accepted: 26 November 2013
© European Union 2013

Abstract We report new geophysical observations on the distribution of subsurface structures associated with monogenetic volcanism in the Garrotxa volcanic field (Northern Spain). As part of the Catalan Volcanic Zone, this Quaternary volcanic field is associated with the European rifts system. It contains the most recent and best preserved volcanic edifices of the Catalan Volcanic Zone with 38 monogenetic volcanoes identified in the Garrotxa Natural Park. We conducted new gravimetric and self-potential surveys to enhance our understanding of the relationship between the local geology and the spatial distribution of the monogenetic volcanoes. The main finding of this study is that the central part of the volcanic field is dominated by a broad negative Bouguer anomaly of around -0.5 mGal, within which a series of gravity minima are found with amplitudes of up to -2.3 mGal. Inverse modelling of the Bouguer data suggests

that surficial low-density material dominates the volcanic field, most likely associated with effusive and explosive surface deposits. In contrast, an arcuate cluster of gravity minima to the NW of the Croscat volcano, the youngest volcano of this zone, is modelled by vertically extended low-density bodies, which we interpret as a complex ensemble of fault damage zones and the roots of young scoria cones. A ground-water infiltration zone identified by a self-potential anomaly is associated with a steep horizontal Bouguer gravity gradient and interpreted as a fault zone and/or magmatic fissure, which fed the most recent volcanic activity in the Garrotxa. Gravimetric and self-potential data are well correlated and indicate a control on the locations of scoria cones by NNE–SSW and NNW–SSE striking tectonic features, which intersect the main structural boundaries of the study area to the north and south. Our interpretation of the data is that faults facilitated magma ascent to the surface. Our findings have major implications for understanding the relationship between subsurface structures and potential future volcanic activity in the Garrotxa volcanic field.

Editorial responsibility: T. Nishimura

Electronic supplementary material The online version of this article (doi:10.1007/s00445-013-0788-0) contains supplementary material, which is available to authorized users.

S. Barde-Cabusson (✉) · J. Martí · X. Bolós · A. Geyer · E. Ronchin · A. Sánchez
Institute of Earth Sciences Jaume Almera, ICTJA-CSIC, Lluís Sole i Sabaris s/n, 08028 Barcelona, Spain
e-mail: s.barde.cabusson@gmail.com

J. Gottsmann
Department of Earth Sciences, University of Bristol, Wills Memorial Building, Queens Road, Bristol BS8 1RJ, UK

A. G. Camacho
Instituto de Geociencias (CSIC, UCM), Plaza de Ciencias 3,
28040 Madrid, Spain

L. Planagumà
Tosca, Environment Services of Education, Casal dels Volcans, Av.
Santa Coloma, 17800 Olot, Spain

Keywords Self-potential · Gravimetry · Garrotxa · Structural control · Monogenetic volcanism

Introduction

The temporal and spatial distribution of monogenetic volcanoes and the probability of future activity in monogenetic volcanic fields are subjects of increasing interest (e.g. Scandone 1979; Connor and Hill 1995; Connor et al. 2000; Alberico et al. 2002; Martin et al. 2003; Valentine and Perry 2006; Alberico et al. 2008). Statistical analyses indicate that deep and near-surface geological structures may control the distribution of magmatic complexes and volcanic vents

(Zhang and Lutz 1989; Lutz and Gutmann 1995; Paulsen and Wilson 2010), but geological structures are often hidden and their identification from surface geology alone can be difficult. Statistical, numerical and geological studies are ideally combined with geophysical investigations to build geologically meaningful models (Kiyosugi et al. 2010; Cebrià et al. 2011). In addition, geophysical methods have already been shown to be useful in studying dispersed volcanic fields and their relation to local tectonics (e.g. Rout et al. 1993 with detailed gravity and aeromagnetic studies on the Auckland volcanic field, New Zealand; Blakely et al. 1997 with gravity data on the Cascade Range, Oregon and California; Connor et al. 2000 with a combination of gravity data and magnetic data at Yucca Mountain (Nevada); Kiyosugi et al. 2010 with P-wave tomography from the Abu Monogenetic Volcano Group, Japan).

In a monogenetic volcanic field, from one eruption to another, magma must be transported from source to surface at different places. Depending on stress conditions, magma injection parameters and geometry, pre-existing crustal fractures may influence the propagation of magmas (Valentine and Krogh 2006; Gaffney et al. 2007; Wetmore et al. 2009). In a set of analogue experiments, Le Corvec et al. (2013) investigate the conditions leading a dyke to interact with pre-existing fractures into the crust, by varying (1) the volume of injected magma, (2) the distance between a dike and a pre-existing fracture and (3) the impact of a deviatoric stress. They find that, in nature, the interaction between propagating dikes and pre-existing fractures is likely to occur when the horizontal distance that separates them becomes less than about 200 m, and they determine that dikes with a volume less than about 10^{-2} km^3 would experience a decrease in their propagation velocity owing to the presence of surrounding fractures.

The Garrotxa monogenetic volcanic field is part of the Catalan Volcanic Zone (Martí et al. 1992) and hosts one of the Spanish Peninsula's youngest volcanic fields (Fig. 1). The Catalan Volcanic Zone is itself part of a major European belt of young volcanic zones and rift valleys (Wilson and Downes 1991) including the Eger graben and the Rhone–Rhine valley systems. Despite eruptive activity as recently as 10 ka BP (Cebrià et al. 2000), the hazard potential of the Garrotxa volcanic field has been little studied and needs to be accurately assessed. Most of the volcanic activity of the Garrotxa took place along a WNW–ESE trending depression, corresponding to an eroded anticline of Eocene rocks (Martí et al. 2011; Fig. 1). The volcanic activity within the Garrotxa volcanic field is concentrated along structural lineaments (Martí et al. 2011; Cimarelli et al. 2013). Martí et al. (2011) described the main characteristics of the volcanism and the stratigraphic sequences of some key volcanic edifices in this area. They conclude that the main cause of the complex eruptive behaviour observed in the Garrotxa volcanic field resides in the

lithological, structural and hydrogeological characteristics of the substrate beneath the volcanoes. However, knowledge of the subsurface architecture from geophysical data has so far only been available on a regional scale.

Here, we present results from a study of the subsurface structure beneath the Garrotxa volcanic field using new gravity and self-potential data to assess the relationship between the distribution of volcanic landforms and the subsurface structure of the field (Fig. 2).

Field investigations, data post-processing and modelling

Joint gravimetric and GPS surveys

Gravimetric data were obtained over 80 km^2 in the Natural Park of La Garrotxa, including all volcanic edifices outside the township of Olot. The survey area extends roughly between the townships of Olot and Santa Pau and follows the east–west elongated depression where most of the volcanic edifices are built (Fig. 1).

Data were collected in September 2007 and March 2008 at 205 individual benchmarks (Fig. 2). Maximum distance between individual benchmarks in the central zone was about 1.5 km, and average distance between benchmarks around volcanic vents was $<500 \text{ m}$. Gravimetric measurements were performed using an automated Burris gravimeter (B-028). Data at each benchmark were obtained by averaging a data stream from the gravimeter collected automatically by a handheld controller. The data collection is unbiased by the operator as the process of data collection and processing to an observed gravity value is automated by the system. Individual measurements were obtained at an instrumental repeatability of better than 6 muGal ($1 \text{ muGal} = 10^{-8} \text{ m/s}^2$). Data at benchmarks was recorded relative to a reference located at 4665916mN, 459604 mE (m, UTM 31 N, ED50).

We calculated the complete Bouguer anomaly (with terrain correction to a distance of 60 km). Raw data was reduced for the effects of instrument drift (approximately linear at -37.5 muGal/day), Solid Earth tides, latitude variations, difference of elevation between individual benchmarks and terrain effects using standard procedures. A terrain density of $2,450 \text{ kg/m}^3$ was derived based on a minimum correlation between observed gravity variations and topography, inferred from digital elevation data of 15 m spatial resolution. This mathematically derived density value is in broad agreement with the densities of sedimentary surface rocks of the area. Gravity data are reported relative to absolute gravity reference value calculated theoretically at $980,240 \text{ mGal}$ (see supplementary Table 1).

Benchmark locations and elevations were determined using a Global Satellite Navigation System composed of two LEICA SR20 Global Positioning System (GPS) single-

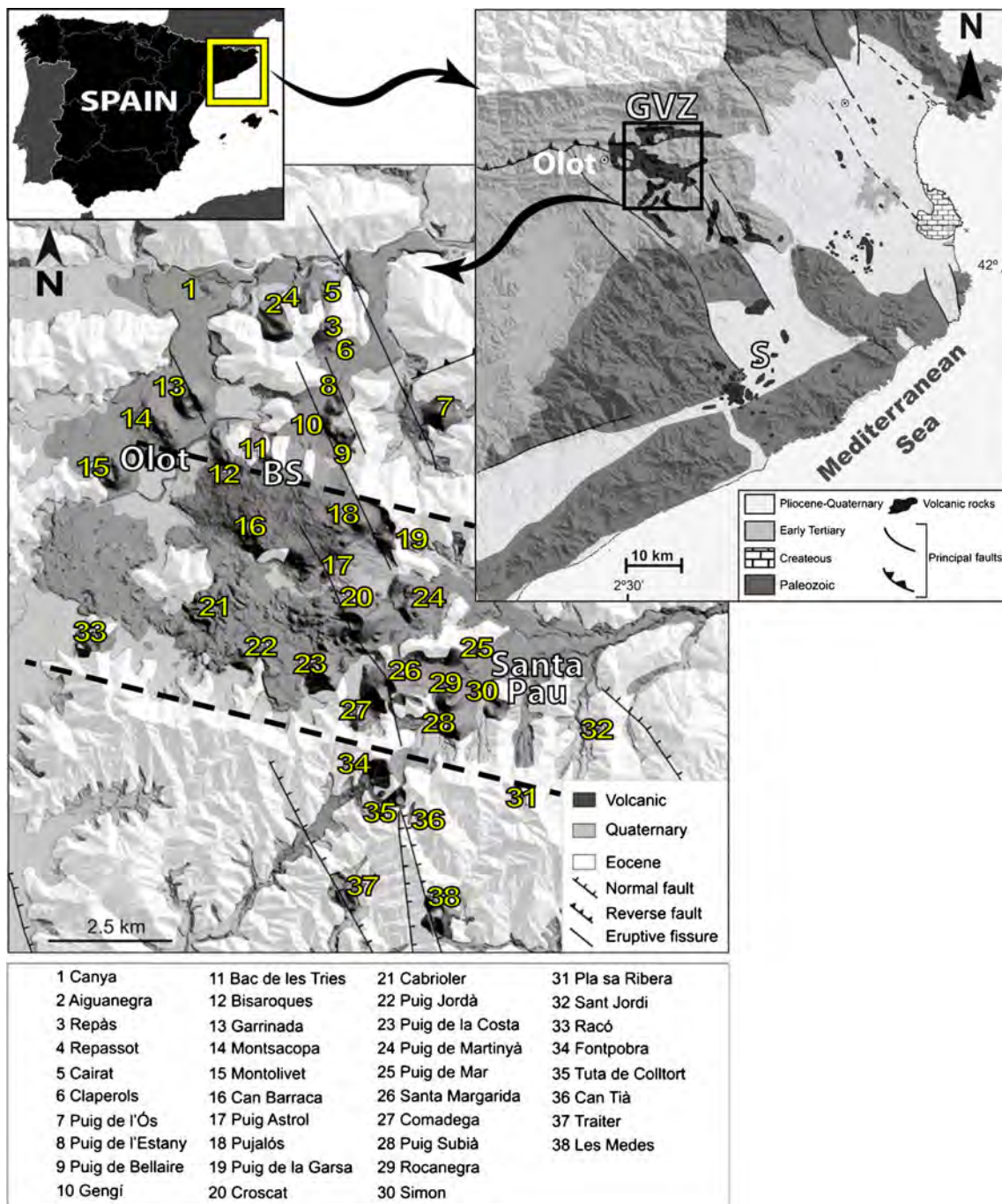


Fig. 1 Index and simplified geological and structural map of the studied area (modified from Martí et al. 2011). *BS* stands for Batet de la Serra village, and *black dashed lines* highlight the Garrotxa eroded anticline

depression. *Upper right inset* Simplified geological map of the Catalan Volcanic Zone and its surroundings (modified from Guérin et al. 1985). *GVZ* Garrotxa Volcanic Zone, *S* La Selva

frequency receivers. GPS data were collected simultaneously at benchmarks and at a reference station. The reference included an antenna mounted on a metal pole, which was fixed to the ground by a buried socket and a data logger. In total, we recorded more than 100 h of reference data at 10-s intervals. The roving receiver collected data in static mode from an antenna, which was carried on a pole housed in a backpack. GPS observation times varied inversely with signal quality

between 6 and 30 min. One operator took GPS measurements at each benchmark, while another operated the gravimeter.

Benchmark locations were calculated with respect to the reference using LEICA SKIPRO software. We obtained an average precision on benchmark locations of <0.5 and 1 m in the horizontal and vertical, respectively. This precision is sufficient to correct the gravimetric data for the effect of elevation changes from benchmark to benchmark over the

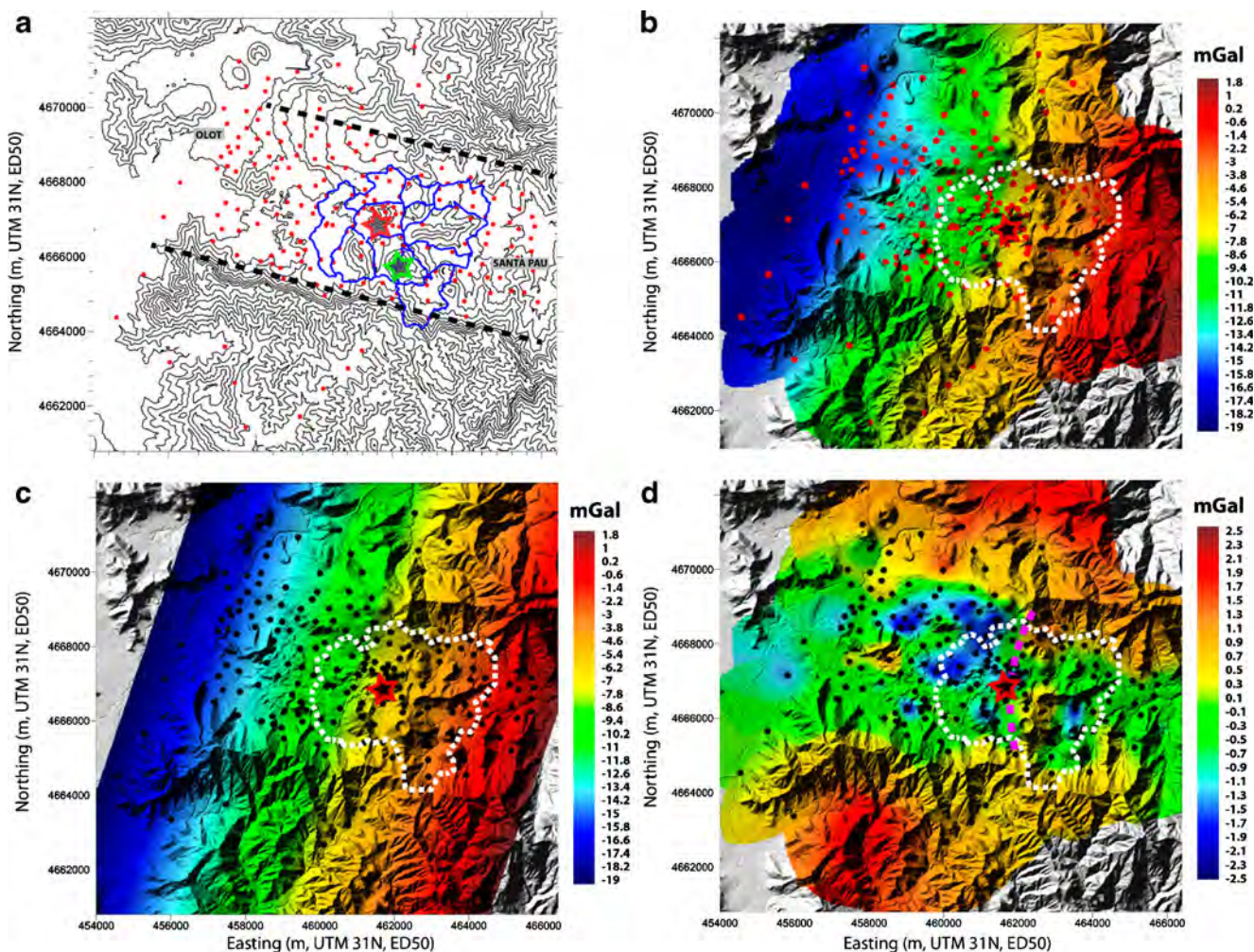


Fig. 2 **a** Topographic contours for the area, overlain by the gravity data benchmarks (*red dots*) and the self-potential data points (*blue dots*). **b** Bouguer anomaly map and index for the self-potential map (*white dashed line*). **c** Regional anomaly. **d** Residual gravity map obtained by subtracting the regional anomaly from the observed one; this residual

anomaly is built to extract the short-wavelength signal. The *pink dashed line* highlights a steep gravity gradient described in the text. *Red and black dots* Gravimetry-survey benchmarks, *red star* Crosca volcano, *green star* Santa Margarida cone. Coordinates in metres (UTM31N–ED50)

survey area in order to obtain a resolution of Bouguer gravity variations <1 mGal ($=10^{-5}$ m/s²), which is deemed appropriate for the study. This contrasts with existing regional Bouguer anomaly data, which is associated with an uncertainty of at least a factor of 5 higher.

Gravimetric data uncertainties and adjustment of geodetic reference frames

Error analysis gives a mean precision of the differential gravity values of ± 21 μ Gal, which represents an excellent value for structural gravimetric observations. Nevertheless, final anomaly data also contain uncertainties coming from elevation data and from terrain corrections. We estimate a precision level of 0.3 μ Gal, for this combined data. Some complexities in processing the terrain effect arise from differences between the geodetic reference frame of the survey (ellipsoidal WGS84) and the reference frame of available digital

topographic data (local reference frame with geoidal orthometric heights). We applied a mathematical correlation procedure to compare Northing, Easting and ellipsoidal height values of both frames. Fixing several reference points in either framework, we were able to derive the following relationships to match the DEM framework to our GPS positions and vice versa:

1. Easting=EastingDEM-88 m
2. Northing=NorthingDEM-220.8 m
3. Geoid height=ellipsoidal heights from GPS measurements+47.1 m.

Three-dimensional (3D) positions of benchmarks between our GPS data and the available digital elevation data are thus offset according to the following shift values:

$$dz = 47.1 \text{ m} \quad dx = 88.0 \text{ m} \quad dy = 220.8 \text{ m}$$

The value of dz of 47.1 m clearly corresponds to the height of the geoid in the zone (orthometric to geometric height translation). The values for dx and dy would correspond to a translation or horizontal discrepancy between the two reference systems. Cross-correlating both datasets, we obtain an average vertical precision of the digital elevation data of 2.52 m, which appears a reasonable value given that the DEM is based on gridded data with 15 m precision. Supplementary Table 1 gives details on UTM benchmark coordinates (Zone T31), GPS heights and correlation with available digital elevation data of the survey area as well as the obtained gravity data.

3D inversion of Bouguer gravity anomaly data

We performed a non-linear inversion of resulting local Bouguer anomaly data to construct a 3D model of the anomalous sub-surface density distribution (Fig. 3). The inversion routine is described in detail in Gottsmann et al. (2008) and Camacho et al. (2011) including sensitivity tests. In summary, the inversion constructs a subsurface model defined by a 3D aggregation of M parallelepiped cells, which are filled, in a “growth” process, by means of prescribed positive and/or negative density contrasts.

We addressed the problem of non-uniqueness by adopting a mixed minimisation condition, based on model “fitness”

(least square fitness) and “smoothness” (total anomalous mass):

$$\mathbf{v}^T \mathbf{Q}_D^{-1} \mathbf{v} + \lambda \mathbf{m}^T \mathbf{Q}_M^{-1} \mathbf{m} = \min \quad (1)$$

where $\mathbf{m} = (\Delta\rho_1, \dots, \Delta\rho_M)^T$ (superscript T denotes transpose of a matrix) are density contrast values for the M cells of the model, $\mathbf{v} = (v_1, \dots, v_N)^T$ are residual values for the N data points, \mathbf{Q}_D is an a priori covariance matrix for uncertainties of the gravity data, \mathbf{Q}_M is an a priori covariance matrix for uncertainties of the model parameters, and λ is a factor for selected balance fitness/smoothness of the model (Camacho et al. 2011).

Key for the inversion is the selection of an optimal balance between data “fitness” (least-square fitness) and model “smoothness” (total anomalous mass) expressed by the dimensional optimisation factor λ . For low values of λ , the inversion results in the generation of an excessively complex model of the subsurface structure with very good fit to the data. For high values of λ , the inversion produces a simple model but with poor fit to the data. L -curve criterion is a popular approach to select the trade-off parameter (e.g., Aster et al. 2004). We adopt the optimisation procedure proposed in Camacho et al. (2011) as producing uncorrelated inversion residuals. In fact, for too high a value of λ , model residuals are large and auto-correlated with respect to their

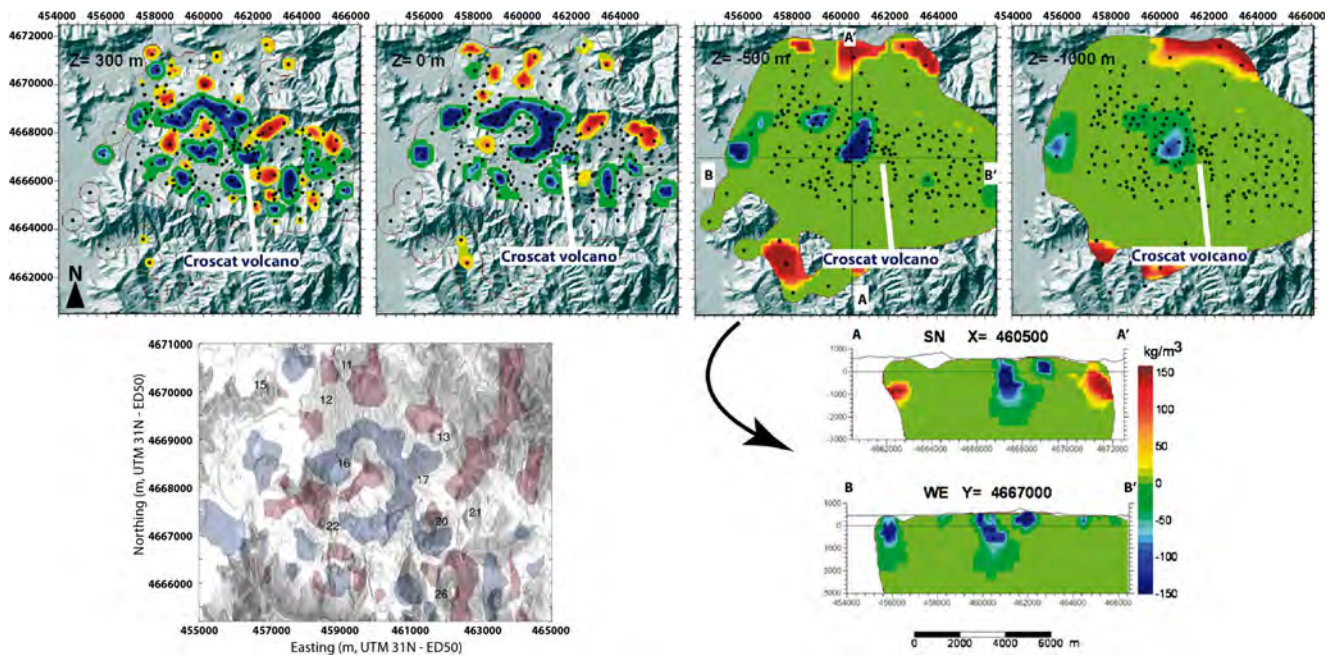


Fig. 3 Horizontal and vertical sections through the preferred density anomaly model of the Garrotxa depression (*upper panel and lower right-hand side*). *Lower left-hand side* depicts the modelled distribution of anomalous density bodies overlain by a digital elevation model. Isopycnic surfaces show the $+120 \text{ kg/m}^3$ (*red*) and -120 kg/m^3 (*blue*) contrasts. Numbers of volcanoes refer to those shown in Fig. 1. The low-density bodies are interpreted to result from a combination of tectonic

lineaments and the sub-volcanic roots of the dominant volcanic landforms in the Garrotxa monogenetic volcanic field. High-density bodies in the centre of the modelling domain are interpreted as surficial features of the landforms such as lava flows. High-density bodies at the periphery of the modelling domain are poorly constrained due to low data coverage. Coordinates in meters (UTM31N–ED50)

mutual distance. For too low a value of λ , model residuals show negative values of autocorrelation for small distances due to accounting for noise. The optimal value satisfies the condition of a zero autocorrelation of residuals with respect to the mutual distance between benchmarks.

Self-potential survey

The self-potential method measures the distribution of the electric potential at the surface of Earth or in boreholes, with respect to a reference electrode. Sources of self-potential fields include chemical potential gradients (Maineult et al. 2005, 2006), redox potentials (Linde and Revil 2007), rapid fluid disruption (Johnston et al. 2001) and electrokinetic conversion associated with fluid movement through porous materials (the so-called streaming potential). In active volcanic areas, the main source of self-potential variations is related to the flow of groundwater (e.g. Massenet and Pham 1985; Ishido et al. 1997; Bedrosian et al. 2007; Barde-Cabusson et al. 2009; Mauri et al. 2010; Pearson et al. 2012).

We used a pair of non-polarizing Cu/CuSO₄ electrodes. The microporous nature of the end contacts of these electrodes (made of a low-permeability wood) avoids leakage of the CuSO₄ solution during contact with the ground. The difference of electrical potential between a fixed reference and a moving electrode was measured with a calibrated high impedance voltmeter (Extech EX520, sensitivity of 0.1 mV, input impedance >10 M Ω).

Before and after each series of measurements, the reference electrode and the moving electrode were put face-to-face to check that the difference of potential between the two electrodes was <2 mV (if this is not the case, the static value is removed to all the measurements). For each self-potential measurement, the value of the electrical resistance was also measured prior the self-potential measurement in order to check the quality of the electrical contact between the scanning electrode and the ground (less than a few tens kilohms).

Self-potential measurements were obtained with a 300-m-long wire connecting the two electrodes. We performed a series of closed profiles between Olot and Santa Pau (2,073 measurements). The distance between two successive measurement stations was 20 m. Using a long cable avoids cumulative errors by changing the reference too often along the same profile. As the profiles are several kilometres long, a new reference station was established every 300 m. After the survey, the entire self-potential dataset was corrected using the first reference station as the unique reference. Usually, the 0 mV reference for self-potential measurements is taken at the sea or a water table as it provides a constant value in time. Because no such stable reference was available and self-potential is intrinsically a relative measurement, our self-potential data set is referenced arbitrarily to a point northeast of Santa Margarida (Fig. 1). A closure correction (below

50 mV for eight profiles and as much as 100 mV for three profiles) was applied to distribute the calculated data drift linearly on the profiles forming the dataset in order to limit cumulative errors.

Measurements of self-potential were only carried out in a small part of the area investigated by gravimetric measurements. Our aim was to test if near-surface structures such as fracture and faults have corresponding expressions at greater depth as revealed by the inversion of the gravimetric data and if the joint application of these potential field techniques in the Garrotxa yields useful insights.

Results

Local gravity anomaly

Figure 2b shows the resultant gravity anomaly data for the survey area with values between -19 and 2 mGal. The gravity data appears to follow a strong linear trend, which we modelled with a horizontal slope of 1,928 μ Gal/km and azimuth N108°E (Fig. 2c). We attribute this trend to regional large wavelength deep-seated geological structures associated with the topography of the metamorphic basement below a thrust belt at the SE part of the Pyrenees (Martinez et al. 1997). In order to derive the local gravity anomaly data (Bouguer anomaly), we subtracted the predicted gravity anomaly of the regional component from the observed data. The resultant anomaly map is given in Fig. 2d.

The obtained Bouguer anomaly map shows a range in gravity variations in the survey area between -2.5 and +2.5 mGal. Neutral to mildly negative (up to -0.7 mGal) gravity anomalies dominate a central elongated sector striking WNW-ESE and following the Garrotxa depression, which hosts the volcanic zone. A pronounced negative gravity anomaly with amplitudes of up to -2.5 mGal lays in the central part of the survey area bordering the high ground to the north. There is, however, no indication for a spatially extended large amplitude and coherent low-density structure beneath the entire volcanic zone, but rather for a series of spatially concentrated low-density bodies. The overall surficial shape of the dominant gravity-low resembles a horseshoe, which opens towards the SW (Fig. 2d).

Parts of the area dominated by low gravity values correspond to prominent volcanic edifices such as, the Croscat, Can Barraca, Puig Astrol and Pujalós volcanoes (see Figs. 1 and 2d with Croscat taken as a reference for localization). The anomaly is clearly bounded to the North (by areas of higher topography) as well as to the East with a steep horizontal gravity gradient towards neutral gravity. This transition occurs across a line striking roughly N-S (pink dashed line in Fig. 2d).

In addition, a linear element of relative higher gravity (+0.3 to +0.7 mGal; depicted by yellow colors in Fig. 2d; roughly at

4 666 000 mN and 463,000 mE) separates two zones with negative anomalies. This gravity high strikes NNE–SSW, coincides with a break in slope from the volcanic centres towards the town of Santa Pau and runs roughly parallel to the Eastern border of the dominant negative horseshoe-shaped gravity anomaly.

Gravity inversion results

The resultant gravity model is illustrated in Fig. 3, and the distribution of inversion residuals is shown in Fig. 4. Anomalous density contrasts range between -150 and 150 kg/m^3 , where neutral contrasts with terrain rocks are expressed by values of 0 kg/m^3 .

Bodies of positive and negative density contrasts dominate the near surface of the volcanic field. However, only low-density bodies modelled in the centre of the survey area and underlying major volcanic landforms (predominantly scoria cones) appear to be rooted at greater depth with traceable extents to depths greater than -500 m . In particular, the size and extent of the dominant low-density bodies beneath the Croscat cone and its adjacent NW side are revealed. The lower left hand of Fig. 3 depicts the modelled distribution of

anomalous density bodies overlain by a digital elevation model. Isopycnic surfaces show the $+120 \text{ kg/m}^3$ (red) and -120 kg/m^3 (blue) contrasts (see Fig. 1 for numbered volcano names).

Self-potential

The most striking feature of the self-potential map is a sharp transition in the self-potential values from east to west, where the lowest values are registered (Fig. 5a). This transition takes place along a NNE–SSW axis in the northern part of the study area and along a NNW–SSE axis south of the Croscat volcanic cone. The NNW–SSE axis is outlined by sharp self-potential spatial variations northwest of the Croscat cone, south of the Croscat cone and a more gradual variation through the Santa Margarida cone. The self-potential map shows a total variation of $\sim 340 \text{ mV}$. Maximum self-potential values have been measured in the eastern half of the study area with poor spatial variations ($<30 \text{ mV}$) and no specific pattern identified through the orientation of the self-potential isolines. In this sector, however, as it coincides with a negative gravity anomaly ($\sim -1.7 \text{ mGal}$; Fig. 5b), we note the presence of a low self-potential minimum ($<20 \text{ mV}$ under the local values) just

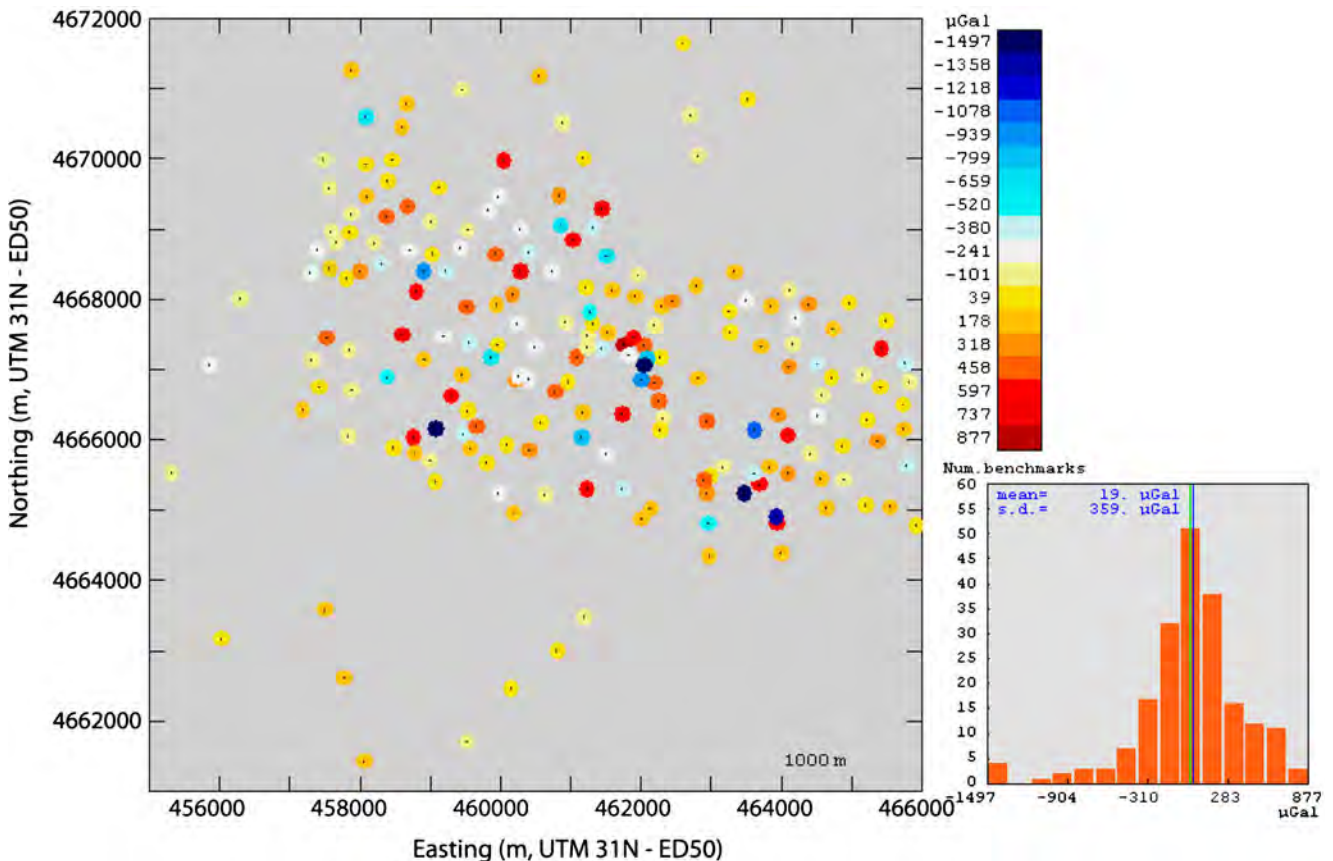
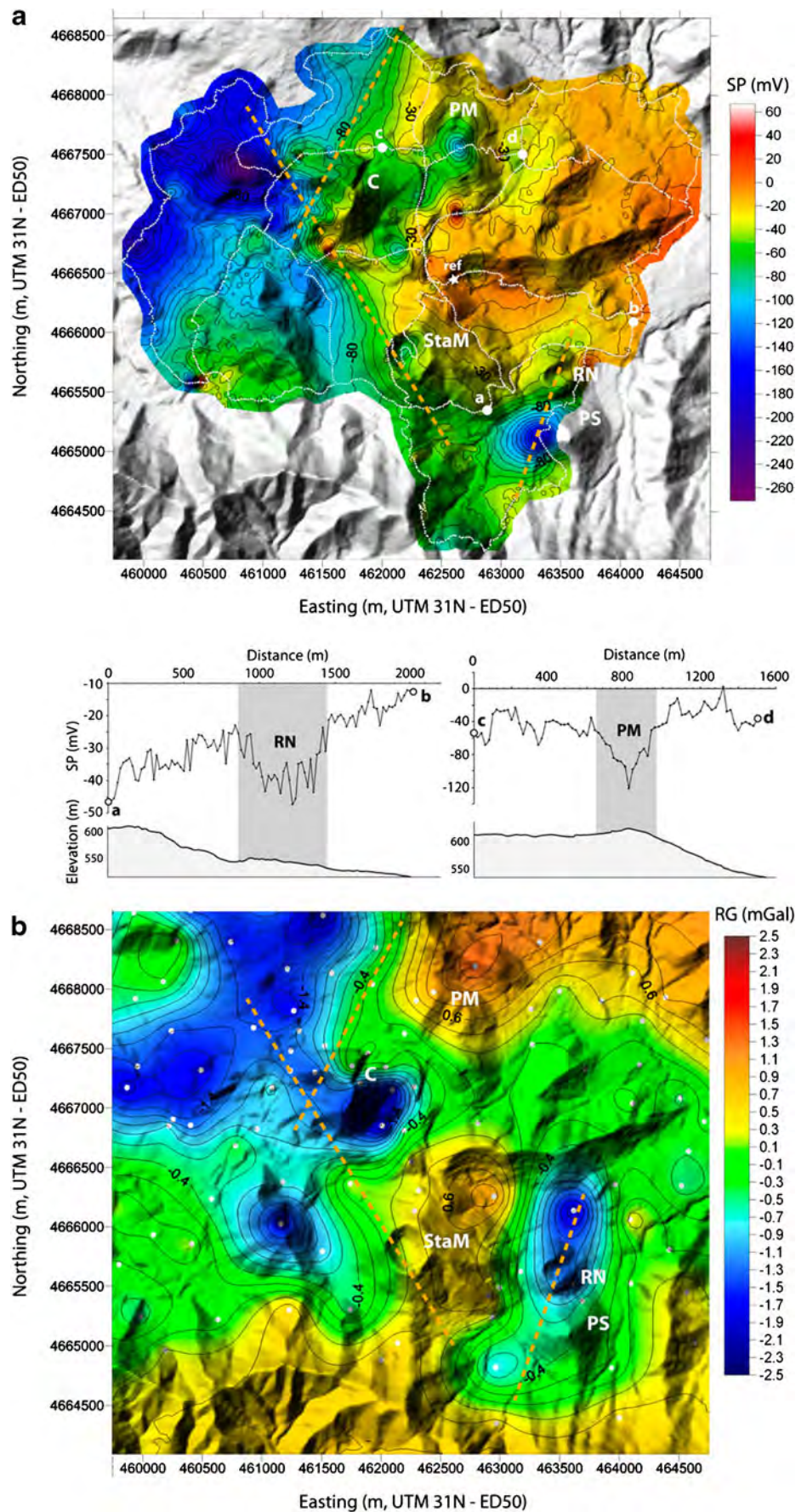


Fig. 4 Map showing the distribution of the inversion residuals as a proxy for the quality of fit of the model to the observations. The mean residual is 0.019 mGal with a standard deviation of 0.359 mGal , reflecting the best fit to the data as well as satisfying constraints of model smoothness ($\lambda=40$)

Fig. 5 **a** Self-potential map overlain on a digital elevation model. In the lower part, two SP vs distance graphs and corresponding topography (ab and cd). **b** Residual gravity anomaly map in the same area. Note how both self-potential and gravimetric data highlight NNE–SSW and NNW–SSE lineaments (orange broken lines). *ref* stands for the SP reference point, *C* Croscat, *PM* Puig de Martinyà, *StaM* Santa Margarida, *RN* Rocanegra, *PS* Puig Subià



north of the Rocanegra scoria cone. This variation is less than the background noise in the area, but it is clearly above the local noise (see profile a–b in Fig. 5a).

The Puig Subià cone shows a strong self-potential minimum of 150 mV below the surrounding background self-potential.

A self-potential vs elevation graph of the whole dataset (Fig. 6) shows different distributions of the measurements for the eastern and western parts of the map, separated by the NNE–SSW and NNW–SSE lineations identified with self-potential. The eastern zone shows a linear trend with a self-potential vs elevation gradient of -0.19 mV/m, typical of hydrogeological zones on volcanoes (e.g. Lénat 2007). This contrasts with data from the western zone, which does not follow a particular trend. Only the isolated minima or maxima registered in the eastern part of the map diverge from this trend. As an example, the self-potential measurements corresponding to the strong minimum registered on Puig Subià plot outside of the hydrogeological trend (Fig. 6). At the south-western end of the map the self-potential signal tends to increase again. Additionally, some small-scale (a few tens of metres wide) self-potential minima or maxima are visible along single profiles. In particular, a self-potential minimum has been mapped in the Puig de Martinyà area (see profile c–d in Fig. 5a).

The NNE–SSW and NNW–SSE self-potential axes coincide with the orientation of the residual gravity anomaly isolines corresponding to the gravity lows reported in the previous section (Fig. 5). Overall we find an excellent correlation between the gravity and self-potential anomalies as depicted in Fig. 7.

Discussion

Distribution of volcanism related to local tectonics from gravity and self-potential data

The localized gravity lows (Fig. 2d) are interpreted to result from relatively low rock densities. These densities could reflect either volcanic surface deposits or rocks of the shallow plumbing system of individual volcanic centres. The rather abrupt change from neutral to both pronounced negative and positive gravity values and vice versa (horizontal gravity gradients $> \pm 1$ mGal/km) might indicate a structural confinement of the main anomalous density zones by conjugated faults. The data allow us to suggest a WNW–ESE orientation, which finds expression in the main structural lineaments of the Garrotxa graben. In addition, NNE–SSW and NNW–SSE axes are highlighted in the central part of the volcanic field (Fig. 5). Although the self-potential data covers only part of the gravimetry map, it supports the same NNE–SSW and NNW–SSE orientations with the strong transition observed from east to west (100 mV over a few hundred metres). The NNW–SSE axis matches the lineament drawn by the gravity high near Croscat and Santa Margarida cones (Fig. 5). Martí et al. (2011) interpret the Santa Margarida/Croscat/La Pomareda alignment as the result of a single eruptive episode along a NNW–SSE trending, 3 km long fissure. Our data provides geophysical evidence for a correlation between volcanism and tectonic structures, which may imply a structural control on magma at depth, establishing a basis for interpreting the self-potential variations associated with gravity anomalies in our study area.

The north-western sector of the self-potential map presents another sharp variation highlighting a NNE–SSW lineament.

Fig. 6 Plot of the self-potential data as a function of elevation. A global trend illustrates the correlation between SP and elevation in the eastern zone of the SP map, with a SP/elevation gradient of -0.19 mV m⁻¹, while this correlation does not exist in the western zone. Only punctual minima or maxima registered in the eastern part of the SP map plot outside this trend, as exemplified by the Puig Subià minimum (blue squares)

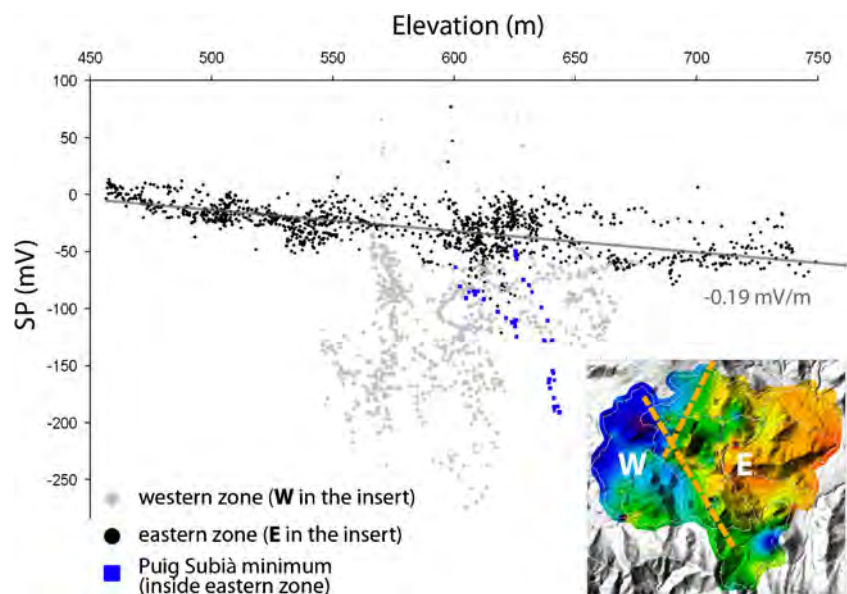
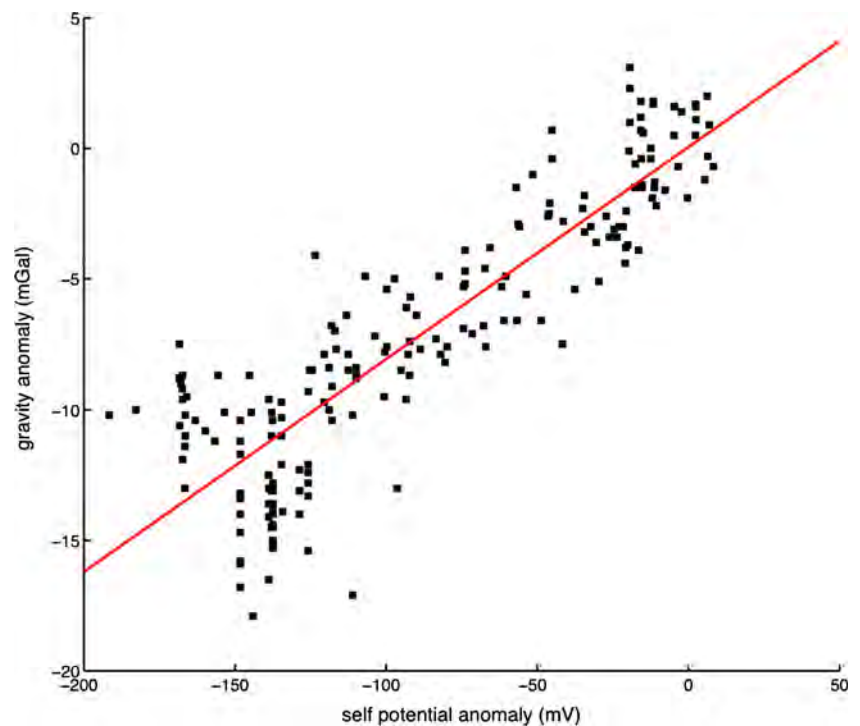


Fig. 7 There is a positive linear relationship between the gravity and self potential anomalies with a regression coefficient $R=0.88$. Due to different locations of the individual measurement points for the two techniques, the SP data have been interpolated at the gravity benchmark to test for a possible correlation



This coincides with the eastern limit of the north-western negative gravity anomaly (Fig. 5). No volcanic edifice is evident along this lineament, but our geophysical data might indicate the presence of a NNE–SSW-oriented structural boundary, similar to the NNW–SSE axis detected between the Crosat and Santa Margarida volcanoes. The former can be interpreted as a fault zone or a zone of failed shallow intrusions along an existing structural anisotropy. Due to the substantial vegetation cover and poor accessibility, there is a lack of precise geological data on the extent of surface deposits from individual eruptions or indeed small-scale volcanic edifices in this area. Volcanological field observations to the north and south of the Crosat volcano indicate that there is indeed no correlation between the spatial distribution of the surface deposits and the spatial limits of the geophysical structures. The stark difference in self-potential values between the western and eastern zone (Fig. 6) suggests lateral heterogeneity of the medium (Lénat 2007). This indicates that the corresponding NNW–SSE and NNE–SSW lineaments might not simply mark eruptive fissures but may indicate faults separating two blocks with different hydrogeological properties and/or different global resistivity values. The presence of pre-existing faults is not necessary to explain the observed self-potential signal because the presence of dykes might impede groundwater movement, creating this contrast between the eastern and the western zones. Both interpretations, independently or combined, are compatible with the results.

North of the Rocanegra cone, the eastern negative gravity anomaly (Fig. 5) is associated with a weak self-potential

minimum showing a sharp variation at the limits (see profile a–b in Fig. 5). This minimum is of ~ 20 mV with respect to the surrounding area, which is significantly higher than the signal noise along the corresponding profile. South of Rocanegra, on the Puig Subià cone, we also measured a strong self-potential minimum of ~ 150 mV. Again, no relationship could be established with the surface lithology. These self-potential minima are thought to be related to preferential meteoric infiltration or to a sharp lateral resistivity variation. The association and sharp limits of the self-potential minima and the negative gravity anomaly might indicate a structural limit such as a fault or a fissure, guiding infiltration of groundwater. The respective location of Rocanegra and Puig Subià, two well-preserved volcanic edifices, establish a NNE–SSW alignment with the measured anomalies. This direction and the similar preservation state of the two cones are consistent with a genetic link between them along a NNE–SSW oriented structural weakness (Fig. 5).

It is interesting to note that volcanic edifices occur only within the depression formed by the eroded anticline. Wetmore et al. (2009) discuss the relationship between intrusions and folding on local scale and give the example of the Trachyte Mesa intrusion (Utah, USA), which was emplaced into a series of northeast trending upright and open folds formed during the Jurassic. The fold axes strike sub-parallel to the long axis of the Trachyte Mesa intrusion, and the geometry of the basal contact of the intrusion appears to follow the morphology of the fold limbs. The majority of the intrusion is confined within the axis of a syncline bounded by anticlines on either side. The authors suggest that both pre-

existing structures and the density of the magma relative to that of the host rocks fundamentally controlled the emplacement of this intrusion. In the case of the Garrotxa volcanic field, we cannot unambiguously establish a causal relationship between the anticline and the volcanic activity, but note that there are strong indications for the presence of structural lineaments that cut across the anticline and contributed to the localisation of magma pathways (see below).

Density anomaly models of volcanic roots

The 3D density anomaly model shows a dominant body of negative density contrast, with an annulus of isolated density lows of similar amplitude (up to -150 kg/m^3). The centre of the main anomalous body is located $\sim 1 \text{ km}$ WNW of the $\sim 14 \text{ ka}$ Croscat volcano, the youngest volcano in this area (Puiguriguer et al. 2012). The -2 mGal Bouguer anomaly is explained in the model by a coherent arcuate and rather shallow-seated (to depths of around sea level) low-density structure. The anomaly is well defined by numerous gravity stations and its diameter at the surface is about 2 km . Its northern border appears buried beneath the morphological high of the plateau between Batet de la Serra village and Pujalos volcano (Fig. 1). Beneath the main central depression of the Garrotxa (between Olot and the Croscat cone), the anomaly is modelled for an optimisation factor $\lambda=40$ by a shallow zone extending at least 1 km deep over a zone about 1.5 km wide and characterized by up to -150 kg/m^3 density contrast (see cross-sections in Fig. 3). A possible explanation of this dominant structure is that it represents a combination of the (pyroclastic) sub-volcanic root of the surficial scoria cones and fault/fissure damage zones. The portions of these structures beneath Batet de la Serra village and Pujalos volcano appear to be shallow intrusions branching from the main low-density bodies, which fed the scoria cones in the central depression as depicted in the N–S cross-section and by the -120 kg/m^3 isopycnic surfaces (Fig. 3). The roughly NNE–SSW extension of the western arc and the roughly NNW–SSE extension of the eastern arc may delineate magma pathways along the dominant structural features of the Garrotxa. It is perhaps interesting to note that the deeper portions of the low-density bodies resemble cylindrical geometries, which may delineate the shallow magmatic feeder systems of individual volcanoes in the western part of the study (near Olot), as well as the scoria cone cluster at the centre of the volcanic field (Croscat and its neighbouring volcanoes to the SW and W). From west to east, the Garrinada, Can Barraca, Cabrioler, Puig Jorda, Puig de la Costa, Croscat, Puig Subià, Rocanegra, Puig de Mar and Simon volcanoes are modelled to contain low-density roots to several hundred metres depth.

The origin of the main low-density body near Croscat deserves further examination. First, it appears that the cluster of volcanic cones in the centre of the Garrotxa has been fed by a common fault-bounded magmatic feeder system from which

conduit-like structures fan away at surficial levels ($<1,000 \text{ m}$ depth) to feed monogenetic volcanoes of the central zone. Second, the stratigraphic record of the Croscat edifice shows evidence for violent Strombolian activity during its generation (Marti et al. 2011). This implies an increase in intensity of eruption, inferred to result from deepening of the fragmentation level. Therefore, in addition to a tectonic origin for the low-density structure, the body could also be a testament of pyroclastic roots beneath the cones.

In contrast to Croscat, a pronounced negative density body is absent beneath Santa Margarida volcano, which appears bounded in the north by a high-density body next to the low-density volume beneath Croscat. Such a sharp change in density contrasts is striking and our interpretation is that a NNE–SSW trending fault zone and potentially a second zone striking perpendicular to it separates the plumbing systems of Croscat and Santa Margarida, masking a potential low-density root beneath Santa Margarida. In addition, the eruptive history of Santa Margarida volcano is profoundly different from that of Croscat. Santa Margarida is almost exclusively built of phreatomagmatic lithic-rich deposits from surges. The absence of a dominant density low beneath Santa Margarida could also result from a fundamentally different fragmentation process of its magma, which according to its stratigraphic record never attained the substantial violent Strombolian character that its neighbour Croscat did (Marti et al. 2011).

Volcano-tectonics of the Garrotxa monogenetic field

The main lineaments identified by the geophysical study intersect the edges of the depression formed by the Garrotxa eroded anticline (Martinez et al. 1997). The NNW–SSE trending lineaments run parallel to major regional structures expressed by major normal faults (see insert in Fig. 1). One could thus envisage a mini-(half) graben almost perpendicular to the main WNW–ESE striking eroded anticline defining the location of the central volcanic zone of the Garrotxa, between Olot and Santa Pau. In order to explain the negative density contrasts, a substantial amount of pyroclastic material or porous lavas with lower than average bulk densities must be present. In this context and based on the data and modelling presented herein, we surmise that the presence and location of the volcanic centres is tectonically controlled by a network of conjugate faults intersecting the anticline axis.

Conclusions

The main finding of this study is that the central part of the Garrotxa volcanic field is underlain by low-density material. Porous volcanoclastic deposits including the pyroclastic roots of volcanic edifices in combination with fault and fissure damage zones appear to be the main candidates to explain

the observed gravity anomalies. Volcanism appears to be controlled by NNE–SSW and NNW–SSE tectonic structures identified by both gravimetric and self-potential data. The Croscat, Santa Margarida and Roca Negra volcanoes lie atop a conjugated fault system. The combination of the two geophysical methods has helped us to explore and link the surficial expressions of monogenetic volcanism and characteristic fault/fissure zones of the volcanic field with magma pathways and their sub-surface structures to depths of about 1 km. Identification of such volcano-morpho-tectonic structures and their mutual relationships is critical for better understanding the dynamics of monogenetic volcanic fields. Our study demonstrates the close link between tectonic structures and magma pathways in the evolution of the Garrotxa volcanic field with potential to guide future eruptive activity. This subject is of substantial interest for the assessment of causes and consequences of future volcano-tectonic unrest and volcanic reactivation in the Garrotxa and other monogenetic volcanic fields.

Acknowledgments We thank the Natural Park of the La Garrotxa Volcanic Zone and its staff for their support throughout this study. SBC acknowledges the JAE-Doc postdoctoral personal grant program of Consejo Superior de Investigaciones Científicas (JAEDoc_09_01319), JG acknowledges funding from a Royal Society University Research Fellowship and an International Joint Project grant with JM and AG acknowledges her post-doctoral Juan de la Cierva Grant (JCI-2010-06092). X. Bolós has been funded by grant Beca d’investigació “Oriol de Bolós” en Ciències Naturals (Olot, Spain). AGC has been supported by the MICINN research project AYA2010-17448. The work was also partially supported by the European Commission (FP7 Theme: ENV.2011.1.3.3-1; grant 282759: “VUELCO”). We sincerely thank the Executive Editor James D. L. White, Editor Takeshi Nishimura, and reviewers Charles Connor and Koki Aizawa for their constructive and helpful comments on our manuscript.

References

- Alberico I, Lirer L, Petrosino P, Scandone R (2002) A methodology for the evaluation of long-term volcanic risk from pyroclastic flows in Campi Flegrei (Italy). *J Volcanol Geotherm Res* 116:63–78
- Alberico I, Lirer L, Petrosino P, Scandone R (2008) Volcanic hazard and risk assessment from pyroclastic flows at Ischia island (southern Italy). *J Volcanol Geotherm Res* 171:118–136
- Aster R, Borchers B, Thurber C (2004) Parameter estimation and inverse problems. Elsevier Academic, Amsterdam, 301 pp.
- Barde-Cabusson S, Levieux G, Lénat JF, Finizola A, Revil A, Chaput M, Dumont S, Duputel Z, Guy A, Mathieu L, Saumet S, Sorbadère F, Vieille M (2009) Transient self-potential anomalies associated with recent lava flows at Piton de la Fournaise volcano (Réunion Island, Indian Ocean). *J Volcanol Geotherm Res* 187:158–166. doi:10.1016/j.jvolgeores.2009.09.003
- Bedrosian PA, Unsworth MJ, Johnston MJS (2007) Hydrothermal circulation at Mount St. Helens determined by self-potential measurements. *J Volcanol Geotherm Res* 160:137–146
- Blakely RJ, Christiansen RL, Guffanti M, Wells RE, Donnelly-Nolan JM, Muffler LJP, Clynne MA, Smith JG (1997) Gravity anomalies, Quaternary vents, and Quaternary faults in the southern Cascade Range, Oregon and California: implications for arc and backarc evolution. *J Geophys Res* 102(B10):22513–22527
- Camacho AG, Fernandez J, Gottsmann J (2011) A new gravity inversion method for multiple subhorizontal discontinuity interfaces and shallow basins. *J Geophys Res* 116:B02413. doi:10.1029/2010JB008023
- Cebrià JM, López-Ruiz J, Doblas M, Oyarzun R, Hertogen J, Benito R (2000) Geochemistry of the Quaternary alkali basalts of Garrotxa (NE Volcanic Province, Spain): a case of double enrichment of the mantle lithosphere. *J Volcanol Geotherm Res* 112:175–187
- Cebrià JM, Martín-Escorza C, López-Ruiz J, Morán-Zenteno DJ, Martiny BM (2011) Numerical recognition of alignments in monogenetic volcanic areas: examples from the Michoacán–Guanajuato volcanic field in Mexico and Calatrava in Spain. *J Volcanol Geotherm Res* 201:73–82. doi:10.1016/j.jvolgeores.2010.07.016
- Cimarelli C, Di Traglia F, de Rita D, Gimeno Torrente D, Fernandez Turiel JL (2013) Space–time evolution of monogenetic volcanism in the mafic Garrotxa volcanic field (NE Iberian Peninsula). *Bull Volcanol* 75:758. doi:10.1007/s00445-013-0758-6
- Connor CB, Hill BE (1995) Three nonhomogeneous Poisson models for the probability of basaltic volcanism: application to the Yucca Mountain region, Nevada. *J Geophys Res* 100:10107–10125
- Connor CB, Stamatakis JA, Ferrill DA, Hill BE, Ofoegbu GI, Conway FM, Sagar B, Trapp J (2000) Geologic factors controlling patterns of small-volume basaltic volcanism: application to a volcanic hazards assessment at Yucca Mountain, Nevada. *J Geophys Res* 105:417–432
- Gaffney ES, Damjanac B, Valentine GA (2007) Localization of volcanic activity: 2. Effects of pre-existing structure. *Earth Planet. Sci Lett* 263(3–4):323–338
- Gottsmann J, Camacho AG, Martí J, Wooller L, Fernandez J, Garcia A, Rymer H (2008) Shallow structure beneath the Central Volcanic Complex of Tenerife from new gravity data: Implications for its evolution and recent reactivation. *Phys Earth Planet Inter* 168(3–4): 212–230
- Guérin G, Behamoun G, Mallarach JM (1985) Un exemple de fusió parcial en medi continental. El vulcanisme quaternari de la Garrotxa. Publicació del Museu Comarcal de la Garrotxa, Vitrina 19–26
- Ishido T, Kiruchi T, Matsushima N, Yano Y, Nakao S, Sugihara M, Toshi T, Takakura S, Ogawa Y (1997) Repeated self-potential profiling of Izu-Oshima Volcano, Japan. *J Geomagn Geoelectr* 49:1267–1278
- Johnston MJS, Byerlee JD, Lockner D (2001) Rapid fluid disruption: a source of self-potential anomalies on volcanoes. *J Geophys Res* 106(B3):4327–4335
- Kiyosugi K, Connor CB, Zhao D, Connor LJ, Tanaka K (2010) Relationships between volcano distribution, crustal structure, and P-wave tomography: an example from the Abu Monogenetic Volcano Group, SW Japan. *Bull Volcanol* 72:331–340. doi:10.1007/s00445-009-0316-4
- Le Corvec N, Menand T, Lindsay J (2013) Interaction of ascending magma with pre-existing crustal fractures in monogenetic basaltic volcanism: an experimental approach. *J Geophys Res* 118:968–984. doi:10.1002/jgrb.50142
- Lénat JF (2007) Retrieving self-potential anomalies in a complex volcanic environment: an SP/elevation gradient approach. *Near Surf Geophys* 5:161–170
- Linde N, Revil A (2007) Comment on “Electrical tomography of La Soufrière de Guadeloupe Volcano: Field experiments, 1D inversion and qualitative interpretation”, by F. Nicollin et al. *Earth Planet Sci Lett* 258:619–622. doi:10.1016/j.epsl.2006.02.020
- Lutz TM, Gutmann JT (1995) An improved method for determining and characterizing alignments of pointlike features and its implications for the Pinacate volcanic field, Sonora, Mexico. *J Geophys Res* 100(B9):17659–17670
- Maineult A, Bernabé Y, Ackerer P (2005) Detection of advected concentration and pH fronts from self-potential measurements. *J Geophys Res* 110:B11205. doi:10.1029/2005JB003824

- Maineult A, Bernabé Y, Ackerer P (2006) Detection of advected, reacting redox fronts from self-potential measurements. *J Contam Hydrol* 86: 32–52
- Martí J, Mitjavila J, Roca E, Aparicio A (1992) Cenozoic magmatism of the Valencia trough (Western Mediterranean): relation between structural evolution and Volcanism. *Tectonophysics* 203:145–166
- Martí J, Ll P, Geyer A, Canal E, Pedrazzi D (2011) Complex interaction between Strombolian and phreatomagmatic eruptions in the Quaternary monogenetic volcanism of the Catalan Volcanic Zone (NE of Spain). *J Volcanol Geotherm Res* 201(1–4):178–193. doi:10.1016/j.jvolgeores.2010.12.009
- Martin AJ, Takahashi M, Umeda K, Yusa Y (2003) Probabilistic methods for estimating the long-term spatial characteristics of monogenetic volcanoes in Japan. *Acta Geophys Pol* 51:271–291
- Martinez A, Rivero L, Casas A (1997) Integrated gravity and seismic interpretation of duplex structures and imbricate thrust systems in the southeastern Pyrenees (NE Spain). *Tectonophysics* 282:303–329
- Massenet F, Pham VN (1985) Experimental and theoretical basis of self-potential phenomena in volcanic areas with reference to results obtained on Mount Etna (Sicily). *Earth Planet Sci Lett* 73:415–429
- Mauri G, Williams-Jones G, Saracco G (2010) Depth determinations of shallow hydrothermal systems by self-potential and multi-scale wavelet tomography. *J Volcanol Geotherm Res* 191(3):233–244
- Paulsen TS, Wilson TJ (2010) New criteria for systematic mapping and reliability assessment of monogenetic volcanic vent alignments and elongate volcanic vents for crustal stress analyses. *Tectonophysics* 482(1):16–28
- Pearson SCP, Kiyosugi K, Lehto HL, Saballos JA, Connor CB, Sanford WE (2012) Integrated geophysical and hydrothermal models of flank degassing and fluid flow at Masaya volcano, Nicaragua. *Geochem Geophys Geosyst* 13: Q05011. doi:10.1029/2012GC004117
- Puiguirguier M, Alcalde G, Bassols E, Burjachs F, Exposito I, Planaguma L, Sana M, Yll E (2012) C-14 dating of the last Croscat volcano eruption (Garrotxa Region, NE Iberian Peninsula). *Geol Acta* 10(1): 43–47
- Rout DJ, Cassidy J, Locke CA, Smith IE (1993) Geophysical evidence for temporal and structural relationships within the monogenetic basalt volcanoes of the Auckland volcanic field, northern New Zealand. *J Volcanol Geotherm Res* 57(1):71–83
- Scandone R (1979) Preliminary evaluation of the volcanic hazard in the southern valley of Mexico. *Geofis Int* 18:21–35
- Valentine GA, Perry FV (2006) Decreasing magmatic footprints of individual volcanoes in a waning basaltic field. *Geophys Res Lett* 33: L14305. doi:10.1029/2006GL026743
- Valentine GA, Krogh KEC (2006) Emplacement of shallow dikes and sills beneath a small basaltic volcanic center—the role of pre-existing structure (Paiute Ridge, southern Nevada, USA). *Earth Planet Sci Lett* 246(3–4):217–230
- Wetmore PH, Connor CB, Kruse SE, Callihan S, Pignotta G, Stremtan C, Burke A (2009) Geometry of the Trachyte Mesa intrusion, Henry Mountains, Utah: Implications for the emplacement of small melt volumes into the upper crust. *Geochem Geophys Geosyst* 10: Q08006. doi:10.1029/2009GC002469
- Wilson M, Downes H (1991) Tertiary-Quaternary extension-related alkaline magmatism in Western and Central Europe. *J Petrol* 32(4): 811–849
- Zhang D, Lutz T (1989) Structural control of igneous complexes and kimberlites: a new statistical method. *Tectonophysics* 159:137–148

APPENDIX 3

Geophysical exploration on the subsurface geology of La Garrotxa monogenetic Volcanic Field (NE Iberian Peninsula)

Geophysical exploration on the subsurface geology of La Garrotxa monogenetic volcanic field (NE Iberian Peninsula)

Xavier Bolós · Stéphanie Barde-Cabusson ·
Dario Pedrazzi · Joan Martí · Albert Casas ·
Raúl Lovera · Daniel Nadal-Sala

Received: 7 February 2014 / Accepted: 4 June 2014
© Springer-Verlag Berlin Heidelberg 2014

Abstract We applied self-potential (SP) and electrical resistivity tomography (ERT) to the exploration of the uppermost part of the substrate geology and shallow structure of La Garrotxa monogenetic volcanic field, part of the European Neogene–Quaternary volcanic province. The aim of the study was to improve knowledge of the shallowest part of the feeding system of these monogenetic volcanoes and of its relationship with the subsurface geology. This study complements previous geophysical studies carried out at a less detailed scale and aimed at identifying deeper structures, and together will constitute the basis to establish volcanic susceptibility in La Garrotxa. SP study complemented previous smaller-scale studies and targeted key areas where ERT could be conducted. The main new results include the generation of resistivity models identifying dykes and faults associated with several monogenetic cones. The combined results confirm that shallow tectonics controlling the distribution of the foci of eruptive activity in this volcanic zone mainly correspond to NNW–SSE and accessorially by NNE–SSW Neogene extensional fissures and faults and concretely show the associated magmatic

intrusions. These structures coincide with the deeper ones identified in previous studies, and show that previous Alpine tectonic structures played no apparent role in controlling the loci of this volcanism. Moreover, the results obtained show that the changes in eruption dynamics occurring at different vents located at relatively short distances in this volcanic area are controlled by shallow stratigraphical, structural and hydrogeological differences underneath these monogenetic volcanoes.

Keywords Monogenetic volcanism · Garrotxa volcanic field · Electrical resistivity tomography · Self-potential · Subsurface geology · Feeding system

Introduction

Monogenetic volcanism is characterised by the formation of volcanoes that extrude small amounts of magma in each eruption (0.01–0.2 km³) (Walker 2000). These short-lived eruptions are often grouped in volcanic fields (Connor and Conway 2000; Walker 2000; Valentine and Gregg 2008) and are common under a variety of geodynamic conditions (Francis 1993; Connor and Conway 2000; Walker 2000). A particular feature of this type of volcanism is the great variety of resulting eruptive styles, morphologies and deposits (Houghton et al. 1999; Connor and Conway 2000; Parfitt 2004; Valentine and Gregg 2008). This diversity is caused by compositional changes (e.g. volatile content), magma supply rate, local tectonics (e.g. stress fields, degree of fracturing, basement mechanical behaviour) or by the hydrogeological characteristics of the substrate (e.g. Vespermann and Schmincke 2000; Walker 2000; Martí et al. 2011; Bolós et al. 2012; Pedrazzi et al. 2014). A good example of the great diversity found in monogenetic volcanic fields

X. Bolós (✉) · S. Barde-Cabusson · D. Pedrazzi · J. Martí
Group of Volcanology, Institute of Earth Sciences Jaume Almera,
SIMGEO (UB-CSIC), ICTJA-CSIC, c/Lluís Solé i Sabarís s/n,
08028 Barcelona, Spain
e-mail: xbolos@ictja.csic.es

A. Casas · R. Lovera
Economic and Environmental Geology and Hydrology Group,
Department of Geochemistry, Petrology and Geophysical
Prospecting, Faculty of Geology, University of Barcelona,
Martí Franqués s/n, 08028 Barcelona, Spain

D. Nadal-Sala
Ecology Department, University of Barcelona, Diagonal 645,
08028 Barcelona, Spain

is the European Cenozoic Rift System, which encompasses several different volcanic areas, all related to the same geodynamic environment but with different local tectonics (Wilson and Downes 1991, 1992; Downes 2001; Dèzes et al. 2004).

The location and distribution of monogenetic volcanic fields depend on the size and shape of the magmatic source, i.e. it is governed by regional geodynamics. However, the distribution of the eruptive vents within each volcanic field is the result of the geological structure and stress fields found in the upper crust at the moment of activity in each location (Zhang and Lutz 1989; Connor and Conway 2000; Cebrià et al. 2011).

The factors controlling the precursory activity in monogenetic volcanic fields are still poorly understood, and so eruptions in these systems are difficult to forecast. In monogenetic volcanism, each new eruption creates a different vent, suggesting that volcanic susceptibility contains a high degree of randomness and that accurate spatial forecasting is at best highly uncertain. Recent studies of monogenetic volcanism reveal how sensitive magma migration is to changes in regional and/or local stress fields caused by tectonic or lithological contrasts (e.g. former magmatic intrusions) (Martí et al. 2013). This may induce variations in the pattern of further magma movements and thus affect the location of future eruption sites.

The spatial distribution of eruptive vents may help reveal fracture patterns. At depth, magma rises towards the surface following the path that is normal to the minimum stress in the area (Connor and Conway 2000; Gudmundsson 2006; Cebrià et al. 2011). Near to the Earth's surface, it may become increasingly influenced by pre-existing structures and, for example, be captured by pre-existing faults and joints (e.g. Valentine and Gregg 2008; Le Corvec et al. 2013). Therefore, knowledge of regional and local tectonic controls and structures and the position of the eruptive vents is essential for understanding past volcanism. The relationship between the position of past eruptive focuses and these controls and structures will be important for determining the location of future vents (Martí and Felpeto 2010).

Geophysical exploration and more specifically geoelectrical methods have been used in the last decades to investigate structural geology and the feeding system in different volcanic areas around the world. For example, in New Zealand, Nishi et al. (1996) applied self-potential (SP) surveys to study the hydrothermal system of White Island Volcano. Bibby et al. (1998) used electrical resistivity imaging to characterise the upper crust of the Taupo Volcanic Zone. In Italy, Di Maio et al. (1998, 2000) applied electrical and electromagnetic methods to study the structure of Mount Somma and Campi Flegrei. In Japan, Hase et al. (2005) studied the hydrothermal system beneath Aso volcano

with SP and resistivity measurements. In Massif Central of France, Portal et al. (2013) explored the inner structure of Puy de Dôme volcano from electrical resistivity tomography (ERT), gravity and muon imaging. These studies and others referenced therein have proven the efficiency of geoelectrical methods for studying the structure and geology of volcanoes.

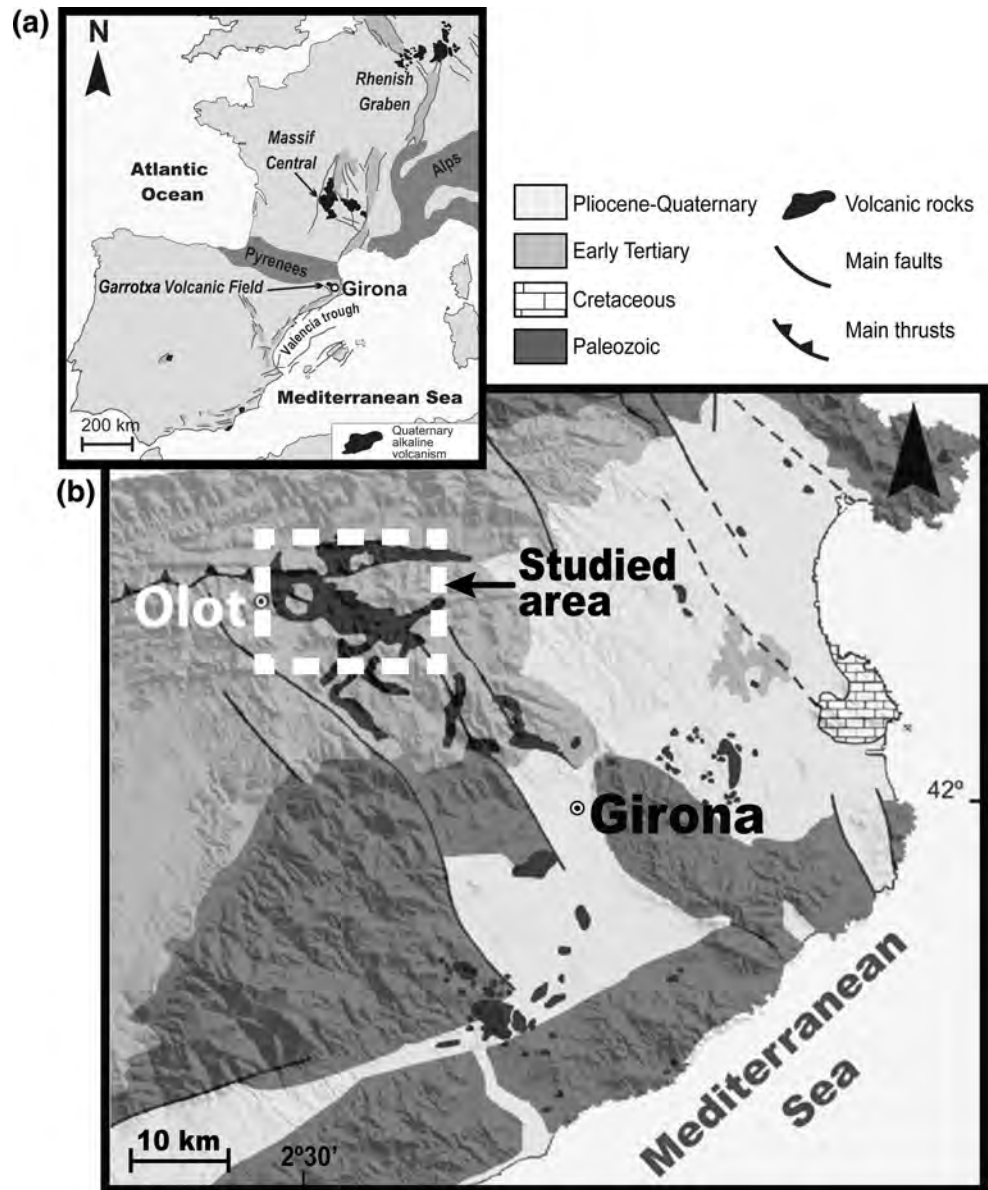
A previous geophysical study has been performed in La Garrotxa volcanic field (GVF) by Barde-Cabusson et al. (2014) dealing with deeper structures (up to 3 km in depth) associated with the volcanism of this area. This study was based mainly on the application of gravimetry and SP techniques and revealed interesting features of the internal structure of the area (e.g. the presence of low density bodies associated with the main Neogene fault and fissure systems). However, this study did not clarify the superficial aspects of the possible control exercised by the substrate geology or identify any shallow structural features. Thus, in order to obtain a much better resolution of the shallower structures of this area, a new geophysical survey was carried out that covered a greater area than the previous SP survey and undertook ERT surveys throughout the whole area. The SP data confirm and complement previous results, which, combined with the new electrical tomography data, offer a more detailed picture of the substrate geology and structure beneath the volcanoes of La Garrotxa.

In this paper, we describe the methodology used to conduct the field surveys and to process the data gathered, and then present the data obtained. We interpret the geological meaning of the data and, finally, discuss their relevance to subsoil geology in highly built-up areas and/or areas covered by dense vegetation. We identify the local shallow tectonic controls operating on the distribution of eruptive vents in the GVF and situate them in a more complex regional context.

Geological setting

The GVF is part of the Catalan Volcanic Zone (CVZ) (NE Spain), one of the Quaternary alkaline volcanic provinces associated with the intraplate European Cenozoic Rift System (Martí et al. 1992; Downes 2001; Dèzes et al. 2004) (Fig. 1). It covers an area of about 600 km² and is located between the cities of Olot and Girona (Fig. 1). This basaltic volcanic field contains over 50 cones including cinder and scoria cones, tuff rings and maars, ranging in age from 0.7 Ma to early Holocene (Martí et al. 2011). Materials from the upper Palaeozoic, Eocene and Quaternary characterise the substrate. The volcanism of the GVF is mainly represented by alkaline rocks with poorly evolved magmas, i.e. basalts and basanites (Araña et al. 1983; Cebrià et al. 2000). A notable feature of this area is the presence

Fig. 1 **a** Simplified map of the distribution of the volcanism in the European Cenozoic Rift System. **b** Simplified geological map of the Catalan Volcanic Zone (modified from Guérin et al. 1985)



of mantle xenoliths and lower crust cumulates (Araña et al. 1983; López-Ruiz and Rodríguez-Badiola 1985; Martí et al. 1992; Neumann et al. 1999; Cebrià et al. 2000), which suggests that some of the eruptive fissures and faults reached quite deeply into the lithosphere and that some were the same regional normal faults which bound the area's horsts and grabens (Martí et al. 2011).

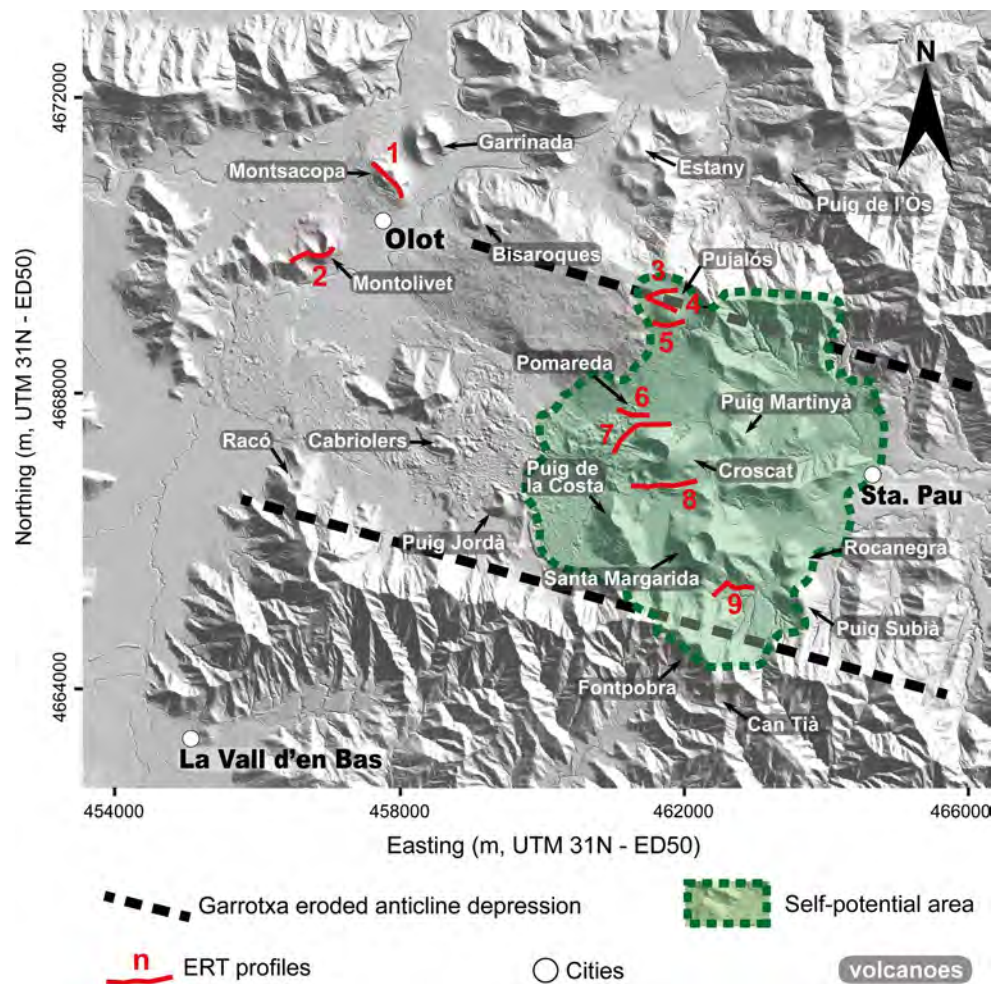
The GVF is laterally limited by two main NNW–SSE fault systems: the Llorà Fault to the east and the Amer Fault to the west, which are thought to be responsible for the distribution of the area's volcanism and its fluvial network (Saula et al. 1995; Martí et al. 2011; Bolós et al. 2012; Cimarelli et al. 2013). Most of the volcanoes in the study area are located between the towns of Olot and Santa Pau (Fig. 2). They stand on folded Eocene basement,

characterised by conglomerates, sandstones, marls, clays and gypsum (Bracons and Bellmunt formations) that outcrops as an eroded anticline with an E–W axial plane. This anticline and the reverse faults described in the area were formed during the Alpine Orogeny (Martinez et al. 1997) (Fig. 2).

Methods

The study area extends roughly between the towns of Olot and Santa Pau, both inside and outside the elongated E–W-eroded anticline depression in which most of the volcanic edifices of the GVF are situated (Fig. 2). The study involved the application of SP and ERT, which generated

Fig. 2 Digital elevation model of the study area, with location of the self-potential and ERT profiles described in this study



data that, in conjunction with existing geological data, enabled us to map geological units and to delineate structural limits at the surface and in the substrate below the volcanic edifices. The SP measurements focused on a number of key volcanic edifices and provided surface information to a resolution of 20 m, thereby allowing the main structural limits to be identified; the ERT profiles, on the other hand, provided 2D geological, structural and hydrogeological information at depth.

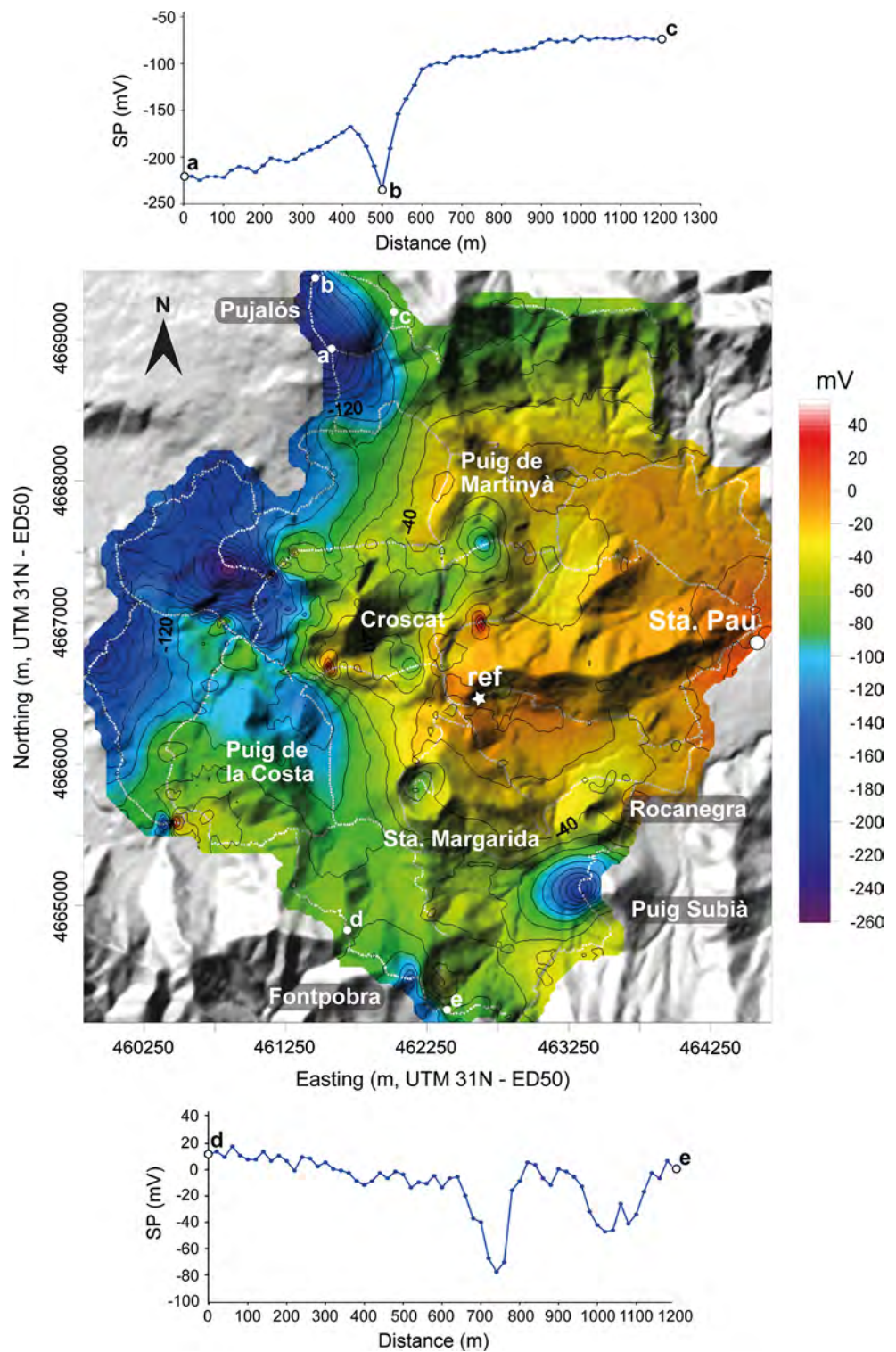
The main mechanism responsible of SP signals in volcanic terrains is the electrokinetic effect. This mechanism produces a positive electrical potential in the flow direction. When the groundwater moves through a porous rock matrix or in fractures and discontinuities of the substrate, electrochemical interactions occur at the interface between a mineral and the pore water. In normal pH conditions, the surface of silicate and aluminosilicates is negatively charged and the zeta-potential is negative. In order to maintain a global electro neutrality in the system, the electrical double (or triple) layer theory says that the diffuse layer has a net charge of opposite sign (positive) to the surface charge of the mineral. In this way, the positive electrical charges are

dragged by groundwater in the direction of the flow, creating positive SP anomalies over discharge areas and negative anomalies over recharge areas (e.g. Revil 2002).

The SP map drawn by Barde-Cabusson et al. (2014) was completed by means of 474 new measurements in additional profiles that covered a total of 10 km. All the SP measurements were made with a high impedance voltmeter (Extech EX520, sensitivity of 0.1 mV, input impedance >10 M Ω) using two non-polarised Cu/CuSO₄ electrodes and a 300 m section of cable. The difference in potential between the reference electrode, which was placed at the start of the profile, and the moving electrode was measured. In all, the SP surveys correspond to a series of profiles involving a total of 2,547 measurements with a distance of 20 m between successive stations. Additional data were corrected for closure errors based on the previous SP dataset correction with a single reference (Fig. 3; for details of the field methodology, see Barde-Cabusson et al. 2014).

Electrical resistivity methods are based on the principle that the distribution of electrical potential in the ground around a current-carrying electrode depends on the electrical resistivities and distribution of the surrounding rocks.

Fig. 3 Self-potential map. In the *upper* and *lower* part of the figure, the two SP versus distance graphs correspond on the map to the ‘*abc*’ and ‘*de*’ profiles. *White dots* show the location of the SP measuring stations. Coordinates in UTM—31 N—ED50



Resistivity measurements are commonly used for investigating various types of subsurface exploration problems. As a general principle, the acquisition techniques consist in measuring, between two electrodes (M, N), the difference of potential generated by the electrical current which is injected into the ground via two other electrodes (the

transmitting line AB). ERT surveys are normally carried out with multi-electrode resistivity systems. Such surveys use a number of electrodes deployed in a straight line at equal intervals and computer-controlled system is then used to select the active electrodes for each electrode set-up automatically (Griffiths and Barker 1993). This allows

a large number of measurements to be taken and 2D resistivity high-resolution data can be obtained very quickly. The ERT data were acquired with an Iris Syscal Pro resistivity system. A Wenner–Schlumberger electrode configuration was used with 48 electrodes connected to a 470 m section of cable (10 m between electrodes) that enabled us to obtain a maximum depth of investigation of 100 m. The main reason for choosing a mixed Wenner–Schlumberger array in areas where both types of geological structures (vertical and horizontal) are expected to occur is because better results might be obtained. The signal strength of this hybrid array is weaker than the one provided by the Wenner array, but the depth of investigation is increased and lateral coverage is improved (Martorana et al. 2009). Besides, in the Wenner–Schlumberger configuration, the measured voltage signal drops to the level of electrical noise as the distance between the current electrodes becomes very large while keeping the potential dipole length constant. This is because the measured potential signal in the Schlumberger array is inversely proportional to the square of the current electrode spacing, whereas in the dipole–dipole array the measured potential signal is inversely proportional to the third power of the current electrode spacing.

A total of nine ERT profiles of different lengths were obtained from 16 acquisitions using 470-m-long sections (Fig. 2). The roll-along method was used to obtain five of the profiles (profiles 1, 2, 7, 8 and 9). Profiles 7 and 8 consisted of three sections with half the cable length overlapping, giving each a total length of 950 m, while profiles 1, 2, and 9 were composed of two sections, each with a total length of 710 m. Finally, four profiles (3, 4, 5 and 6) consisted of individual sections.

The data obtained were interpreted using an inversion process to provide a resistivity section that approximates the actual subsurface structure and to locate their boundaries spatially below the surface of the site. The apparent electrical resistivity data acquired in the field were processed with the Res2dinv software from GEOTOMO© (Loke 2002), which is based on the smoothness-constrained, nonlinear least-squares optimisation technique, was used to obtain the interpretative model. The inversion algorithm is an iteratively reweighted least-squared method based on the Gauss–Newton method; in addition, the Jacobian matrix of partial derivatives is always recalculated using the finite-element method. The first step in the inversion is the estimation of an initial model. Next, the solution is iteratively improved by varying the model parameters to minimise the discrepancies between the observed and the calculated responses. The inversion programme uses a 2D model divided into a number of rectangular blocks (pixels of inversion models), whose arrangement is made according to the distribution of the

data points in the pseudo-section (Loke and Barker 1996). In the model, we also included topographical information obtained from the digital elevation model (DEM) to a resolution of 15×15 m from Catalan Geographic Institute (<http://www.icc.cat>). The RMS error (representation of the reproducibility of the data from the inverted model) was in most cases $<7\%$ but increased in the roll-along profiles.

Results

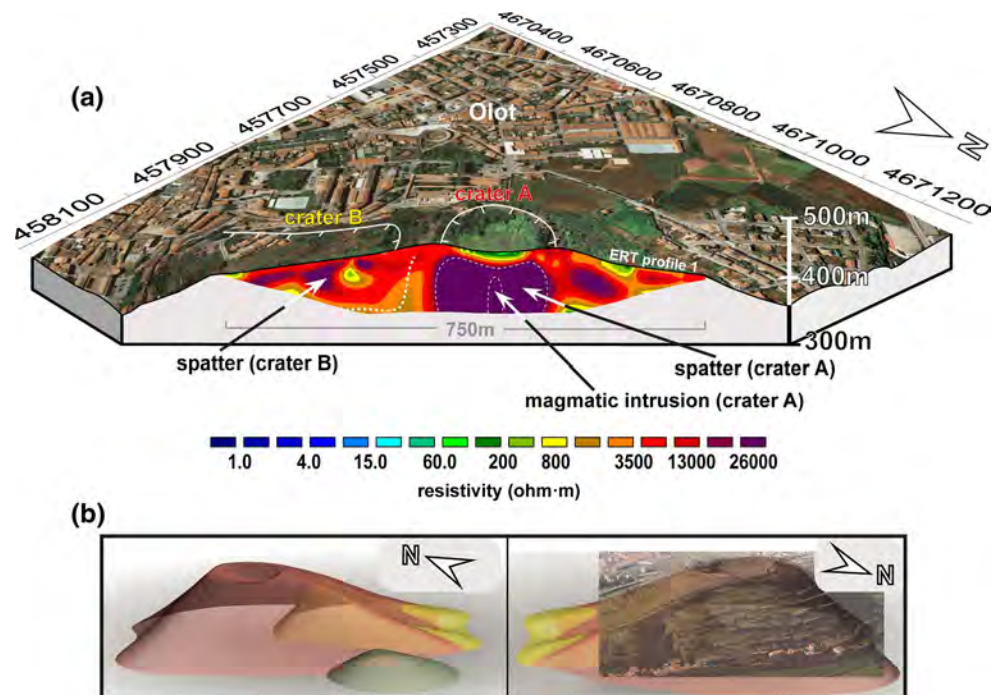
Self-potential map

The SP map (Fig. 3) shows a total variation of ~ 300 mV. The main feature of the map is the transition from east to west: in the east, low amplitude SP spatial variation (<30 mV) is observed, while in the west the SP isolines are oriented NNW–SSE and NNE–SSW. Additional more isolated negative SP peaks are visible at Rocanegra Strombolian volcano, Puig Subià and Puig Martinyà (Fig. 3). One of the most significant features of this new SP map is the abrupt E–W transition (with the lowest values recorded on the western side) observable in the northern sector centred on the Pujalós volcano. In the southernmost part of the map, the new data that complement the data generated by Barde-Cabusson et al. (2014) show a continuation of the NNW–SSE lineament crossing the volcanoes of Croscat and Santa Margarida (Fig. 3). This area corresponds to the southern high point of the anticline, where a normal fault and pyroclastic deposits from the Fontpobra volcano are found (IGC; 1:25,000, <http://www.igc.cat>).

Electrical resistivity tomography

ERT profiles show in some cases excessively high resistivity values, ranging from $<10 \Omega\text{m}$ to hundreds of thousands of Ωm . These high resistivities are generated by the inversion process in Res2dinv when strong resistivity contrasts exist close to the surface. This occurs if materials with very low resistivity such as clay, silt and organic soils come into contact in parallel with materials with very high resistivity (Loke 2002). For this reason, we chose a colour scale whose maximum corresponds to values of resistivity $>26,000 \Omega\text{m}$, the value measured for the massive basaltic intrusions that outcrop in the field that were the highest measured in the area. This enabled us to provide a more realistic picture of the subsurface repartitioning of the resistivity. In Res2dinv, however, we imposed a cell width of half the unit electrode spacing, which allowed us to obtain optimal results in profiles with high contrasts in resistivity (Loke 2002).

Fig. 4 **a** Orthophotograph overlaid on a 3D block diagram of ERT profile 1 corresponding to Montsacopa volcano (RMS error 5.7 %). **b** 3D interpretation model showing the overlapping cones inside the edifice. Coordinates in UTM—31 N—ED50



Profile 1: Montsacopa volcano

Profile 1 was carried out through the central part of the Montsacopa edifice (Fig. 4) in a NNW–SSE direction. It is characterised by resistivity values from ~ 100 to over $26,000 \Omega\text{m}$. The lowest values are visible in the shallowest part of the high resistivity intrusive and spatter products below the volcano's crater A. In the south-eastern half of the profile, high values of resistivity are interrupted by a small zone of lower resistivities (Fig. 4) corresponding to another hidden crater (crater B) (Bolós 2009; Barde-Cabusson et al. 2013). These craters are aligned in a NNW–SSE direction.

Profile 2: Montolivet volcano

An E–W profile was conducted on the southern side of the Montolivet volcano. Profile 2 (Fig. 5) reveals a zone of high resistivity ($>1,000 \Omega\text{m}$) located mainly in the eastern half of the edifice, with a thickness of over 80 m. The deepest part of this profile had lower resistivity values ($\sim 60\text{--}1,000 \Omega\text{m}$) that define a horizontal interface with the upper resistive layer. This deep layer continues in the western part of the volcano, where the values are also lower ($\sim 20\text{--}200 \Omega\text{m}$), and is separated from the eastern high resistivity zone by an interface dipping 45° eastwards in the cross section defined by the ERT profile.

Profiles 3, 4 and 5: Pujalós volcano

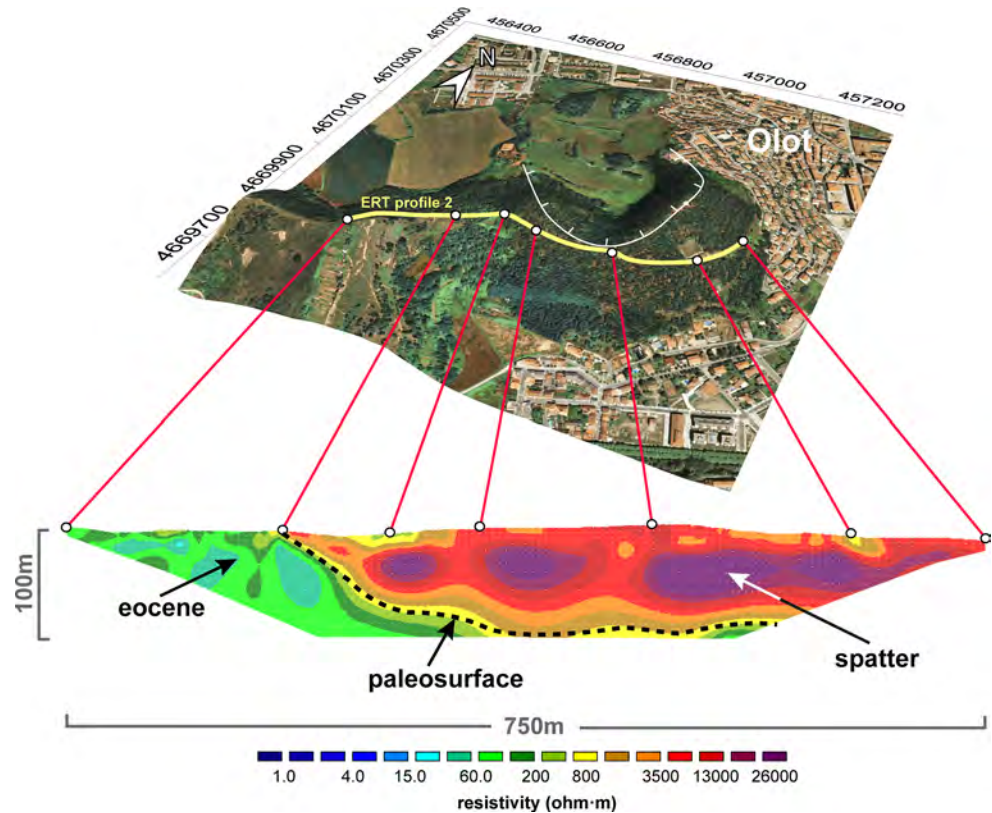
Three profiles were carried out on the Pujalós volcano as a means of comparing results with variations in the SP.

Profile 3 in the northern part of the volcano (Fig. 6a, b) cuts across the NNW–SSE lineament shown by the SP. This profile reveals a shallow conductive layer ($40\text{--}400 \Omega\text{m}$) overlaying a resistive layer ($>1,000 \Omega\text{m}$) that continues to the maximum depth of exploration in the western half of the profile, but narrows eastwards to a thickness of ~ 40 m (Fig. 6b). Profile 4 was acquired through the centre of the volcanic cone (Fig. 6a, c) and obtained a resistivity model that is very similar to that from profile 3 (Fig. 6b). Profile 5 was located in the southern part of the volcano and crosses the NNW–SSE SP lineament described above (Fig. 6a, d). Although the repartition of the resistivity is not as clear in this ERT model as in the two previous profiles, an irregular resistive layer is seen to extend from a depth of 50 m to the maximum depth of the exploration. In the upper part, a less resistive layer is sometimes interrupted in places by resistive bodies connected to the deeper layer and sometimes also to the topography surface. Strombolian fallout deposits and spatter facies have been observed on the surface, coinciding geographically with the high resistivity values in the shallow part of these profiles.

Profile 6: La Pomareda spatter cone

Profile 6 cuts across the Pomareda volcano in an E–W direction (Fig. 2) and has the highest resistivity values ($\sim 13,000$ to $\sim 26,000 \Omega\text{m}$) detected at the surface in the study area (Fig. 7). In the field, this unit corresponds to massive basaltic lava flows and spatter deposits. A 15- to 20-m-thick layer appears to be connected to the deepest part of the resistivity model

Fig. 5 *Top*: orthophotograph overlaid on a digital elevation model with the location of ERT profile 2 (yellow line) corresponding to Montolivet volcano. *Bottom*: ERT model (RMS error 3.0 %). Coordinates in UTM—31 N—ED50



via a narrow channel reaching $\sim 4,000 \Omega\text{m}$. This channel crosses a less resistive layer ($400\text{--}2,000 \Omega\text{m}$) and joins a deep, high resistivity horizontal layer with values that range from $\sim 2,000 \Omega\text{m}$ in the west to $\sim 10,000 \Omega\text{m}$ in the east (Fig. 7).

Profiles 7 and 8: Croscat volcano

Profile 7 (Fig. 8) was carried out in an E–W direction (Fig. 2) on the northern side of the volcano, and it was composed of three different sections that were processed jointly. It has a high inversion error (RMS = 22.5 %) due to the poor quality of the measurements carried out in the western part of the profile. We processed each section separately and found RMS errors of 11.9, 15.2 and 35.8 % from east to west, respectively, indicating that the data from the westernmost section is the least reliable. One of the main elements of the profile is observed in its centre (Fig. 8, zone A), where a resistive body shows values over $20,000 \Omega\text{m}$. This body is elongated and rises vertically from the base of the resistivity model almost to the topography surface. Its lateral contacts are well defined on both sides and there is a sharp lateral transition of the resistivity. In the cross section, this body is $\sim 30 \text{ m}$ thick in its shallowest part and $\sim 60 \text{ m}$ thick at depth. In the westernmost part of the profile, its resistivity values are of the same order of magnitude (Fig. 8, zone B); this area is quite homogeneous from the surface to the maximum depth of exploration (Fig. 8).

Profile 8 has the same direction as profile 7 (E–W) and it is located on the southern side of the volcano (Fig. 9). A resistive body borders the western part of the profile (Fig. 9, zone A) and extends from the maximum depth of exploration (here $\sim 70 \text{ m}$) to the topography surface. Due to the presence of a main road, we were unable to extend the profile further to the west to gain a better idea of the geometry of this resistive body. A few metres to the east a resistive bulge with no continuity at depth coincides with the deposits of Croscat's secondary crater (Fig. 9, zone B). Throughout the rest of the profile, a 30- to 15-m-thick resistive level ($1,000\text{--}13,000 \Omega\text{m}$) overlies a more conductive layer ($50\text{--}1,000 \Omega\text{m}$). In the easternmost part of the profile, these layers appear to be shifted downwards by $\sim 10 \text{ m}$, thereby defining a western and an eastern block. This separation also coincides with a discrete break-in-slope in the topography. The eastern block is overlain by a conductive layer that is just a few metres thick. The deepest layer has the highest conductive values encountered in the profile (reaching values $< 4 \Omega\text{m}$) (Fig. 9, zone C), a whole order of magnitude lower than the corresponding layer in the western block.

Profile 9: Santa Margarida volcano

Profile 9 is located on the south of Santa Margarida volcano (Fig. 10). With an RMS error of 11 % after six iterations,

Fig. 6 **a** Orthophotograph overlaid on a digital elevation model with the location of the ERT profiles (red lines). **b–d** 3D block diagrams of Pujalós volcano, showing the corresponding SP mapping on the surface and ERT profiles 3 (RMS error 2.9 %), 4 (RMS error 15.2 %) and 5 (RMS error 3.7 %) in the cross section. White dotted lines show the location of the SP measurements. White dashed line identifies the SP lineation. Coordinates in UTM—31 N—ED50

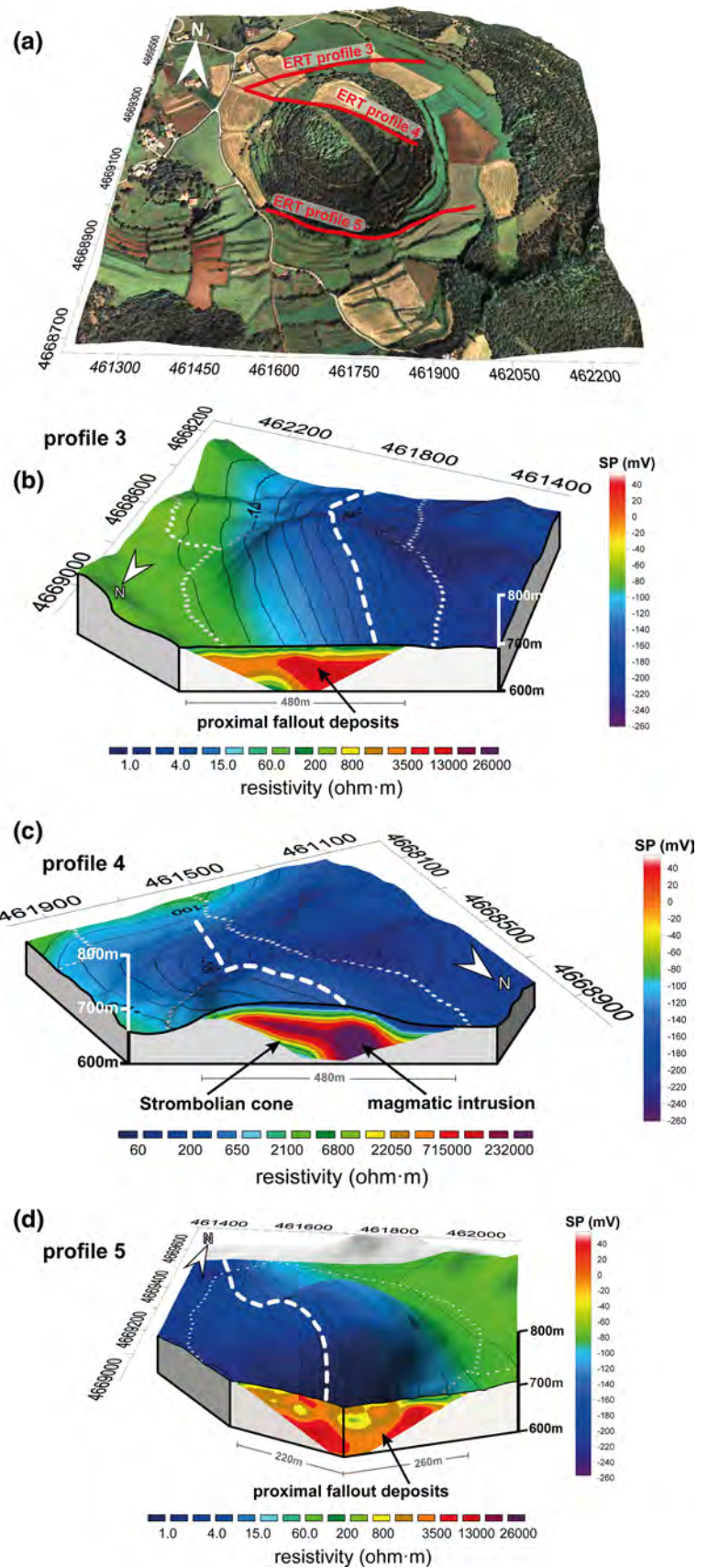
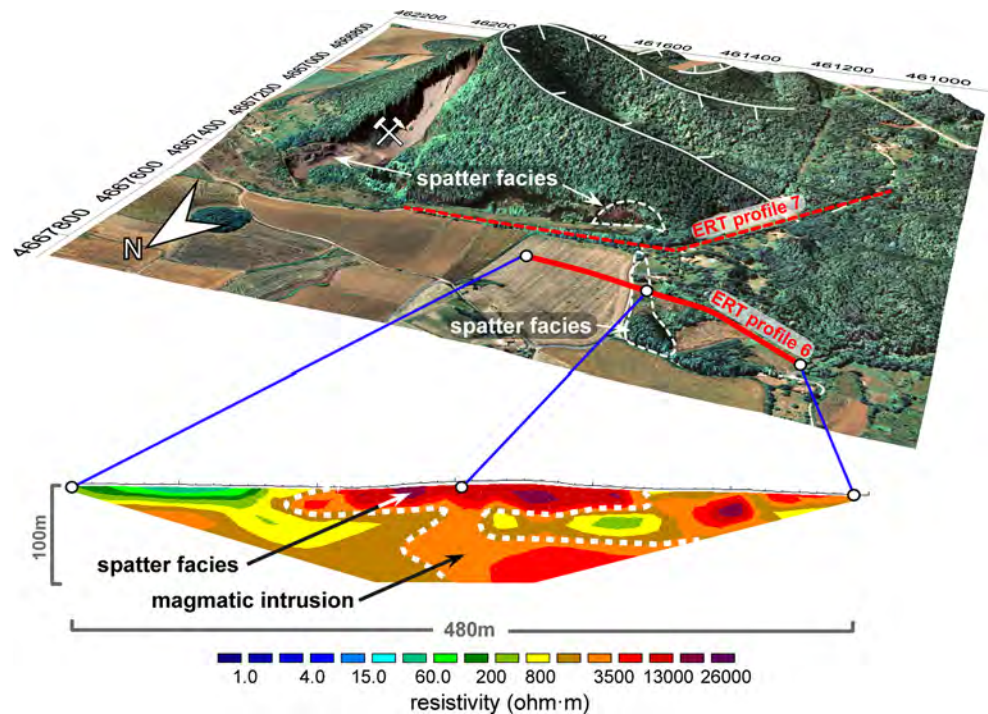


Fig. 7 *Top*: orthophotograph overlaid on a digital elevation model with the location of ERT profile 6 corresponding to Pomareda volcano (red line). *Bottom*: ERT model (RMS error 5.5 %). Coordinates in UTM—31 N—ED50



this profile may be unreliable since it also included a lot of unrealistic data points that we removed during processing with Res2dinv. The distribution of the resistivity is not as clear as in the other resistivity models. Nevertheless, the most interesting feature here is probably the observation of a resistive body at a depth of about 70 m in the east of a resistive body ($>10,000 \Omega\text{m}$), possibly connected to shallower layers along a narrow pathway (Fig. 10, zone A).

Discussion

Interpretations of the new SP map enable us to identify structures that were subsequently observed in two dimensions in the high-resolution ERT profiles. Surface geological information was also useful for interpreting the ERT profiles.

As proposed by Barde-Cabusson et al. (2014; Fig. 5a), the main observed features are the NNW–SSE and NNE–SSW trends that show up in the SP, suggesting that the volcanic field is structurally confined by this conjugated fault system that favoured magma ascent. This hypothesis is confirmed by the ERT profiles performed in the directions described above. We identified several very shallow intrusive bodies aligned along the profiles whose cross sections are geometrically more or less vertical which narrow near the surface, and which are characterised by high resistivity values. This is fully compatible with the presence of feeder dykes. In the northern part of the map, at least two of the three ERT profiles (i.e. profiles 3 and 4) from Pujalós

volcano (Fig. 6) reveal resistive bodies that continue beyond the maximum depth of exploration. Although the distribution of the resistivity in the third southern profile (profile 5) is less clear, the direction of the line joining the main resistive bodies detected in these profiles matches the NNW–SSE SP trend detected in this volcano. Figure 3 contains a graph of SP versus distance passing north of Pujalós that shows a clear negative peak corresponding geographically to the location of the resistive body in profile 3 that is not present in the SP profile passing south of this volcano. This peak cannot be explained by the nonlinearity of the SP profile in the north and could be a consequence of meteoric water infiltration along a structural limit covered by impermeable material in the south. We believe that profiles 3 and 4 merely reveal the upper part of the feeder dyke as it flares on reaching the topography surface (Valentine 2012; Barde-Cabusson et al. 2013).

The Santa Margarida-Crosca-La Pomareda alignment in the central part of the study area was described by Martí et al. (2011) as the result of a single eruptive episode occurring along a 3-km-long fissure system. Our study provides geophysical and geological evidence supporting this idea. La Pomareda ERT (profile 6) was performed across the inferred fissure zone (Fig. 7) and generated high resistivity values that can be related to outcropping spatter facies. At depth, the resistive channel connecting the spatter at the surface to the deepest zone can be interpreted as the feeder dyke that supplied the eruption. The resistivity values obtained for this channel ($\sim 3,500 \Omega\text{m}$) are lower than those obtained for the resistive bodies found along the

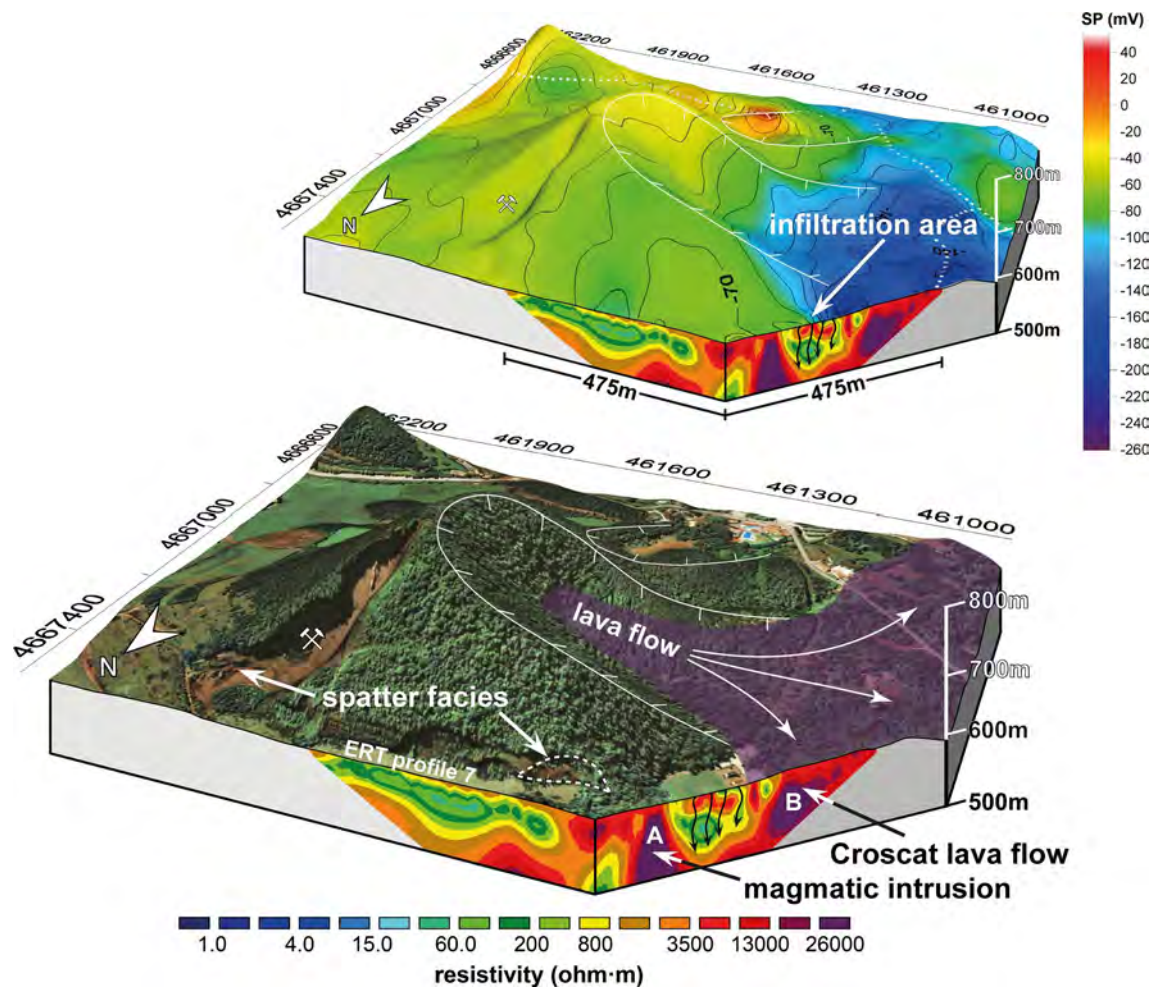


Fig. 8 3D block diagrams for ERT profile 7 located on the northern side of Croscat volcano. The *upper* part of the figure shows the surface SP map overlaid on a digital elevation model. In the *lower* part,

an orthophotograph is overlaid on the same digital elevation model. The corresponding ERT profile is presented in the cross section (RMS error 22.5 %). Coordinates in UTM—31 N—ED50

same fissure near Croscat volcano. It is important to bear in mind, however, that the Pomareda spatter cone forms a smaller edifice than Croscat. These observations suggest that the magma flow rate—and thus the intensity of the eruptive activity—was lower at this point on the fissure. Croscat, built on the same eruptive fissure, is a complex volcano with several vents and several eruptive phases including violent Strombolian and phreatomagmatic episodes (Martí and Mallarach 1987; Martí et al. 2011). The ERT profiles performed north and south of this volcano (Figs. 8, 9, respectively) exhibit resistive bodies that are compatible with the presence of a feeder dyke aligned with the Pomareda volcano in a NNW–SSE direction (Fig. 11). At the surface, a spatter facies was found in profile 7 and a secondary cone is visible near profile 8. The westernmost resistive body described in profile 7 matches a lava flow that occurred during the final phase of Croscat’s eruption (Fig. 8). An important feature observable in the eastern part

of profile 8 (Fig. 9) is a clear shift of ~10 m at the base of the upper resistive layer, which has been mapped as fall-out deposits and a lava flow from Croscat (Cimarelli et al. 2013). These volcanic deposits probably cover a pre-existing normal fault that affects the underlying Eocene units and is revealed only by a small break-in-slope visible in the surface topography. In the eastern block, the underlying unit is clearly more conductive than in the western block due to the presence of an aquifer confined to the west by the fault plane (Figs. 9, 11). This fault is likely a conjugate of a Neogene fault mapped 200 m to the southeast (IGC; 1:25,000, <http://www.igc.cat>) or a prolongation of the same. Its presence has important implications for understanding eruptive dynamics in monogenetic volcanic fields since it may explain why hydro magmatic and Strombolian activity can take place simultaneously or within short time spans, in close proximity to each other or even in the same edifice (e.g. Martí et al. 2011; Pedrazzi et al. 2014). Thus,

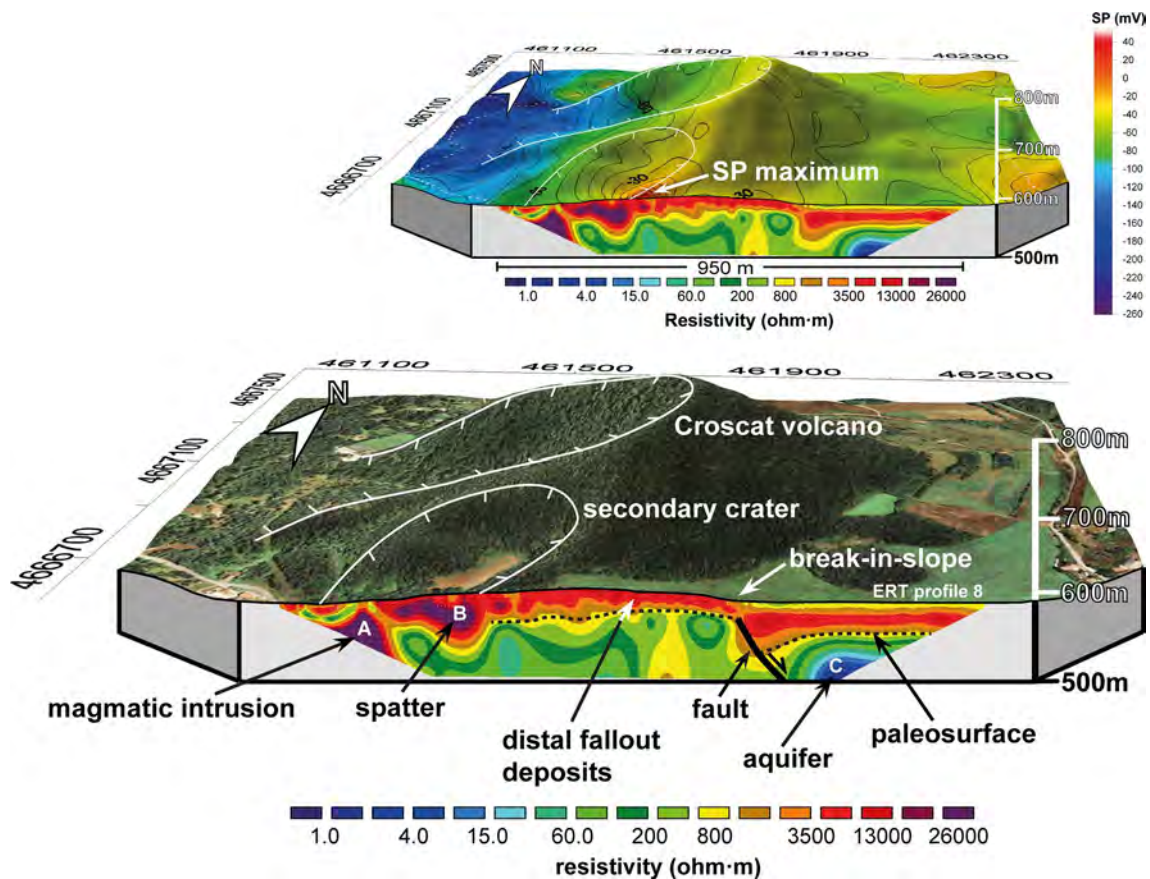


Fig. 9 3D block diagrams for ERT profile 8 located on the southern side of Croscat volcano. The *upper* part of the figure shows the surface SP map overlaid on a digital elevation model. In the *lower* part,

an orthophotograph is overlaid on the same digital elevation model. The corresponding ERT profile is presented in the cross section (RMS error 11.7 %). Coordinates in UTM—31 N—ED50

tectonic limits may play an important role in defining the diversity of monogenetic volcanoes owing to their impact on hydrogeology at shallow depths. In the eastern part of profile 9 (Fig. 10) in the south of this area, a resistive body ($>10,000 \Omega\text{m}$) is present at a depth of 70 m. This body is aligned with Santa Margarida-Croscat-La Pomareda fissure system; therefore, it correspond presumably to a magmatic intrusion, which did not reach the surface in this profile.

The area of Olot ERT profile 1 (Fig. 4) performed on the Montsacopa volcano has already been described by Barde-Cabusson (2013). The present study confirms that in addition to the obvious crater on its summit, and there is a hidden vent located on the south-eastern flank of this volcano, as suggested by Bolós (2009). These two coalescent cones are aligned in a NNW–SSE direction. Montsacopa, and the two other volcanic edifices within the city of Olot (Garrinada and Montolivet) all have several vents that define three separate NNW–SSE lines which reflect the direction of their corresponding eruptive fissures (Martí et al. 2011). This finding contrasts with previous studies that assumed that the eruptions of Montsacopa, Garrinada

and Montolivet were located along a single NE–SW fissure (Calderón et al. 1906; San Miguel de la Cámara 1918; Malarach and Riera 1981; Gisbert et al. 2009).

ERT profile 2 crosses the southern flank of Montolivet and the outcropping Eocene basement (Bellmunt Formation) that is characterised by conglomerates, sandstones and clays. The Bellmunt Formation appears in the profiles as shades of green ($\sim 20\text{--}500 \Omega\text{m}$) only on the western side and at depth (Fig. 5). The transition towards the high resistivity values of the Montolivet volcanic deposits defines the pre-eruptive topography. The highest resistivity values have no continuity at depth, which suggests that this area is characterised only by proximal facies deposits and that this profile (profile 2) did not cross the feeder dyke (Fig. 5). Nevertheless, the horseshoe-shaped depression of Montolivet's crater indicates that the feeder fracture runs in a NNW–SSE direction (i.e. fault-strike breaching, Tibaldi 1995), as seen in other areas (Corazzato and Tibaldi 2006). Differently, Croscat's crater is open to the west, even though all the data obtained show that it is associated with a NNW–SSE fault. Crater breaching

Fig. 10 *Top*: orthophotograph overlaid on a digital elevation model with the location of ERT profile 9 on the southern side of Santa Margarida volcano (*red line*). *Bottom*: ERT model (RMS error 11.0 %). Coordinates in UTM—31 N—ED50

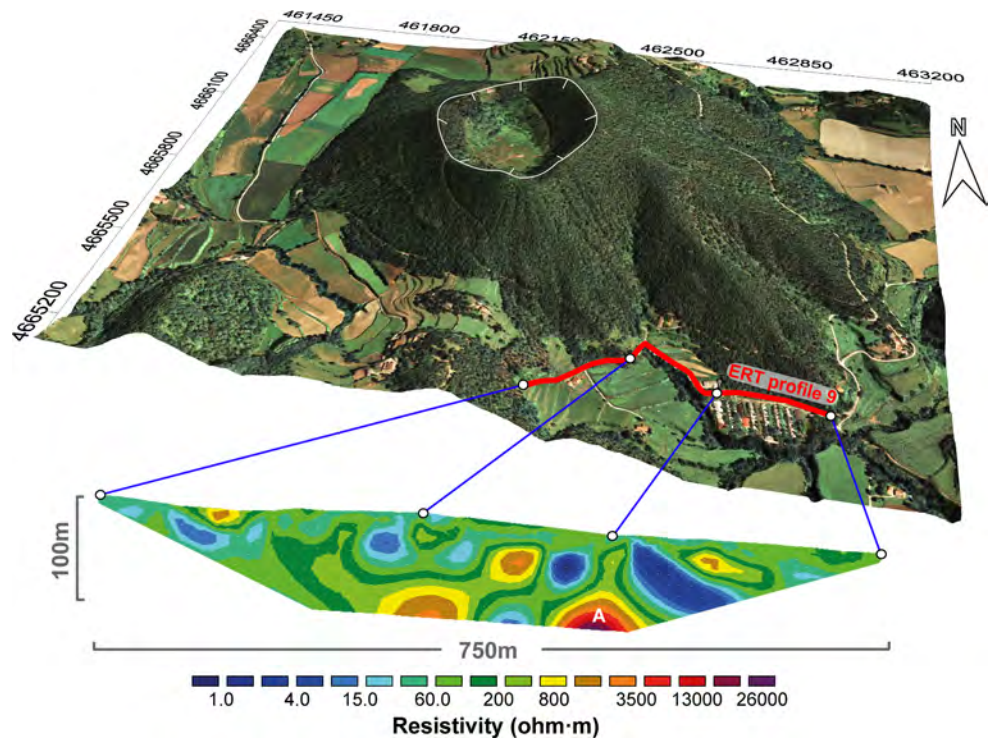
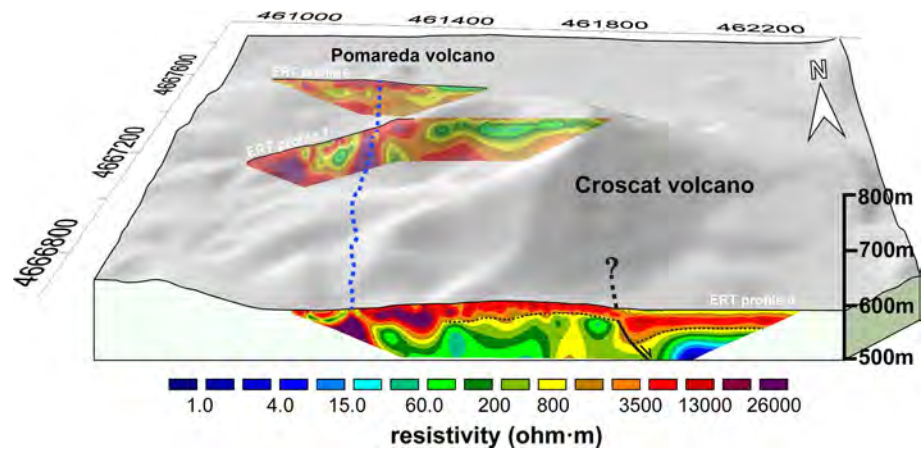


Fig. 11 3D block diagram of Croscat and Pomareda volcanoes showing ERT profiles 6, 7 and 8. The *blue dashed line* highlights a NNW–SSE eruptive fissure



might coincide with fracture propagation (e.g. Montolivet volcano) or with the weakest zone of the cone (e.g. Croschat volcano) (see Tibaldi 1995). The NNW–SSE direction determined for the nearby Montsacopa and Garrinada volcanoes tends to support this interpretation of Montolivet. A hypothesis that explains why the feeder dyke is not visible in the ERT profile is that the edifice of Montolivet was in fact built at the south-eastern tip of the fissure.

Two main fault systems were identified in the study area: an E–W compressive fault system formed during the Alpine Orogeny and a NNW–SSE normal fault system formed during the current extensive context (Martinez et al. 1997). The data obtained suggest that volcanism in the area is controlled by the recent extensive fault system and that

the Alpine system played no role in controlling magma ascent and/or eruptions. These NNW–SSE normal faults are almost perpendicular to the limits of the E–W depression formed by the Garrotxa anticline.

The Pujalós and the Fontpobra volcanoes provide key information on the faults associated with the GVF volcanism. Both are located outside the depression of La Garrotxa, very close to the northern and southern limits of the anticline, respectively. However, ERT (in the case of Pujalós) and SP (Pujalós and Fontpobra) suggest the presence of NNW–SSE eruptive fissures, which would indicate that the tectonic limits associated with the Alpine Orogeny did not determine the volcanic intrusions in the GVF.

Conclusions

New geophysical data were combined with field geological information to explore the subsurface geology and structure of the monogenetic GVF. We identified feeder dykes and structural limits associated with known eruptive vents. The information derived for the subsurface provides data that is useful for interpreting the influence of shallow geological and structural settings on the eruptive dynamics of this monogenetic volcanic field and has interesting implications for similar volcanic zones.

The NNW–SSE direction highlighted by previous SP and gravimetric studies was targeted by the ERT. The 2D images obtained with this method reveal the existence of high resistivity bodies corresponding to NNW–SSE-running feeder dykes that confirm the role played by NNW–SSE tectonic structures in the volcanic manifestations in the area. In addition, the same direction is observed for the Pujalós and Fontpobra eruptive fissures, although both volcanoes are located in the vicinity of the limits of the anticline, respectively, in the northern and southern part of the study area. This suggests that Alpine tectonic structures such as the anticline and the associated regional faults were not implicated in the formation of these two volcanoes. This conclusion can be extended to the whole area given the distribution of the dykes that have been identified and available geological and geophysical data.

In ERT profile 8, we identified a normal fault confining an aquifer to the west. This configuration could have a number of different consequences on eruptive dynamics depending on the path followed by future intrusions. Both phreatomagmatic and Strombolian activity could take place simultaneously or within a short time span, in close proximity or even in the same volcanic edifice, depending on whether or not the intrusion interacts with the aquifer. The existence of such a configuration could explain the variety of eruptive dynamics in the monogenetic GVF and in other volcanic fields of similar characteristics without any need for change in the composition of the magma.

The results of this paper will help assess the volcanic susceptibility of the area and increase understanding of the influence of local geology on the distribution and dynamics of the eruptive activity in this area and in monogenetic fields in general.

Acknowledgments This study was partially funded by the *Beca Ciutat d'Olot en Ciències Naturals* and the European Commission (FT7 Theme: ENV.2011.1.3.3-1; Grant 282759: “VUELCO”). S. Barde-Cabusson was funded by JAE-Doc Program (JAE-Doc_09_01319). We are grateful to La Garrotxa Volcanic Zone Natural Park and its staff for their support throughout this study. We would like to thank Llorenç Planagumà for his logistical help during this research. Thanks are also due to Núria Bagués, David Granados, Guillem Serra and Joan Puigferrer for their assistance in the field. We are also grateful to Editors Prof. Wolf-Christian Dullo and

Christoph Breitzkreuz, and two anonymous reviewers for their constructive reviews of this manuscript. The English text was corrected by Michael Lockwood.

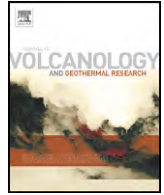
References

- Araña V, Aparicio A, Martín-Escorza C, García Cacho L, Ortiz R, Vaquer R, Barberi F, Ferrara G, Albert J, Gassiot X (1983) El volcanismo Neógeno-Cuaternario de Catalunya: caracteres estructurales, petrológicos y geodinámicos. *Acta Geol Hisp* 18:1–17
- Barde-Cabusson S, Bolós X, Pedrazzi D, Lovera R, Serra G, Martí J, Casas A (2013) Electrical resistivity tomography revealing the internal structure of monogenetic volcanoes. *Geophys Res Lett* 40:2544–2549. doi:10.1002/grl.50538
- Barde-Cabusson S, Gottsmann J, Martí J, Bolós X, Camacho A, Geyer A, Planagumà L, Ronchin E, Sánchez A (2014) Some insights on the structural control of monogenetic volcanism from gravity and self-potential measurements. *Bull Volcanol* 76:788. doi:10.1007/s00445-013-0788-0
- Bibby HM, Caldwell TG, Risk GF (1998) Electrical resistivity image of the upper crust within the Taupo Volcanic Zone, New Zealand. *J Geophys Res* 103:9665–9680
- Bolós X (2009) Characterization of the Montsacopa volcano and its surroundings (in English, Spanish, and Catalan). <http://bit.ly/ZqkAaY>, Garrotxa Volcanic Natural Parc, Olot, Spain
- Bolós X, Barde-Cabusson S, Pedrazzi D, Martí J, Casas A, Himi M, Lovera R (2012) Investigation of the inner structure of La Crosa de Sant Dalmaï maar (Catalan Volcanic Zone, Spain). *J Volcanol Geoth Res* 247–248:37–48. doi:10.1016/j.jvolgeores.2012.08.003
- Calderón S, Cazorro M, Fernández Navarro L (1906) Memoria sobre las formaciones volcánicas de la provincia de Gerona. *Memorias de Real Sociedad Española de Historia Natural*, t. IV, memoria 5ª, Madrid, pp 165–489
- Catalan Geographic Institute (ICC) (2013) Digital elevation model 15 × 15 m. <http://www.icc.cat/>. Accessed 3 Dec 2013
- Catalan Geologic Institute (IGC) (2013) Carta Volcanològica de la Zona Volcànica de la Garrotxa, 1:25,000. <http://www.igc.cat/>. Accessed 3 Dec 2013
- Cebrià JM, López-Ruiz J, Doblás M, Oyarzun R, Hertogen J, Benito R (2000) Geochemistry of the quaternary alkali basalts of Garrotxa (NE Volcanic Province, Spain): a case of double enrichment of the mantle lithosphere. *J Volcanol Geoth Res* 112:175–187
- Cebrià JM, Martín-Escorza C, López-Ruiz J, Morán-Zenteno DJ, Martiny BM (2011) Numerical recognition of alignments in monogenetic volcanic areas: examples from the Michoacán-Guanajuato volcanic field in Mexico and Calatrava in Spain. *J Volcanol Geoth Res* 201:73–82
- Cimarelli C, Di Tragia F, de Rita D, Gimeno Torrente D, Fernandez Turiel JL (2013) Space-time evolution of monogenetic volcanism in the mafic Garrotxa volcanic field (NE Iberian Peninsula). *Bull Volcanol* 75:758. doi:10.1007/s00445-013-0758-6
- Connor CB, Conway FM (2000) Basaltic volcanic fields. In: Sigurdsson H (ed) *Encyclopedia of volcanoes*. Academic Press, San Francisco, pp 331–343
- Corazzato C, Tibaldi A (2006) Fracture control on type, morphology and distribution of parasitic volcanic cones: an example from Mt. Etna Italy. *J Volcanol Geoth Res* 158:177–194
- Dèzes P, Schmid SM, Ziegler PA (2004) Evolution of the European Cenozoic rift system: interaction of the alpine and pyrenean orogens with their foreland lithosphere. *Tectonophysics* 389:1–33
- Di Maio R, Mauriello P, Patella D, Petrillo L, Piscitelli S, Siniscalchi A (1998) Electric and electromagnetic outline of the mount Somma-Vesuvius structural setting. *J Volcanol Geoth Res* 82:219–238

- Di Maio R, Patella D, Petrillo Z, Siniscalchi A, Cecere G, De Martino P (2000) Application of electric and electromagnetic methods to the definition of the Campi Flegrei caldera (Italy). *Annali di Geofisica* 43:375–390. Catalan Geographic Institute. Digital Elevation model, Garrotxa area. <http://www.icc.cat/>. Accessed 10 Oct 2013
- Downes H (2001) Formation and modification of the shallow sub-continental lithospheric mantle: a review of geochemical evidence from ultramafic xenolith suites and tectonically emplaced ultramafic massifs of Western and Central Europe. *J Petrol* 42:233–250
- Francis PW (1993) *Volcanoes: a planetary perspective*. Clarendon Press, Oxford
- Gisbert G, Gimeno D, Fernandez-Turiel JL (2009) Eruptive mechanisms of the Puig de La Garrinada volcano (Olot, Garrotxa volcanic field, Northeastern Spain): a methodological study based on proximal pyroclastic deposits. *J Volcanol Geoth Res* 180:259–276
- Griffiths DH, Barker RD (1993) Two-dimensional resistivity imaging and modelling in areas of complex geology. *J Appl Geophys* 29:211–226
- Gudmundsson A (2006) How local stresses control magma-chamber ruptures, dyke injections, and eruptions in composite volcanoes. *Earth Sci Rev* 79:1–31
- Guérin G, Behamoun G, Mallarach JM (1985) Un exemple de fusió parcial en medi continental. El vulcanisme quaternari de la Garrotxa. Publicació del Museu Comarcal de la Garrotxa, Vitrina, 19–26
- Hase H, Hashimoto T, Sakanaka S, Kanda W, Tanaka Y (2005) Hydrothermal system beneath Aso volcano as inferred from self-potential mapping and resistivity structure. *J Volcanol Geoth Res* 143:259–277
- Houghton BF, Wilson CJN, Smith IEM (1999) Shallow-seated controls on styles of explosive basaltic volcanism: a case study from New Zealand. *J Volcanol Geoth Res* 91:97–120
- Le Corvec N, Menand T, Lindsay J (2013) Interaction of ascending magma with pre-existing crustal fractures in monogenetic basaltic volcanism: an experimental approach. *J Geophys Res Solid Earth* 118:968–984. doi:10.1002/jgrb.50142
- Loke MH (2002) Res2dinv ver. 3.54. Rapid 2-D resistivity and IP inversion using the least square method. Geotomo Software
- Loke MH, Barker RD (1996) Rapid least-squares inversion of apparent resistivity pseudo sections by a quasi-Newton method. *Geophys Prospect* 44:131–152
- López-Ruiz J, Rodríguez-Badiola E (1985) La región volcánica Mio-Pleistocena del NE de España. *Estud Geol* 41:105–126
- Mallarach JM, Riera M (1981) *Els volcans olotins i el seu paisatge*. Editorial Serpa, Barcelona; 250 pp
- Martí J, Felpeto A (2010) Methodology for the computation of volcanic susceptibility: an example mafic and felsic eruptions on Tenerife (Canary Islands). *J Volcanol Geoth Res* 195:69–77
- Martí J, Mallarach JM (1987) Erupciones hidromagmáticas en el vulcanismo cuaternario de Olot. *Estud Geol* 43:31–40
- Martí J, Mitjavila J, Roca E, Aparicio A (1992) Cenozoic magmatism of the Valencia trough (Western Mediterranean): relation between structural evolution and Volcanism. *Tectonophysics* 203:145–166
- Martí J, Ll Planagumà, Geyer A, Canal E, Pedrazzi D (2011) Complex interaction between Strombolian and phreatomagmatic eruptions in the quaternary monogenetic volcanism of the Catalan Volcanic Zone (NE of Spain). *J Volcanol Geoth Res* 201(1–4):178–193
- Martí J, Pinel V, López C, Geyer A, Abella R, Tárraga M, Blanco MJ, Castro A, Rodríguez C (2013) Causes and mechanisms of the 2011–2012 El Hierro (Canary Islands) submarine eruption. *J Geophys Res Solid Earth* 118:823–839. doi:10.1002/jgrb.50087
- Martinez A, Rivero L, Casas A (1997) Integrated gravity and seismic interpretation of duplex structures and imbricate thrust systems in the southeastern Pyrenees (NE Spain). *Tectonophysics* 282:303–329
- Martorana R, Fiandaca G, Casas A, Cosentino PL (2009) Comparative tests on different multi-electrode arrays using models in near-surface geophysics. *J Geophys Eng* 6:1–20
- Neumann ER, Martí J, Mitjavila J, Wulff-Pedersen E (1999) Origin and implications of mafic xenoliths associated with Cenozoic extension-related volcanism in the València Trough, NE Spain. *Mineral Petrol* 65:113–139
- Nishi Y, Ishido T, Matsushima N, Ogawa Y, Tosha T, Myazaki J, Yasuda A, Scott BJ, Sherburn S, Bromley C (1996) Self-Potential and audio-magnetotelluric survey in White Island Volcano. New Zealand Geothermal Workshop
- Parfitt EA (2004) A discussion on the mechanisms of explosive basaltic eruptions. *J Volcanol Geoth Res* 134:77–107
- Pedrazzi D, Bolós X, Martí J (2014) Phreatomagmatic volcanism in complex hydrogeological environments: La Crosa de Sant Dalmau maar (Catalan Volcanic Zone, Geoshpere, NE Spain). doi:10.1130/GES00959.1
- Portal A, Labazuy P, Lénat JF, Béné S, Boivin P, Busato E, Cârloganu C, Combaret C, Dupieux P, Fehr F, Gay P, Laktineh I, Miallier D, Mirabito L, Niess V, Vulpesu B (2013) Inner structure of the Puy de Dôme volcano: cross-comparison of geophysical models (ERT, gravimetry, muon imaging). *Geosci Instrum Method Data Syst* 2:47–54
- Revil A (2002) Comment on “Rapid fluid disruption: a source for self-potential anomalies on volcanoes” by M. J. S. Johnston, J. D. Byerlee, and D. Lockner. *J Geophys Res* 107 (B8). doi:10.1029/2001JB000788
- San Miguel de la Cámara M (1918) El vulcanismo en España. *Boletín de la Real Academia de Ciencias y Artes de Barcelona* 244–254
- Saula E, Picart J, Mató E, Llenas M, Losantos M, Berasategui X, Agustí J (1995) Evolución geodinámica de la fosa del Empordà y de las Sierras Transversales. *Acta Geol Hisp* 29:55–75
- Tibaldi A (1995) Morphology of pyroclastic cones and tectonics. *J Geophys Res* 100:24521–24535
- Valentine GA (2012) Shallow plumbing systems for small-volume basaltic volcanoes, 2: evidence from crustal xenoliths at scoria cones and maars. *J Volcanol Geoth Res* 223–224:47–63. doi:10.1016/j.jvolgeores.2012.01.012
- Valentine GA, Gregg TKP (2008) Continental basaltic volcanism: process and problems. *J Volcanol Geoth Res* 177:857–873
- Vespermann D, Schmincke HU (2000) Scoria cones and tuff rings. In: Sigurdsson H (ed) *Encyclopedia of volcanoes*. Academic Press, San Diego, pp 683–694
- Walker GPL (2000) Basaltic volcanoes and volcanic systems. In: Sigurdsson H (ed) *Encyclopedia of volcanoes*. Academic Press, San Francisco, CA, pp 283–289
- Wilson M, Downes H (1991) Tertiary-quaternary extension-related alkaninmagmatism in Western and Central Europe. *J Petrol* 32:811–849
- Wilson M, Downes H (1992) Mafic alkaline magmatism associated with the European Cenozoic rift system. *Tectonophysics* 208:173–182
- Zhang D, Lutz T (1989) Structural control of igneous complexes and kimberlites: a new statistical method. *Tectonophysics* 159:137–148

APPENDIX 4

**Investigation of the inner structure of La Crosa de Sant Dalmai
maar (Catalan Volcanic Zone, Spain)**



Investigation of the inner structure of La Crosa de Sant Dalmai maar (Catalan Volcanic Zone, Spain)

Xavier Bolós ^{a,*}, Stéphanie Barde-Cabusson ^a, Dario Pedrazzi ^a, Joan Martí ^a, Albert Casas ^b, Mahjoub Himi ^{b,c}, Raúl Lovera ^b

^a Group of Volcanology, Institute of Earth Sciences "Jaume Almera" (GVB-CSIC), SIMGEO (UB-CSIC), Lluís Solé i Sabarís s/n, 08028 Barcelona, Spain

^b Economic and Environmental Geology and Hydrology Group, Department of Geochemistry, Petrology and Geological Prospecting, Faculty of Geology, University of Barcelona, Martí i Franquès s/n, Barcelona, Spain

^c Ecole Nationale des Sciences Appliquées d'Al Hoceima (ENSAH), University Mohammed Premier, Ajdir, Al Hoceima, Morocco

ARTICLE INFO

Article history:

Received 21 March 2012

Accepted 7 August 2012

Available online 18 August 2012

Keywords:

Catalan Volcanic Zone

Maar-diatreme

Goelectrical methods

Gravity survey

Magnetic survey

Drill core

ABSTRACT

La Crosa de Sant Dalmai volcano is the largest volcanic edifice of the Catalan Volcanic Zone (NE Spain). It is a very well preserved maar-type structure, 1.5 km in diameter, excavated at the contact between a hard substrate and a soft substrate formed by Palaeozoic granites and Pliocene and Quaternary gravels, respectively. In order to infer the uppermost inner structure of La Crosa de Sant Dalmai maar and to characterise its main geological and tectonic constraints, we have performed a multiparametric geophysical study including gravimetry, magnetometry, self-potential, and electrical resistivity tomography. The results obtained together with a field geology revision and additional geological data from two drill cores, provide a detailed picture of the post-eruptive maar infill sequence as well as of the uppermost part of the maar-diatreme structure. This information helps in understanding the origin and subsequent evolution of the volcano, which included an alternation of phreatomagmatic and Strombolian phases. Geophysical data show that the last Strombolian phase, which culminated with the formation of a scoria cone inside the maar, was associated with a NW–SE trending regional fault. The little erosion and degradation of the original tephra ring suggest a much younger age of La Crosa de Sant Dalmai maar than was previously stated.

© 2012 Elsevier B.V. All rights reserved.

1. Introduction

Phreatomagmatic explosions result from brief, near-surface magma/water interactions occurring during the ascent of magma towards the surface, which leads to violent explosions (Lorenz, 1973; Sheridan and Wohletz, 1981, 1983; Wohletz, 1983). Unlike magmatic eruptions that are entirely controlled by the composition and physical properties of the magma (i.e. volatile content, viscosity), phreatomagmatic eruptions may vary considerably depending on external factors such as the stratigraphic, structural and hydrogeological characteristics of the substrate through which the volcanoes are emplaced. Phreatomagmatism is common in all subaerial volcanic settings as continental rifts, active continental volcanic island arc, foreland basins, late orogenic intermontane basins of orogenic belts, basin and range, cratons, and hot spots (Lorenz, 2007). In monogenetic volcanic fields, as well as in polygenetic volcanoes, a large variety of volcanic morphologies and eruption sequences can be observed associated with this type of volcanism (Wohletz and Sheridan, 1983).

A maar is a type of phreatomagmatic volcanic structure characterised by the formation of a tephra ring due to the accumulation of

pyroclastic deposits around a circular crater, whose floor lies below the pre-eruption ground surface (Lorenz, 1973, 2007; Lorenz and Kurszlaukis, 2007; White and Ross, 2011). The presence of meteoric water and/or groundwater, after the eruption's end, might lead to the development of a lake inside the crater (Schmincke, 1988; Büchel, 1993). Due to the surface geomorphology and the internal structure, these volcanoes are called maar-diatremes. The term used is descriptive and not genetic, so it does not refer to any specific place or suite of processes (Lorenz, 1975, 1986). The maar-diatreme volcanoes, although representing examples of monogenetic activity, represent a significant degree of hazard, as has been shown by past eruptions with a number of human casualties in the historical record around the world (White and Ross, 2011).

The reconstruction of the internal structure of individual young maar-diatreme systems can only be based on geophysical studies and drill cores and other type of mechanical excavations. In deeply eroded systems it is possible to observe the deepest parts of the diatreme but the uppermost sections have been lost in most cases. Therefore, to get an idealised picture of the maar-diatreme system it is necessary to combine both approaches.

This study is aimed at obtaining a 3D geological model of the internal structure of the topmost part of La Crosa de Sant Dalmai maar, in the Catalan Volcanic Zone (NE Spain), in order to determine the structure of the

* Corresponding author.

E-mail address: xbolos@ictja.csic.es (X. Bolós).

substrate below the tephra ring and the post-eruptive infill sequence of the maar crater and the uppermost level inside the diatreme. In order to accomplish this objective we applied several geophysical techniques, including gravity, magnetic, self-potential and electrical resistivity tomography methods. These methods combined with field geology and the study of samples from two drill cores located inside the maar-crater, provided the necessary information to image the shallow internal structure of the La Crosa de Sant Dalmai maar-diatreme volcano.

2. Geological setting and general characteristics of La Crosa de Sant Dalmai

The Catalan Volcanic Zone (CVZ), situated in the NE part of the Iberian Peninsula (Girona Province), is one of the Quaternary alkaline volcanic provinces belonging to the European Cenozoic Rift System (Martí et al., 1992; Dèzes et al., 2004) (Fig. 1). The CVZ ranges in age from > 12 Ma to early Holocene and it is mainly represented by alkali basalts and basanites (Martí et al., 1992; Cebriá et al., 2000).

This basaltic monogenetic volcanic zone comprises more than 50 well preserved monogenetic cones including scoria cones, tuff cones, tephra rings, and maars. The area has traditionally been divided into three different sub-zones: L'Empordà to the Northeast (12–8 Ma), La

Selva (7.9–1.7 Ma) to the South and La Garrotxa (0.5–0.01 Ma) to the West (Araña et al., 1983; Martí et al., 1992) (Fig. 1). In the CVZ volcanism, small-sized cinder cones formed along widely dispersed fissure zones during monogenetic, short-lived eruptions. Hydromagmatic events were also common. Each eruption was probably caused by an individual batch of magma that was transported rapidly from the source region, each batch representing the products of an individual partial melting event (Martí et al., 1992, 2011).

La Crosa de Sant Dalmai maar belongs to the La Selva subzone, which corresponds to a tectonic depression bounded by an ENE–WSW and a NW–SE fault system (Fig. 1). The basement of this area consists of granites and metamorphic rocks of Palaeozoic age, which crop out defining a nonconformity with the Pliocene and Quaternary sediments. These last filled the La Selva depression with variable thicknesses of 35 to 200 m in the Sant Dalmai area (Trilla and Pallí, 1977; Barnolas et al., 1979). The volcanic deposits cover an area of about 7 km² among the municipalities of Aiguaviva and Sant Dalmai, 2 km northwest of the Girona airport, overlying basement and Pliocene and Quaternary rocks (Fig. 2).

The ejecta of this maar volcano are mostly composed of phreatomagmatic deposits that form a circular tephra ring around a shallow crater 1250 m in diameter and a few tens of metres in depth. The tephra ring is asymmetrical, being higher in the west

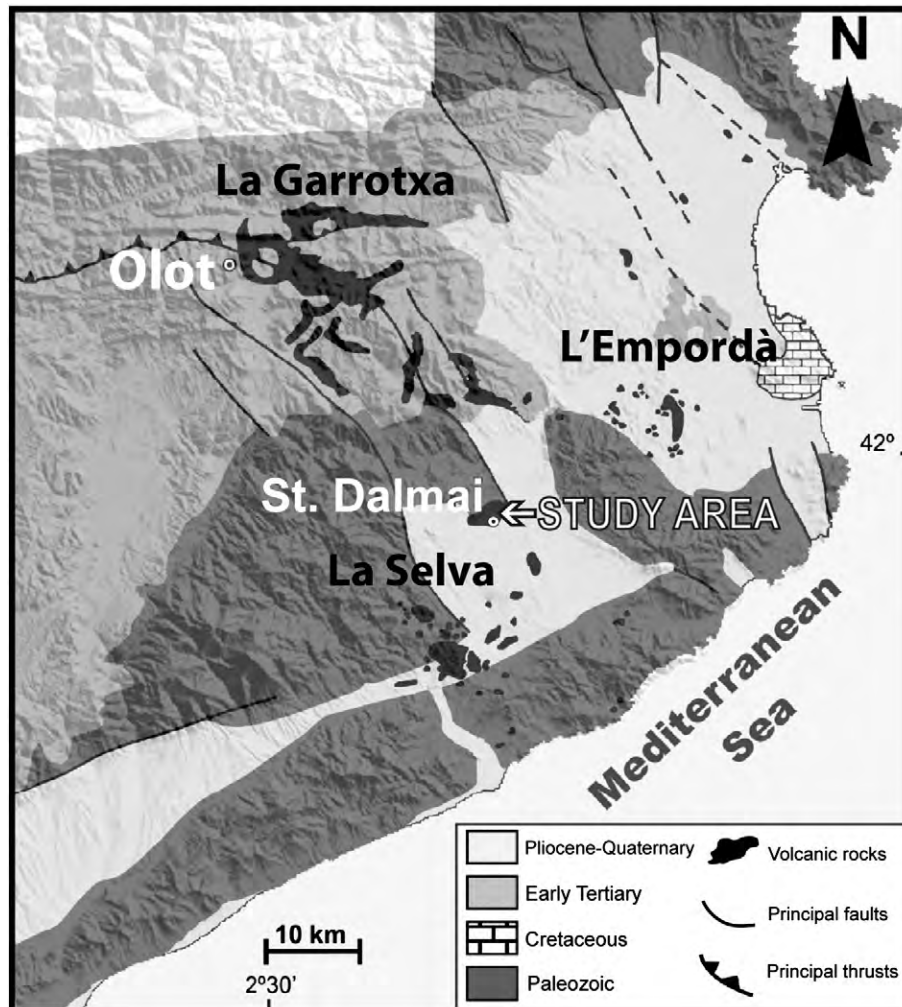


Fig. 1. Simplified geological map of the Catalan Volcanic Zone and its surroundings. Location of La Garrotxa, La Selva and L'Empordà volcanic fields. (Modified from Guérin et al., 1986)

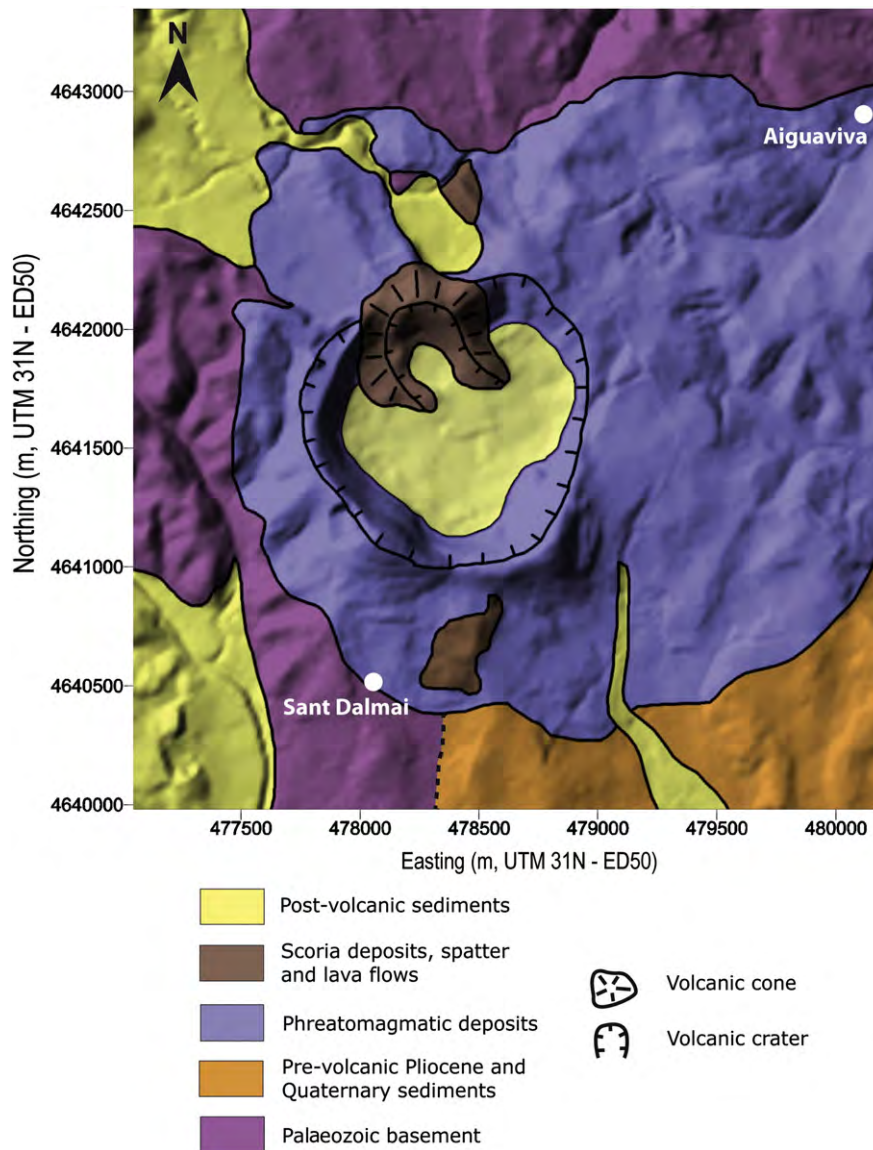


Fig. 2. Geological map of la Crosa de Sant Dalmai volcano. Coordinates in metres (UTM31N – ED50). Topographic base is taken from the ICC, at 1:5000 scale. The mapping of the deposits has been developed from the simplified map of Martí and Mallarach (1987) and analysis from new outcrops in the field. The figure shows the main crater and the scoria cone the latter formed during the final stages of activity of the volcano, along with the extent of the phreatomagmatic deposits.

(maximum height of 50 m), where the internal and external slopes are also steeper, than in the east (maximum height of 30 m). Also, the deposits surrounding the rim show a wider distribution towards the east (Fig. 2). The succession of deposits shows the same stratigraphy all around the tephra ring but not in equal proportions. They reached distances of nearly 4 km towards the east and only of a few hundred metres towards the west. This asymmetrical distribution of the deposits was attributed to different strength of the rocks that form the substrate at each side below the volcano (Martí et al., 1986). The initial topography, the direction of the wind during the eruption, and the possible inclination of the eruptive conduit could also have influenced the distribution of the deposits around the vent (e.g. Büchel and Lorenz, 1993).

The lowermost unit of the succession of deposits of La Crosa de Sant Dalmai volcano is not fully exposed and corresponds to >1 m thick coarse lithic-rich breccia with blocks up to 70 cm in diameter. The lithics consist of granites and schists with subordinate scoria lapilli and cauliflower bombs (Pedrazzi, et al., 2012). Above them lies

a 10 m thick uniform sequence of lithic-rich deposits alternating with crudely stratified, coarse-grained pyroclastic surge deposits. The next unit in the stratigraphic succession is a 1 m thick Strombolian, non-welded scoria lapilli deposit, which is followed by 8 m thick sequence of alternating units of lithic-rich breccia and pyroclastic surges. The eruption ended with a new Strombolian episode from a new vent opened at the interior of the maar. This episode formed a small scoria cone partially overlapping the maar tephra ring and a lava flow emplaced inside the maar (see below). As most maar-diatreme volcanoes are related to basic magmas, most final magmatic phases inside maar craters lead to the formation of scoria cones or even lava lakes in a final magmatic phase (Lorenz, 2007).

The age of this volcano is not well constrained. Although it is located in the La Selva sector where most of the outcropping volcanic rocks have ages older than 1.7 Ma (Araña et al., 1983), it is evident from the state of preservation of its morphology and juvenile components that La Crosa de Sant Dalmai volcano might be younger.

3. Methodology

The methodology used to carry out this work comprises multi-disciplinary tasks. A preliminary geological map of the area at 1:5000 scale was produced starting from the one elaborated by Martí, et al. (1986) and conducting new field work (Fig. 2). This allowed us to understand field relationships among the different geological units, to determine the extent of the deposits, and to identify the most significant geomorphological features. All the geological information collected was incorporated into a georeferenced database and processed through a Geographical Information System managed by ©Global Mapper 12.00 and Arcgis 9.2 (© ESRI) software. The projection system of coordinates used was the ED50 DATUM, UTM 31 N.

Additional geological data came from two drill cores (S1 and S2, Fig. 3). S1, reaching a depth of 15 m, was made in December 2009 at the western side of La Crosa de Sant Dalmai maar crater. S2, with a total depth of 61 m, was made in April 2012 at the north-eastern side of the maar crater (Fig. 3) The data collected from these cores were helpful in studying the post-eruptive sedimentary fill of the crater and correlating these deposits with the resistivity profiles obtained through the electrical resistivity tomography (ERT) (Fig. 3).

Subsequently, various geophysical techniques, including gravity, magnetics, self-potential and electrical resistivity tomography, were applied. Some unpublished data from several geophysical surveys carried out in 1995 by some of the authors of this publication already

existed. We incorporated these data into this study and in some cases they were recollected and reprocessed.

The gravity survey covered a total area of 8 km² inside and around La Crosa de Sant Dalmai maar, and included a total of 158 stations. Gravity readings were taken with a Lacoste and Romberg G831 gravimeter and referred to the IGSN-71 international gravity system. Station altitude was measured with an Air HB-1A high precision quartz altimeter or derived from ± 0.1 m benchmarks. The gravity data were corrected for effects caused by variations in latitude, elevation, topography, instrumental drift and earth tides caused by the sun and moon. The corrected values generated Bouguer anomalies, which represent the gravity effect of crustal and shallower geological structures. In order to get the residual anomaly, due to the local density changes, it was necessary to subtract the regional component that in this area shows a well defined west–east trend with values ranging from -0.2 to -4.4 mGal that mostly express the depth of the Moho discontinuity (Casas et al., 1986).

Total field magnetic measurements were performed in 1995 with a proton magnetometer Geometrics model G-816. In this study we used the 226 original stations without adding new measurements. The correction for diurnal variation was previously performed on the data set and as with the gravity data, a regional field was defined from stations distant from the volcano and subtracted to give the residual anomaly. After this step, the magnetic data were interpolated to a regular grid. The residual values are around the zero level far away from the volcano indicating a successful removal of the regional field.

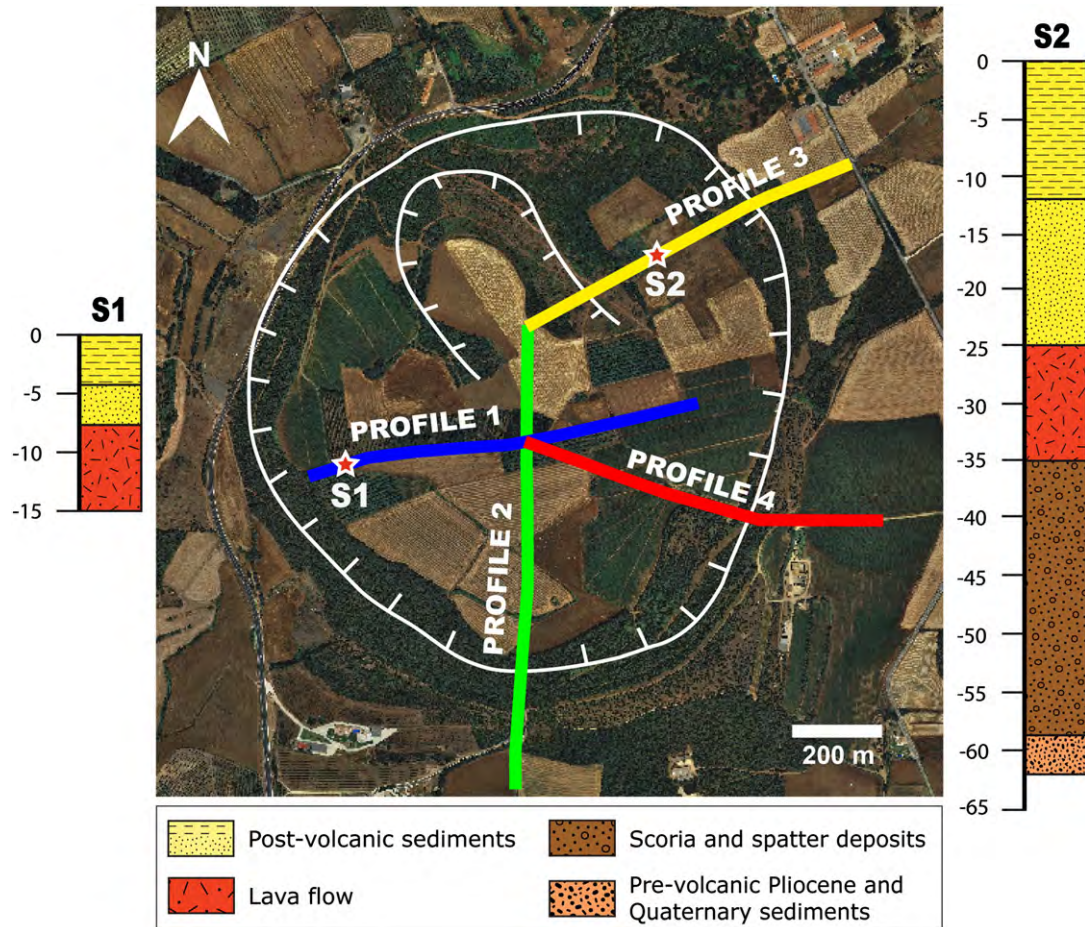


Fig. 3. Orthophotomap from the Institut Cartogràfic de Catalunya (ICC) web site, showing the location of each ERT profile. It also shows the location of the two drill cores (S1 and S2) and their respective synthetic stratigraphic sections.

The self-potential (SP) measurements were made with a high impedance voltmeter ($\sim 10\text{ M}\Omega$) with a sensitivity of 0.1 mV, using two non-polarised Cu/CuSO₄ electrodes and a 300 m long cable. The difference of potential was measured between the reference electrode, which was placed at the beginning of the profile and the moving electrode. The measurements were performed every 20 m with several profiles forming an interconnected network covering the entire surface of the crater of La Crosa de Sant Dalmai. During the measurements, the reference and moving electrodes were switched every few hundred metres in order to avoid the systematic error due to electrode offset. In the data-processing we applied a closure correction along the profiles, in order to limit cumulative errors.

The electrical resistivity tomography (ERT) is a technique in which the process of data acquisition is fully automated. This allows performing a great number of measurements, obtaining 2D resistivity high resolution data in a short time. The electrical resistivity data were acquired with an Iris Syscal Pro resistivity system. The electrode configuration was the Wenner-Schlumberger array using 48 electrodes connected to a 470 m long cable (10 m spacing between electrodes), obtaining a maximum depth of investigation of about 100 m. The main reason for choosing a Wenner-Schlumberger electrode array was the good relationship between signal intensity and good horizontal and vertical sensitivity analysis (Binley and Kemna, 2005).

We used the roll-along method to complete some of the profiles (Fig. 3). Profile 1 and profile 3 were composed of two sections overlapping on one-third of the cable length, resulting in 800 m long profiles. Profile 4 sections overlapped on half of the cable length giving a total length of 710 m. Finally, the two sections composing profile 2 did not share any electrode.

The apparent electrical resistivity data acquired in the field were processed with the RES2DINV software from GEOTOMO© (Loke, 2002) including topography information. The topography was obtained from the Digital Elevation Model (DEM) of $15 \times 15\text{ m}$ resolution from Institut Cartogràfic de Catalunya. In all our profiles the RMS error, indicator of the reliability of the inversion, was less than 7%, giving a high viability for the resistivity models obtained (Loke and Barker, 1996).

4. Results

4.1. Geological data

The geological map in Fig. 2 shows that the maar is located near the nonconformity between Palaeozoic basement (mainly outcropping at the northern and western side of the map) and the pre-volcanic Pliocene and Quaternary sediments, which fill La Selva depression mainly at the southern side. The maar pyroclastic deposits show an asymmetrical distribution mostly extending towards the east for more than 4 km (Martí et al., 1986). The tephra ring morphology and deposits around the crater are very well preserved as well as the Strombolian cone located on the northern side of the maar crater (Fig. 2).

Relevant geological information was also obtained from the analysis of the two drill cores S1 and S2 (Fig. 3). S1 shows a phreatic water table at a depth of 10 m. The first 7.6 m below the crater floor are composed of alternating fine-grained silt and clay deposits. Deeper, the drilling encounters a basaltic lava flow from the final Strombolian episode related to La Crosa de Sant Dalmai eruption. S2 shows a phreatic water table at a depth of 18 m. The first 12 m of the core are composed of fine silt and clay deposits, and the following 14 m show grained sand and colluvial deposits from the tephra ring and the Strombolian cone. The basaltic lava flow appears at a depth of 26 m and shows a total thickness of 10 m. Below, there is a 20 m thick succession of alternating fine and coarse-grained lapilli beds from the intra-maar Strombolian cone. At a depth of 61 m, S2 shows Pliocene and Quaternary sediments containing organic material, which correspond to the contact between the diatreme and the substratum.

4.2. Gravimetry

The residual Bouguer anomaly map (Fig. 4c) shows slightly negative to neutral values in the western sector of the map, increasing towards the east, up to 3.5 mGal. The global pattern in the eastern sector shows a NW–SE orientation. The map shows negative values for the stations located right on the rim of the tephra cone. In the north, a minimum is centred on the ring, where the Strombolian scoria cone was emplaced. In the south another minimum coincides with the thicker deposits of the tephra ring. Inside the maar, neutral values are found while reaching the central area. The gravity model of the maar structure has not been developed because the main gravity signature is a circular gravity low produced by the accumulation of pyroclastic material and there is no evidence of the deep root of the structure.

4.3. Magnetometry

The resulting magnetometry map (Fig. 5) shows the distribution of the local magnetic field for the superficial geological layers. The surface structures detected by this method correspond to rocks with a high proportion of magnetic minerals. Concentric magnetic isolines characterise the interior of the maar crater, with an increase from 1600 nT along the ring to 3200 nT toward the central area. A magnetic maximum is measured at the northern side of the maar, on the eastern side of the Strombolian cone rim with values up to 5000 nT.

4.4. Self-potential (SP)

The SP map (Fig. 6) shows an increase of 120 mV from SW to NE, describing a sharp transition highlighting a NW–SE lineament across the maar. The northern end of this lineament overlaps the magnetic anomaly high centred on the Strombolian edifice located at the northern side of the maar crater. In the western side the maar no significant variation of self-potential is observed.

4.5. Electrical resistivity tomography (ERT)

ERT models show high resistivity values (1000 $\Omega\cdot\text{m}$ to more than 8000 $\Omega\cdot\text{m}$) matching the areas where the profiles cut the tephra ring (Fig. 7). Inside the main crater the profiles show a ~ 10 to 20 m thick superficial planar layer of low resistivity (10 $\Omega\cdot\text{m}$ to 200 $\Omega\cdot\text{m}$) (Fig. 7).

In profiles 1 and 2, this layer overlies a thick high resistivity layer (~ 2000 to 5000 $\Omega\cdot\text{m}$) visible until the maximum depth of investigation. However, in the last 20 m, resistivity tends to be lower so that we can estimate the thickness of this layer at $\sim 60\text{ m}$.

Profile 3 crosses the eastern flank of the Strombolian cone and the eastern side of the maar rim. We observe a high resistivity body (from 2000 to more than 8000 $\Omega\cdot\text{m}$) in the Strombolian cone area. This resistive zone spreads from 30 m under the surface and is rooted beyond the depth of investigation. Between the Strombolian cone and the maar rim (from 380 to 520 m distance on the resistivity model) the conductive superficial layer overlies a resistive layer, slightly thinner than the one described in profiles 1 and 2. This resistive layer overlies a conductive layer (a few $\Omega\cdot\text{m}$ to 100 $\Omega\cdot\text{m}$), visible until depth of investigation.

In profile 4, high resistivity in the tephra ring narrows from 30 m under the topography and extends at depth. Inside the maar, under the superficial low resistivity layer encountered in all the profiles, lies a resistive layer. As well as in profile 3, it is thinner than those encountered in the same position on profiles 1 and 2. At greater depth the resistivity lowers to $\sim 100\text{ }\Omega\cdot\text{m}$.

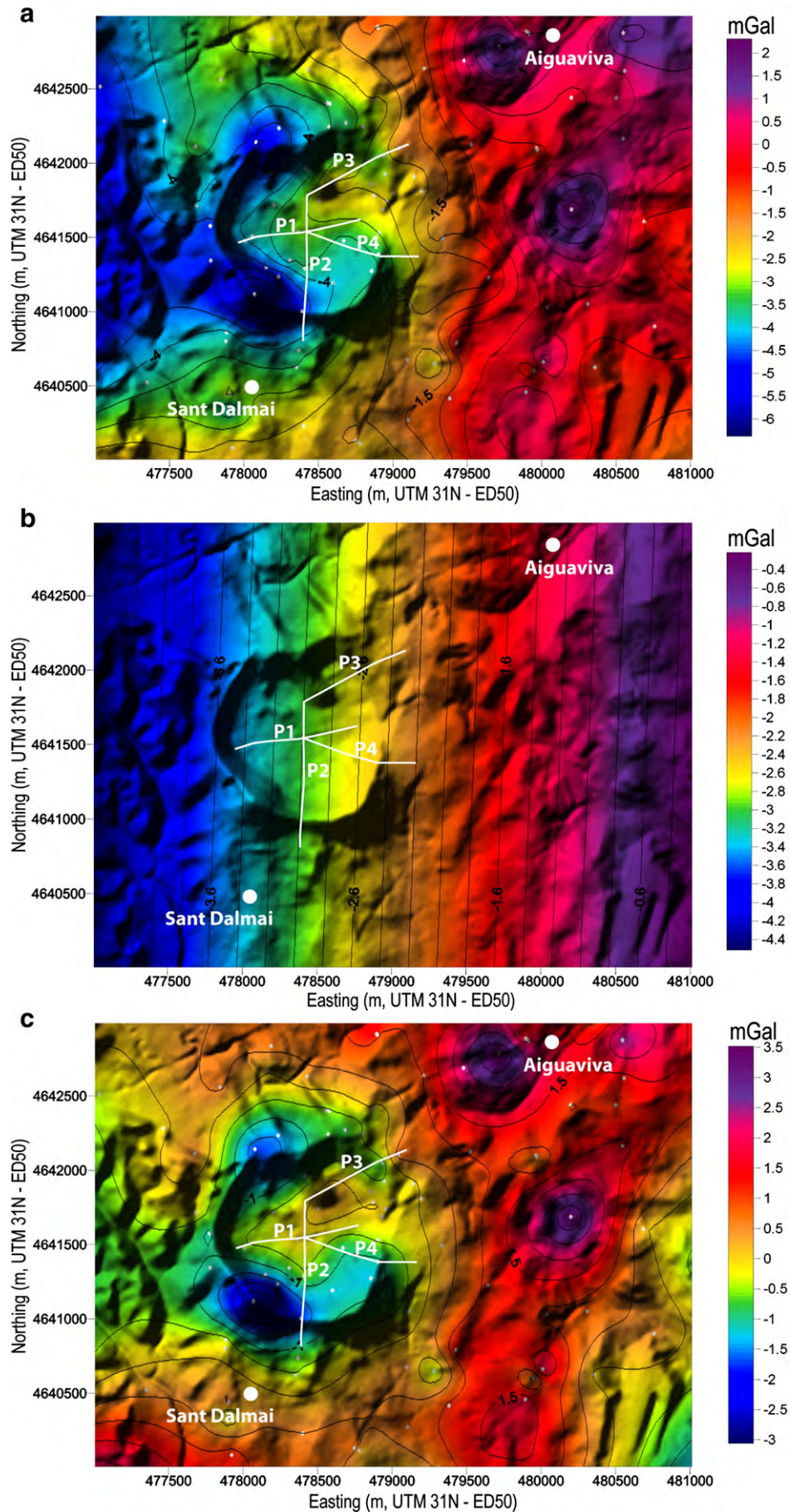


Fig. 4. a. Bouguer anomaly map; b. regional anomaly; c. residual gravity map obtained by subtracting the regional anomaly from the Bouguer anomaly map. Coordinates in metres (UTM31N – ED50). In white: location of ERT the profiles P1, P2, P3, and P4. Small white dots correspond to the gravimetry stations.

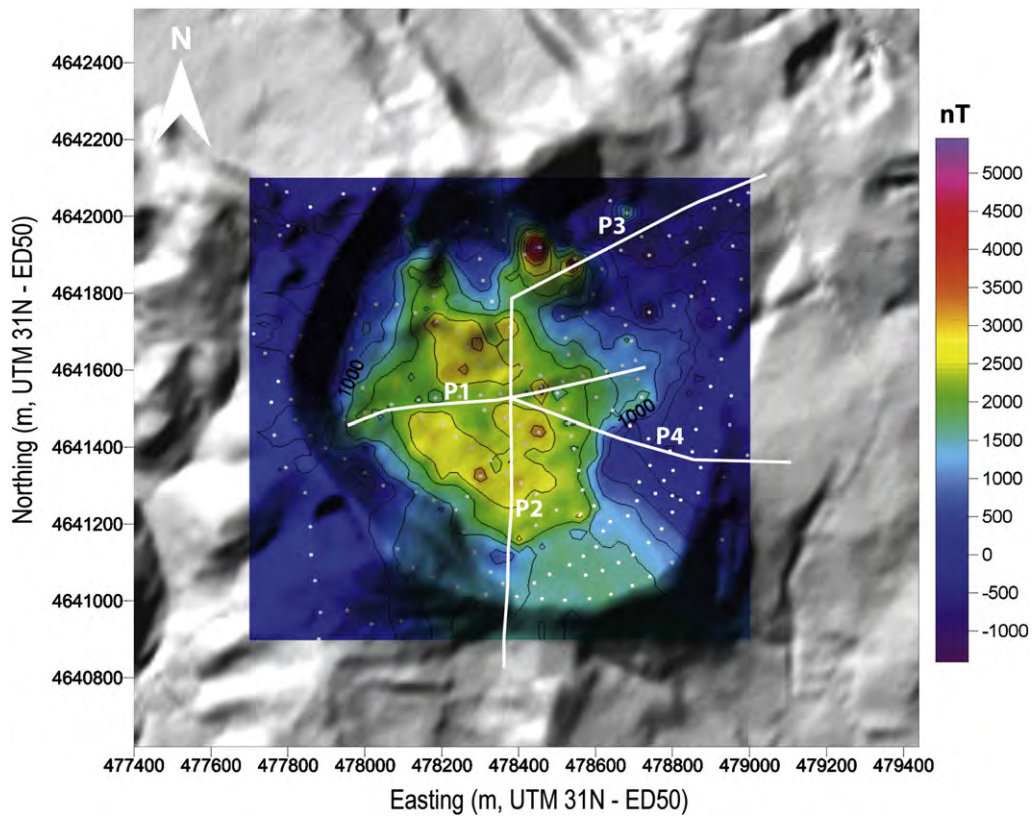


Fig. 5. Residual total field magnetic anomaly map. The white dots correspond to the measurements. The white lines show the location of ERT profiles (P).

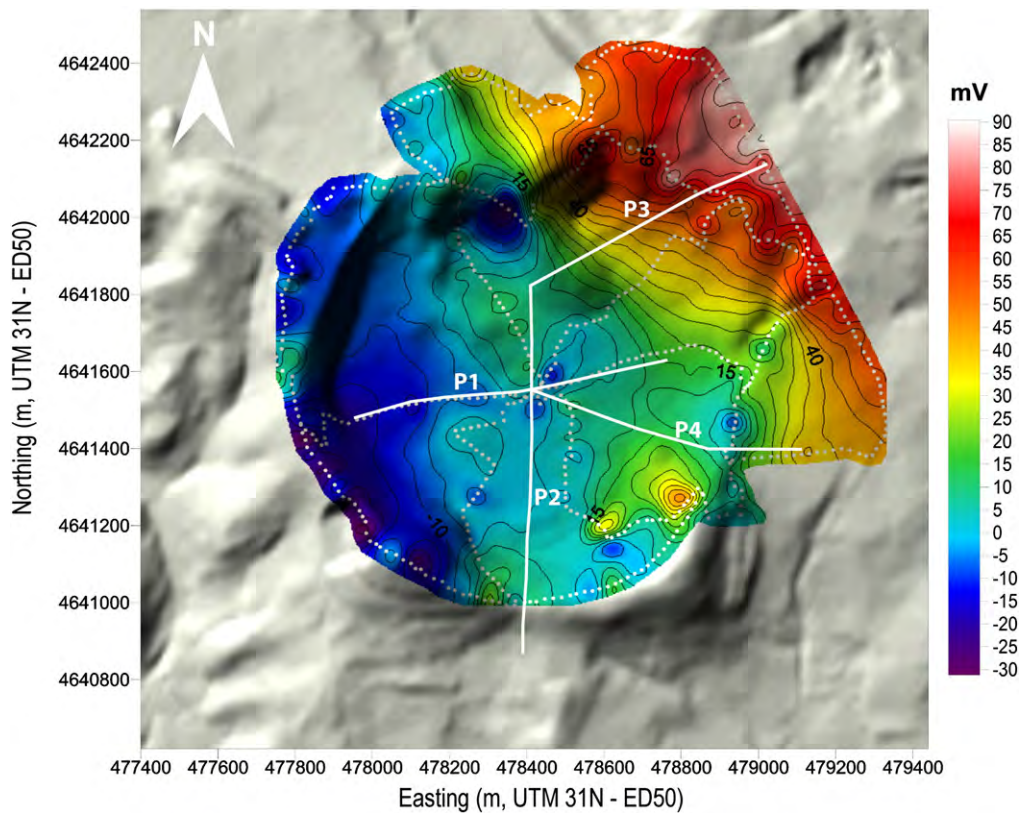


Fig. 6. Self-potential map. The white dots correspond to the measurements. The white lines show the location of ERT profiles (P).

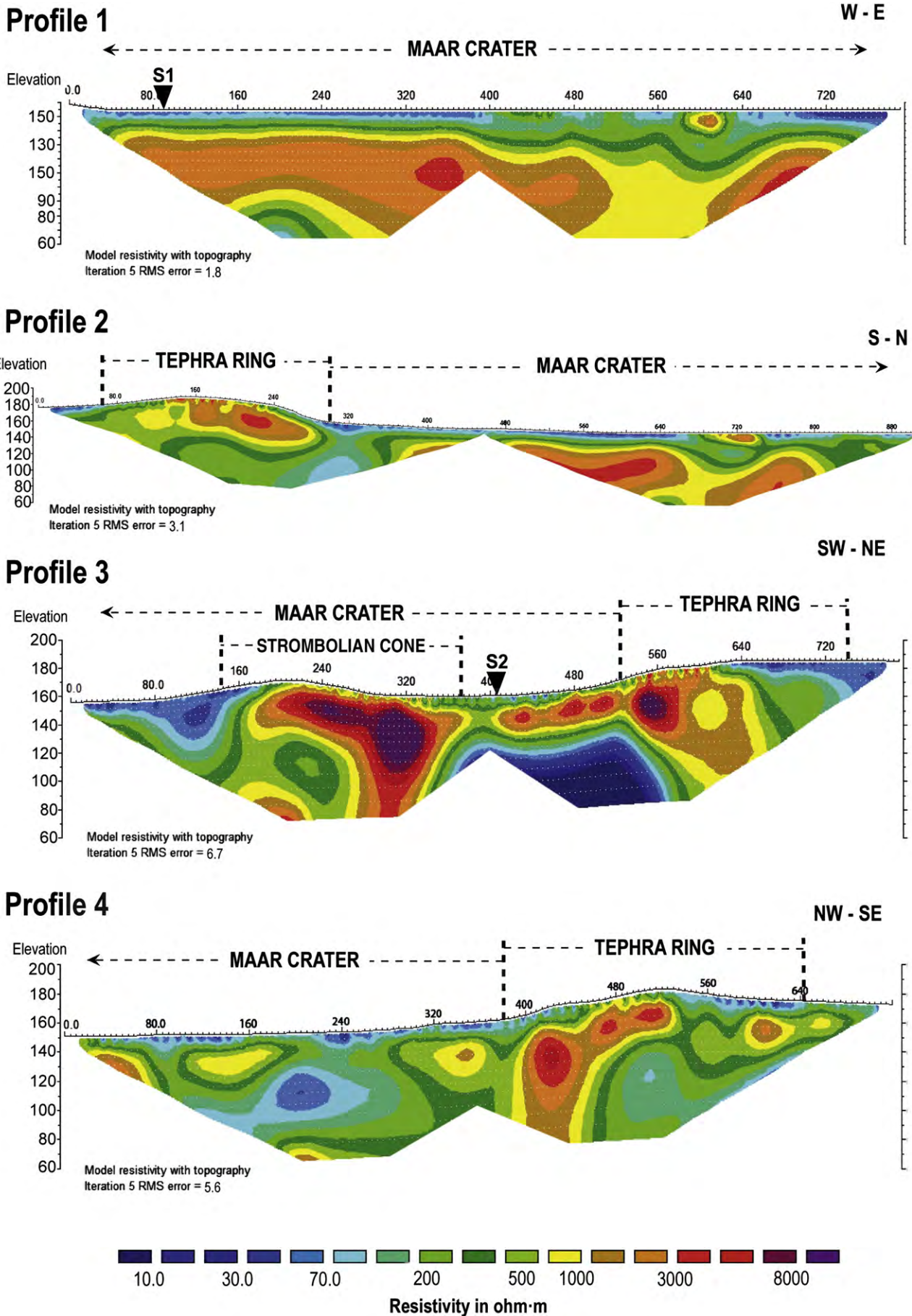


Fig. 7. ERT models with topography.

5. Discussion

5.1. Phreatomagmatic activity

The residual gravity anomaly map shows negative anomalies coinciding with resistive structures imaged with ERT. The southwest main gravity anomaly reaches values of about -2.5 mGal and coincides with an area of maximum accumulation of poorly consolidated pyroclastic materials, i.e. unwelded breccia, that form the tephra ring. This

is consistent with the high resistivity observed in the tephra ring as this material is highly vesiculated. This physical characteristic confers a high resistivity to these levels.

5.2. Strombolian activity

The strong gravity anomaly located at the northern side of the tephra ring shows negative values of up to -2 mGal. This anomaly marks the zone of maximum accumulation of scoria deposits belonging to the

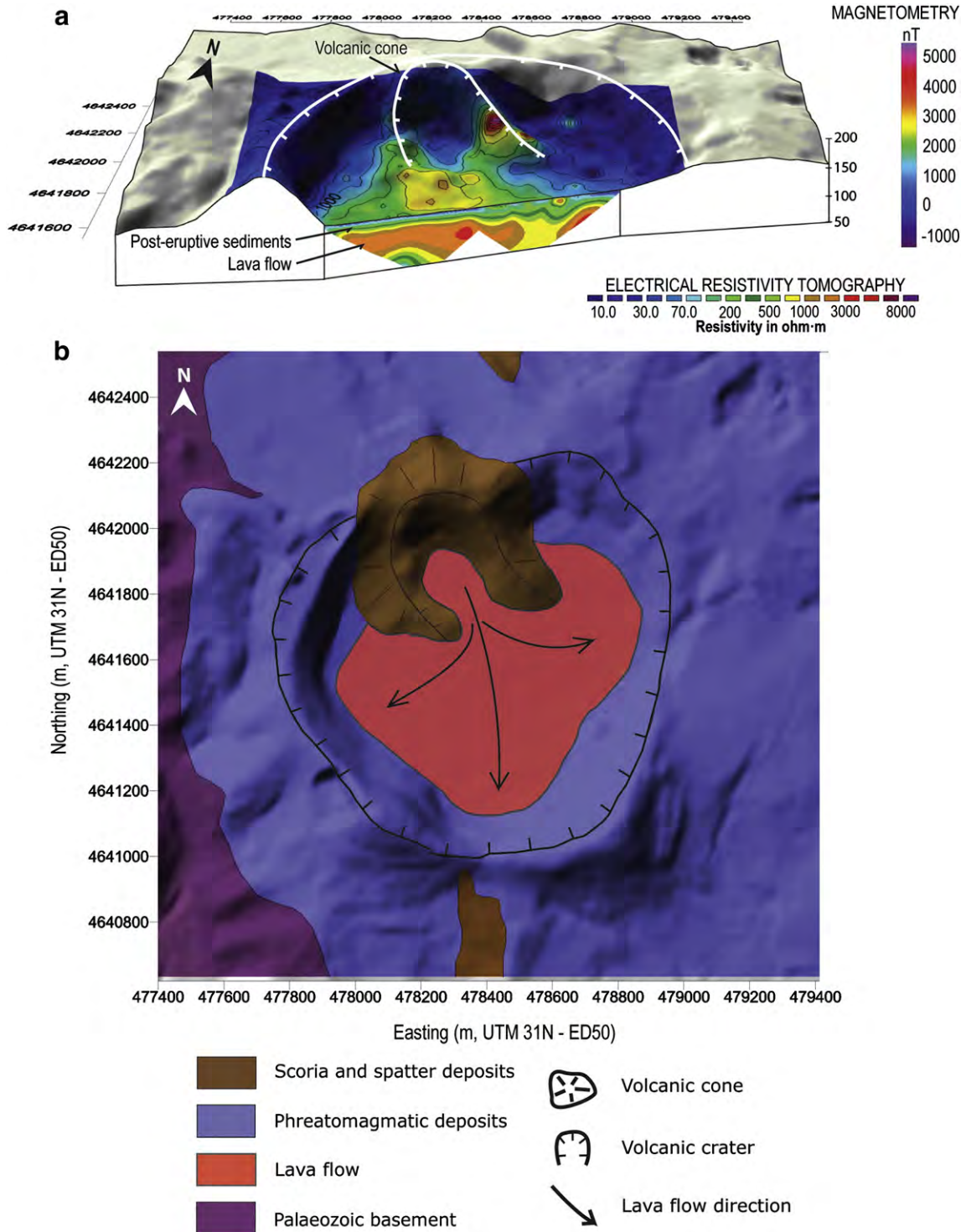


Fig. 8. a) 3D block diagram of the residual total field magnetic anomaly map and the ERT profile 1. b) Mapping of the interpreted lava flow.

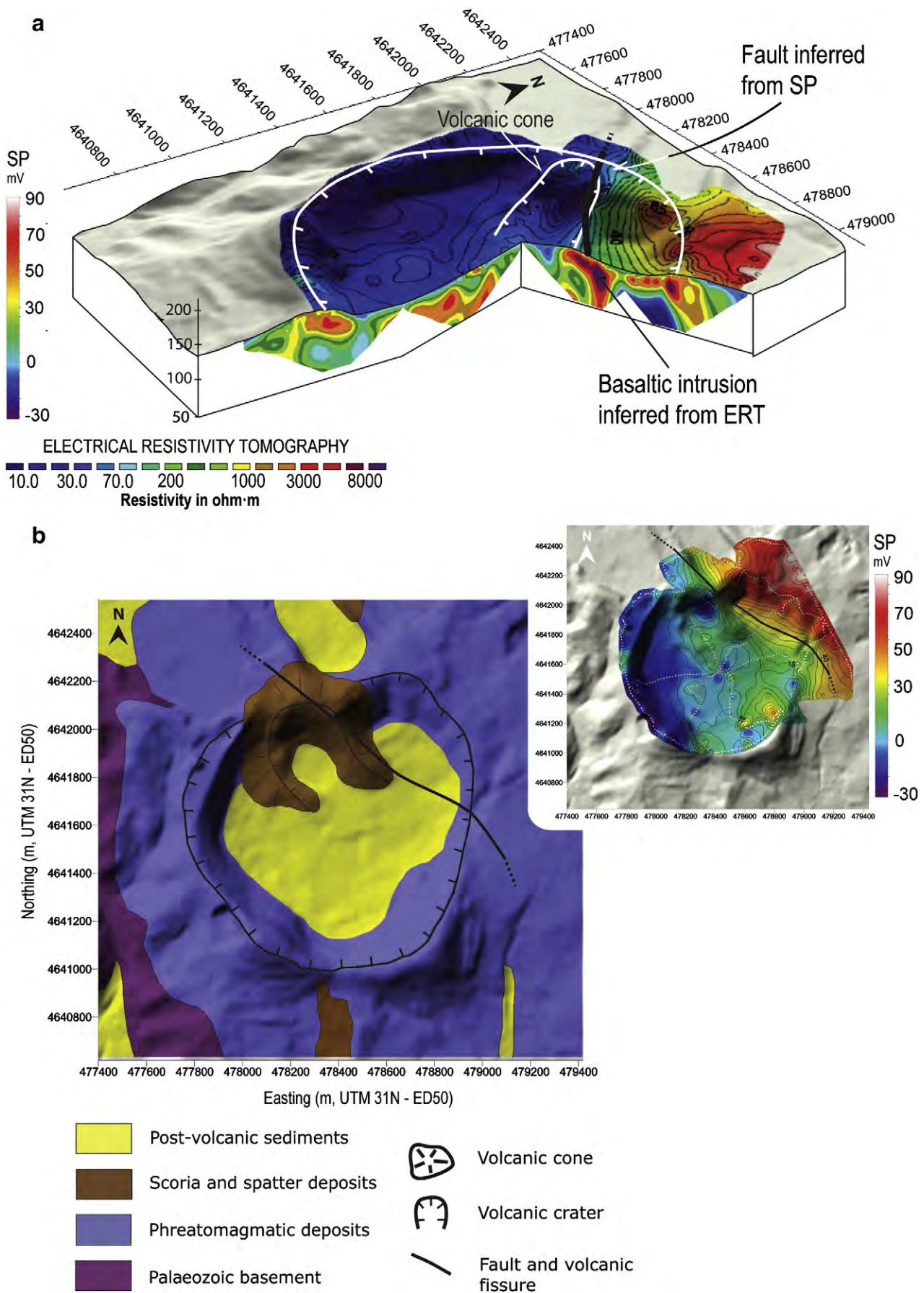


Fig. 9. a) 3D block diagram of the self-potential and the ERT profiles 2 and 3. b) NW-SE fault inferred from self-potential, in the upper right corner, and located on the geological map.

Strombolian cone formed inside the maar crater. Resistivity profile 3, crossing the Strombolian cone more in the South, gives high resistivity values. The shape of the corresponding resistivity body, narrowing from 30 m under the topographic surface might correspond to the base of the Strombolian cone, highlighting the former depth of the maar crater before the Strombolian episode in this part of the crater. The resistive root found under the Strombolian cone might correspond to the eruptive conduit or a secondary dyke.

The ERT images show an area inside the maar crater ranging from 1100 to 3000 $\Omega\cdot\text{m}$ (coloured orange and red in Fig. 8a). This is interpreted to correspond to the basaltic lava flow emitted during the Strombolian phase at the end of La Crosa de Sant Dalmai eruption, and which was also intersected by the drill core S1 (see position in Fig. 3). In some places, this basaltic lava flow is detected until the maximum depth of investigation of the ERT profiles (95 m). The positive magnetic anomaly covers almost the whole maar crater, outlining the extent of the lava below the post-maar sediments (Fig. 8b). In the eastern part of the maar crater floor, no significant magnetic anomaly is detected while the S2 drill core shows the presence of the lava flow at a depth of 26 m, with a thickness of 10 m. The lava flow is not detected by the magnetic measurements probably because it is thin and located too deep for the resolution of the method.

5.3. Post-eruptive phase

The drill cores show that the post-volcanic infill sequence of the maar crater has an average thickness of 10 m in the eastern part of the maar, and 26 m in the north-western zone. This is in the order of magnitude of the 10–25 m thick superficial conductive layer observed in the ERT models. These data indicate that the corresponding post-maar sediments (ranging from $\sim 30 \Omega\cdot\text{m}$ to 500 $\Omega\cdot\text{m}$) form a regular layer extending in the whole maar crater around the Strombolian cone, burying the associated lava flow (Fig. 8).

5.4. Geological control on the eruptive activity

The SP map displays a sharp transition from negative (-25 mV) to positive values (75 mV), following a NW–SE trend. This lineament may be interpreted as a fault associated with the regional trend, guiding the ascending magma (Fig. 1). The resistive body (2000 to more than 8000 $\Omega\cdot\text{m}$) detected at depth in the ERT profile 3 and rooted below the maximum depth of investigation is located on this fault (Fig. 9). We interpret this high resistivity root as a basaltic intrusion that fed the last episode of La Crosa de Sant Dalmai eruption, i.e. the last Strombolian phase. It is difficult to estimate the dimensions of this intrusion (eruptive conduit or secondary dyke). Our ERT data provide only 2 day information and the resolution decreases exponentially with depth making difficult concluding on the nature of this intrusion. However, the superficial section of this intrusion could be estimated between 20 and 30 m wide. This is not concordant with the usual dyke dimensions in such small volcanic edifices. However, White and Ross (2011) and Lefebvre et al. (2012) show that dykes can widen through several processes near the surface and produce such large superficial intrusions from a dyke or from the coalescence of dyke segments.

The problem is whether this fracture also controlled the ascent of magma in the phreatomagmatic phases corresponding to the opening and development of the maar crater and its diatreme. Although the deeper internal structure of the diatreme cannot be defined with the geophysical methods we have applied in this study, it is possible to know the geological unit where the phreatomagmatic explosions occurred. This may be done by simply looking at the populations of the lithic fragments present in the maar deposits, which correspond exclusively to Palaeozoic granites. These fragments are decimetric to less than 1 mm in size, show angular to subangular shapes, and in some cases are strongly hydrothermally altered. These lithic fragments

were directly broken and ejected from the Palaeozoic substrate of the volcano by the phreatomagmatic explosions. This suggests that the maar-forming explosions and, therefore, the magma/water interaction did not occur at the contact between the Palaeozoic basement and the Pliocene and Quaternary infill of the La Selva depression as was initially suggested by Martí et al. (1986), but occurred directly in an aquifer located in the fractured granitic basement (Pedrazzi et al., 2012).

Therefore, if the fracture detected with SP is the main pathway by which the magma ascended to the surface, this should be branched into the granite causing interaction of ascending magma with its aquifer, thus generating violent explosions leading to the formation of the maar and its diatreme. Later, after the maar-diatreme formation, the rise and eruption of the magma would be restricted to the main fracture without the possibility of interacting with the granite aquifer, probably already exhausted, resulting in a final purely Strombolian phase.

Finally, it is important to mention that the geophysical imaging of the maar confirms the lack of significant erosion and modification of its original morphology. This is demonstrated by the preservation of the original slopes of the tephra ring and also by the scarcity of breccia deposits inside the crater, which suggests that little remobilisation of the tephra ring deposits has occurred since its formation. All this suggests that the age of the La Crosa de Sant Dalmai volcano is younger than stated previously for the La Selva sub-zone (7.9–1.7 Ma, Araña, et al. (1983)).

6. Conclusions

Combining new geophysical and geological data we have been able to elaborate a 3D model of the internal structure of the uppermost part of La Crosa de Sant Dalmai maar-diatreme system (Fig. 10), the largest volcano of the Catalan Volcanic Zone. This model helps in understanding the influence of the pre-eruptive basement on the phreatomagmatic and Strombolian activity that constructed the volcanic edifice and the characteristics of the post-eruptive deposits that infill the maar crater. In particular, we have been able to determine 1) the elevation of the maar crater floor under the Strombolian cone; 2) the extension of the lava flow formed during this last Strombolian episode, which is now buried under a 10 to 20 m thick post eruptive sedimentary layer; 3) the presence of a NW–SE lineament interpreted as a fault associated with the regional trend; and 4) the control exerted by this fault on the location of the Strombolian cone, whilst the phreatomagmatic activity resulted from the interaction with an aquifer in the granitic basement.

This multiparametric geophysical and geological research has provided relevant information on the upper structure of La Crosa de Sant Dalmai maar, offering important clues to understand its formation and evolution. However, the applied geophysical methods do not always have sufficient spatial resolution and depth of investigation, so there are still some questions about the deeper part of the diatreme, for which exploration other methods such as pole-dipole ERT profiles or seismic reflection profiles should be used.

Acknowledgements

This study has been partially funded by the grants CGL2010-12338-E and CGL2009-07025 (subprogram BTE). We thank Lluís Motjé (Consortium of the Crosa de Sant Dalmai: management of field geology at the Crosa volcanic area) for his great logistical support all along the field work. We also thank Olaya García, Adelina Geyer, Stefania Bartolini, Llorenç Planagumà, Silvina Guzmán, Ismael Casado, and Anna Sanchez for their assistance in the field. We are grateful to the Editor, Prof. Lionel Wilson, and Prof. Volker Lorenz and one anonymous referee for the constructive reviews of our manuscript.

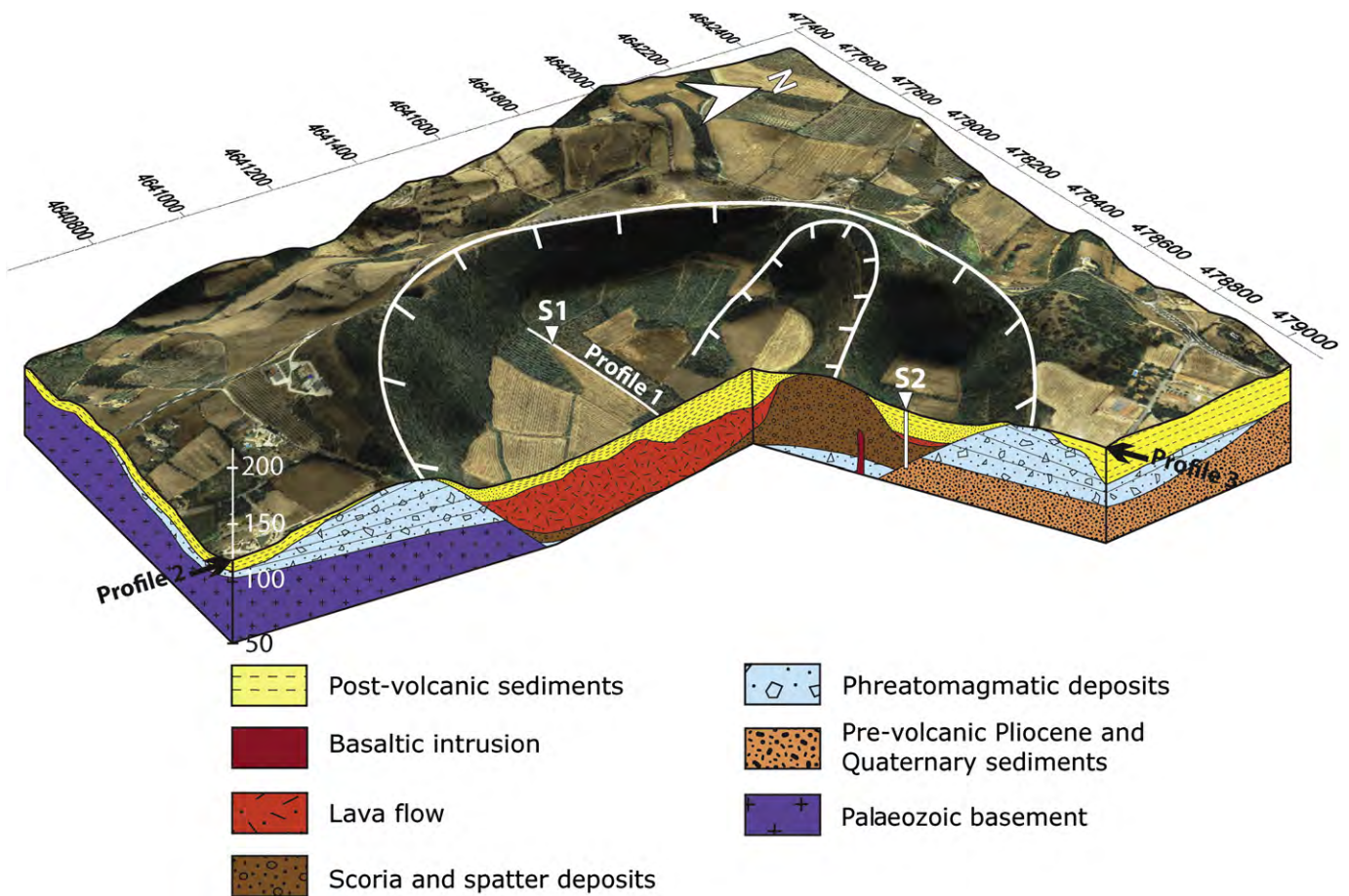


Fig. 10. Synthetic 3D model. Orthophotomap overlapped on the DEM with geologic interpretation through cross sections corresponding to ERT profile 2 (N–S direction) and 3 (SW–NE direction). The locations of S1 and S2 drillings are indicated.

References

- Araña, V., Aparicio, A., Martín-Escorza, C., García Cacho, L., Ortiz, R., Vaquer, R., Barberi, F., Ferrara, G., Albert, J., Gassiot, X., 1983. El volcanismo Neógeno-Cuaternario de Catalunya: caracteres estructurales, petrológicos y geodinámicos. *Acta Geologica Hispánica* 18, 1–17.
- Barnolas, A., García, A., Muelas, A., Soubrier, J., Pallí, Ll., Carreras, J., Martínez, F., Quesada, C., Ruiz, C., 1979. Mapa Geológico de España. E. 1:50000. Santa Coloma de Farners.
- Binley, A., Kemna, A., 2005. DC resistivity and induced polarization methods. In: Rubin, Y., Hubbard, S. (Eds.), *Hydrogeophysics*. Springer, New York, pp. 129–156.
- Büchel, G., 1993. Maars of the Westeifel, Germany. In: Negendank, J.F.K., Zolitschka, B. (Eds.), *Paleolimnology of European Maar Lakes*. Lecture Notes in Earth Sciences, vol. 49. Springer, Berlin, Heidelberg, pp. 1–13.
- Büchel, G., Lorenz, V., 1993. Syn- and post-eruptive mechanism of the Alaska Ukinrek Maars in 1977. In: Negendank, J.F.W., Zolitschka, B. (Eds.), *Paleolimnology of European Maar Lakes*. Lecture Notes in Earth Sciences, 49. Springer, Berlin, Heidelberg, pp. 15–60.
- Casas, A., Torné, M., Banda, E., 1986. Mapa gravimètric de Catalunya 1:500000. Servei Geològic de Catalunya. Dpt. De Política Territorial i Obres Públiques.
- Cebrià, J.M., López-Ruiz, J., Doblas, M., Oyarzun, R., Hertogen, J., Benito, R., 2000. Geochemistry of the Quaternary alkali basalts of Garrotxa (NE Volcanic Province, Spain): a case of double enrichment of the mantle lithosphere. *Journal of Volcanology and Geothermal Research* 102 (3–4), 217–235.
- Dèzes, P., Schmid, S.M., Ziegler, P.A., 2004. Evolution of the European Cenozoic Rift System: interaction of the Alpine and Pyrenean orogens with their foreland lithosphere. *Tectonophysics* 389, 1–33.
- Digital Elevation model. Sant Dalmai zone. <http://www.icc.cat/>, Last date of access 27 February, 2012.
- Guérin, G., Benhamou, G., Mallarach, J.M., 1986. Un exemple de fusió parcial en medi continental. El vulcanisme quaternari de Catalunya. *Vitrina* 1, 20–26.
- Lefebvre, N.S., White, J.D.L., Kjarsgaard, B.A., 2012. Spatter-dike reveals subterranean magma diversions: consequences for small multivent basaltic eruptions. *Geology* 40, 423–426.
- Loke, M.H., 2002. RES2DINV ver. 3.54. Rapid 2-D resistivity and IP inversion using the least square method. Geotomo Software.
- Loke, M.H., Barker, R.D., 1996. Practical techniques for 3D resistivity surveys and data inversion. *Geophysical Prospecting* 44 (3), 499–523.
- Lorenz, V., 1973. On the formation of maars. *Bulletin Volcanologique* 37 (2), 183–204.
- Lorenz, V., 1975. Formation of phreatomagmatic maar-diatreme volcanoes and its relevance to kimberlite diatremes. *Physics and Chemistry of the Earth* 9, 17–27.
- Lorenz, V., 1986. On the growth of maars and diatremes and its relevance to the formation of tuff rings. *Bulletin of Volcanology* 48 (5), 265–274.
- Lorenz, V., 2007. Syn- and post-eruptive hazards of maar-diatreme-volcanoes. *Journal of Volcanology and Geothermal Research* 150, 285–312.
- Lorenz, V., Kurszlaukis, S., 2007. Root zone processes in the phreatomagmatic pipe emplacement model and consequences for the evolution of maar-diatreme volcanoes. *Journal of Volcanology and Geothermal Research* 159 (1–3), 4–32.
- Martí, J., Mallarach, J.M., 1987. Erupciones hidromagmáticas en el volcanismo cuaternario de Olot. *Estudios Geológicos* 43, 31–40.
- Martí, J., Ortiz, R., Claudin, F., Mallarach, J.M., 1986. Mecanismos eruptivos del volcán de la Closa de Sant Dalmai (Prov. Girona). *Anales de Física* (82), 143–153 Vol. esp. serie B.
- Martí, J., Mitjavila, J., Roca, E., Aparicio, A., 1992. Cenozoic magmatism of the Valencia trough (western Mediterranean): relationship between structural evolution and volcanism. *Tectonophysics* 203 (1–4), 145–165.
- Martí, J., Planagumà, L., Geyer, A., Canal, E., Pedrazzi, D., 2011. Complex interaction between Strombolian and phreatomagmatic eruptions in the Quaternary monogenetic volcanism of the Catalan Volcanic Zone (NE of Spain). *Journal of Volcanology and Geothermal Research* 201 (1–4), 178–193.
- Pedrazzi, D., Martí, J., Bolós, X., 2012. Interaction between Strombolian and phreatomagmatic eruptions in the Catalan Volcanic Field: La Closa de Sant Dalmai maar. *Volcandpark International Congress, Olot, Spain*, pp. 22–52.
- Schmincke, H.-U., 1988. *Vulkane im Laacher See-Gebiet, ihre Entstehung und heutige Bedeutung*. Doris Bode Verlag, Haltern, pp. 1–119.
- Sheridan, M.F., Wohletz, K.H., 1981. Hydrovolcanic explosions: the systematics of water-pyroclast equilibrium. *Science* 212, 1387–1389.
- Sheridan, M.F., Wohletz, K.H., 1983. Hydrovolcanism: basic considerations and review. *Journal of Volcanology and Geothermal Research* 17 (1–4), 1–29.
- Trilla, J., Pallí, L., 1977. Vulnerabilidad a la polución como temática hidrogeológica. Aplicación en una zona de los alrededores de Girona. *Cámara of. de Com. e Ind. Girona*, p. 75.
- White, J.D.L., Ross, P.-S., 2011. Maar-diatreme volcanoes: a review. *Journal of Volcanology and Geothermal Research* 201 (1–4), 1–29.
- Wohletz, K.H., 1983. Mechanisms of hydrovolcanic pyroclast formation: grain-size, scanning electron microscopy, and experimental studies. *Journal of Volcanology and Geothermal Research* 17 (1–4), 31–63.
- Wohletz, K.H., Sheridan, M.F., 1983. Hydrovolcanic explosions II, evolution of basaltic tuff rings and tuff cones. *American Journal of Science* 283 (5), 385–413.

APPENDIX 5

Electrical resistivity tomography revealing the internal structure of monogenetic volcanoes

Electrical resistivity tomography revealing the internal structure of monogenetic volcanoes

Stéphanie Barde-Cabusson,¹ Xavier Bolós,¹ Dario Pedrazzi,¹ Raul Lovera,² Guillem Serra,³ Joan Martí,¹ and Albert Casas²

Received 22 March 2013; revised 2 May 2013; accepted 6 May 2013.

[1] Eruptive activity of individual monogenetic volcanoes usually lasts a few days or weeks. However, their short lifetime does not always mean that their dynamics and structure are simple. Monogenetic cones construction is rarely witnessed from the beginning to the end, and conditions for observing their internal structure are hardly reached. We provide high-resolution electrical resistivity sections (10 m electrode spacing) of three monogenetic cones from northeastern Spain, comparing our results to geological observations to interpret their underground continuation. The 100 m maximum depth of exploration provides information on almost the entire edifices, highlighting the relationships between Strombolian and hydromagmatic deposits in two multiphase edifices. A main observation is a column of distinct resistivity centered on the Puig d'Adri volcano, which we interpret as the eruptive conduit. This method can provide valuable information on the past volcanic dynamics of monogenetic volcanic fields, which has real implications for the forecast of future activity.
Citation: Barde-Cabusson, S., X. Bolós, D. Pedrazzi, R. Lovera, G. Serra, J. Martí, and A. Casas (2013), Electrical resistivity tomography revealing the internal structure of monogenetic volcanoes, *Geophys. Res. Lett.*, 40, doi:10.1002/grl.50538.

1. Introduction

[2] Monogenetic volcanoes are small volcanic edifices built-up in a short period of time, (e.g., few hours or days in the East-Izu monogenetic volcano group and several years for Jorullo in 1759~1766 and Parícutín in 1943~1952), so that their complexity is sometimes underestimated [*De la Cruz-Reyna and Yokoyama*, 2011]. Monogenetic volcanic edifices go from simple one-phase volcanoes to complex edifices built from several distinct phases of activity [*Walker*, 2000; *Valentine and Gregg*, 2008]. A complex eruptive dynamics can, for example, result in the accumulation of highly vesicular scoria (Strombolian-style explosive events) and compact, fine-enriched ash (phreatomagmatic

explosive events), forming a complex layercake-style edifice alternating horizons of different electric resistivity material in a reduced space. This makes high-resolution electrical resistivity tomography (ERT) a valuable tool to investigate the internal structure of monogenetic volcanoes. In contrast with polygenetic volcanoes and despite being the most common type of activity, eruptions giving birth to monogenetic volcanoes are much less witnessed and less described in scientific reports [*Kereszturi and Németh*, 2012]. Only a few events of this type have occurred worldwide in historical times such as Al Madinah (1256), Jorullo (1759~1766) and Parícutín (1943~1952), and the Ukinrek maar (1977) [*De la Cruz-Reyna and Yokoyama*, 2011; *Kereszturi and Németh*, 2012]. Monogenetic cones can be weathered, exhibiting part of their internal structure. *Mathieu et al.* [2008] presented natural examples of monogenetic cones from the Chaîne des Puys (French Massif Central) and of parasitic cones from the northeast rift of Teide (Canary Islands) where the shape of shallow volcanic intrusions are well-preserved. Other examples exist [e.g., *Geshi et al.*, 2011]; however, no unified model or similar attempted to connect field observations of this type with some geophysical approach until now.

[3] *Valentine* [2012] used crustal xenoliths to study the shallow plumbing systems of small-volume scoria cones and maars. In particular, he showed that their conduits or dikes flare mainly in the uppermost ~150 m of the crust.

[4] Geophysics has been successfully used to model [*Cassidy et al.*, 2007; *Mrlina et al.*, 2009; *Blaikie et al.*, 2012] or to image [e.g., *Gebhardt et al.*, 2011; *Martín-Serrano et al.*, 2009; *Bolós et al.*, 2012] the subsurface structure of maar volcanoes. ERT was applied on polygenetic volcanoes, providing valuable information on their structure and hydrothermal systems [e.g., *Revil et al.*, 2008, 2011]. *Portal et al.* [2013] also presented preliminary results on a model of monogenetic dome using joint interpretation of ERT, gravimetry, and muonic imagery models. However, a detailed study of the internal structure of monogenetic volcanoes remains poorly documented, particularly edifices built up after multiple phases of activity.

[5] The Catalan Volcanic Zone (CVZ), at the north of Spain (Figure 1a), is mostly unknown compared to the contemporaneous alkaline volcanism in other parts of western and central Europe (Cenozoic alkaline volcanism in the Rhenish massif and Rhinegraben of Germany, the Massif Central of France, and the western Pannonian Basin in Eastern Europe; e.g., *Downes* [2001]) but it offers an excellent opportunity for a detailed exploration of monogenetic volcanoes' internal structure. In this study, we present ERT models from three monogenetic volcanoes giving a detailed image of the entire edifices. Key observations are made from the two more complex edifices because they offer the most important diversity of deposits and structural features.

¹Institute of Earth Sciences Jaume Almera, ICTJA-CSIC, Lluís Sole i Sabaris s/n, Barcelona, Spain.

²Economic and Environmental Geology and Hydrology Group, Department of Geochemistry, Petrology and Geological Prospecting, Faculty of Geology, University of Barcelona, Barcelona, Spain.

³Polytechnic University of Catalonia, Barcelona, Spain.

Corresponding author: S. Barde-Cabusson, Institute of Earth Sciences Jaume Almera, ICTJA-CSIC, Lluís Sole i Sabaris s/n, 08028 Barcelona, Spain. (sbarde@ictja.csic.es)

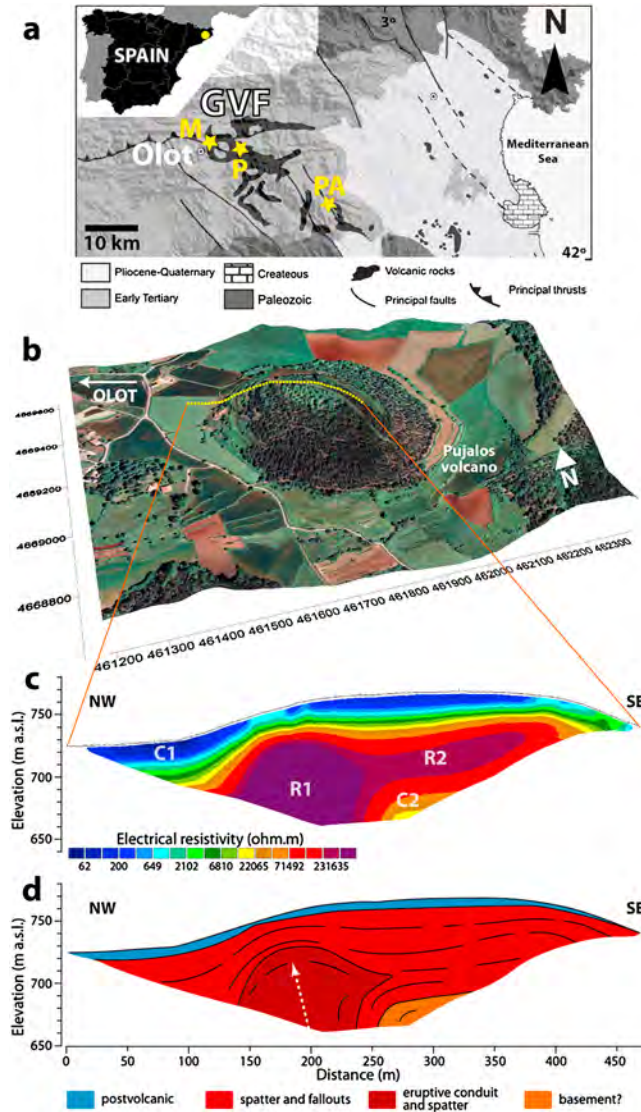


Figure 1. (a) Localization maps of the Garrotxa volcanic field (GVF) and of our three monogenetic volcanoes: Pujalós (P), Montsacopa (M), and Puig d’Adri (PA) volcanoes (modified from *Martí et al.* [2011]). (b) Orthophotography of the Pujalós volcano, a monogenetic Strombolian volcano, overlaid on a digital Elevation Model with localization of the ERT profile (yellow dotted line). (c) ERT model (RMS error 15.2% after five iterations). R and C stands for resistive and conductive bodies or layers respectively. (d) Geological interpretation.

2. Monogenetic Volcanism in the Garrotxa Volcanic Field

[6] The CVZ is one of the Quaternary alkaline volcanic provinces of the European rifts system [*Martí et al.*, 1992, 2011]. It has been active during the last 12 Ma and the volcanism is mainly characterized by alkali basalts and basanites. Inside the CVZ, the Garrotxa volcanic field is a subzone registering the latest volcanic activity (0.5–0.01 Ma) [*Araña et al.*, 1983; *Martí et al.*, 1992]. It comprises more than 50 well-preserved monogenetic volcanoes including scoria cones, tephra rings, and maars. Some of these eruptions alternated Strombolian and hydromagmatic phases, giving rise to complex stratigraphic successions not only within the monogenetic field but also at the scale of individual edifices [*Martí and Mallarach*, 1987; *Martí et al.*, 2011; *Pedrazzi and Martí*, 2011; *Bolós et al.*, 2012]. *Martí et al.* [2011] classify monogenetic volcanoes depending on

whether or not hydromagmatic activity contributed to their construction. Volcanoes exclusively derived from magmatic activity correspond to scoria cones with occasional lava flows while volcanic cones including hydromagmatic activity, although morphologically similar to scoria cones, are much more complex. They may alternate phreatic, phreatomagmatic, and Strombolian phases, generating a wide diversity of pyroclastic density currents and fallout deposits, including explosive and effusive episodes.

3. Data Acquisition and Processing

[7] Multielectrode ERT was used to obtain 2-D resistivity high-resolution data on three monogenetic volcanoes from the Garrotxa volcanic field. We used an Iris Syscal Pro resistivity system with 48 electrodes connected to a 470 m long cable (10 m electrode spacing) in Wenner-Schlumberger configuration (maximum depth of investigation of about

100 m). We used the roll-along method to complete some of the profiles. No reciprocal measurements were taken but data quality was assessed by averaging or stacking several measurements and very good quality factors were obtained ($q < 3.5\%$). Low contact resistances of the electrodes were achieved because of the high moisture of the soils and the special design of the stainless steel electrodes directly in contact with the multicore cable (maximum values $< 3 \text{ k}\Omega$). Current injected was automatically adjusted by the system to optimize the input voltage and to ensure the best signal-to-noise ratio. The maximum power of the instrument is 800 V and the maximum current is 320 mA at 2.5 k Ω contact resistance. In our survey, depending on the distance between current electrodes, the current intensity ranged from 275 to 5 mA. The typical standard deviation was less than 1% with maximum standard deviation values lower than 3.5%.

[8] The resistivity data were inverted with RES2DINV [Loke, 2002]. Covariance matrix is commonly used to assess the accuracy of the inversion for models that consist of a small number of parameters but RES2DINV, like most nonlinear inversion programs, carries out an optimization process that tries to reduce the difference between the calculated and measured apparent resistivity values. The inversion routine used by the program is based on the smoothness-constrained least-squares method [de Groot-Hedlin and Constable, 1990; Sasaki, 1992] which allows to adjust the damping factor. This parameter is designed to accommodate noisier data sets, without which the inversion attempts to fit noise as data and becomes unstable. A larger damping factor was used for the Pujalós volcano data set (Figure 1). When data show large resistivity variations near the surface, it is also recommended to use a model where the cell width is half the unit electrode spacing. This was applied to the Pujalós and Montsacopa profiles. This strategy allowed us to improve the results but RMS error, estimating the difference between the calculated and measured apparent resistivity, was still high for Pujalós. The results are discussed taking this fact into account.

4. Results

[9] The following results relate to our three example monogenetic volcanoes. A first ERT profile was performed on the Pujalós volcano, near the city of Olot, in the Garrotxa volcanic field (Figure 1). The ERT cable was laid out from the northwestern side of the Pujalós, passing through the summit up to the southeastern flank (Figure 1b). The resistivity model (Figure 1c) shows a globally simple distribution of the resistivity. We found a superficial conductive layer C1 ($< 650 \text{ }\Omega\cdot\text{m}$), 10 to 20 m thick, and slightly thicker beyond the fields located at the NW of the cone. A rounded resistive body R1 ($> 250,000 \text{ }\Omega\cdot\text{m}$) appears at ~ 30 m depth. R1 is offset with respect to the cone summit and extends beyond the maximum depth of investigation. This resistive body seems to be connected to the SE with an elongated shape of slightly lower resistivity values that follows a 15° slope (R2). Under this layer, the resistivity values decrease progressively up to one order of magnitude (C2).

[10] The second test was performed in the same area, on Montsacopa, a volcano located inside the city of Olot itself. This volcano presents a NW-SE elongated shape with a

well-preserved circular crater in the summit (crater B in Figure 2a). A previous study based on stratigraphy indicates the presence of a second eruptive vent (crater A in Figure 2a) on the SE flank [Bolós, 2009]. Our ERT profile (Figure 2b) covers the volcano nearly from one extreme to the other, crossing the two craters. This 710 m long profile is composed of two sections acquired with a roll-along of half the cable length. After four iterations, the data inversion gave a good RMS error value of 5.7%. The most striking feature is a 150 m wide high-resistivity body R3 ($> 200,000 \text{ }\Omega\cdot\text{m}$) under crater B. It presents a concave upper limit, nearly vertical laterals, and extends beyond the maximum depth of exploration. On top of this body lies a lenticular conductive body marked as C3, ~ 20 m thick at its maximum (~ 950 to $100 \text{ }\Omega\cdot\text{m}$). At the NW we observe a resistive elongated body (R4), dipping NW at an angle of 20° . It is surrounded by lower resistivity values (~ 3000 to $300 \text{ }\Omega\cdot\text{m}$). The resistivity distribution in the SE flank is more complex. It shows a few meters-thick superficial layer, displaying resistivity $< 3000 \text{ }\Omega\cdot\text{m}$. It overlays an irregular resistive layer with several tens of thousands $\Omega\cdot\text{m}$ resistivity (R5). Surrounded by these high-resistivity values, the model shows a drop-shaped zone C4, of lower resistivity ($\sim 1000 \text{ }\Omega\cdot\text{m}$). Deeper, the inversion model shows resistivity values of about $3000 \text{ }\Omega\cdot\text{m}$.

[11] Still in the Garrotxa, we acquired a third ERT profile on the Puig d'Adri volcano (Figures 2d, 2e, 2f, and 1a for localization). These data were acquired along three sections overlapping by half the cable length, i.e., we obtained a profile of 950 m in total. After five iterations we obtained an RMS error of 6.1% for this model, confirming the quality of the inversion. The eastern part of the resistivity model shows several layers identified through their respective resistivity. In particular, we can notice the presence of a horizontal conductive layer ($< 400 \text{ }\Omega\cdot\text{m}$) at depth (C5). Going upward, an area of 1000 to $3000 \text{ }\Omega\cdot\text{m}$ seems to change progressively from horizontal to $\sim 20^\circ$ dip. It lays under a more resistive (up to $8000 \text{ }\Omega\cdot\text{m}$) 20 m thick layer (R6). The rest of the resistivity model is occupied by a large resistive unit, R7, ($> 4000 \text{ }\Omega\cdot\text{m}$) overlaid by a conductive layer ($< 400 \text{ }\Omega\cdot\text{m}$). The resistive unit displays a V-shaped base, intersected by the lower limit of the model. Nearly in the center of the V, a less-resistive (light-red color in Figure 2e) vertical column connects the deepest layer to the surface. At 100 m to the west the conductive superficial layer enters deeper into the resistive unit. This last follows the slope of the western flank, forming a thick resistive layer (R8).

5. Discussion

[12] Our three example monogenetic volcanoes are a good illustration of the difference made by Martí *et al.* [2011] concerning monogenetic volcanoes affected or not by hydromagmatic phases during their construction. For the three sites, the water table is located in the sedimentary basement, at depths greater than our maximum depth of exploration so that we do not take it into account in the interpretation. Available geological information describes the Pujalós volcano as a scoria cone, possibly originating a lava flow covering an area of about 6 km^2 to the west [JGC *et al.*, 2007]. Despite the elevated RMS error (15.2% after five iterations), the resistivity model seems to fit well this description (Figure 1). Moreover, a strong likeness exists with natural

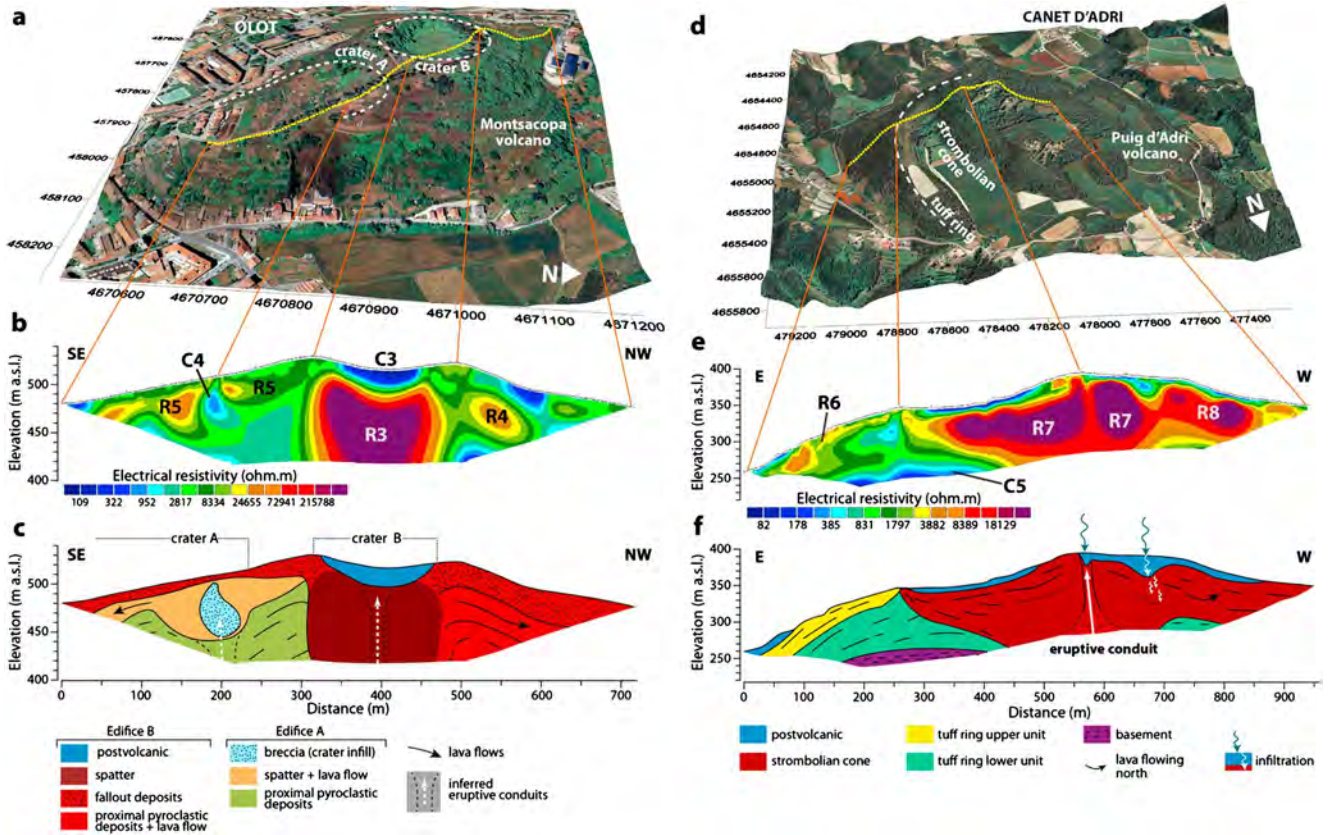


Figure 2. The Montsacopa and Puig d’Adri volcanoes, two complex monogenetic volcanoes built by hydromagmatic and Strombolian activity. (a and d) Orthophotography overlaid on a digital elevation model with localization of the ERT profile (yellow dotted line). (b and e) ERT model (vertical exaggeration 1.17, RMS error 5.7% after four iterations for Montsacopa and vertical exaggeration 1.17, RMS error 6.1% after five iterations for Puig d’Adri). R and C stands for resistive and conductive units respectively. (c and f) Geological interpretation.

examples from eroded areas such as the one we observed in El Hierro (Canary Islands, Spain). Figure 3 shows two buried monogenetic cones intersected by a vertical scarp on the coast of El Hierro. This situation allows observing a cross-section of both cones with their feeding dykes enlarging to flattened rounded massive units at the center of the volcanoes. This would correspond to the resistive heart R1 of the Pujalós volcano (Figure 1c). The conduit enlarging in the very superficial part of the eruptive system is quite compatible with conclusions made by *Valentine* [2012]. It can be interpreted as spatter deposits, which are the most proximal products to volcanic vents and directly connected to the eruptive conduit. In the Pujalós, resistive layer R2 can be compared to the stratified accumulation of scoria visible in the monogenetic cones of El Hierro. The resistivity values decreasing at depth (C2) may correspond to the basement, dipping NW. Because of the position of the profile we cannot confirm or infer the presence of a lava flow to the west. Finally, the conductive superficial layer C1 corresponds to the postvolcanic cover, thicker in the northwestern cultivated fields area.

[13] The repartition of the resistivity inside Montsacopa and Puig d’Adri appears more complex than for the Pujalós volcano, reflecting their more complex eruptive histories. Montsacopa shows a sequence involving a Strombolian phase at the beginning and a hydromagmatic one at the end [*Marti et al.*, 2011]. In addition to the summit well-visible

crater, stratigraphical study of the volcanic deposits suggest the existence of a hidden vent on the southeastern flank [*Bolós*, 2009], which is confirmed by ERT. In the SE flank, we interpret the lower resistivity body C4 as crater A infill, i.e., breccias associated to Strombolian explosions (Figure 2b). This unit is likely surrounded by spatter deposits (R5). The connection with a feeding conduit is not visible on the tomogram, most probably because the profile is offset on a side of the crater. The continuation of R5 to the SE can be interpreted as a lava flow (Figure 2c). Under this system, the lower resistivity values may correspond to material with a higher open porosity and/or alteration [*Loke*, 2002]. According to the position of this unit in the edifice, it is compatible with fallout deposits that can be associated to the early activity of crater A. These deposits may have been cut-off to the NW by an explosion giving birth to crater B. This ~150 m wide cavity was likely filled by welded deposits forming R3 high-resistivity body. However, note that the inversion process may be affected by superficial strong resistivity contrasts [*Loke*, 2002] and the resistivity values of this body may be overestimated. These rocks being inaccessible and no similar rocks outcropping, no laboratory measurement of the real resistivity could be performed. The lenticular conductive layer C3 consists of postvolcanic products filling crater B. The NW flank of the volcano can be interpreted as an accumulation of proximal fallout deposits associated to crater B, with intercalation of more resistive lava flows (R4).

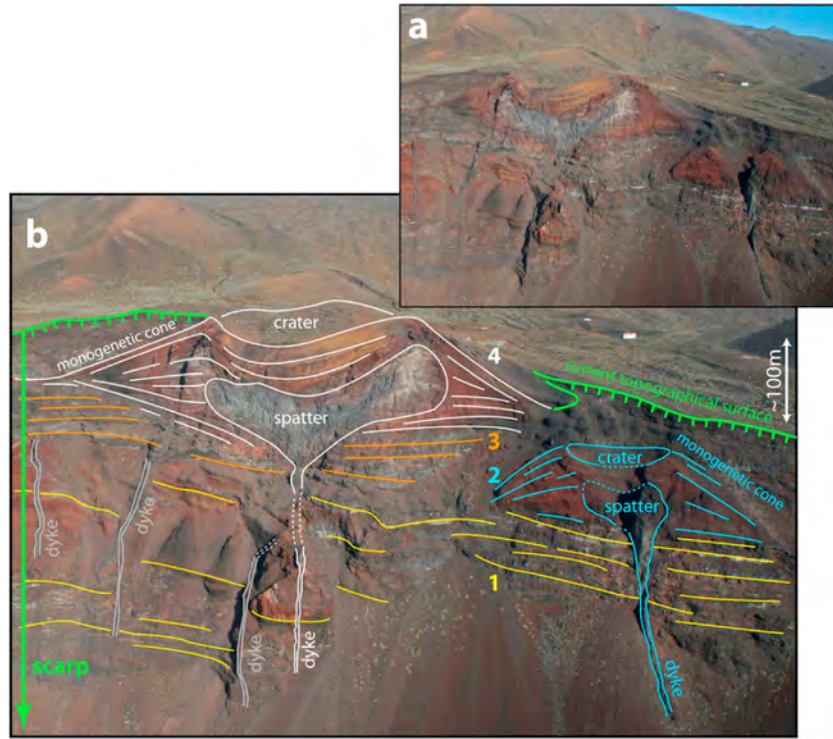


Figure 3. (a) Photography of two monogenetic cones intersected by a cliff at the western point of El Hierro (Canary Islands, Spain). (b) Interpretation. Numbers associated to a color code corresponds to a chronological order.

Indeed, outcrops at the NW of the volcano, close to our profile, show a superposition of two lava flows attributed to the activity of Montsacopa [Bolós, 2009].

[14] Martí *et al.* [2011] describe a complex eruptive history for the Puig d’Adri volcano, involving successive hydromagmatic and Strombolian phases. On the corresponding ERT profile the hydromagmatic deposits of the eastern side of the profile and the Strombolian deposits inside the limits of the tuff-cone [Pujadas *et al.*, 1997; Martí *et al.*, 2011] are well-identifiable (Figures 2e and 2f). In the east, the successive layers of different resistivity values correspond, from the surface to the base, to postvolcanic deposits on two hydromagmatic units. The upper hydromagmatic deposits (R6) show higher resistivity values with respect to the underlying deposits possibly because of a higher degree of compaction, reducing its permeability and then its water content. The underlying tuff ring deposits (Figure 2f) consist mainly of surges, explosion breccias, and a pyroclastic flow [Martí *et al.*, 2011]. Conductive layer C5, visible at the inferior limit of the tomogram, likely corresponds to marls and sandstones constituting the basement. Its spatial relationship with both the hydromagmatic and Strombolian units and its resistivity, are fully compatible with this interpretation. The most uncommon observation provided by our ERT data concerns the Strombolian unit, represented in red tones in Figure 2f and corresponding to the highest resistivity values. A less-resistive 10 to 20 m large column occupies a central position inside the Strombolian cone and connects the deep layer to the surface. We believe that this lower resistivity values correspond to an accumulation of brecciated material partly consolidated, plugging the feeding conduit of the Strombolian cone. To our knowledge this is the first time that this has been shown with geophysical imaging. Finally, we interpret R8, at the western side of the profile, as the two lava

flows described by Martí *et al.* [2011] that caused the breaching of the northwestern flank of the scoria cone. The underlying deposits are likely to be attributed to the hydromagmatic anterior phase. The interface between the lava flows and the Strombolian cone may constitute a preferential path for meteoric water infiltration, triggering progressive weathering of rocks and thus leading to decrease the resistivity. This would explain the deepening of the conductive superficial layer observed (blue arrow in Figure 2f). A similar explanation can be proposed for the slight deepening of the conductive superficial layer into the eruptive conduit, even if we are here at the limit of the spatial resolution of the ERT measurements.

6. Conclusion

[15] We show that volcanic cones exclusively derived from magmatic activity, built by the accumulation of scoria with occasional emission of lava flows, are easily distinguished from more complex edifices affected by hydromagmatic phases. ERT offers a strong advantage regarding spatial resolution and depth of exploration with respect to other geophysical methods, for the study of monogenetic volcanoes. With complementary surface geological observations either on site or using other natural examples, we could highlight various elements of the structure of these volcanoes and evidence several types of volcanic products such as (1) spatter deposits in the central part of the cones, (2) contrasts between hydromagmatic and Strombolian deposits, (3) buried lava flows, (4) the hidden eruptive vent of the Montsacopa volcano, and (5) the eruptive conduit of the Puig d’Adri Strombolian cone. We think that high-resolution ERT is a powerful tool for the study of the internal structure of monogenetic volcanoes. The detailed structural and geological

interpretation of such data is a valuable contribution to enhance knowledge about volcanic hazards in monogenetic volcanic fields in general. Because this method gives information about the past volcanic dynamics, it is particularly interesting for the forecast of future activity in a given monogenetic volcanic field.

[16] **Acknowledgments.** S. Barde-Cabusson was funded by JAE-Doc Program (JAEDoc_09_01319). This study was partially funded by the European Commission (FP7 Theme: ENV.2011.1.3.3-1; grant 282759; “VUELCO”), and by the grant *Beca d’investigació “Oriol de Bolós” en Ciències Naturals* (Olot, Spain). We thank the Natural Park of the Garrotxa Volcanic Zone for its support. We sincerely thank the Editor Andrew Newman, Karoly Nemeth and an anonymous reviewer for the improvements made from their comments.

[17] The Editor thanks Karoly Nemeth and an anonymous reviewer for their assistance in evaluating this paper.

References

- Araña, V., A. Aparicio, C. Martín-Escorza, L. García Cacho, R. Ortiz, R. Vaquer, F. Barberi, G. Ferrara, J. Albert, and X. Gassiot (1983), El volcanismo Neógeno-Cuaternario de Catalunya: caracteres estructurales, petrológicos y geodinámicos, *Acta Geol. Hisp.*, *18*, 1–17.
- Blaikie, T. N., L. Ailleres, R. A. F. Cas, and P. G. Betts (2012), Three-dimensional potential field modelling of a multi-vent maar-diatreme - The Lake Coragulac maar, Newer Volcanics Province, south-eastern Australia, *J. Volcanol. Geoth. Res.*, *235–236*, 70–83, doi:10.1016/j.jvolgeores.2012.05.002.
- Bolós, X. (2009), Characterization of the Montsacopa volcano and its surroundings (in English, Spanish, and Catalan). Web access <http://bit.ly/ZqkAaY>, Garrotxa Volcanic Natural Parc, Olot, Spain.
- Bolós, X., S. Barde-Cabusson, D. Pedrazzi, J. Martí, A. Casas, M. Himi, and R. Lovera (2012), Investigation of the inner structure of La Crosa de Sant Dalmai maar (Catalan Volcanic Zone, Spain), *J. Volcanol. Geoth. Res.*, *247–248*, 37–48, doi:10.1016/j.jvolgeores.2012.08.003.
- Cassidy, J., S. J. France, and C. A. Locke (2007), Gravity and magnetic investigation of maar volcanoes, Auckland volcanic field, New Zealand, *J. Volcanol. Geoth. Res.*, *159*, 153–163, doi:10.1016/j.jvolgeores.2006.06.007.
- De la Cruz-Reyna, S., and I. Yokoyama (2011), A geophysical characterization of monogenetic volcanism, *Geophys. Int.*, *50*(4), 465–484.
- Downes, H. (2001), Formation and modification of the shallow subcontinental lithospheric mantle: a review of geochemical evidence from ultramafic xenolith suites and tectonically emplaced ultramafic massifs of Western and Central Europe, *J. Petrol.*, *42*, 233–250.
- Gebhardt, A. C., M. De Batist, F. Niessen, F. S. Anselmetti, D. Ariztegui, T. Haberzettl, C. Kopsch, C. Ohlendorf, and B. Zolitschka (2011), Deciphering lake and maar geometries from seismic refraction and reflection surveys in Laguna Potrok Aike (southern Patagonia, Argentina), *J. Volcanol. Geoth. Res.*, *201*, 357–363, doi:10.1016/j.jvolgeores.2010.12.019.
- Geshi, N., K. Németh, and T. Oikawa (2011), Growth of phreatomagmatic explosion craters: A model inferred from Suoana crater in Miyakejima Volcano, Japan, *J. Volcanol. Geoth. Res.*, *201*(1–4), 30–38, doi:10.1016/j.jvolgeores.2010.11.012.
- de Groot-Hedlin, C., and S. Constable (1990), Occam’s inversion to generate smooth, two-dimensional models from magnetotelluric data, *Geophysics*, *55*, 1613–1624.
- Institut Geològic de Catalunya (IGC), Institut Cartogràfic de Catalunya (ICC), and Parc Natural de la Zona Volcànica de la Garrotxa (PNZVG) (2007), Carta Vulcanològica de la Zona Volcànica de la Garrotxa, 1:25.000, Ed.: Institut Cartogràfic de Catalunya, Barcelona.
- Kereszturi G., and K. Németh (2012), Monogenetic Basaltic Volcanoes: Genetic Classification, Growth, Geomorphology and Degradation, in *Updates in Volcanology - New Advances in Understanding Volcanic Systems*, edited by K. Nemeth, Jeddah, Kingdom of Saudi Arabia, ISBN: 978-953-51-0915-0, InTech, doi:10.5772/51387.
- Loke, M. H. (2002). RES2DINV ver. 3.54. Rapid 2-D resistivity and IP inversion using the least square method. Geotomo Software.
- Martí, J., and J. M. Mallarach (1987), Erupciones hidromagmáticas en el volcanismo cuaternario de Olot, *Estudios Geológicos*, *43*, 31–40.
- Martí, J., J. Mitjavila, E. Roca, and A. Aparicio (1992), Cenozoic magmatism of the Valencia trough (Western Mediterranean): relation between structural evolution and Volcanism, *Tectonophysics*, *203*, 145–166.
- Martí, J., L. Planagumà, A. Geyer, E. Canal, and D. Pedrazzi (2011), Complex interaction between Strombolian and phreatomagmatic eruptions in the Quaternary monogenetic volcanism of the Catalan Volcanic Zone (NE of Spain), *J. Volcanol. Geoth. Res.*, *201*(1–4), 178–193.
- Martín-Serrano, A., J. Vegas, A. García-Cortés, L. Galán, J. L. Gallardo-Millán, S. Martín-Alfageme, F. M. Rubio, P. I. Ibarra, A. Granda, A. Pérez-González, and J. L. García-Lobón (2009), Morphotectonic setting of maar lakes in the Campo de Calatrava Volcanic Field (Central Spain, SW Europe), *Sediment. Geol.*, *222*, 52–63.
- Mathieu, L., B. van Wyk de Vries, E. P. Holohan, and V. R. Troll (2008), Dykes, cups, saucers and sills: Analogue experiments on magma intrusion into brittle rocks, *Earth Planet. Sci. Lett.*, *271*(1–4), 1–13, doi:10.1016/j.epsl.2008.02.020.
- Mrlina, J., H. Kämpf, C. Kroner, J. Mingram, M. Stebich, A. Brauer, W. H. Geissler, J. Kallmeyer, H. Matthes, and M. Seidl (2009), Discovery of the first Quaternary maar in the Bohemian Massif, Central Europe, based on combined geophysical and geological surveys, *J. Volcanol. Geoth. Res.*, *182*, 97–112, doi:10.1016/j.jvolgeores.2009.01.027.
- Pedrazzi, D., and J. Martí (2011), Interaction between Strombolian and phreatomagmatic eruptions in the monogenetic volcanic fields of the Iberian Peninsula and Lanzarote Island, A. Rittmann Conference, Nicolosi (Catania), 7–9 June 2011.
- Portal, A., et al. (2013), Inner structure of the Puy de Dôme volcano: cross-comparison of geophysical models (ERT, gravimetry, muon imaging), *Geosci. Instrum. Method. Data Syst.*, *2*, 47–54, doi:10.5194/gi-2-47-2013.
- Pujadas, A., L. Pallí, D. Brusi, and C. Roqué (1997), *El Vulcanisme de la Vall de Llèmena*, Universitat de Girona, Spain (Eds.).
- Revil, A., et al. (2008), Inner structure of La Fossa di Vulcano (Vulcano Island, southern Tyrrhenian Sea, Italy) revealed by high resolution electric resistivity tomography coupled with self-potential, temperature, and soil CO₂ diffuse degassing measurements, *J. Geophys. Res.*, *113*, B07207, doi:10.1029/2007JB005394.
- Revil, A., et al. (2011), Hydrogeology of Stromboli volcano, Aeolian Islands (Italy) from the interpretation of resistivity tomograms, self-potential, soil temperature, and soil CO₂ concentration measurements, *Geophys. J. Int.*, *186*, 1078–1094, doi:10.1111/j.1365-246X.2011.05112.x.
- Sasaki, Y. (1992), Resolution of resistivity tomography inferred from numerical simulation, *Geophys. Prospect.*, *40*, 453–464.
- Valentine, G. A. (2012), Shallow plumbing systems for small-volume basaltic volcanoes, 2: Evidence from crustal xenoliths at scoria cones and maars, *J. Volcanol. Geoth. Res.*, *223–224*, 47–63, doi:10.1016/j.jvolgeores.2012.01.012.
- Valentine, G. A., and T. K. P. Gregg (2008), Continental basaltic volcanism—process and problems, *J. Volcanol. Geoth. Res.*, *177*, 857–873.
- Walker, G. P. L. (2000), Basaltic volcanoes and volcanic systems, in *Encyclopedia of Volcanoes*, edited by Sigurdsson, H., pp. 283–289, Academic Press, San Francisco (CA).

APPENDIX 6

Volcanic stratigraphy of the Quaternary La Garrotxa Volcanic Field (NE Iberian Peninsula)



**Volcanic stratigraphy of the Quaternary La Garrotxa
Volcanic Field (NE Iberian Peninsula)**

Journal:	<i>Journal of Quaternary Science</i>
Manuscript ID:	JQS-13-0100.R1
Wiley - Manuscript type:	Research Article
Date Submitted by the Author:	n/a
Complete List of Authors:	Bolós, Xavier; CSIC, ICTJA Planagumà, Llorenç; Tosca S.A. Serveis d'Educació Ambiental, Martí, Joan; CSIC, ICTJA
Keywords:	Quaternary volcanism, volcano-stratigraphy, monogenetic volcanism, Garrotxa volcanic field, hazard assessment

SCHOLARONE™
Manuscripts

1
2 1
3
4 2
5
6 3
7
8 4
9
10 5 **Volcanic stratigraphy of the Quaternary La Garrotxa Volcanic Field (NE Iberian Peninsula)**
11
12 6
13
14
15 7 Xavier Bolós¹, Llorenç Planagumà², Joan Martí¹
16
17 8
18
19 9 1. Institute of Earth Sciences Jaume Almera, CSIC. Group of Volcanology, SIMGEO (UB-CSIC),
20
21 10 c/Lluis Sole Sabaris s/n, 08028 Barcelona, Spain.
22
23
24 11
25
26 12 2. Tosca Environmental Services. Parc Natural de la Zona Volcànica de la Garrotxa, c/Santa
27
28 13 Coloma, 17800 Olot, Spain.
29
30
31 14
32
33 15
34
35 16 Corresponding author: Xavier Bolós (xbolos@ictja.csic.es)
36
37 17
38
39 18
40
41 19 Submitted to: Journal of Quaternary Science
42
43
44 20
45
46 21
47
48
49
50
51
52
53
54
55
56
57
58
59
60

1
2
3
4
5
6
7
8
9
10
11
12
13
14
15
16
17
18
19
20
21
22
23
24
25
26
27
28
29
30
31
32
33
34
35
36
37
38
39
40
41
42
43
44
45
46
47
48
49
50
51
52
53
54
55
56
57
58
59
60

22 **Abstract**

23 The monogenetic Quaternary La Garrotxa Volcanic Field forms part of the Catalan Volcanic Zone
24 (NE Iberian Peninsula), one of the alkaline volcanic provinces of the European rift system. It
25 harbours in total more than 50 basaltic monogenetic cones that range in age from the Middle
26 Pleistocene to the early Holocene and include cinder and scoria cones, lava flows, tuff rings and
27 maars. This study is the result of 10 years work, during which we conducted extensive fieldwork,
28 including the study of ephemeral outcrops and the stratigraphic logging of new water wells and
29 geotechnical drill holes, taking also into account the existing information gathered by recent
30 geophysical studies that have applied shallow geophysical methods to establish the substrate
31 geology of this volcanic field. As a result we have obtained a comprehensive volcanic stratigraphy
32 of the area that identifies the products of each single eruption, their relative stratigraphy and their
33 surface area. This volcanic stratigraphy constitutes an essential tool for understanding the evolution
34 of this volcanic field and for establishing a correct volcanic hazard assessment of the area, but it
35 also provides a precise reference for the Quaternary tephrochronology of the lake sediments in
36 neighbouring areas.

37
38 **KEYWORDS:** Quaternary volcanism, volcano-stratigraphy, monogenetic volcanism, Garrotxa
39 volcanic field, hazard assessment

40 Introduction

41 Volcanic terrains are characterised by the complex stratigraphic relationships of their
42 products whose causes include, variously, the extremely rapid depositional rates compared with
43 conventional sub-aerial and submarine sedimentary environments, the friable character of many
44 volcanic deposits, which facilitate their rapid erosion, the contrasting influence of topography on
45 the emplacement of volcanic products, and rapid changes in facies. Such complexity constitutes one
46 of the main obstacles when reconstructing the geological evolution of volcanic areas. This is even
47 more problematic in highly urbanised areas where construction activities modify the original
48 morphology of the area and hide many natural features, and where deposits are often lost to
49 quarrying. This may impose a limitation to construct a volcanic hazard model from such active
50 volcanic areas, as establishing correct stratigraphic relationships may be challenged due to the
51 ignorance of part of the volcanological record.

52 The stratigraphic and volcanological evolution of the different volcanic fields of the Neogene-
53 Quaternary volcanism associated with the European Cenozoic Rift System are still poorly known.
54 Although several detailed petrological and geochemical studies of this magmatic episode have been
55 conducted in recent decades aimed at understanding its petrogenesis and geodynamic constraints
56 (Wilson and Downes, 1991, 1992, 2006; Hoernle et al., 1995; Wilson and Bianchini, 1999; Wilson
57 and Petterson, 2001; Lustrino and Wilson, 2007), the eruptive history and geochronology of the
58 different areas where this volcanic activity occurred, are not well constrained. In many cases this
59 has hindered the definition of the evolution of the volcanism in each area, thereby generating
60 uncertainty around the relative age of volcanic episodes and recurrence cycles. It also complicates
61 any comprehensive hazard assessment in these areas, some of which have been active into Mid-
62 Holocene.

63 One of the least studied of these recent European volcanic areas is the Catalan Volcanic
64 Zone (Martí et al., 1992) located in the northeast of the Iberian Peninsula. Its activity started over 12
65 Ma ago and continued until the early Holocene. The Quaternary La Garrotxa Volcanic Field (GVF)

1
2 66 (Martí et al., 2011) is the youngest (Middle Pleistocene to early Holocene) and best preserved of
3
4 67 these volcanic areas. However, its surface outcrops are just part of the complex geology that has
5
6 68 been constructed during the over 700 ka of intermittent volcanism in this area. In this paper we
7
8 69 present a comprehensive volcanic stratigraphy of the GVF. This work is based on ten years of
9
10 70 systematic recognition and characterisation of all ephemeral outcrops exposed on construction sites
11
12 71 and data from all new wells and geotechnical boreholes. Geological data have been complemented
13
14 72 with results from recent geophysical studies on the substrate geology of the GVF (Bolós et al.,
15
16 73 2012, in press; Barde-Cabusson et al., 2013, 2014;), in order to obtain a more precise picture of the
17
18 74 subsoil geology of the area and to better define the corresponding stratigraphic relationships. We
19
20 75 describe the results obtained and discuss their implications for the study of the evolution of this
21
22 76 volcanic area and for assessing potential hazard and tephrochronological correlations in the area.
23
24
25
26
27

28 78 **Geological setting**

29
30 79 Situated in the northeast of the Iberian Peninsula, the Garrotxa Volcanic Field (GVF) is
31
32
33 80 part of the Catalan Volcanic Zone and one of the provinces of the Neogene–Quaternary alkaline
34
35 81 volcanism associated with the European rift system. It covers about 600 km² and is located between
36
37 82 the cities of Olot and Girona (Fig. 1). This basaltic volcanic field contains over 50 cones (including
38
39 83 both cinder and scoria cones), lava flows, tuff rings and maars dating from the Middle Pleistocene
40
41 84 to early Holocene that rest on upper Palaeozoic granites and schists, or on sedimentary Eocene and
42
43 85 Quaternary substrates. Available petrological and geochemical data indicate that the products of this
44
45 86 volcanic region range from strongly silica-undersaturated to nearly silica-saturated compositions
46
47 87 (Araña et al., 1983; López-Ruiz and Rodríguez-Badiola, 1985; Cebriá et al., 2000; Martí et al.,
48
49 88 1992). This region comprises a suite of intracontinental leucite, basanites, nepheline basanites and
50
51 89 alkali olivine basalts, which in most cases represent primary or nearly primary liquids (Cebriá et al.,
52
53 90 2000). The geochemical characteristics of these lavas are very similar to the analogous petrologic
54
55 91 types of other Cenozoic volcanics of Europe, which are intermediate between HIMU, DM and EM1
56
57
58
59
60

1
2
3
4
5
6
7
8
9
10
11
12
13
14
15
16
17
18
19
20
21
22
23
24
25
26
27
28
29
30
31
32
33
34
35
36
37
38
39
40
41
42
43
44
45
46
47
48
49
50
51
52
53
54
55
56
57
58
59
60

92 (Cebriá et al., 2000; Downes, 2001).

93 The GVF embraces two geographically distinct zones, the larger one located in the north in
94 the area of La Garrotxa and a southerly area that contains fewer but larger and more complex
95 volcanic edifices (Martí et al., 2011) (Fig. 1). Although both corresponding to tectonically
96 controlled depressions, the northern zone has a substrate of thick layers of Tertiary and Quaternary
97 sediments, whereas the southern zone is floored by unconsolidated Quaternary sediments in
98 combination with the Palaeozoic basement.

99 Volcanic activity in the GVF is characterised by numerous small cinder cones built during
100 short-lived monogenetic eruptions along tectonic related volcanic fissures. The total volume of
101 extruded magma in each eruption was between 0.01 and 0.2 km³ (DRE). Strombolian and
102 phreatomagmatic episodes alternated in most of these eruptions and gave rise to complex
103 stratigraphic sequences composed of a broad range of pyroclastic deposits (Martí et al., 2011;
104 Cimarelli et al., 2013). The eruption sequences differ from one cone to another and demonstrate that
105 the eruptions did not follow a common pattern, particularly in cases of magma/water interaction.
106 This complex eruptive behaviour may be related to the differing stratigraphic, structural and
107 hydrogeological characteristics of the substrate below each volcano rather than to any differences in
108 the physicochemistry of the erupting magmas, which are generally fairly homogeneous throughout
109 the GVF (Martí et al., 2011).

110 The eruptive fissures that controlled the volcanic activity in the GVF correspond to NNW-
111 SSE and NNE-SSW oriented Neogene tectonic structures (Cimarelli et al., 2013; Barde-Cabusson et
112 al., 2013, 2014; Bolós et al., in press). This suggests that the ascent and eruption of the magmas
113 originated at the base of the lithosphere (Martí et al., 1992) was guided by the same regional faults
114 system that bound the area's horsts and grabens. This explains the high magma ascent velocities
115 (0.2m/s) found in these volcanic materials, which together with the presence of mantle xenoliths
116 and lower crust cumulates suggest that some of the eruptive fissures and faults extended to the base
117 of the lithosphere (Martí et al., 1992).

1
2 118 An important part of the northern zone of the GVF now lies underneath the city of Olot
3
4 119 (almost 40,000 inhabitants), a highly industrialised and urbanised area covering about 30 km². The
5
6 120 deposits of the five recent volcanic cones (Montolivet, Montsacopa, La Garrinada, Bisaroques and
7
8 121 Ca l'Isidret) located in the middle of the city (Fig. 2) have been partially covered by or removed due
9
10 122 to urban and industrial construction. Furthermore, a dense carpet of vegetation covers other parts of
11
12 123 the GVF and thus the surface geology of the area is not always visible. Traditionally, these factors
13
14 124 have hampered geological mapping and stratigraphic correlations and in part explain the incomplete
15
16 125 knowledge of the volcanological evolution of this area.
17
18
19
20 126

21 127 **Methodology**

22
23
24 128 The lack of continuous outcrops due to partial erosion of the deposits, coverage by younger
25
26 129 products and/or human-induced modification of terrains due construction activities, as well as the
27
28 130 apparent similarity of most of these deposits, mean that stratigraphic correlation and the
29
30 131 determination of the relative ages of these outcrops is not a straightforward task. To sort out these
31
32 132 limitations we carried out extensive fieldwork including the study of ephemeral outcrops and the
33
34 133 stratigraphic logging of water wells and geotechnical drill holes (Fig. 3). In addition, we also
35
36 134 considered the existing information gathered by recent geophysical studies that have applied
37
38 135 shallow geophysical methods to establish the substrate geology of the GVF (Bolós et al., 2012, in
39
40 136 press; Barde-Cabusson et al., 2013, 2014). Finally, we also used basic petrology and geochemistry
41
42 137 including mineral chemistry to identify possible fingerprints that could establish a precise
43
44 138 correlation between these deposits and determine their relative stratigraphy, as it has been done in
45
46 139 similar studies (e.g.: García et al., 2014). However, in this case the results obtained were not
47
48 140 relevant to establish a systematic distinction of deposits from different eruptions based on
49
50 141 petrological criteria, so these results were not considered to establish our volcanic stratigraphy and
51
52 142 are not presented in this study. The use of precise petrological fingerprints with this type of volcanic
53
54 143 rock would require a much more detailed petrological study, which is beyond the main purpose of
55
56
57
58
59
60

1
2
3
4
5
6
7
8
9
10
11
12
13
14
15
16
17
18
19
20
21
22
23
24
25
26
27
28
29
30
31
32
33
34
35
36
37
38
39
40
41
42
43
44
45
46
47
48
49
50
51
52
53
54
55
56
57
58
59
60

144 this study.

145 We used as a reference the geological 1:25,000-scale maps of the Catalan Geological Survey
146 (IGC, 2003, 2007), which were substantially modified by the new data obtained in this work. A
147 shape file containing the new digital geological maps was combined with a 2-m resolution DEM of
148 the area using an open GIS platform (QGIS) to obtain a graphic representation of the volcanic
149 stratigraphy of the area. The legend of the maps includes the relative stratigraphy of the different
150 mappable units that were identified.

151 Field geology consisted of a revision of the existing geological maps and the remapping of
152 certain areas at different scales (1:5000 and 1:1000) using as a basis the topographic maps and
153 orthophotographs produced by the Catalan Geographic Institute (www.icc.cat). These resources
154 permitted us to identify most of the characteristics of the surface geology and, in particular, the
155 contact between the volcanic and non-volcanic units, the superficial extent of the volcanic units, the
156 direction of emplacement and position of vents, and a number of volcanic-related structural
157 lineations.

158 Fieldwork was completed via the study of ephemeral outcrops (Fig. 4) and the stratigraphic
159 logging of water wells and geotechnical drill holes (Fig. 3), which also provided information on the
160 subsoil geology. Construction in built-up areas occasionally exposes new outcrops and large
161 stratigraphic sections. However, the temporary nature of these outcrops is an important drawback
162 and if they are not documented immediately they run the risk of being quickly lost. The same
163 applies to geotechnical boreholes and wells. This information is frequently poorly recorded and
164 often lost among the myriad of documents handled by local administrative bodies.

165 Over the previous ten years we systematically studied most of the ephemeral outcrops in the
166 GVF created by urban, industrial and infrastructure construction, as well as new water wells and
167 geotechnical boreholes. In all, we described and catalogued almost 100 ephemeral outcrops (Fig. 3).
168 The methodology applied consisted of three different steps that were followed in all cases. First, we
169 designed a series of data sheets or templates for the systematic description of each ephemeral

1
2 170 outcrop (Fig. 5) with space for notes on a series of variables including outcrop code, type of
3
4 171 construction work, name of reviewer of the outcrop, location (UTM coordinates), a detailed field
5
6 172 description, photographs, geological cross-sections, a stratigraphic column, an interpretation of the
7
8 173 outcrop in the general geological context of the area, and other relevant observations. Second, we
9
10 174 maintained close links with local authorities and the Catalan Geological Survey to ensure that we
11
12 175 were warned well in advance of any new construction work in the area or any new wells or
13
14 176 boreholes. We also developed a protocol for obtaining information from any public construction
15
16 177 work planned at national level that was to be carried out in the study area. Lastly, all the information
17
18 178 obtained was incorporated into a geographical database developed using an open-access GIS
19
20 179 platform (QGIS, www.qgis.org). A shape file containing all the new digital geological map sections
21
22 180 was created with a 2-m-resolution DEM of the area.
23

24
25
26 181 During the period of data collection we conducted stratigraphic logging of the geotechnical
27
28 182 boreholes and water wells included in this study directly at each site during drilling operations. This
29
30 183 allowed us to identify the different stratigraphic units and to obtain samples that were later studied
31
32 184 at the laboratory. In most cases only cuttings were obtained from the drilling operations but they
33
34 185 permitted to identify the different stratigraphic units with a high degree of accuracy. Also, we
35
36 186 revised and incorporated, when relevant, information from previous boreholes recorded and
37
38 187 classified by the Catalan Geological Survey.
39

40
41 188 The criteria used to establish the relative stratigraphy of the volcanic units were their field
42
43 189 relationships, the stratigraphic relationships observed in boreholes and wells, morphometry-based
44
45 190 relative dating using the degradation of volcanic cones (see Kereszturi et al., 2013), paleomagnetic
46
47 191 correlations (Ll. Planagumà, unpublished data), the degree of alteration (weathering) of the volcanic
48
49 192 materials, the presence of interbedded fluvial terraces, and absolute dates (if available). To estimate
50
51 193 the volume of the deposits corresponding to the products of each eruption we took into account their
52
53 194 spatial distribution and thickness variations. We measured in the laboratory densities from field
54
55 195 samples from all types of volcanic materials (lavas, scoria, lapilli size pyroclasts, juvenile fragments
56
57
58
59
60

1
2 196 in PDC deposits) and obtained an average density for each type. Then, the calculated volumes
3
4 197 where converted into Dense Rock Equivalent volumes using a density of 2,53 for the magma that
5
6 198 we obtained from a glass made from a natural sample (Croscat lava flow) and applying the
7
8 199 equation: $DRE (km^3) = \text{volume of volcanic deposit } (km^3) * \text{density of volcanic deposit } (kg/m^3) /$
9
10 200 $\text{magma density } (kg/m^3)$, for each type of deposit belonging to the same eruption and then adding all
11
12 201 the values to obtain the total volume in DRE for each eruption.

13
14
15 202 To complement the geological information obtained from the field studies, we also took into
16
17 203 account the available geophysical information of the area, including gravity data, self-potential (SP)
18
19 204 maps and electrical resistivity tomography (ERT), obtained in previous studies by the same working
20
21 205 group (Bolós et al., 2012; in press; Barde-Cabusson et al., 2013, 2014). The combined interpretation
22
23 206 of the geological and geophysical data provided detailed information on the internal structure of
24
25 207 certain volcanic cones and the stratigraphy and shallow structure of the substrate on which the
26
27 208 volcanoes were emplaced.

28
29
30 209

31 32 33 210 **Volcanic stratigraphy vs. conventional stratigraphy**

34
35 211 Before presenting and discussing the results of this study it is worthwhile first analysing the
36
37 212 stratigraphic criteria used in this work. One of the key questions in understanding the evolution of
38
39 213 an active volcano or a recent volcanic field is the volcanic stratigraphy, that is, the stratigraphic and
40
41 214 chronological order in which the products of each eruption appear in the geological record. Volcanic
42
43 215 stratigraphy is an essential part of field studies in volcanic areas everywhere and is necessary for
44
45 216 generating geological maps, reconstructing the volcanological evolution and eruptive dynamics, and
46
47 217 studying the physical volcanology and tephrostratigraphy (Connor, 1990; Nemeth et al., 2001,
48
49 218 2012; Palladino et al., 2010; Branca et al., 2011; Guillbaud et al., 2011; Groppelli and Martí, 2013).

50
51
52 219 Fisher and Schmincke (1984) proposed the use of volcanic activity units combining
53
54 220 stratigraphic and volcanological criteria, a method that has the advantage of directly linking
55
56 221 volcanic activity with the resulting stratigraphic record; the main unit is considered to be the
57
58
59
60

1
2 222 individual eruption (Member) (Table 1). Another advantage of volcanic stratigraphic units is that
3
4 223 they are very useful for understanding the eruptive dynamics of a given eruption or set of eruptions.
5
6 224 However, they do not take into account inter-eruptive phenomena (e.g. debris flow, lahars, etc.),
7
8 225 which may represent important elements in the life of a volcano and can have important
9
10 226 chronological implications (Groppelli and Martí, 2013). Instead of this some authors (e.g. Groppelli
11
12 227 et al., 2005; Giordano et al., 2010; Palladino et al., 2010; Branca et al., 2011; Cimarelli et al., 2013)
13
14 228 prefer to use unconformity related units (synthems) in the study of volcanic successions. These type
15
16 229 of stratigraphic units, initially defined by Chang (1975) and Salvador (1987) for sedimentary
17
18 230 terrains, enable the time evolution of a volcanic area to be correlated with geological events acting
19
20 231 on local, regional or global scales; an example would be the correlation of the timing and styles of
21
22 232 volcanism in a volcanic province with regional tectonics (Palladino et al., 2010). In a similar way,
23
24 233 volcanic activity may lead to the incorporation of a large amount of debris into a sedimentary
25
26 234 system, thereby changing its dynamics and the sedimentation vs. erosional rates (Smith, 1991). All
27
28 235 this may create normally low-rank unconformities in the stratigraphic record of an area that
29
30 236 correspond to distinct volcanological-geological events. However, unconformity based units often
31
32 237 show non-isochronous boundaries. This is the reason why geological units, members, formations
33
34 238 and groups are preferred in many volcano-stratigraphic studies and also in this study.

35
36
37
38
39 239 In the GVF the recorded volcanism dates from the Middle Pleistocene to the early Holocene
40
41 240 (Araña et al., 1983; Guerin et al., 1985; Lewis et al., 2000). During this period no significant
42
43 241 geological changes have been recorded in the region (Martí et al., 1992) and so the observed
44
45 242 stratigraphic unconformities are very local in scale and due to the irregular emplacement of volcanic
46
47 243 products and not to any more widespread geological changes. In addition to this, the lack of
48
49 244 geochronological data hampers the identification of groups of volcanic eruptions that could have
50
51 245 occurred during the same time interval. For these reasons, we chose to use the formal volcano-
52
53 246 stratigraphic unit member - in the sense defined by Fisher and Schminke (1984) – and mapped the
54
55 247 eruptive units associated with each of the volcanic structures of this field.
56
57
58
59
60

1
2 248 Using the member as the fundamental volcano-stratigraphic unit we grouped all the products
3
4 249 of a single eruption into the same stratigraphic member and distinguished each one from those
5
6 250 pertaining to other eruptions or members. In each member, we distinguished different units
7
8 251 corresponding to the products of the different pulses of a single eruption. This permitted us to
9
10 252 characterise the eruption sequences and their mechanisms and understand how volcanism evolved
11
12 253 with time; this in turn enabled us to identify any changes in the eruption style, the location of the
13
14 254 vents, the size of the eruptions, the characteristics of their products, and their relative stratigraphy
15
16 255 (age) and areal extent (Figs. 4 and 5). The information provided in this format is crucial not only
17
18 256 for understanding the evolution of this volcanic area but also for the description of any potential
19
20 257 hazards.
21
22
23
24 258

259 **Results**

260 The main outcome of this study is a new digital volcano-stratigraphic map of the GVF at
261 scale 1:2000, which is summarised in Figs. 6 and 7. These new volcano-stratigraphic framework
262 complements a previous study focused on the description of the successions of deposits
263 characteristic of the GVF volcanoes (Martí et al., 2011), and improves the recent stratigraphy
264 proposed by Cimarelli et al., 2013, which is based on different stratigraphic criteria (synthoms) and
265 is partially incomplete due to the lack of subsoil information and that from the ephemeral outcrops.

266 Table 2 summarises all the stratigraphic members (55 in all) that were identified in this
267 study. The members are placed from the youngest (top) to the oldest (bottom) according to their
268 relative stratigraphy (Fig. 8). Also given is an indication of whether the age is relative (i.e. it was
269 established on the basis of observable stratigraphic relationships) or absolute (i.e. a
270 geochronological – isotopic or paleontologic – date is available), as well as the corresponding
271 reference source and the calculated erupted volumes (in Dense Rock Equivalent, DRE) when
272 available.

273 The precision in establishing the stratigraphic relationships between the volcanic materials

1
2 274 studied decreased progressively with their age, as the younger materials were better exposed and
3
4 275 preserved, and located at shallower depths than the older ones, which were often only accessible
5
6 276 through boreholes and wells or deep ephemeral outcrops. Due to the incomplete exposure some of
7
8 277 the older units could have been missed. However, the systematics used in the construction of this
9
10 278 volcanic stratigraphy will allow the incorporation of new stratigraphic units or the modification of
11
12 279 their relative stratigraphic position in an easy way and without disturbing the rest of the information
13
14 280 included.

15
16
17 281 When the source area or vent of the different volcano-stratigraphic units or members was
18
19 282 plotted on a structural map of the area with the successive numbers of their relative ages (1 for the
20
21 283 youngest, 55 for the oldest) indicated (Fig. 9), it becomes evident that most members are located on
22
23 284 NNW-SSE-oriented Neogene fractures and faults, thereby confirming the findings of other authors
24
25 285 (Martí et al, 2011; Cimarelli et al., 2013; Barde-Cabusson et al., 2014; Bolós et al., in press). These
26
27 286 members have a rather scattered time-space distribution, albeit with a tendency for older eruptions
28
29 287 (Middle Pleistocene) to be concentrated towards the north of the area. However, we observed no
30
31 288 structural indicator that could suggest a similar tendency in the Neogene faults as suggested by
32
33 289 Cimarelli et al (2013). Some of the eruptions developed in multiple phases and with multiple vents
34
35 290 along the same eruption fissure (Martí et al., 2011), and are thus responsible for some of the clusters
36
37 291 of vents that appear in Fig 8. However, a comparison of the different eruptions failed to identify any
38
39 292 apparent concentration of vents at any specific location or at any specific time.

40
41
42 293 The volcanic materials of the studied stratigraphic units consist of lava flows and different
43
44 294 types of fallout and pyroclastic density current deposits derived from Strombolian and
45
46 295 phreatomagmatic eruptions. Martí et al. (2011) pointed out that different eruption sequences,
47
48 296 corresponding either to purely magmatic or phreatomagmatic episodes and alternating Strombolian
49
50 297 and phreatomagmatic phases, characterise the volcanoes of La Garrotxa. However, they did not
51
52 298 identified neither the spatial relationships among the products of the different eruptions nor their
53
54 299 relative stratigraphy. Our field stratigraphic study did not reveal any apparent time or space
55
56
57
58
59
60

1
2 300 variation in the style of volcanism, thereby suggesting that differences in eruptive behaviour could
3
4 301 be related to local variations in the characteristics (e.g. hydrogeology) of the substrate rather than to
5
6 302 geological changes on a major scale.
7

8
9 303 The calculated volumes shown in Table 2 are all minimum estimates of the DRE and
10
11 304 represent the minimum volume of magma erupted in each case and, consequently, the magnitude of
12
13 305 the eruption. Not all calculated volumes have the same degree of accuracy, since not all deposits are
14
15 306 completely exposed. This implies that the record presented here is incomplete and should be treated
16
17 307 with care if used in further studies. The volumes obtained lie between 0.01–0.03 km³. However, a
18
19 308 few eruptions (Crosca (2), Puig Subià (18), Crosca de Sant Dalmai (21), Puig de Banyà del Boc
20
21 309 (32), Garrinada (35), Puig d'Àdri (45) and Puig de l'Ós (51)) generated larger volumes, up to 0.2
22
23 310 km³, in the case of Crosca.
24
25

26 311 Other important results derive from this stratigraphic study at a more local and detailed
27
28 312 level. The use of ephemeral outcrops, wells and boreholes (this work), in combination with results
29
30 313 from the application of shallow geophysical methods (Bolós et al., 2012, in press; Barde-Cabusson,
31
32 314 et al., 2013, 2014), permitted to obtain the volcanic stratigraphy of the highly urbanised – and,
33
34 315 consequently, with a poorly exposed geology – area of Olot (Fig. 9), thus improving previous maps
35
36 316 (Mallarach, 1982; IGC, 2003, 2007; Cimarelli et al., 2013) that could not show the same degree of
37
38 317 detail. In this sector of the GVF we found very complex stratigraphic relationships between the
39
40 318 city's five volcanic cones (Garrinada, Montsacopa, Bisaroques, Ca l'Isidret and Montolivet) (Fig.
41
42 319 10). In previous studies based on the surface geology observable in this built-up area, three of these
43
44 320 volcanoes (Montolivet, Garrinada and Montsacopa) were assumed to belong either to the same
45
46 321 eruption (Calderón et al, 1906; Sant Miguel de la Cámara and Marcet Riba, 1926; Mallarach and
47
48 322 Riera, 1981) or to different eruptions occurring along the same NE-SW fracture (Gisbert et al.,
49
50 323 2009). Our study reveals that, in fact, each cone corresponds to a different eruption, all of which are
51
52 324 situated along NNW-SSE-oriented fissures. The study of the ephemeral outcrops enabled us to
53
54 325 identify the stratigraphic relationships between deposits and discover that each succession of
55
56
57
58
59
60

1
2 326 deposits was separated from the next by stratigraphic discontinuities (i.e. erosion surfaces, and
3
4 327 paleosoils), which suggest that several thousand years elapsed between each eruption. The oldest of
5
6 328 these volcanoes is now thought to be La Garrinada and the youngest Montolivet. In addition, we
7
8 329 identified a previously unrevealed volcanic cone (Ca l'Isidret) that formed from a separate vent
9
10 330 during the eruption of the Bisaroques volcano (Fig. 10). The volcanic fissures that formed these five
11
12 331 cones run all in a NNW-SSE direction, as do most of the other eruptive fissures identified in this
13
14 332 study.

15
16
17 333 Moreover, in the case of La Garrinada, we used an ephemeral outcrop to complete the
18
19 334 stratigraphic sequence partially established by Gisbert et al. (2009), thus providing better constraints
20
21 335 to interpret its eruption sequence. Also, the study of 30 ephemeral outcrops around Montsacopa
22
23 336 (Fig. 11), combined with a revision of existing conventional outcrops, enabled us to identify the
24
25 337 different vents and products generated during its construction, not envisaged in previous studies
26
27 338 (e.g.: Martí et al., 2011; Cimarelli et al., 2013). The construction of this volcano resulted from a
28
29 339 multivent fissural eruption. In total we identified up to five different vents on Montsacopa: a
30
31 340 central cone and crater, which was the only previously known cone, two other vents whose products
32
33 341 are mostly covered by those emitted from the main crater, and scoria deposits that were generated
34
35 342 by two further vents. This multivent eruption included Strombolian and phreatomagmatic phases
36
37 343 that generated a large variety of deposits including fallout, ballistic ejecta, pyroclastic density
38
39 344 currents and lava flows (Fig. 10).

40
41
42 345 Another example of complex multivent fissure fed eruption is illustrated by two of the
43
44 346 largest volcanoes in the GVF, Croscat and Santa Margarida (Figs. 8 and 12). Our results confirm
45
46 347 what was envisaged by Martí et al (2011) in the sense these two volcanoes, together with La
47
48 348 Pomareda scoria vent, formed during the same eruption along the same fissure and showing very
49
50 349 different eruption dynamics. The data obtained in this study from two boreholes and one ephemeral
51
52 350 outcrop confirm the existence of a phreatomagmatic ash layer formed during the opening phase of
53
54 351 the Santa Margarida crater, which is conformably underlying La Pomareda and Croscat successions.
55
56
57
58
59
60

1
2 352 This ash layer lies on a thick paleosoil, thus indicating the existence in this area of a significant
3
4 353 temporal interruption of volcanic activity before this last eruption. These boreholes also show the
5
6 354 existence of more than 100 m of pyroclastic materials from La Pomareda and Crosdat not exposed
7
8 355 at surface, and how the La Pomareda scoria conformably underlies the Crosdat succession (Fig. 8),
9
10 356 mostly formed by an initial scoria and a thick sequence of lapilli size fallout, which mostly extend
11
12 357 towards the east, conformably overlying the Santa Margarida crater and deposits. These
13
14 358 conformable stratigraphic relationships and the absence of paleosoils or erosion surfaces between
15
16 359 the deposits suggest that these three vents, in fact, formed during the same eruption.
17
18
19
20 360

21 361 **Discussion and conclusions**

22
23
24 362 The study of ephemeral outcrops and the stratigraphic logging of water wells and
25
26 363 geotechnical drill holes, combined with surface geology and results from shallow geophysical
27
28 364 studies, proves to be an efficient way of reconstructing the geology and volcanic stratigraphy of
29
30 365 recent volcanic fields and, in particular, of highly urbanised areas in which increasing construction
31
32 366 and the occupation of the soil hamper direct observation. The pioneering work conducted in La
33
34 367 Garrotxa Volcanic Field, studying and cataloguing all new ephemeral outcrops and water wells and
35
36 368 geotechnical boreholes (almost 100) over a period of ten years, has enabled us to (i) establish a
37
38 369 detailed stratigraphy of the whole volcanic succession, from the Middle Pleistocene to the early
39
40 370 Holocene, (ii) complete a detailed volcanological map of this volcanic field (which includes the city
41
42 371 of Olot), and (iii) reinterpret a number of eruptive events. Likewise, our knowledge of the relative
43
44 372 geochronology and extension of the most recent volcanic deposits has also improved. Despite
45
46 373 revealing no clear pattern of the time-space evolution of this volcanism without a more precise
47
48 374 statistical analysis, a concentration of the oldest eruptions towards the north and east of the area can
49
50 375 be inferred from the results. Most of the volcanic eruptions (members) identified in this study
51
52 376 concentrate in what we refer to as the northern sector of the GVF (Fig. 6) and far fewer are found in
53
54 377 the southern sector (Fig. 7). This difference in the concentrations of the volcanic vents between the
55
56
57
58
59
60

1
2 378 two sectors is not time-controlled since eruptions of similar ages have occurred in both sectors (see
3
4 379 Table 2).

5
6 380 Despite their complexity, we observed no major geological changes in the area that could
7
8 381 justify the stratigraphic relationships in the volcanic materials of the GVF. We attribute all the
9
10 382 observed stratigraphic discontinuities and unconformities to either minor, inter-eruptive and syn-
11
12 383 eruptive erosional and depositional episodes, to non-depositional hiatus corresponding to the non-
13
14 384 uniform aerial distribution of the volcanic materials erupting from the vents, or – above all – to the
15
16 385 fact that volcanic materials do not always emplace according to the principle of superposition, in
17
18 386 particular when younger materials emplace on deeply eroded older ones. The style of the volcanism
19
20 387 does not show any significant variation along the stratigraphic succession. The differences observed
21
22 388 in the deduced eruption sequences (e.g. the alternation of Strombolian and phreatomagmatic phases)
23
24 389 (see Martí et al 2011 and Cimarelli et al 2013) of the different members should be interpreted as due
25
26 390 to local variations in the characteristics of the substrate rather than to any geological changes on a
27
28 391 major scale. Similarly, the volume of erupted magma in those cases for which it could be calculated
29
30 392 is mostly of the order of $0.02 \text{ km}^3 \pm 0.01$, which indicates that most of the eruptions were low
31
32 393 magnitude monogenetic eruptions. The trends and outliers observed in these estimated volumes
33
34 394 require a more detailed investigation that was beyond the scope of this study.

35
36
37
38
39 395 At a more detailed level, the results obtained help demonstrate the importance of access to
40
41 396 the subsoil geology if a correct interpretation of such a complex stratigraphic succession, marked by
42
43 397 multiple but relatively small and irregularly distributed depositional (and erosional) events, is to be
44
45 398 attempted; this is the case of many Quaternary monogenetic volcanic fields and, in particular, in
46
47 399 highly urbanised areas. In this study we were able to identify the volcanic stratigraphy buried below
48
49 400 the city of Olot and other sectors of the volcanic field, thereby providing a correct interpretation that
50
51 401 previously had always depended on incomplete observations. This complicates the reconstruction of
52
53 402 the eruption dynamics and may induce significant miscalculations in hazard assessments due to
54
55 403 errors in the inferred eruptive scenarios resulting from a lack of geological information from built-
56
57
58
59
60

1
2 404 up areas.

3
4 405 In conclusion, the proposed volcanic stratigraphy offers the basis on which to built further
5
6 406 studies on the GVF. It also provides a precise reference for the Quaternary tephrochronology of the
7
8 407 lake sediments in neighbouring areas. The role of these studies in the reconstruction of the
9
10 408 palaeoclimate histories is important to understand sedimentological variability and climate change.
11
12 409 In the case of northeastern Iberian Peninsula the presence of Late Pleistocene tephra layers coming
13
14 410 from the GVF in some lake sediments (e.g. Högbig et al., 2012) help to establish stratigraphic and
15
16 411 geochronological markers. A precise correlation with eruptive episodes identified in this study will
17
18 412 provide a constraint for the Pleistocene evolution of this area, but will also contribute to better
19
20 413 estimate the size of these eruption by characterising more precisely their areal extend and volume of
21
22 414 erupted magma. Finally, studies like this one represent a step forward in the preservation of the
23
24 415 geological heritage of areas such as the GVF, by providing the basic knowledge on their evolution
25
26 416 but also by enhancing the importance of their geological values in front of potential threats imposed
27
28 417 by the demographic expansion of modern societies.
29
30
31

32 418

33
34
35 419 **Acknowledgements:**

36 420

37
38
39 421 This study was partially funded by the *Beca Ciutat d'Olot* and the European Commission (FT7
40
41 422 Theme: ENV.2011.1.3.3-1; Grant 282759: "VUELCO"). We would like to thank La Garrotxa
42
43 423 Volcanic Zone Natural Park for their support and logistical help during this research. With thank
44
45 424 Shan Cronin, Patrick Bachelery and Antonio Brum da Silveira for their throughout and constructive
46
47 425 reviews. The English text was corrected by Michael Lockwood.
48
49

50 426

51 427

52
53
54
55 428 **REFERENCES**

56
57 429 Araña, V., Aparicio, A., Martín-Escorza, C., García Cacho, L., Ortiz, R., Vaquer, R., Barberi, F.,
58
59
60

- 1
2 430 Ferrara, G., Albert, J., Gassiot, X., 1983. El volcanismo Neógeno-Cuaternario de Catalunya:
3
4 431 caracteres estructurales, petrológicos y geodinámicos. *Acta Geologica Hispánica* 18, 1–17.
5
6 432 Barde-Cabusson, S., Bolós, X., Pedrazzi, D., Lovera, R., Serra, G., Martí, J., Casas, A., 2013.
7
8 433 Electric resistivity tomography revealing the internal structure of monogenetic volcanoes.
9
10 434 *Geophysical Research Journal*, 40, 1–6, doi:10.1002/grl.50538.
11
12 435 Barde-Cabusson, S., Gottsmann, J., Martí, J., Bolós, X., Camacho, A., Geyer, A., Planagumà, Ll.,
13
14 436 Ronchin, E., Sánchez, A., 2014. New insights on a monogenetic volcanic field from gravity
15
16 437 and self-potential measurements. *Bulletin of Volcanology*, 76:788. doi:[10. 1007/ s00445-013-](https://doi.org/10.1007/s00445-013-0788-0)
17
18 438 [0788-0](https://doi.org/10.1007/s00445-013-0788-0)
19
20
21 439 Branca S., Coltelli M., Groppelli G., Lentini F., 2011. Geological map of Etna volcano, 1:50,000
22
23 440 scale, *Italian Journal of Geoscience*, 130, n. 3, pp. 265-291.
24
25
26 441 Bolós, A., 1925. L'estació paleontològica del Pont de Ferro i algunes consideracions sobre el
27
28 442 vulcanisme olotí. *But. ICHN*, 2^a sèrie. V, 4. Barcelona.
29
30
31 443 Bolós, X., Barde-Cabusson, S., Pedrazzi, D., Martí, J., Casas, A., Himi, M., Lovera, R., 2012.
32
33 444 Investigation of the inner structure of La Crosa de Sant Dalmai maar (Catalan Volcanic Zone,
34
35 445 Spain). *Journal of Volcanology and Geothermal Research* 247–248, 37-48.
36
37
38 446 Bolós, X., Barde-Cabusson, S., Pedrazzi, D., Martí, J., Casas, A., Lovera, R., Nadal-Sala, D., in
39
40 447 press. Geophysical exploration on the subsurface geology of La Garrotxa monogenetic
41
42 448 Volcanic Field (NE Iberian Peninsula). *International Journal of Earth Science*.
43
44
45
46 449 Burjachs, F., 1985. Evolució de la vegetació i paleoclimatologia des de fa més de 85.000 anys a la
47
48 450 regió d'Olot. Anàlisi pol·línica del Pla de l'Estany (Sant Joan les Fonts, la Garrotxa). *Vitrina:*
49
50 451 publicació del Museu Comarcal de la Garrotxa, a Recerca Científica del Parc Natural de la
51
52 452 Zona Volcànica de la Garrotxa. 1982-1992. 1, 49-56.
53
54
55 453 Cebriá. J. M., López-Ruiz, J., Doblas, M., Oyarzun, R., Hertogen, J., Benito, R., 2000.
56
57 454 Geochemistry of the Quaternary alkali basalts of Garrotxa (NE Volcanic Province, Spain): a
58
59
60

- 1
2 455 case of double enrichment of the mantle lithosphere. *Journal of Volcanology and Geothermal*
3
4 456 *Research*, 112, 175-187.
- 5
6
7 457 Calderón, S., Cazorro, M., Fernández Navarro, L., 1906. Memoria sobre las formaciones volcánicas
8
9 458 de la provincia de Gerona. *Memorias de Real Sociedad Española de Historia Natural*, t. IV,
10
11 459 memoria 5^a, Madrid, 165–489.
- 12
13 460 Cimarelli, C., Di Traglia, F., de Rita, D., Gimeno Torrente, D., Fernandez Turiel, J.L., 2013. Space–
14
15 461 time evolution of monogenetic volcanism in the mafic Garrotxa Volcanic Field (NE Iberian
16
17 462 Peninsula). *Bulletin of Volcanology* 75, 758.
- 18
19
20 463 Chang K.H., 1975. Unconformity bounded stratigraphic units, *Geological Society of America*
21
22 464 *Bulletin*, 86, 11, 1544-1552,
- 23
24
25 465 Connor, C.B., 1990. Cinder cone clustering in the TransMexican volcanic belt: implication for
26
27 466 structural and petrologic models. *Journal of Geophysical Research* 95, 19395–19405
- 28
29
30 467 Di Traglia, F., Cimarelli, C., de Rita, D., Gimeno Torrente, D., 2009. Changing eruptive styles in
31
32 468 basaltic explosive volcanism: examples from Croscat complex scoria cone, Garrotxa Volcanic
33
34 469 Field (NE Iberian Peninsula). *Journal of Volcanology and Geothermal Research* 180, 89–109.
- 35
36 470 Donville, B., 1973. *Géologie Néogène et ages des éruptions volcaniques de la Catalogne orientale*.
37
38 471 *These doct. Fac. Sciences. Université Paul Sabatier. Tolosa de Llenguadoc*.
- 39
40
41 472 Downes, H., 2001. Formation and modification of the shallow sub-continental lithospheric mantle:
42
43 473 a review of geochemical evidence from ultramafic xenolith suites and tectonically emplaced
44
45 474 ultramafic massifs of Western and Central Europe. *Journal of Petrology*, 42, 233-250.
- 46
47 475 Fisher, R.V., Schmincke, H.U., 1984. *Pyroclastic rocks*, Springer Verlag, 472 pp.
- 48
49
50 476 García, O., Guzmán, S., Martí, J., 2014. Stratigraphic correlation of Holocene phonolitic explosive
51
52 477 episodes of the Teide–Pico Viejo Volcanic Complex, Tenerife. *Journal of the Geological*
53
54 478 *Society*, London 86. <http://dx.doi.org/10.1144/jgs2013-086>
- 55
56
57 479 Gisbert, G., Gimeno, D., Fernandez-Turiel, J.L., 2009. Eruptive mechanisms of the Puig de La
58
59 480 Garrinada volcano (Olot, Garrotxa volcanic field, Northeastern Spain): a methodological study
60

- 1
2 481 based on proximal pyroclastic deposits. *Journal of Volcanology and Geothermal Research* 180,
3
4 482 259–276.
- 5
6 483 Giordano G., Mattei M., Funicello F., 2010. Geological map of the Colli Albani Volcano, in
7
8 484 Funicello F. Giordano G. (Eds), *The Colli Albano Volcano*, Special Publication of IAVCEI, 3,
9
10 485 Geological Society, London.
- 11
12
13 486 GropPELLI G., Norini G., 2005. From geological map to volcanic hazard evaluation on Mount Etna,
14
15 487 Italy: Methodology and examples based on GIS analyses, in J.C. Thouret, C. Ollier, B. Joyce
16
17 488 (Eds), *Zeitschrift für Geomorphologie*, Special Issue on “Volcanic landforms, processes and
18
19 489 hazards”, vol. 140, pp. 167-179.
- 20
21
22 490 GropPELLI, G., Martí, J., 2013. Volcanic Stratigraphy – State of the art. Proceedings of STRATI 2013,
23
24 491 First International Congress on Stratigraphy, Ciências de la Terra (UNL), Lisboa, 18, 99-104.
- 25
26 492 Guérin, G., Behamoun, G., Mallarach, J.M., 1985. Un exemple de fusió parcial en medi continental.
27
28 493 El vulcanisme quaternari de la Garrotxa. Publicació del Museu Comarcal de la Garrotxa,
29
30 494 Vitrina 1, 19–26.
- 31
32
33 495 Guérin, G., Valladas, G., 1980. Un exemple de fusió parcial en medi continental. El vulcanisme
34
35 496 quaternari de la Garrotxa. Thermoluminescence dating of volcanic plagioclases. *Nature*, 286,
36
37 497 697-699.
- 38
39
40 498 Guilbaud, M.N, Siebe, C., Layer, P., Salinas, S., Castro-Govea, R., Garduño-Monroy, V.H., Le
41
42 499 Corvec, N., 2011. Geology, geochronology, tectonic setting of the Jorullo volcano region,
43
44 500 Michoacán, México. *Journal of Volcanology and Geothermal Research* 201, 97–112
- 45
46 501 Hedberg, H.D. (ed.), 1976, *International Stratigraphic Guide - A guide to stratigraphic classification,*
47
48 502 *terminology, and procedure*, 1st edition. Wiley & Sons, Inc., 200 pp.
- 49
50
51 503 Höbig, N., Weber, M. E., Kehl, M., Weniger, G. C., Julià, R., Melles, M., Fu□löp, R. H., Vogel,
52
53 504 H., Reicherter, K., 2012. Lake Banyoles (northeastern Spain): A Last Glacial to Holocene
54
55 505 multi-proxy study with regard to environmental variability and human occupation. *Quaternary*
56
57 506 *International*, 274, 205-218.
- 58
59
60

- 1
2 507 Hoernle, K., Zhang, Y.S., Graham, D., 1995. Seismic and geochemical evidence for large-scale
3
4 508 mantle upwelling beneath the eastern Atlantic and western and central Europe. *Nature* 374,
5
6 509 34–9.
7
8 510 IGC (Institut Geològic de Catalunya), 2003. Cartografia Temàtica. Sèrie Mapa Geològic de
9
10 511 Catalunya. Olot. Available at
11
12 512 http://www1.igc.cat/web/gcontent/pdf/mapes/igc_GT1_257q12_75x22_v1g.pdf
13
14
15 513 IGC (Institut Geològic de Catalunya), 2007. Carta vulcanològica de la Zona Volcànica de La
16
17 514 Garrotxa. Institut Geològic de Catalunya. scale 1:25,000
18
19 515 Kereszturi, G., Geyer, A., Martí, J., Nemeth, K., Dóniz-Pérez, F. J., 2013. Evaluation of
20
21 516 morphometry-based dating of monogenetic volcanoes—a case study from Bandas del Sur,
22
23 517 Tenerife (Canary Islands). *Bulletin of Volcanology* 75:734 DOI 10.1007/s00445-013-0734-1
24
25
26 518 Lewis, C. L., Vergés, J., Marzo, M. 2000. High mountains in a zone of extended crust: Insights into
27
28 519 the Neogeno-Quaternary topographic development of Northeastern Iberia. *Tectonics*, 19, 86-
29
30 520 102
31
32
33 521 López-Ruiz, J., Rodríguez-Badiola, E., 1985. La región volcánica Mio-Pleistocena del NE de
34
35 522 España. *Estudios Geológicos*, 41, 105-126.
36
37 523 Lustrino, M., Wilson, M., 2007. The circum-Mediterranean anorogenic Cenozoic igneous province.
38
39 524 *Earth-Science Reviews* 81 1–65
40
41
42 525 Mallarach, J.M., 1982. Carta geològica de la regió volcànica d'Olot. *Litologia i geomorfologia*.
43
44 526 1120.000. Ed Maber, Ajuntament d'Olot.
45
46 527 Mallarach, J.M., 1984. Nota sobre les darreres erupcions volcàniques quaternàries olotines. *Revista*
47
48 528 *de Girona*. Núm. 107.
49
50 529 Mallarach, J.M., 1998. El vulcanisme prehistòric de Catalunya *Revista de Girona*. Núm. 107. 322.
51
52
53 530 Mallarach, J.M., Riera, M., 1981. *Els volcans olotins i el seu paisatge*. Editorial Serpa, Barcelona.
54
55 531 250 pp.
56
57 532 Martí, J., Mallarach, J.M., 1987. Erupciones hidromagmáticas en el volcanismo cuaternario de Olot.
58
59
60

- 1
2 533 Estudios Geológicos 43, 31–40.
3
4 534 Martí, J., Mitjavila, J., Roca, E., Aparicio, A., 1992. Cenozoic magmatism of the Valencia trough
5
6 535 (Western Mediterranean): relation between structural evolution and Volcanism.
7
8 536 Tectonophysics 203, 145–166.
9
10 537 Martí, J., Planagumà, L., Geyer, A., Canal, E., Pedrazzi, D., 2011. Complex interaction between
11
12 538 Strombolian and phreatomagmatic eruptions in the Quaternary monogenetic volcanism of the
13
14 539 Catalan Volcanic Zone (NE of Spain). Journal of Volcanology and Geothermal Research 201,
15
16 540 178–193.
17
18 541 Murphy M.A., Salvador A., (eds.), 1999. *International Stratigraphic Guide -An abridged edition*,
19
20 542 Episodes, 22, no. 4, pp. 255-271.
21
22
23
24 543 Nemeth, K., Martin, U., Harangi, S., 2001. Miocene phreatomagmatic volcanism at Tihany
25
26 544 (Pannonian Basin, Hungary). Journal of Volcanology and Geothermal Research 111 (1–4),
27
28 545 111–135.
29
30
31 546 Nemeth, K., Cronin, S. J., Smith, I. E. M., Flores, J. A., 2012. Amplified hazard of small-volume
32
33 547 monogenetic eruptions due to environmental controls, Orakei Basin, Auckland Volcanic Field,
34
35 548 New Zealand. Bulletin of Volcanology, DOI 10.1007/s00445-012-0653-6
36
37
38 549 Owen, D., 2009. How to use stratigraphic terminology in papers, illustrations, and talks.
39
40 550 Stratigraphy, 6, 106-116.
41
42
43 551 Palladino D.M., Simei S., Sottili G., Trigila R., 2010. Integrated approach for the reconstruction of
44
45 552 stratigraphy and geology of Quaternary volcanic terrains: an application to the Vulsini
46
47 553 Volcanoes (central Italy), in G. Gropelli & L. Viereck-Goette (Eds.), Stratigraphy and geology
48
49 554 of volcanic areas, The Geological Society of America Special Paper 464, pp. 63-84.
50
51
52 555 Salvador A., 1987. Unconformity-bounded stratigraphic units. Geological Society of America
53
54 556 Bulletin, 98, 232-237.
55
56
57 557 Salvador A. (Ed.), 1994, *International Stratigraphic Guide. A guide to stratigraphic classification*,
58
59
60

- 1
2 558 *terminology, and procedure*. The International Union of Geological Sciences and the
3
4 559 Geological Society of America, 214 pp.
5
6
7 560 San Miguel de la Cámara, M., Marcet Riba, J., 1926. Región Volcánica de Olot, Extracto de la Guía
8
9 561 “Cataluña” Excursión C-4, XIV Congreso Geológico Internacional, Imprenta Sobrinos de
10
11 562 López Robert y Cia., Barcelona, 39–214.
12
13 563 Wilson, M., Bianchini, G., 1999. Tertiary–Quaternary magmatism within the Mediterranean and
14
15 564 surrounding regions. In: Durand, B., Jolivet, L., Horvath, F., Seranne, M. (Eds.), *The*
16
17 565 *Mediterranean Basins: Tertiary extension within the Alpine Orogen*. Geological Society of
18
19 566 London, vol. 156, pp. 141–168.
20
21
22 567 Wilson, M., Downes, H., 1991. Tertiary–Quaternary extension related alkaline magmatism in
23
24 568 western and central Europe. *Journal of Petrology*. 32, 811–849.
25
26
27 569 Wilson, M., Downes, H., 1992. Mafic alkaline magmatism associated with the European Cenozoic
28
29 570 rift system. *Tectonophysics* 208, 173– 182.
30
31 571 Wilson, M., Downes, H., 2006. Tertiary–Quaternary intra-plate magmatism in Europe and its
32
33 572 relationship to mantle dynamics. In: Gee, D., Stephenson, R. (eds.) *European Lithosphere*
34
35 573 *Dynamics*, Geological Society of London Memoire 32, 147–166.
36
37
38 574 Wilson, M., Patterson, R., 2001. Intraplate magmatism related to short wavelength convective
39
40 575 instabilities in the upper mantle: evidence from the Tertiary–Quaternary volcanic province of
41
42 576 western and central Europe. In: Ernst, R.E., Buchan, K.L. (Eds.), *Mantle Plumes: Their*
43
44 577 *Identification Through Time*. Geological Society of America Special Paper, vol. 352, pp. 37–
45
46 578 58.
47
48
49
50
51
52
53
54
55
56
57
58
59
60

1
2 579 **List of figures**
3

4 580 Figure 1. Map of the study area. a) Simplified map of the distribution of the European rift system.

5
6 581 b) Simplified geological map of the Catalan Volcanic Zone (Modified from Guérin et al., 1985). c)

7
8
9 582 Geographic distribution of the Garrotxa Quaternary volcanic field
10

11
12 583
13

14 584 Figure 2. Aerial view of the city of Olot and its volcanic cones.
15

16 585
17
18

19 586 Figure 3. Location of the studied ephemeral outcrops, water wells and geotechnical drill holes.
20

21 587
22

23 588 Figure 4. Example of an ephemeral outcrop (left) from Montsacopa member, visible during the
24
25 construction of a new building.
26

27 589
28 590
29

30 591 Figure 5. Data sheet designed for the systematic study and cataloguing of ephemeral outcrops (see
31
32 text for explanation).
33

34 593
35
36

37 594 Figure 6. Volcanic stratigraphy map of the northern sector of the Garrotxa Volcanic Field. A
38
39 different colour based on the RGB scale was assigned to each member and different kinds of
40
41 hatching were used to indicate different types of deposits (PDCs, lava flows, fallout, etc.). Numbers
42
43 correspond to the stratigraphic order of Table 2. Numbers missing in this legend correspond to non-
44
45 mappable (i.e.: only observable in boreholes and wells) stratigraphic units.
46
47 598

48 599
49

50 600 Figure 7. Volcanic stratigraphy map of the southern sector of the Garrotxa Volcanic Field.
51

52 601
53
54

55 602 Figure 8. Correlation of the main stratigraphic members identified in the northern sector of the
56

57 603 GVF. Colours of different units are the same than in Fig. 6. In grey, units not observable at surface
58
59
60

1
2 604 (i.e.: only visible in boreholes and wells). Numbers of different members as listed in Table 2. See
3
4 605 Figures 1 and 3 for location of the stratigraphic logs.

5
6 606

7
8 607 Figure 9. Map of the vents and source areas of the different eruptions (members) listed in Table 2.

9
10 608

11
12 609 Figure 10. a) Geological map of the Olot area made by the Catalan Geological Survey (IGC, 2007).

13
14 610 (b) Main urbanised area (violet colour) and location of the studied ephemeral outcrops and
15
16 611 boreholes. c) New geological map of the Olot area made in this study.

17
18
19 612

20
21 613 Figure 11. Field photographs showing Montsacopa deposits and their the stratigraphic relationships.

22
23 614 Upper) Conformable contact between Strombolian (lapilli scoria) and phreatomagmatic (PDC)

24
25 615 deposits from the main cone building phase of the Montsacopa eruption. Lower) Syn-eruptive

26
27 616 succession formed by welded scoria (spatter) at the base and a lava flow on top erupted from a

28
29 617 marginal vent with an intercalated distal fallout deposits from the main Montsacopa vent.

30
31
32 618

33
34 619 Figure 12. New geological map (this study) and cross section showing the stratigraphic correlation

35
36 620 (modified from Martí et al. 2011) of the central sector of the Garrotxa Volcanic Field obtained

37
38 621 through the study of ephemeral outcrops and the stratigraphic logging of wells.

39
40
41
42 622
43
44
45
46
47
48
49
50
51
52
53
54
55
56
57
58
59
60

623 **List of tables**

624 Table 1. Volcanic activity units and formal volcano-stratigraphic units (modified from Fisher and
625 Schmincke, 1984).

626

627 Table 2. Volcanic stratigraphy of the La Garrotxa Volcanic Field. Source: (1) Burjachs (1983). C14
628 dating. (2) Guérin and Valladas (1980). Thermoluminescence dating of volcanic plagioclases. (3)
629 Guerin i Benhamou (1985). Thermoluminescence dating of volcanic plagioclases and K/Ar Isotopic
630 dating. (4) Bolós A. (1925). Relative dating by biostratigraphy. (5) Pedrazzi et al. (2014). U-Th and
631 C14 dating. (6) Mallarach, JM. (1981, 1982, 1998). Relative dating by stratigraphy. (7) Donville
632 (1973). K/Ar Isotopic dating. (8) Lewis, C (2000). Ar/Ar Isotopic dating. (9) Gómez B. (personal
633 communication, 2014) Thermoluminescence (TL) dating of sediments.

634

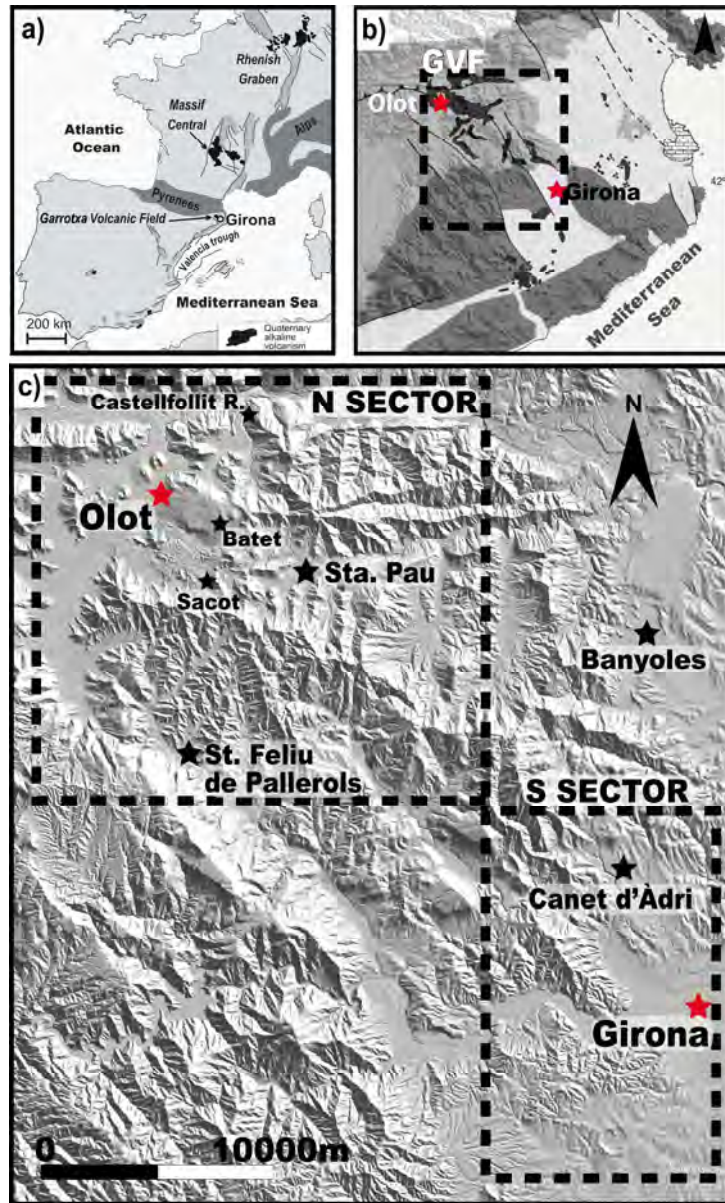


Figure 1. Map of the study area. a) Simplified map of the distribution of the European rift system. b) Simplified geological map of the Catalan Volcanic Zone (Modified from Guérin et al., 1985). c) Geographic distribution of the Garrotxa Quaternary volcanic field.
261x431mm (300 x 300 DPI)

1
2
3
4
5
6
7
8
9
10
11
12
13
14
15
16
17
18
19
20
21
22
23
24
25
26
27
28
29
30
31
32
33
34
35
36
37
38
39
40
41
42
43
44
45
46
47
48
49
50
51
52
53
54
55
56
57
58
59
60



Figure 2. Aerial view of the city of Olot and its volcanic cones.
203x152mm (300 x 300 DPI)

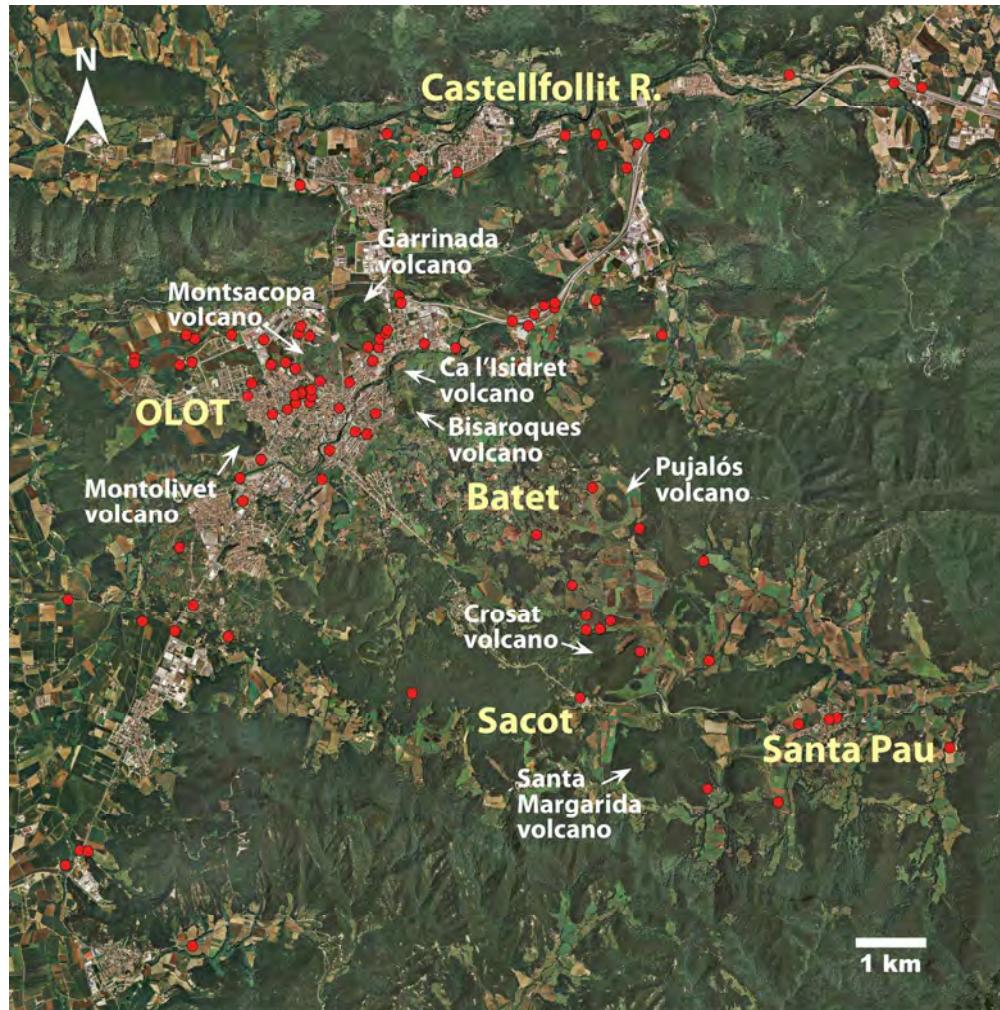


Figure 3. Location of the studied ephemeral outcrops, water wells and geotechnical drill holes.
147x149mm (300 x 300 DPI)

1
2
3
4
5
6
7
8
9
10
11
12
13
14
15
16
17
18
19
20
21
22
23
24
25
26
27
28
29
30
31
32
33
34
35
36
37
38
39
40
41
42
43
44
45
46
47
48
49
50
51
52
53
54
55
56
57
58
59
60

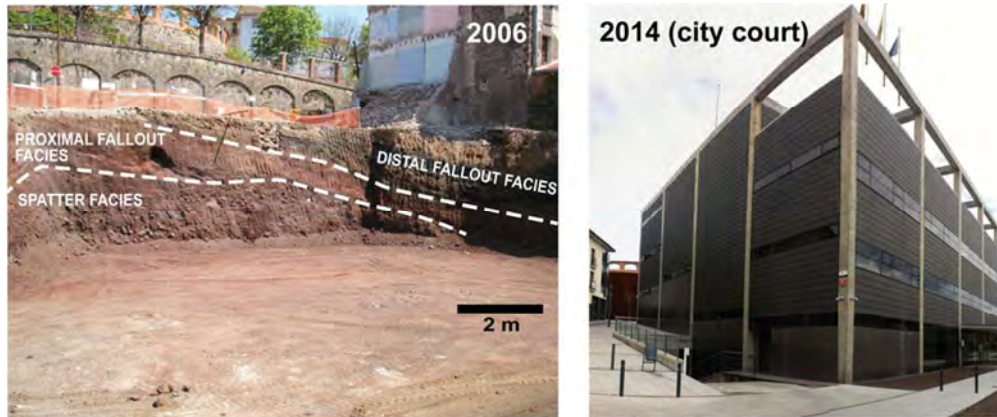


Figure 4. Example of an ephemeral outcrop (left) from Montsacopa member, visible during the construction of a new building.
80x33mm (300 x 300 DPI)

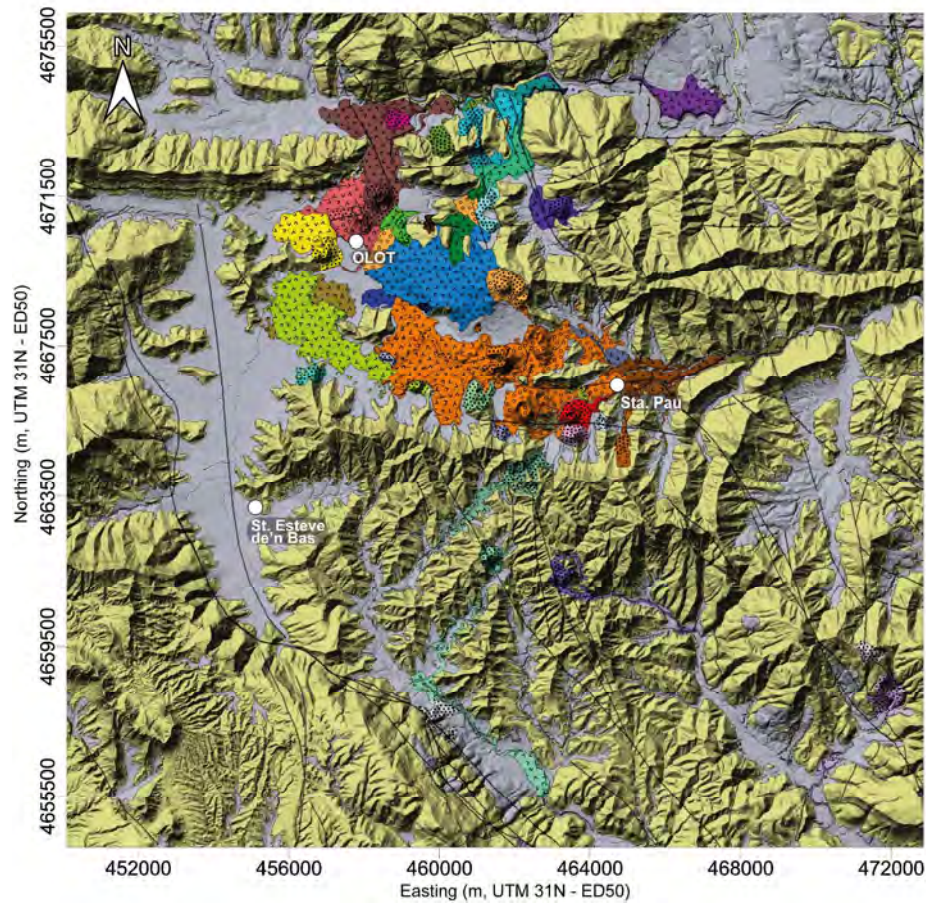


Figure 6. Volcanic stratigraphy map of the northern sector of the Garrotxa Volcanic Field. A different colour based on the RGB scale was assigned to each member and different kinds of hatching were used to indicate different types of deposits (PDCs, lava flows, fallout, etc.). Numbers correspond to the stratigraphic order of Table 2. Numbers missing in this legend correspond to non-mappable (i.e.: only observable in boreholes and wells) stratigraphic units.

204x193mm (300 x 300 DPI)



Figure 6. Volcanic stratigraphy map of the northern sector of the Garrotxa Volcanic Field. A different colour based on the RGB scale was assigned to each member and different kinds of hatching were used to indicate different types of deposits (PDCs, lava flows, fallout, etc.). Numbers correspond to the stratigraphic order of Table 2. Numbers missing in this legend correspond to non-mappable (i.e.: only observable in boreholes and wells) stratigraphic units.

224x289mm (300 x 300 DPI)

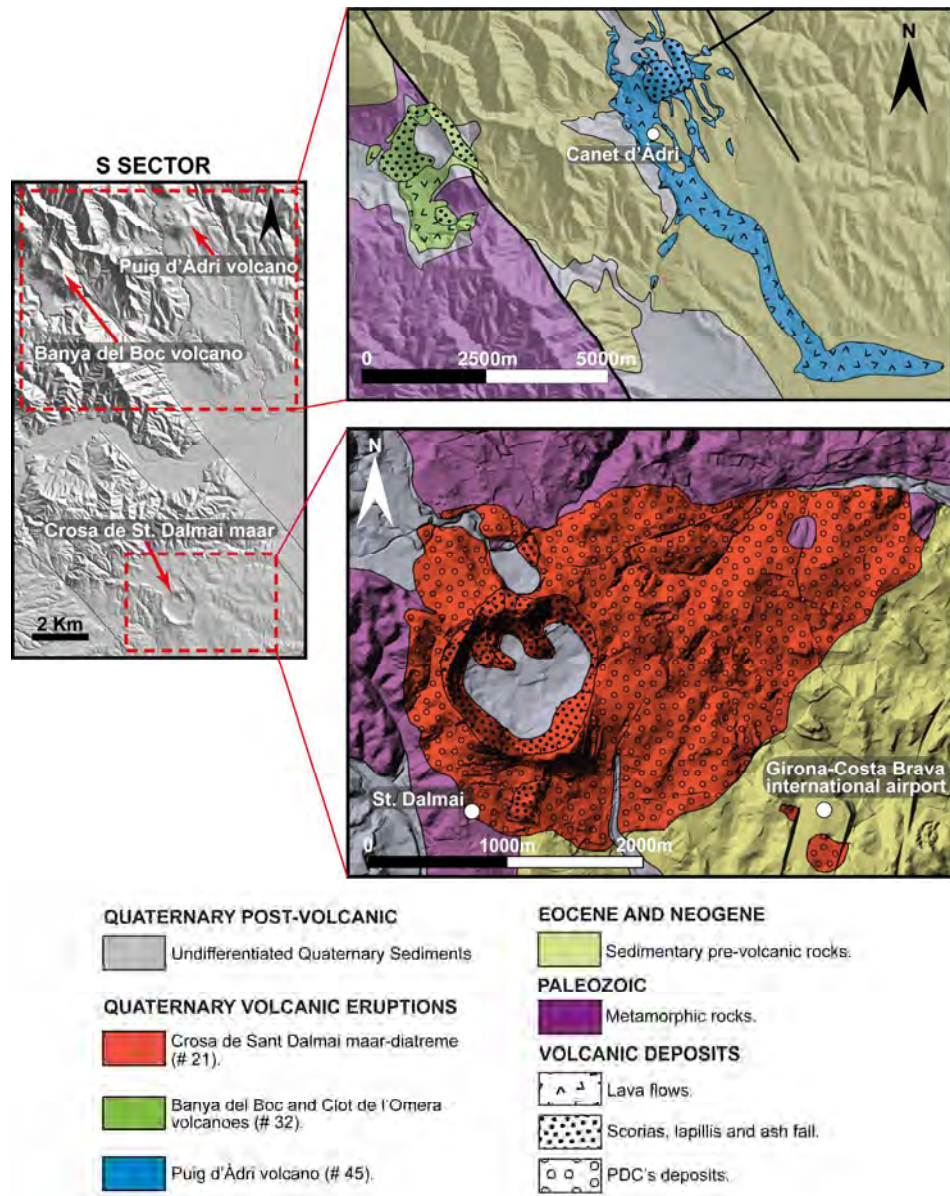


Figure 7. Volcanic stratigraphy map of the southern sector of the Garrotxa Volcanic Field. 243x308mm (300 x 300 DPI)

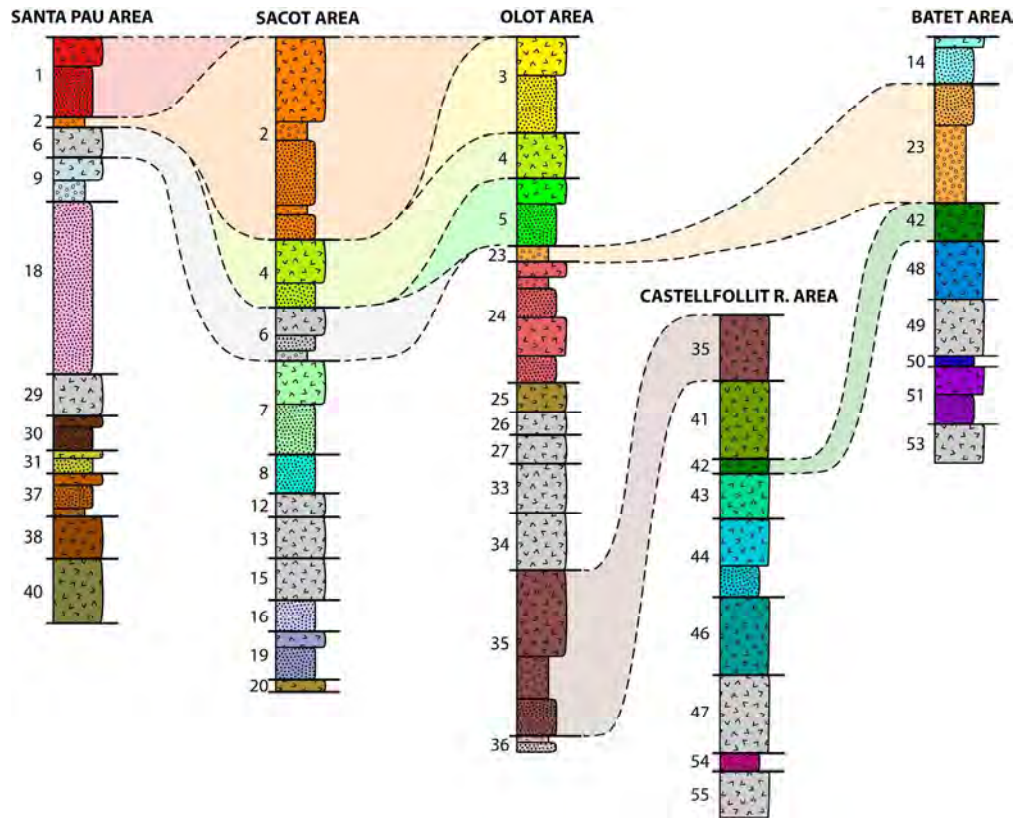


Figure 8. Correlation of the main stratigraphic members identified in the northern sector of the GVF. Colours of different units are the same than in Fig. 6. In grey, units not observable at surface (i.e.: only visible in boreholes and wells). Numbers of different members as listed in Table 2. See Figures 1 and 3 for location of the stratigraphic logs.
185x150mm (300 x 300 DPI)

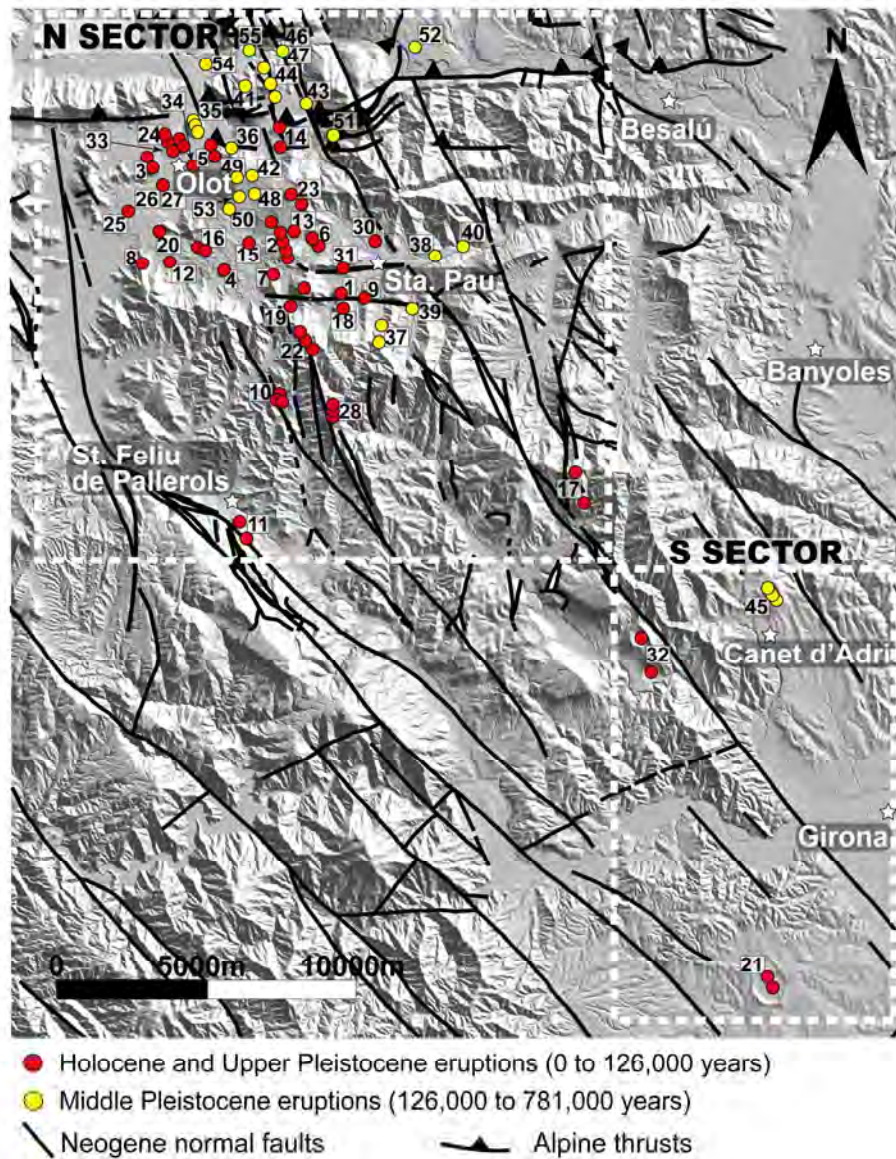


Figure 9. Map of the vents and source areas of the different eruptions (members) listed in Table 2.
225x272mm (300 x 300 DPI)

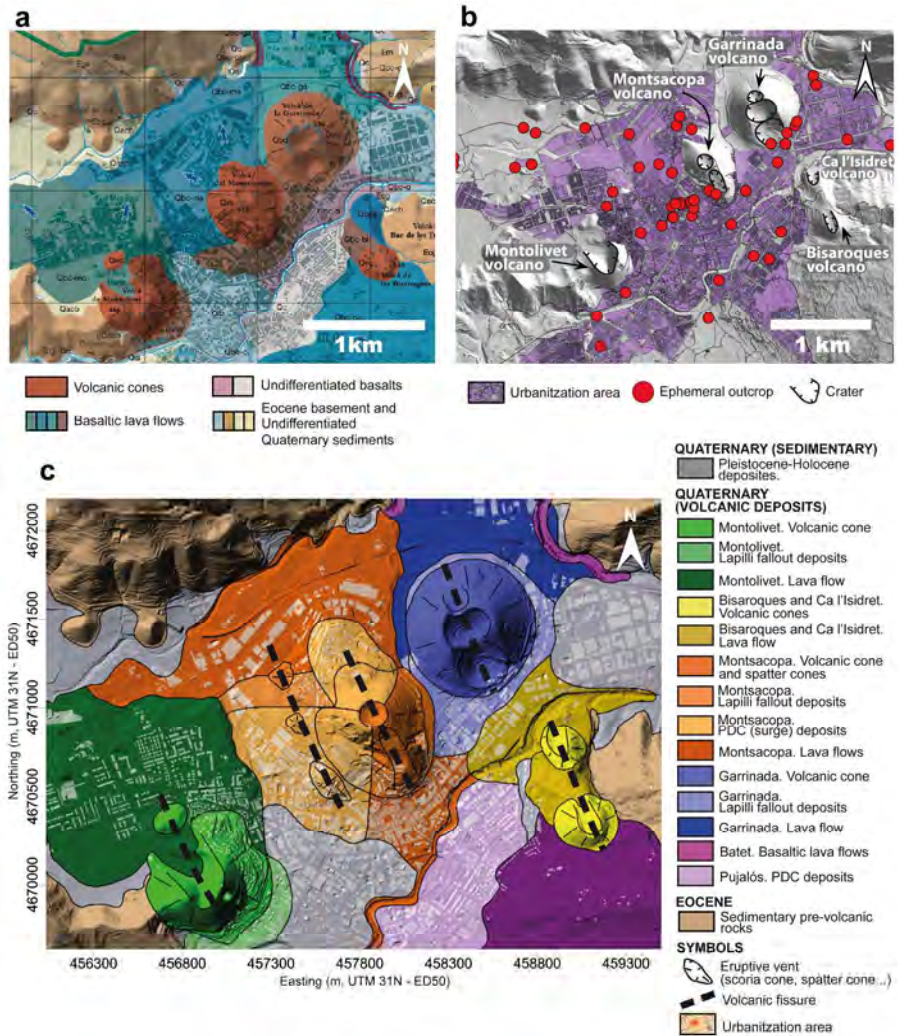


Figure 10. a) Geological map of the Olot area made by the Catalan Geological Survey (IGC, 2007). (b) Main urbanised area (violet colour) and location of the studied ephemeral outcrops and boreholes. c) New geological map of the Olot area made in this study. 217x224mm (300 x 300 DPI)

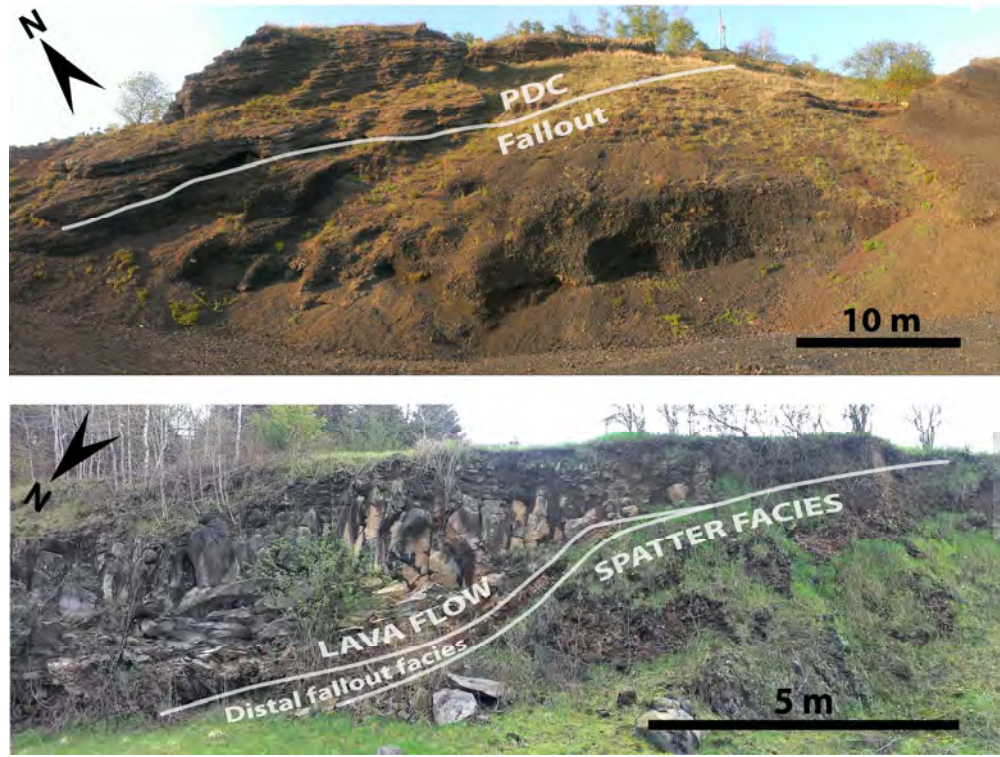


Figure 11. Field photographs showing Montsacopa deposits and their the stratigraphic relationships. Upper) Conformable contact between Strombolian (lapilli scoria) and phreatomagmatic (PDC) deposits from the main cone building phase of the Montsacopa eruption. Lower) Syn-eruptive succession formed by welded scoria (spatter) at the base and a lava flow on top erupted from a marginal vent with an intercalated distal fallout deposits from the main Montsacopa vent.

179x134mm (300 x 300 DPI)

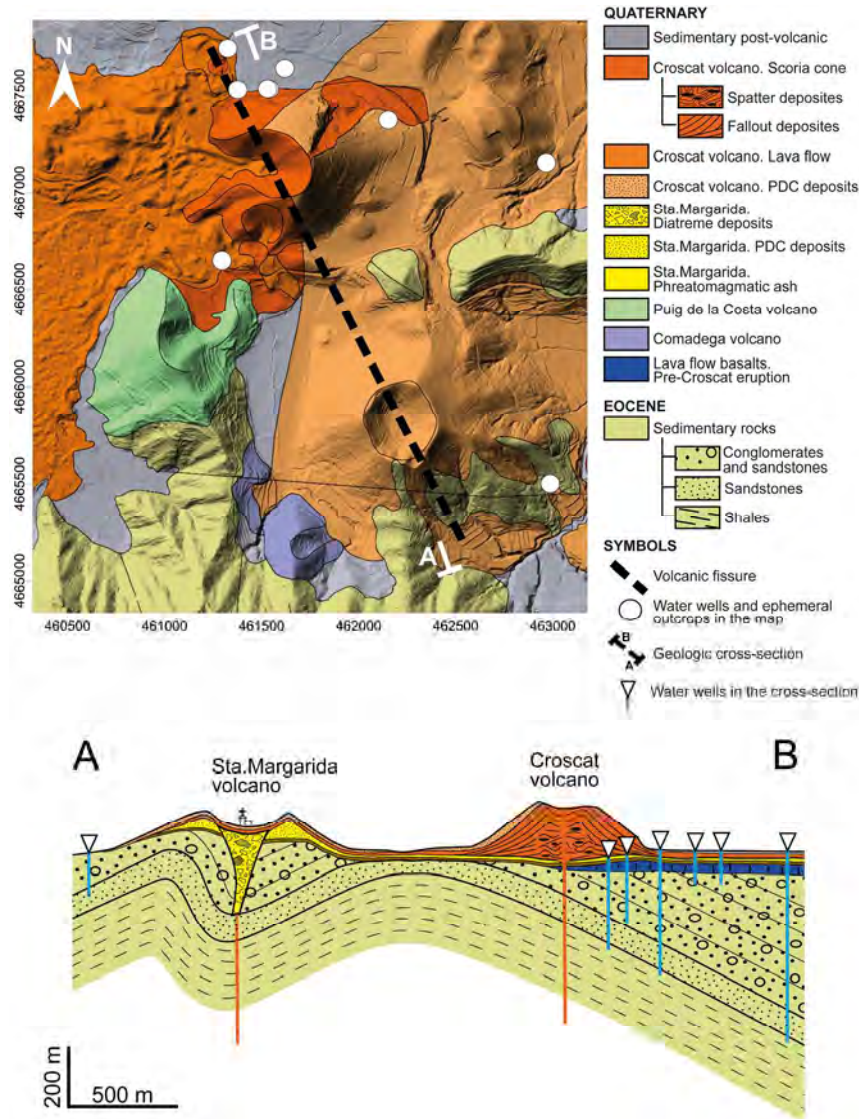


Figure 12. New geological map (this study) and cross section showing the stratigraphic correlation (modified from Martí et al. 2011) of the central sector of the Garrotxa Volcanic Field obtained through the study of ephemeral outcrops and the stratigraphic logging of wells.
240x270mm (300 x 300 DPI)

Volcanic Activity Units	Duration	Products and Volcanic Landforms	General Genetic designation	Volcano-stratigraphic Units (Formal units)
Eruptive pulse	seconds, minutes	Single airfall bed, PDC deposit, lahar, lava flow, etc	Eruption units (one or several beds, bedding sets, flows, ...)	Bed or level
Eruptive phase (several pulses)	minutes, hours, days	One or several deposits (several beds) of airfall, PDC, lava flows, lahars	One or several deposits (several beds) corresponding to a particular eruption dynamics	Unit
Eruption (several phases)	days, months, years	Succession of volcanic deposits of any nature (airfall, PDCs, lahars, lava flows, etc	Sequence of volcanic and related deposits formed during the same eruption	Member
Eruptive epoch (includes several eruptions and inter-eruptive - calm- episodes)	tens, hundreds or thousands of years	Single poligenetic volcanoes (stratovolcanoes, shield volcanoes, calderas, etc) or single monogenetic volcanic fields	Multiple members that may be grouped in cycles, depending on age, composition, eruptive style, etc	Formation
Eruptive period (includes several epochs and calm periods)	thousands or millions of years	Volcanic fields and regions consisting of many volcanoes and volcanic forms	Multiple Formations	Group

Time period	Relative Stratigraphy (from younger to older)	Age	Member	Source	Description	DRE (Km ³)
Holocene	1	Relative	Rocanegra volcano	(1)	These deposits overlie the Croscat volcano (# 2) phreatomagmatic deposits and are not covered by the Croscat volcano fallout.	0,01
	2	11.5 – 13 ka	Santa Margarida – Croscat – Pomareda eruptive fissure	(2) (3)		0,18
Upper Pleistocene	3	Relative < 18000	Montolivet volcano	(4)	These deposits overlie those of Montsacopa volcano (# 24), which in turn overlay La Garrinada (# 35) volcano deposits.	0,02
	4	17.1 ka	Puig Jordà volcano	(2) (3)	Lava flow with rootless volcanoes, locally known as Bosc de Tosca.	0,03
	5	Relative	Bisaroques and Ca l'Isidret volcanoes		Young aspect and poorly eroded materials overlying La Garrinada (# 35) volcano deposits.	0,01
	6	Relative	Puig de Martinyà volcano		There is a paleosoil that separates these deposits from the Croscat volcano (# 2) deposits.	
	7	Relative	Puig de la Costa volcano (Lava flow below Croscat volcano member (# 2))		Several lava flows were recognised in the Croscat borehole (see Figs. 8 and 12) below the Croscat and Puig Martinyà (# 6) deposits. The uppermost lava flow can be stratigraphically correlated with the Puig de la Costa volcano, so it should be younger than 30 ka.	
	8	Relative	Racó volcano			0,02
	9	28.1 ka	Simon volcano and Santa Pau lava flow	(2)	Santa Pau lava flow could be related to the Simon volcano according to its location and stratigraphic position.	
	10	30 to 46.3 ka	Traiter volcano	(2)		0,03
	11	Relative	Sant Marc and Puig Roig volcano			
	12	Relative	Lava flow below Bosc de Tosca		Appears underlying the Bosc de Tosca (Puig Jordà volcano (# 4)) lava flow and Racó volcano (# 8) deposits.	
	13	Relative	Pla de Massandell borehole upper lava flow			
	14	Relative (< 45 ka)	L'Estany and Bellaire volcanoes	(1)		0,02

15	Relative	Pla de Massandell borehole lower lava flow			
16	Relative	Cabriolers volcanoes			
17	Relative	Puig de Granollers volcano			0,03
18	Relative	Puig Subià volcano		Its deposits appear below the Santa Pau lava flow (# 9).	0.1 – 0.2
19	Relative	Comadega volcano		Underlying deposits from Croscat and Santa Margarida (# 2) and other volcanoes deposits in the Santa Pau area.	
20	Relative	La Moixina lava flow			
21	43 - 120 ka	Crosa de Sant Dalmai volcano	(1) (5)		0,13
22	73.5 ka	Fontpobra, Can Tià and Coll Tort volcanoes	(2)		0,03
23	Relative	Pujalós volcano			0,03-0.07
24	Relative	Volcà del Montsacopa		Its deposits overlay La Garrinada volcano (# 35) and are covered by thus from the Bisaroques and Ca l'Isidret volcanoes (# 5).	0.02-0.06
25	Relative	Pla de Llacs lava flow			
26	Relative	Pla d'Olot lava flow		Below Pla de Llacs (# 25). Only observable in boreholes.	
27	Relative	Pla d'Olot lava flows		Undetermined number of lava flows that fill the Olot depression.	
28	100 ka	Puig de les Medes and Puig Rodó volcanoes	(2)		0,02
29	Relative	Lava flow in borehole at Croscat northern flank			
30	110 ka	Pla de les Tries lava flow	(2)		
31	110 ka	Puig de Mar volcano	(6) (2) (7) (6) (2) (7)		
32	121 ka	Puig de la Banya del Boch and Clot de l'Omera volcanoes	(2) (3)		
33	Relative	Olot 2 lava flow		Only observable in boreholes.	
34	Relative	Olot 1 lava flow		Only observable in boreholes.	

Middle Pleistocene

35	133 ka	Garrinada volcano	(2) (8)		0,08
36	Relative	Bac de les Tries volcano		Deposits observable below la Garrinada volcano (# 35).	
37	Relative	Pla sa Ribera volcano			
38	Relative	Riu Ser lava flow 2		Appearing above the Riu Ser lava flow 1 (# 40).	
39	Relative	Vall dels Arcs phreatomagmatic deposits		Underlying the Riu Ser lava flow 2 (# 39).	
40	Relative	Riu Ser lava flow 1			
41	150 ka	Sant Joan les Fonts lava flow and Aiguanegra volcano	(8)		
42	Relative	Sant Cosme lava flow (from Batet)		Above the Funoses lava flow (# 42).	
43	Relative	Les Funoses lava flow		Above the Castellfollit lava flows (# 46 and # 47).	
44	Relative	Cairat-Repàs-Claperols eruptive fissure			
45	168 ka	Puig d'Àdri volcano	(9)		0,09
46	192 ka	Castellfollit de la Roca upper lava flow	(8)		
47	217 ka	Castellfollit de la Roca lower lava flow	(8)		
48	Relative	Batet upper lava flows			
49	247 ka	Batet middle lava flows	(2)		
50	Relative	Barraca volcano		These products are covered by the Batet lavas (# 48 and # 49).	
51	250 ka	Puig de l'Òs volcano	(8)		0,02
52	Relative	Sant Jaume de Llierca lava flow			
53	Relative	Batet lower lava flows		Lava flows identified in a borehole at the Batet high (Fig. 3).	
54	Relative	La Canya volcano			
55	590 – 700 ka	Sant Joan les Fonts lava flows	(8)	The oldest lava emission recognised in this volcanic field.	

Appendix 6.1. Acceptance proof of the paper

Journal of Quaternary Science

Decision Letter (JQS-13-0100.R2)

From: a.j.long@durham.ac.uk
To: xbolos@ictja.csic.es
CC:
Subject: Journal of Quaternary Science - Decision on Manuscript ID JQS-13-0100.R2
Body: 18-May-2014

Dear Mr Bolós,

It is a pleasure to accept your manuscript entitled "Volcanic stratigraphy of the Quaternary La Garrotxa Volcanic Field (NE Iberian Peninsula)" in its current form for publication in Journal of Quaternary Science.


Your article cannot be published until you have signed the appropriate license agreement. In due course you will receive an email from Wiley's Author Services system which will ask you to log in and will present you with the appropriate licence for completion.

Thank you for your fine contribution.



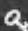

Sincerely,

Prof. Antony Long
a.j.long@durham.ac.uk
Journal of Quaternary Science

Date Sent: 18-May-2014

 Close Window

© Thomson Reuters | © ScholarOne, Inc., 2014. All Rights Reserved.
ScholarOne Manuscripts and ScholarOne are registered trademarks of ScholarOne, Inc.
ScholarOne Manuscripts Patents #7,257,767 and #7,263,655.

 @ScholarOneNews |  System Requirements |  Privacy Statement |  Terms of Use

APPENDIX 7

Volcano-structural analysis of La Garrotxa Volcanic Field (NE of Iberia): implications on the plumbing system

Manuscript Number:

Title: Volcano-structural analysis of La Garrotxa Volcanic Field (NE Iberia): implications for the plumbing system

Article Type: Research Paper

Keywords: Volcano-structural; Garrotxa Volcanic Field; monogenetic volcanism; magma ascent rates; plumbing system

Corresponding Author: Mr. Xavier Bolós, M.D.

Corresponding Author's Institution: ICTJA-CSIC

First Author: Xavier Bolós, M.D.

Order of Authors: Xavier Bolós, M.D.; Joan Martí; Laura Becerril; Llorenç Planagumà; Pablo Grosse; Stéphanie Barde-Cabusson

Abstract: The Garrotxa Volcanic Field is related to the Neogene-Quaternary European Rift system and is the youngest representation of monogenetic volcanism in the Iberian Peninsula. It encompasses over 50 well-preserved volcanoes in an area of about 600 km² lying between the cities of Olot and Girona (NE Spain). In this paper we investigate the relationship between the Neogene extensional tectonics and the spatial distribution of the volcanoes in the area. The analysis includes the geostatistical distribution of faults, fissures and vents, as well as morpho-structural lineaments, and the morphometrical analysis of volcanic cones and craters. As well, we use the location of the regional seismicity registered since 1978 and the sites of freshwater springs and mantle-derived gases as indicators of active faults and open fractures. Finally, we consider the location of the volcanoes with ultramafic xenoliths as a way of identifying the deepest fractures in the zone and estimating magma ascent velocities. The results obtained show that this volcanic area consists of an extensional basin delimited by two principal faults that permitted the ascent of magma from either the source region or from shallower reservoirs located at the base of the crust. Towards the upper part of the crust, magma transport was captured by shallow extensional secondary faults whose formation is linked to the slight transtensional movement of the main bounding faults. Our study provides evidence of how the local stress field and contrasts in rheology could have controlled magma migration, which suggests that precise knowledge of the stress configuration and distribution of rheological and structural discontinuities in such regions is crucial in the forecasting of monogenetic volcanism.



MINISTERIO
DE ECONOMÍA
Y COMPETITIVIDAD



INSTITUTE OF EARTH SCIENCES JAUME ALMERA (ICTJA)

Barcelona, May 23, 2014

Dear Editor of Tectonophysics,

Please find enclosed the manuscript entitled "**Volcano-structural analysis of La Garrotxa Volcanic Field (NE Iberia): implications for the plumbing system**", by Xavier Bolós, Joan Martí, Laura Becerril, Llorenç Planagumà, Pablo Grosse, Stéphanie Barde-Cabusson, which we would like to submit for publication to Tectonophysics.

This research paper focuses on the Quaternary La Garrotxa Volcanic Field, the youngest sector of the Catalan Volcanic Zone (NE of Spain), a still poorly known part of the European Volcanic Rifts System. We conducted a detailed volcano-structural analysis of this volcanic field, including geostatistical distribution of faults, fissures and vents, morpho-structural lineaments identified by remote sensing, a morphometrical analysis of the volcanic cones and craters, location of regional seismic events recorded in the area (since 1978), and mantle derived gases in springs and water wells, as a guide to identify active faults and open fractures and to define the structural controls of this volcanism. The results obtained from this paper have permitted to understand how magma was transported into the lithosphere and erupted at the surface, and represent an essential tool for a correct volcanic hazard assessment of this volcanic field.

The manuscript satisfies the Tectonophysics mission statement in the sense that it deals with an important, but still poorly studied, Quaternary volcanic episode in Europe, but also because it describes a methodology for establishing the tectonic controls and the origin of this monogenetic volcanism that will be useful for being applied to other areas with similar problems.

On behalf of the Authors

Sincerely,

Xavier Bolós

Volcano-structural analysis of La Garrotxa Volcanic Field (NE Iberia): implications for the plumbing system

Corresponding author: X. Bolós

Abstract

The Garrotxa Volcanic Field is related to the Neogene-Quaternary European Rift system and is the youngest representation of monogenetic volcanism in the Iberian Peninsula. It encompasses over 50 well-preserved volcanoes in an area of about 600 km² lying between the cities of Olot and Girona (NE Spain). In this paper we investigate the relationship between the Neogene extensional tectonics and the spatial distribution of the volcanoes in the area. The analysis includes the geostatistical distribution of faults, fissures and vents, as well as morpho-structural lineaments, and the morphometrical analysis of volcanic cones and craters. As well, we use the location of the regional seismicity registered since 1978 and the sites of freshwater springs and mantle-derived gases as indicators of active faults and open fractures. Finally, we consider the location of the volcanoes with ultramafic xenoliths as a way of identifying the deepest fractures in the zone and estimating magma ascent velocities. The results obtained show that this volcanic area consists of an extensional basin delimited by two principal faults that permitted the ascent of magma from either the source region or from shallower reservoirs located at the base of the crust. Towards the upper part of the crust, magma transport was captured by shallow extensional secondary faults whose formation is linked to the slight transtensional movement of the main bounding faults. Our study provides evidence of how the local stress field and contrasts in rheology could have controlled magma migration, which suggests that precise knowledge of the stress configuration and distribution of rheological and structural discontinuities in such regions is crucial in the forecasting of monogenetic volcanism.

**Volcano-structural analysis of La Garrotxa Volcanic Field (NE Iberia):
implications for the plumbing system**

Corresponding author: X. Bolós

HIGHLIGHTS

- Analyses of structural elements, vents, seismicity, freshwater springs and gases
- Xenoliths to identify the deepest fractures and estimate magma ascent velocities.
- Transtensional main faults determine spatial distribution of the Garrotxa volcanism
- Magma transport in the upper part crust is captured by extensional secondary faults

1 **Volcano-structural analysis of La Garrotxa Volcanic Field (NE Iberia):**
2 **implications for the plumbing system**

3

4 Xavier Bolós¹, Joan Martí¹, Laura Becerril¹, Llorenç Planagumà², Pablo Grosse³,
5 Stéphanie Barde-Cabusson¹

6

7 1) Institute of Earth Sciences Jaume Almera, ICTJA-CSIC, Group of Volcanology.

8 SIMGEO (UB-CSIC) Lluís Solé i Sabarís s/n, 08028, Barcelona, Spain.

9 2) Tosca Environmental Services. Parc Natural de la Zona Volcànica de la Garrotxa,
10 c/Santa Coloma, 17800 Olot, Spain.

11 3) CONICET and Fundación Miguel Lillo, Tucumán, Argentina.

12

13 Corresponding author: Xavier Bolós (xavier.bolos@gmail.com)

14

15 **Abstract**

16

17 The Garrotxa Volcanic Field is related to the Neogene-Quaternary European Rift system
18 and is the youngest representation of monogenetic volcanism in the Iberian Peninsula.

19 It encompasses over 50 well-preserved volcanoes in an area of about 600 km² lying
20 between the cities of Olot and Girona (NE Spain). In this paper we investigate the
21 relationship between the Neogene extensional tectonics and the spatial distribution of
22 the volcanoes in the area. The analysis includes the geostatistical distribution of faults,
23 fissures and vents, as well as morpho-structural lineaments, and the morphometrical
24 analysis of volcanic cones and craters. As well, we use the location of the regional
25 seismicity registered since 1978 and the sites of freshwater springs and mantle-derived

26 gases as indicators of active faults and open fractures. Finally, we consider the location
27 of the volcanoes with ultramafic xenoliths as a way of identifying the deepest fractures
28 in the zone and estimating magma ascent velocities. The results obtained show that this
29 volcanic area consists of an extensional basin delimited by two principal faults that
30 permitted the ascent of magma from either the source region or from shallower
31 reservoirs located at the base of the crust. Towards the upper part of the crust, magma
32 transport was captured by shallow extensional secondary faults whose formation is
33 linked to the slight transtensional movement of the main bounding faults. Our study
34 provides evidence of how the local stress field and contrasts in rheology could have
35 controlled magma migration, which suggests that precise knowledge of the stress
36 configuration and distribution of rheological and structural discontinuities in such
37 regions is crucial in the forecasting of monogenetic volcanism.

38

39

40 **Keywords:** Volcano-structural, Garrotxa Volcanic Field, monogenetic volcanism,
41 magma ascent rates, plumbing system

42

43

44 **1. Introduction**

45

46 Basaltic monogenetic volcanic fields related to rift zones are found world-over
47 and are expressed on the Earth's surface by the alignments of pyroclastic cones and
48 vents and parallel faults and eruptive fissures (Fiske and Jackson, 1972; Walker, 1999).
49 A volcanic eruption signals the end of the process whereby magma rises from its source
50 in the upper mantle to the surface (e.g. Brenna et al., 2011; McGee et al., 2011). The

51 final geometry of the magma pathway towards the surface is directly controlled by the
52 stress field and always follows a path normal to the minimum stress and parallel to the
53 maximum principal stress (Rubin, 1995; Connor and Conway, 2000; Gudmundsson and
54 Philipp, 2006, Cebrià et al., 2011; Le Corvec et al., 2013). In monogenetic volcanic
55 fields the distributions and magnitudes of different stress fields can be related to the
56 tectonic and gravitational forces that, in turn, are linked to (a) basement geometry, (b)
57 local topography, (c) stress changes occurring during dyke propagation, and (d) stress
58 barriers related to structural discontinuities and rheological changes in stratigraphic
59 successions (Gretener, 1969; Clemens and Mawer, 1992; Gudmundsson, 2003; Tibaldi,
60 2003; Acocella and Tibaldi, 2005; Gudmundsson and Philipp, 2006; Kavanagh et al.,
61 2006; Tibaldi et al., 2014). Deciphering the potential pathways that magma uses to
62 reach the surface is of crucial importance when conducting hazard assessment in
63 volcanic areas.

64 The complexity of subsurface plumbing systems in monogenetic volcanic fields
65 ensures that such systems are difficult to predict and rarely accessible for study and so
66 other methods are needed for understanding the structural setting of a volcanic area and
67 the pathways used by magma on its ascent to the Earth's surface. Over the last twenty
68 years, several geophysical studies have been devoted to geostructural characterisations
69 of the feeding systems of monogenetic volcanic areas (or, more generally, of active
70 volcanic districts) (e.g. Nishi et al., 1996; Bibby et al., 1998; Di Maio et al., 1998, 2000;
71 Portal et al., 2013; Blaikie et al 2014). In La Garrotxa Volcanic Field geophysical
72 studies of this type have been conducted in recent years and have been successful in
73 describing the stratigraphy of the area and the shallow structure beneath the volcanic
74 deposits (Bolós et al., 2012, 2014a, 2014b; Barde-Cabusson et al., 2013, 2014). Results
75 have confirmed in general terms that this volcanism is mainly controlled by NW-SE

76 faults that are the very faults that control the post-Alpine structural evolution of the
77 area. However, the exact structural control and the role played by the major and
78 subordinated faults in determining the distribution of vents and the frequency and size
79 of the eruptions is not known.

80 In order to improve our understanding of the structural constraints of La
81 Garrotxa volcanism we combined the results of these previous geophysical works with
82 new volcano-structural analysis that includes data on the geostatistical distribution of
83 faults, fissures and eruptive vents, the identification of morpho-structural lineaments by
84 remote sensing, and a morphometrical analysis of the field's volcanic cones and craters.
85 In addition, we took into account all of the epicentres of regional seismic events
86 recorded by the Geological Survey of Catalonia (IGC) since 1978, as well as the
87 distribution of CO₂-rich freshwater springs, and springs and wells with high radon
88 levels, as a guide to active faults and open fractures, respectively. Finally, we analysed
89 the distribution of upper mantle xenoliths and lower crust cumulates as an indication of
90 the depth reached by certain fractures and faults, and used the largest of these enclaves
91 to estimate magma ascent velocities. The data obtained was combined into a conceptual
92 model describing how magma was transported from source to the surface in La
93 Garrotxa Volcanic Field, which can bring some clues for such processes in other
94 monogenetic volcanic fields.

95

96

97 **2. Geological setting**

98

99 Mafic alkaline volcanism is widely distributed along the European Cenozoic Rift
100 System that comprises four main volcanic areas: the Rhenohercynian in Germany, the

101 western Panonian Basin in Eastern Europe, the Massif Central in France and the
102 Valencia Trough in Spain (Ziegler, 1992; Downes, 2001; Dèzes et al, 2004, Michon and
103 Merle, 2005). The study area is part of the Valencia Trough, a NE-SW-oriented Neogene
104 basin lying offshore between the Iberian Peninsula and the Balearic promontory in
105 northeastern Spain (Fig. 1). The most important concentration of Middle Miocene-to-
106 recent volcanism in the Valencia Trough is found in the Catalan Volcanic zone (CVZ) in
107 the NE Iberian Peninsula (Martí et al., 1992; Martí et al., 2011). This area is
108 characterised by a series of graben and horst structures that have controlled Neogene-
109 Quaternary volcanism and sedimentation.

110 The most recent episode in this volcanism corresponds to La Garrotxa Volcanic
111 Field (GVF) (0.7 Ma to early Holocene) (Araña et al., 1983; Bolós et al., 2014b). This
112 field covers an area of about 600 km² located between the cities of Olot and Girona
113 (Fig. 1) and is bounded by two regional conjugated Neogene normal faults with a
114 transtensional component (Goula et al., 1999; Olivera et al., 2003): the Amer Fault to
115 the east and the Llorà Fault to the west. These two faults are responsible for the
116 distribution of the area's volcanism, as well as its seismicity and fluvial network (Saula
117 et al., 1996; Martí et al., 2011; Cimarelli et al., 2013; Barde-Cabusson et al 2014). The
118 northern part of this volcanic field is limited by an E-W reverse fault system, which is
119 not related to the subsequent magmatism. The GVF contains over 50 well-preserved
120 cones, the main concentration being located in the northern sector of the area (Fig. 1).
121 The morphologies of these volcanoes include cinder and scoria cones, spatter cones, tuff
122 rings and maars, and in composition mainly correspond to basanites and alkaline basalts
123 (Araña et al., 1983; Cebrià et al., 2000; Martí et al., 1992). Some volcanoes contain
124 ultramafic to mafic xenoliths including pyroxenites, melanogabbros, amphibolites and
125 spinel lherzolites, of which the pyroxenites are the most abundant (Llobera, 1983;

126 Neumann et al., 1999, Bianchini et al., 2007; Galán et al., 2008). Pressure and
127 temperature estimates suggest that the pyroxenites, melanogabbros and amphibolites
128 may have crystallised in magma chambers located at the crust–mantle boundary
129 (Neumann et al., 1999), which, according to geophysical estimates, are located at a
130 depth of ~30 km (Fernández et al., 1990; Gallart et al., 1984, 1991); on the other hand,
131 the spinel lherzolites may derive from the source region in the asthenospheric mantle
132 (Bianchini et al., 2007).

133

134

135 **3. Methodology**

136

137 New fieldwork and remote sensing analyses were conducted in order to identify
138 and measure the main volcano-structural features such as vents lineaments, fissures and
139 faults (Fig. 2). Structural mapping was performed with the software ArcGIS 10 by
140 ESRI[®] at a scale of 1:5 000 using orthophotographs (1:2500), aerial photographs (1:18
141 000) and Digital Elevation Models (DEM; 5- and 2-m resolutions) produced by the
142 Cartographic Institute of Catalonia (ICC; www.icc.cat). Geological maps produced by
143 the Geological Survey of Spain and Geological Survey of Catalonia (IGME; 1:50 000,
144 <http://cuarzo.igme.es/sigeco/>, 2011; IGC; 1:25 000; www.igc.cat) were also used. The
145 morpho-tectonic analysis included the determination and comparison of lineaments
146 obtained from orthophotomaps and different illumination-shaded relief DEMs, as well
147 as a statistical analysis of the length and orientation of lineations. To avoid any artefact
148 that could be attributed to the lighting direction of the DEM we used different lighting
149 models. We also analysed the profile and direction of several streams and rivers in order

150 to detect abrupt changes in slope direction that could be related to tectonic movements
151 (Fig. 3).

152 Eruptive vents were mapped as individual points of magma emission on the
153 surface, which allowed us to delineate eruptive fissures corresponding to lines
154 connecting volcanic vents opened during the same eruption (e.g. Tibaldi; 1995, Paulsen
155 and Wilson, 2010; Becerril et al., 2013). Fieldwork allowed us to verify the number of
156 existing vents and to check fissure lengths and strikes.

157 A morphometrical analysis of the most representative well-preserved volcanoes
158 was also performed. We analysed a total of 28 cones and craters in both the northern and
159 southern sectors of the GVF using a DEM with resolutions of 2 and 5 m, respectively.
160 The cone and crater outlines were manually delimited by consulting slope breaks and
161 geological maps. Morphometric parameters of each cone and crater were extracted
162 using the MORVOLC program (Grosse et al., 2009, 2012). The following parameters
163 were considered: (a) Ellipticity Index (EI) of the cone and crater outlines (EI is a
164 measure of elongation equal to:

$$165 \quad EI = (\pi * (L/2)^2) / A \quad (1)$$

166 where L is the maximum/major outline axis and A is the outline area), (b) the average EI
167 of the closed elevation contours (at 5 m equidistance) within the cone base, (c) the
168 major axis azimuths of the cone and crater outlines, (d) the circular average azimuth of
169 the major axes of the closed elevation contours within the cone, and (e) the calculated
170 azimuth and direction of breaching in breached craters.

171 A statistical analysis based on the nearest-neighbour concept (see Cebrià et al.,
172 2011) was applied to eruptive vents in order to obtain the angles of the lines that
173 connect all pairs of eruptive vents. Previous studies have demonstrated that the main
174 lineaments obtained from the union of eruptive vents can reveal stress field patterns

175 (Lutz, 1986; Cebrià et al., 2011). To carry out this analysis we considered lineaments of
176 up to 12 km in maximum length, corresponding to the maximum distance between two
177 eruptive vents inside the northern sector. We choose this sector since it has the major
178 concentration of volcanoes (Fig. 4).

179 No outcropping dykes were identified in the studied area due to its recent age
180 and lack of significant erosion. However, several feeder dykes hidden by their own
181 deposits were identified using Electric Resistivity Tomography (Bolós et al., 2012,
182 2014a). Preliminary interpretations of geological maps were carried out in order to
183 compile and to check previous mapped faults (IGC and IGME geological maps) and to
184 identify new ones. Stress patterns were also obtained from the drainage network map
185 extracted using a DEM spatial analysis. Rose diagrams of fissures, faults and drainage
186 networks were performed with the software Stereonet 8.8.4 (Cardozo and Allmendinger,
187 2013). We also took into account the distribution of the main freshwater springs existing
188 in the study area (Fig. 5) to indicate the presence of open fractures and faults. We
189 georeferenced a total of 254 springs shown on the topographic maps of the Catalan
190 Geographic Institute (www.icc.cat), along with others identified during fieldwork. High
191 concentrations of endogenous gases (i.e. radon, CO₂) in freshwater springs are assumed
192 to indicate the presence of deep fractures with high permeability values (Wattananikorn
193 et al., 1998; Kresic, 2010), which is this case where they are directly linked to active
194 Quaternary faults (Zarroca et al., 2012). In a small part of the study area (southern
195 sector; 463216, 4646403 (UTM 31N - ED50)) we also used 12 measurements of CO₂ in
196 freshwater springs taken by Zarroca et al. (2012). In the northern part of the study area
197 (449194, 4662424 (UTM 31N - ED50)), Moreno et al. (2014) catalogued 53
198 groundwater radon measurements in water wells and springs. All these data were
199 incorporated into a database and are presented in this work, together with data from

200 other springs (Fig. 5).

201 The location of seismic events was also incorporated into the dataset used in this
202 study (Fig. 6). Although seismic events are not that abundant in the northeastern part of
203 the Iberian Peninsula, it was possible to collect accurate data regarding the earthquakes
204 recorded since 1978 by the Geological Survey of Catalonia (www.igc.cat). This data
205 provides information regarding the current tectonic stresses in the GVF. We compiled
206 the location, depth and magnitude of the seismic events; locations of seismic events
207 were represented on the structural map. The average distance between seismic stations
208 is 30 km and data pertaining to earthquakes located within this network have an
209 accuracy of 2–3 km for epicentres and 5 km for depths (Goula et al., 1999).

210 The presence of upper-mantle and lower-crust xenoliths in volcanic products has
211 been used as an indicator of the depth of magma pathways and to estimate magma
212 ascent velocities (Parsons et al., 1980; Peterson and Hildreth, 1989; Hildreth and
213 Tange, 1998; Mattsson 2012; Jankovics et al., 2013). In this study we
214 mapped the distribution of the volcanoes containing lower-crust xenoliths, mantle-
215 derived xenoliths or both (Fig. 7) as a way of estimating the depth of the fractures and
216 faults through which magma is transported to the surface. Calculations of magma ascent
217 velocities were made on the basis of the assumption that magma (melt) was – in
218 rheological and petrological terms – similar throughout the study area (i.e. basalts and
219 basanites) (Araña et al., 1983; Cebriá et al., 2000; Martí et al., 1992), although the
220 distribution of xenoliths does in fact vary. In addition, we assumed that during its ascent
221 the magma did not undergo any significant temperature variations, as has been
222 suggested by Cimarelli et al. (2012), and that its rheology was close to that of a
223 Newtonian fluid, as should occur in the case of a magma of this composition with a
224 crystal content of less than 15% (see Vona et al, 2011). With these assumptions in mind,

225 we applied the method of Spera (1980, 1984), which defines:

$$226 \quad Re_n = \frac{\rho_l u_n R_n}{\eta_l} \quad (2)$$

$$227 \quad u_n = \left(\frac{8R_n \Delta\rho g}{3C_d \rho_l} \right)^{1/2} \quad (3)$$

228 where η_l , u_n , R_n , $\Delta\rho$, ρ_l , g and C_d represent the Newtonian viscosity, nodule settling
229 velocity, radius, density difference between melt and xenolith, density of melt, gravity
230 value, and drag coefficient, respectively. C_d is related to the nodule settling velocity and
231 hence to Re_n . For our samples we considered $Re_n > 0.1$ and therefore we applied:

$$232 \quad C_d = 18Re_n^{-3/5} \quad (4)$$

233 In order to estimate the minimum ascent rate we took into account the maximum
234 size of xenoliths found in the area. The density of the melt was measured from natural
235 rock glass by remelting a representative sample in a Pt crucible at 1400° C for 5 hours in
236 an open atmosphere to remove vesiculation. The density obtained was 2.53 g/cm³.
237 Finally, we used the method of Vona et al. (2011) to estimate the viscosity (40 to 50
238 Pa.s).

239

240

241 **4. Results**

242 Although the GVF is constrained above all between two Neogene faults, the
243 Amer and Llorà faults, there are a few other volcanic outcrops and vents located outside
244 these structural limits, mainly east of the Llorà fault (Fig. 2). No vents are directly
245 located on the Amer and Llorà faults. All the vents identified in this study are located on
246 subordinated faults. In the field it is clear that the majority of volcanic deposits have
247 not been affected by the Neogene faults. Only the main Amer fault affects the central
248 sector of the volcanic deposits (Fig. 8). Most of the volcanic deposits located in the

249 north of the study area cover the basement rocks, which prevents the subordinate faults
250 in this zone from being identified. Towards the north, a set of E-W reverse faults and
251 thrusts formed during the Alpine Orogeny delimits the volcanic field but is intersected
252 (crossed) by the same NW-SW Neogene fault system that constrains the volcanic field
253 further to the south (Fig. 2) (Table 1, Supp. material).

254 A total of 67 eruptive vents were mapped in the study area and are represented
255 on our map (Fig. 2) by points corresponding to the middle of the craters of isolated
256 cinder cones and of coalescent cinder cones that belong to the same eruptive fissure.
257 The majority of eruptive vents (83.5%) are located in the northern sector of the GVF,
258 around the city of Olot (Fig. 2), while only a few (16.5%) are located in the southern
259 sector (Fig. 2) (Table 1, Supp. material). However, the volcanoes in the southern sector
260 are larger and emitted more magma than those in the northern sector (Bolós et al.,
261 2014a). Several volcanic deposits that cannot be associated with any eruptive vent,
262 either because they have been eroded or covered by more recent volcanic materials,
263 were not considered in our structural analysis.

264 The alignments defined by 44 eruptive vents allowed us to infer up to 19
265 eruptive fissures (Fig. 2). All fissures have the same trend, with a strike average of
266 \sim N155°E; the exception is a fissure with a strike of N29°E subparallel to a related. The
267 longest fissure was measured at \sim 3050 m and is located in the central area of the
268 northern sector (Pomareda - Croscat - Santa Margarida eruptive fissure) (Pm-Cr-Sta.M
269 in Fig. 2), and was recognized through geological fieldwork and geophysical studies
270 (Barde-Cabusson et al., 2013; Barde-Cabusson et al., 2014). The shortest fissure
271 measures 287 m and the average fissure length is 968 m, although most fissures
272 measure between 400 and 1200 m (Table 1, Supp. material).

273 The 28 analysed cones have basal widths between 160 and 1430 m (average 610

274 m) and heights between 20 and 170 m (average 73 m). 23 of the 28 cones have visible
275 craters, with some cones having 2 or 3 coalescing craters. Additionally, 4 craters not
276 associated to any cone, were also mapped. Of a total of 36 analysed craters, 21 are
277 breached. Closed craters have widths between 40 and 390 m (average 220 m; excluding
278 one large crater with a width of 1160 m) and depths between 5 and 60 m (average 20
279 m). Cone bases EI vary between 1.2 and 2.1, and for the closed crater outlines between
280 1.2 and 1.5; EI average of elevation contours vary between 1.3 and 4.9. Elongation
281 azimuths of the cone bases, closed crater outlines and elevation contours, together with
282 breaching directions of the breached craters, defines two orientation trends: a main NW-
283 SE to NNW-SSE trend (with crater breaching mostly to the NNW), and a secondary
284 NE-SW trend (with crater breaching towards the NE) (see Table 2 in Supp. material).

285 The analysis of the drainage network also allowed us to distinguish different
286 trends that confirm the main structural features of the area; the four principal stream
287 directions identified were NW-SE, NE-SW, N-S and E-W (Fig. 3).

288 In order to obtain an unbiased analysis of the main direction of the alignments,
289 we performed a statistical study based on the nearest-neighbour concept. The results
290 obtained show a lineament distribution that clearly follows a NNW-SSE trend (Fig. 4).
291 Secondary directions ranging from NE-SW to E-W were also obtained.

292 The majority of freshwater springs identified and plotted on the structural map
293 coincide with the main tectonic elements such as Neogene faults and the Alpine reverse
294 faults (Fig 5). However, a few springs are not associated to any structural element.
295 Moreno et al. (2014) analysed the endogenous gas content of springs and water wells in
296 the northern part of the study area. A total of 41 measurements of water radon
297 concentration with values between 16.7 and 7.1 Bq.l⁻¹ were made, with most located on
298 the Amer and Llorà faults and others on other Neogene secondary faults (Fig. 5). As

299 well, Zarroca et al. (2012) measured a total of 12 CO₂-rich springs located in the
300 southern part of our study area on the central part of the Amer fault (Fig.5). The
301 emissions of CO₂ in this area are clearly measurable in the field as sustained bubbling
302 in freshwater springs.

303 A total of 144 seismic events have been recorded in the GVF since 1978 (Fig. 6)
304 and are mostly distributed along the Neogene faults clustered between the Amer and
305 Llorà faults. Moreover, there is a greater density of seismic events in the central part of
306 the Amer fault that coincides with high CO₂ emissions. The maximum earthquake
307 magnitude registered in this period was 3.5 (local magnitude) in 1983 on the Amer fault
308 (Fig. 6) (Table 3, Supp. material). Despite the low present-day seismicity, a swarm of
309 powerful earthquakes that took place in 1427-1428 with epicentral intensities ranging
310 between VI and VIII has been attributed to a movement of the Amer fault (Fontserè and
311 Iglésies, 1971; Goula et al., 1999; Olivera et al., 2003, 2006; Perea, 2009; Zarroca et al.,
312 2012).

313 As explained above, we also considered the distribution of mantle-derived
314 xenolith and crustal cumulates as a way of indicating the depth of the faults and fissures
315 through which they were transported to the surface, and of estimating magma ascent
316 velocities. The distribution of all ultramafic xenoliths found in the area along with their
317 maximum sizes is shown in Figure 7. We observed that the presence of xenoliths is
318 related to the volcanoes located near – but not on – the main Llorà fault. In the area with
319 the greatest density of volcanic cones (northern area), only three volcanoes (Rocanegra,
320 La Garrinada and La Canya; see Fig. 7) have ultramafic xenoliths, whilst in the southern
321 sector all the volcanoes have this type of xenoliths. Moreover, we observed that the
322 presence of upper-mantle cumulates (i.e. spinel lherzolites) coincides with the volcanoes
323 that have xenoliths, whereas the presence of lower-crust cumulates (i.e.

324 Pyroxenites/Amphybolites) is restricted to volcanoes located in the northern sector and
325 just one volcano in the south sector (Puig de la Banya del Boc; see Fig. 7). The
326 maximum sizes of the ultramafic xenoliths found in the GVF correspond to pyroxenites,
327 with diameters of up to 80 cm (Fig. 9). However, most xenoliths range in size from a
328 few centimetres to 20 cm in diameter, for both mantle-derived nodules and lower-crust
329 cumulates. Velocities of 0.19 to 0.21 m/s have been obtained using equations 2, 3, 4,
330 assuming a Newtonian viscosity of 40–50 Pa.s, the largest xenolith encountered (80
331 cm), a melt density of 2.53 g/cm³, a xenolith density of 3.55 g/cm³, and a gravity value
332 of 9.8 m/s². The velocities obtained are in accordance with those suggested for other
333 monogenetic volcanic fields (Zab and Odnar, 1998; Sparks et al.,
334 2006; Mattsson, 2012; Harangi et al., 2013; Jankovics et al., 2013).

335

336

337 **5. Discussion and conclusions**

338

339 The morphological and structural data presented above reveal that the evolution
340 of the GVF has been mostly controlled by two major Neogene faults, the Amer and
341 Llorà faults. They are both oriented NW-SE as are most of the major post-Alpine
342 extensional faults that have defined a horst and graben structural pattern in NE Iberia.
343 However, most of the eruptive fissures and secondary structural lineaments identified in
344 this study show a NNW-SSE trend that runs slightly obliquely to the main faults.

345 The pattern shown by the eruptive fissures and subordinated structural
346 lineaments is compatible with a slight dextral transtensional component in the two main
347 faults, as previously suggested by previous studies (Goula et al., 1999; Olivera et al.,
348 2003) and indicates that magma ascent in the uppermost crust and subsequent eruptions

349 were controlled by these subordinated fissures. This structural configuration would have
350 favoured the opening of these fractures and the transport of magma through them, at
351 least in the final pre-eruptive stages. Similar behaviour has been described in other
352 volcanic zones (e.g. Karakhanian et al., 2002). However, it is not clear how deep these
353 fractures are nor what exactly was their role in transporting magma from deeper levels.

354 The presence of mantle-derived xenoliths and lower-crust cumulates suggests
355 that the magmas that erupted in the GVF came either directly from the source region in
356 the upper mantle or from intermediate reservoirs located at the base of the crust. No
357 evidence exists for the presence of shallower reservoirs under this volcanic field. This is
358 also confirmed by existing petrological and geochemical data (Martí et al., 1992;
359 Neuman et al., 1999; Cebriá et al., 2000). Therefore, what remains to be discerned is
360 how deep the structures observed on the surface extend and how they were used by
361 magma to reach the surface. It is worth noting that most of the area's freshwater springs
362 are associated with relatively shallow stratigraphic or structural discontinuities, while
363 the presence of high radon and CO₂ concentrations mainly occurs along the major
364 Neogene faults (Moreno et al., 2014; Zarroca et al., 2012), thereby indicating that the
365 deep circulation of these mantle-derived gases is permitted through these faults
366 (Redondo and Yélamos, 2005; Zarroca et al., 2012). Likewise, the recorded seismicity
367 also reveals that Neogene faults have been active recently, mainly along the Amer fault.
368 Finally, the obtained magma ascent rates indicate that only a relatively short time was
369 required for magma to reach the surface, thereby suggesting the existence of preferential
370 pathways for magma when ascending from source or accumulation regions to the
371 eruption sites.

372 Taking into account all this evidence we speculate that the Llorà fault played the
373 most important role in driving magma from the source region, either to the base of the

374 crust where magma occasionally accumulated (underplating) and differentiated or
375 directly to much shallower levels where it was captured by the subordinated fractures
376 that allowed it to erupt to the surface. As indicated by the presence of lower-crust
377 cumulates and the location of vents and eruptive fissures, the extraction of magma from
378 the lower crust reservoir(s) was mainly controlled by the Llorà fault and, to a lesser
379 extent, by the Amer fault, which would have acted as a conjugate major fault reaching
380 down the base of the crust. Shallow subordinated fractures to the Amer fault would have
381 also captured the ascending magma in its last stages and have controlled its eruption to
382 the surface (Fig. 10).

383 Confirming the proposed model would require the undertaking of a detailed
384 petrological study, which is beyond the purpose of this paper. However, the fact that the
385 mantle-derived xenoliths and the largest lower-crust cumulates are restricted to the vents
386 related to the Llorà fault is strong support for this model. Likewise, the volcanoes
387 associated with this fault have the largest erupted volumes (Bolós et al., 2014b) of all
388 volcanoes in this volcanic field, which also suggests that the Llorà fault was the main
389 magma pathway.

390 The reason why magma eruptions have occurred through different NNW-SSE
391 eruptive fissures during the history of the GVF – despite its constant and common
392 feeding system at depth – seems to be related to the role played by these subordinate
393 shallow fractures. They captured magma during the final stages of its ascent to the
394 surface and so determined the point of each eruption. The shallow character of these
395 fractures suggests that the local stress field, which was mostly controlled by the
396 movement of the two main (Llorà and Amer) faults, only made a weak contribution.
397 Under these circumstances, these shallow fractures could be easily sealed by residual
398 magma that solidified within and it was easier for a new eruptive episode to open a

399 fresh fracture than to reuse a previously sealed one. The sealing of these eruptive
400 fissures by intruding magma would also obstruct the circulation of the endogenous
401 gases, as is shown in the northern sector around Olot, where most eruptive vents have
402 no associated volcanic gas emissions. This would also suggest – in accordance with the
403 intermittent character of this volcanism (Martí et al., 1992) – that each eruptive episode
404 corresponds to an intermittent reactivation of the main fault system every 5 000 – 20
405 000 years. These tectonic reactivations would permit the ascent of deep magma and the
406 opening of subordinate fractures in the uppermost crust, which would erupt on the
407 surface each time in a different location in the volcanic field. Volcanism in the GVF is
408 mainly concentrated in its northern sector, which suggests that the basin in this area is
409 larger, where the accumulation of post-Alpine sediments is thicker. Moreover, the
410 difference in basement lithology between the northern (Tertiary and Quaternary
411 sediments) and southern (Paleaeozoic granites and schists) sectors of the volcanic field
412 may also have played a significant role in controlling the ability for magma to find
413 pathways to reach the surface. The fact that there is no magmatism north of the GVF
414 may be due to the important increase in thickness of the crust due to the Alpine Orogeny
415 (Fig. 2).

416 Although the GVF is the best-preserved area in the Catalan Volcanic zone, it is
417 not the only one containing important volumes of volcanic rocks. Older zones such as
418 the Empordà or La Selva (Araña et al., 1983; Martí et al., 1992) also have numerous
419 volcanic features that can be observed on the surface (highly eroded outcrops) or in the
420 subsoil in seismic profiles and gravity and aeromagnetic maps (Casas et al., 1986;
421 Zeyen and Banda, 1988). The tectonic evolution of the area has been controlled by a
422 similar system of Neogene NW-SE-oriented faults, which seems to have evolved over
423 time from NE to SW. We believe that a similar model to the one proposed in this study

424 for the GVF could be applied to other areas in the Catalan Volcanic Zone.

425 In conclusion, the GVF provides a good example of the structural complexity
426 that governs monogenetic volcanism. Although magma ascent from the depths has
427 always been controlled by the same Neogene extensional fault system that reaches the
428 base of the lithosphere, magma transport in the uppermost crust and the eruptions were
429 controlled by subordinated fractures originating in response to the transtensional
430 component of the main faults. These shallow fractures were sealed by the remaining
431 magma after each eruption and so new fractures had to be opened in each new eruptive
432 episode, probably in association with a sporadic reactivation of the main faults. The
433 model proposed has important implications for hazard assessment as this pattern of
434 magma flow makes this type of volcanism largely unpredictable in terms of the eruption
435 location since the exact position of new vents does not necessarily follow a statistically
436 pre-defined law. Any point located in the area affected by the tectonic stresses
437 constrained by the two main faults could host a new vent if no major basement
438 rheological discontinuities exist. Moreover, the calculated ascent velocities imply that
439 magma may travel either from the source region in the mantle or from the base of the
440 crust to the surface in just a few days, as has been proposed in other monogenetic fields.
441 It is likely that most of this journey occurred aseismically due to the relatively large
442 dimensions of the path provided by the main faults and the absence of shear movement
443 between the fault planes, as occurred in the 2011-2012 El Hierro eruption (Martí et al.,
444 2013). Only when magma had to open the shallow subordinate fractures did the
445 hydraulic fracturing cause any shallow seismicity that could warn of the imminence of
446 the eruption. Therefore, precise knowledge of the stress configuration and distribution
447 of rheological and structural discontinuities in monogenetic fields is crucial when
448 attempting to forecast monogenetic volcanism.

449

450

451 **Acknowledgments**

452

453 This study was partially funded by the European Commission (FT7 Theme:
454 ENV.2011.1.3.3-1; Grant 282759: "VUELCO") and Beca Ciutat d'Olot en Ciències
455 Naturals. We are grateful to La Garrotxa Volcanic Zone Natural Park for their support
456 throughout this study. We would like to thank Emilio Casciello, Núria Bagués, Joan
457 Andujar, Pierangelo Romano, Dario Pedrazzi, Daniele Giordano, Jorge Pedro Galve,
458 Xavier Castelltort and Daniel Nadal for their suggestions during this research. We also
459 thank Enric Vinyals for providing us with unpublished information on seismic studies in
460 the study area. The English text was corrected by Michael Lockwood.

461

462

463 **References**

464

- 465 Acocella, V., Tibaldi, A., 2005. Dike propagation driven by volcano collapse: a general
466 model tested at Stromboli, Italy. *Geophysical Research Letters* 32.
- 467 Araña, V., Aparicio, A., Martín Escorza, C., García Cacho, L., Ortiz, R., Vaquer, R.,
468 Barberi, F., Ferrara, G., Albert, J., Gassiot, X., 1983. Neogene-Quaternary
469 volcanism of Catalunya: structural, petrological, and geodynamic characteristics.
470 *Acta Geol. Hisp.* 18, 1-17.
- 471 Barde-Cabusson, S., Bolós, X., Pedrazzi, D., Lovera, R., Serra, G., Martí, J., Casas, A.,
472 2013. Electrical resistivity tomography revealing the internal structure of
473 monogenetic volcanoes. *Geophysical Research Letters* 40, 2544-2549.

474 Barde-Cabusson, S., Gottsman, J., Martí, J., Bolós, X., Camacho, A.G., Geyer, A.,
475 Planagumà, L., Ronchin, E., Sanchez, A., 2014. Structural control of monogenetic
476 volcanism in the Garrotxa volcanic field (Northeastern Spain) from gravity and
477 self-potential measurements. *Bulletin of Volcanology* 76, 788.

478 Becerril, L., Cappello, A., Galindo, I., Neri, M., Del Negro, C., 2013. Spatial probability
479 distribution of future volcanic eruptions at El Hierro Island (Canary Islands,
480 Spain). *Journal of Volcanology and Geothermal Research* 257, 21-30.

481 Bibby H. M., Caldwell T. G., Risk G. F., 1998: Electrical resistivity image of the upper
482 crust within the Taupo Volcanic Zone, New Zealand. *Journal Geophysical*
483 *Research*, 103, 9665-9680.

484 Bianchini, G., Beccaluva, L., Bonadiman, C., Nowell, G., Pearson, G., Siena, F., Wilson,
485 M., 2007. Evidence of diverse depletion and metasomatic events in harzburgite–
486 lherzolite mantle xenoliths from the Iberian plate (Olot, NE Spain) implications for
487 lithosphere accretionary processes. *Lithos* 94, 25-45.

488 Blaikie, T. N., Ailleres, L., Betts, P. G., Cas, R.A.F., 2014, A geophysical comparison of
489 the diatremes of simple and complex maar volcanoes, Newer Volcanics Province,
490 south-eastern Australia. *Journal of Volcanology and Geothermal Research* 276
491 (2014) 64–81

492 Bolós, X., Barde-Cabusson, S., Pedrazzi, D., Martí, J., Casas, A., Himi, M., Lovera, R.,
493 2012. Investigation of the inner structure of La Crosa de Sant Dalmai maar
494 (Catalan Volcanic Zone, Spain). *Journal of Volcanology and Geothermal Research*
495 247–248, 37-48.

496 Bolós, X., Barde-Cabusson, S., Pedrazzi, D., Martí, J., Casas, A., Lovera, R., Nadal-
497 Sala, D., 2014a (in press). Geophysical exploration on the subsurface geology of

498 La Garrotxa monogenetic Volcanic Field (NE Iberian Peninsula). *International*
499 *Journal of Earth Science*.

500 Bolós, X., Planagumà, L., Martí, J., 2014b (in press). Volcanic stratigraphy and
501 evolution of the Quaternary monogenetic volcanism in the Catalan Volcanic Zone
502 (NE Spain). *Journal of Quaternary Science*.

503 Brenna, M., Cronin, S.J., Németh, K., Smith, I.E.M., Sohn, Y.K., 2011. The influence of
504 magma plumbing complexity on monogenetic eruptions, Jeju Island, Korea. *Terra*
505 *Nova* 23(2), 70-75.

506 Catalan Geographic Institute (ICC). <http://www.icc.cat/>. Accessed 15 January 2014

507 Catalan Geologic Institute (IGC). <http://www.igc.cat/>. Accessed 15 January 2014

508 Cardozo, N., Allmendinger, R.W., 2013. Spherical projections with OSXStereonet
509 *Computers & Geosciences* 51, 193-205.

510 Casas, A., Torné, M., Banda, E., 1986. Mapa gravimètric de Catalunya 1:500000. Servei
511 Geològic de Catalunya . Dpt. De Política Territorial i Obres Públiques.

512 Cebrià, J.M., López-Ruiz, J., Doblas, M., Oyarzun, R., Hertogen, J., Benito, R., 2000.
513 Geochemistry of the Quaternary alkali basalts of Garrotxa (NE Volcanic Province,
514 Spain): a case of double enrichment of the mantle lithosphere. *Journal of*
515 *Volcanology and Geothermal Research* 102, 217-235.

516 Cebrià, J.M., Martín-Escorza, C., López-Ruiz, J., Morán-Zenteno, D.J., Martiny, B.M.,
517 2011. Numerical recognition of alignments in monogenetic volcanic areas:
518 Examples from the Michoacán-Guanajuato Volcanic Field in Mexico and
519 Calatrava in Spain. *Journal of Volcanology and Geothermal Research* 201, 73-82.

520 Cimarelli, C., Di Tragia, F., de Rita, D., Gimeno Torrente, D., Fernandez Turiel, J.L.,
521 2013. Space–time evolution of monogenetic volcanism in the mafic Garrotxa
522 Volcanic Field (NE Iberian Peninsula). *Bulletin of Volcanology* 75, 758.

523 Cimarelli, C., Di Traglia, F., Taddeucci, J., 2012. Basaltic scoria textures from a zoned
524 conduit as precursors to violent Strombolian activity. *Geology* 38, 439-442.

525 Clemens, J.D., Mawer, C.K., 1992. Granitic magma transport by fracture propagation.
526 *Tectonophysics* 204, 339-360.

527 Connor, C.B., Conway, F.M., 2000. Basaltic volcanic fields. In: Sigurdsson, H.,
528 Houghton, B.F., McNutt, S.R., Rymer H., Stix J. (Editors), *Encyclopedia of*
529 *Volcanoes*. Academic Press, San Diego, p. 331–343.

530 Dèzes, P., Schmid, S.M., Ziegler, P.A., 2004. Evolution of the European Cenozoic Rift
531 System: interaction of the Alpine and Pyrenean orogens with their foreland
532 lithosphere. *Tectonophysics* 389, 1–33.

533 Di Maio, R., Mauriello, P., Patella, D., Petrillo, Z., Piscitelli, S., Siniscalchi, A., 1998.
534 Electric and electromagnetic outline of the Mount Somma-Vesuvius structural
535 setting. *Journal of Volcanology and Geothermal Research*, 82, 219-238.

536 Di Maio R., Patella D., Petrillo Z., Siniscalchi A., Cecere G., De Martino P., 2000:
537 Application of electric and electromagnetic methods to the definition of the
538 Campi Flegrei caldera (Italy). *Annali di Geofisica*, 43, 375-390.

539 Downes, H., 2001. Formation and modification of the shallow sub-continental
540 lithospheric mantle: a review of geochemical evidence from ultramafic xenolith
541 suites and tectonically emplaced ultramafic massifs of Western and Central
542 Europe. *Journal of Petrology* 42, 233-250.

543 Fernández, M., Torné, M., Zeyen, H., 1990. Lithospheric thermal structure of NE Spain
544 and the North-Balearic basin. *Journal of Geodynamics* 12, 253–267.

545 Fiske, R.S., Jackson, E.D., 1972. Orientation and growth of Hawaiian volcanic rifts: the
546 effect of regional structure and gravitational stresses. *Proc. R. Soc. Lond.* 329,
547 299-326.

548 Fontserè, E., Iglésies, J., 1971. Recopilació de dades sísmiques de les terres catalanes
549 entre 1100 i 1906. Fundació Salvador Vives Casajuana, Barcelona, 548.

550 Galán, G., Oliveras, V., Paterson, B.A., 2008. Types of metasomatism in mantle
551 xenoliths enclosed in Neogene–Quaternary alkaline mafic lavas from Catalonia
552 (NE Spain). *Geological Society of London* 293, 121-153.

553 Gallart, J., Olivera, C., Correig, A., 1984. Aproximación geofísica a la zona volcánica de
554 Olot (Girona). *Estudio local de sismicidad. Revista de Geofísica* 40, 205-226.

555 Gallart, J., Pous, J., Boix, F., Hirn, A., 1991. Geophysical constraints on the structure of
556 the Olot Volcanic Area, north-eastern Iberian Peninsula. *Journal of Volcanology
557 and Geothermal Research* 47, 33–44.

558 Goula, X., Olivera, C., Fleta, J., Grellet, B., Lindo, R., Rivera, L.A., Cisternas, A.,
559 Carbon, D., 1999. Present and recent stress regime in the eastern part of the
560 Pyrenees. *Tectonophysics* 308, 487–502.

561 Gretener, P.E., 1969. On the mechanics of the intrusion of sills. *Canadian Journal of
562 Earth Sciences* 6, 1415–1419.

563 Grosse, P., van Wyk de Vries, B., Petrinovic, I.A., Euillades, P.A., Alvarado, G., 2009.
564 Morphometry and evolution of arc volcanoes. *Geology* 37, 651–654.

565 Gudmundsson, A., 2003. Surface stresses associated with arrested dykes in rift
566 zones. *Bulletin of Volcanology* 65, 606-619.

567 Grosse, P., B. van Wyk de Vries, P. A. Euillades, M. Kervyn, and I. Petrinovic (2012),
568 Systematic morphometric characterization of volcanic edifices using digital
569 elevation models, *Geomorphology*, 136, 114–131,
570 doi:10.1016/j.geomorph.2011.06.001.

571 Gudmundsson, A., Philipp, S.L., 2006. How local stress fields prevent volcanic
572 eruptions. *J. Volcanol. Geotherm. Res.* 158, 257-268.

573 Guérin, G., Behamoun, G., Mallarach, J.M., 1985. Un exemple de fusió parcial en medi
574 continental. El vulcanisme quaternari de la Garrotxa. Publicació del Museu
575 Comarcal de la Garrotxa, Vitrina 1, 19–26.

576 Harangi, S., Sági, T., Seghedi, I., Ntaflos, T., 2013. Origin of basaltic magmas of
577 Perşani volcanic field, Romania: a combined whole rock and mineral scale
578 investigation. *Lithos* 180-181, 43–57 (in this issue).

579 IGME, 2011. Continuous Digital Geological Map of Spain, Canary Islands, 1:25.000,
580 <http://cuarzo.igme.es/sigeco/>. Accessed 15 January 2014

581 Jankovics, M.É., Dobosi, G., Embey-Isztin, A., Kiss, B., Sági, T., Harangi, S., Ntaflos,
582 T., 2013. Origin and ascent history of unusually crystal-rich alkaline
583 basaltic magmas from the western Pannonian Basin. *Bulletin of Volcanology* 75,
584 1–23. DOI 10.1007/s00445-013-0749-7

585 Karakhanian, A., Djr bashian, R., Trifonov, V., Philip, H., Arakelian, S., 2002
586 holocene-historical volcanism and active faults as natural risk factors for Armenia
587 and adjacent countries. *Journal of Volcanology and Geothermal Research* 113,
588 319-344

589 Kavanagh, J.L., Menand, T., Sparks, R.S.J., 2006. An experimental investigation of sill
590 formation and propagation in layered elastic media. *Earth Planetary Science*
591 *Letters* 245, 799-813.

592 Lu gel, A., 1998. Reactions between mantle xenoliths and host magma beneath La
593 Palma (Canary Islands): constraints on magma ascent rates and crustal reservoirs.
594 *Contrib Mineral Petrol* 131(2):237–257

595 Kresic, N., 2010. Types and classifications of springs, in: Kresic, N., Stevanovic, Z.
596 (Eds.), *Groundwater Hydrology of Springs: Engineering, Theory, Management*
597 *and Sustainability*. Butterworth-Heinemann, p. 592.

598 Le Corvec, N., Menand, T., Lindsay, J., 2013. Spatial distribution and alignments of
599 volcanic centers: Clues to the formation of monogenetic volcanic fields. *Earth-*
600 *Science Reviews* 124, 96-114.

601 Llobera, P., 1983. Petrologia de los enclaves del volcán Roca Negra (Olot, NE España).
602 *Acta Geològica Hispànica* 18, 19-25.

603 Lutz, T.M., 1986. An analysis of the orientations of large-scale crustal structures: a
604 statistical approach based on areal distributions of pointlike feature. *Journal of*
605 *Geophysical Research* 91 (B1), 421–434.

606 Martí, J., Mitjavila, J., Roca, E., Aparicio, A., 1992. Cenozoic magmatism of the
607 Valencia trough(western Mediterranean): relationship between structural evolution
608 and volcanism. *Tectonophysics* 203, 145-165.

609 Martí, J., Planagumà, L., Geyer, A., Canal, E., Pedrazzi, D., 2011. Complex interaction
610 between Strombolian and phreatomagmatic eruptions in the Quaternary
611 monogenetic volcanism of the Catalan Volcanic Zone (NE of Spain). *Journal of*
612 *Volcanology and Geothermal Research* 201, 178-193.

613 Martí, J., Pinel, V., López, C., Geyer, A., Abella, R., Tárraga, M., Blanco, M.J., Castro,
614 A., Rodríguez, C., 2013. Causes and mechanisms of the 2011-2012 El Hierro
615 (Canary Islands) submarine eruption, *J. Geophys. Res. Solid Earth*, 118, 823–839,
616 doi:10.1002/jgrb.50087.

617 Mattsson, H.B., 2012. Rapid magma ascent and short eruption durations in the Lake
618 Natron–Engaruka monogenetic volcanic field (Tanzania): a case study of the
619 olivine melilititic Pello Hill scoria cone. *Journal of Volcanology and Geothermal*
620 *Research* 247–248, 16–25.

621 McGee, L., Beier, C., Smith, I., Turner, S., 2011. Dynamics of melting beneath a
622 smallscale basaltic system: a U-Th–Ra study from Rangitoto volcano, Auckland
623 volcanic field, New Zealand. *Contributions to Mineralogy and Petrology*, 1-17.

624 Michon L. Merle O. 5. Discussion on “Evolution of the European Cenozoic Rift
625 System: interaction of the Alpine and Pyrenean orogens with their foreland
626 lithosphere”. *ectonophysics* 5 -256.

627 Moreno, V., Bach, J., Baixeras, C., Font, L., 2014. Radon levels in groundwaters and
628 natural radioactivity in soils of the volcanic region of La Garrotxa, Spain. *Journal*
629 *of Environmental Radioactivity* 128, 1-8.

630 Neumann, E.R., Martí, J., Mitjavila, J., Wulff-Pedersen, E., 1999. Origin and
631 implications of marie xenoliths associated with Cenozoic extension-related
632 volcanism in the Valencia Trough, NE Spain. *Minerology and Petrology* 65, 113-
633 139.

634 Nishi Y., Ishido T., Matsushima N., Ogawa Y., Tosha T., Myazaki J., Yasuda A., Scott
635 B.J., Sherbum S., Bromley C., 1996: Self-Potential and audio-magnetotelluric
636 survey in White Island Volcano. *New Zealand Geothermal Workshop*
637 (<http://www.geothermal-energy.org/pdf/IGAstandard/NZGW/1996/Nishi.pdf>).

638 Olivera, C., Fleta, J., Susagna, T., Figueras, S., Goula, X., Roca, A., 2003. Seismicity
639 and recent deformations in the northeastern of the Iberian Peninsula. *Física de la*
640 *Tierra* 15, 111-114.

641 Olivera, C., Redondo, E., Lambert, J., Riera Melis, A., Roca, A., 2006. Els terratrèmols
642 dels segles XIV i XV a Catalunya. *Institut Cartogràfic de Catalunya, Barcelona*
643 *Monografies no. 30, 407.*

644 Paulsen, T.S., Wilson, T.J., 2010. New criteria for systematic mapping and reliability
645 assessment of monogenetic volcanic vent alignments and elongate volcanic vents
646 for crustal stress analyses. *Tectonophysics* 482, 16–28.

647 Perea, H., 2009. The Catalan seismic crisis (1427 and 1428; NE Iberian Peninsula):
648 Geological sources and earthquake triggering. *Journal of Geodynamics* 47, 259-
649 270.

650 Portal, A., Labazuy, P., Lénat, J.F., Béné, S., Boivin, P., Busato, E., Cârloganu, C.,
651 Combaret, C., Dupieux, P., Fehr, F., Gay, P., Laktineh, I., Miallier, D., Mirabito, L.,
652 Niess, V., Vulpescu, B., 2013. Inner structure of the Puy de Dôme volcano: cross-
653 comparison of geophysical models (ERT, gravimetry, muon imaging). *Geosci.*
654 *Instrum. Method. Data Syst.* 2, 47–54. Revil A (2002)

655 Rubin, A.M., 1995. Propagation of magma-filled cracks. *Annual Review of Earth &*
656 *Planetary Sciences* 23, 287-336.

657 Sachs, P.M., Stange, S., 1993. Fast assimilation of xenoliths in mag-mas. *J Geophys Res*
658 98(B11): 19741-19754

659 Saula, E., Picart, J., Mató, E., Llenas, M., Losantos, M., Berasategui, X., Agustí, J.,
660 1996. Evolución geodinámica de la fosa del Empordà y de las Sierras
661 Transversales. *Acta Geologica Hispánica* 29, 55–75.

662 Sparks, R.S.J., Pinkerton, H., Macdonald, R., 1977. The transport of xenoliths in
663 magmas. *Earth Planet Sci Lett* 35(2):234–238.

664 Sparks, R.S.J., Baker, L., Brown, R.J., Field, M., Schumacher, J., Stripp, G., Walters, A.,
665 2006. Dynamical constraints on kimberlite volcanism. *J Volcanol Geotherm Res*
666 155(1–2):18–48.

667 Spera, F.J., 1980. Aspects of magma transport, in: Hargraves, R.B. (Ed.), *Physics of*
668 *magmatic processes*. Princeton University Press, p. 265-323.

669 Spera, F.J., 1984. Carbon dioxide in petrogenesis III: role of volatiles in the ascent of
670 alkaline magma with special reference to xenolith-bearing mafic lavas. *Contrib.*
671 *Mineral. Petrol.* 88, 217-232.

672 Szabó, C., Bodnar, R.J., 1996. Changing magma ascent rates in the Nógrád–Gömör
673 volcanic field, Northern Hungary/Southern Slovakia: evidence from CO₂-rich
674 fluid inclusions in metasomatized upper mantle xenoliths. *Petrology* 4(3):221–230

675 Tibaldi, A., 1995. Morphology of pyroclastic cones and tectonics. *Journal of*
676 *Geophysical Research* 100.

677 Tibaldi, A., 2003. Influence of cone morphology on dykes, Stromboli, Italy. *Journal of*
678 *Volcanology and Geothermal Research* 126, 79-95.

679 Tibaldi, A., Bonali, F.L., Corazzato, C., 2014. The diverging volcanic rift system.
680 *Tectonophysics* 611, 94-113.

681 Tsuchiyama, A., 1986. Melting and dissolution kinetics: application to partial melting
682 and dissolution of xenoliths. *J Geophys Res* 91(B9): 9395-9406

683 Vona, A., Romano, C., Dinwell, D.B., Giordano, D., 2011. The rheology of crystal-
684 bearing basaltic magmas from Stromboli and Etna. *Geochimica et Cosmochimica*
685 *Acta* 75, 3214–3236.

686 Walker, G.P.L., 1999. Volcanic rift zones and their intrusion swarms. *Journal of*
687 *Volcanology and Geothermal Research* 94, 21–34.

688 Wattananikorn, K., Kanaree, M., Wiboolsake, S., 1998. Soil gas radon as an earthquake
689 precursor: some considerations on data improvement. *Radiate Measurements* 29,
690 593-598.

691 Zarroca, M., Linares, R., Bach, J., Roqué, C., Moreno, V., Font, L., Baixeras, C., 2012.
692 Integrated geophysics and soil gas profiles as a tool to characterize active faults:

693 the Amer fault example (Pyrenees, NE Spain). *Environment Earth Science* 67,
694 889-910.

695 Zeyen, H. J. Banda, E., 1988. Geophysical mapping in Catalonia. Aeromagnetic map.
696 *Rev. Soc. Geol. España*, 1, (1-2), 73-79.

697 Ziegler, P.A., 1992. European Cenozoic rift system. In: P.A. Ziegler (ed), *Geodynamics*
698 *of Rifting, Volume I. Case History Studies on Rift: Europe and Asia.*
699 *Tectonophysics*, 208:91-111.

700 **Figure captions**

701

702 Figure 1. Location of the study area. a) Simplified map of the distribution of the
703 European rift system. b) Simplified geological map of the Catalan Volcanic Zone
704 (modified from Guérin et al., 1985). c) Geographic distribution of La Garrotxa
705 Quaternary volcanic field.

706

707 Figure 2. Volcano-structural map of La Garrotxa Volcanic Field. a) Rose diagram of
708 faults; Neogene faults are represented in dark grey and Alpine reverse faults in light
709 grey. b) Rose diagram of eruptive fissures.

710

711 Figure 3. Drainage network of La Garrotxa Volcanic Field. Trends are represented in a
712 rose diagram.

713

714 Figure 4. Eruptive vent lineaments obtained using the nearest-neighbour technique. The
715 rose diagram shows the distribution of the alignments.

716

717 Figure 5. Map of freshwater springs (blue dots) and water radon concentrations (purple
718 stars) obtained by Moreno et al. (2014), and CO₂-rich springs (blue stars) obtained by
719 Zarroca et al. (2012).

720

721 Figure 6. Epicentral map of regional seismic events recorded by the Geological Survey
722 of Catalonia (IGC) since 1978.

723

724 Figure 7. Volcano-structural map with the distribution of all ultramafic xenoliths (upper-
725 mantle and lower-crust xenoliths) found in the study area, with an indication of their
726 maximum size. a: La Canya; b: La Garrinada; c: Rocanegra; d: Puig de la Banya del
727 Boc.

728

729 Figure 8. Outcrops of Quaternary volcanic deposits affected by the Amer fault.

730

731 Figure 9. Photograph of the largest xenolith (pyroxenite) found in the study area (Banya
732 del Boc volcano, southern sector of the GVF, see Fig. 7).

733

734 Figure 10. Schematic representation of the relationships between regional/local tectonic
735 faulting and the plumbing system of La Garrotxa Volcanic Field. (Right) cross section.
736 (Left) top view.

737

738 **Supplementary material**

739

740 Table 1. Summary of the structural data.

741 Table 2. Summary of the morphometric data. ND: not determined. * Azimuth of crater
742 alignment.

743 Table 3. Seismic events recorded by the Geological Survey of Catalonia (IGC) since

744 1978. ND: not determined.

Figure 1

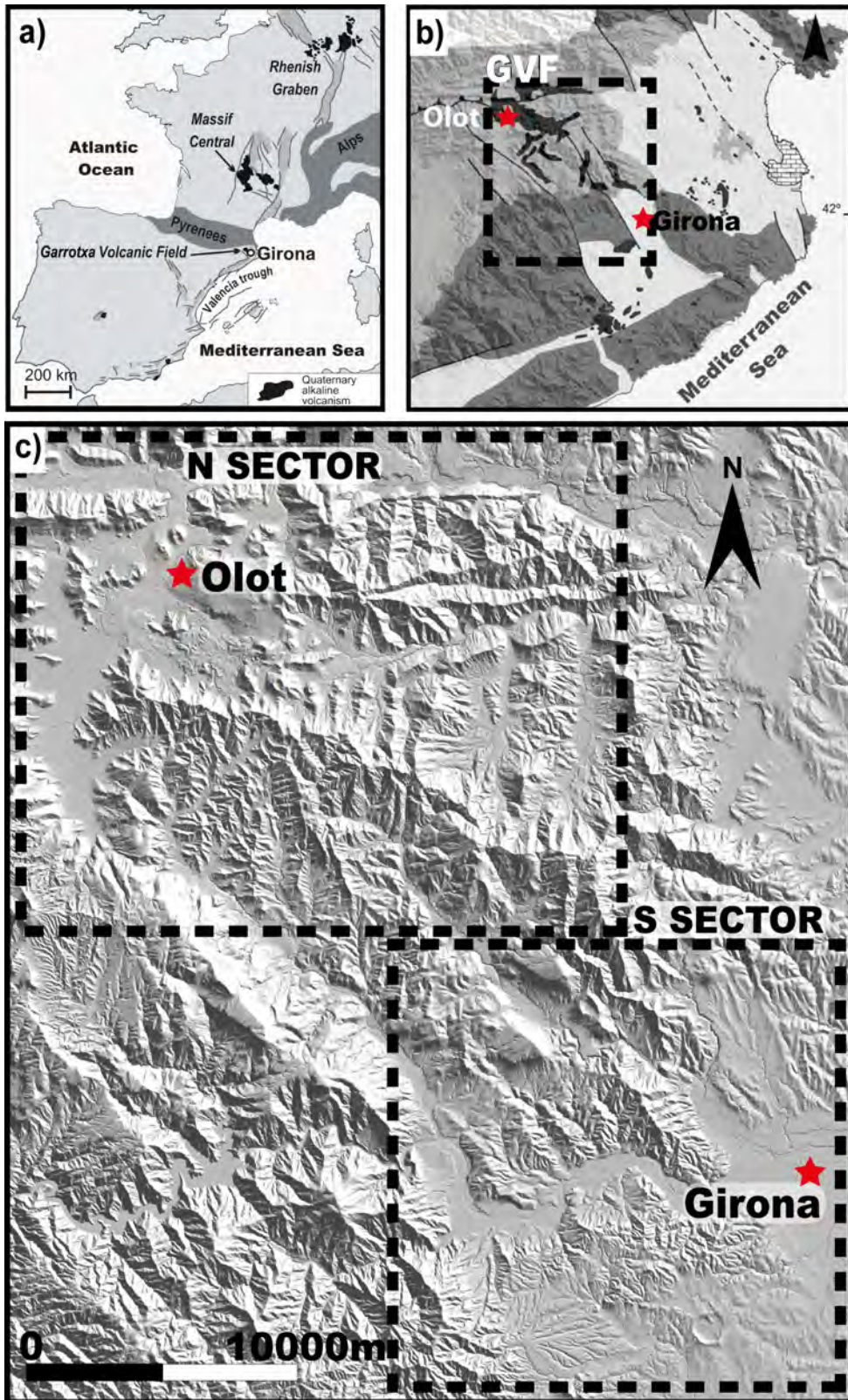
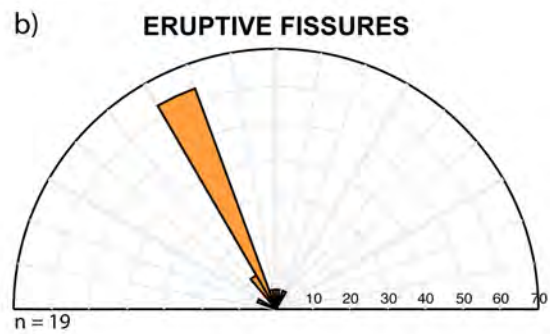
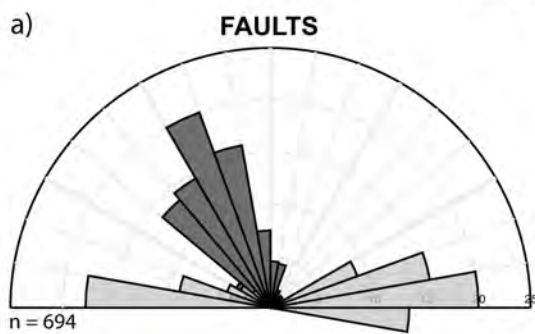
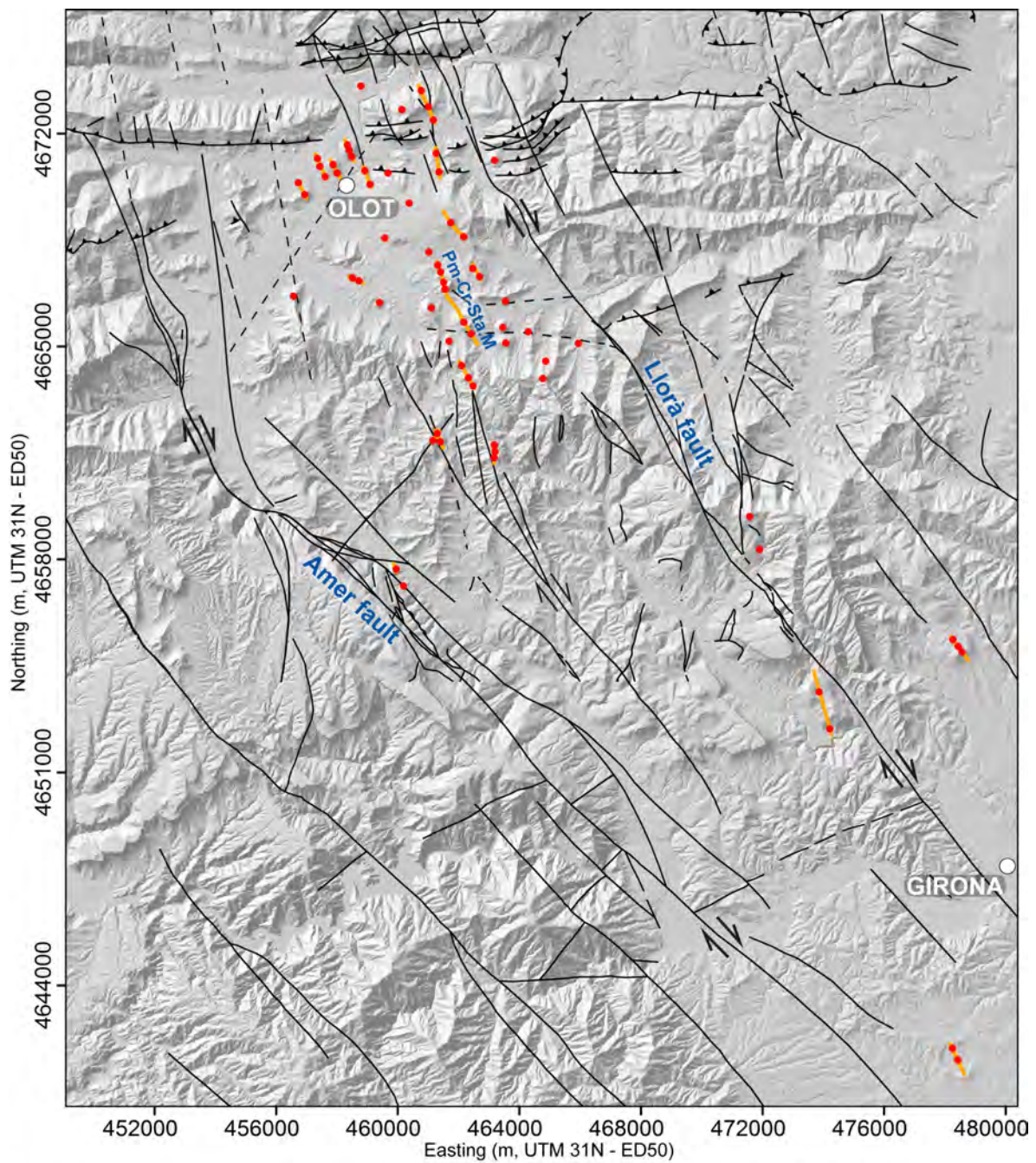


Figure 2



- Eruptive vents
- Eruptive fissures
- Normal and transensional Neogene faults
- - - Inferred faults
- ▲ Reverse Alpine faults
- Main cities

Figure 3

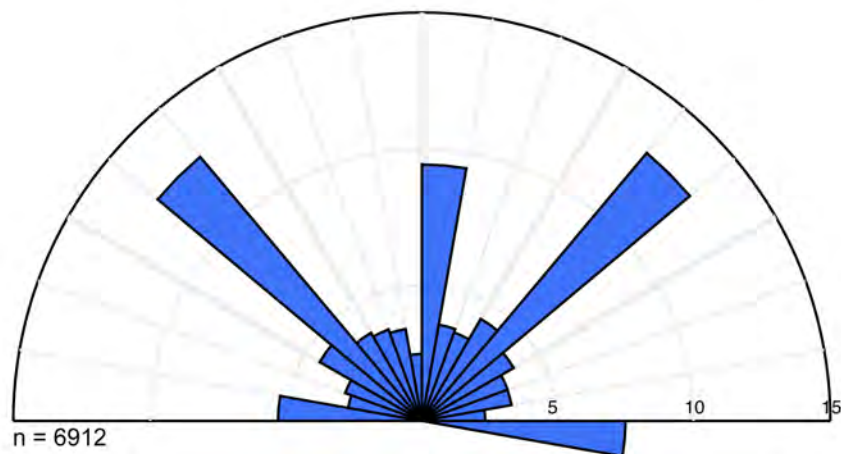
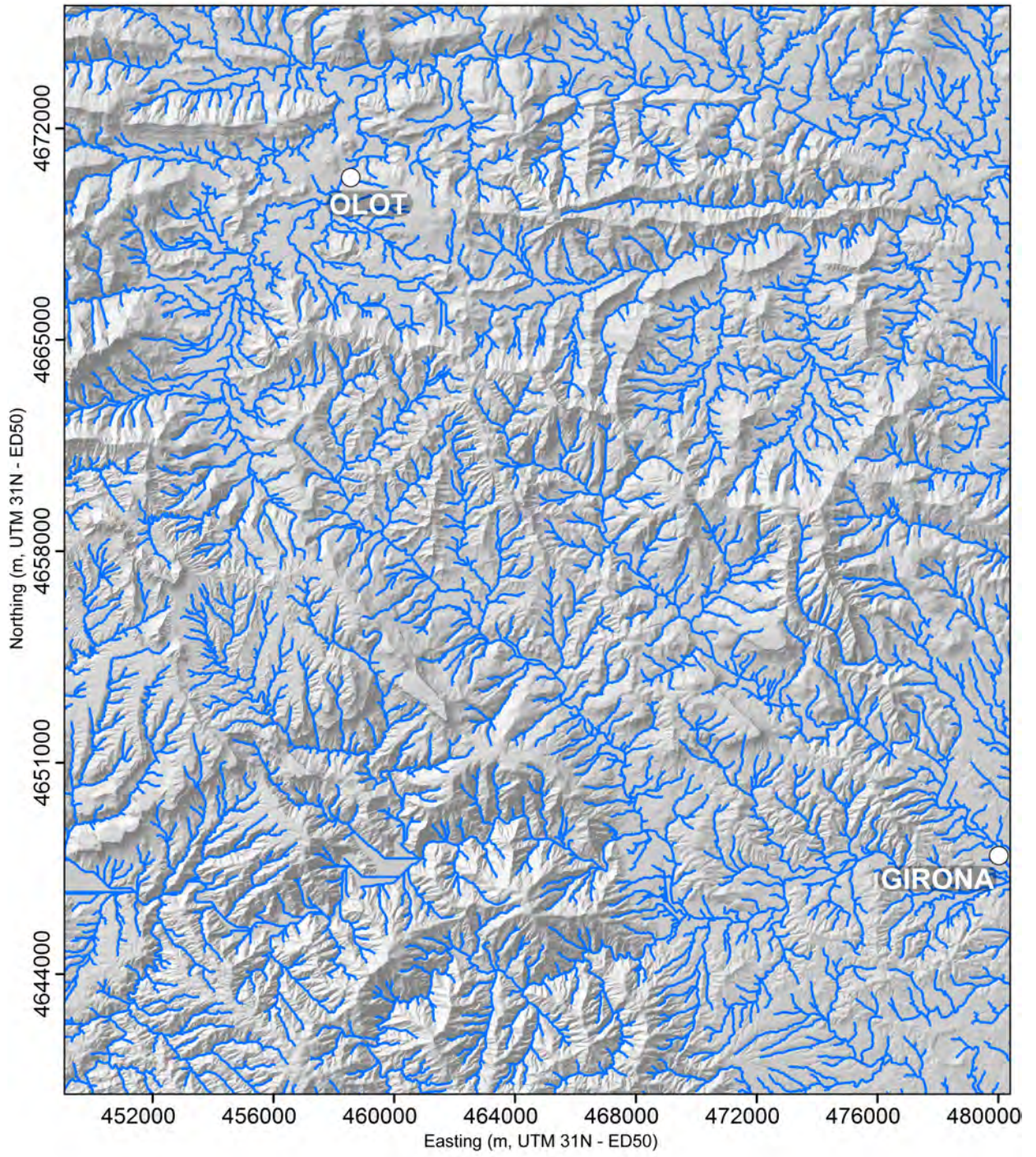


Figure 4

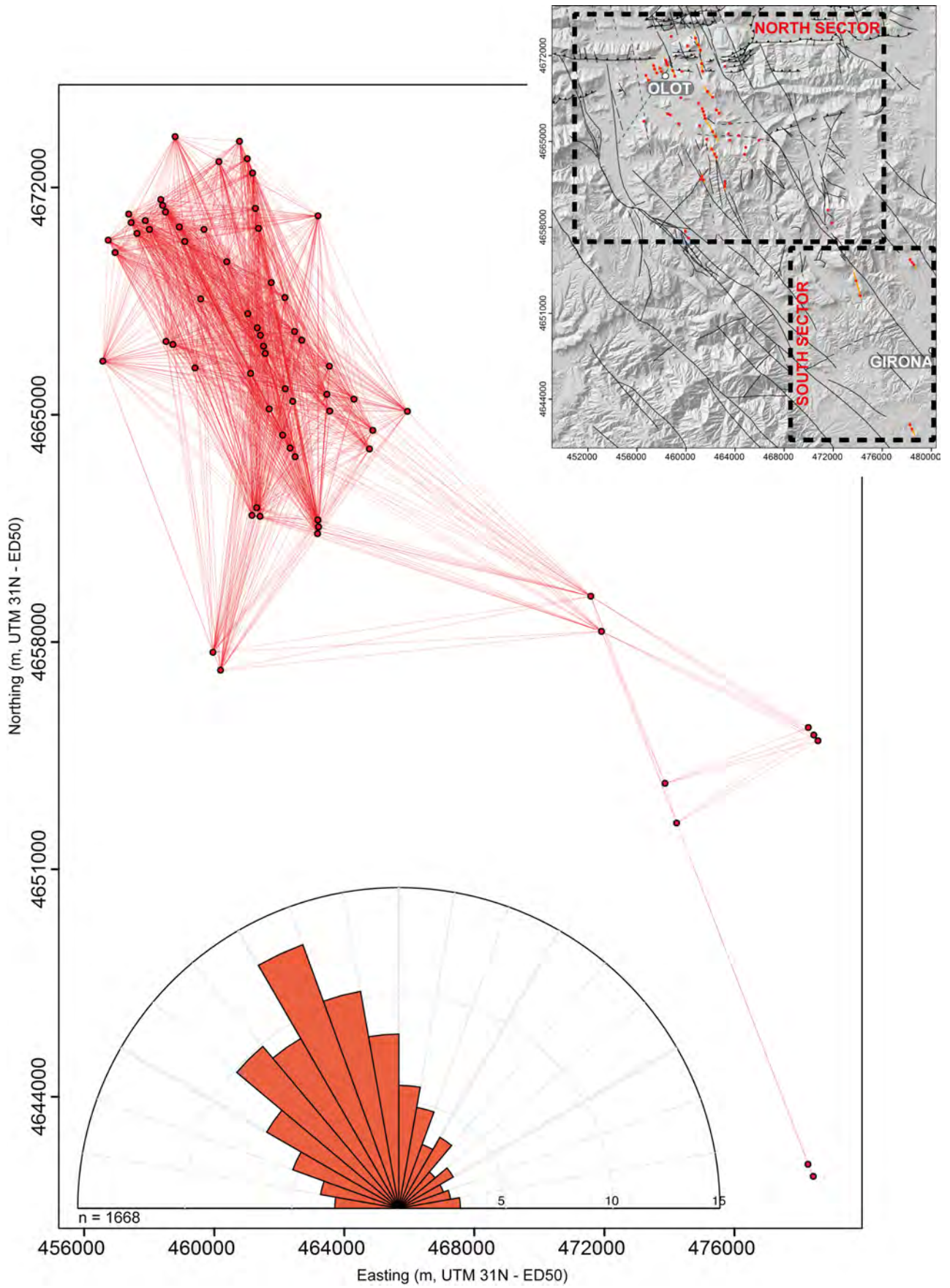
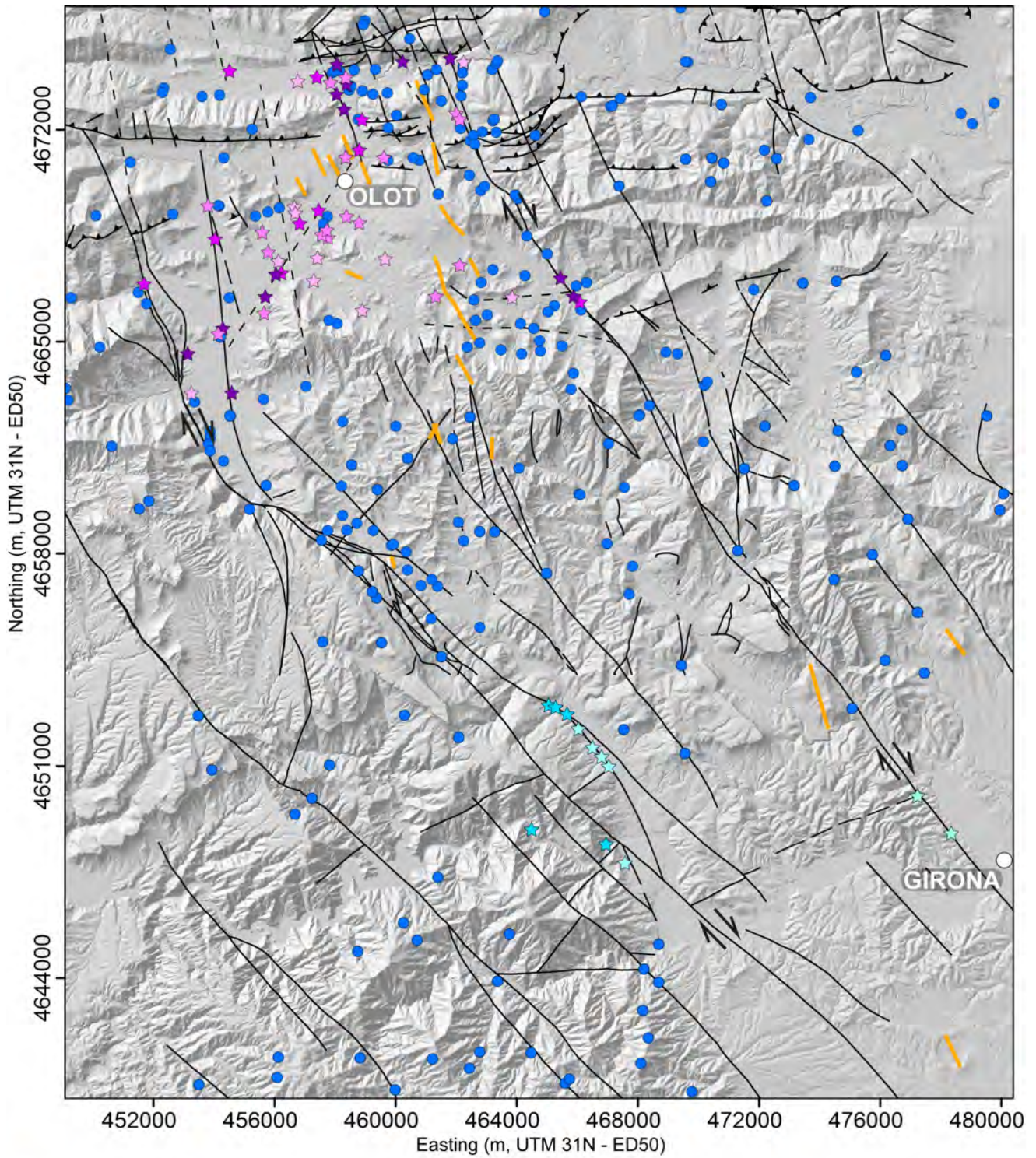
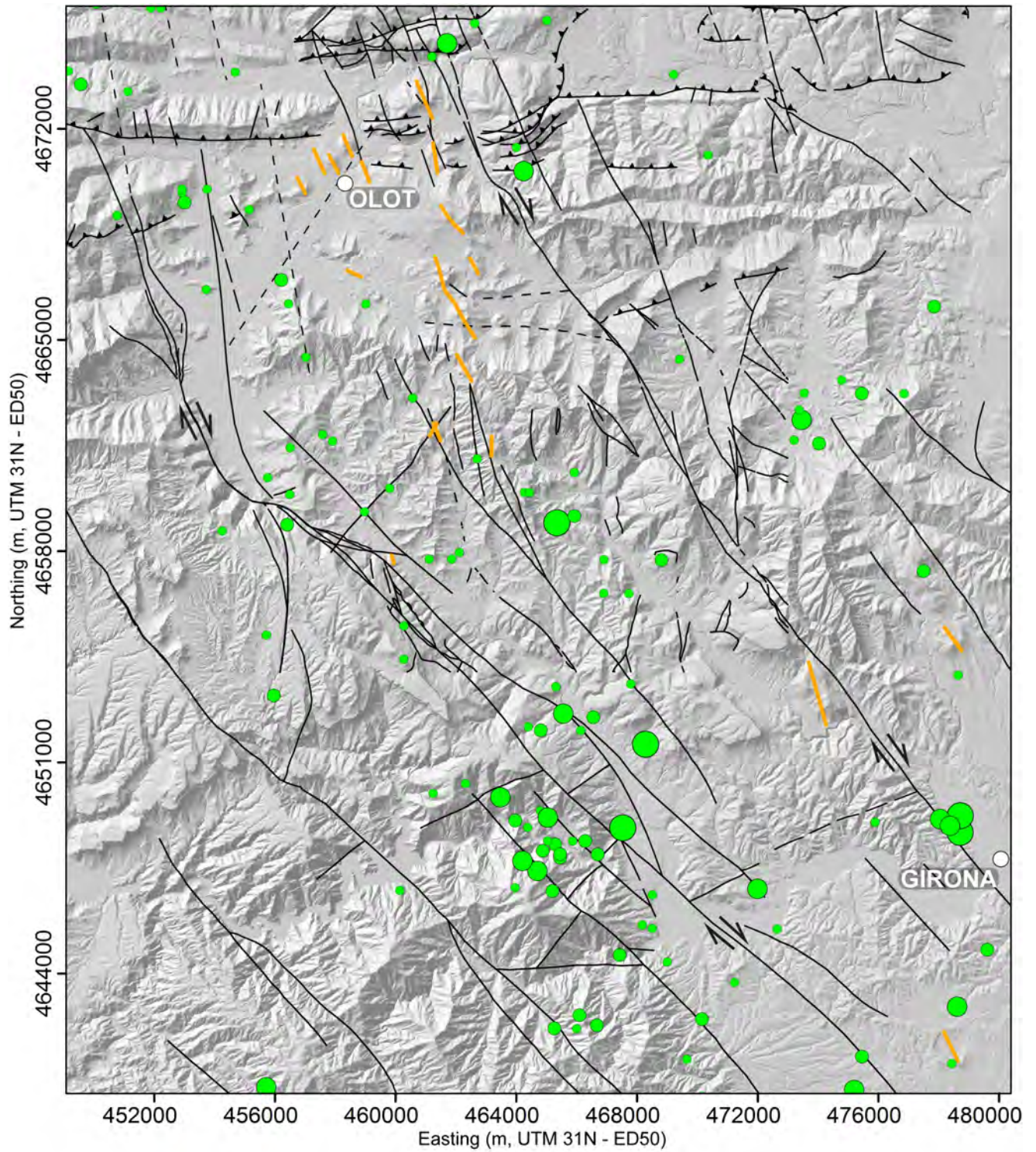


Figure 5



- | | |
|--|--|
| ● Water springs (icc.cat + fieldwork) | — Eruptive fissures |
| ★ Water radon concentration over $16.7 \text{ Bq}\cdot\text{l}^{-1}$ (Moreno et al., 2014) | — Normal and transtensional Neogene faults |
| ★ Water radon concentration between 11.4 and $16.7 \text{ Bq}\cdot\text{l}^{-1}$ (Moreno et al., 2014) | - - - Inferred faults |
| ★ Water radon concentration between 7.1 and $11.4 \text{ Bq}\cdot\text{l}^{-1}$ (Moreno et al., 2014) | ↔ Reverse Alpine faults |
| ★ Water radon concentration under $7.1 \text{ Bq}\cdot\text{l}^{-1}$ (Moreno et al., 2014) | ○ Main cities |
| ★ CO_2 - rich springs (Zarroca et al., 2012) | |
| ★ Springs with limited CO_2 (Zarroca et al., 2012) | |

Figure 6












-  Eruptive fissures
-  Normal and transensional Neogene faults
-  Inferred faults
-  Reverse Alpine faults
-  Main cities
- Epicenters 1978 - 2014 (Magnitudes)**
 -  M < 1
 -  1 ≤ M < 2
 -  2 ≤ M < 3
 -  M ≥ 3

Figure 7

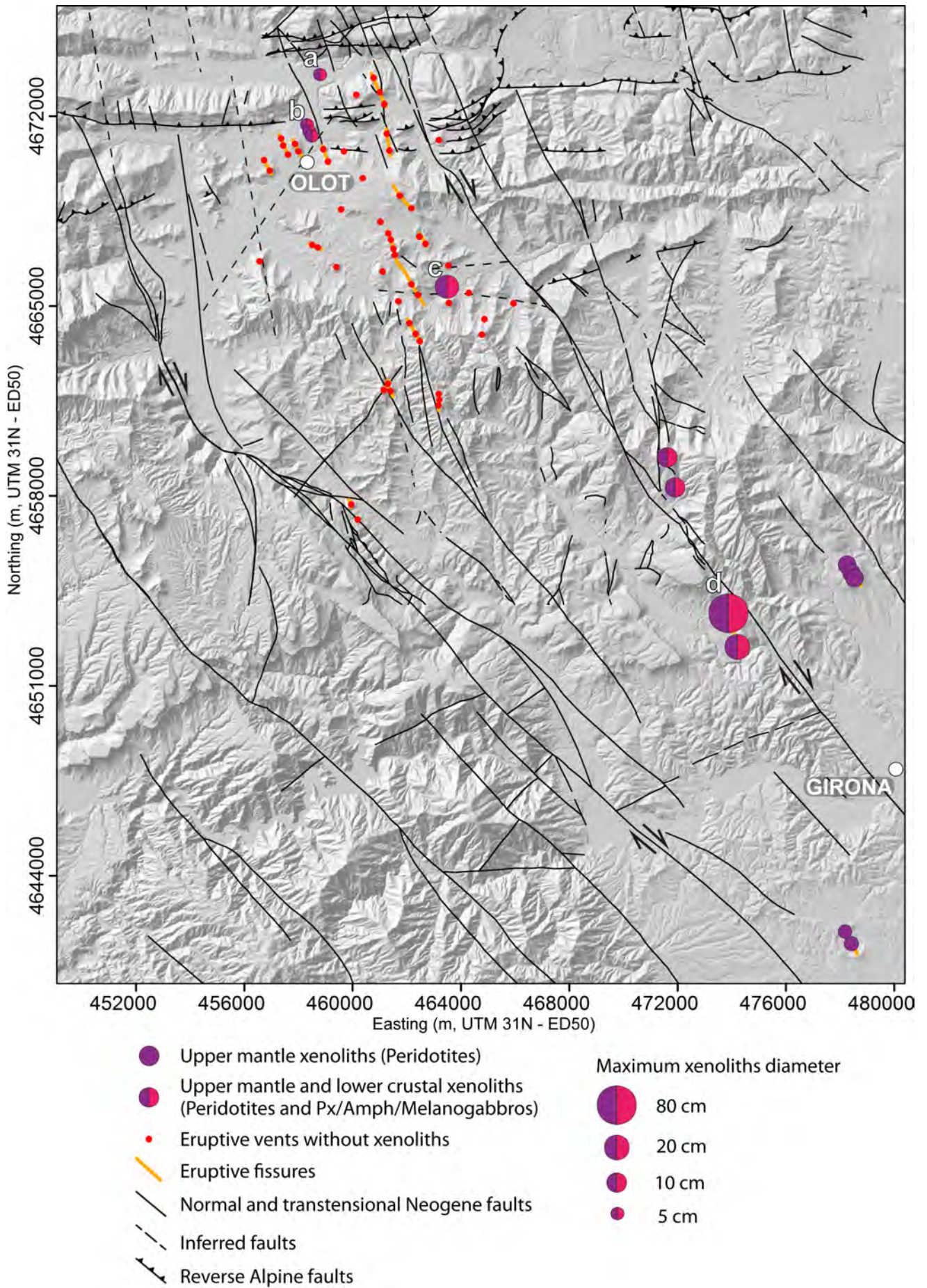


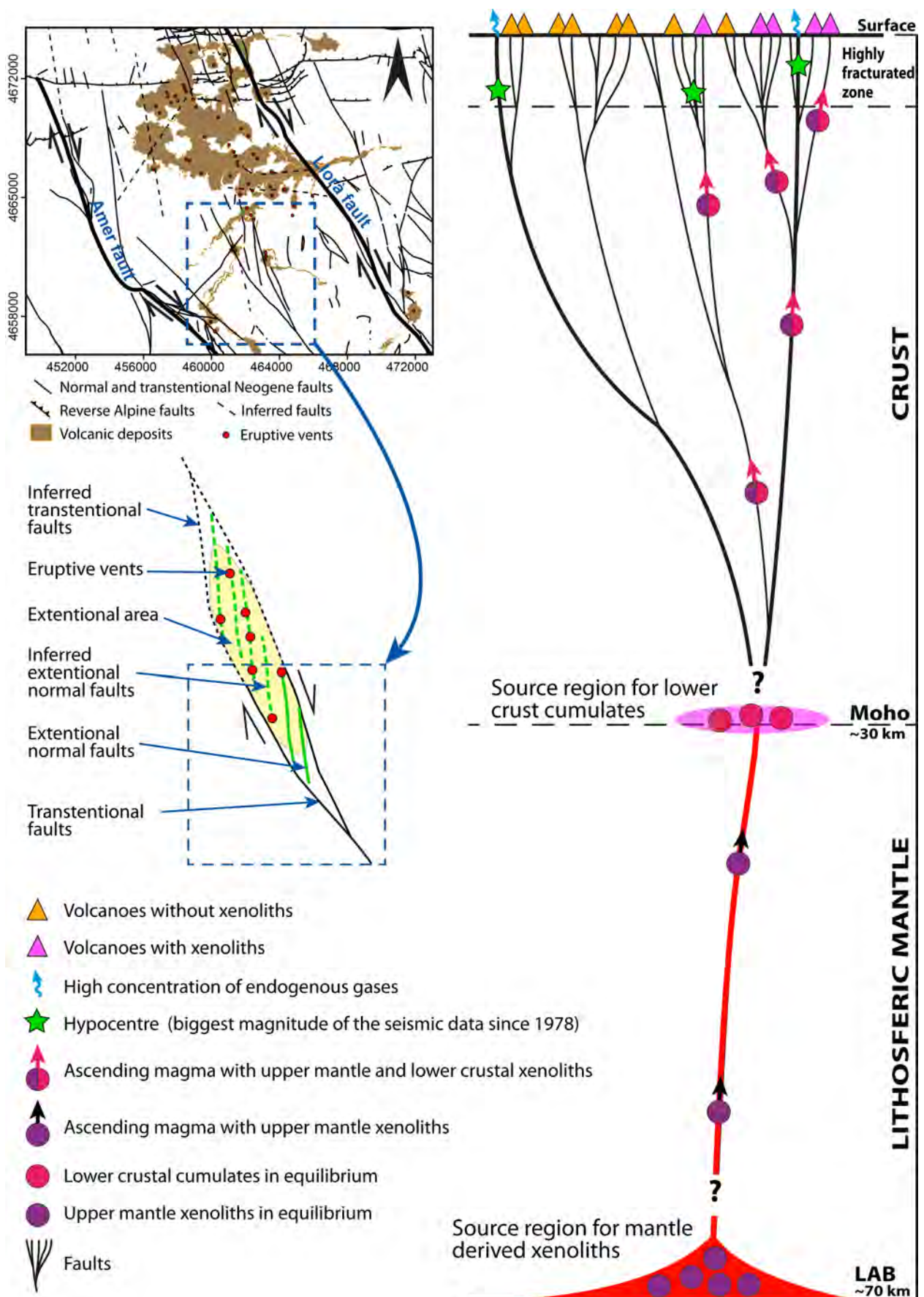
Figure 8






Figure 9



Figure 10



Appendix 7.1. Proof of delivery of the paper

TECTONOPHYSICS  Contact us  Help  'My EES Hub' available for consolidated users ... [more](#)

[home](#) | [main menu](#) | [submit paper](#) | [guide for authors](#) | [register](#) | [change details](#) | [log out](#) Username: [xavier.bolos@gmail.com](#)
Switch To: [Author](#) | Go to: [My EES Hub](#) Version: [EES 2014.3](#)

Submissions Being Processed for Author Xavier Bolós, M.D.

Page: 1 of 1 (1 total submissions) Display results per page.

Action	Manuscript Number	Title	Initial Date Submitted	Status Date	Current Status
Action Links	TECTO9652	Volcano-structural analysis of La Garrotxa Volcanic Field (NE Iberia): implications for the plumbing system	23 May 2014	24 May 2014	Under Review

Page: 1 of 1 (1 total submissions) Display results per page.

[<< Author Main Menu](#)